David Moe Almenningen

Synthetic Efforts to Investigate Structure-Property Relationships in Dyes for Dye-Sensitized Solar Cells

Doctoral thesis

David Moe Almenningen

NTNU
Norwegian University of
Science and Technology
Thesis for the degree of
Philosophiae Doctor
Faculty of Natural Sciences
Department of Chemistry

Doctoral theses at NTNU, 2022:300

NTNU
Norwegian University of
Science and Technology

NTNU
Norwegian University of
Science and Technology

NTNU

David Moe Almenningen

Synthetic Efforts to Investigate Structure-Property Relationships in Dyes for Dye-Sensitized Solar Cells

Thesis for the degree of Philosophiae Doctor

Trondheim, October 2022

Norwegian University of Science and Technology
Faculty of Natural Sciences
Department of Chemistry

NTNU
Norwegian University of
Science and Technology

PRINTED IN
NORWAY
NO - 1598

NORDIC SWAN ECOLABEL

Printed matter
2041 0731

Acknowledgments

First and foremost, I wish to express my most sincere gratitude to **Odd Reidar**. Thank you for always believing in me, and for the freedom you have given me to choose my own path forwards. The genuine care you have for every member of your research group is obvious, and has made working with you during my master's and PhD studies something I will remember fondly. I am very grateful to my co-supervisor **Bård** for all the good discussions we have had on chemistry, writing manuscripts, and more importantly football. I value your constant good mood, it is very infectious. If my list of thanks to **Audun** was to be complete, it would cover unseemly amounts of space. Instead I will attempt to express my gratitude via this metaphor: Working in the solar cell lab after you has been like skiing (on fluorine-free skis) in perfectly prepared tracks. In addition, a big thanks is due for **Henrik**. You have been a joy to work with and your EIS expertise has been key in completing this project. **Solon**, your taste in music and your help with electrochemistry have both been first rate.

A heartfelt thanks is extended to all my collaborators who I have been fortunate to work with. I am also very fortunate to have received help from the excellent technical staff at the Faculty. A special mention goes out to **Roger**, your constant supply of chemicals and encouragements have made life in the lab as smooth as it can be.

Thanks to the "veierom" wrecking crew **Johnson**, **Big Fred**, **The CEO**, **Audi**, **AC**, **Voksne Thomas**, **Mel**, **Shanno**, **Sim1**, and **Prince Andrew**. I could not dream of a finer cohort. Your combined expertise in chemistry and in having a good time has proven invaluable in dealing with challenges provided by lab-work or global pandemics. I am thankful for my office-mate **Helgi** and his unique dry/dark humor, which has made spending time in the office writing considerably more fun. Thank you to **Cecilie** who proofreaded this thesis. I am also thankful for helpful discussions with **The K-Man**, both those related to science and those related to climbing betas. I want to thank all master's students that I have been lucky to supervise, and to past and present member of the solar cell lab. I have always looked forward to spending time in the lab due to the super environment that exists there.

My whole life I have been very fortunate to have excellent friends, your support

and the good times we have together mean the world to me. No one mentioned, no one forgotten. Another source of constant support is my family, for which I am very grateful. **Solveig**, den omsorgen du syner for dei rundt deg er ein dagleg inspirasjon for meg. My parents **Eldbjørg** and **Ole Erik** have taught me countless valuable lessons, but perhaps most crucially that "it's nice to be important, but more important to be nice". My sisters **Maria** and **Anna** are the funniest people I know, and are the true inspiration behind the naming of some of my compounds (**DMA** = David, Maria, Anna).

Last but most of all, I am grateful to **Vilde**. Whatever we have had to face from the ups-and-downs associated with doing a PhD or making it through a global pandemic, overcoming these things with you has made it considerably easier and considerably more worthwhile. Islands in the stream, that is what we are.

"What's really important here," I whispered loudly to myself "is not the big things other people have thought up, but the small things you, yourself have."

Haruki Murakami,
Sputnik Sweetheart

Abstract

With the backdrop of human-induced global warming in mind, the need for sustainable energy has never been larger. The Intergovernmental Panel on Climate Change presented in their recent assessment report that global warming already has had adverse effects on nature and people beyond natural variability. The release of greenhouse gases from human activity is no longer a problem for the future, the consequences can be felt already today.

Sustainable energy sources such as nuclear, hydroelectric, wind, wave, and solar cells technology will have to carry the brunt of the energy production for the future. Putting serious research effort into improving the viability of these technologies will be important in the transition to sustainable energy production. This thesis concerns the development of a solar cell technology, more specifically the dye-sensitized solar cell (DSSC).

The dye-sensitized solar cell, a technology that recently turned 30 years since its original report in 1991, has shown great promise for multiple applications. The typical DSSC is comprised of a simple sandwich structure of a photoanode and a counter electrode with a redox shuttle carrying the charge between these. The crucial photoanode is made up of a mesoporous semiconductor material, typically TiO_2. The semiconductor is coated by a dye that absorbs light and injects electrons to the semiconductor. Although it is less efficient compared to the conventional silicon solar cell under standard solar illumination, the DSSC still have some unique properties making it a fascinating topic to devote attention to. In recent years, it has been established that the DSSC is the most efficient technology for low light harvesting. This trait means that the DSSC can be used under indoor lighting to power the ever-increasing market of consumer electronic devices and sensors. Another strength associated with the DSSC is the aesthetically pleasing aspect of transparent solar cells and the possibility of deciding the color of the finished device. Dye development is absolutely central to achieving DSSCs with these illustrious properties. The topic of this thesis is precisely this, to develop novel dyes for use in DSSC. The main focus is to use organic synthesis to prepare libraries of dyes and look for successful traits to guide design of future dyes.

In Paper I-III, the electronic system of the dyes was scrutinized. The investigation of oligothiophene π-spacers in phenothiazine dyes presented in Paper I revealed that the dye without any π-spacer was the most efficient dye when implemented in a DSSC. The highest photocurrent was produced by the terthiophene linked dye, which laid the foundation for Paper II. The library of terthiophene linked triarylamine dyes found that the fully fused terthiophene dye was the most efficient in a Cu regenerated device. The study on planarizing the triarylamine donor shown in Paper III, highlighted the importance of the geometry on optical and electron transport properties. The conventional phenothiazine motif displayed superior photovoltaic properties over the triarylamine dyes in an iodine regenerated device. The fully planarized double phenoxazine donor with its excellent absorption properties failed to convert them to efficient solar cell performance.

In Paper IV and V, the goal was to improve the packing ability of the dyes on the surface of TiO_2 with minimal influence on the optoelectronic properties of the compounds. In Paper IV the first account of covalently attaching the common anti-aggregation additive chenodeoxycholic acid (CDCA) to a dye was presented. This modification improved the quality of the dye monolayer on TiO_2, and it was established that the optimal ratio of CDCA to dye on the semiconductor surface was larger than one. Hoping to improve the viability of this strategy by employing a simpler blocking unit, in Paper V two ethyladamantyl decorated dyes were considered. Both these dyes displayed improved photovoltages compared to the unmodified reference dye. However, the adamantyl decorated π-spacer displayed deleterious interactions when paired with the anti-aggregation additive CDCA, which led to significantly increased elcectron loss processes.
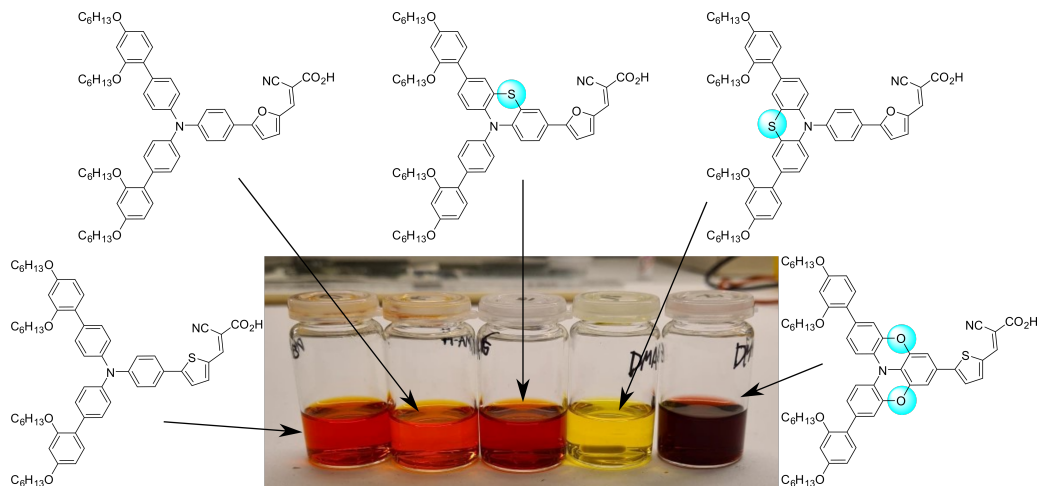
The image from Paper III shows the effect that a single atom or two can have on the absorption properties of the dyes. Equally as important is the placement of the atoms.

Samandrag

Med menneskeskapt global oppvarming som bakteppe, har behovet for berekraftig energi aldri vore større. FNs klimapanel (IPCC) presenterte i deira nye hovudrapport at global oppvarming allereie har hatt skadelege effektar på natur og menneske forbi naturleg variasjon. Utslepp av drivhusgassar frå menneskeleg aktivitet er ikkje lenger eit problem for framtida, konsekvensane er merkbare allereie no.

Berekraftige energikjelder som atom-, vatn-, vind-, og bølgekraft vil i lag med solcelleteknologi måtte stå for mesteparten av energiproduksjonen i framtida. Det vil difor vera viktig å drive omfattande forsking for å auke konkurransedyktigheita til desse teknologiane for å gjennomføre overgangen til berekraftig energiproduksjon. Denne doktorgradsoppgåva omhandlar utviklinga av ein solcelleteknologi, meir spesifikt omhandlar den fargestoffbaserte solceller kalla DSSC.

Fargestoffbaserte solceller er ein teknologi som nyleg fylte 30 år sidan den originalt vart introdusert i 1991, og har vist stort potensial for fleire applikasjonar. Den typiske DSSC-strukturen består av ein fotoanode og ein motelektrode som omgir eit redoksmateriale som bær ladninga mellom elektrodane. Fotoanoden består av eit mesoporøst halvleiarmateriale, som oftast TiO_2. Dette er dekka med fargestoff som absorberer lys og injiserer elektron til halvleiaren. Sjølv om DSSC-teknologien er mindre effektiv under standard sollys enn konvensjonelle silisium solceller, så er det mange unike eigenskapar knytt til DSSC som gjer den til eit fascinerande forskingsobjekt. I dei siste åra så har det blitt vist at DSSC er den mest effektive teknologien under svak belysing. Denne eigenskapen gjer DSSC til ein ettertrakta energikjelde for den stadig aukande marknaden for forbrukarelektronikk og sensorar. Ein annan styrke assosiert med DSSC er den estetiske faktoren knytt til gjennomsiktige solceller og høvet til å bestemme fargen til den ferdige solcella. Utvikling av nye fargestoff har vore heilt essensielt for å oppnå DSSC med desse strålande eigenskapane. Temaet på denne oppgåva er nettopp det, å utvikle nye fargestoff til bruk i DSSC. Hovudfokuset er å bruke organisk syntese som eit verkty for å framstille samlingar av nye fargestoff. Desse samlingane skal så brukast for å leite etter nyttige trekk som kan styre design av framtidige fargestoff.

I Artikkel I-III, vart det elektroniske systemet til fargestoffa granska. Undersøkinga av oligotiofen π-bruer i fenotiazin fargestoff, presentert i Artikkel I, avslørte at fargestoffet utan π-bru var det mest effektive for bruk i DSSC. Den høgaste straumen vart målt frå eit fargestoff med tertiofen π-bru, dette vart grunnlaget for Artikkel II. Samlinga med tertiofen-linka fargestoff viste at den fullstendig samankopla tertiofenen var den mest effektive i ei kopar-regenerert solcelle. Studien på planarisering av triarylamindonoren, vist i Artikkel III, understreka viktigheita av geometrien til fargestoffet både på optiske og elektrontransport eigenskapar. Den konvensjonelle fenotiazin-strukturen utklassa triarylamin-fargestoffa med tanke på effektivitet i ei jod-regenerert solcelle. Den fullstendig planariserte doble fenoxazin donoren viste framifrå absorbsjonseigenskapar, men lukkast ikkje i å konvertere dei til effektiv solcelleytelse.

I Artikkel IV og V var målet å forbetre evnen fargestoffa har til å dekke overflata på TiO$_2$, men samstundes påverke dei optoelektroniske eigenskapane til sambindingane minimalt. I Artikkel IV viste me dei fyrste fargestoffa med det vanlege anti-aggregeringstoffet *chenodeoxycholic acid* (CDCA) kovalent bundne til seg. Denne modifikasjonen forbetra fargestofflaget på TiO$_2$, og det vart vist at det optimale forholdet mellom CDCA og fargestoff på overflata av halvleiaren er større enn ein. Med håp om å forbetra nytteverdien til denne strategien ved å bruke ein enklare blokkeringsmodifikasjon, vart to fargestoff substituert med etyladamantyl testa til dette føremålet i Artikkel V. Begge desse fargestoffa viste forbetra spenning samanlikna med referansefargestoffet utan etyladamantyl. Fargestoffet med adamantyl-substituert π-bru viste øydeleggjande interaksjonar då det vart brukt i lag med anti-aggregeringstoffet CDCA, noko som førte til ein auke i elektrontapsprosessar.
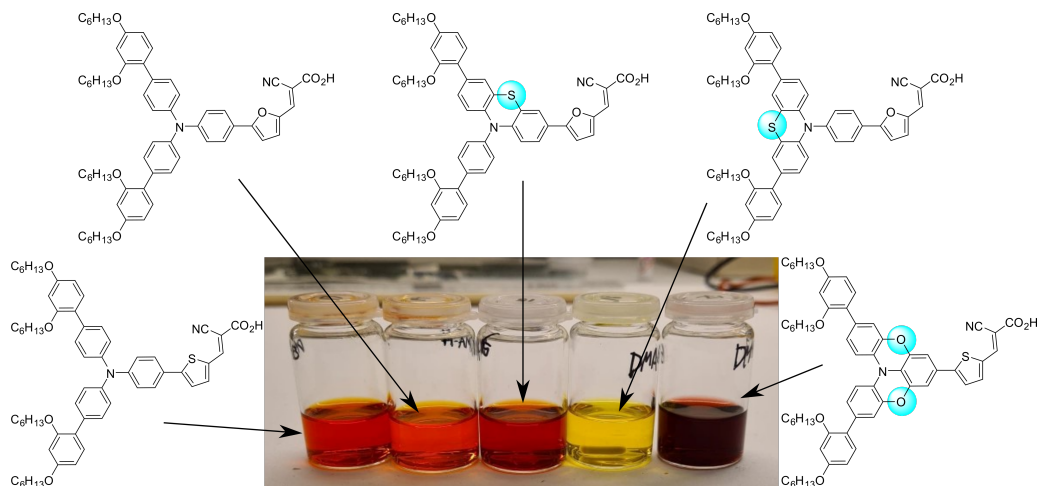
Biletet frå Artikkel III syner effekten som eit einskild atom eller to kan ha på absorbsjonseigenskapane til fargestoffa. Like viktig er likevel plasseringa av desse atoma.

Contents

List of Papers

Papers included in this thesis

I. **D. M. Almenningen**, H. E. Hansen, M. F. Vold, A. F. Buene, V. Venka-traman, S. Sunde, B. H. Hoff and O. R. Gautun,

Effect of thiophene-based π-spacers on N-arylphenothiazine dyes for dye-sensitized solar cells,

Dyes and Pigments **185** 108951 (2021).

Contribution: Synthesis and characterization of dyes — preparation and characterization of DSSCs — paper drafting, review and editing

II. **D. M. Almenningen**, H. E. Hansen, A. F. Buene, B. H. Hoff and O. R. Gautun,

Effect of seven different terthiophene π-spacers on dye performance in dye-sensitized solar cells,

Submitted to Dyes and Pigments

Contribution: Design, synthesis and characterization of dyes — preparation and characterization of DSSCs — paper drafting, review and editing

III. **D. M. Almenningen**, V. M. Engh, E. A. Strømsodd, H. E. Hansen, A. F. Buene, B. H. Hoff and O. R. Gautun,

Synthetic Efforts to Investigate the Effect of Planarizing the Triarylamine Geometry in Dyes for Dye-Sensitized Solar Cells,

ACS Omega **7** 22046 (2022).

Contribution: Design, synthesis and characterization of dyes **3,7-PTZ-Fu** and **POZPOZ-Th** — preparation and characterization of DSSCs — paper drafting, review and editing

IV. A. F. Buene, **D. M. Almenningen**, A. Hagfeldt, O. R. Gautun and B. H. Hoff,

First Report of Chenodeoxycholic Acid–Substituted Dyes Improving the Dye Monolayer Quality in Dye-Sensitized Solar Cells,

Solar RRL, **4** 1900569 (2020).
DOI: 10.1002/solr.201900569

Contribution: Synthesis of dyes C_6 and C_3 — paper review and editing

V. **D. M. Almenningen**, B. S. Haga, H. E. Hansen, A. F. Buene, B. H. Hoff and O. R. Gautun,

Adamantyl Side-Chains as Anti-aggregating Moieties in Dyes for Dye-Sensitized Solar Cells,

Chemistry - A European Journal *Accepted article* (2022).
DOI: 10.1002/chem.202201726

Contribution: Designed the dyes and supervised the synthesis of them — Preparation and characterization of DSSCs — paper drafting, review and editing

Papers not included in this thesis

VI. A. E. Yemene, V. Venkatraman, **D. M. Almenningen**, B. H. Hoff and O. R. Gautun

Synthesis of Novel 3,6-Dithienyl Diketopyrrolopyrrole Dyes by Direct C-H Arylation,

Molecules, **25** 2349 (2020).
DOI: 10.3390/molecules25102349

VII. A. F. Buene and **D. M. Almenningen**

Phenothiazine and phenoxazine sensitizers for dye-sensitized solar cells – an investigative review of two complete dye classes,

Journal of Materials Chemistry C, **9** 11974 (2021).

VIII. N. Gudim, M. Mikhailov, E. A. Knyazeva, **D. M. Almenningen**, L. V. Mikhalchenko, S. Economopoulos and O. A. Rakitin

Monitoring the dependence of photovoltaic properties of dye-sensitized solar cells from the structure of D-A-π-A type sensitizers with 9-(p-tolyl)-2, 3, 4, 4a, 9, 9a-hexahydro-1H-1, 4-methanocarbazole donor building block,

Molecular Systems Design & Engineering, (2022).

List of Abbreviations and Symbols

ϵ Molar extinction coefficient

λ_{max} Absorption maximum

$\phi_{\text{AM 1.5G}}$ Photon flux from AM 1.5G irradiance

Φ_{col} Electron collection efficiency

Φ_{inj} Electron injection efficiency

Φ_{LHE} Light-harvesting efficiency

θ_z Zenith angle

A   Absorbance

ADAA   1-Adamantane acetic acid

AM   Air mass

AR6   Assessment Report 6

AZA   2-azaadamantan-N-oxyl

CB   Conduction band

CDCA   Chenodeoxycholic acid

CE   Counter electrode

CIGS   Copper indium gallium diselenide

CPDT   Cyclopenta[1,2-b:5,4-b']dithiophene

CV   Cyclic voltammetry

DSSC   Dye-sensitized solar cell

E_{0-0} Optical band gap

EIS   Electrochemical impedance spectroscopy

Fc   Ferrocene

FF   Fill factor

FMO   Frontier molecular orbitals

FTO   Fluorine doped tin oxide

HOMO   Highest occupied molecular orbital

ICT   Intramolecular charge transfer

IEA   International Energy Agency

IoT   Internet-of-things

IPCC   Intergovernmental Panel on Climate Change

IPCE   Incident photon to current conversion efficiency

J_{max} Current density at maximum power

J_{sc} Short-circuit current density

LiTFSI   Lithium bis(trifluoromethane)sulfonimide

LUMO   Lowest unoccupied molecular orbital

MLCT   Metal-to-ligand charge transfer

MO   Molecular orbital

NHE   Normal hydrogen electrode

NREL   National Renewable Energy Laboratory

OFET   Organic field-effect transistor

OLED   Organic light-emitting diode

OPV   Organic Photovoltaics

P_{in} Incident power

P_{max} Maximum power

PCE   Power conversion efficiency

PEC   Photoelectrochemical cell

PEDOT Poly(3,4-ethylenedioxythiophene)

Phen 1,10-Phenanthroline

PL Photoluminescence

POZ Phenoxazine

PSC Perovskite solar cell

PTZ Phenothiazine

PV Photovoltaic

QDSSC Quantum dot-sensitized solar cell

R_s Series resistance

R_{Pt} Counter electrode charge transfer resistance

r_{rec} Recombination resistance

r_{tr} Transport resistance

SHE Standard hydrogen electrode

ssDSSC Solid-state dye-sensitized solar cell

TAA Triarylamine

TBA Tetrabutylammonium

TBP 4-*tert*-Butylpyridine

tmby 4,4',6,6'-Tetramethyl-2,2'-bipyridine

TPA Triphenylamine

V_{max} Voltage at maximum power

V_{oc} Open-circuit voltage

VB Valence band

WE Working electrode

Z_D Warburg diffusion impedance

Preface

This thesis is submitted to the Norwegian University of Science and Technology (NTNU) as a partial fulfillment of the requirements for the degree of Philosophiae Doctor. The PhD period lasted from August 2018 to August 2022, and included the equivalent of one year teaching duties and 30 ECTS of coursework, corresponding to approximately six months. The work is structured as a collection of papers, and the finished papers and manuscripts are found in the appendix. Four out of the five papers are accepted for publication, while Paper II is provided as the manuscript submitted to the journal Dyes and Pigments.

The work was supported by the Department of Chemistry at NTNU. The main supervisor was Ass. Prof. Odd Reidar Gautun (NTNU) and the co-supervisor was Prof. Bård Helge Hoff (NTNU).

David Moe Almenningen
Trondheim, September 2022

Aim of the Thesis

Approaching the task of improving the DSSC technology as an organic chemist, the most prudent way to do so is probably through organic chemistry. The main goal of this thesis was to use organic synthesis as a tool to prepare sets of dyes that can illuminate useful structure-property relationships. With the wealth of organic synthesis knowledge available at the department it has been possible to prepare larger sets of dyes for fundamental studies, introduce novel dye design concepts, and target elusive dye structures. The working method chosen for this thesis can be briefly summarized as follows:

- Design and synthesize novel dye libraries from practical synthesis routes.

- Characterize the optoelectronic properties of the dyes and prepare DSSC devices to evaluate their photovoltaic properties.

- Relate the optoelectronic and photovoltaic properties to dye structure, where electrochemical impedance spectroscopy served as the main tool to elucidate the effect on electron transfer processes.

- Pursue interesting observations and develop on lead dye structures.

As the second PhD candidate working on the DSSC project at NTNU, another important goal was to expand on the brilliant work put into establishing fabrication equipment and procedures. The key objective was to make state-of-the-art DSSCs employing one-electron metal complex redox shuttles in the solar cell lab in Trondheim.

1 Introduction

This chapter is intended to provide the reader with a background for the work presented in Chapter 2. The structure of this chapter resembles that of an onion where you peel away one layer after the other to get to the core. Starting in Section 1.1, the topic of photovoltaics (PV) and its prospects as a future energy source is covered. In Section 1.2 the dye-sensitized solar cell (DSSC) and its intricacies is presented. Section 1.3 concerns the dyes responsible for the light harvesting in DSSCs, where a special focus is given to the fully organic dyes. The final Section 1.4 covers vital aspects related to the organic synthesis of the dyes presented in this thesis.

1.1 Photovoltaics

This thesis concerns the synthesis of organic dyes for DSSCs, with the goal of understanding and hopefully improving the photovoltaic performance of the solar cells. But first, the fundamentals of photovoltaics, and what the prospects of these technologies are needs to be considered. Briefly, photovoltaics are technologies concerned with the direct conversion of sunlight to energy. However, before exploring these technologies further in this thesis, the need for these technologies must be motivated.

1.1.1 Why do we need photovoltaics?

"Human-induced climate change has caused widespread adverse impacts and damages to nature and people, beyond natural climate variability." This is one of the verdicts presented by the Intergovernmental Panel on Climate Change (IPCC) in their most recent assessment report (AR6).[1] The consequences of anthropogenic greenhouse gases in the atmosphere are no longer a problem for the future, its effects are already felt today.

To lessen the adverse impacts brought on by climate change, the United Nations have through the Paris Agreement set out to limit the temperature increase to 1.5 °C.[2] To reach this goal, it is important that more sustainable energy sources are made available and competitive to fossil fuels. Sustainable energy sources

should be naturally replenished and not contribute further to increasing anthropogenic global warming. It is natural to consider the Sun when seeking to meet these criteria. Sustainable energy sources such as hydroelectricity, wind and wave power all depend on the Sun as their origin of power. The direct conversion of solar radiation to electric energy through the photovoltaic effect is probably the technology most likely to meet the present and future energy demands.

The Sun as an energy source has tremendous potential. The surface of the Earth is radiated with $1.2 \cdot 10^{17}$ W,[3] meaning that the yearly energy demand on earth is met in less than one hour. However, the radiation from the Sun that reaches the ground is dependent on daily and yearly variations. In addition, the atmosphere is also highly influential in determining the amount of solar energy that reaches Earth's surface. As shown in Figure 1.1 where the black line illustrates the energy that reaches the top of the atmosphere, while the red and blue lines represent the solar spectrum after passing through the atmosphere and reaching the surface. The reduction in incident energy occurs due to scattering of the sunlight and absorption by chemicals in the atmosphere (O_3/H_2O/CO_2).
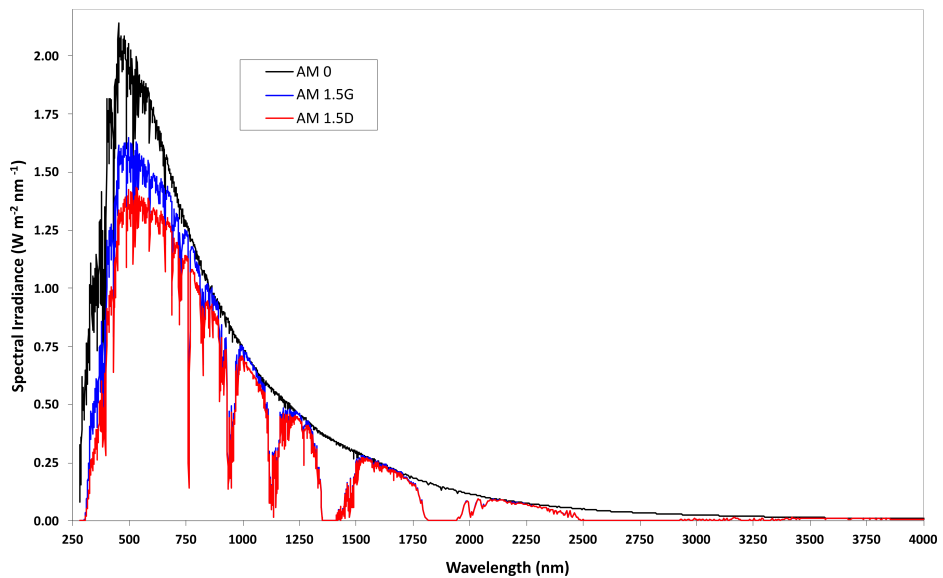

Figure 1.1: The irradiance of the AM 0 (black line), AM 1.5G (blue line), AM 1.5D (red line) spectra (ASTM G173-03). The data is provided by NREL (*https://www.nrel.gov/grid/solar-resource/spectra-am1.5.html* accessed 02. 05. 2022.)

The effect of Earth's atmosphere on the amount of sunlight reaching its surface has been accounted for by introducing the concept *air mass* (AM). This is illustrated in Figure 1.2. The air mass depends on the relative length of the path of the sunlight through the atmosphere. The shortest length corresponds to the Sun being at zenith, here the air mass is 1 (AM 1.0). Outside of Earth's atmosphere the air mass is 0 (AM 0). To approximate the air mass in other cases,

the relation $1/\cos(\theta_z)$ is used, where θ_z is the zenith angle of the Sun. Figure 1.1 also demonstrates the difference between measuring only the direct sunlight on Earth's surface (red curve) and including the diffuse radiation from light scattering and ground reflection (blue curve). The latter considerations are referred to as the Global (G) spectrum, and are used in the "standard" solar spectrum AM 1.5 Global (AM 1.5G). An air mass of 1.5 equals the irradiation at a zenith angle of 48.2°, corresponding to mid-latitude countries. The AM 1.5G solar spectrum corresponds to an incident irradiance of 1 kW m^{-2}, referred to as 1 sun.[3]
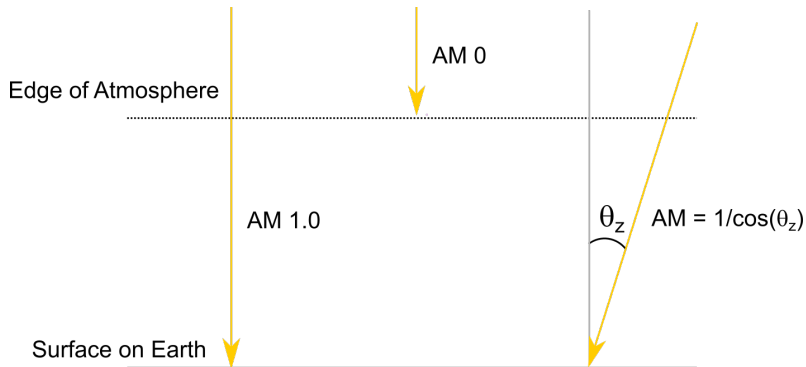

Figure 1.2: The effect of atmosphere on the attainable sunlight is expressed in air mass (AM).

According to the International Energy Agency (IEA), the worlds energy demands is projected to increase by 17% within 2040.[4] The increase in energy demand should be met by an increased sustainable energy production. Having established the credentials of the Sun as a source for sustainable energy production for the next 5 billion years, the next topic that will be devoted attention is how to harvest it through the photovoltaic effect.

1.1.2   What is photovoltaics?

Edmond Becquerel has been heralded as the inventor of the field of photovoltaics for his discovery of current being produced from a silver chloride coated platinum electrode in an electrolyte under solar illumination.[5] His discovery of the photovoltaic effect in 1839 laid the foundation for a whole new way of harvesting energy from the Sun. Prior to this discovery, the only *direct* use of solar energy was seen through the thermal properties of sunlight for heating and drying. The next major contribution to the field of photovoltaics was made by Adams and Day in 1876, where they presented a selenium-platinum junction capable of producing current under solar illumination.[6] Although the photovoltaic effect had been established for more than 100 years, the modern solar cell was not invented until 1954. That was the year when Chapin, Fuller and Pearson presented the first silicon *p-n* junction photovoltaic device.[7]

The silicon p-n junction solar cell has since its origin in 1954 become a mature technology with Si-wafer based technologies making up 95% of all production in the PV-market.[8] During the last 10 years, the average efficiency of Si-based photovoltaic modules has increased from 15% to 20%, and the energy payback time for these PV-systems in northern Europe has become as low as 1.2 years.[8] Integral to the Si-wafer solar cell is ultra-pure silicon, the purity requirement for solar-grade silicon is 99.9999%. The most common way to produce ultra-pure silicon is through the Czochralski process, invented by Jan Czochralski in 1918.[9] In this crystallization process, Si is melted at 1414 °C and a seed crystal of silicon is brought in contact with the melt. As crystallization begins, the seed is pulled out slowly, thus forming an ingot of single-crystal silicon. The ingot is then cut into wafers to form the substrates for the solar cells, resulting in loss of ultra-pure silicon material during the cutting process. Recent work from Fraunhofer ISE on the development of epitaxially grown silicon addresses the material loss issue,[10] and brings promise of even more cost-effective photovoltaics.

Ultra-pure silicon on its own does not achieve high-efficiency photovoltaic devices, as this operates almost as an insulator due to the restricted movement of electrons in the filled valence band (VB).[3] For the silicon semiconductor to conduct electricity it needs to be doped by phosphorus (*n-type*) and boron (*p-type*). The phosphorus atoms (or other group 5 atoms) have five outer electrons and four of these are used to fill the valence band of the semiconductor. The remaining electron is donated to the conduction band (CB) of the semiconductor, making the Si-crystal a conductor. The nomenclature *n-type* refers to the charge carrier being a negatively charged electron. The introduction of boron atoms (or other group 3 atoms) have the opposite effect, where the three outer electrons are insufficient to fill the valence band of Si. The missing electron is referred to as a *hole* and can be considered a positively charged charge carrier, thus explaining the *p-type* nomenclature.

For the semiconductor to operate as a solar cell, a p-n junction needs to be formed by making an interface between the n and p region of the semiconductor. Across the junction a strong electrical field is formed, and the surplus electrons in the n region are pulled to the p side of the junction, and the holes are pulled in the opposite direction. Another vital aspect of the photovoltaic performance of silicon p-n junction solar cells is the light absorption by the semiconductor. Once a photon with energy larger than the band gap of the semiconductor strikes the solar cell, it may be absorbed and promote an excitation of an electron in the valence band to the conduction band. This process generates an *electron-hole pair* which is expertly separated across the electrical field of the p-n junction. This explains how charge generated under illumination is extracted and collected as electric current. A schematic representation of the working principles is shown in Figure 1.3 a).
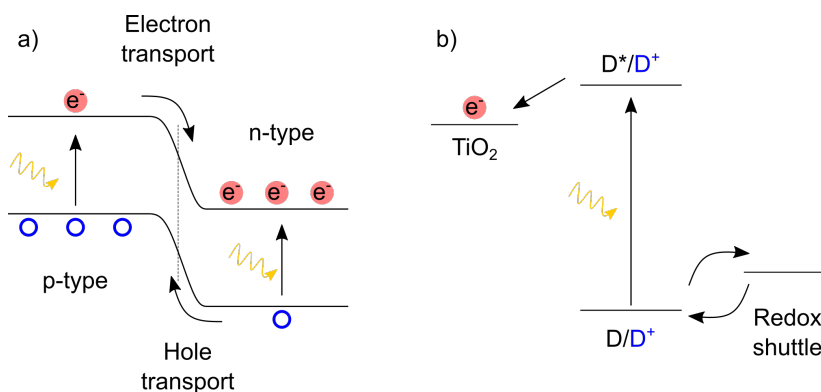
Figure 1.3: a) The working principles of a silicon *p-n* junction solar cell. b) The working principles of the photoelectrochemical dye-sensitized solar cell.

The thorough introduction to the working principles of *p-n* junction solar cells is made here to clarify the distinction between the traditional photovoltaic cell and the photoelectrochemical cell (PEC). The working principles of a DSSC, which is a photoelectrochemical cell, are shown in Figure 1.3 b). Though the inner workings of this technology will be covered more extensively in Section 1.2. To complicate matters more, both these technologies rely on the photovoltaic effect where incident light generates electron-hole pairs that can be separated across a semiconductor junction.[11] The main difference between the two solar cell technologies is that the PEC contains a redox shuttle that carries the moving charge, and electrochemical reactions occur on the redox shuttle/electrode interface(s).[12] Conversely, the PV solar cell is a fully solid-state device where electrons and holes carry the moving charge, and no chemical change occurs under operation.

With the immense amount of energy supplied to Earth from the Sun each day, it is no wonder that the invention of the first solar cell in 1954 sparked tremendous research and innovation efforts in the field of photovoltaics. The stages of development are categorized into generations of photovoltaics, where the crystalline silicon solar cells, along with GaAs solar cells, are referred to as first generation. Monocrystalline Si cells have reached a power-conversion efficiency (PCE) of 26.7% in the laboratory.[8] The second generation photovoltaics comprises the thin-film technologies such as cadmium telluride (CdTe), copper indium gallium diselenide (CIGS), and amorphous silicon (a-Si). The development of the PCE of these technologies is presented in Figure 1.4, which is a chart of all the highest PCE-values confirmed by independent recognized test labs. The third generation photovoltaics is the group of emerging photovoltaic technologies such as quantum dot sensitized solar cells (QDSSC),[13] organic photovoltaics (OPV),[14] perovskite solar cells (PSC),[15] and dye-sensitized solar cells (DSSC).[16] Particularly promising among these emerging technologies is the perovskite solar cell, from its original report of 9.7% PCE in 2012[17] it has reached a confirmed efficiency of 25.5% in 2022.[8]
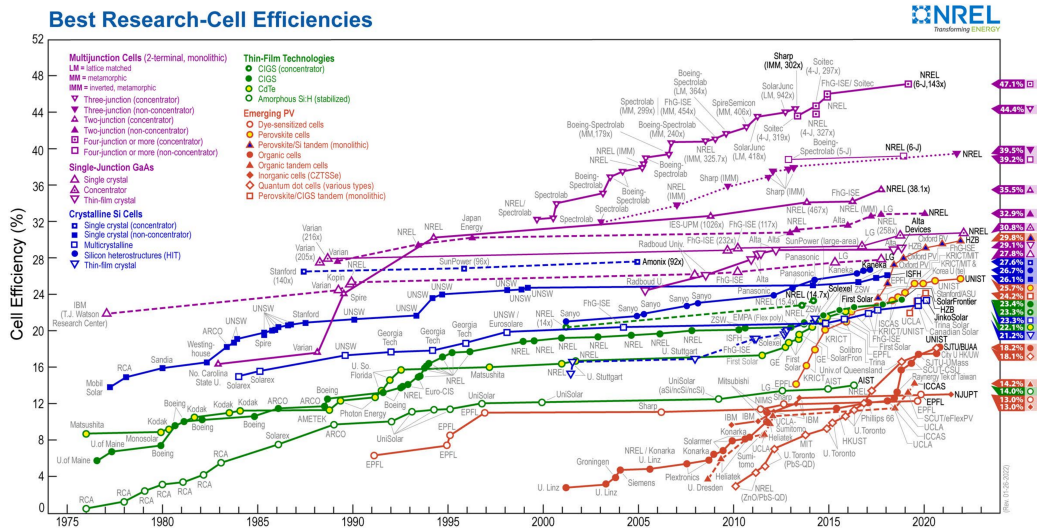
Figure 1.4: The NREL best-research cell efficiency chart. This plot is courtesy of the National Renewable Energy Laboratory, Golden, CO. (https://www.nrel.gov/pv/cell-efficiency.html) (04.05.2022)

With the fundamental concepts of photovoltaics covered in the above text, the prospect for these technologies to produce sustainable energy is apparent. The following section takes a closer look at one technology, the dye-sensitized solar cell. Although Figure 1.4 places the DSSC in joint last place in terms of PCE, the DSSC has many illustrious properties that will be covered in detail. And in any case, if more of the energy demand is to be met by photovoltaics it is beneficial to explore all technologies and not just the most efficient ones.

1.2 Dye-sensitized solar cells

The dye-sensitized solar cell was first presented in 1991, in the seminal paper by O'Regan and Grätzel.[18] Based on the distinction between the PV and PEC solar cell presented in Section 1.1.2, it is possible to attribute one of the DSSC's most alluring aspects to its photoelectrochemical nature. The light absorption of a DSSC is governed by the dye while the charge transport is carried out by the semiconductor and redox shuttle. In the silicon solar cells, the semiconductor has to be tailored to achieve both light absorption and charge transport simultaneously. The implication of this for the DSSC is that the charge transport and charge generation can be optimized by modifying separate parts of the solar cell. The multi-faceted nature of the DSSC has attracted a wide range of science disciplines such as materials scientists studying electrode materials, electrochemists developing the redox shuttles, or organic chemists preparing novel dyes for light harvesting. Before addressing the state-of-the-art DSSC, a quick overview of the

history of the technology is in place.

1.2.1 History of the DSSC

The first reports of a device resembling the DSSC, was presented in the pioneering work of Tributsch and Gerischer in the late 1960s.[19–21] Their work involved dye-sensitized ZnO crystals in contact with an electrolyte. Photocurrents were measured when this system was irradiated with light of a wavelength that the dye absorbed. The authors were also able to establish that the mechanism behind this photocurrent is the direct electron transfer from the excited dye molecule to the conduction band of the semiconductor.[21] This discovery laid the foundation for developing solar cells capable of separating the photogenerated electron-hole pair without an internal electrical field. In 1985, Desilvestro *et al.* demonstrated an unprecedented 44% incident-photon-to-current conversion efficiency (IPCE) by utilizing colloidal polycrystalline TiO_2 electrodes sensitized by a ruthenium complex dye.[22] The use of a mesoporous TiO_2 electrode with a high internal surface area, as presented in the original DSSC paper by O'Regan and Grätzel,[18] significantly improved the PCE to 7.9% and proved the feasibility of the technology for practical applications.
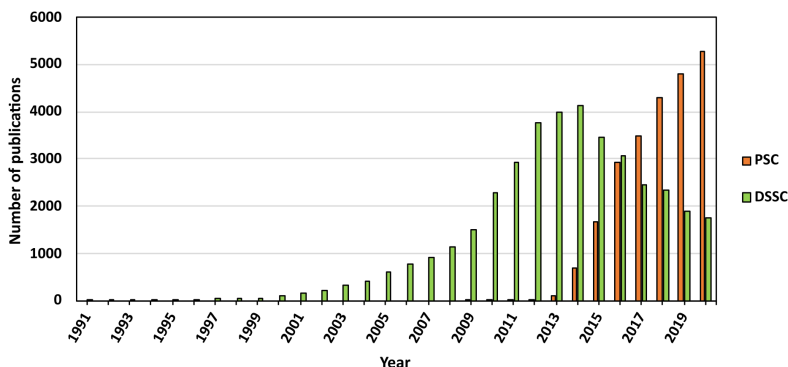

Figure 1.5: The number of publications per year concerning the concepts *dye-sensitized solar cells* (DSSC) and *perovskite solar cells* (PSC). This figure is adapted from Buene, 2021.[23]

As demonstrated in Figure 1.5, the DSSC has been extensively studied since its origin in 1991. The decline in publications in recent years is commonly attributed to the increase of research on the spin-off technology perovskite solar cells.[23] Two years after the DSSC proof-of-concept was presented, the synthesis of the novel ruthenium complex dye **N3** saw the efficiency rise to 10% (see Figure 1.6).[24] High-efficiency devices were for a long period of time associated with ruthenium complexes such as **N3**, its tetrabutyl ammonium salt analog **N719**, and the black dye **N749**.[25] In 2014, the fully organic dye **RK-1** was able to match the high-efficiency performance of **N719** in a DSSC device regenerated by an iodine redox
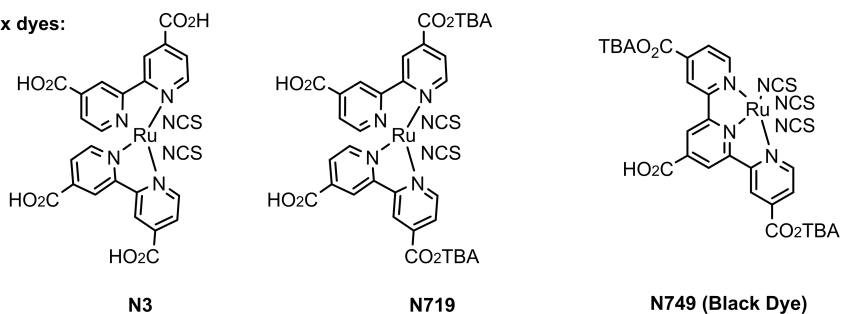
shuttle.[26] The library of cobalt complex redox mediators presented by Feldt *et al.*[27] in 2010, and their successful performance with the organic dye **D35** (see Figure 1.20) marked the beginning of a new era where the fully organic dyes replaced the ruthenium complexes as the state-of-the-art sensitizers. Utilizing the new cobalt complexes with more positive redox potentials than the iodine redox shuttle, the photovoltage of the DSSCs finally exceeded 1 V.[28] In 2015, the PCE record for DSSCs was set by Kakiage *et al.*,[29] following their report of a device co-sensitized by two organic dyes (**ADEKA-1** and **LEG4**) and employing a cobalt redox shuttle reaching a PCE of 14.3%. Ever since the publication by Freitag *et al.*[30] in 2016, the copper complex redox shuttle has become a mainstay for the modern DSSC due to its minimized overpotential losses. The record for most efficient photovoltaic technology under ambient light illumination was set by a copper-based DSSC in 2018, when the DSSC reported by Cao *et al.*[31] reached a PCE of 32% under ambient light. The novel dye **MS5** reported by Zhang *et al.*[32] in 2021 is a striking example of how important dye development is to improve DSSC performance. A DSSC sensitized by this dye was able to achieve an excellent photovoltage of 1.24 V, and while used as a co-sensitizer along with **XY1b** the record for ambient light photovoltaics was broken once more with a PCE of 34.5%.

This brief overview of the history is by no means extensive enough to encompass all the excellent work that has been done to develop the DSSC technology. However, it explains how the DSSC came to be, and the journey it has taken from a promising new photovoltaic technology to being established as the most efficient ambient light harvesting technology. Although the DSSC is not as efficient as other PV technologies under 1 sun AM 1.5G illumination, the excellent ambient light PCE makes the DSSC promising for powering the ever-increasing internet-of-things (IoT) applications with indoor lighting.[33] Having covered improvements made to the DSSC through development of new components and materials, it is only natural that the next section covers in detail the parts that constitutes the DSSC.
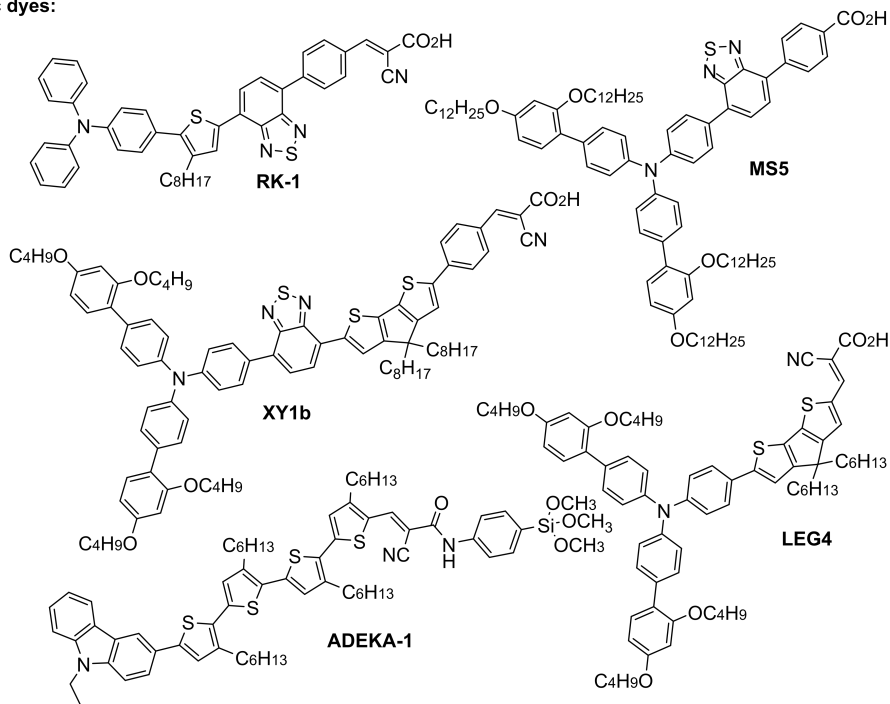
1.2.2   Components and materials of the DSSC

Before this overview of materials and components found in a DSSC, it is important to specify that it only addresses the *n*-type DSSC. The "DSSC architecture" has been utilized in other devices that, although similar, are distinct from the conventional *n*-type DSSC. Examples of such technologies are the *p*-type DSSC,[34] artificial photosynthesis,[35] solid-state DSSC (ssDSSC),[36] dye-sensitized photoelectrolysis,[37] and perovskite solar cells (PSC).[38] Unless specified otherwise in this text, the term DSSC refers to the "conventional" *n*-type DSSC with a liquid electrolyte redox shuttle. A schematic representation of such a device and its components are shown in Figure 1.7.

Ru complex dyes:

N3   **N719**   **N749 (Black Dye)**

Organic dyes:

RK-1   **MS5**   **XY1b**   **LEG4**   **ADEKA-1**

Redox shuttles

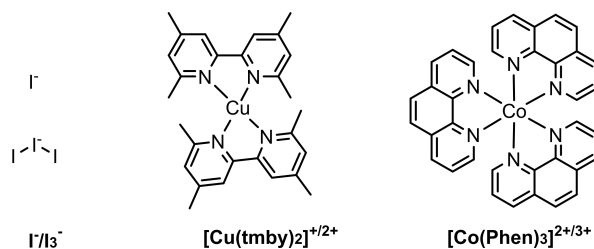I^-/I_3^- $[Cu(tmby)_2]^{+/2+}$ $[Co(Phen)_3]^{2+/3+}$

Figure 1.6: An overview of some of the most efficient dyes in DSSC history and their according redox shuttles. The Ru complex dyes and **RK-1** proved highly efficient with the I^-/I_3^- redox shuttle. A co-sensitized device with **XY1b** and **MS5** and regenerated by the $[Cu(tmby)_2]^{+/2+}$ set the record PCE under ambient light conditions. The combination of **ADEKA-1** and **LEG4** along with the $[Co(Phen)_3]^{2+/3+}$ redox shuttle is the most efficient DSSC to date.
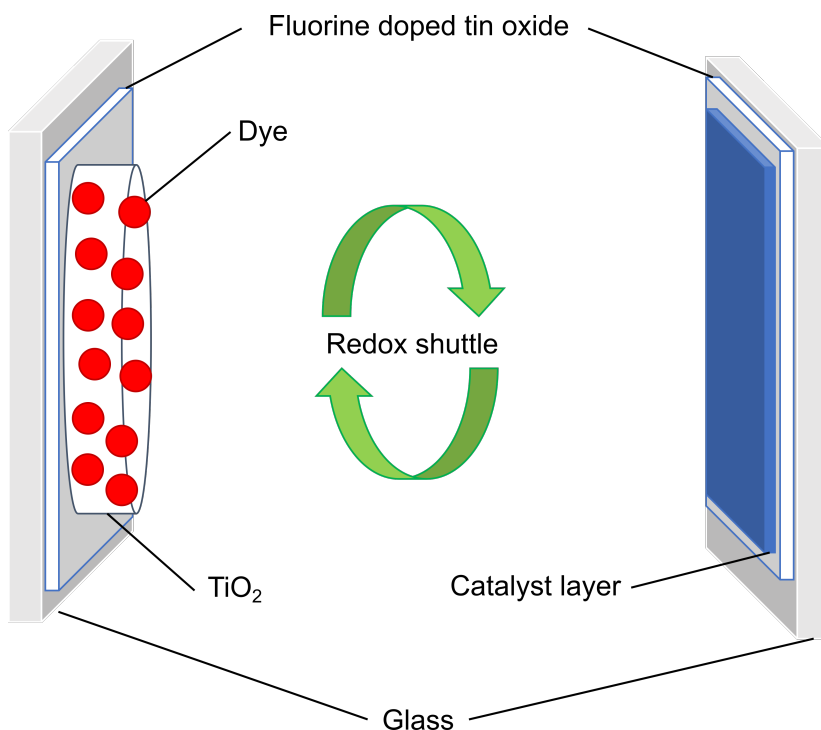
Figure 1.7: A schematic representation of the different components found in a typical *n*-type liquid electrolyte DSSC.

Glass substrate

The typical DSSC is a sandwich cell where the working and counter electrodes are arranged face-to-face. The substrate for these electrodes is frequently glass coated with fluorine-doped tin oxide (FTO).[39] The FTO glass is suitable for the DSSC application because of its high solar light transmittance, low sheet resistance, and good thermal stability.

Metal oxide semiconductor

Although ZnO was the original material used by Gerischer and Tributsch in the 1960s,[19] it was the introduction of mesoporous TiO_2 as the semiconductor material that revolutionized the DSSC and made it a feasible technology.[18] Since then, TiO_2 has been the preferred semiconductor metal oxide for DSSC. The TiO_2 crystal form *anatase* is preferred over the more thermodynamically stable form, *brookite*, because anatase has a higher conduction band edge leading to a higher Fermi level.

The typical working electrode (WE) is first equipped with a blocking layer of TiO_2 to reduce the contact between the FTO and the redox shuttle. The subsequent TiO_2 layers are fabricated by screen printing techniques to control the thickness of the semiconductor layers. The "active" TiO_2 layers are made from

nanocrystals of TiO_2 where the particle sizes are in the 10-50 nm range. The size of the TiO_2 nanocrystals and the thickness of the active layer are customized to fit the redox shuttle of the DSSC. For the I^-/I_3^- redox shuttle, a ~10 μm thick layer of TiO_2 with ~20 nm particle size is used. For the diffusion limited Co and Cu complexes, a thinner ~4 μm TiO_2 layer with ~30 nm sized particles is used. Recently, Velore *et al.*[40] demonstrated the mass transport issues that arises in Cu-based DSSC devices with too thick active layers. On top of the active layer it is common to deposit a "light scattering" layer consisting of ~400 nm TiO_2 particles. The scattering layer reflects light that is not absorbed by the active layer back into the light harvester and improves the PCE of the devices.[41] Finally, the electrodes are submerged in an aqueous $TiCl_4$ solution to deposit a thin layer of TiO_2 on the mesoporous TiO_2. This treatment increases the roughness and the surface area of the mesoporous TiO_2, and improves the dye loading.[42]

Dye

The role of the dye in a DSSC is so vital to this thesis that an entire section (Section 1.3) is devoted to it, and will therefore only be discussed briefly here. The dye is attached to the metal oxide semiconductor. A high surface area of the mesoporous TiO_2 is required to provide enough adsorption sites for the dyes. The dyes used in DSSCs can be tuned to fit different redox shuttles, match different light sources, or display different colors. Historically, the metal complex dyes fit the I^-/I_3^- redox shuttle best, while organic dyes are best for Co and Cu redox shuttles.

Redox shuttle

In a liquid redox shuttle it is common to use an organic solvent to dissolve the redox couple components along with various additives. The most important criteria when selecting a redox shuttle, is that there is sufficient driving force between the redox potential of the shuttle and the oxidation potential of the dyes. This way, an efficient dye regeneration is ensured. Additives such as 4-t-butylpyridine (TBP) shifts the CB of TiO_2 towards higher energy levels and increase the photovoltage.[43] Conversely, addition of lithium salts, such as lithium bis(trifluoromethane)sulfonimide (LiTFSI), shift the CB of TiO_2 towards lower energy levels. Resulting in an increased rate of electron injection from the dye, and improvement of the photocurrent.[44] The merits and disadvantages of the iodine redox shuttle *vs.* the Co and Cu complex redox shuttles are presented below.

Iodine redox shuttle: The I^-/I_3^- redox shuttle has been a highly successful redox shuttle for several decades and has several attractive features. The small molecular size enables high diffusion, in pair with the high solubility in many solvents that allows for high concentrations, and high charge conductivity. The low redox potential of ~0.40 V *vs.* the standard hydrogen electrode (SHE)[45] makes

it possible to regenerate most dyes. However, the low redox potential limits the attainable photovoltage from DSSCs using this redox shuttle and has motivated the search for new redox shuttles with higher redox potentials.

Co and Cu complex redox shuttle: A library of cobalt complexes was reported by Feldt *et al.*[46] with redox potentials ranging from 0.34-1.20 V *vs.* normal hydrogen electrode (NHE), while the library of copper complexes reported by Saygili *et al.*[47] found the redox potential in the range of 0.87-0.97 V *vs.* SHE. In other words, the Co and Cu complex redox shuttles meet the brief of having higher redox potentials than the I^-/I_3^- redox shuttle and thereby improve the attainable photovoltage. The record PCE in a I^-/I_3^- DSSC of 12.4% was achieved with a photovoltage of 0.775 V,[48] while the record PCE in a $Co^{2+/3+}$ DSSC of 14.3% produced a photovoltage of 1.01 V.[29] An astounding photovoltage of 1.24 V was achieved in a DSSC employing $Cu^{1+/2+}$ complex redox shuttles.[32] Although the higher redox potentials have realized higher photovoltages in the DSSC, the metal coordination complexes also undergo recombination with electrons in the TiO_2 more rapidly. This increase in recombination enforces a stricter requirement on dye design, where efficient dyes have to provide an umbrella-effect that prevents the redox shuttle from approaching the TiO_2 surface.[49]

Counter electrode catalyst layer

The FTO glass on its own has a very high interfacial charge transfer resistance and needs to be coated with a catalyst to ensure efficient electron transfer to the redox shuttle.[50] Deposition of a thin layer of Pt is the most common catalyst layer for the I^-/I_3^- redox shuttle. For the metal complex redox shuttles, poly(3,4-ethylenedioxythiophene) (PEDOT) show reduced charge transfer resistances and higher PCEs.[51]

1.2.3 Operating principles of the DSSC

"The DSSC is a good example of a molecular system where the function of the overall device is better than the sum of properties of its components."[16] This quote from the comprehensive review by Hagfeldt *et al.* on the DSSC motivates the transition from looking at the individual components to understanding how they operate together. Figure 1.8 shows the basic electron transfer processes occurring in a DSSC.
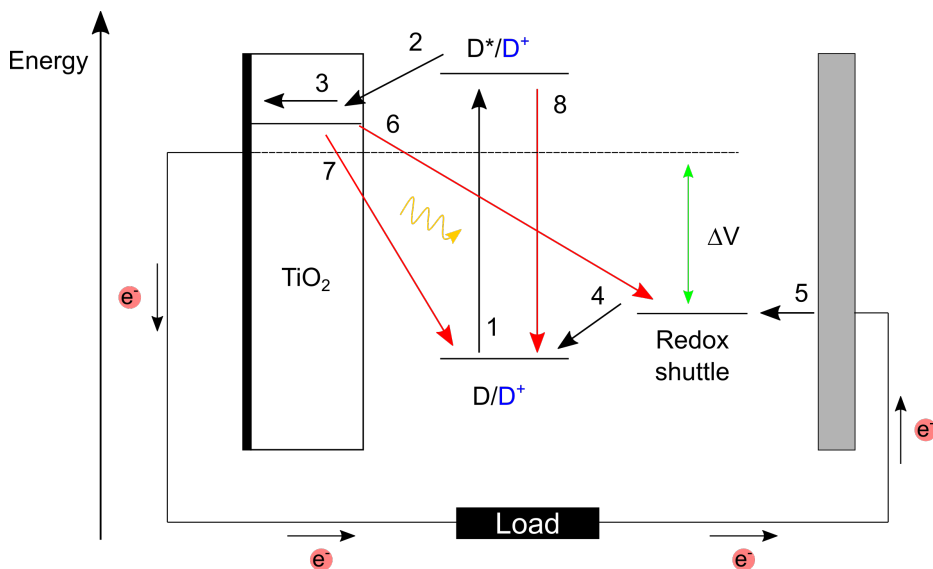
Figure 1.8: The electron transfer processes occurring in a DSSC: 1 - photoexcitation of the dye, 2 - electron injection, 3 - electron transport through TiO_2, 4 - regeneration of the dye, 5 - regeneration of the redox shuttle. The loss processes are labeled with red arrows: 6 - recombination of electrons in TiO_2 with the redox shuttle, 7 - recombination of electrons in TiO_2 with the oxidized dye, 8 - excited state decay. The difference between the Fermi level of TiO_2 and the redox potential of the redox shuttle is indicated with the green arrow and defines the attainable photovoltage.

Photoexcitation of the dye (process 1): Once the dye is hit with a photon of energy that exceeds the band gap of the dye, the photon may be absorbed. The absorbed energy of the photon promotes the excitation of an electron from the highest occupied molecular orbital (HOMO) to the lowest unoccupied molecular orbital (LUMO). The process is shown in Eq. 1.1, where D is the dye, hν is the energy of a photon, and D* is the excited dye.

$$D + h\nu \rightarrow D^* \tag{1.1}$$

Electron injection (process 2): Given that the energy level of the LUMO is sufficiently higher than the conduction band edge of TiO_2, an electron can be injected from the LUMO of the dye to the CB of the semiconductor as shown in Eq. 1.2. Increasing the energy difference between the LUMO of the dye and the CB of TiO_2 increases the injection rate.[52]

$$D^* \rightarrow D^+ + e^-_{TiO_2} \tag{1.2}$$

Electron transport through TiO_2 (process 3): The electron is transported through the mesoporous network of TiO_2 to be collected at the FTO and further transported through an external circuit. The transport of electrons through the TiO_2

is generally explained by a multiple trapping model with an exponential trap distribution below the CB.[53]
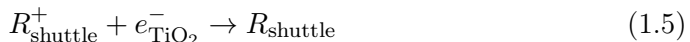
Regeneration of the dye (process 4): The oxidized dye species produced in Eq. 1.2 is regenerated by the redox shuttle. The process is shown in Eq. 1.3, where $R_{shuttle}$ is the electron transferring redox shuttle. For this process to occur there has to be a sufficient driving force between the redox potential of the redox shuttle and the oxidation potential of the dye. Different driving force requirements have been established for different redox shuttles. For the I^-/I_3^- redox shuttle, a 50-60 mV driving force is needed for efficient regeneration.[16] The large driving force requirements are attributed to initial regeneration involving the I^-/I_2^- redox couple with a higher potential than I^-/I_3^-. For the $Co^{2+/3+}$ redox shuttle a driving force of 25 mV has been shown to ensure a 84% dye regeneration.[46] A driving force of merely 10 mV has been established to be the requirement for efficient organic dye regeneration using the $Cu^{1+/2+}$ redox shuttle.[47]

$$D^+ + R_{shuttle} \rightarrow D + R_{shuttle}^+ \tag{1.3}$$

Regeneration of the redox shuttle (process 5): The oxidized species of the redox shuttle is regenerated by the transfer of an electron from the counter electrode (CE), as shown in Eq. 1.4.

$$R_{shuttle}^+ + e_{CE}^- \rightarrow R_{shuttle} \tag{1.4}$$

Recombination of electrons in TiO$_2$ with the redox shuttle (process 6): The recombining of electrons in the CB of TiO_2 with oxidants in the redox shuttle is a highly unwanted loss process in the DSSC. The process is shown in Eq. 1.5. This prevents the electrons from being collected in the external circuit and reduces the attainable photocurrent. It also lowers the Fermi level of the semiconductor, which in turn lowers the attainable photovoltage.[54] The obtainable photovoltage is the difference in energy between the Fermi level of TiO_2 and the redox potential of the redox shuttle. Both the choice of dye and the choice of redox shuttle have been shown to influence the rate of this recombination process. The use of sulfur-containing heterocyclic compounds in the dye forms sulfur-iodine complexes near the surface of TiO_2 and promotes recombination with the I^-/I_3^- redox shuttle.[55] The one-electron Co and Cu complex redox shuttles also undergo a more rapid recombination compared to the I^-/I_3^- redox shuttle.[27,49,56]

$$R_{shuttle}^+ + e_{TiO_2}^- \rightarrow R_{shuttle} \tag{1.5}$$

Recombination of electrons in TiO$_2$ with the oxidized dye (process 7): The electrons in the CB of TiO_2 recombine with oxidized dye species and regenerate it, as shown in Eq. 1.6. This recombination process is less investigated than the one shown in Eq. 1.5, but it has been shown to be independent of TiO_2 particle size.[57]

$$D^+ + e^-_{\text{TiO}_2} \rightarrow D \qquad (1.6)$$

Excited state decay (process 8): The excited dye molecule returns to its ground state and releases the energy as heat, as shown in Eq. 1.7.

$$D^* \rightarrow D + h\nu \qquad (1.7)$$

1.2.4 Characterization techniques for the DSSC

Proper and preferably standardized characterization methods are crucial to evaluate the effect of altering the components in a DSSC.[54] As demonstrated in Section 1.2.2, the DSSC consists of several critical components required for successful operation of the DSSC. These components need to be characterized before assembling the solar cell to get an estimate of how the photovoltaic device will perform. Techniques that establish the energy levels of the dyes or measure the absorption/emission properties of the dyes are particularly important to the work presented herein. Combining the components to form complete devices tend to complicate characterization, in particular when investigating how the components affect each other under illumination. Characterization methods that measure device performance, and techniques that investigate how the electron transfer processes are affected by the dye are given special attention below.

Characterization techniques for the DSSC device

JV measurements: Perhaps the most obvious criteria to evaluate the merit of new dyes is whether they improve the PCE of the solar cell. The PCE of a device is found by performing JV measurements of the complete DSSC under 1 sun AM 1.5G illumination. By performing a voltage scan from short circuit conditions ($V = 0$) to open circuit conditions ($J = 0$), the performance parameters short circuit current density (J_{sc}), open circuit voltage (V_{oc}), and fill factor (FF) are obtained. The efficiency of the solar cell is the ratio of the maximum power output divided by the power from the incident irradiation, and can be expressed through the performance parameters as follows

$$\text{PCE} = \frac{P_{\text{max}}}{P_{\text{in}}} = \frac{J_{\text{sc}} V_{\text{oc}} \text{FF}}{P_{\text{in}}}. \qquad (1.8)$$

The power from incident irradiation P_{in} is 100 mW cm^{-2} for the 1 sun AM 1.5G solar spectrum. The fill factor is the ratio between power output at maximum power and the product of J_{sc} and V_{oc} as follows

$$\text{FF} = \frac{J_{\text{max}} V_{\text{max}}}{J_{\text{sc}} V_{\text{oc}}}. \qquad (1.9)$$

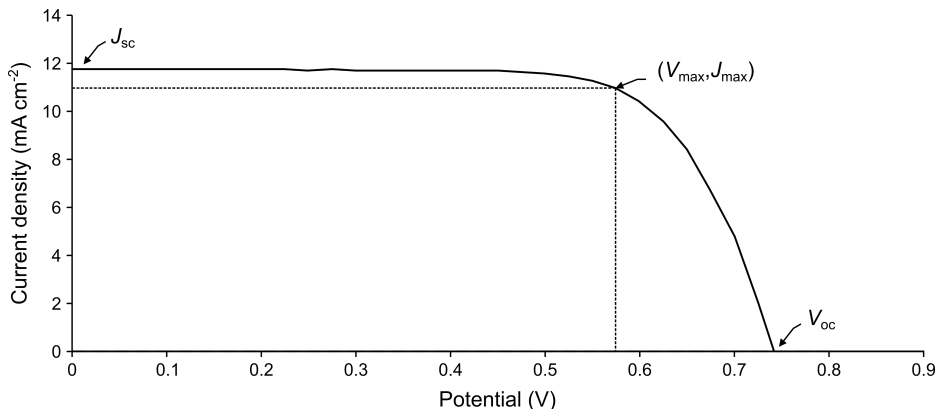An example of a JV curve obtained under 1 sun AM 1.5G solar illumination is shown in Figure 1.9.

Figure 1.9: An example of a JV curve from the **N719** DSSC in paper III.[58]

Although the measurement is simple to perform and understand, reports of mischaracterized solar cells are still frequent.[59] As improvements in PCE of only 1% can be considered significant breakthroughs, it is imperative that the direction for future photovoltaic research efforts is founded on correctly characterized solar cells. A striking example of incorrect characterization was uncovered by Buene *et al.*[60] when they reproduced the champion phenothiazine dye (**Dye 2**) and found that its performance in the original report was exaggerated. Yang *et al.*[61] propose the following set of conditions for reliable evaluation of DSSCs: 1) The AM 1.5G light source should be calibrated with a reference solar cell. 2) The delay time between each voltage step should be sufficient for the cell to reach equilibrium. 3) The test DSSC should be covered with a mask that has an aperture area that is slightly smaller than the area of active TiO_2. 4) The temperature should be stable at 25 °C during the measurements. 5) Record claims should be certified by an independent qualified public test centre.

IPCE measurements: Incident photon to current conversion efficiency (IPCE) measures the spectral response of the solar cell and quantifies how much light of a given wavelength is converted to collected current. The IPCE is calculated as follows

$$\text{IPCE}(\lambda) = \frac{J_{\text{sc}}(\lambda)}{e\Phi(\lambda)} = \frac{1240}{\lambda}\frac{J_{\text{sc}}(\lambda)}{P_{\text{in}}(\lambda)}. \tag{1.10}$$

Where e is the elemental charge and $\Phi(\lambda)$ is the photon flux of a given wavelength. The IPCE can also be expressed as the product of the efficiency of process 1, 2, and 3 in Figure 1.8. The expression for IPCE is then converted to

$$\text{IPCE}(\lambda) = \Phi_{\text{LHE}}(\lambda)\Phi_{\text{inj}}(\lambda)\Phi_{\text{col}}(\lambda), \tag{1.11}$$

18

where Φ_{LHE} is the light harvesting efficiency, Φ_{inj} is the electron injection efficiency, and Φ_{col} is the electron collection efficiency. The expression shown in Eq. 1.11 can be a quite useful starting point when trying to identify which process in the solar cell is the bottleneck. The IPCE-spectrum obtained can be integrated with respect to the AM 1.5G photon flux and provide the "theoretical" $J_{\text{sc, IPCE}}$ of the device as follows

$$J_{\text{sc, IPCE}} = \int \text{IPCE}(\lambda) \cdot e \cdot \phi_{\text{AM 1.5G}}(\lambda) \mathrm{d}\lambda, \tag{1.12}$$

where $\phi_{\text{AM 1.5G}}$ is the photon flux from the AM 1.5G solar spectrum. Large discrepancies between $J_{\text{sc, IPCE}}$ and the measured J_{sc} can indicate calibration issues in either the solar simulator or the IPCE measuring device. Christians *et al.*[62] suggest that discrepancies exceeding 20% call for further experimental explanation. To avoid presenting exaggerated J_{sc} values from 1 sun AM 1.5G *JV* measurements, it is good practice to check their validity against the calculated $J_{\text{sc, IPCE}}$. An example of an IPCE spectrum and the corresponding integrated current density is shown in Figure 1.10.
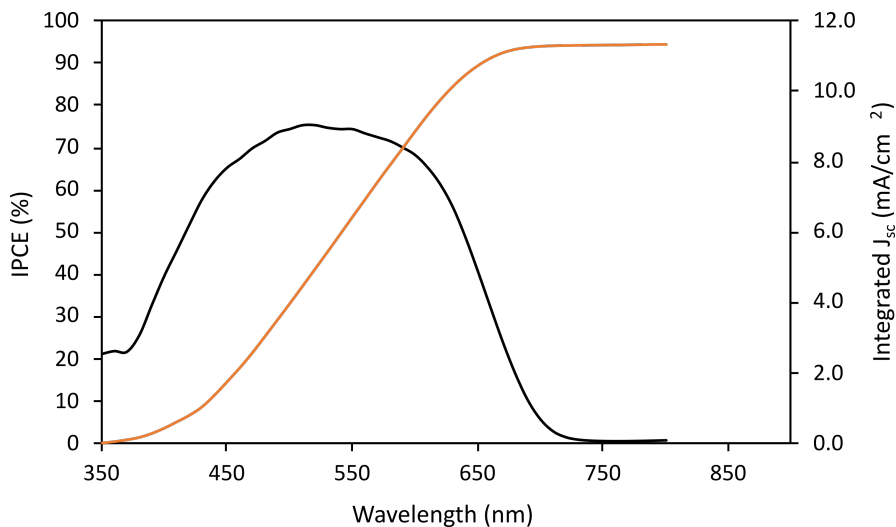
Figure 1.10: An example of an IPCE spectrum (black line, left axis) and the integrated current density (orange line, right axis) for a DSSC sensitized with the dye **Y123** from paper II.

Electrochemical impedance spectroscopy measurements: Electrochemical impedance spectroscopy (EIS) is a powerful tool to investigate electron transfers across interfaces. As the DSSC contain several interfaces where electrons are transferred, the EIS methodology has been used successfully to investigate the processes outlined in Figure 1.8. To perform EIS on the solar cell, a small oscillating voltage signal $(V_{\text{AC}}(\omega, t))$ is superimposed on the DC voltage of the cell.[63] The AC current response $(i_{\text{AC}}(\omega, t))$ is then measured while scanning the signal frequency over a

range, which yields the impedance spectrum $Z_{\mathrm{DSSC}}(\omega)$ as follows

$$Z_{\mathrm{DSSC}}(\omega) = \frac{V_{\mathrm{AC}}(\omega, t)}{i_{\mathrm{AC}}(\omega, t)}. \tag{1.13}$$

The impedance data of the DSSC can be interpreted by equivalent circuit models consisting of resistive and capacitive elements in the DSSC.[64] An illustration of this model is shown in Figure 1.11. This model makes it is possible to gather information about the resistance of the individual components in the DSSC from EIS measurements. The information obtained from EIS is so closely related to the actual operation of the DSSC and its JV curve that it is possible to quantitatively predict the JV curve from the EIS data. There are two approaches to reproduce the JV curve from EIS data, the first is based on the electron diffusion model[65] where the resistance modelling is performed as a function of current density.[63] The second approach is based on the transmission line model where the resistance modelling is performed as function of the cell voltage.[66]
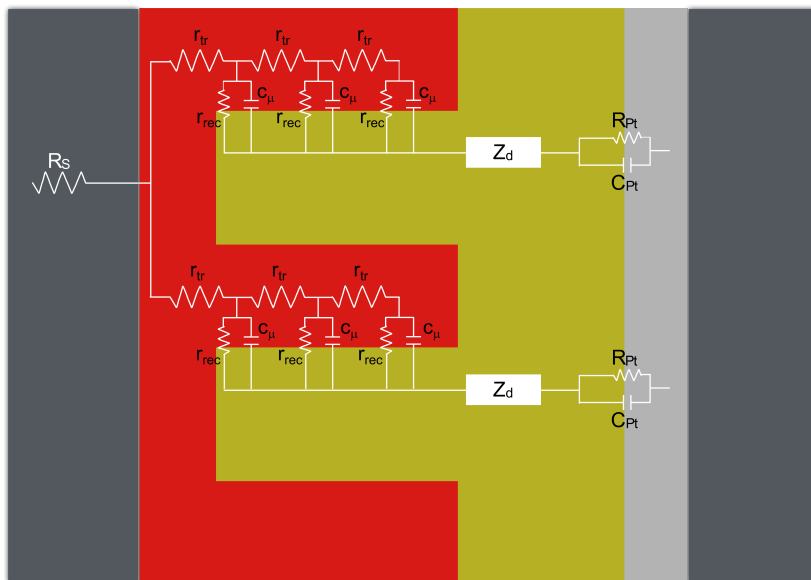
Figure 1.11: The equivalent circuit of a dye-sensitized solar cell superimposed on a simple model of the cell itself. The circuit consists of an ohmic series resistance (R_{s}), a transmission line model with the associated transport resistances (r_{tr}) and recombination resistances (r_{rec}), a finite-diffusion Warburg element (Z_{D}), and an RC-circuit with a charge transfer resistance (R_{Pt}). The figure is adapted from Paper I.[67]

A typical representation of the EIS measurement is the complex plane plot, for which an example is shown in Figure 1.12. In this plot the negative of the imaginary part of the impedance is shown as a function of the real part of the impedance. The distance from the origin to the first semicircle represents the

series resistance (R_s) of the DSSC. The small first semicircle represents the charge transfer resistance (R_Pt) from the counter electrode to the redox shuttle. The large second semicircle originates from the resistance of the TiO$_2$ film ($R_\mathrm{TiO_2}$) and includes the transport resistance (r_tr) and recombination resistance (r_rec). The recombination resistance should be higher than the transport resistance to obtain high-efficiency devices. The effective electron diffusion length L_n is used as a measure of the competition between charge recombination and charge collection.[68] The effective electron diffusion length can be obtained from the recombination and transport resistance as follows

$$L_n = L\sqrt{\frac{r_\mathrm{rec}}{r_\mathrm{tr}}}, \tag{1.14}$$

where L is the TiO$_2$ film thickness. The barely visible shoulder on the large semicircle represents impedance from diffusion (Z_D) of the charge carriers in the redox shuttle. Figure 1.12 shows the difference in performing EIS measurements in the dark *vs.* under illumination. Performing the measurements in the dark will ensure that the recombination resistance measures only recombination between electrons in TiO$_2$ and the the redox shuttle (process 6 in Figure 1.8). Under illumination, oxidized dye species are also present and offer an additional pathway for recombination (process 7 in Figure 1.8).
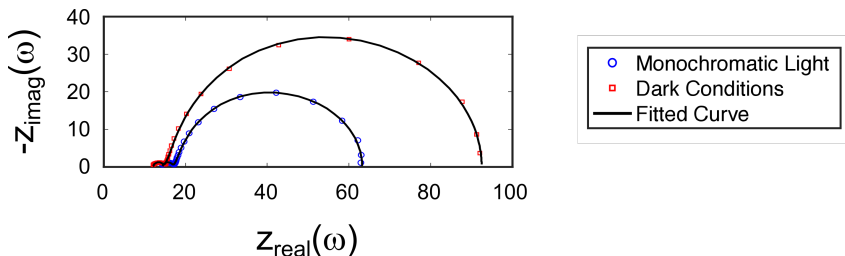
Figure 1.12: The complex plane plot of **DMA-0** at open circuit voltage from Paper I.[67]

Characterization techniques for the DSSC dyes

UV/Vis spectroscopy: When novel dyes are prepared for use in a DSSC, knowledge about the absorption properties of the dye is essential. Measuring the absorbance of diluted dye solutions over a wide range of wavelengths yields the UV/Vis spectrum of the the dye. An example of such a spectrum is shown in Figure 1.13. If the concentration of the diluted dye solution is known, then the molar extinction coefficient of the dye ϵ is readily available from Beer-Lamberts law:

$$\epsilon = \frac{A}{l \cdot C}, \tag{1.15}$$

where A is the measured absorbance, l is the optical path length, and C is the concentration of the solution. This relation is also useful for dye loading experiments

to evaluate the amount of dye absorbed to the TiO$_2$ electrode. By submerging dye-stained TiO$_2$ electrodes in a basic solution (frequently 40 mM TBA(OH) in THF) the dye is desorbed from the TiO$_2$. UV/Vis measurements performed on the solution of desorbed dye along with ϵ obtained from a known concentration of the dye in the basic solution, is enough information to work out the amount of dye desorbed from the TiO$_2$.

Due to the transparent nature of the nanocrystals of TiO$_2$ it is also possible to perform UV/Vis measurements of the dye-stained TiO$_2$ films. This allows for an evaluation of the absorption properties of the dye in a setting that more closely resembles the setting of the dye under DSSC operation. When measuring absorption of the dye on the TiO$_2$ film it is common to observe a blue shift of the absorption maxima compared to the dye in solution. This blue shift is commonly attributed to formation of dye-aggregates on the TiO$_2$ surface and the deprotonation of the anchoring group after the dye is bound to TiO$_2$.[69,70]
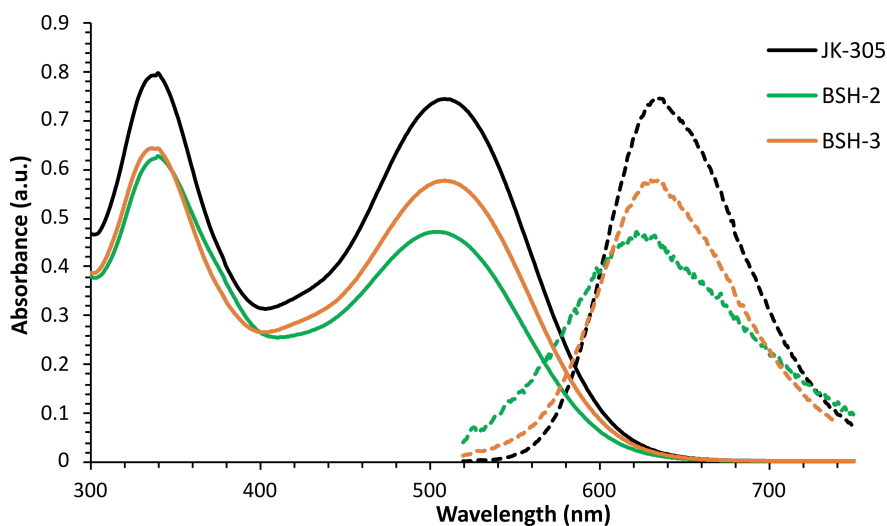
Figure 1.13: An example of UV/Vis spectra (left) and normalized emission spectra (right) of the **JK-305**, **BSH-2**, and **BSH-3** dyes from Paper V.[71] The intersection between these spectra gives the optical band gap of the dye, E_{0-0}.

Fluorescence spectroscopy: The fluorescence spectroscopy technique, also known as photoluminescence (PL) spectroscopy or emission spectroscopy, provides information about the fluorescence properties of the dyes. This is typically done by irradiating the dye in solution with light of wavelength that corresponds to the maximum absorption. The fluorescence emitted from the dye is then measured over a range of wavelengths. An example of a fluorescence spectrum is shown in Figure 1.13. The difference between the absorption maximum and emission maximum is referred to as the Stokes shift, which is a measure of how much energy is lost from the absorbed photon to the emitted photon. Fluorescence spectroscopy

is particularly useful along with UV/Vis spectroscopy to determine the optical band gap of a dye. The intersection between the normalized absorption spectrum and the normalized fluorescence spectrum gives the optical band gap, E_{0-0} from the Planck-Einstein relation:

$$E_{0-0} = \frac{h \cdot c}{\lambda} = \frac{1240}{\lambda} \tag{1.16}$$

wher h is the Planck constant, c is the speed of light and λ is the wavelength of intersection.

Cyclic voltammetry: Knowing the driving force for regeneration of the dye by electron transfer from the redox shuttle is crucial for justifying the choice of dye and redox shuttle pairing. The driving force is the difference in energy level between the redox potential of the redox shuttle and the oxidation potential of the dye. A common way to determine the oxidation potential of the dyes is through cyclic voltammetry (CV) experiments. A typical set-up for CV experiments is a three-electrode system submerged in a supporting electrolyte.[72] The three electrodes are the working electrode, the counter electrode, and the reference electrode. The supporting electrolyte is typically a salt dissolved in an organic solvent. The solvent must have an electrochemical window suitable for the potentials investigated. The CV experiments are ran by applying a scanning voltage across the three-electrode system and measuring the observed current. By reversing the scan at a certain potential, the complete cyclic voltammogram is obtained as shown in Figure 1.14. If the oxidation is reversible, the oxidation potential is given as the average of the peak obtained from the forward scan and the peak obtained from the reverse scan.[72] The terminology oxidation potential refers here to the potential required to oxidize the sensitizer.

Wang *et al.*[73] demonstrated the possibility of doing CV experiments on dye-stained TiO_2 electrodes. This has since been used to obtain measurements that more closely represent the dye under operation in a DSSC.[74] Ferdowsi *et al.*[75] showed a 180 mV difference in oxidation potential measured from the dye dissolved in the electrolyte and the dye-stained electrode. This discrepancy highlights the usefulness of performing measurements of the dye oxidation potential on dye-stained TiO_2 electrodes. To calibrate the reference electrode in the CV experiments, it is common to measure the redox potential of ferrocene in the same supporting electrolyte. The oxidation potential of the dyes can in this way be presented as V *vs.* SHE by the estimated redox potential of ferrocene at 0.624 V *vs.* SHE.[76]

By establishing the energy level for the LUMO of the dye, the driving force for electron injection is also established. The LUMO of the dye is readily estimated as

$$E_{\text{LUMO}} = E_{\text{ox}} - E_{0-0}, \tag{1.17}$$

given that the oxidation potential and optical band gap is known.
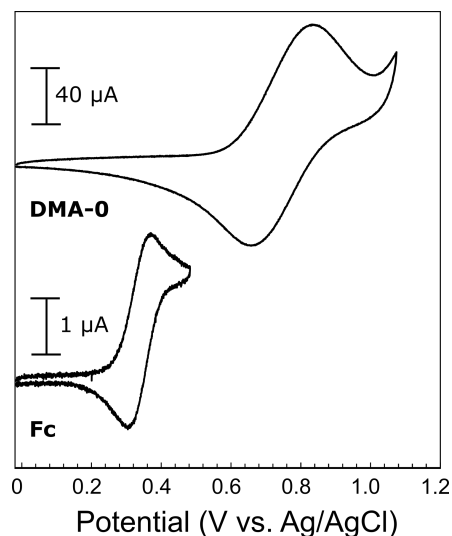
Figure 1.14: An example of a cyclic voltammogram of the dye **DMA-0** and the ferrocene (Fc) reference from Paper I.[67]

1.3 Dyes for DSSC

The dye in a DSSC has the crucial role of absorbing photons from the solar irradiation and injecting electrons from the excited state to the CB of TiO_2. Over the years, dye designs have been extensively studied and countless molecular structures have been proposed and investigated. From the huge variation of dyes reported, it can be difficult to identify a common ground for the different design principles, however the dyes all seek to meet the following criteria:[16]

I. **Absorption properties:** The absorption of the dye should be broad in order to cover as much of the solar spectrum as possible. Alternatively, in a co-sensitization approach, the dye should be tailored to a specific absorption region that complements the other dye(s). In addition, the dye should have a high molecular extinction coefficient to be employed successfully with the thin TiO_2 layers used for Co and Cu redox shuttles.

II. **Energy level requirements:** The HOMO and LUMO energy levels of the dye should be compatible with the semiconductor material and redox shuttle that is used. The LUMO should be higher in energy than the conduction band of TiO_2 to ensure a favorable driving force for electron injection. The HOMO of the dye needs to be more positive than the redox potential of the redox shuttle to provide an efficient regeneration of the oxidized dyes.

III. **Chemical requirements:** The dyes should have anchoring groups (COOH, H_2PO_3, SO_3H, etc.) that strongly binds the dye to the metal oxide surface.

In addition, dyes should possess sterically bulky groups that prevent unfavorable dye aggregation on the TiO_2 surface. These sterically bulky groups should also act as an umbrella for the TiO_2 and prevent the I_3^-, Co^{3+} and Cu^{2+} species in the redox shuttle from recombining with electrons in the semiconductor.

IV. **Stability requirements:** The dye should be photostable and tolerate the electrochemical and thermal stress it will be subjected to under DSSC operation.

As previously mentioned, the Ru complex dyes were the state-of-the-art sensitizers for a long time. They displayed excellent photovoltaic performance when paired with an iodine redox shuttle. They met all the criteria listed above and displayed particularly broad IPCE spectra resulting in high photocurrents upwards of 20 mA cm^{-2}.[25,77–79] The transition from the iodine redox shuttle to the metal complex redox shuttles saw these dyes fall out of favor largely due to two factors. The first factor is the generally low molar extinction coefficients of the Ru complex dyes that prevents them from being as efficient in the thinner TiO_2 electrodes required by the Co and Cu redox shuttles.[39] The second factor is the TiO_2 surface protection that these dyes provide is typically quite limited compared to the organic dyes. This makes the Ru complex dyes more plagued by electron recombination from TiO_2 to Co^{3+} or Cu^{2+} (process 6 in Figure 1.8). Inclusion of 2-hexylthiophene and perfluoroalkyl chains on the Ru complex dye **51-57dht.1** (see Figure 1.15) yielded a 9.53% PCE in cobalt redox shuttle and proved that they can be made compatible with the metal complex redox shuttles.[80] Another drawback associated with the Ru complex dyes is the limited abundance and the high cost associated with the noble metal.

1.3.1 Organic dyes for DSSC

Seeking to address the problems associated with the Ru complex dyes, is the organic dyes. The organic dyes are made from earth-abundant materials, display higher molar extinction coefficients, and can be easily modified to provide surface isolation. Additionally, organic dyes present unique opportunities to target interesting functionalities such as in the photochromic dye **NPI**[81] (see Figure 1.16) or the dye **VG20-C$_{16}$**[82] that absorbs light beyond 800 nm, rendering it transparent to the human eye. Organic dyes are often also referred to as metal-free dyes, by that referring to all dyes that do not follow the metal-to-ligand charge transfer (MLCT) excitation mechanism of the transition metal complex dyes. This sees the category of zinc porphyrin dyes grouped along with organic dyes and not as metal complex dyes. These dyes typically follow an intramolecular charge transfer (ICT) excitation mechanism where photoexcitation leads to an electron transfer from the donor (D) to the acceptor (A).[83]
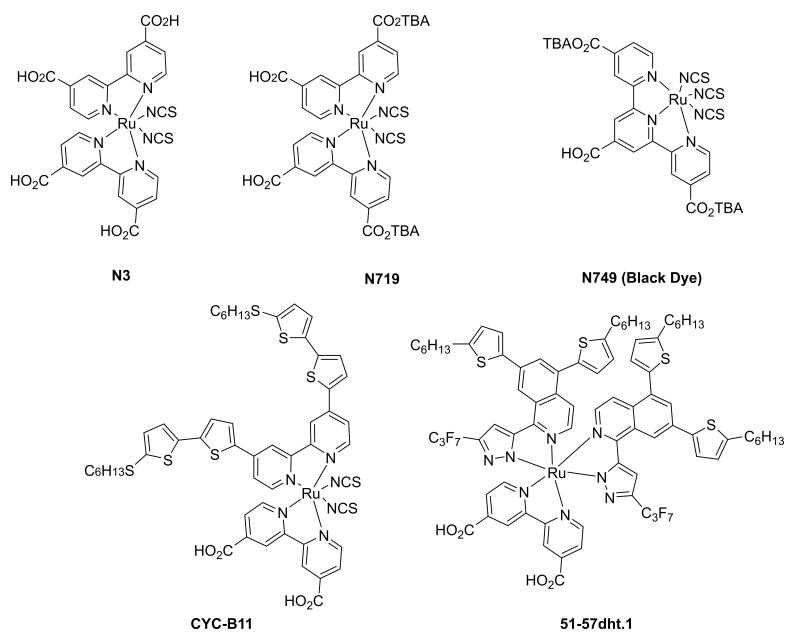
Figure 1.15: Collection of successful Ru-complex dyes. The dyes **N3**, **N719**, **N749**, and **CYC**-**B11** have demonstrated excellent performances with the iodine redox shuttle.[24,25,77] The dye **51-57dht.1** has shown good performance in pairing with a Co redox shuttle.[80]
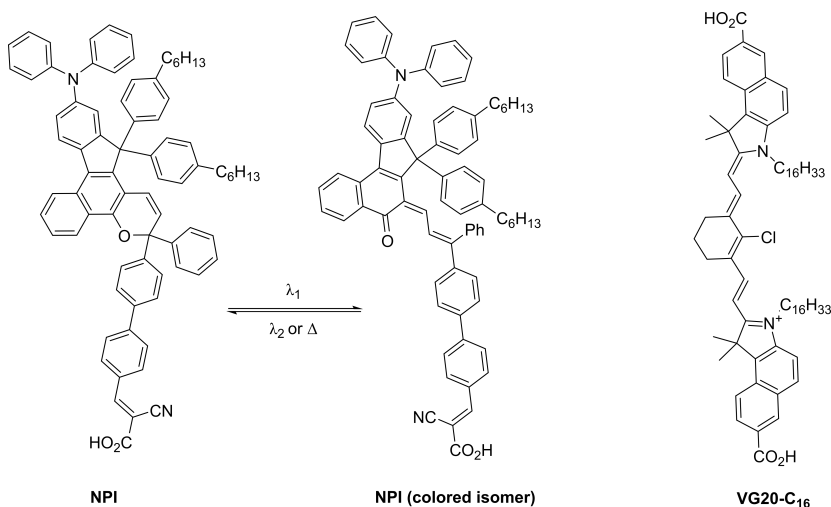

Figure 1.16: Organic dyes offer the ability to target unique properties. The dye **NPI** is photochromic and will display considerably different absorption properties under illumination *vs.* in the dark.[81] The dye **VG20**-**C**$_{16}$ absorbs light not visible to the human eye, rendering the DSSC devices transparent.[82]

Although the molar extinction coefficients are higher than that of the Ru complex dyes, the organic dyes tend to lack the spectral width of their metal complex

counterparts. The dye **RK-1** (see Figure 1.17) is an example of an organic dye that is able to match the photovoltaic performance of the Ru complex **N719** in an iodine redox shuttle. However, the IPCE onset of the organic dye is still blue shifted by ∼100 nm compared to the Ru complex.[26] To take advantage of the beneficial properties associated with the organic dyes and still ensure a wide absorption it is common to co-sensitize the TiO_2 electrode with multiple dyes. The record DSSC performances of Co and Cu redox shuttle devices both stem from co-sensitized devices.[29,32] This highlights the possibility for organic dyes to be tuned to absorb the light in certain spectral regions and cover a wider range of the solar spectrum through co-sensitization. The tuning of organic dyes follow some predictable trends that will be presented in the following text.
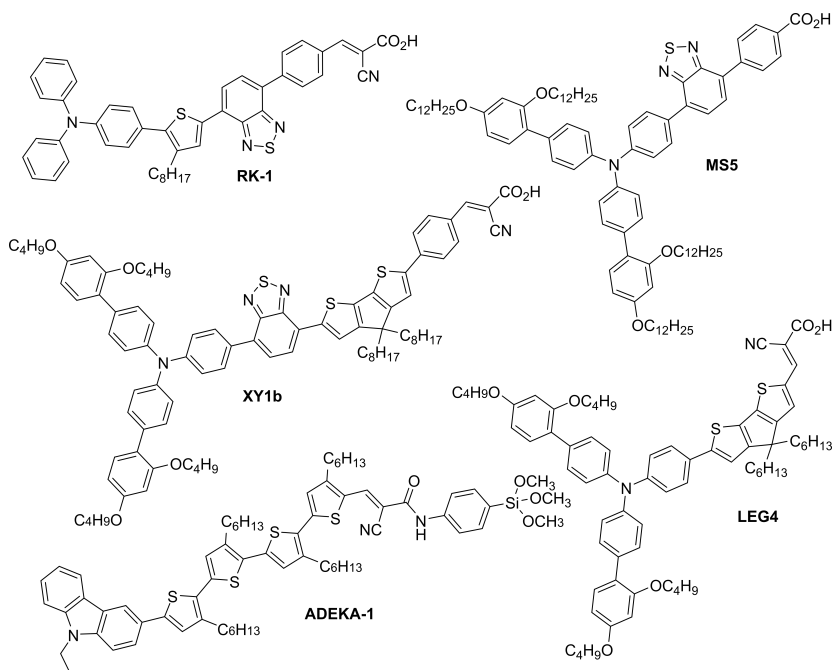
Figure 1.17: Representative organic dyes for the different redox shuttles. The dye **RK-1** displayed a PCE of 10.2% in an iodine based redox shuttle.[26] The co-sensitization of **MS5** and **XY1b** displayed a 13.5% PCE in a Cu based redox shuttle.[32] The most efficient DSSC to date is the result of co-sensitization of **ADEKA-1** and **LEG4** achieving a PCE of 14.3% in a Co based redox shuttle.[29]

Property tuning of dyes for DSSC

The unique possibility to tailor molecular properties of organic π-conjugated molecules with respect to energy levels of the frontier molecular orbitals (FMO) or their optical properties is an inherent strength of organic dyes. The ability to customize the properties of the organic π-conjugated molecules has seen them being implemented in a variety of optoelectronic technologies such as light-emitting diodes (OLED),[84]

organic photovoltaic cells (OPV),[85] and field-effect transistors (OFET).[86]

The tuning of these molecules properties follow a set of fairly established structure-property relationships[87] that will be discussed below. Often referred to as push-pull molecules or D-π-A compounds, where D signifies an electron donor, π represents a π-conjugated system, and A is an electron acceptor. A push-pull system is made by fitting the π-conjugated system with a donor and an acceptor on either side, which facilitate an intramolecular charge transfer (ICT). The interaction between the donor and acceptor forms a new molecular orbital (MO).[88] The electrons in the new MO are more easily excited. Adopting the D-π-A structure locates the HOMO predominantly around the donor of the dye, while the LUMO is located around the acceptor. In Figure 1.18, the electron density of the HOMO and LUMO of two phenothiazine dyes are displayed. Upon excitation, the ICT shift the electron density from the donor to the acceptor. The donor-acceptor interaction determines the ICT and the corresponding optical properties and its HOMO-LUMO gap.[89] The D-A interaction can be tuned by the "strength" of the donor and acceptor, the extension and nature of the π-conjugated spacer, and the planarity of the aromatic system.
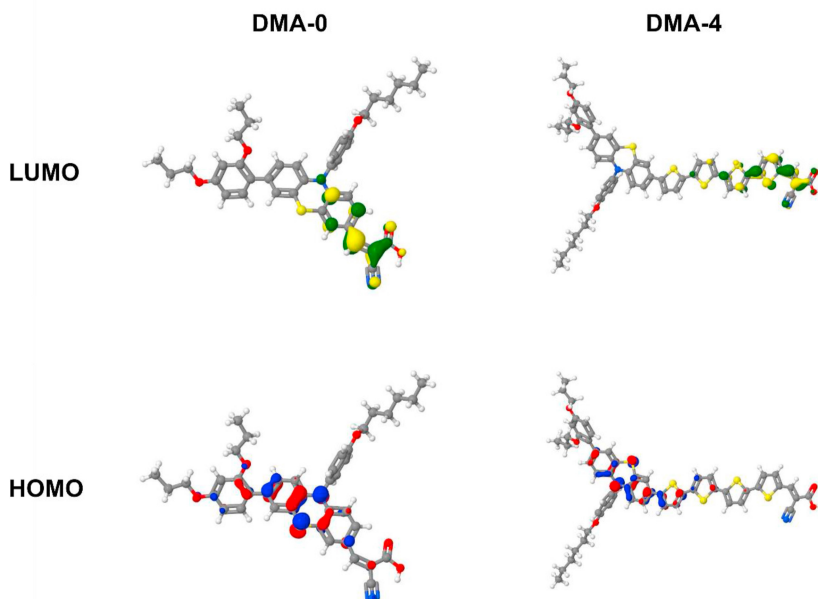
Figure 1.18: The isodensity plot of **DMA-0** and **DMA-4** which locates the HOMO near the phenothiazine donor and the LUMO on the cyanoacrylic acid acceptor. The figure is from Paper I.[67]

Increasing the strength of the donor typically refers to increasing the electron donating ability of the donor either through an inductive or a resonance effect

or a combination of both. The Hammet σ_p parameter can be used to predict the strength of an electron donor.[90] A study on tuning the FMO energy levels through the donor by Kúlhanek *et al.*[91] showed that it had a profound effect on the HOMO, but that the LUMO was largely unaffected. Going from a "hydrogen donor" to a ferrocenyl donor lifted the HOMO level from -6.15 eV to -4.87 eV, while the LUMO was only shifted from -2.78 eV to -2.67 eV. This highlights the quite precise tuning efforts possible for push-pull molecules. Würthner *et al.*[92] demonstrated that increased donating ability led to a red shift of the absorption maximum, λ_{max}. An array of donors have been prepared and evaluated for use in dyes for DSSC such as coumarine,[93] indoline,[94] carbazole,[95] phenothiazine,[23] and triarylamine[96] to name a few. The donating strength of common donors in DSSC dyes has been estimated by Ndaleh *et al.*[97] by comparing the onset of absorption for a library of dyes. In terms of increasing strength the order is carbazole < aryl-substituted triphenylamine < alkoxy-substituted triphenylamine < indoline. A density functional theory (DFT) study on 13 different donors found the chrysene donor to be the weakest and the *N,N*-dialkylaniline to be the strongest donor.[98]

Tuning the optoelectronic properties of D-π-A compounds through the acceptor is also possible. Altering the acceptor mainly affects the energy level of the LUMO,[87] which complements the HOMO-tuning possible through the donor. A library of thiophene-compounds with various acceptors presented by Bürckstümmer *et al.*[99] displayed the possibility of tuning the absorption across the entire visible spectrum by only altering the acceptor unit. In dyes for DSSC, the acceptor also plays the role of anchoring group that has to be able to covalently bind to the TiO$_2$ surface. The most conventional anchoring group for the DSSC dyes is the cyanoacrylic acid group comprised of two electron-accepting units (CN and COOH). Other acceptor groups have also been evaluated such as tropolone,[100] hydroxamic acid,[101] silyl ethers,[102] and benzoic acid[103,104] and found to improve stability or PCE of DSSCs. Despite their reduced absorption properties, benzoic acid analogs have been found to outperform their cyanoacrylic counterparts due to allowing a higher dye loading on the TiO$_2$ surface.[105]

The π-spacer is also a vital part in determining the absorption properties of dyes. Hagberg *et al.*[106] showed that expanding the π-conjugated system by incorporation of vinylene and thiophene resulted in an increasingly red shifted λ_{max} with increasingly sized aromatic system. However, the larger π-spacers did not yield increased PCE-values, as they also facilitated recombination of electrons in TiO$_2$ with triiodide in the redox shuttle. A series of triarylamine dyes presented by Liu *et al.*[107] were linked with 1-4 successive thiophene units in the π-spacer, and revealed a similar effect where the largest aromatic system displayed the widest absorption. The dye with four thiophenes in the π-spacer also proved to be the most efficient in a DSSC, but produced a considerably lower V_{oc} than the dye with only one thiophene. Buene *et al.*[108] prepared a library of 11 phenothiazine dyes and found that 5-membered aromatic rings outperformed 6-membered ones, and that no π-spacer performed better than all dyes, except one that was linked with

furan. In other words, Tuning the dye through the π-spacer lead to a mixed bag of results. The increased size of the aromatic system typically tend to red shift the absorption, although there are reports of terthiophenes displaying red shifted λ_{max} compared to quaterthiophenes in a push-pull system.[109,110] The incorporation of π-spacers is commonly associated with reduction of photovoltages, which makes tuning through the π-spacer a careful balancing act between optimizing the photocurrent without too detrimental drops in photovoltage. The reduced photovoltage can be attributed to a shift in the conduction band,[111,112] and to the formation of sulfur-iodine complexes near the surface of TiO_2.[55,113]

Modifying the planarity of the aromatic system also has a profound impact on the optoelectronic properties. Increasing the planarity of the system strengthens the interaction between donor and acceptor, and the smaller reorganizational energy of the planar system benefits the ICT.[114] Increasing the planarity of the donor has shown to improve the ICT,[115] lower the energy level of HOMO,[116] and improve the interfacial charge transfer processes occuring in the DSSC.[117] Binding the phenyl rings of the common triarylamine donor with methylene[118] and diarylmethylene[119] has also proved to be a successful strategy for improving the PCE compared to the "free" triarylamines. Increasing the planarity of the π-spacer is another beneficial approach to improve the properties of dyes.[56] As seen in Figure 1.17, the planar cyclopentadithiophene (CPDT) is found in two of the champion dyes **XY1b** and **LEG4**. The library of dyes presented by Gabrielsson *et al.* showed a considerable red shift of λ_{max} and improved photocurrent as a result of switching from an unmodified bithiophene spacer to a planar CPDT spacer.[56] Due to the success of the CPDT unit, an array of planarized thiophene compounds have been prepared and evaluated as π-spacers.[120–123] The planar N-annulated perylenes showed great promise as π-spacers,[124,125] but even more when used as planar donors reaching an impressive performance of 12.5% PCE in a Co-based DSSC.[126]

In addition to tuning the dye performance through the aromatic system, it is also important to consider the implications of varying the side chains attached to the dyes. Dyes are frequently fitted with side chains to aid their solubility, circumvent aggregation, and insulate the surface of TiO_2 from the redox shuttle. As previously discussed, there is a massive opportunity in expanding and planarizing the conjugated system of dyes to improve their light harvesting. Although one drawback is that big planar aromatic systems leave the dyes susceptible to form unwanted H-aggregates.[127] These aggregates blue shift the absorption and promote excited state quenching, both of which are detrimental to dye-performance. Several studies show improved performances from increasing the bulkiness of the side chains.[32,128,129] A theoretical study presented by Pastore and Angelis[130] revealed that dye dimers was the most stable conformation for the least steric dyes, while the more steric dyes were separated with a Ti atom between them. The side chains also influence the rate of recombination between electrons in the TiO_2 and oxidants in the redox shuttle. By replacing methoxy side chains with hexyloxy

side chains, Xu *et al.*[131] demonstrated an improvement in PCE from 5.93% to 7.05%, which they attributed to a reduced rate of recombination. However, it has also been shown that overlong alkyl chains can retard the redox shuttle in the regeneration of the oxidized dye species.[132] Additionally, an increased size of the side chains will reduce dye loading. Much like tuning the dye's properties through the aromatic system, the optimization of dye side chains is a careful balancing act.

Following this brief overview of concepts related to property tuning of dyes for use in DSSC, the attention is turned to how they have been applied in the literature of the two main class of dyes investigated in this thesis; the phenothiazine and triarylamine dyes.

Phenothiazine dyes

The patent by Heinrich Caro in 1877 (German patent no. DE-18771866) presented the synthesis of the dye and malaria drug *methylene blue*, and represented the first account of a phenothiazine compound. Six years later came the report of the first successful preparation of $10H$-phenothiazine.[133] Phenothiazine is a heterocyclic compound made up of three rings linked together as anthracene, where the central ring contains a sulfur and a nitrogen atom bridging the peripheral phenyl rings. Due to the heteroatoms in the central ring, the structure of phenothiazine possesses a ~150° angle between the plane of the two phenyl rings.[134,135] This structure is called the butterfly structure. The radical cation of phenothiazine is reported to be planar.[136] This leads to the amusing consequence that the butterfly structure is "flapping" its phenyl rings upon repeated oxidation and re-reduction, as expected to happen in an electrochemical device such as the DSSC.

The first DSSC phenothiazine dye, **T2-1** (see Figure 1.19), was reported by Tian *et al.*[137] in 2007 and served as one of the early metal-free dye scaffolds (see Figure 1.19). Owing to its low oxidation potential, phenothiazine is an interesting compound for electrochemical purposes. Phenothiazine had, therefore, seen some use in the DSSC field prior to being used as the donor of an organic dye. Tethering phenothiazine to a Ru-complex dye allowed phenothiazine to donate electrons into the metal centre and locate the positive charge further away. This reduced the back transfer of electrons from TiO_2 to the oxidized dye.[138] Phenothiazine also improved PCE when used as a co-mediator in an early study on Co redox shuttles.[139] Currently the predominant use of phenothiazine in the field of DSSC is as a donor or auxiliary donor in dyes. The topic of phenothiazine dyes has been reviewed on several occasions with respect to photovoltaic performance,[140,141] optoelectronic properties,[142,143] and synthesis.[144] A collection of some of the most notable dyes discussed in this section is shown in Figure 1.19. Most recently, the entire class of phenothiazine dyes and their analogs the phenoxazine dyes were investigated by Buene and Almenningen.[23] The following contains a brief overview of the key findings with regards to property tuning.
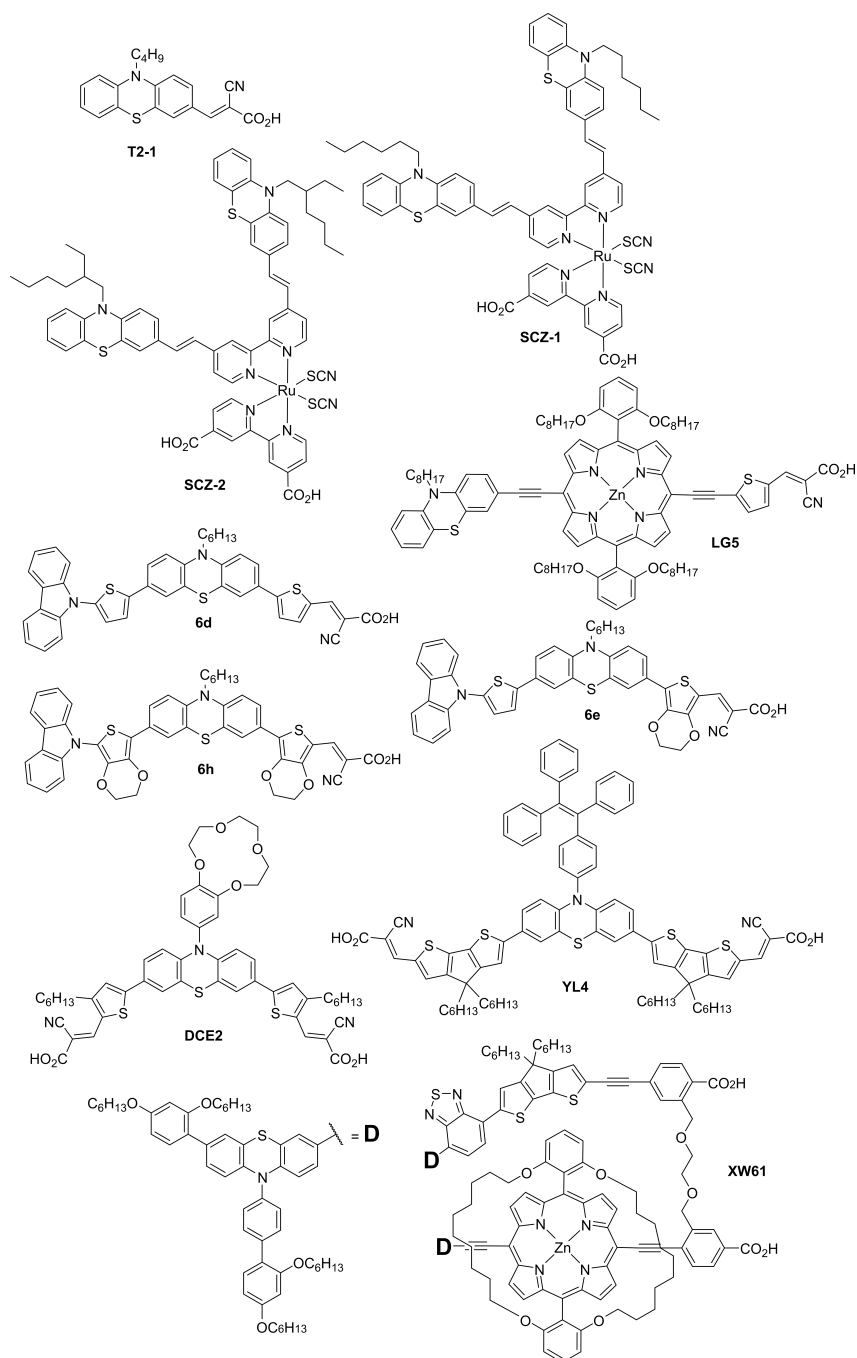
Figure 1.19: The structure of a selection of phenothiazine dyes including the original dye **T2-1**.[137] Also shown is the successful use of phenothiazine as an auxiliary donor in **SCZ-1**, **SCZ-2**,[145] and **LG5**.[146] The use of π-spacer in a successful manner is demonstrated in the dyes **6d**, **6e**, and **6h**,[147] and in the double anchored dyes **YL4**[148] and **DCE2**.[149] The recently reported double chromophore **XW61** is currently the most efficient organic dye in an iodine redox shuttle.[48]

Phenothiazine dyes are frequently fitted with auxiliary donors making D-D-A or D-D-π-A motifs. These modifications generally improve the photovoltaic performance compared to their non-modified analogs. The mechanism behind these improvements appear to be a combination of an electronic effect and a steric effect. A common trait of the successful auxiliary donors used for phenothiazine dyes is that they possess large alkyl chains of six carbons or longer that prevents aggregation and retards recombination.[150–152] The oxidation potentials of the dyes are also lowered by incorporation of auxiliary donors, compared to dyes without auxiliary donors.[60,151,153–155] The lowered oxidation potential suggests that the auxiliary donors increase electron density on phenothiazine and in turn improve its donor strength.[87] The use of phenothiazine as an auxiliary donor itself has proved perhaps even more potent. Demonstrated by the Ru complex dyes **SCZ-1** and **SCZ-2**,[145] and the Zn porphyrin dye **LG5**,[146] all of which surpass 10% PCE and make up some of the most efficient phenothiazine dyes reported to date.

Introducing π-spacers to phenothiazine has shown to give some quite effective dyes such as **6d**, **6e** and **6h**, all displaying PCEs exceeding 8%.[147] In addition, the highly efficient double anchoring phenothiazine dyes **YL4**[148] and **DCE2**[149] are both fitted with π-spacers. The phenothiazine scaffold appears very well-suited for double anchoring purposes. In available direct comparisons, the double anchor configuration is as good, or better, than the single anchor analog in all cases.[156–161] Expanding on the success of the double-anchored dyes is the tethered dye **XW61** comprised of two linked phenothiazine dyes, which currently is the most efficient organic dye in an iodine redox shuttle at 12.4% PCE.[48] Incorporation of π-spacers is, as previously mentioned, associated with loss of photovoltage, and this is also observed for phenothiazine dyes, where direct comparisons reveal higher V_{oc} for the dyes without π-spacers.[108,111,137,153,162]

Triarylamine dyes

The merits of the triarylamine scaffold for use in dyes for DSSC is unquestionable. Figure 1.17 shows highly successful organic dyes for the three major redox shuttles, and the triphenylamine/triarylamine donor is found in four out of five dyes. The donor is comprised of an amine linked to three phenyl groups for the triphenylamine (TPA) dyes. In the case of triarylamine (TAA) dyes, the donor is embellished with additional auxiliary aryl donor groups. The triphenylamine fragment holds a propeller shape where the plane of the phenyl rings are all $\sim$70-75° out of plane from each other.[163] The non-planar shape of triphenylamine is beneficial for preventing aggregation of the dyes.[96] The first synthesis of triphenylamine was reported in 1873 by Merz and Weith.[164] The original report of triphenylamine dyes for DSSC by Kitamura *et al.*[165] in 2004 (see Figure 1.20), described the dyes **1b** and **2b**.
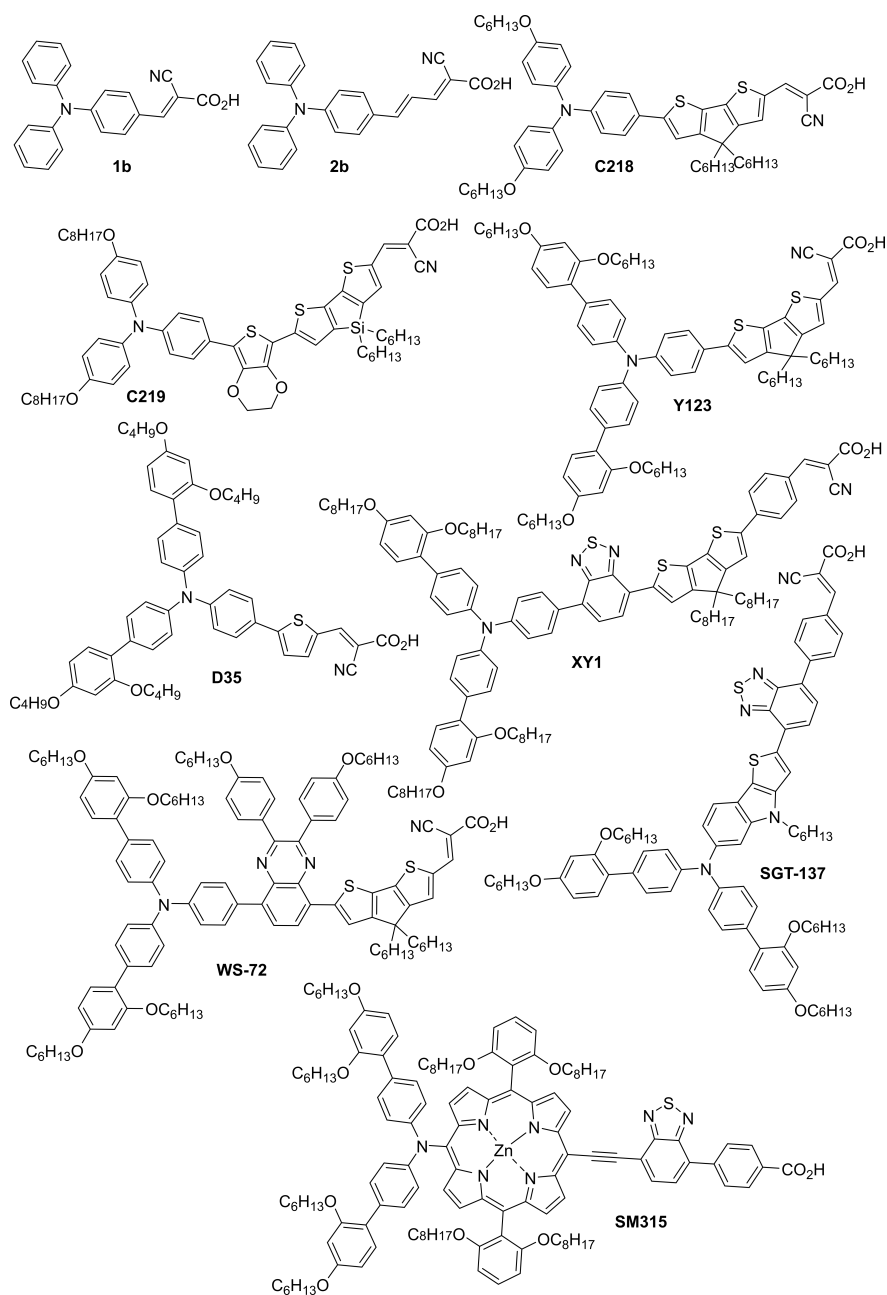
Figure 1.20: The structure of a selection of triphenylamine/triarylamine dyes including the original dyes **1b** and **2b**,[165] and **D35**.[166] Also shown are the two analogs **C218** and **Y123**, where the latter displayed a 10-fold increase in electron lifetime in a Co redox shuttle.[167] The π-spacer has been used to extend the absorption of triarylamine dyes as shown by **C219**,[168] **XY1**,[169] **WS-72**,[170] and **SGT-137**.[171] The dye **SM315** demonstrates the combination of the triarylamine donor and a porphyrin donor.[172]

Unmodified triphenylamine can serve excellently as a donor on its own, as demonstrated by the DSSC achieving 10.2% PCE when sensitized by the dye **RK-1**[26] (Figure 1.17). The alkyloxy substituted triphenylamine dye **C219** was also able to produce PCE values above 10%.[168] It should be noted, however, that these strong performances were measured in a I^-/I_3^- device, and that for Co and Cu redox shuttles an extra surface protection found in the triarylamine donor is desired. The work presented by Yella *et al.*[167] found a 10-fold increase in electron lifetime for the tetraalkoxy substituted TAA dye **Y123** compared to the dialkoxy substituted TPA dye **C218** in a Co regenerated device. This resulted in a considerably higher photovoltage and improved photovoltaic performance for the dye **Y123**, despite the fact that TPA is considered a stronger electron donor than TAA.[97,167]

The tetraalkoxy substituted triarylamine donor motif is commonly referred to as the Hagfeldt donor,[49,173] and is found in three out of the five champion dyes in Figure 1.17. In 2009, the famous **D35** dye was prepared by Hagberg *et al.*,[166] which later was used to demonstrate the possibility of using one-electron metal complex redox shuttles with only the dye providing surface insulation.[27] When **D35** was used as a co-sensitizer along with **XY1** in a Cu regenerated DSSC, an excellent PCE of 11.3% was achieved.[169] As previously mentioned, the triarylamine donor is found to have a mediocre donor strength. As shown in Figure 1.20 it is frequently modified with large π-spacers to ensure sufficient absorption properties. An example of such a dye is **WS-72** with its quinoxaline and CPDT π-spacer it is capable of producing a PCE of 11.6% in a single dye device.[170] By modifying the triarylamine scaffold to encompass a thieno$[3, 2 - b]$indole unit, the π-spacer was planarized efficiently and the dye **SGT-137** displayed a very wide IPCE-spectrum.[171] A tandem DSSC device with the dye **SGT-137** in one layer and a porphyrin dye in another layer, displayed a PCE of 14.6%. The Hagfeldt donor has also been used to great effect on a porphyrin scaffold as exemplified by the dye **SM315** achieving a PCE of 13%.[172] The co-sensitization of the dyes **MS5** and **XY1b** (see Figure 1.17) that achieved a PCE of 13.5% further highlights the excellent compatibility between the tetraalkoxy substituted triarylamine donor and the state-of-the-art copper complex redox shuttles.[32]

1.4 Organic synthesis of dyes for DSSC

One of the inherent strengths of organic dyes is that they are easily designed and synthesized. While *easy* might not be the word the author would choose to describe the task of synthesizing novel organic dyes, it is true that these syntheses are largely founded on an abundance of well-described and well-understood methods for preparing and purifying novel organic compounds. The following section focuses on a selection of strategies for preparing phenothiazine and triarylamine dyes. An introduction to five key reactions for preparing dyes is also given.

1.4.1 Synthetic strategies
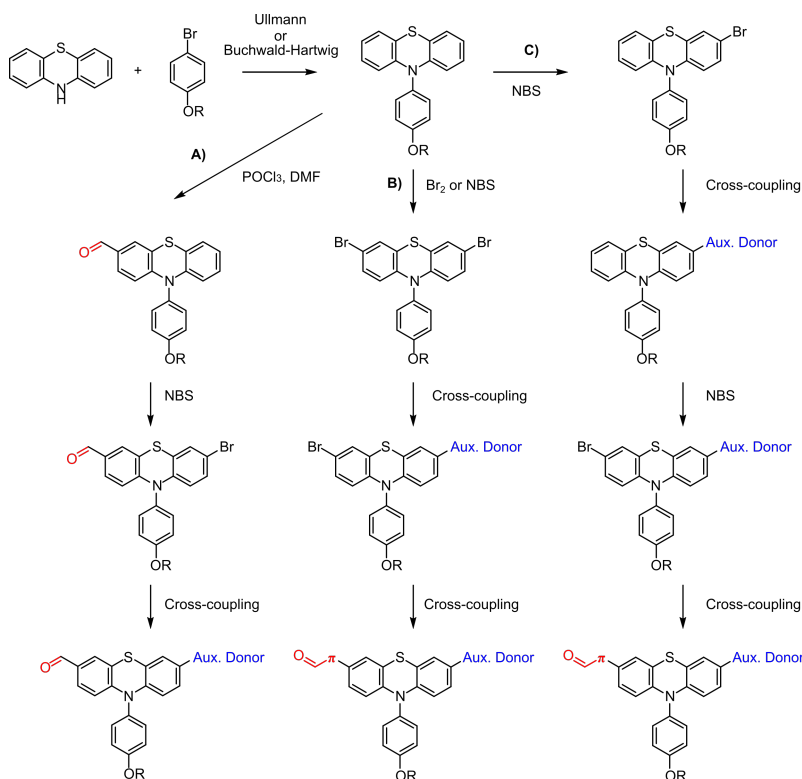
Scheme 1.1: Synthetic strategies for preparing phenothiazine dyes. Following route **A)** a wide range of D'-D-A dyes has been prepared.[67,174,175] Route **B)** is a very common route for preparing D'-D-π-A dyes.[111,158,176] Route **C)** avoids a non-selective Suzuki-Miyaura cross-coupling step at the cost of a slightly longer synthesis route, and was used in preparation of dyes for Paper I.[67]

Phenothiazine dyes. The presented synthesis strategies concerns the preparation of *N*-aryl substituted phenothiazine dyes. The first step in the preparation of *N*-aryl substituted phenothiazine dyes is commonly the functionalization of the amine in an Ullmann or Buchwald-Hartwig coupling. In contrast, the first step in the synthesis of *N*-alkyl substituted phenothiazine dyes is commonly a bromination to take advantage of the highly crystalline 3,7-dibromo-10H-phenothiazine in a scalable purification process.[60,108,154] Introducing the bromide prior to the metal-catalyzed C-N coupling reactions used for preparing *N*-aryl substituted phenothiazine is undesirable due to the loss of selectivity this would cause. Following the cross-coupling, the phenothiazine is subjected to a functionalization. For this step, formylation, dibromination, and monobromination have all been proven to be successful approaches. Phenothiazine is a forgiving scaffold to work with due to the resonance stabilization that the lone pair on nitrogen provides for the arenium

ion formed during the electrophilic aromatic substitutions (EAS). This allows for selective modifications on the 3- and 7-position on the phenothiazine moiety by EAS reactions. An outline of the strategies used for preparing N-aryl substituted phenothiazine dyes is shown in Scheme 1.1.
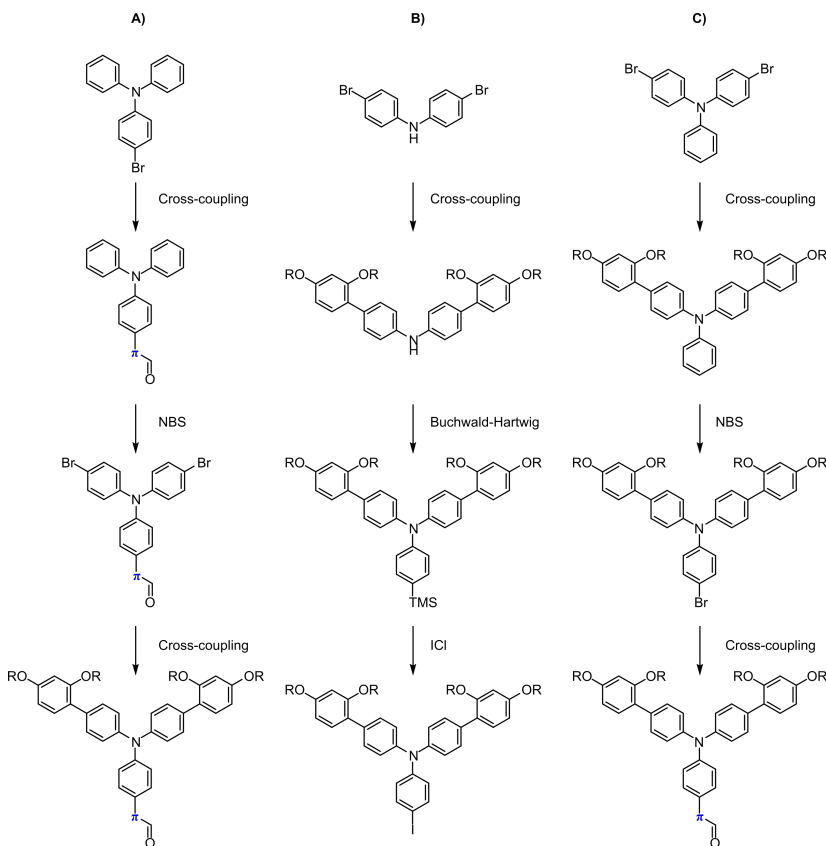
Scheme 1.2: Synthetic strategies for preparing triarylamine dyes. Route **A)** involves introducing the π-spacer in the first step of the synthesis, this route has been chosen on numerous occasions.[166,177,178] An exciting approach involving the conversion of TMS to I is shown in route **B)**, and avoiding any selectivity issues.[179] The completion of the donor first approach is shown in route **C)**, this has found use in several reports of triarylamine dyes.[56,180–182]

Triarylamine dyes. The same advantages observed for the phenothiazine scaffold with regards to EAS selectivity can also be seen for the triarylamine dyes. The central amine group directs substitutions in a selective manner to the *para*-position. Multiple routes to the triarylamine donor exists, as shown in Scheme 1.2. Highlighting the prevalent nature of the triarylamine donor is the fact that the advanced fully functionalized boronic ester of the tetraalkoxysubstituted triarylamine donor is commercially available (*dyenamo.se/dyenamo_building_blocks* accessed 05.06.2022). The original synthesis of **D35** followed synthesis route **A)** in Scheme 1.2, where the monobrominated triphenylamine is coupled with the

π-spacer in the first step.[166] Bromination and a subsequent Suzuki-Miyaura cross-coupling yields the finished dye precursor. Recently, Baumann *et al.*[173] reported the synthesis of an iodinated triarylamine donor fragment following a synthesis route **B)**, which does not rely on selective halogenation steps. Instead it relies on converting the trimethylsilyl (TMS) group to iodide in the ultimate step.[179] Route **C)** resembles **A)** except that the order of the cross-coupling steps is reversed and the auxiliary alkoxyphenyl groups are introduced first. Performing the reactions in this order reduces the risk associated with the potentially labile aldehyde group.

1.4.2 Classical textbook reactions

Electrophilic aromatic substitution (EAS)

As shown in the above discussion on synthesis strategies, the EAS reaction is quite common in the preparation of dyes. Working with electron rich aromatic compounds such as phenothiazine means that the EAS reactions can be performed in good rates, and also with selective substitutions due to the resonance stabilization provided by the lone pair on nitrogen.[183] Working with activated aromatics also allows for bromination reactions using N-bromosuccinimide (NBS) as the brominating agent at room temperature, permitting mild and regiospecific brominations.[184] A proposed mechanism for the bromination of a phenothiazine compound with NBS is shown in Scheme 1.3. For less activated compounds, catalysis with either HCl,[185] HClO$_4$,[186] or NH$_4$OAc[187] has proven useful for bromination using NBS.
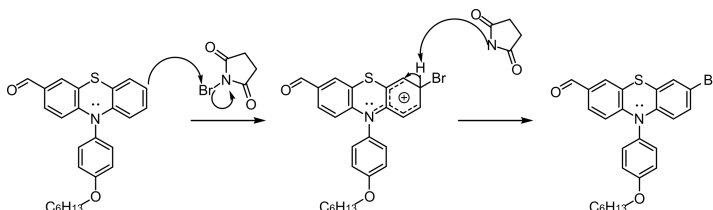
Scheme 1.3: Proposed mechanism for the bromination of a phenothiazine compound.

Another highly useful and common EAS reaction for the synthesis of dyes is the Vilsmeier-Haack formylation.[188] Mixing N,N-dialkylamide with phosphorus oxychloride forms the chloroiminium ion, which is the electrophile in the reaction. Electron rich aromatics such as thiophenes, phenothiazines, or arylamines will undergo a reaction following the EAS mechanism with the chloroiminium electrophile and produce aromatic formyl or acyl compounds depending on the N,N-dialkylamide chosen.[189] The Vilsmeier-Haack formylation has been a vital reaction for the preparation of dyes and their associated building blocks in the color industry. Approximately 2000 tons of Vilsmeier-Haack products were produced industrially in 1996.[190]

Knoevenagel condensation

Installing the cyanoacrylic acid anchoring group is carried out using the Knoevenagel condensation.[191] The reaction involves aldehydes or ketones and an activated methylene compound that, in the presence of a weak base, produces α,β unsaturated dicarbonyls or similar compounds. There exist several proposed mechanisms for this base catalyzed aldol-type reaction. If the base is a tertiary amine, it is proposed that the first step is a deprotonation of the activated methylene compound forming an enolate intermediate.[192] The enolate then acts as a nucleophile on the aldehyde or ketone that yields the desired product after dehydration. If the amine is primary or secondary, the mechanism begins with the aldehyde and the amine condensing to an iminium salt. The iminium salt then undergoes a reaction with the enolate. After elimination of the amine, the α,β unsaturated product is formed.[193] A proposed mechanism for the Knoevenagel condensation used to prepare the dyes in this thesis is shown in Scheme 1.4.
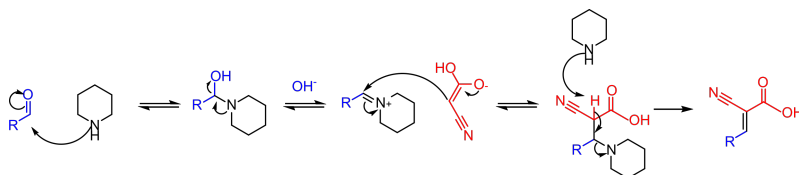
Scheme 1.4: Proposed mechanism for the Knoevenagel condensation.[193]

When using a methylene compound with two different substituents for the condensation with an aldehyde, a mixture of geometric isomers could be expected. As the mechanism for the condensation consists of several reversible steps, the major product formed is usually the most thermodynamically stable isomer.[194] Following this reasoning, it is expected that the cyanoacrylic acid will adopt an E-configuration with the least steric interaction between the aromatic system and the carboxylic acid. The E-configuration is reported almost exclusively in all reports of new cyanoacrylic acid dyes, but few demonstrate experimental evidence that support this. Experimental evidence that support the E-isomer as the favored isomer is found in NMR studies,[195] and crystallographic studies[196] on related compounds. Hong *et al.*[197] demonstrated that a mixture of E and Z configuration in dyes for DSSC is obtained from using a methylene compound with two substituent of comparable size (trifluoromethyl acrylic acid). Upon separation of the two isomers, it was discovered that the configuration with carboxylic acid *trans* to the aromatic system was more efficient (4.1% PCE) than the opposite (1.4% PCE).

1.4.3 Modern transition-metal catalyzed reactions

Suzuki-Miyaura cross-coupling

The Pd-catalyzed coupling of alkenyl boranes with aryl halides reported by Suzuki and Miyaura in 1979,[198] laid the foundation for what would later be known as the Suzuki-Miyaura cross-coupling. This reaction has been established as a "workhorse" in modern organic chemistry, and is frequently used to form new C-C bonds in the synthesis of novel dyes. Owing to its prevalence, a plethora of coupling partners, both boronic compounds and aryl halides are commercially available. The reaction has since its origin been the subject of research aimed at improving it, such as developing novel catalysts that facilitate the coupling of tricky substrates,[199–201] or developing methods that allow coupling of sp^3-hybridized alkyl halides that would normally undergo β-hydride elimination instead of transmetalation.[202,203]

The precise mechanism for the Suzuki-Miyaura reaction is still debated, a proposed mechanism is shown in Scheme 1.5.[204] The first step is the *oxidative addition* step where the aryl halide is added to the $Pd^{(0)}$ catalyst, making a $Pd^{(II)}$ complex. A mechanistic study found this to be the rate determining step (RDS) when coupling aryl bromides, while for aryl iodides, transmetallation was the RDS.[205] By increasing the size of the halide, the C-X bond is weakened and thus the rate of oxidative addition is improved. Also, electron withdrawing groups on the aryl halide will facilitate the oxidative addition.[206] In addition, the use of electron rich phosphine ligands is beneficial for improving the rate of this step.[201]

The next step is the *metathesis* step, where the halide on the Pd complex is replaced by the base (in an aqueous Suzuki-Miyaura reaction it is OH^-). The next step is the *transmetallation* step, where the aryl boronic acid transfers the aryl group to the Pd-center in exchange for the base. Recent studies have shown that, contrary to popular belief, the transmetallation step is not dependent on forming a four-coordinate boronate beforehand. In fact, Ar'B(OH)$_3^-$ is unreactive compared to Ar'B(OH)$_2$.[207,208] The ultimate step is the *reductive elimination* where the C-C σ-bond is formed and the $Pd^{(0)}$ catalyst is regenerated. The rate of reductive elimination is reduced by increasing the electron density of the phosphine ligands, making the optimization of catalyst a balancing act to accomodate both oxidative addition and reductive elimination. Employing sterically demanding ligands has been shown to speed up reductive elimination,[209] making electron-rich and bulky ligands favorable for use in this reaction.
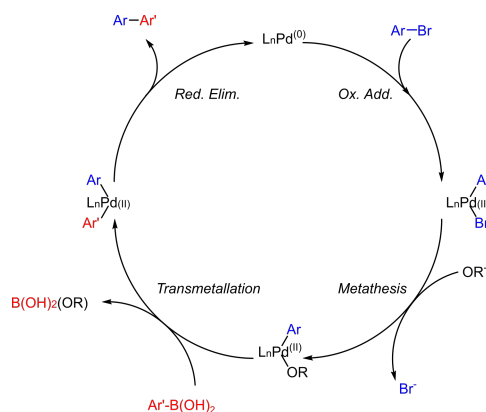
Scheme 1.5: Proposed mechanism for the Suzuki-Miyaura reaction.[204]
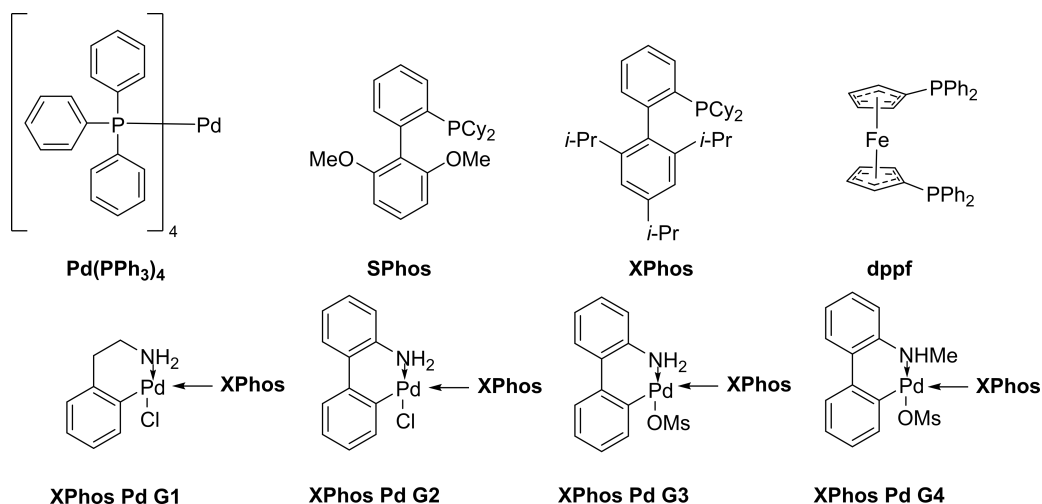
Figure 1.21: The "standard" Pd-catalyst $Pd(PPh_3)_4$ used in the pioneering work by Suzuki and Miyaura.[198] The structure of some potent ligands (**SPhos**,[210] **XPhos**,[211] and **dppf**[212]) for Pd-catalyzed reactions is shown, along with the four generations of commercially available **XPhos** precatalysts.[199,213–215]

A wealth of electron-rich and steric ligands for the Pd-catalysts have been reported, and are now commercially available (see Figure 1.21). The ligand **SPhos** is prepared from a one-pot reaction starting with 1,3-dimethoxybenzene,[216] and has been proven efficient in preparing sterically tricky tetra-*ortho*-substituted biaryls.[210] The **XPhos** ligand is particularly interesting for dye synthesis due to its proven efficiency for coupling thiophene boronic acids.[211] Four generations of precatalysts based on the **XPhos** ligand has been made commercially available, following development from the Buchwald group.[199,213–215] The goal of these precatalysts is to form the catalytically active species under milder conditions to further increase the scope of the Suzuki-Miyaura reaction and other Pd-catalyzed

reactions. The bidendate ferrocene ligand **dppf**[212] is interesting because the ligand is not electron-rich nor sterically hindered, yet the ligand is still highly effective due to the wide bite-angle of the ligand that reduces the angle between the two aryl groups (Ar and Ar') and accelerates reductive elimination.[217]

Following the Pd-catalyzed reaction mechanism, several competing reactions are present. Most notorious is perhaps *homo-coupling* and *deboronation* of the aryl boronate, and *dehalogenation* of the aryl halide. A possible mechanism for dehalogenation is metathesis with a solvent such as methanol. The resulting complex is susceptible to β-H elimination forming the ArPdH complex and subsequently Ar-H.[218] Homo-coupling of aryl boronates is thought to be caused by Pd$^{(0)}$ being oxidized by oxygen forming a Ar'PdOR complex.[219] This complex reacts with another equivalent of the aryl boronate forming the complex Ar'PdAr' and subsequently Ar'-Ar'. Particularly troubling for dye synthesis is the unstable nature of five-membered heteroaromatic boronates (e.g. thiophene/furan) where these decompose to Ar'-H at elevated temperatures and over a wide pH-range.[220]

Miyaura borylation

Having covered the vital Suzuki-Miyaura cross-coupling, the need for synthetic approaches to prepare aromatic boron compounds is apparent. The standard approach is lithiation of an aromatic halide and quenching with a boronic electrophile to prepare aromatic boronates. Ishiyama *et al.*[221] presented in 1995 an alternative approach to prepare arylboronic esters that relies on Pd-catalysis. The approach is known as Miyaura borylation, and offers an alternative that omits the use of strong alkyl lithium bases and thereby increases the functional group tolerance and safety considerably. Development of novel catalysts expanded the scope of the reaction to include aryl chlorides where previously only bromides and iodides were reactive.[222] Further optimization of the catalyst improved the atom efficiency of the reaction by enabling reactions with pinacol borane (H-BPin) instead of the traditional bis(pinacolato)diboron (B$_2$Pin$_2$) reagent.[223] Recent developments made to the reaction has made the synthesis of aryl boronic acids possible from aryl halides, where previously only boronic esters were available.[224,225] Examples of direct C-H borylation to form aryl boronic esters from iridium-catalysis also exist in the literature.[226,227]

A proposed mechanism for the Pd-catalyzed borylation is shown in Scheme 1.6. The mechanism starts as expected with an *oxidative addition* of the aryl halide to the Pd-catalyst. Murata *et al.*[228] proposed a three-step catalytic cycle involving *transmetallation* and *reductive elimination* to arrive at the aryl boronic compound. A DFT study performed by Lam *et al.*[229] questioned the possibility of the transmetallation step relying on deprotonation of H-BPin due to the hydridic nature of the B-H bond. Instead they proposed a four-step catalytic cycle involving an *amine assisted ionization* making a cationic intermediate. Their calculations found that this pathway was energetically favored over the previously

proposed transmetalation mechanism. Pinacol borane is involved in the *metathesis* step producing the finished boronic ester, and transferring the hydride to the Pd-catalyst. Ultimately, the amine contributes in the *reductive elimination* by deprotonating the Pd complex and regenerating the catalyst.
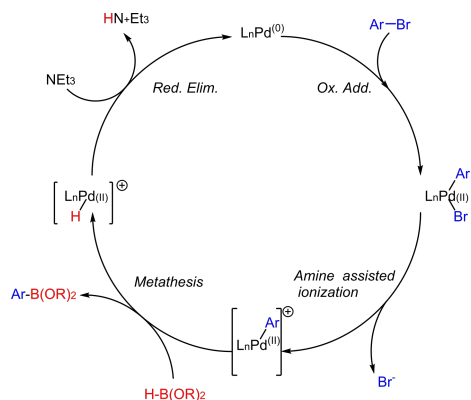
Scheme 1.6: Proposed mechanism for the Miyaura borylation reaction.[229]

Buchwald-Hartwig amination

Robust procedures for forming C-N bonds on aromatic compounds is of great significance in the toolbox of an organic dye chemist. The traditional approach of nucleophilic aromatic substitution is limited to aryl halides that are sufficiently activated with electron withdrawing groups. Ullmann type couplings relying on Cu-catalysis is another proven method for preparing arylamines.[230,231] The Ullmann type C-N couplings often require high temperatures, suffer from homo-coupling of the aryl halides, and are substrate specific.[232] The Pd-catalyzed C-N cross-coupling reaction known as the Buchwald-Hartwig amination is a more general and milder method for preparing arylamines. The reaction is named after its co-discoverers which both concurrently reported the first Pd-catalyzed coupling of free amines and aryl halides in 1995.[233,234] Both the original papers highlighted the need for a strong base to deprotonate the Pd-coordinated amine forming an amide.[235] Developments made to the catalyst system have expanded the scope of the reaction to unreactive substrates such as aryl chlorides and amides.[199,235,236]

A proposed mechanism for the reaction is shown in Scheme 1.7. The first step is *oxidative addition* of the aryl halide, before two different routes to the Pd-amide intermediate is proposed. The first route suggest the formation of a $Pd^{(II)}$-alkoxide intermediate via a *metathesis* step, before a reaction with the amine yields the desired Pd-amide.[232] The second route involves the coordination of amine to Pd before the base forms the amide and a displacement of the halide yields the Pd-aryl amide complex.[237] The final step is a *reductive elimination* yielding the finished arylamine and regenerating the Pd-catalyst.
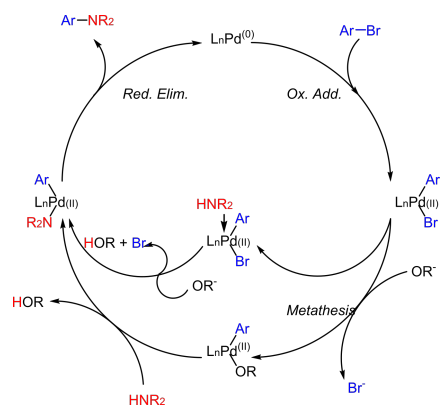
Scheme 1.7: Proposed mechanism for the Buchwald-Hartwig reaction.[232,237]

2 Results and Discussion of Papers

In this chapter, the body of work that represents the foundation of this thesis is presented. Special attention is given to the background or reasoning behind each study presented, as well as how the different studies relate to each other. This chapter is not extensive enough to cover all the details presented in the individual papers, nor is it intended to, instead the reader is referred to the appendix for a full account of the papers.

As outlined in Figure 2.1, Paper I-III concerns modifications done on the π-conjugated system of the dyes, while Paper IV-V present alterations done to the side chains. Although the properties of the dyes studied in the first set of papers are more affected by the modifications than the ones in the last set, the overall goal is still the same: To use organic synthesis as a tool to prepare dyes with unique structures and establish useful structure-property relationship data for DSSC-dyes.

Paper I
Paper II
Paper III

Altering:
- Electronic system
Affecting:
- Absorption properties
- Frontier orbital energy levels

Affecting:
- Photovoltaic performance
- Aggregation
- Charge recombination

Paper IV
Paper V

Altering:
- Side-chains
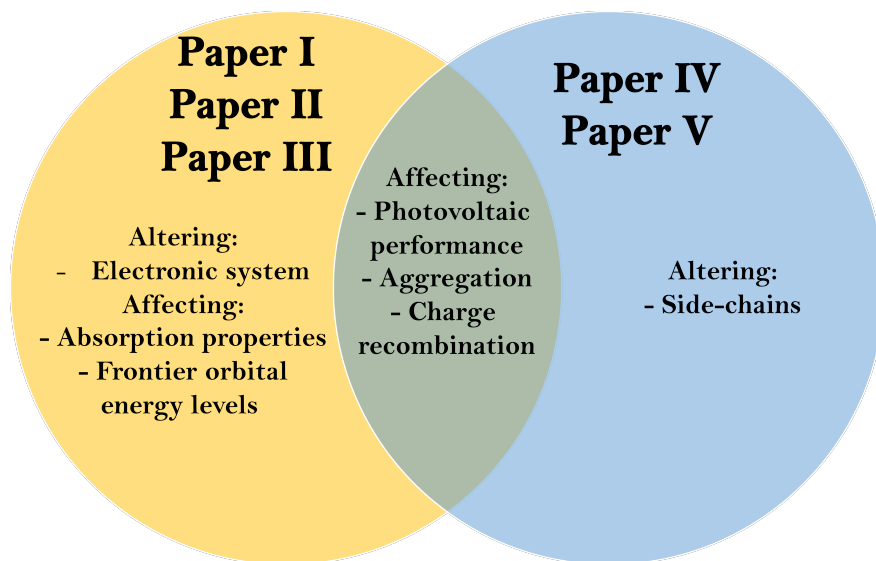
Figure 2.1: A simplified scheme of how the different papers relate to each other.

2.1 Paper I: Effect of thiophene-based π-spacers on N-arylphenothiazine dyes for dye-sensitized solar cells

In paper I, the main goal was to investigate the effect of extending the thiophene π-spacer on a set of phenothiazine dyes.[67] The study picks up on the previous π-spacer study by Buene *et al.*[108] where it was established that the photocurrent gained from a single thiophene did not outweigh the loss of photovoltage. The dye without π-spacer performed better than the one linked with thiophene. By successively expanding the size of the π-spacer from none to four consecutive thiophene units, we aimed to establish whether the longer π-spacers would be able to generate a sufficiently high photocurrent to offset the loss in photovoltage. The structure of the dyes investigated is shown in Table 2.1. The synthesis of the larger dyes (**DMA-3** and **DMA-4**) was particularly troublesome due to the poor solubility of these dyes. As a result, the yields for the synthesis of these dyes were lower than the other dyes in the series. From the series of dyes, we were able to see the expected increase in photocurrent in response to the inreasingly sized thiophene π-spacers from zero to three consecutive π-spacers. Surprisingly, the dye linked with a quaterthiophene π-spacer produced the lowest photocurrent of the series, showing that aggregation of large aromatic systems on the surface of TiO_2 has a profound effect on the DSSC performance. The dye without any π-spacer proved to be the most efficient in this study due to its excellent photovoltage 0.83 V in a I^-/I_3^- redox shuttle, although the dyes furnished with a single thiophene and bithiophene produced comparable PCE-values.

The results from this study show that there are no universal answers to optimizing the π-spacer for all donors. A series of coumarine dyes presented by Hara *et al.*[238] found the bithiophene spacer to outperform thiophene and terthiophene in terms of PCE. Conversely, Liu *et al.*[107] found that photovoltaic performance increased with increasing the size of the π-spacer all the way to a quaterthiophene in a series of triphenylamine dyes. The effect of the π-spacer has been extensively studied both experimentally and theoretically, and the mechanism behind the voltage loss is well understood. i) The larger π-spacers increase the dipole moment which down shift the Fermi level of TiO_2.[112] ii) The lessened influence of the donor increase the acidity of the carboxylic acid and the increased protonation lower the conduction band edge.[23] iii) Sulfur-containing heterocycles (such as thiophene) form sulfur-iodine complexes near the surface of TiO_2 and lower the Fermi level through an increased rate of recombination.[55] The first two mechanisms likely explain why different donors show different trends with regards to the optimal π-spacer size. The last mechanism can be avoided by not using the I^-/I_3^- redox shuttle.

DMA-0 : π = "Nothing"

DMA-1 : π =

DMA-2 : π =

DMA-3 : π =
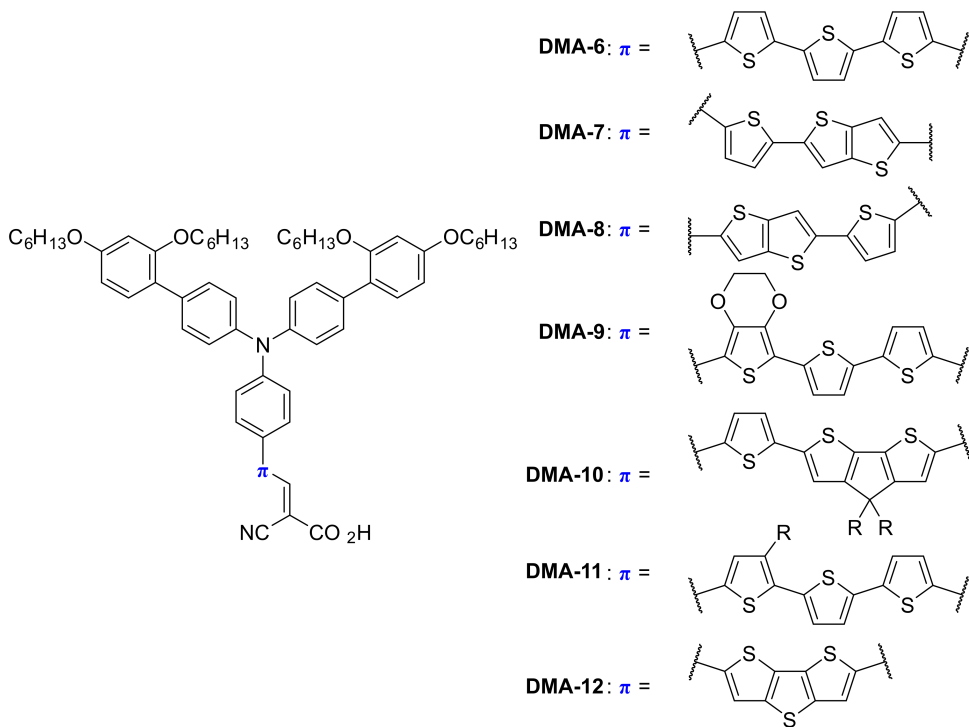
DMA-4 : π =

DMA-5 : π =
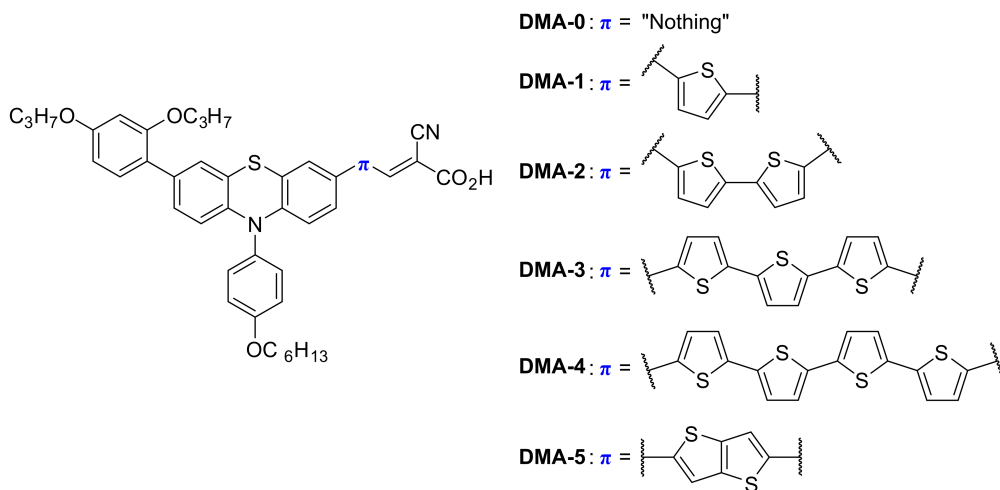
Table 2.1: The structure of the dyes investigated. Also shown in the absorption maximum of the dye when sensitized on TiO$_2$, the oxidation potential, and the photovoltaic parameters.

Dye	λ_{max,TiO_2} (nm)	E_{ox} (V *vs.* SHE)	J_{sc} (mA cm^{-2})	V_{oc} (V)	FF (-)	PCE (%)
DMA-0	444	1.04	10.1	0.83	0.68	5.7
DMA-1	379	0.93	10.6	0.77	0.69	5.6
DMA-2	421	0.95	10.9	0.77	0.67	5.6
DMA-3	419	0.96	11.0	0.70	0.68	5.2
DMA-4	441	0.92	7.3	0.63	0.68	3.1
DMA-5	402	0.92	10.3	0.74	0.69	5.3

The results from EIS showed that the recombination resistance decreased with increasing size of the π-spacer. The facilitation of recombination by larger π-spacers and the observed drop in photovoltages support the formation of sulfur-iodine complex mechanism. This led us to design a set of sensitizers that could harness the excellent light absorption of the terthiophene π-spacer while using a redox shuttle that prevents the sulfur-iodine interactions.

2.2 Paper II: Effect of terthiophene-based π-spacers on triarylamine dyes for dye-sensitized solar cells

Paper II was, as previously mentioned, a follow-up study on Paper I. The aim of this study was to establish whether it was possible to retain the high photocurrent of the dye **DMA-3** and achieve high photovoltages in an iodine-free redox shuttle. To employ a Cu redox shuttle, the phenothiazine donor was replaced with the prevalent tetraalkoxy substituted triarylamine donor. The secondary objective was to identify successful molecular traits of terthiophene π-spacers. A library of seven novel terthiophene dyes was prepared to achieve this. The structures of the dyes are shown in Table 2.2. The convergent/divergent synthesis approach reported by Gabrielsson *et al.*[56] proved highly suitable to prepare the novel dyes. Two dyes from the library prepared (**DMA-9** and **DMA-10**), displayed considerably better absorption properties than the rest, but as a consequence their oxidation potentials were lowered too much to be utilized effectively in the Cu redox shuttle. The dye **DMA-10** is an analogue to the highly successful **Y123**[239] dye, differing only in an additional thiophene between the CPDT and donor unit. The extra thiophene unit of **DMA-10** did not significantly alter the absorption of the dye in solution, but red shifted λ_{max} slightly when adsorbed on TiO$_2$. Photovoltaic characterization revealed that the hexyl substituted terthiophene and the fully fused terthiophene were the most successful π-spacer designs. Sensitizing the dyes on electrodes employing a thicker active TiO$_2$ layer resulted in a considerable drop in photovoltaic performance.

The reduction of the aromatic system by incorporating fused bithiophene and fused terthiophene had negligible effect on the λ_{max} compared to the unmodified terthiophene (**DMA-6**). This suggest that the increased planarity of these spacers likely counteract the effect of reducing the size of the π-conjugated system. Another interesting observation is that all the modified π-spacers led to reduced optical band gaps compared to the unmodified terthiophene spacer. The reduced performance of the devices that employed a thicker TiO$_2$ is attributed to mass transport issues of the redox shuttle. Velore *et al.*[40] showed that by going from 4 μm to 8 μm TiO$_2$ the PCE almost halved under 1 sun AM 1.5G illumination. They also found that the dye configuration that formed the closest packed dye layers were affected the most by varying the thickness due to it blocking the redox shuttle the most. Following this logic, the two most efficient dyes **DMA-11** and **DMA-12** were also the ones that formed the most closely-packed dye layers.

Considering that the terthiophene dyes presented in this paper did not yield the expected high photocurrents seen for the phenothiazine dye, it might be attributed to differences in the donor unit. The main difference in the donor of Paper I and Paper II is the sulfur bridge between two phenyl rings on phenothiazine. In paper III we look closer at the significance of this and other heteroatom bridge possibilities on the triarylamine scaffold, and try to establish effect of these.

DMA-6: π =

DMA-7: π =

DMA-8: π =

DMA-9: π =

DMA-10: π =

DMA-11: π =

DMA-12: π =

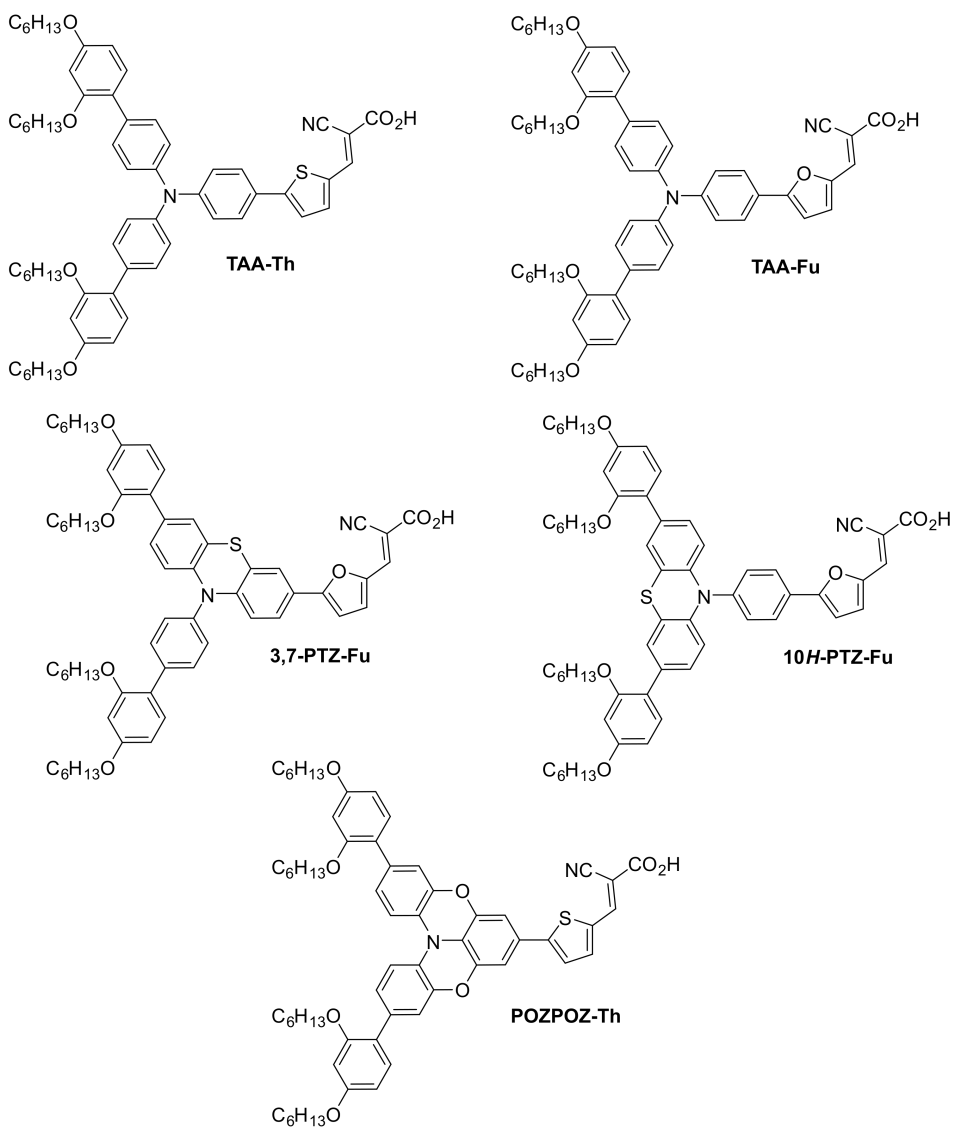C$_6$H$_{13}$O OC$_6$H$_{13}$ C$_6$H$_{13}$O OC$_6$H$_{13}$
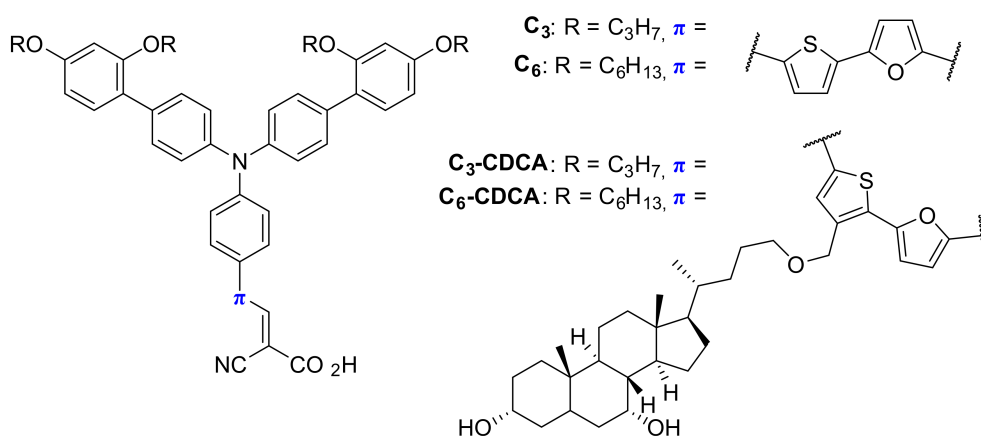
N

π

NC CO$_2$H

Table 2.2: The structure of the dyes investigated. Also shown in the absorption maximum of the dye when sensitized on TiO$_2$, the oxidation potential, and the photovoltaic parameters.

Dye	λ_{max,TiO_2} (nm)	E_{ox} (V *vs.* SHE)	J_{sc}^a (mA cm^{-2})	V_{oc}^a (V)	FF^a (-)	PCE^a (%)
DMA-6	459	1.09	6.1	0.89	0.61	3.3
DMA-7	465	1.10	5.1	0.87	0.63	2.8
DMA-8	464	1.10	6.4	0.91	0.59	3.4
DMA-9	488	0.96	3.1	0.78	0.55	1.3
DMA-10	498	1.01	5.9	0.83	0.68	3.3
DMA-11	451	1.05	7.0	0.94	0.62	4.1
DMA-12	456	1.11	7.0	0.95	0.66	4.4

^{a} *Values obtained from the 4.5 μm TiO$_2$ devices.*

2.3 Paper III: Synthetic Efforts to Investigate the Effect of Planarizing the Triarylamine Geometry in Dyes for Dye-Sensitized Solar Cells

In this paper, we prepared two triarylamine dyes, two phenothiazine dyes, and a double phenoxazine dye to investigate the effect of the heteroatom bridges. The structures of these dyes are shown in Table 2.3. The preparation of these dyes turned out to be quite complicated, and required carefully designed synthesis routes. Particularly challenging was the synthesis of **POZPOZ-Th**, which of course limits any practical applications of these dyes. Bridging the central phenyl rings of the triarylamine unit is bound to increase the planarity of the donor, and improved the absorption properties of **3,7-PTZ-Fu** and **POZPOZ-Th** compared to their triarylamine analogs. The dye **10H-PTZ-Fu**, with its drastically reduced absorption, showed the importance of keeping the aromatic system of the donor and acceptor in the same plane. The planarized donors also had their oxidation potentials lowered too much to be utilized in pairing with a Cu redox shuttle.

By using the λ_{onset} on TiO$_2$ estimation method for evaluating donor strength,[97] we found the following trend of increasing strength: 10H-PTZ < TAA < 3,7-PTZ < POZPOZ. However, the superior donating strength of the double phenoxazine did not translate into increased photovoltaic performance, as the dye **POZPOZ-Th** displays the worst PCE in the series. Reviewing the results of the EIS measurements showed that this dye displayed an irregular behavior and lowered recombination resistances at applied voltages below V_{oc}. This shows that the fully planarized dye design provides less surface protection than the other dyes in the series. Conversely, both the phenothiazine dyes showed sign of improved surface protection compared to the triarylamine dyes. The recombination resistances of both these dyes were slightly higher than their triarylamine analog, and the effective electron diffusion length was considerably improved. This demonstrates that the sulfur bridge in phenothiazine improves the ratio of electrons being collected in the external circuit to the number of electrons recombining with the redox shuttle. The dye **3,7-PTZ-Fu** outperformed all the dyes in the series in terms of PCE, which shows the merit of this donor over the triarylamine donor. Although this only holds when employing a I$^-$/I$_3^-$ redox shuttle.

The dyes presented in this study showed how alterations done to the aromatic system can influence the optical properties and energy levels of the dyes significantly. For the next two papers, the goal was completely opposite, where we aimed to alter dye structure without influencing the optical and electronic properties at all.
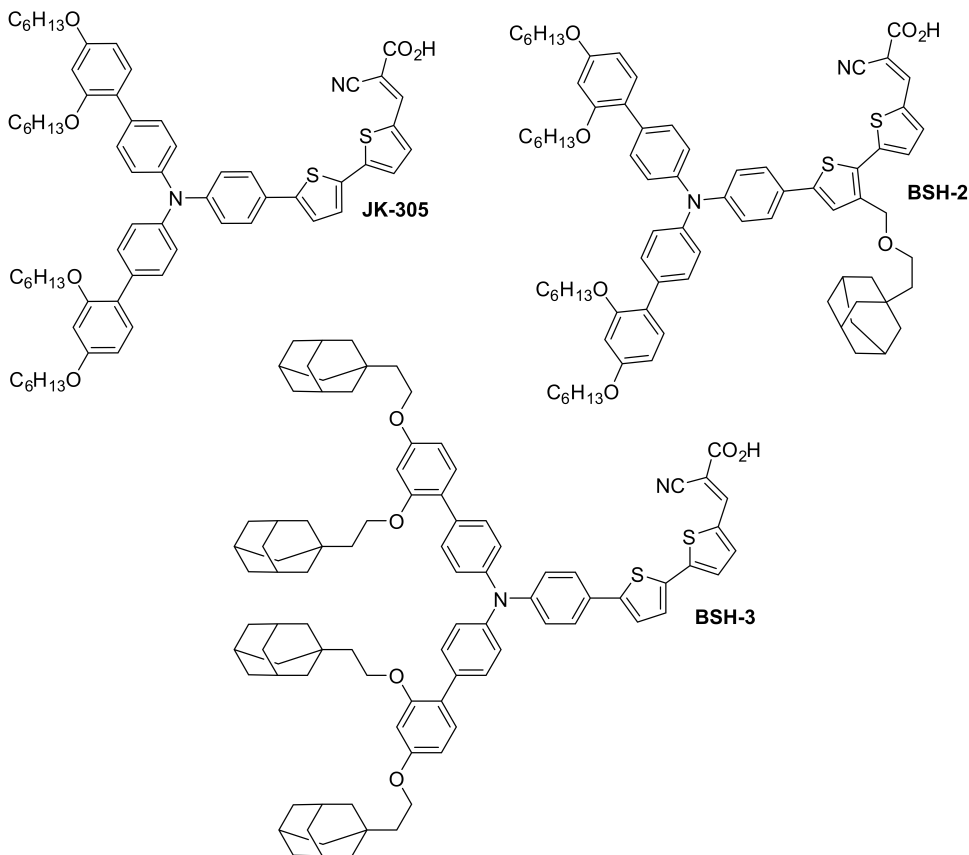
Table 2.3: The structure of the dyes investigated. Also shown in the absorption maximum of the dye when sensitized on TiO_2, the oxidation potential, and the photovoltaic parameters.

Dye	λ_{max,TiO_2} (nm)	E_{ox} (V *vs.* SHE)	J_{sc} (mA cm^{-2})	V_{oc} (mV)	FF (-)	PCE (%)
TAA-Th	464	1.13	7.5	829	0.66	4.1
TAA-Fu	462	1.10	7.7	869	0.70	4.7
3,7-PTZ-Fu	466	0.97	8.8	838	0.70	5.2
10*H*-PTZ-Fu	461	0.91	4.9	839	0.77	3.1
POZPOZ-Th	522	0.96	5.8	673	0.59	2.3

2.4 Paper IV: First Report of Chenodeoxycholic Acid –Substituted Dyes Improving the Dye Monolayer Quality in Dye-Sensitized Solar Cells

The topic of this paper is the prospect of covalently attaching chenodeoxycholic acid (CDCA) to the dyes as shown in Table 2.4.[180] The bile acid CDCA has been used as an anti-aggregation additive in staining solutions for DSSC since 1993.[240] The carboxylic acid group of CDCA allows it to attach itself to TiO_2 and interpose the aggregating dyes. When using CDCA to space out the dyes on the semiconductor surface there is limited control of the distribution, and no way to ensure an isotropic layer of dye and additive. Our synthesis of the dyes involved preparing advanced triarylamine boronic ester fragments and coupling them with π-spacer building blocks. To evaluate the effect of the CDCA substitution, we used two different π-spacer fragments, either with or without the CDCA-substitution. When measuring the optical and electrochemical properties we found that the CDCA-substitution was quite inert, and only minor differences between the dyes was observed.

Table 2.4: The structure of the dyes investigated. Also shown in the absorption maximum of the dye when sensitized on TiO_2, the oxidation potential, and the photovoltaic parameters.

Dye	λ_{max,TiO_2} (nm)	E_{ox} (V $vs.$ SHE)	J_{sc}[a] (mA cm^{-2})	V_{oc}[a] (mV)	FF[a] (-)	PCE[a] (%)
C$_3$	442	1.09	7.6	962	0.73	5.4
C$_6$	445	1.12	7.6	1000	0.74	5.7
C$_3$-CDCA	448	1.11	7.1	1013	0.73	5.3
C$_6$-CDCA	451	1.11	8.0	1035	0.74	6.2

[a] *Values from the 4 + 2 μm TiO_2 devices with 10 eq. CDCA.*

Due to the fairly consistent optical and electronic properties of the dyes, we could more precisely isolate the performance difference of the dyes to the steric effect of the CDCA-substituent. This allowed us to develop the performance measurement sensitizer quantum efficiency (SQE), which is a dye-loading adjusted IPCE spectrum. This measurement looks at the efficiency of the individual dye molecule. We found that the CDCA-substituted dyes clearly outperformed the reference dyes in terms of SQE. We attributed this difference to a superior molecular environment for the CDCA-dyes in the dye monolayer. We also observed that the V_{oc} dropped with increasing concentrations of "free" CDCA, which we believe is caused by the increased protonation of TiO_2 downshifting the Fermi level of the semiconductor. In contrast to what we observed in Paper II, we also saw an increase in performance when employing thicker active TiO_2. We observed a linear dependence when measuring the J_{sc} as a function of light intensity, which would suggest that these devices were not mass transport limited.

The introduction of CDCA to the thiophene unit was largely a success and was carried out in 4 steps where the yields were quantitative for each step. Still, we asked ourselves whether we could do more with less and increase the practical potential of this concept by using a simpler more compact blocking unit.

2.5 Paper V: Adamantyl Side-Chains as Anti-aggregating Moieties in Dyes for Dye-Sensitized Solar Cells

Taking inspiration from the results in Paper IV, we set out to investigate whether a more compact anti-aggregation unit could achieve similar results. We prepared two novel dyes **BSH-2** and **BSH-3** that were decorated by ethyladamantyl substitutions as shown in Table 2.5. The adamantane moiety is a hydrocarbon comprised of three fused cyclohexane rings in a rigid, but strain free system,[241] and is perhaps most known for its frequent use in antiviral drugs.[242] In DSSCs the adamantane structure has been used on a couple of occasions previously: 1-Adamantane acetic acid (ADAA) has been evaluated as an anti-aggregation additive akin to CDCA,[240] the nitroxide radical 2-azaadamantan-N-oxyl (AZA) has been tested as a redox shuttle,[243] and AZA has been used in a tandem redox shuttle along with a Co complex to achieve photovoltage above 1 V.[244] The synthesis of the π-spacer **BSH-2** followed the route we made for the $\mathbf{C_3/C_6}$-**CDCA** dyes, but it was made simpler due to the chemical nature of the substituent not needing protecting groups. The donor of **BSH-3** was done following the exact same synthesis route as the previous triarylamine dyes presented herein. The effect of the adamantyl substitutions were evaluated against the non-modified triarylamine dye **JK-305**.[245]

C6H13O

CO2H

NC

S

S

JK-305

C6H13O

C6H13O

N

C6H13O

C6H13O

C6H13O

CO2H

NC

S

S

O

BSH-2

O

O

N

O

CO2H

NC

S

S

O

BSH-3

Table 2.5: The structure of the dyes investigated. Also shown in the absorption maximum of the dye when sensitized on TiO_2, the oxidation potential, and the photovoltaic parameters.

Dye	λ_{max,TiO_2} (nm)	E_{ox} (V *vs.* SHE)	J_{sc} (mA cm^{-2})	V_{oc} (mV)	FF (-)	PCE (%)
JK-305	454	1.10	8.6	1035	0.64	5.7
+ CDCA	-	-	8.4	972	0.70	5.8
+ ADAA	-	-	7.5	955	0.55	3.9
BSH-2	453	1.11	8.2	1067	0.63	5.5
+ CDCA	-	-	7.4	975	0.49	3.5
BSH-3	456	1.14	7.9	1045	0.45	3.7
+ CDCA	-	-	8.3	1054	0.69	6.1

Fortunately, the dyes produced displayed the same behavior as the dyes presented in Paper IV where the modifications had minimal impact on the optical and electronic properties. The photovoltaic performance of the dyes was measured in devices with and without any anti-aggregation additives to be able to

compare how these dyes behave compared to the CDCA-dyes in Paper IV. In the CDCA-free devices, we observed considerably better performances from the dye with a standard hexyloxy substituted triarylamine donor. EIS measurements revealed worse recombination resistances from the adamantyl decorated donor, by that explaining why this dye performed worse than the other dyes. However, when the devices were prepared with CDCA, another picture revealed itself. The dye **BSH-3** displayed a drastic improvement in performance, while the opposite was the case for **BSH-2** where a considerable reduction in performance was noted. The improvement observed for **BSH-3** was attributed to the excellent recombination resistance measured. The incorporation of CDCA in staining solution has previously been noted to provide surface isolation.[246] Surprisingly, the introduction of CDCA reduced the recombination resistance of **BSH-2**. This suggest that the adamantyl moiety on the π-spacer produced some deleterious interactions with CDCA on the surface of TiO_2.

2.6   Organic synthesis of the dyes

The foundation for this thesis has been organic synthesis as a tool to prepare dyes that will expand the current understanding of structure-property relationships for dyes. As a result, considerable synthetic efforts have been put forward. The following section presents some of the key considerations that can be made when reviewing the organic synthesis performed.

Synthesis of N-arylphenothiazine dyes: The preparation of *N*-arylphenothiazine dyes was performed in both Paper I and Paper III. The synthetic route chosen was different for the two papers, the two pathways are shown in Scheme 2.1. The synthesis route that was used to prepare **DMA-1** consists of seven steps, and yielded the finished dye in an overall yield of 14%. The two selective brominations using NBS are absolutely crucial for the success of this strategy, and is founded on the protocols for preparing and purifying brominated *N*-arylphenothiazines developed by Bejan *et al.*[247] The last bromination reaction still yields a mixture of brominated and unreacted phenothiazines that in our hands proved inseparable. As a consequence, the brominated and subsequent borylated intermediates are not isolated following this synthesis route. The synthetic strategy presented in Paper III is comparatively more convoluted, and **3,7-PTZ-Fu** was prepared in a worse overall yield of 2%. Still, there are some merits to this strategy. The first step is a bromination using Br_2 based on affordable starting materials, which can be carried out in quite large scale due to facile re-crystallization of the dibrominated phenothiazine. The first step in the synthesis of **DMA-1** relies on Pd-catalysis, along with the need to perform SiO_2 column chromatography, limits the scale of this reaction. Following the route in Paper III, all the intermediates were also isolated and characterized.
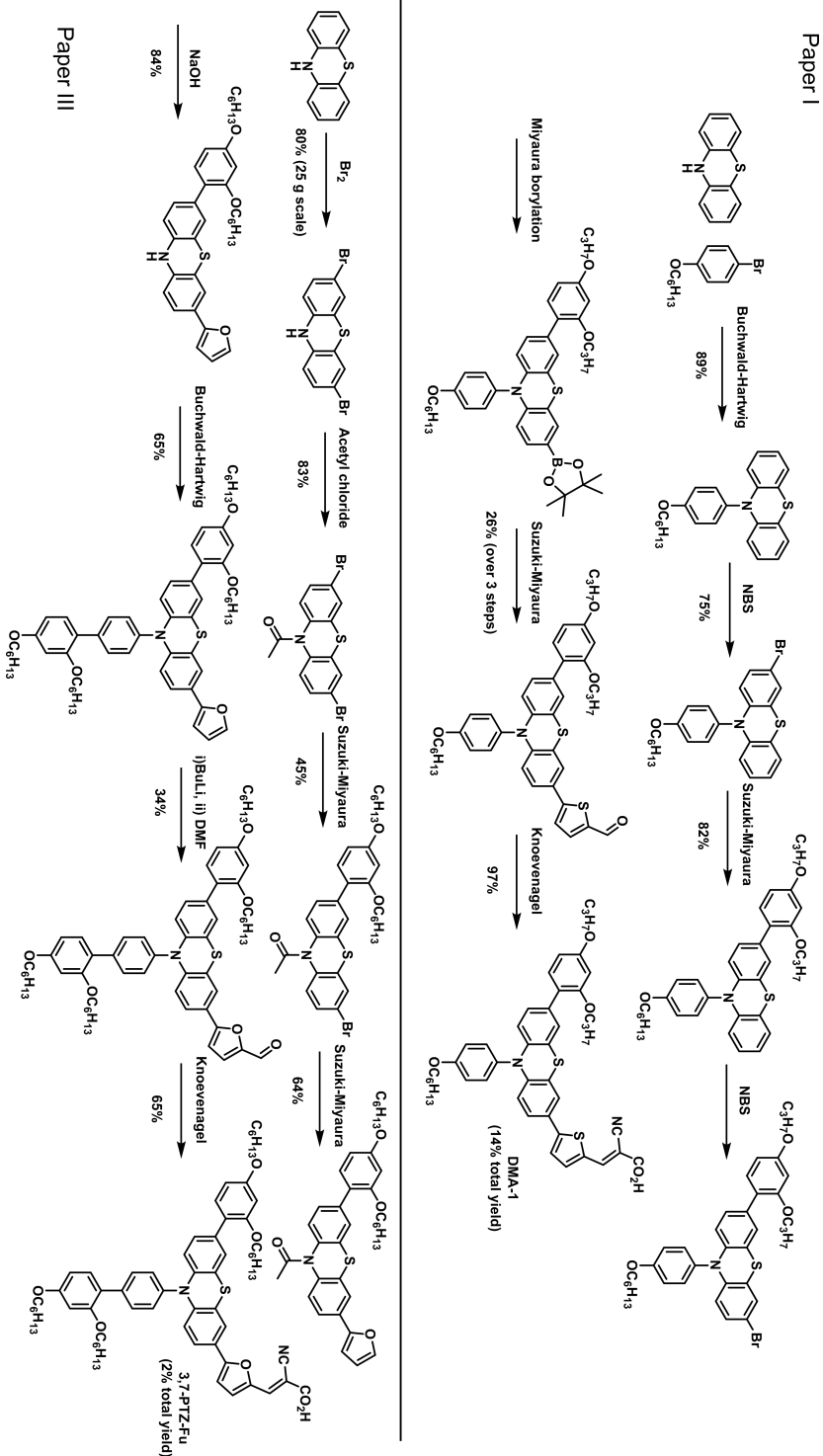
Scheme 2.1: A comparison of two different synthesis routes to prepare *N*-arylphenothiazine dyes presented in Paper I[67] and III.[58]

Synthesis of π-spacers with large substituents: Common for the last two papers is the preparation of π-spacers with bulky substituents. The synthesis of the finished coupling partners for the Suzuki-Miyaura cross-coupling with the donor moiety is shown in Scheme 2.2. Also included is the synthesis of the hexyl substituted analogue prepared by Gabrielsson *et al.*[56] The first cross-coupling reactions were carried out in larger yields for both the CDCA substituted and adamantyl substituted thiophenes compared to the hexyl substituted thiophene. This suggests that the additional bulk of the CDCA and adamantyl moieties do not interfere with the reaction. This is supported by the fact that the un-substituted π-spacer prepared in Paper IV was isolated in a yield of 48%, which is considerably lower than the yield of the CDCA-substituted biaryl. Due to the unstable nature of the furan boronic acid, we used 3 equivalents of it in the cross-coupling presented in Paper IV to achieve satisfactory yields. Switching the catalyst system to XPhos Pd G3 afforded the coupled product in a 54% yield, using only 1.5 equivalents of boronic acid. A curious observation is the reduced yield obtained from the bromination steps of the π-spacers in Paper IV and V. The low yield observed in Paper IV is due to a challenging purification, where parts of the crude product decomposed during column chromatography.
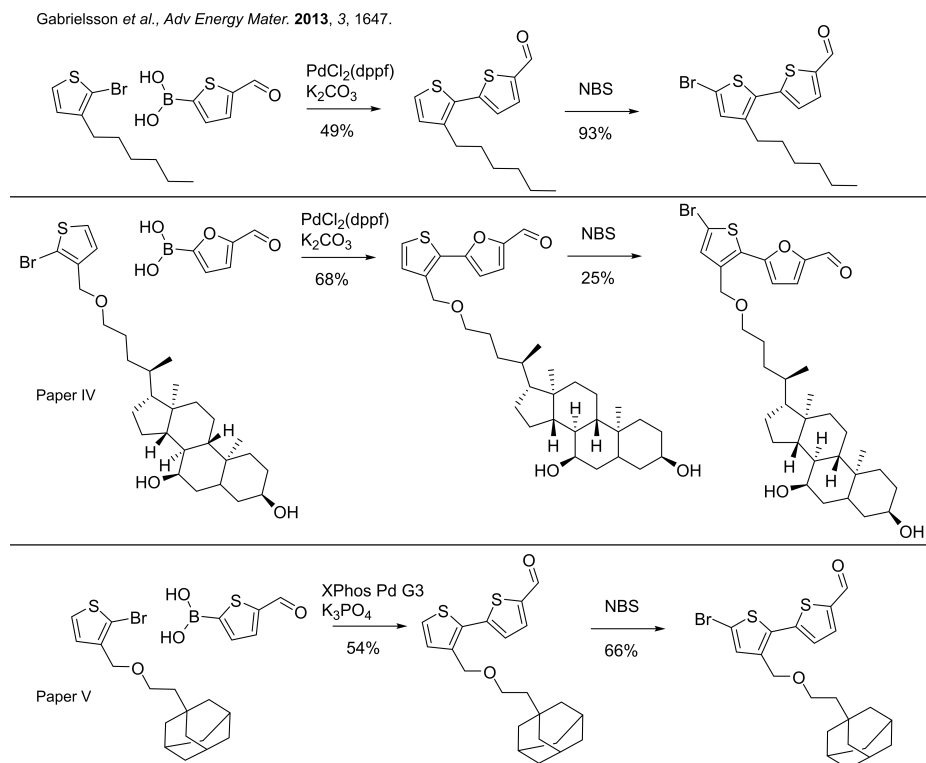
Scheme 2.2: A comparison of π-spacer syntheses presented by Gabrielsson *et al.*,[56] and in Paper IV[180] and V.[71]
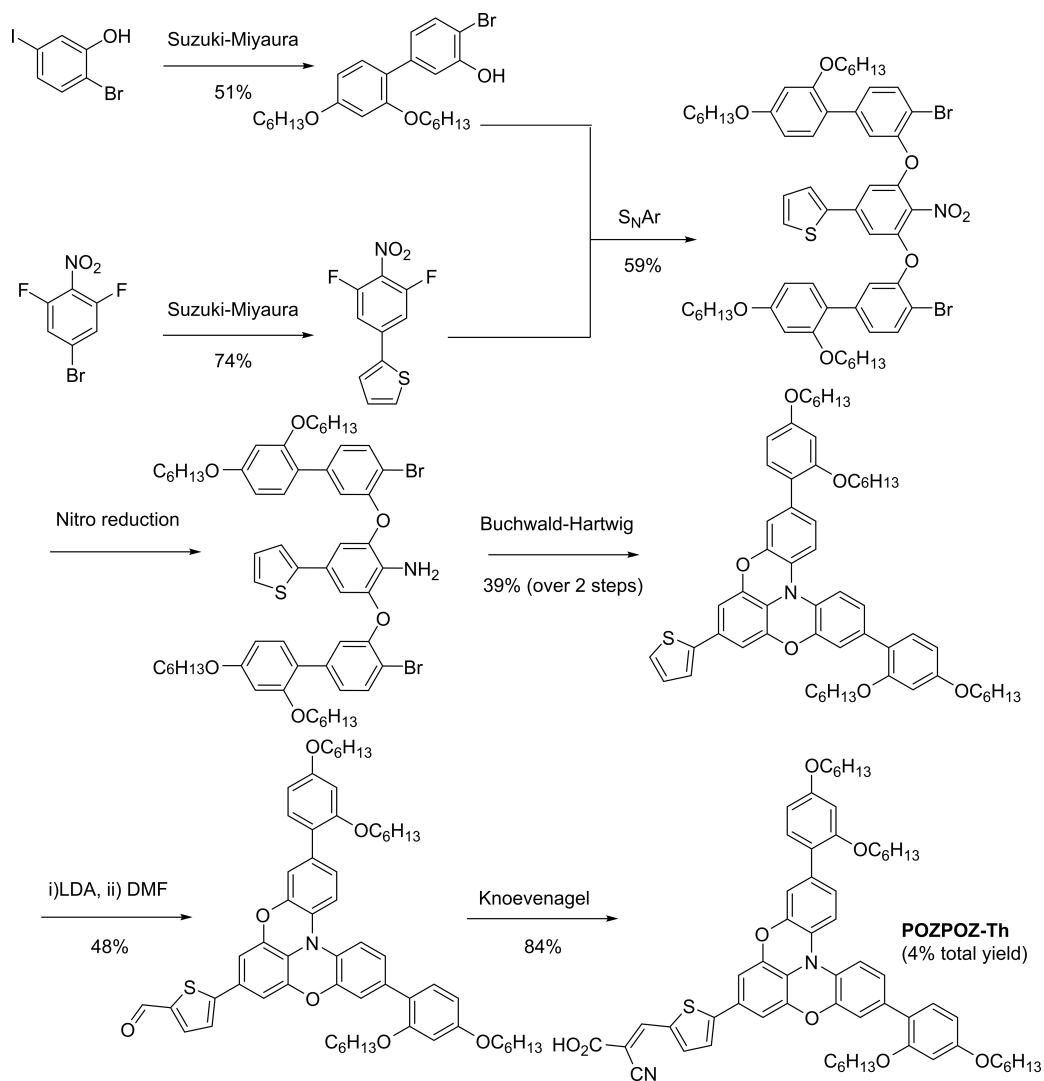
Scheme 2.3: The synthesis of the dye **POZPOZ-Th** presented in Paper III.[58] This synthesis route differs from other routes presented in this thesis because there are no selective halogenation steps involved.

*Synthesis of **POZPOZ-Th**:* The preparation of the double phenoxazine dye **POZPOZ-Th** is arguably the greatest synthetic challenge presented in this thesis. The central fragment, the double phenoxazine, differed from the similar phenothiazine and triarylamine fragments in terms of selectivity for the EAS reaction. Because of this, the original synthesis route, which relied on selectively brominating this moiety, was discarded in favor of the strategy shown in Scheme 2.3. The synthesis route shown in this scheme is not reliant on any selective halogenation reactions. Omitting the use of selective bromination reactions is a considerable limitation to the synthesis of a dye, as all other dye syntheses presented in this

thesis depend on at least one of these reactions at some point. In the synthesis presented in Scheme 2.3, all the halides required for the cross-coupling reactions are found in the starting materials. Although the finished dye turned out to be quite disappointing in terms of PCE, the synthesis route presented here could be of use for others looking to selectively functionalize the double phenoxazine moiety. Several studies are devoted to harnessing the double phenoxazine motif for use in organic hole transporting materials,[248–250] phosphorescent Ir complexes,[251,252] and thermochromic dyes.[253]

3 Conclusions

The aim of this thesis was to expand the knowledge of structure-property relationships in dyes for DSSC. This was done by preparing families of dyes aimed at unravelling a certain aspect of dye design.

The investigation of oligothiophene π-spacers led to the realization that "no π-spacer" was the most efficient dye design for the phenothiazine dyes investigated. The superior performance of the dye without a π-spacer was largely attributed to its high photovoltage. The iterative expansion of the π-spacer yielded the expected red shift of absorption and improved photocurrents. However, introducing the quaterthiophene resulted in a severely diminished photocurrent and PCE compared to the other dyes. The recombination resistance was lowered with the increasingly sized oligothiophene linker, providing a possible explanation as to why the photovoltage was lowered by lengthening the π-spacer. The results from this study coincide with results from other research groups where the formation of sulfur-iodine complexes is seen as a mechanism behind the voltage drops of thiophene compounds in iodine redox shuttles.

The following π-spacer investigation was founded on seven novel triarylamine dyes with different terthiophene linkers, each prepared following a convergent/divergent synthesis approach. Characterization of the optical properties revealed that the ethylenedioxythiophene (**DMA-9**) and cyclopentadithiophene (**DMA-10**) modified dyes displayed particularly red shifted spectra compared to the non-modified terthiophene dye (**DMA-6**). However, the two former dyes were found incompatible with the copper redox shuttle. The two most efficient dyes were established to be the hexyl substituted dye (**DMA-11**) and the fully fused terthiophene dye (**DMA-12**). The preparation and characterization of two different sets of DSSC devices with different thicknesses of active TiO_2 (4.5 μm and 9 μm) revealed a considerably better performance from the 4.5 μm devices. The devices with 9 μm TiO_2 were described by Gerischer impedance, meaning that there is strong recombination and low electron collection efficiency. The drastic improvement of dyes **DMA-11** and **DMA-12** in going from a 9 μm to a 4.5 μm device suggest that these dyes form the most closely packed dye layer on TiO_2, as they hindered the diffusion of the redox shuttle the most in the 9 μm device.

The bridge between triarylamine dyes and phenothiazine dyes was established

both metaphorically and synthetically in our investigation on planarization of the triarylamine donor. Through synthetic efforts, four different donor geometries spanning from the "free" triarylamine to the fully planarized double phenoxazine were prepared. The fully planar **POZPOZ-Th** displayed considerably improved optical properties, and the width of the IPCE-spectrum matched that of the benchmark Ru complex dye **N719** albeit at a considerably reduced intensity. However, the planar dye was considerably worse at blocking recombination than the other dyes in this series, and at lower applied voltages it was approaching Gerischer impedance. This highlighted the need for some out-of-plane geometry present on the donor to provide surface protection. The butterfly configuration of phenothiazine proved to be as good, or even slightly better than the propeller shape of triarylamine with regards to blocking recombination. For the effective electron diffusion length, a clear advantage was noted for the phenothiazine dyes. While encouraging for the class of phenothiazine dyes, the superior photovoltaic performance of the **3,7-PTZ-Fu** dye over the triarylamine dyes is not expected to be transferable to a state-of-the-art copper regenerated device.

Seeking to target novel dye design concepts, the first report of covalently attaching the anti-aggregating additive CDCA to a dye molecule was presented. This design allowed an isotropic distribution of dye and CDCA on the surface of TiO_2, which is not possible following the conventional approach of adding CDCA to the staining solution. Comparing the two reference sensitizers without CDCA-modification, an improved photovoltage was observed for the dye with the longest alkyl chains. The hexyloxy substituted dye blocked recombination better than the propoxy substitution, and supporting the improved photovoltages noted for C_6. In DSSCs prepared without additional "free" CDCA added to the staining solution, there were no benefit from the CDCA substitution. In devices that were added 10 equivalents of "free" CDCA, several advantages were observed. The C_3**-CDCA** dye displayed similar performances to the non-modified dye, but with higher photovoltages. The C_6**-CDCA** dye improved both photovoltage and PCE compared to the non-modified reference dye. The improved performance of the CDCA-modified dyes upon addition of "free" CDCA suggests that the optimal ratio of CDCA to dye on the surface of TiO_2 is larger than one.

The incorporation of ethyladamantyl side chains was also presented for the first time in dyes for DSSC following our synthetic efforts. The adamantyl substituted dyes displayed improved photovoltages compared to the non-modified reference dye in all cases. The dye **BSH-2** with its adamantyl decorated π-spacer displayed a considerably inferior photovoltaic performance once CDCA was introduced to the staining solution, indicating that the two steric functionalities suffer from deleterious interactions. The combination of **BSH-2** and CDCA resulted in the facilitation of recombination. The combination of the reference dye **JK-305** and adamantyl acetic acid also turned out to facilitate recombination. The adamantyl decorated donor **BSH-3** enjoyed a considerable boost to PCE upon addition of CDCA to the staining solution, and the recombination resistance was consider-

ably improved. This device displayed an improved performance compared to the hexyl substituted donor, indicating that the adamantyl donor of **BSH-3** might be successfully implemented in other dyes.

Reviewing the library of the 25 dyes prepared and characterized in this thesis, a few considerations can be made. In an iodine redox shuttle, the phenothiazine donor is more efficient than the triarylamine donor. Additionally, phenothiazine proved to give better effective electron diffusion lengths. Keeping in mind that the state-of-the-art Cu redox shuttles are more susceptible to recombination than the iodine redox shuttle, finding a way to harness phenothiazine dyes in copper regenerated devices would hold some merit. In the library of dyes already prepared, the dye **DMA-0** presents an interesting prospect for use as a co-sensitizer in a Cu regenerated DSSC. Successful co-sensitization approaches are frequently the combination of a "wide-absorption" dye and a "high-voltage" dye, the epitome of which is seen in the **XY1b**/**MS5** device previously discussed. The dye **DMA-0** with its oxidation potential of 1.04 V *vs.* SHE is compatible with most Cu redox shuttles. With its proven anti-recombination properties it could serve as a "high-voltage" dye, and to the best of the authors knowledge be the first phenothiazine dye in a Cu DSSC.

The performance of the individual dyes might overall be considered a little disappointing. Some of the reason behind this is the quality of fabrication equipment, procedure, and materials involved in making the DSSCs. The benchmark dyes **N719** and **Y123** typically achieves PCEs in excess of 6% in the studies we present, and is a testament to the potential to improve our fabrication procedure. Also by choosing to prepare libraries of target compounds to look for successful traits, the chance of preparing ineffective compounds is always present. Although not desirable, there are valuable lessons to be learned from "failed" dye designs also. An example of such a lesson is found in Paper II where the two isomeric dyes reveal a considerable reduction in PCE in the dye with the fused bithiophene α to the acceptor (**DMA-7**) compared to employing the fused bithiophene α to the donor (**DMA-8**).

Ultimately, the library of dyes prepared offer a unique opportunity to look for traits across the five different studies. By applying the λ_{onset} on TiO$_2$ method to dyes with the same π-spacer and acceptor, the donor strength can be estimated. From Paper III, the onset of absorption for the thiophene linked and furan linked dye was found fairly similar. As such, the foundation for this comparison will be all dyes linked with a single thiophene or furan unit. This gives the following estimate of donor strength **POZPOZ-Th**$\gg$**3,7-PTZ-Fu**$>$**TAA-Th**$\approx$**TAA-Fu**$>$**10H-PTZ-Fu**$>$**DMA-1**. Applying the same approach on all the dyes with the same donor, would provide an estimate for "π-spacer strength". Reviewing all the dyes with the hexyloxy substituted triarylamine donor gives the following order **DMA-9**$>$**DMA-10**$>$**DMA-6**$>$**Y123**$\approx$**DMA-7**$\approx$**DMA-8**$\approx$**DMA-11**$>$**DMA-12**$\approx$**BSH-2**$\approx$**JK-305**$\approx$**C$_6$**$>$**C$_6$-CDCA**$\approx$**TAA-Th**$\approx$**TAA-Fu**.

3.1 Future work

As previously mentioned, the investigation of phenothiazine dyes as a co-sensitizer for use in state-of-the-art Cu DSSC devices could hold some merit. The dye **DMA-0** is for instance a promising starting point for such an investigation. Alternatively, preparing a **MS5/DMA-0** hybrid as shown in Figure 3.1, could provide a significant surface protection.

Our covalent CDCA-linking strategy could be of use for dyes that are strongly affected by aggregation. The previously mentioned near-infrared absorbing dye **VG20-C$_{16}$** is an example of such a dye, where the optimized performance for this dye is found using a $1/500$ ratio of dye to CDCA. Preparing the CDCA substituted dye **VG20-CDCA** (see Figure 3.1) could aid in reducing the formation of dye aggregates.

The adamantyl-substitutions invariably increased the photovoltage of the DSSC devices compared to the standard alkyl-substituted dye. Attempting to harness this property in the design of future dyes could lead to improved photovoltaic performances. Replacing the donor of a wide-absorption dye such as **XY1** with the donor of **BSH-3** could be an interesting study to see if the excellent photocurrent is retained, but with improved photovoltages.
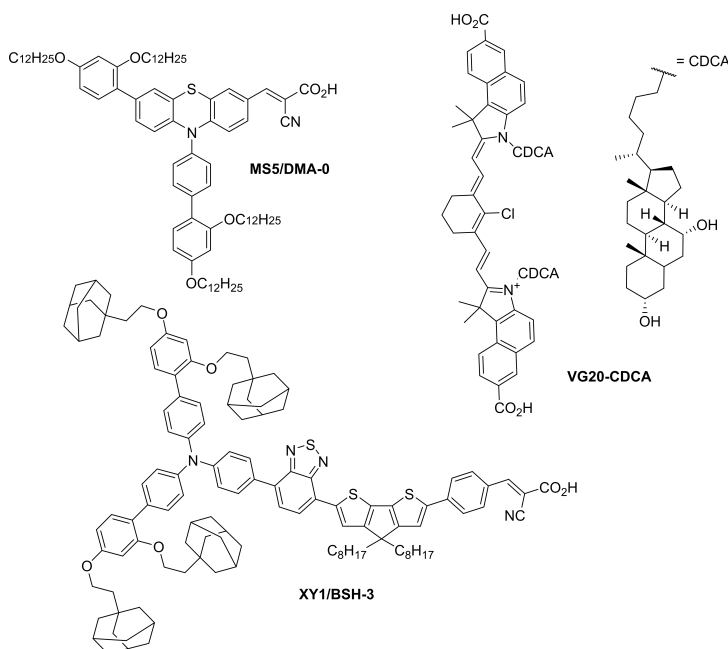
Figure 3.1: The dye **MS5/DMA-0** aims to provide excellent recombination blocking, key to the success of this design is the lack of π-spacer that would render the phenothiazine incompatible with Cu redox shuttles. **VG20-CDCA** is decorated with two CDCA-units to prevent aggregation. **XY1/BSH-3** targets high photocurrents and high photovoltages.

References

[1] H.-O. Pörtner, D. Roberts, M. Tignor, E. Poloczanska, K. Mintenbeck, A. Alegría, S. L. M. Craig, S. Löschke, V. Möller, A. Okem, and B. Rama. IPCC, 2022: Climate Change 2022: Impacts, Adaptation, and Vulnerability, 2022.

[2] Paris Agreement, https://unfccc.int/sites/default/files/english_paris_agreement.pdf (accessed May 02, 2022).

[3] T. Markvart. 2nd. Wiley, Solar Electricity, 2000.

[4] International Energy Agency (IEA), Key World Energy Statistics 2021, https://www.iea.org/reports/key-world-energy-statistics-2021, 2021.

[5] E. Becquerel. *Comptes Rendus* **9** (1839), 561–567.

[6] W. G. Adams and R. E. Day. *Proc. R. Soc. Lond.* **25** (1877), 113–117.

[7] D. M. Chapin, C. S. Fuller, and G. L. Pearson. *J. Appl. Phys* **25** (1954), 676–677.

[8] S. Philipps. Fraunhofer ISE, Photovoltaics Report, 2022.

[9] J. Czochralski. *Z. Phys. Chem.* **92U** (1918), 219–221.

[10] N. Milenkovic, M. Drießen, B. Steinhauser, J. Benick, S. Lindekugel, M. Hermle, S. Janz, and S. Reber. In: *2016 IEEE 43rd Photovoltaic Specialists Conference (PVSC)*. 2016, 0058–0061.

[11] B. A. Gregg and M. C. Hanna. *J. Appl. Phys* **93** (2003), 3605–3614.

[12] M. D. Archer. *Phys. E: Low-Dimens. Syst. Nanostructures* **14** (2002), 61–64.

[13] Z. Du, M. Artemyev, J. Wang, and J. Tang. *J. Mater. Chem. A* **7** (2019), 2464–2489.

[14] O. Inganäs. *Adv. Mater.* **30** (2018), 1800388.

[15] M. I. H. Ansari, A. Qurashi, and M. K. Nazeeruddin. *J. Photochem. Photobiol. C: Photochem. Rev.* **35** (2018), 1–24.

[16] A. Hagfeldt, G. Boschloo, L. Sun, L. Kloo, and H. Pettersson.
      Chem. Rev. **110** (2010), 6595–6663.

[17] H.-S. Kim, C.-R. Lee, J.-H. Im, K.-B. Lee, T. Moehl, A. Marchioro,
      S.-J. Moon, R. Humphry-Baker, J.-H. Yum, J. E. Moser, M. Grätzel, and
      N.-G. Park. *Sci. Rep.* **2** (2012), 591.

[18] B. O'Regan and M. Grätzel. *Nature* **353** (1991), 737–740.

[19] H. Gerischer, M. E. Michel-Beyerle, F. Rebentrost, and H. Tributsch.
      Electrochim. Acta **13** (1968), 1509–1515.

[20] H. Gerischer and H. Tributsch.
      Ber. Bunsenges. Phys. Chem. **72** (1968), 437–445.

[21] H. Tributsch and H. Gerischer.
      Ber. Bunsenges. Phys. Chem. **73** (1969), 251–260.

[22] J. Desilvestro, M. Graetzel, L. Kavan, J. Moser, and J. Augustynski.
      J. Am. Chem. Soc. **107** (1985), 2988–2990.

[23] A. F. Buene and D. M. Almenningen.
      J. Mater. Chem. C **9** (2021), 11974–11994.

[24] M. K. Nazeeruddin, A. Kay, I. Rodicio, R. Humphry-Baker, E. Mueller,
      P. Liska, N. Vlachopoulos, and M. Graetzel.
      J. Am. Chem. Soc. **115** (1993), 6382–6390.

[25] M. K. Nazeeruddin, P. Péchy, T. Renouard, S. M. Zakeeruddin,
      R. Humphry-Baker, P. Comte, P. Liska, L. Cevey, E. Costa, V. Shklover,
      L. Spiccia, G. B. Deacon, C. A. Bignozzi, and M. Grätzel.
      J. Am. Chem. Soc. **123** (2001), 1613–1624.

[26] D. Joly, L. Pellejà, S. Narbey, F. Oswald, J. Chiron, J. N. Clifford,
      E. Palomares, and R. Demadrille. *Sci. Rep.* **4** (2014), 4033.

[27] S. M. Feldt, E. A. Gibson, E. Gabrielsson, L. Sun, G. Boschloo, and
      A. Hagfeldt. *J. Am. Chem. Soc.* **132** (2010), 16714–16724.

[28] S. M. Feldt, G. Wang, G. Boschloo, and A. Hagfeldt.
      J Phys. Chem. C **115** (2011), 21500–21507.

[29] K. Kakiage, Y. Aoyama, T. Yano, K. Oya, J.-i. Fujisawa, and M. Hanaya.
      ChemComm **51** (2015), 15894–15897.

[30] M. Freitag, F. Giordano, W. Yang, M. Pazoki, Y. Hao, B. Zietz,
      M. Grätzel, A. Hagfeldt, and G. Boschloo.
      J Phys. Chem. C **120** (2016), 9595–9603.

[31] Y. Cao, Y. Liu, S. M. Zakeeruddin, A. Hagfeldt, and M. Grätzel.
      Joule **2** (2018), 1108–1117.

[32] D. Zhang, M. Stojanovic, Y. Ren, Y. Cao, F. T. Eickemeyer, E. Socie, N. Vlachopoulos, J. E. Moser, S. M. Zakeeruddin, A. Hagfeldt, and M. Grätzel. *Nat. Commun.* **12** (2021), 1777.

[33] H. Michaels, I. Benesperi, and M. Freitag. *Chem. Sci.* **12** (2021), 5002–5015.

[34] L. Zhang, G. Boschloo, L. Hammarström, and H. Tian. *Phys. Chem. Chem. Phys.* **18** (2016), 5080–5085.

[35] B. Zhang and L. Sun. *Chem. Soc. Rev.* **48** (2019), 2216–2264.

[36] M. Stojanović, N. Flores-Diaz, Y. Ren, N. Vlachopoulos, L. Pfeifer, Z. Shen, Y. Liu, S. M. Zakeeruddin, J. V. Milić, and A. Hagfeldt. *Helv. Chim. Acta* **104** (2021), e2000230.

[37] S. Yun, N. Vlachopoulos, A. Qurashi, S. Ahmad, and A. Hagfeldt. *Chem. Soc. Rev.* **48** (2019), 3705–3722.

[38] S. Sahare, H. D. Pham, D. Angmo, P. Ghoderao, J. MacLeod, S. B. Khan, S.-L. Lee, S. P. Singh, and P. Sonar. *Adv. Energy Mater.* **11** (2021), 2101085.

[39] A. B. Muñoz-García, I. Benesperi, G. Boschloo, J. J. Concepcion, J. H. Delcamp, E. A. Gibson, G. J. Meyer, M. Pavone, H. Pettersson, A. Hagfeldt, and M. Freitag. *Chem. Soc. Rev.* **50** (2021), 12450–12550.

[40] J. Velore, S. C. Pradhan, T. W. Hamann, A. Hagfeldt, K. N. N. Unni, and S. Soman. *ACS Appl. Energy Mater.* **5** (2022), 2647–2654.

[41] C. Hora, F. Santos, M. G. F. Sales, D. Ivanou, and A. Mendes. *ACS Sustain. Chem. Eng.* **7** (2019), 13464–13470.

[42] S. Ito, P. Liska, P. Comte, R. Charvet, P. Péchy, U. Bach, L. Schmidt-Mende, S. M. Zakeeruddin, A. Kay, M. K. Nazeeruddin, and M. Grätzel. *ChemComm* (2005), 4351–4353.

[43] G. Boschloo, L. Häggman, and A. Hagfeldt. *J Phys. Chem. B* **110** (2006), 13144–13150.

[44] J. Wu, Z. Lan, J. Lin, M. Huang, Y. Huang, L. Fan, and G. Luo. *Chem. Rev.* **115** (2015), 2136–2173.

[45] A. Kay, R. Humphry-Baker, and M. Graetzel. *J. Phys. Chem.* **98** (1994), 952–959.

[46] S. M. Feldt, P. W. Lohse, F. Kessler, M. K. Nazeeruddin, M. Grätzel, G. Boschloo, and A. Hagfeldt. *Phys. Chem. Chem. Phys.* **15** (2013), 7087–7097.

[47] Y. Saygili, M. Söderberg, N. Pellet, F. Giordano, Y. Cao, A. B. Muñoz-García, S. M. Zakeeruddin, N. Vlachopoulos, M. Pavone, G. Boschloo, L. Kavan, J. E. Moser, M. Grätzel, A. Hagfeldt, and M. Freitag. *J. Am. Chem. Soc.* **138** (2016), 15087–15096.

[48] K. Zeng, Y. Chen, W.-H. Zhu, H. Tian, and Y. Xie.
J. Am. Chem. Soc. **142** (2020), 5154–5161.

[49] A. Baumann, C. Curiac, and J. H. Delcamp.
ChemSusChem **13** (2020), 2503–2512.

[50] A. Hauch and A. Georg. *Electrochim. Acta* **46** (2001), 3457–3466.

[51] H. Ellis, N. Vlachopoulos, L. Häggman, C. Perruchot, M. Jouini,
G. Boschloo, and A. Hagfeldt. *Electrochim. Acta* **107** (2013), 45–51.

[52] S. E. Koops, B. C. O'Regan, P. R. F. Barnes, and J. R. Durrant.
J. Am. Chem. Soc. **131** (2009), 4808–4818.

[53] A. J. Frank, N. Kopidakis, and J. van de Lagemaat.
Coord. Chem. Rev. **248** (2004), 1165–1179.

[54] M. Pazoki, U. B. Cappel, E. M. J. Johansson, A. Hagfeldt, and
G. Boschloo. *Energy Environ. Sci.* **10** (2017), 672–709.

[55] M. Zhang, J. Liu, Y. Wang, D. Zhou, and P. Wang.
Chem. Sci. **2** (2011), 1401–1406.

[56] E. Gabrielsson, H. Ellis, S. Feldt, H. Tian, G. Boschloo, A. Hagfeldt, and
L. Sun. *Adv. Energy Mater.* **3** (2013), 1647–1656.

[57] I. Martini, J. H. Hodak, and G. V. Hartland.
J Phys. Chem. B **103** (1999), 9104–9111.

[58] D. M. Almenningen, V. M. Engh, E. A. Strømsodd, H. E. Hansen,
A. F. Buene, B. H. Hoff, and O. R. Gautun.
ACS Omega **7** (2022), 22046–22057.

[59] H. J. Snaith. *Nat. Photonics* **6** (2012), 337–340.

[60] A. F. Buene, E. E. Ose, A. Zakariassen, A. Hagfeldt, and B. Hoff.
J. Mater. Chem. A (2019).

[61] X. Yang, M. Yanagida, and L. Han. *Energy Environ. Sci.* **6** (2013), 54–66.

[62] J. A. Christians, J. S. Manser, and P. V. Kamat.
J. Phys. Chem. Lett. **6** (2015), 852–857.

[63] J. Halme, P. Vahermaa, K. Miettunen, and P. Lund.
Adv. Mater. **22** (2010), E210–E234.

[64] F. Fabregat-Santiago, J. Bisquert, G. Garcia-Belmonte, G. Boschloo, and
A. Hagfeldt. *Sol. Energy Mater. Sol. Cells* **87** (2005), 117–131.

[65] S. Soedergren, A. Hagfeldt, J. Olsson, and S.-E. Lindquist.
J Phys. Chem. **98** (1994), 5552–5556.

[66] F. Fabregat-Santiago, J. Bisquert, E. Palomares, L. Otero, D. Kuang,
S. M. Zakeeruddin, and M. Grätzel.
J Phys. Chem. C **111** (2007), 6550–6560.

[67] D. M. Almenningen, H. E. Hansen, M. F. Vold, A. F. Buene,
V. Venkatraman, S. Sunde, B. H. Hoff, and O. R. Gautun.
Dyes Pigm. **185** (2021), 108951.

[68] Q. Wang, S. Ito, M. Grätzel, F. Fabregat-Santiago, I. Mora-Seró,
J. Bisquert, T. Bessho, and H. Imai.
J Phys. Chem. B **110** (2006), 25210–25221.

[69] H. Tian, X. Yang, R. Chen, R. Zhang, A. Hagfeldt, and L. Sun.
J Phys. Chem. C **112** (2008), 11023–11033.

[70] T. Dentani, Y. Kubota, K. Funabiki, J. Jin, T. Yoshida, H. Minoura,
H. Miura, and M. Matsui. *New J. Chem.* **33** (2009), 93–101.

[71] D. M. Almenningen, B. S. Haga, H. E. Hansen, A. F. Buene, B. H. Hoff,
and O. R. Gautun. *Chem. Eur. J.* **n/a** (2022).

[72] N. Elgrishi, K. J. Rountree, B. D. McCarthy, E. S. Rountree,
T. T. Eisenhart, and J. L. Dempsey. *J. Chem. Educ.* **95** (2018), 197–206.

[73] Q. Wang, S. M. Zakeeruddin, J. Cremer, P. Bäuerle, R. Humphry-Baker,
and M. Grätzel. *J. Am. Chem. Soc.* **127** (2005), 5706–5713.

[74] A. F. Buene, A. Hagfeldt, and B. H. Hoff. *Dyes Pigm.* **169** (2019), 66–72.

[75] P. Ferdowsi, Y. Saygili, W. Zhang, T. Edvinson, L. Kavan, J. Mokhtari,
S. M. Zakeeruddin, M. Graetzel, and A. Hagfeldt.
ChemSusChem **11** (2018), 494–502.

[76] V. V. Pavlishchuk and A. W. Addison.
Inorganica Chim. Acta **298** (2000), 97–102.

[77] C.-Y. Chen, M. Wang, J.-Y. Li, N. Pootrakulchote, L. Alibabaei,
C.-h. Ngoc-le, J.-D. Decoppet, J.-H. Tsai, C. Grätzel, C.-G. Wu,
S. M. Zakeeruddin, and M. Grätzel. *ACS Nano* **3** (2009), 3103–3109.

[78] H. Ozawa, Y. Okuyama, and H. Arakawa.
Dalton Trans. **41** (2012), 5137–5139.

[79] H. Ozawa, T. Sugiura, T. Kuroda, K. Nozawa, and H. Arakawa.
J. Mater. Chem. A **4** (2016), 1762–1770.

[80] K.-L. Wu, A. J. Huckaba, J. N. Clifford, Y.-W. Yang, A. Yella,
E. Palomares, M. Grätzel, Y. Chi, and M. K. Nazeeruddin.
Inorg. Chem. **55** (2016), 7388–7395.

[81] Q. Huaulmé, V. M. Mwalukuku, D. Joly, J. Liotier, Y. Kervella,
P. Maldivi, S. Narbey, F. Oswald, A. J. Riquelme, J. A. Anta, and
R. Demadrille. *Nat. Energy* **5** (2020), 468–477.

[82] W. Naim, V. Novelli, I. Nikolinakos, N. Barbero, I. Dzeba, F. Grifoni,
Y. Ren, T. Alnasser, A. Velardo, R. Borrelli, S. Haacke,
S. M. Zakeeruddin, M. Graetzel, C. Barolo, and F. Sauvage.
JACS Au **1** (2021), 409–426.

[83] A. Błaszczyk. *Dyes Pigm.* **149** (2018), 707–718.

[84] N. T. Kalyani and S. J. Dhoble.
      Renew. Sust. Energ. Rev. **16** (2012), 2696–2723.

[85] K. A. Mazzio and C. K. Luscombe. *Chem. Soc. Rev.* **44** (2015), 78–90.

[86] L. Torsi, M. Magliulo, K. Manoli, and G. Palazzo.
      Chem. Soc. Rev. **42** (2013), 8612–8628.

[87] F. Bureš. *RSC Adv.* **4** (2014), 58826–58851.

[88] H. Meier. *Angew. Chem. Int. Ed.* **44** (2005), 2482–2506.

[89] D. F. Perepichka and M. R. Bryce.
      Angew. Chem. Int. Ed. **44** (2005), 5370–5373.

[90] C. Hansch, A. Leo, and R. W. Taft. *Chem. Rev.* **91** (1991), 165–195.

[91] J. Kulhánek, F. Bureš, A. Wojciechowski, M. Makowska-Janusik,
      E. Gondek, and I. V. Kityk. *J Phys. Chem. A* **114** (2010), 9440–9446.

[92] F. Würthner, F. Effenberger, R. Wortmann, and P. Krämer.
      Chem. Phys. **173** (1993), 305–314.

[93] Z.-S. Wang, Y. Cui, K. Hara, Y. Dan-oh, C. Kasada, and A. Shinpo.
      Adv. Mater. **19** (2007), 1138–1141.

[94] Y. Wu, M. Marszalek, S. M. Zakeeruddin, Q. Zhang, H. Tian, M. Grätzel,
      and W. Zhu. *Energy Environ. Sci.* **5** (2012), 8261–8272.

[95] N. Koumura, Z.-S. Wang, S. Mori, M. Miyashita, E. Suzuki, and K. Hara.
      J. Am. Chem. Soc. **128** (2006), 14256–14257.

[96] J. Wang, K. Liu, L. Ma, and X. Zhan.
      Chem. Rev. **116** (2016), 14675–14725.

[97] D. N. D. Ndaleh, D. Nugegoda, J. Watson, H. Cheema, and
      J. H. Delcamp. *Dyes Pigm.* **187** (2021), 109074.

[98] V. V. Divya and C. H. Suresh. *New J. Chem.* **44** (2020), 7200–7209.

[99] H. Bürckstümmer, E. V. Tulyakova, M. Deppisch, M. R. Lenze,
      N. M. Kronenberg, M. Gsänger, M. Stolte, K. Meerholz, and F. Würthner.
      Angew. Chem. Int. Ed. **50** (2011), 11628–11632.

[100] T. Higashino, Y. Fujimori, K. Sugiura, Y. Tsuji, S. Ito, and H. Imahori.
      Angew. Chem. Int. Ed. **54** (2015), 9052–9056.

[101] T. Higashino, Y. Kurumisawa, N. Cai, Y. Fujimori, Y. Tsuji, S. Nimura,
      D. M. Packwood, J. Park, and H. Imahori.
      ChemSusChem **10** (2017), 3347–3351.

[102] T. Higashino, S. Nimura, K. Sugiura, Y. Kurumisawa, Y. Tsuji, and
      H. Imahori. *ACS Omega* **2** (2017), 6958–6967.

[103] Y. Liu, Y. Cao, W. Zhang, M. Stojanovic, M. I. Dar, P. Péchy, Y. Saygili, A. Hagfeldt, S. M. Zakeeruddin, and M. Grätzel. *Angew. Chem. Int. Ed.* **57** (2018), 14125–14128.

[104] Z. Yang, C. Liu, K. Li, J. M. Cole, C. Shao, and D. Cao. *ACS Appl. Energy Mater.* **1** (2018), 1435–1444.

[105] J. Li, Y. Ding, S. Liu, W. Ding, D. Fang, H. Chen, Y. Jiao, B. Mi, W. Xu, and Z. Gao. *Synth. Met.* **287** (2022), 117067.

[106] D. P. Hagberg, T. Marinado, K. M. Karlsson, K. Nonomura, P. Qin, G. Boschloo, T. Brinck, A. Hagfeldt, and L. Sun. *J. Org. Chem.* **72** (2007), 9550–9556.

[107] J. Liu, R. Li, X. Si, D. Zhou, Y. Shi, Y. Wang, X. Jing, and P. Wang. *Energy Environ. Sci.* **3** (2010), 1924–1928.

[108] A. F. Buene, N. Uggerud, S. P. Economopoulos, O. R. Gautun, and B. H. Hoff. *Dyes Pigm.* **151** (2018), 263–271.

[109] M. M. Oliva, J. Casado, M. M. M. Raposo, A. M. C. Fonseca, H. Hartmann, V. Hernández, and J. T. L. Navarrete. *J. Org. Chem.* **71** (2006), 7509–7520.

[110] M. M. Raposo, A. C. Fonseca, and G. Kirsch. *Tetrahedron* **60** (2004), 4071–4078.

[111] A. F. Buene, N. Boholm, A. Hagfeldt, and B. Hoff. *New J. Chem.* (2019).

[112] E. Ronca, M. Pastore, L. Belpassi, F. Tarantelli, and F. D. Angelis. *Energy Environ. Sci.* **6** (2013), 183–193.

[113] Y. K. Eom, S. H. Kang, I. T. Choi, E. Kim, J. Kim, M. J. Ju, and H. K. Kim. *RSC Adv.* **5** (2015), 80859–80870.

[114] S. Chaurasia, C.-J. Liang, Y.-S. Yen, and J. T. Lin. *J. Mater. Chem. C* **3** (2015), 9765–9780.

[115] J.-H. Park, D. G. Nam, B.-M. Kim, M. Y. Jin, D.-H. Roh, H. S. Jung, D. H. Ryu, and T.-H. Kwon. *ACS Energy Lett.* **2** (2017), 1810–1817.

[116] Y. Liu, X. Zhang, C. Li, Y. Tian, F. Zhang, Y. Wang, W. Wu, and B. Liu. *J Phys. Chem. C* **123** (2019), 13531–13537.

[117] L. Tian, Y. Wang, Y. Zhang, X. Li, W. Wu, and B. Liu. *ACS Appl. Energy Mater.* **4** (2021), 242–248.

[118] K. Do, D. Kim, N. Cho, S. Paek, K. Song, and J. Ko. *Org. Lett.* **14** (2012), 222–225.

[119] F. Wu, S. Zhao, L. T. L. Lee, M. Wang, T. Chen, and L. Zhu. *Tetrahedron Lett.* **56** (2015), 1233–1238.

[120] N. Cai, R. Li, Y. Wang, M. Zhang, and P. Wang. *Energy Environ. Sci.* **6** (2013), 139–147.

[121] L. Cai, T. Moehl, S.-J. Moon, J.-D. Decoppet, R. Humphry-Baker, Z. Xue, L. Bin, S. M. Zakeeruddin, and M. Grätzel. *Org. Lett.* **16** (2014), 106–109.

[122] H. Li, T. M. Koh, Y. Hao, F. Zhou, Y. Abe, H. Su, A. Hagfeldt, and A. C. Grimsdale. *ChemSusChem* **7** (2014), 3396–3406.

[123] N. Zhou, K. Prabakaran, B. Lee, S. H. Chang, B. Harutyunyan, P. Guo, M. R. Butler, A. Timalsina, M. J. Bedzyk, M. A. Ratner, S. Vegiraju, S. Yau, C.-G. Wu, R. P. H. Chang, A. Facchetti, M.-C. Chen, and T. J. Marks. *J. Am. Chem. Soc.* **137** (2015), 4414–4423.

[124] L. Yang, Y. Ren, Z. Yao, C. Yan, W. Ma, and P. Wang. *J Phys. Chem. C* **119** (2015), 980–988.

[125] C. Yan, W. Ma, Y. Ren, M. Zhang, and P. Wang. *ACS Appl. Mater. Interfaces* **7** (2015), 801–809.

[126] Z. Yao, M. Zhang, H. Wu, L. Yang, R. Li, and P. Wang. *J. Am. Chem. Soc.* **137** (2015), 3799–3802.

[127] L. Zhang and J. M. Cole. *J. Mater. Chem. A* **5** (2017), 19541–19559.

[128] J. Wang, S. Liu, Z. Chai, K. Chang, M. Fang, M. Han, Y. Wang, S. Li, H. Han, Q. Li, and Z. Li. *J. Mater. Chem. A* **6** (2018), 22256–22265.

[129] D. Joly, M. Godfroy, L. Pellejà, Y. Kervella, P. Maldivi, S. Narbey, F. Oswald, E. Palomares, and R. Demadrille. *J. Mater. Chem. A* **5** (2017), 6122–6130.

[130] M. Pastore and F. D. Angelis. *ACS Nano* **4** (2010), 556–562.

[131] M. Xu, R. Li, N. Pootrakulchote, D. Shi, J. Guo, Z. Yi, S. M. Zakeeruddin, M. Grätzel, and P. Wang. *J Phys. Chem. C* **112** (2008), 19770–19776.

[132] J. E. Kroeze, N. Hirata, S. Koops, M. K. Nazeeruddin, L. Schmidt-Mende, M. Grätzel, and J. R. Durrant. *J. Am. Chem. Soc.* **128** (2006), 16376–16383.

[133] A. Bernthsen. *Ber. Dtsch. Chem. Ges.* **16** (1883), 2896–2904.

[134] J. J. H. McDowell. *Acta. Crystallogr. B* **32** (1976), 5–10.

[135] Y. Aouine, A. Alami, A. El Hallaoui, A. Elachqar, and H. Zouihri. *Acta Crystallogr. E* **66** (2010), o2830.

[136] D. Pan and D. L. Phillips. *J Phys. Chem. A* **103** (1999), 4737–4743.

[137] H. Tian, X. Yang, R. Chen, Y. Pan, L. Li, A. Hagfeldt, and L. Sun. *ChemComm* (2007), 3741–3743.

[138] R. Argazzi, C. A. Bignozzi, T. A. Heimer, F. N. Castellano, and G. J. Meyer. *J. Phys. Chem. B* **101** (1997), 2591–2597.

[139] S. Cazzanti, S. Caramori, R. Argazzi, C. M. Elliott, and C. A. Bignozzi.
J. Am. Chem. Soc. **128** (2006), 9996–9997.

[140] J.-S. Luo, Z.-Q. Wan, and C.-Y. Jia.
Chin. Chem. Lett. **27** (2016), 1304–1318.

[141] Z.-S. Huang, H. Meier, and D. Cao.
J. Mater. Chem. C **4** (2016), 2404–2426.

[142] I. J. Al-Busaidi, A. Haque, N. K. A. Rasbi, and M. S. Khan.
Synth. Met. **257** (2019), 116189.

[143] D. Devadiga, M. Selvakumar, P. Shetty, M. S. Santosh,
R. S. Chandrabose, and S. Karazhanov.
Int. J. Energy Res. **45** (2021), 6584–6643.

[144] S. N. Al-Ghamdi, H. A. Al-Ghamdi, R. M. El-Shishtawy, and A. M. Asiri.
Dyes Pigm. **194** (2021), 109638.

[145] Z. She, Y. Cheng, L. Zhang, X. Li, D. Wu, Q. Guo, J. Lan, R. Wang, and
J. You. *ACS Appl. Mater. Interfaces* **7** (2015), 27831–27837.

[146] N. V. Krishna, J. V. S. Krishna, S. P. Singh, L. Giribabu, L. Han,
I. Bedja, R. K. Gupta, and A. Islam.
J Phys. Chem. C **121** (2017), 6464–6477.

[147] W. Wang, X. Li, J. Lan, D. Wu, R. Wang, and J. You.
J. Org. Chem. **83** (2018), 8114–8126.

[148] C.-T. Li, Y.-L. Kuo, C. H. P. Kumar, P.-T. Huang, and J. T. Lin.
J. Mater. Chem. A **7** (2019), 23225–23233.

[149] C.-T. Li, F.-L. Wu, C.-J. Liang, K.-C. Ho, and J. T. Lin.
J. Mater. Chem. A **5** (2017), 7586–7594.

[150] X. Zhang, F. Gou, D. Zhao, J. Shi, H. Gao, Z. Zhu, and H. Jing.
J. Power Sources **324** (2016), 484–491.

[151] S. Wang, H. Wang, J. Guo, H. Tang, and J. Zhao.
Dyes Pigm. **109** (2014), 96–104.

[152] T. Hua, Z.-S. Huang, K. Cai, L. Wang, H. Tang, H. Meier, and D. Cao.
Electrochim. Acta **302** (2019), 225–233.

[153] X. Zhang, F. Gou, J. Shi, H. Gao, C. Xu, Z. Zhu, and H. Jing.
RSC Adv. **6** (2016), 106380–106386.

[154] A. F. Buene, M. Christensen, and B. H. Hoff. *Molecules* **24** (2019).

[155] H.-H. Gao, X. Qian, W.-Y. Chang, S.-S. Wang, Y.-Z. Zhu, and
J.-Y. Zheng. *J. Power Sources* **307** (2016), 866–874.

[156] S. S. Park, Y. S. Won, Y. C. Choi, and J. H. Kim.
Energy Fuels **23** (2009), 3732–3736.

[157] S. Yellappa, W. A. Webre, H. B. Gobeze, A. Middleton, C. B. KC, and
       F. D'Souza. *ChemPlusChem* **82** (2017), 896–903.

[158] Z. Iqbal, W.-Q. Wu, H. Zhang, L. Han, X. Fang, L. Wang, D.-B. Kuang,
       H. Meier, and D. Cao. *Org. Electron.* **14** (2013), 2662–2672.

[159] M. Mao, X. Zhang, L. Cao, Y. Tong, and G. Wu.
       Dyes Pigm. **117** (2015), 28–36.

[160] Y. S. Yang, H. D. Kim, J.-H. Ryu, K. K. Kim, S. S. Park, K.-S. Ahn, and
       J. H. Kim. *Synth. Met.* **161** (2011), 850–855.

[161] W.-I. Hung, Y.-Y. Liao, C.-Y. Hsu, H.-H. Chou, T.-H. Lee, W.-S. Kao,
       and J. T. Lin. *Chem. Asian J.* **9** (2014), 357–366.

[162] Y.-D. Lin, B.-Y. Ke, Y. J. Chang, P.-T. Chou, K.-L. Liau, C.-Y. Liu, and
       T. J. Chow. *J. Mater. Chem. A* **3** (2015), 16831–16842.

[163] A. N. Sobolev, V. K. Belsky, I. P. Romm, N. Y. Chernikova, and
       E. N. Guryanova. *Acta. Crystallogr. C* **41** (1985), 967–971.

[164] V. Merz and W. Weith. *Ber. Dtsch. Chem. Ges.* **6** (1873), 1511–1520.

[165] T. Kitamura, M. Ikeda, K. Shigaki, T. Inoue, N. A. Anderson, X. Ai,
       T. Lian, and S. Yanagida. *Chem. Mater.* **16** (2004), 1806–1812.

[166] D. P. Hagberg, X. Jiang, E. Gabrielsson, M. Linder, T. Marinado,
       T. Brinck, A. Hagfeldt, and L. Sun.
       J. Mater. Chem. **19** (2009), 7232–7238.

[167] A. Yella, R. Humphry-Baker, B. F. E. Curchod, N. A. Astani,
       J. Teuscher, L. E. Polander, S. Mathew, J.-E. Moser, I. Tavernelli,
       U. Rothlisberger, M. Grätzel, M. K. Nazeeruddin, and J. Frey.
       Chem. Mater. **25** (2013), 2733–2739.

[168] W. Zeng, Y. Cao, Y. Bai, Y. Wang, Y. Shi, M. Zhang, F. Wang, C. Pan,
       and P. Wang. *Chem. Mater.* **22** (2010), 1915–1925.

[169] M. Freitag, J. Teuscher, Y. Saygili, X. Zhang, F. Giordano, P. Liska,
       J. Hua, S. M. Zakeeruddin, J. E. Moser, M. Grätzel, and A. Hagfeldt.
       Nat. Photonics **11** (2017), 372–378.

[170] W. Zhang, Y. Wu, H. W. Bahng, Y. Cao, C. Yi, Y. Saygili, J. Luo,
       Y. Liu, L. Kavan, J. E. Moser, A. Hagfeldt, H. Tian, S. M. Zakeeruddin,
       W.-H. Zhu, and M. Grätzel. *Energy Environ. Sci.* **11** (2018), 1779–1787.

[171] Y. K. Eom, S. H. Kang, I. T. Choi, Y. Yoo, J. Kim, and H. K. Kim.
       J. Mater. Chem. A **5** (2017), 2297–2308.

[172] S. Mathew, A. Yella, P. Gao, R. Humphry-Baker, B. F. E. Curchod,
       N. Ashari-Astani, I. Tavernelli, U. Rothlisberger, M. K. Nazeeruddin, and
       M. Grätzel. *Nat. Chem.* **6** (2014), 242–247.

[173] A. Baumann, H. Cheema, M. A. Sabuj, L. E. McNamara, Y. Zhang, A. Peddapuram, S. T. Nguyen, D. L. Watkins, N. I. Hammer, N. Rai, and J. H. Delcamp. *Phys. Chem. Chem. Phys.* **20** (2018), 17859–17870.

[174] Z. Iqbal, W.-Q. Wu, D.-B. Kuang, L. Wang, H. Meier, and D. Cao. *Dyes Pigm.* **96** (2013), 722–731.

[175] R. Y.-Y. Lin, F.-L. Wu, C.-T. Li, P.-Y. Chen, K.-C. Ho, and J. T. Lin. *ChemSusChem* **8** (2015), 2503–2513.

[176] Z. Iqbal, W.-Q. Wu, Z.-S. Huang, L. Wang, D.-B. Kuang, H. Meier, and D. Cao. *Dyes Pigm.* **124** (2016), 63–71.

[177] H. Tian, E. Gabrielsson, P. W. Lohse, N. Vlachopoulos, L. Kloo, A. Hagfeldt, and L. Sun. *Energy Environ. Sci.* **5** (2012), 9752–9755.

[178] X. Zhang, J. Mao, D. Wang, X. Li, J. Yang, Z. Shen, W. Wu, J. Li, H. Ågren, and J. Hua. *ACS Appl. Mater. Interfaces* **7** (2015), 2760–2771.

[179] A. Baumann, J. Watson, and J. H. Delcamp. *ChemSusChem* **13** (2020), 283–286.

[180] A. F. Buene, D. M. Almenningen, A. Hagfeldt, O. R. Gautun, and B. H. Hoff. *Sol. RRL* **4** (2020), 1900569.

[181] X. Zhang, Y. Xu, F. Giordano, M. Schreier, N. Pellet, Y. Hu, C. Yi, N. Robertson, J. Hua, S. M. Zakeeruddin, H. Tian, and M. Grätzel. *J. Am. Chem. Soc.* **138** (2016), 10742–10745.

[182] W. Sharmoukh, J. Cong, J. Gao, P. Liu, Q. Daniel, and L. Kloo. *ACS Omega* **3** (2018), 3819–3829.

[183] H.-S. Chiou, P. C. Reeves, and E. R. Biehl. *J. Heterocycl. Chem.* **13** (1976), 77–82.

[184] M. C. Carreno, J. L. G. Ruano, G. Sanz, M. A. Toledo, and A. Urbano. *J. Org. Chem.* **60** (1995), 5328–5331.

[185] B. Andersh, D. L. Murphy, and R. J. Olson. *Synth. Commun.* **30** (2000), 2091–2098.

[186] Y. Goldberg and H. Alper. *J. Org. Chem.* **58** (1993), 3072–3075.

[187] B. Das, K. Venkateswarlu, A. Majhi, V. Siddaiah, and K. R. Reddy. *J. Mol. Catal. A Chem.* **267** (2007), 30–33.

[188] A. Vilsmeier and A. Haack. *Ber. Dtsch. Chem. Ges.* **60** (1927), 119–122.

[189] G. Jones and S. P. Stanforth. In: *Organic Reactions.* John Wiley Sons, Ltd, 2004. Chap. 1, 1–330.

[190] G. Seybold. *J. Prakt. Chem.* **338** (1996), 392–396.

[191] E. Knoevenagel. *Ber. Dtsch. Chem. Ges.* **29** (1896), 172–174.

[192] A. C. O. Hann and A. Lapworth. *J. Chem. Soc., Trans.* **85** (1904), 46–56.

[193] L. Kurti and B. Czakó. Elsevier, Strategic applications of named reactions in organic synthesis, 2005.

[194] R. Tanikaga, N. Konya, and A. Kaji. *Chem. Lett.* **14** (1985), 1583–1586.

[195] H. Cho, T. Iwashita, M. Hamaguchi, and Y. Oyama. *Chem. Pharm. Bull.* **39** (1991), 3341–3342.

[196] A. E. Maadi, C. L. Matthiesen, P. Ershadi, J. Baker, D. M. Herron, and E. M. Holt. *J. Chem. Crystallogr.* **33** (2003), 757–763.

[197] J. Hong, H. Lai, Y. Liu, C. Yuan, Y. Li, P. Liu, and Q. Fang. *RSC Adv.* **3** (2013), 1069–1072.

[198] N. Miyaura and A. Suzuki. *J. Chem. Soc., ChemComm* (1979), 866–867.

[199] N. C. Bruno, M. T. Tudge, and S. L. Buchwald. *Chem. Sci.* **4** (2013), 916–920.

[200] A. F. Littke and G. C. Fu. *Angew. Chem. Int. Ed.* **37** (1998), 3387–3388.

[201] J. P. Wolfe, R. A. Singer, B. H. Yang, and S. L. Buchwald. *J. Am. Chem. Soc.* **121** (1999), 9550–9561.

[202] M. R. Netherton, C. Dai, K. Neuschütz, and G. C. Fu. *J. Am. Chem. Soc.* **123** (2001), 10099–10100.

[203] J. H. Kirchhoff, C. Dai, and G. C. Fu. *Angew. Chem. Int. Ed.* **41** (2002), 1945–1947.

[204] A. Suzuki. *J. Organomet. Chem.* **576** (1999), 147–168.

[205] G. B. Smith, G. C. Dezeny, D. L. Hughes, A. O. King, and T. R. Verhoeven. *J. Org. Chem.* **59** (1994), 8151–8156.

[206] L. S. Hegedus and R. Macomber. University Science Books, 1994.

[207] C. Amatore, A. Jutand, and G. L. Duc. *Chem. Eur. J.* **17** (2011), 2492–2503.

[208] B. P. Carrow and J. F. Hartwig. *J. Am. Chem. Soc.* **133** (2011), 2116–2119.

[209] G. Mann, Q. Shelby, A. H. Roy, and J. F. Hartwig. *Organometallics* **22** (2003), 2775–2789.

[210] S. D. Walker, T. E. Barder, J. R. Martinelli, and S. L. Buchwald. *Angew. Chem. Int. Ed.* **43** (2004), 1871–1876.

[211] K. Billingsley and S. L. Buchwald. *J. Am. Chem. Soc.* **129** (2007), 3358–3366.

[212] M. S. Driver and J. F. Hartwig. *J. Am. Chem. Soc.* **118** (1996), 7217–7218.

[213] M. R. Biscoe, B. P. Fors, and S. L. Buchwald. *J. Am. Chem. Soc.* **130** (2008), 6686–6687.

[214] T. Kinzel, Y. Zhang, and S. L. Buchwald.
J. Am. Chem. Soc. **132** (2010), 14073–14075.

[215] N. C. Bruno, N. Niljianskul, and S. L. Buchwald.
J. Org. Chem. **79** (2014), 4161–4166.

[216] R. Martin and S. L. Buchwald. *Acc. Chem. Res.* **41** (2008), 1461–1473.

[217] D. Blakemore. Chapter 1 Suzuki–Miyaura Coupling, The Royal Society of
Chemistry, 2016, 1–69.

[218] Z. Ahmadi and J. S. McIndoe. *ChemComm* **49** (2013), 11488–11490.

[219] C. Adamo, C. Amatore, I. Ciofini, A. Jutand, and H. Lakmini.
J. Am. Chem. Soc. **128** (2006), 6829–6836.

[220] P. A. Cox, A. G. Leach, A. D. Campbell, and G. C. Lloyd-Jones.
J. Am. Chem. Soc. **138** (2016), 9145–9157.

[221] T. Ishiyama, M. Murata, and N. Miyaura.
J. Org. Chem. **60** (1995), 7508–7510.

[222] K. L. Billingsley, T. E. Barder, and S. L. Buchwald.
Angew. Chem. Int. Ed. **46** (2007), 5359–5363.

[223] K. L. Billingsley and S. L. Buchwald.
J. Org. Chem. **73** (2008), 5589–5591.

[224] G. A. Molander, S. L. J. Trice, and S. D. Dreher.
J. Am. Chem. Soc. **132** (2010), 17701–17703.

[225] G. A. Molander, S. L. J. Trice, S. M. Kennedy, S. D. Dreher, and
M. T. Tudge. *J. Am. Chem. Soc.* **134** (2012), 11667–11673.

[226] T. Ishiyama, J. Takagi, Y. Yonekawa, J. F. Hartwig, and N. Miyaura.
Adv. Synth. Catal. **345** (2003), 1103–1106.

[227] M. A. Larsen and J. F. Hartwig.
J. Am. Chem. Soc. **136** (2014), 4287–4299.

[228] M. Murata, T. Oyama, S. Watanabe, and Y. Masuda.
J. Org. Chem. **65** (2000), 164–168.

[229] K. C. Lam, T. B. Marder, and Z. Lin.
Organometallics **29** (2010), 1849–1857.

[230] K. Kunz, U. Scholz, and D. Ganzer. *Synlett* **2003** (2003), 2428–2439.

[231] J. Lindley. *Tetrahedron* **40** (1984), 1433–1456.

[232] J. F. Hartwig. *Angew. Chem. Int. Ed.* **37** (1998), 2046–2067.

[233] A. S. Guram, R. A. Rennels, and S. L. Buchwald.
Angew. Chem. Int. Ed. **34** (1995), 1348–1350.

[234] J. Louie and J. F. Hartwig. *Tetrahedron Lett.* **36** (1995), 3609–3612.

[235] J. Yin and S. L. Buchwald. *J. Am. Chem. Soc.* **124** (2002), 6043–6048.

[236] K. W. Anderson, R. E. Tundel, T. Ikawa, R. A. Altman, and S. L. Buchwald. *Angew. Chem. Int. Ed.* **45** (2006), 6523–6527.

[237] S. Shekhar, P. Ryberg, J. F. Hartwig, J. S. Mathew, D. G. Blackmond, E. R. Strieter, and S. L. Buchwald. *J. Am. Chem. Soc.* **128** (2006), 3584–3591.

[238] K. Hara, Z.-S. Wang, T. Sato, A. Furube, R. Katoh, H. Sugihara, Y. Dan-oh, C. Kasada, A. Shinpo, and S. Suga. *J Phys. Chem. B* **109** (2005), 15476–15482.

[239] H. N. Tsao, C. Yi, T. Moehl, J.-H. Yum, S. M. Zakeeruddin, M. K. Nazeeruddin, and M. Grätzel. *ChemSusChem* **4** (2011), 591–594.

[240] A. Kay and M. Graetzel. *J. Phys. Chem.* **97** (1993), 6272–6277.

[241] R. C. Fort and P. von R Schleyer. *Chem. Rev.* **64** (1964), 277–300.

[242] L. Wanka, K. Iqbal, and P. R. Schreiner. *Chem. Rev.* **113** (2013), 3516–3604.

[243] F. Kato, A. Kikuchi, T. Okuyama, K. Oyaizu, and H. Nishide. *Angew. Chem. Int. Ed.* **51** (2012), 10177–10180.

[244] N. Flores-Díaz, H.-w. Bahng, N. Vlachopoulos, J. E. Moser, S. M. Zakeeruddin, M. Grätzel, and A. Hagfeldt. *J. Mater. Chem. A* **7** (2019), 10998–11006.

[245] K. Lim, M. J. Ju, J. Song, I. T. Choi, K. Do, H. Choi, K. Song, H. K. Kim, and J. Ko. *ChemSusChem* **6** (2013), 1425–1431.

[246] P. Salvatori, G. Marotta, A. Cinti, C. Anselmi, E. Mosconi, and F. D. Angelis. *J Phys. Chem. C* **117** (2013), 3874–3887.

[247] A. Bejan, S. Shova, M.-D. Damaceanu, B. C. Simionescu, and L. Marin. *Cryst. Growth Des.* **16** (2016), 3716–3730.

[248] A. Wakamiya, H. Nishimura, T. Fukushima, F. Suzuki, A. Saeki, S. Seki, I. Osaka, T. Sasamori, M. Murata, Y. Murata, and H. Kaji. *Angew. Chem. Int. Ed.* **53** (2014), 5800–5804.

[249] H. Nishimura, Y. Hasegawa, A. Wakamiya, and Y. Murata. *Chem. Lett.* **46** (2017), 817–820.

[250] M. A. Truong, J. Lee, T. Nakamura, J.-Y. Seo, M. Jung, M. Ozaki, A. Shimazaki, N. Shioya, T. Hasegawa, Y. Murata, S. M. Zakeeruddin, M. Grätzel, R. Murdey, and A. Wakamiya. *Chem. Eur. J.* **25** (2019), 6741–6752.

[251] Q. Li, C. Shi, X. Zhang, P. Tao, Q. Zhao, and A. Yuan. *Eur. J. Inorg. Chem* **2019** (2019), 1343–1348.

[252] Q. Li, X. Zhang, Y. Cao, C. Shi, P. Tao, Q. Zhao, and A. Yuan.
       Dalton Trans. **48** (2019), 4596–4601.

[253] K. Okino, D. Sakamaki, and S. Seki. *ACS Mater. Lett.* **1** (2019), 25–29.

Papers

Paper I

D. M. Almenningen, H. E. Hansen, M. F. Vold, A. F. Buene, V. Venkatraman, S. Sunde, B. H. Hoff and O. R. Gautun

Effect of thiophene-based π-spacers on N-arylphenothiazine dyes for dye-sensitized solar cells,

Paper I

Effect of thiophene-based π-spacers on *N*-arylphenothiazine dyes for dye-sensitized solar cells

David Moe Almenningen [a], Henrik Erring Hansen [b], Martin Furru Vold [a], Audun Formo Buene [a], Vishwesh Venkatraman [a], Svein Sunde [b], Bård Helge Hoff [a], Odd Reidar Gautun [a],*

[a] *Department of Chemistry, Norwegian University of Science and Technology, Høgskoleringen 5, NO-7491, Trondheim, Norway*
[b] *Department of Materials Science and Engineering, Norwegian University of Science and Technology, Sem Sælands Vei 12, NO-7491, Trondheim, Norway*

ARTICLE INFO

ABSTRACT

To study the effect of π-spacers on dye performance in DSSC, five novel phenothiazine dyes have been prepared where the number of successive thiophenes in the π-spacer was increased from zero to four. Additionally, a dye bearing thieno[3,2-*b*]thiophene was synthesized, and compared to its unfused bithiophene analogue. When the number of thiophenes were two or more the light absorption properties was significantly better in the region 400–550 nm compared to the dye without a π-spacer. DSSC device testing revealed that the reference dye without a π-spacer gave the best overall performance producing a power conversion efficiency of 5.7% (J_{SC} = 10.1 mA cm^{-2}, V_{OC} = 0.83 V, FF = 0.68), attributed to the superior V_{OC} of this dye. The incorporation of one and two thiophenes resulted in a similar performance as the reference, while incorporation of larger oligothiophenes proved to be deleterious to DSSC-performance. Electrochemical impedance spectroscopy indicates that the voltage drops and performance loss associated with these dyes are due to more facile recombination.

1. Introduction

The nascence of dye-sensitized solar cells (DSSC), brought on by O'Regan and Grätzel in 1991, established a novel photovoltaic technology with unique and promising properties [1]. Traits such as their transparency make DSSC interesting for building integrated photovoltaics (BIPV) [2], they can be made using flexible materials allowing them to be integrated on cloth and wearable devices [3], and their power conversion efficiency under low-light conditions exceed that of the established GaAs solar cells proving their viability for low-power applications [4]. Moreover, Hardin et al. estimate that a competitive price of US$0.20–0.30 W^{-1} can be achieved [5], which is an additional driving force for continued research in this field.

Fully organic dyes for DSSC vary greatly in chemical structure, but most of them adopt some variety of a D-π-A structural motif. Such molecules are constituted of an electron rich donor (D), a π-conjugated linker (π), and an electron acceptor (A) [6]. This architecture facilitates a charge separation upon excitation where electron density is moved from the donor part to the acceptor. Through molecular engineering of the dye structure it is possible to customize the properties of the chromophore. It has been shown that increasing the electron donor properties

raise the energy level of the highest occupied molecular orbital (HOMO), and red-shift the absorption maxima [7–9]. Likewise, it has been shown that stronger electron acceptors also red-shift the UV/Vis adsorption [10], as this will also ensure an efficient internal charge transfer (ICT). For a thorough review of property tuning in D-π-A molecules the reader is referred to the comprehensive paper by Bureš on the topic [11].

The research on new dyes for DSSC has led to an enormous amount of papers on optimizing the different parts of the D-π-A molecule. The only part that is seemingly optimized is the acceptor side, where cyano-acrylic acid is by far the most widely used anchoring group due to its strong electron withdrawing properties as well as the acidic group that binds the dye to TiO$_2$ [12]. There is no clear consensus on the donor. However, triphenylamine-derivatives have displayed good photovoltaic properties in numerous reports [4,13,14]. With regards to the π-linker a number of promising and different candidates have been synthesized and assessed [15–18]. A DSSC co-sensitized by two fully organic dyes (ADEKA-1 and LEG4 see Fig. 1) offer the highest achieved PCE so far at 14.3% [19]. Both of these record dyes are equipped with a thiophene-based linker. Incorporation of thiophene has proven to be useful in broadening the spectral response of chromophores compared to the reference dyes without π-linkers [20,21]. Expanding from thiophene

---

to oligothiophenes further broadens the spectral response as revealed by studies of different donors like coumarin [22], phenothiazine [23], benzo[a]carbazole [24], and triphenylamine [25,26].

A downside of this strategy is the observed drop in photovoltage [22, 26]. Two explanations has been offered for this phenomenon, (i) the electrostatic and charge transfer effect of longer oligothiophenes downshift the conduction band of TiO_2 [27] (ii) the sulfur atom of thiophene and iodine components in the electrolyte interact and form dye-iodine complexes [28]. Ronca et al. performed a theoretical study on a set of known sensitizers [27]. They discovered that significant charge-rearrangement occurred at the dye-titania interface, and demonstrated that longer π-linkers were associated with less efficient charge transfer, leading to a downshift of the conduction band of TiO_2 and a subsequent drop in V_{OC}. This is supported by the work of Rühle et al. who demonstrated that the dipole moment of molecules adsorbed onto TiO_2 had a profound impact on V_{OC} [29]. They found that molecules with a dipole moment pointing away from the TiO_2 surface lowered the energy of the conduction band, decreasing the difference between E_{CB} and E_{redox}. Furthermore the sulfur-iodine interaction theory is supported by the work of Zhang et al., which showed that longer oligothiophenes had a higher probability of forming dye-iodine complexes [28]. Such a phenomenon would accumulate electrolyte species near the titania surface, facilitating recombination at the TiO_2-electrolyte interface. This probably explains why longer oligothiophenes demonstrate higher photovoltages than shorter ones in cobalt-based electrolyte systems, as opposed to the traditional iodine electrolyte [28,30].

Thiophene-derivatives have demonstrated their suitability as π-linkers in organic dyes for DSSC. The most striking example is the co-sensitization of **LEG4** and **ADEKA-1** which led to the current PCE-record for DSSCs, at 14.3% [19], see Fig. 1. The series **T1-T4**, presented by Liu and coworkers, showed that the PCE-values could be improved through

increasing the size of the oligothiophene π-spacer [26]. Our previous work on π-linkers revealed only marginal performance increase using a furan spacer (**AFB-11** in Fig. 1), while the other spacers in the study (**AFB-3,-5,-7**, and **-9**), including thiophene, showed lower efficiency than the reference dye without a π-linker [20]. In view of these conflicting results, we wished to investigate whether longer oligothiophenes can generate sufficiently high photocurrents to offset the associated loss of photovoltage. We have based our comparison on the series of six novel dyes, as shown in Fig. 1. These include one reference dye (**DMA-0**) without any π-spacer. Four dyes (**DMA-1 – DMA-4**) where the π-linker is increased from one to four consecutive 2,5-linked thiophenes. (The dyes **DMA-0 – DMA-4** are named after the number of thiophenes in the π-spacer). Additionally, one dye was synthesized (**DMA-5**) with a rigidified thieno[3,2-*b*]thiophene and also tested.

2. Results and discussion

2.1. Dye synthesis

The dyes in the series all bear the same phenothiazine donor. The hexyloxyphenyl moiety was chosen as the amine substituent to reduce aggregation of the dyes, as this group has been used successfully in previously reported phenothiazine dyes [32,33]. The auxiliary donor chosen for this study was 2,4-dipropoxyphenyl, which was easily introduced by its commercially available boronic acid. The analogous 2, 4-dibutoxyphenyl moiety has proven to be an effective auxiliary donor for triphenylamine dyes [15,34].

The synthesis of the reference dye **DMA-0** was performed through the route shown in Scheme 1. The starting material **1** was prepared according to literary procedures [35,36]. The following two steps of the synthesis were also carried out through a previously reported procedure [37], giving the building block **3** in 53% yield over two steps. The
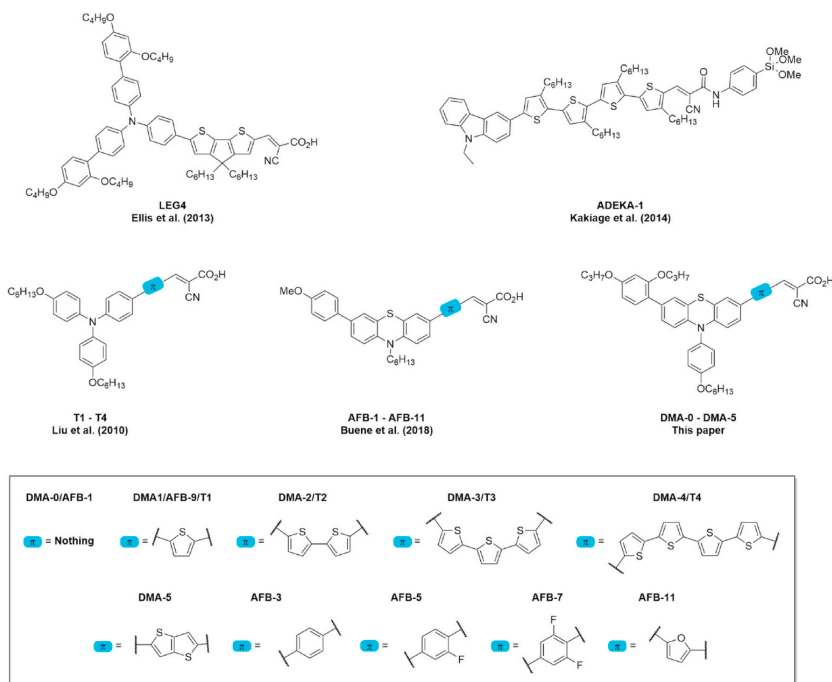
Fig. 1. An assortment of previously synthesized dyes, and the novel dyes presented herein. The dye **LEG4** [15] and **ADEKA-1** [31] are examples of successful dyes employing thiophene-derivatives in the π-spacer. The series **T1-T4** [26] are furnished with increasingly sized oligothiophenes. The π-spacer of **AFB-1 – AFB-11** is varied from nothing to six-membered aromatics to five-membered heteroaromatics.
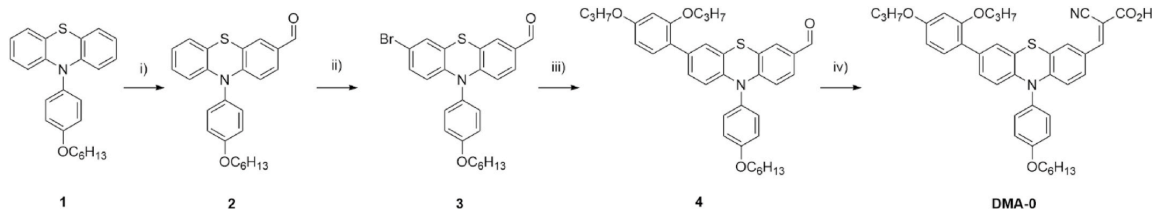
Scheme 1. Synthesis route for the reference dye **DMA-0**. i) POCl$_3$, DMF, ii) NBS, iii) Pd(OAc)$_2$, SPhos, K$_3$PO$_4$, (2,4-dipropoxyphenyl)boronic acid, iv) cyanoacetic acid, piperidine.

brominated phenothiazine was then functionalized with an auxiliary donor through a Suzuki-Miyaura reaction. Following the Knoevenagel condensation procedure reported by Iqbal et al. [21] the cyano-acrylic acid anchor was installed, producing the dye **DMA-0** in a satisfactory yield of 88%.

A selective mono-bromination of **1** using NBS (Scheme 2), allowed for the installment of the 2,4-dipropoxyphenyl auxiliary donor in a subsequent Suzuki-Miyaura cross-coupling. A three-step procedure from **6** to the aldehydes **7–11** was utilized. The first step was a bromination, then a borylation using a procedure described by Billingsley and Buchwald [38] produced the pinacol boronate ester. This was used further in a Suzuki-Miyaura cross-coupling with brominated thiophene carbaldehydes to yield the dye-precursors **7–11** in yields of ~20–40% over three steps. The aforementioned Knoevenagel procedure was employed once more to yield the target dyes **DMA-1 - DMA-5** in yields of 64–97%. The specific synthetic procedures are found in the ESI.

2.2. Photophysical properties

The spectral response of the dyes was studied in solution (DCM, 2 × 10^{-5} M, Fig. 2), and while adsorbed onto TiO$_2$ films (Fig. 3). The data from these experiments are summarized in Table 1. Surprisingly, the reference dye **DMA-0**, without any π-spacer, displayed the second-most redshifted absorption maxima of the dyes in solution (Fig. 2), albeit at the lowest molar extinction coefficient. A blueshift of the absorption maximum by 42 nm, was observed when introducing a thiophene π-linker in **DMA-1**. A similar, although much smaller, hypsochromic shift has been observed in our previous work, where a 4 nm reduction was observed [20].

When comparing the absorption maxima of the dyes in solution

versus the dyes loaded on TiO$_2$-films, a 20–50 nm blueshift was seen for all the dyes. This could be caused by unfavorable dye-aggregation when the dyes were bound to titania [39], as no co-adsorbent CDCA was used for these measurements. Additionally, deprotonation of the dyes also causes blueshift of absorption [40], as shown in Fig. 4. For the reference dye **DMA-0**, the absorption spectrum of the carboxylate is in good accordance with the spectra from the TiO$_2$ film. For **DMA-4** a negligible shift of absorption maximum is seen in the spectrum of the carboxylate. This suggest that there are two different causes for the blueshift seen on TiO$_2$-films for these two dyes. The blueshift of **DMA-0** is largely attributed to deprotonation, meanwhile aggregation is responsible for the blueshift of **DMA-4**. For the remaining dyes in the series there seem to be a combination of these effects causing the blueshifts seen on the TiO$_2$ films. As shown in ESI Fig. S1, deprotonation of the dyes blueshift the dyes, but not to the same extent as seen when sensitized on TiO$_2$.

Extending the π-linker beyond one thiophene-unit redshifted the adsorption maxima for all the dyes in this series. For **DMA-2** a 48 nm redshift was seen (Fig. 2). A distinctly higher absorption in the region 400–550 nm was seen for the dyes bearing two or more thiophenes. A similar trend was seen when we investigated the absorption properties in THF, shown in ESI Fig. S2. As all the sensitizers bear the same donor- and acceptor-moieties, this effect is likely to be explained by the higher conjugation. For the dyes absorbed onto TiO$_2$ this effect was also present, where all the longer oligothiophene dyes displayed better adsorption properties than **DMA-1**. Care should be given with regards to these results, however, as small differences in film thickness as well as dye-loading will affect the absorption measurements.

The optical band gaps were estimated by the intersection of the absorption and normalized emission spectra. The reference dye, **DMA-0**, displayed the lowest band gap of the dyes synthesized, suggesting that
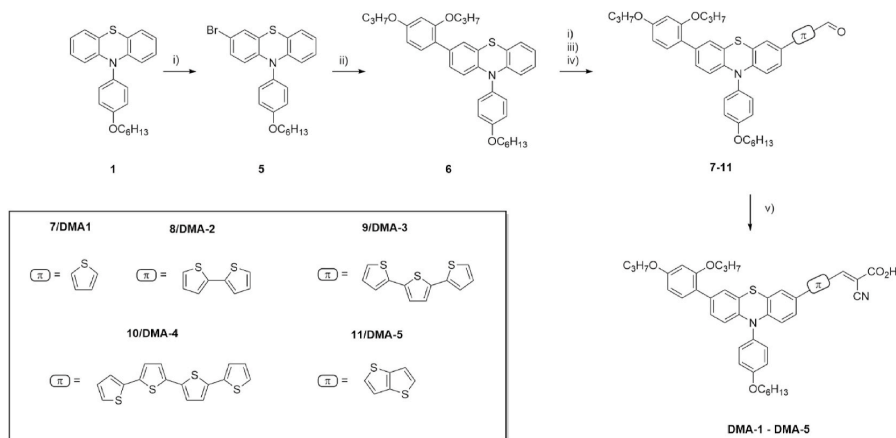
Scheme 2. Synthesis route for the thiophene-containing dyes **DMA-1 – DMA-5**. i) NBS, ii) Pd(OAc)$_2$, SPhos, K$_3$PO$_4$, (2,4-dipropoxyphenyl)boronic acid, iii) PdCl$_2$(CH$_3$CN)$_2$, SPhos, Et$_3$N, pinacol borane, iv) Pd(OAc)$_2$, SPhos, K$_3$PO$_4$, bromo-(thiophene)$_n$ carbaldehyde v) cyanoacetic acid, piperidine.
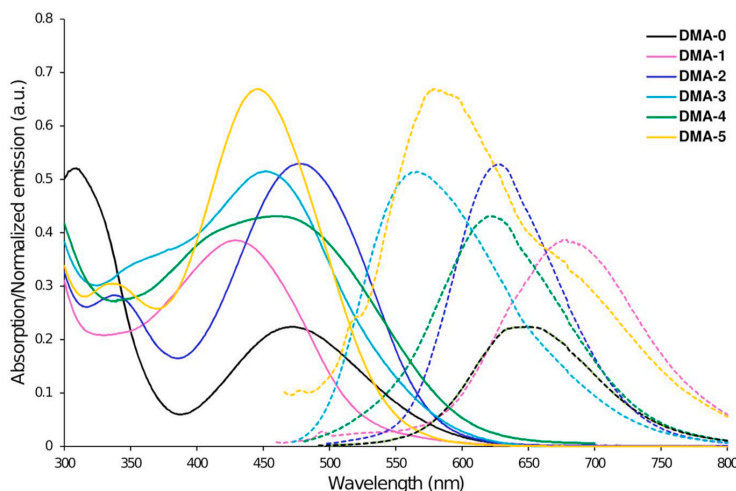
Fig. 2. Absorption and normalized emission spectra of all dyes in DCM solution.
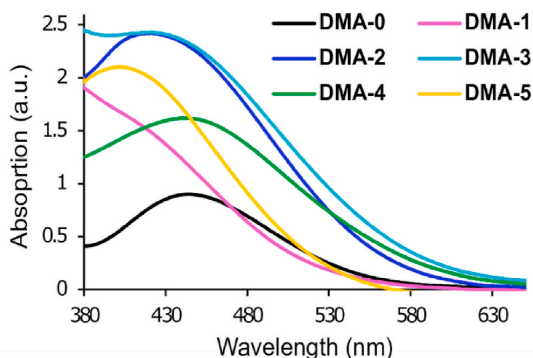
Fig. 3. UV/vis measurements of all dyes on TiO$_2$ films (2.5 μm, 18NR-T, Greatcell Solar).

incorporation of theses π-linkers are negatively affecting the ICT-process of the sensitizers. It is also noteworthy that the terthiophene linker of **DMA-3** increased the band gap significantly, while the band gap of the even larger quaterthiophene-bearing dye, **DMA-4,** was only moderately increased compared to the reference.

2.3. Electrochemical properties

An examination of the frontier orbital energies of **DMA-0** – **DMA-5** was carried out through cyclic voltammetry experiments. The working electrode was a stained TiO$_2$ electrode on FTO, and the counter electrode was a graphite carbon rod. A Ag/AgCl reference electrode was employed with supporting electrolyte 0.1 M LiTFSI in acetonitrile. The oxidation potential of all the dyes was measured vs F$_c^+$/F$_c$, and converted to vs. SHE by 0.624 V as reported by Pavlishchuk and Addison [41]. The recorded CVs are shown in ESI Fig. S3.

The deepest HOMO-level was seen for the reference dye **DMA-0** at 1.04 V vs. SHE (Fig. 5). Introduction of a thiophene π-spacer in dye **DMA-1** elevated the HOMO by 110 mV. This is consistent with previously reported phenothiazine dyes where even a 210 mV increase has been observed [42,43]. Similar HOMO-levels of the dyes was expected for a series of dyes bearing the same donor moiety, while the

Table 1
Photophysical and electrochemical properties of dyes in the series.

Dye	λ_{abs}[a] (nm)	ε (M^{-1}cm^{-1})	Em.[b] (nm)	λ_{abs}[c] on TiO$_2$ (nm)	E$_{0-0}$[d] (eV)	E$_{ox}$[e] (V vs SHE)	E$_{LUMO}$[f] (V)
DMA-0	472	11200	647	444	2.14	1.04	−1.10
DMA-1	430	19300	684	379	2.23	0.93	−1.30
DMA-2	478	26300	632	421	2.18	0.95	−1.23
DMA-3	452	25750	569	419	2.38	0.96	−1.42
DMA-4	461	21550	625	441	2.21	0.92	−1.29
DMA-5	446	33450	587	402	2.40	0.92	−1.48

[a] Maximum of most red-shifted peak.
[b] Emission when ICT band is excited, in DCM solution.
[c] Maximum of most red-shifted peak on TiO$_2$ (2.5 μm, GreatcellSolar 18NR-T).
[d] Calculated from the intersection of the absorption and normalized emission spectra.
[e] Measured vs. F$_c^+$/F$_c$ on stained TiO$_2$ electrodes in acetonitrile with 0.1 M LiTFSI, converted to V vs. SHE by 0.624 V. Scan rate 10 mV s^{-1}.
[f] Calculated from E$_{ox}$-E$_{0-0}$.

LUMO-levels of the dyes varied a lot with the different π-spacers.

The dyes synthesized in this study all displayed sufficiently deep HOMO-levels to be regenerated by the classic iodine redox shuttle. Unfortunately, only one of the dyes reported herein (**DMA-0**) had a sufficiently deep HOMO-level to be comfortably regenerated by the desirable Cu-electrolytes with redox potentials around 0.90 V vs SHE [44].

2.4. Theoretical calculations

Time-dependent density functional theory calculations (TD-DFT) was used to elucidate the electronic properties of the dyes reported herein. Calculations were performed using Gaussian 09 at the CAM-B3LYP/6-31G(d,p) level of theory [45]. The electron distribution of HOMO and LUMO for the two extremes (**DMA-0** and **DMA-4**) is shown in Fig. 6, the remaining dyes are shown in ESI Fig. S4. It was found that
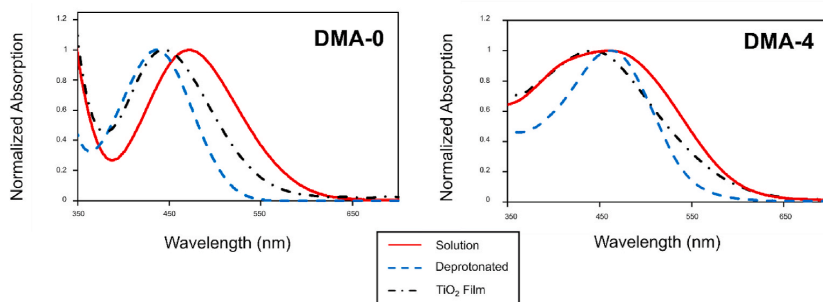
Fig. 4. UV/vis measurements of **DMA-0** and **DMA-4** in solution (DCM), deprotonated in solution, and sensitized on TiO$_2$ films. Deprotonation was carried out by adding a drop of triethylamine to the cuvette.
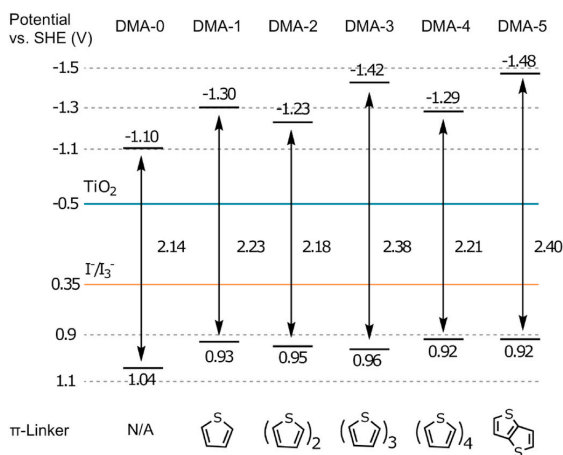
Fig. 5. Energy levels of the frontier orbitals for the sensitizers in this study.

the HOMO is largely located on the phenothiazine-core and the adjacent thiophene-unit for **DMA-1** – **DMA-4**. The LUMOs are found over the cyanoacrylic acid and the thiophenes close to the acceptor. This shows that excitation of the dye molecules moves the electron densities from phenothiazine to the acceptor moiety. This separation of electrons is associated with efficient injection of electron from the acceptor part of the dye to titania.

2.5. Photovoltaic properties

The photovoltaic performance of the dyes was characterized by fabricating three parallel DSSC-devices sensitized with each of the dyes, in addition a **N719** standard for reference. The results are presented in Table 2. The *J-V* curves of the fabricated DSSCs were measured under 1 sun AM 1.5 G illumination, and the best performing parallel was subjected to IPCE-measurements (Fig. 7 and Fig. 8). Integration of the IPCE-spectra over the 1 sun AM 1.5 G spectrum produced theoretical current densities within 20% of what was measured experimentally for all the sensitizers except **DMA-5**. This dye fell narrowly outside the criterion of reasonable correlation proposed by Christians et al. for the field of perovskite solar cells [46].

As also seen in our previous study on the effect of π-linkers on phenothiazine dyes, the reference dye without any spacers performed surprisingly well [20]. In this study **DMA-0** achieved the highest PCE largely owing to its excellent photovoltage with the I$^-$/I$_3^-$ redox electrolyte. An expected photocurrent increase was seen for the iterative

expansion of the oligothiophene moiety in **DMA-1** – **DMA-3**, ultimately achieving a J_{SC} of 11.01 mA/cm^2. To the authors surprise **DMA-4** did not produce a further increase in photocurrent, instead a significant drop in photovoltaic performance was observed. In a similar study, conducted by Liu et al., a series of dyes with a triphenylamine donor produced an ever increasing J_{SC} by increasing the number of thiophenes in the π-linker [26]. However, an increasingly sized aromatic system is more prone to detrimental aggregation effects, which could explain the lackluster J_{SC} of the quaterthiophene dye.

The voltage drops displayed by the thiophene-bearing sensitizers is seen in many studies concerning fully organic dyes for DSSC [26]. A 60 mV decrease of V_{OC} came as a result of inserting a thiophene π-spacer in **DMA-1** compared to the reference dye. Negligible change was seen when comparing the bithiophene to the single thiophene. However, when we installed a third thiophene another 70 mV drop was observed. As expected, the largest oligothiophene, **DMA-4**, produced the lowest photovoltage at 630 mV. This clearly demonstrate the unfortunate side-effect of elongating oligothiophene π-linkers for organic dyes in DSSCs, as a tremendous 200 mV difference between **DMA-4** and the reference dye was seen.

The obtained IPCE-spectra showed the highest maximum for **DMA-0** (Fig. 8). This is in accordance with one of our previous studies where the highest maximum was obtained for a similar reference dye [20]. As expected, the widest action spectra were found for the longest oligothiophenes **DMA-3** and **DMA-4**. The intensity of the spectra was widely different however, where the maximum of the latter was found at 53% down from 77%. The rigidified bithiophene dye (**DMA-5**) also demonstrated an interesting action spectrum, it was considerably more narrow than the unmodified counterpart **DMA-2**. This shows that rigidifying the π-linker does not necessarily yield an improved light-harvesting ability of the dyes.

The dye loading experiment was carried out through desorption of dyes attached to a TiO$_2$-electrode, by immersing the electrode in 40 mM tetrabutylammonium hydroxide (TBA(OH)) in THF. The results shown in Table 2 are averages of two separately desorbed electrodes. The homologous series of **DMA-0** – **DMA-4** displayed a higher loading with increasing molecular size. The amount of dye bearing no linker (**DMA-0**) was approximately a third of the quaterthiophene dye (**DMA-4**). This trend is consistent with our findings from one of our previous studies on phenothiazine sensitizers, where incorporation of a furan linker doubled the dye loading compared to the reference without a π-spacer [47]. The reason for this could be that the dyes with π-spacers are able to compete more favorably with the co-adsorbent CDCA for the absorption sites. The large dyes are also more prone to aggregate, which could also be a significant factor that increase the dye loading of the larger dyes.

DMA-0 **DMA-4**

LUMO

HOMO
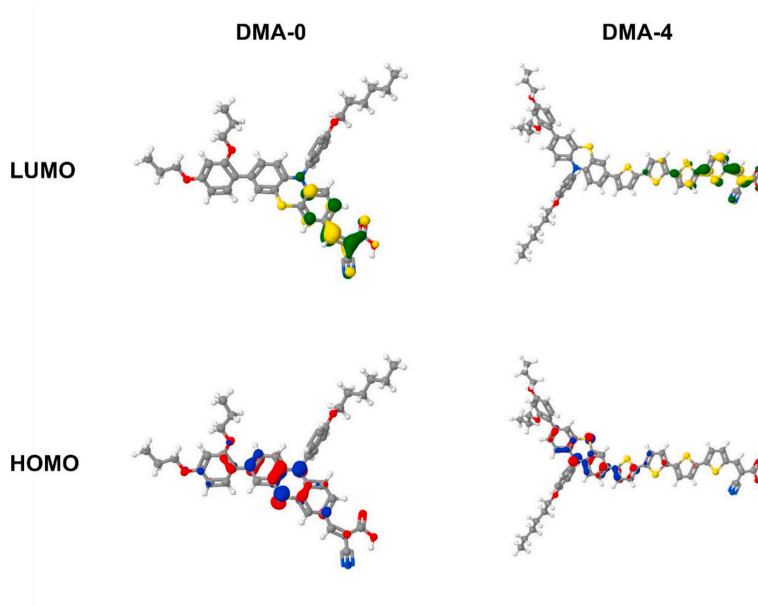
Fig. 6. The frontier orbitals of **DMA-0** and **DMA-4** calculated at the CAM-B3LYP/6-31G(d,p) level.

Table 2

Photovoltaic performance of all dyes under 1 sun AM 1.5G illumination, and from IPCE measurements. Results from dye loading experiments is also included.

Dye	IPCE J_{SC} (mA cm^{-2})[a]	J_{SC} (mA cm^{-2})	V_{OC} (V)	FF	PCE (%)	Dye Loading (10^8 mol cm^{-2})[b]
DMA-0	8.98	10.1 ± 0.2	0.83 ± 0.01	0.68	5.7 ± 0.2	8.3 ± 0.6
DMA-1	9.75	10.6 ± 0.2	0.77 ± 0.01	0.69	5.6 ± 0.2	10.1 ± 0.2
DMA-2	9.58	10.9 ± 0.1	0.772 ± 0.002	0.67 ± 0.01	5.6 ± 0.1	22.7 ± 0.9
DMA-3	10.90	11.0 ± 0.1	0.70 ± 0.01	0.68 ± 0.01	5.2 ± 0.1	24.0 ± 0.4
DMA-4	6.91	7.3 ± 0.1[c]	0.628 ± 0.002[c]	0.68 ± 0.04[c]	3.1 ± 0.2[c]	28.1 ± 0.6
DMA-5	8.09	10.3 ± 0.1	0.74 ± 0.01	0.69 ± 0.01	5.3 ± 0.1	16.5 ± 0.3
N719[d]	14.0	13.2	0.70	0.66	6.1	–

[a] Obtained by integration of the IPCE spectrum over the 1 sun AM 1.5 G spectrum.

[b] Values averaged of two desorbed TiO$_2$-electrodes.

[c] Average values of two cells.

[d] Values from the best-performing device.

2.6. Electrochemical impedance spectroscopy

To investigate the phenomenon of the dropping V_{OC} upon expansion of the π-linker, the dyes **DMA-0 – DMA-4** were analyzed using electrochemical impedance spectroscopy under monochromatic light of 479 nm at different voltages. Impedance data were then used to fit an equivalent circuit (Fig. 9) using non-linear least square fitting with the initial choice of fitting parameters shown in ESI Table S1. The equivalent circuit consists of a transmission line model representing the nano-structured TiO$_2$ anode, an RC-circuit for the faradaic and non-faradaic processes at the cathode, a finite-diffusion Warburg element for the electrolyte diffusion, and a series resistance for the ohmic resistance.
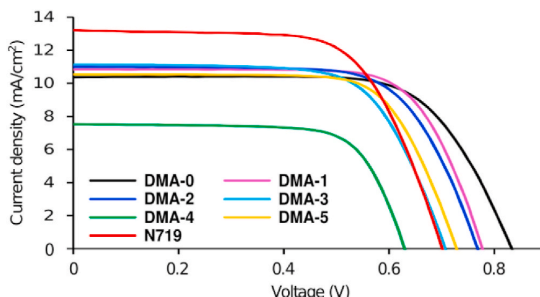
Fig. 7. J-V curves for the best parallel of each dye, obtained under 1 sun AM 1.5G illumination.
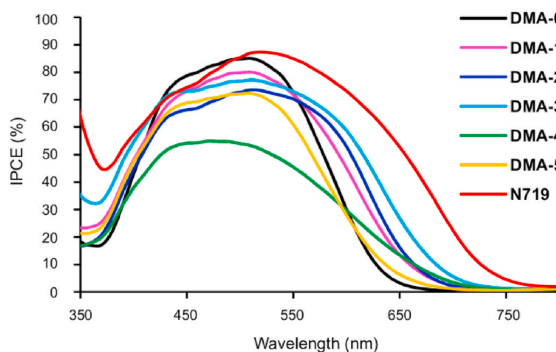
Fig. 8. IPCE spectra of the best performing parallel for each dye.
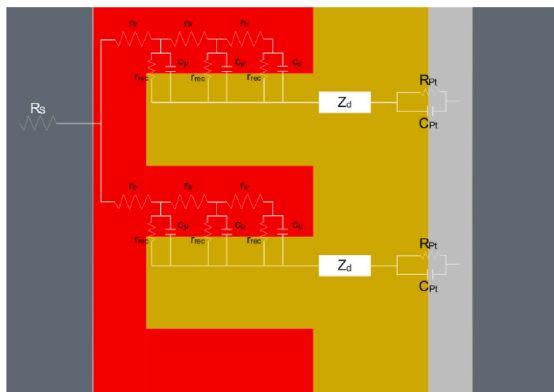
Fig. 9. The equivalent circuit of a dye-sensitized solar cell superimposed on a simple model of the cell itself. The circuit consists of an ohmic series resistance (R_s), a transmission line model with the associated transport resistances (r_{tr}) and recombination resistances (r_{rec}), a finite-diffusion Warburg element (Z_D), and an RC-circuit with a charge transfer resistance (R_{Pt}).

The complete analytical expression for this equivalent circuit is shown in Equation (1).

$$Z = R_s + \frac{R_{RC}}{1 + i\omega R_{RC} C_{RC}} + R_D \frac{\tanh\left[(i\omega/\omega_d)^{1/2}\right]}{(i\omega/\omega_d)^{1/2}}$$
$$+ \left(\frac{R_{tr}R_{rec}}{1 + i\omega/\omega_{rec}}\right)^{1/2} \coth\left[\left(\frac{R_{tr}}{R_{rec}}\right)^{1/2}(1 + i\omega/\omega_{rec})^{1/2}\right] \quad (1)$$

where R_S is the series resistance, R_{RC} and C_{RC} are the resistance and capacitance associated with the RC-circuit at the cathode, R_D is the resistance associated with electrolyte diffusion, R_{tr} is the transport resistance of charges in the semiconductor, and R_{rec} is the recombination resistance between the semiconductor and the electrolyte.

From the fitted impedance parameters, the recombination resistances of the dyes were extracted, and are shown as a function of applied voltage in (Fig. 10a). The results clearly show that the recombination resistance decreases with increasingly sized oligothiophene π-spacers. This might be explained by the higher number of sulfur atoms, causing a higher probability of sulfur-iodine interaction, which in turn promote recombination across the TiO₂-electrolyte interface. Alternatively, it could be caused by clustering/domain formation of aggregated rod-like dyes, giving the electrolyte access to the TiO₂. In any case, the increase in recombination is contributing to lowering the Fermi level of TiO₂, thus reducing the V_{OC} of the devices [48].

The impedance data obtained was also fitted to generate a *J-V* curve
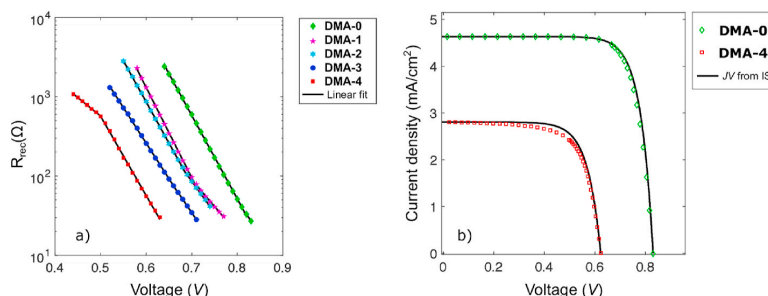
as explained by Fabregat-Santiago et al. [49] The fitted curves and the obtained J-V curves for **DMA-0** and **DMA-4** are shown in (Fig. 10b) and illustrates how **DMA-0** displayed a near perfect overlap, while discrepancies were present for **DMA-4**. This suggest that for **DMA-0** a normal DSSC-behavior was seen where the major resistance element is the recombination. The deviation seen for **DMA-4** is indicative of Gerischer behavior where transport resistance is larger than recombination resistance [50]. This further supports the claim that the voltage drops associated with large oligothiophene π-spacers are caused by a facilitation of recombination. The fitted curves and obtained J-V curves for the homologous series **DMA-0 – DMA-4** (ESI Fig. S6) showed overlapping curves for all dyes except **DMA-4**.

3. Conclusion

The effect of five different thiophene/oligothiophene π-spacers has been investigated and compared to the π-linker free analogue. The dye without π-linker produced the highest photovoltage, while the sensitizers containing mono- and bithiophene produced higher photocurrents without too detrimental voltage drops. Because of this, the PCE-values of **DMA-0 – DMA-2** were quite similar at 5.6–5.7%. The terthiophene dye (**DMA-3**) produced the highest photocurrent, alas the voltage drops associated with larger oligothiophenes led to a significant drop in PCE for this dye. Finally, the dye containing the quaterthiophene π-spacer produced the lowest efficiency out of the dyes tested. Further examination of the dye (**DMA-4**) using impedance measurements showed a Gerischer behavior of the device. In the author's opinion the opportunities that **DMA-3** presents has not yet been fully explored. For instance, modifying the π-spacer with steric functionalities could help preventing the electrolyte from reaching the TiO₂ surface. Such a modification should allow for the dye's promising charge generation to not be weighed down by poor photovoltages.

Overall, we conclude that incorporating thiophene, bithiophene or terthiophene in π-spacers of phenothiazine dyes for DSSC gives no added benefits in terms of PCE, while a significant drop in efficiency is seen for the quaterthiophene containing dye.

4. Experimental

4.1. Materials and reagents

All reactions were performed under inert N₂-atmosphere. The chemicals used were all purchased from Sigma-Aldrich, apart from 2,2':5′,2″-Terthiophene which was purchased from abcr GmbH. A full account of the synthetic procedures is given in the ESI.

4.2. Computational details

Initial 3D geometries of the molecules were generated using

Fig. 10. a) The recombination resistances of the dyes, obtained from EIS under monochromatic light, plotted against applied voltage. b) J-V curves obtained for **DMA-0** (◇) and **DMA-4** (□) under monochromatic light of 479 nm and J-V curves (−) recreated from impedance spectroscopy data.

OpenBabel [51] followed by a semiempirical PM6 Hamiltonian level optimization using MOPAC [52]. Further optimization in solvent (dichloromethane) was carried out using the B3LYP functional and the 6-31G(d,p) basis set. Solvent effects were considered using the using the conductor-like polarizable continuum model. Subsequently, time-dependent density functional theory (TD-DFT) calculations were performed at the CAM-B3LYP/6-31G(d,p) level of theory. The DFT computations were carried out using Gaussian 09 [45].

4.3. Analytical instruments

^{1}H and ^{13}C NMR was performed using either a BRUKER 400 MHz or 600 MHz magnet, the spectra obtained are calibrated against TMS (0 ppm) in CDCl$_3$ or against the residual solvent peak of DMSO-d_6 (2.50/39.52 ppm) or THF-d_8 (3.58/67.57 ppm). The IR-spectra are obtained using a BRUKER Alpha Eco-ATR FTIR spectrometer, the data is reported with wavenumber and according intensity of signal. Mass determination was performed by MS-analysis in positive ionization mode on a Synapt G2-S Q-TOF-instrument for Waters, the samples were ionized by an ASAP-probe (APCI) without prior chromatographic separation. UV–Vis spectroscopy was performed using a Hitachi U-1900 spectrometer, and photoluminescence characterization was carried out on an Edinburgh Instruments FS5-spectrofluorometer.

4.4. Fabrication of dye-sensitized solar cells

The anodes were prepared from FTO glass (NSG10, Nippon Sheet Glass), which was first cleaned in a Deconex 21-solution (2 g/L) under sonication for 45 min. Next the FTO was treated with UV/O$_3$ (Novascan PSD PRO-UV T6) for 15 min. Immersion of the glass in aqueous TiCl$_4$-solution (40 mM) at 70 °C for 2 × 45 min followed by rinsing with deionized water and ethanol was carried out to deposit a blocking layer on the FTO-sample. Pastes of TiO$_2$ were screen printed onto the FTO (mesh count 54, thread diameter 64 mm, area 0.2826 cm^2), first two active layers (18NR-T, Dyesol) were printed, with 5 min heating on a hotplate at 125 °C after each layer. A scattering layer (WER2-O, Dyesol) was ultimately printed, and the TiO$_2$ was sintered in a programmable furnace (Nabertherm LT 9/12) at set temperatures of 125, 250, 325, 450, and 500 °C for 5, 5, 5, 15, and 15 min with a ramping time of 10 min. Upon cooling to room temperature, the anodes were treated with aq. TiCl$_4$ as described earlier. Before staining the electrodes they were annealed at 500 °C for 30 min, using a hot air gun.

The counter electrodes were prepared from TEC10 FTO glass supplied by Sigma Aldrich. Holes were drilled into the electrodes from the FTO-side using a diamond drill bit, this procedure was carried out under water. The glass plates were then cleaned using Deconex 21 (aq., 2 g/L), deionized water, ethanol, and acetone, in an ultrasonic bath for 15 min for each. A solution of H$_2$PtCl$_6$ (10 mM in 2-propanol) was dropcast (5 μL/cm^2) on the FTO before heating at 400 °C for 15 min with a hot air gun formed the catalytic layer of Pt.

The photoanodes were placed in the dye bath while still holding ~80 °C from the annealing-procedure and stored at 30 °C for 15 h. The dye baths were prepared using a mixture of acetonitrile and THF (43/57, v/v) to make a solution of dye and co-adsorbent CDCA, at concentrations of 0.5 mM and 5 mM respectively. The staining of the reference **N719** was done similarly, but the solvent used was in this case ethanol. After the staining of the electrodes, they were rinsed in acetonitrile for 2 min, then sealed to the counter electrode using Surlyn (25 μm, Solaronix) in a drybox. A 4 × 20 s treatment of the cell using a 50 W PTC heat element was sufficient to seal the cells. The electrolyte was vacuum backfilled into the device, the filling-hole was sealed with Surlyn and a glass cover disk, then to complete the devices the exposed electrodes were painted with silver conducting paint (Electrolube, SCP). The electrolyte employed was the A6141 electrolyte, consisting of butylmethylimidazolium iodide (0.60 M), I$_2$ (0.03 M), guanidinium thiocyanate (0.1 M), and *t*-butylpyridine (0.50 M) dissolved in acetonitrile/valeronitrile (85/15, v/v) [53].

The devices used in the impedance measurements were prepared in a similar manner, the only differences being that the FTO glass for the photoanodes were TEC10 from Sigma-Aldrich and the gasket employed was thicker (60 μm, Solaronix).

4.5. Device characterization

J-V curves were obtained under 1 sun illumination AM 1.5G illumination provided by a Sciencetech SP300B solar simulator, calibrated with a Newport Reference Cell (91150 V), connected to a Keithley 2450 SourceMeter. A mask with an active area of 0.238 cm^2 was used on all the *J-V* measurements. IPCE measurements were carried out using a halogen lamp (Ocean Optics HL-2000) and a monochromator (Spectral Products CM110) connected to the Keithley 2450. The devices and the reference photodiode (Thorlabs, FDS100-CAL) were covered with a mask with a size of 0.049 cm^2.

The electrochemical impedance properties were measured in a light-exclusion box containing a Zahner CIMPS QE/IPCE TLS03 tunable light source. The light source was connected to a Zahner XPOT potentiostat, the devices were connected to a Zahner IM6ex potentiostat, both potentiostats were controlled by the Thales software. EIS was performed both in dark conditions and under constant illumination at wavelength 479 nm with an intensity of 12.6 mW/cm^2. For both cases the voltage across the cells was oscillating with an amplitude of 10 mV over a 100 mHz–100 kHz frequency range. The measurements were distributed logarithmically over this range with 8 measurements per decade for frequencies higher than 66 Hz and 3 measurements per decade for frequencies lower than 66 Hz. The results above 66 Hz were also averaged over 20 measurements for every frequency while the results below 66 Hz were averaged over 2 measurements per frequency. The oscillating voltage across the DSSCs had an applied DC-bias during the measurements which was decreased by 10 mV between measurements starting at the open circuit voltage of the cells. All DSSCs were measured 20 times each, with the DC-bias voltage as the variable.

Credit authorship contribution statement

David Moe Almenningen: Investigation, Methodology, Conceptualization, Writing – Original Draft, Visualization. **Henrik Erring Hansen:** Investigation, Methodology, Writing – Review & Editing, Visualization. **Martin Furru Vold:** Investigation. **Audun Formo Buene:** Methodology, Writing – Review & Editing, Visualization. **Vishwesh Venkatraman**: Investigation, Visualization. **Svein Sunde:** Supervision, Writing – Review & Editing. **Bård Helge Hoff:** Supervision, Writing – Review & Editing. **Odd Reidar Gautun:** Supervision, Conceptualization, Writing – Review & Editing.

One additional author has been included for his help with DFT calculations (Dr Vishwesh Venkatraman).

Declaration of competing interest

The authors declare that they have no known competing financial interests or personal relationships that could have appeared to influence the work reported in this paper.

Acknowledgements

Appendix A. Supplementary data

Supplementary data to this article can be found online at https://doi.org/10.1016/j.dyepig.2020.108951.

References

[1] O'Regan B, Grätzel M. A low-cost, high-efficiency solar cell based on dye-sensitized colloidal TiO2 films. Nature 1991;353(6346):737–40.

[2] Snaith HJ, Schmidt-Mende L. Advances in liquid-electrolyte and solid-state dye-sensitized solar cells. Adv Mater 2007;19(20):3187–200.

[3] Yun MJ, Cha SI, Seo SH, Lee DY. Highly flexible dye-sensitized solar cells produced by sewing textile electrodes on cloth. Sci Rep 2014;4:5322.

[4] Cao Y, Liu Y, Zakeeruddin SM, Hagfeldt A, Grätzel M. Direct contact of selective charge extraction layers enables high-efficiency molecular photovoltaics. Joule 2018;2(6):1108–17.

[5] Hardin BE, Snaith HJ, McGehee MD. The renaissance of dye-sensitized solar cells. Nat Photon 2012;6:162.

[6] Hagberg DP, Marinado T, Karlsson KM, Nonomura K, Qin P, Boschloo G, et al. Tuning the HOMO and LUMO energy levels of organic chromophores for dye sensitized solar cells. J Org Chem 2007;72(25):9550–6.

[7] Genin E, Hugues V, Clermont G, Herbivo C, Castro MCR, Comel A, et al. Fluorescence and two-photon absorption of push–pull aryl(bi)thiophenes: structure–property relationships. Photochem Photobiol Sci 2012;11(11):1756–66.

[8] Kulhánek J, Bureš F, Pytela O, Mikysek T, Ludvík J, Růžička A. Push-pull molecules with a systematically extended π-conjugated system featuring 4,5-dicyanoimidazole. Dyes Pigments 2010;85(1):57–65.

[9] Kulhánek J, Bureš F, Wojciechowski A, Makowska-Janusik M, Gondek E, Kityk IV. Optical operation by chromophores featuring 4,5-dicyanoimidazole embedded within poly(methyl methacrylate) matrices. J Phys Chem 2010;114(35):9440–6.

[10] Stiegman AE, Graham E, Perry KJ, Khundkar LR, Cheng LT, Perry JW. The electronic structure and second-order nonlinear optical properties of donor-acceptor acetylenes: a detailed investigation of structure-property relationships. J Am Chem Soc 1991;113(20):7658–66.

[11] Bureš F. Fundamental aspects of property tuning in push–pull molecules. RSC Adv 2014;4(102):58826–51.

[12] Hagfeldt A, Boschloo G, Sun L, Kloo L, Pettersson H. Dye-sensitized solar cells. Chem Rev 2010;110(11):6595–663.

[13] Joly D, Pellejà L, Narbey S, Oswald F, Chiron J, Clifford JN, et al. A robust organic dye for dye sensitized solar cells based on iodine/iodide electrolytes combining high efficiency and outstanding stability. Sci Rep 2014;4:4033.

[14] Tsao HN, Burschka J, Yi C, Kessler F, Nazeeruddin MK, Grätzel M. Influence of the interfacial charge-transfer resistance at the counter electrode in dye-sensitized solar cells employing cobalt redox shuttles. Energy Environ Sci 2011;4(12):4921–4.

[15] Ellis H, Eriksson SK, Feldt SM, Gabrielsson E, Lohse PW, Lindblad R, et al. Linker unit modification of triphenylamine-based organic dyes for efficient cobalt mediated dye-sensitized solar cells. J Phys Chem C 2013;117(41):21029–36.

[16] Yao Z, Wu H, Ren Y, Guo Y, Wang P. A structurally simple perylene dye with ethynylbenzothiadiazole-benzoic acid as the electron acceptor achieves an over 10% power conversion efficiency. Energy Environ Sci 2015;8(5):1438–42.

[17] Yao Z, Yang L, Cai Y, Yan C, Zhang M, Cai N, et al. Rigidifying the π-linker to enhance light absorption of organic dye-sensitized solar cells and influences on charge transfer dynamics. J Phys Chem C 2014;118(6):2977–86.

[18] Hao Y, Saygili Y, Cong J, Eriksson A, Yang W, Zhang J, et al. Novel blue organic dye for dye-sensitized solar cells achieving high efficiency in cobalt-based electrolytes and by Co-sensitization. ACS Appl Mater Interfaces 2016;8(48):32797–804.

[19] Kakiage K, Aoyama Y, Yano T, Oya K, Fujisawa J-i, Hanaya M. Highly-efficient dye-sensitized solar cells with collaborative sensitization by silyl-anchor and carboxy-anchor dyes. Chem Commun 2015;51(88):15894–7.

[20] Buene AF, Uggerud N, Economopoulos SP, Gautun OR, Hoff BH. Effect of π-linkers on phenothiazine sensitizers for dye-sensitized solar cells. Dyes Pigments 2018; 151:263–71.

[21] Iqbal Z, Wu W-Q, Huang Z-S, Wang L, Kuang D-B, Meier H, et al. Trilateral π-conjugation extensions of phenothiazine-based dyes enhance the photovoltaic performance of the dye-sensitized solar cells. Dyes Pigments 2016;124:63–71.

[22] Hara K, Wang Z-S, Sato T, Furube A, Katoh R, Sugihara H, et al. Oligothiophene-containing coumarin dyes for efficient dye-sensitized solar cells. J Phys Chem B 2005;109(32):15476–82.

[23] Gao H-H, Qian X, Chang W-Y, Wang S-S, Zhu Y-Z, Zheng J-Y. Oligothiophene-linked D–π–A type phenothiazine dyes for dye-sensitized solar cells. J Power Sources 2016;307:866–74.

[24] Qian X, Zhu Y-Z, Chang W-Y, Song J, Pan B, Lu L, et al. Benzo[a]carbazole-Based donor−π−acceptor type organic dyes for highly efficient dye-sensitized solar cells. ACS Appl Mater Interfaces 2015;7(17):9015–22.

[25] Li R, Lv X, Shi D, Zhou D, Cheng Y, Zhang G, et al. Dye-sensitized solar cells based on organic sensitizers with different conjugated linkers: furan, bifuran, thiophene, bithiophene, selenophene, and biselenophene. J Phys Chem C 2009;113(17):7469–79.

[26] Liu J, Li R, Si X, Zhou D, Shi Y, Wang Y, et al. Oligothiophene dye-sensitized solar cells. Energy Environ Sci 2010;3(12):1924–8.

[27] Ronca E, Pastore M, Belpassi L, Tarantelli F, De Angelis F. Influence of the dye molecular structure on the TiO2 conduction band in dye-sensitized solar cells: disentangling charge transfer and electrostatic effects. Energy Environ Sci 2013;6(1):183–93.

[28] Zhang M, Liu J, Wang Y, Zhou D, Wang P. Redox couple related influences of π-conjugation extension in organic dye-sensitized mesoscopic solar cells. Chem Sci 2011;2(7):1401–6.

[29] Rühle S, Greenshtein M, Chen SG, Merson A, Pizem H, Sukenik CS, et al. Molecular adjustment of the electronic properties of nanoporous electrodes in dye-sensitized solar cells. J Phys Chem B 2005;109(40):18907–13.

[30] Eom YK, Kang SH, Choi IT, Kim E, Kim J, Ju MJ, et al. New thieno[3,2-b][1] benzothiophene-based organic sensitizers containing π-extended thiophene spacers for efficient dye-sensitized solar cells. RSC Adv 2015;5(98):80859–70.

[31] Kakiage K, Aoyama Y, Yano T, Otsuka T, Kyomen T, Unno M, et al. An achievement of over 12 percent efficiency in an organic dye-sensitized solar cell. Chem Commun 2014;50(48):6379–81.

[32] Hua Y, Lin Lee LT, Zhang C, Zhao J, Chen T, Wong W-Y, et al. Co-sensitization of 3D bulky phenothiazine-cored photosensitizers with planar squaraine dyes for efficient dye-sensitized solar cells. J Mater Chem 2015;3(26):13848–55.

[33] Lin RY-Y, Wu F-L, Li C-T, Chen P-Y, Ho K-C, Lin JT. High-performance aqueous/organic dye-sensitized solar cells based on sensitizers containing triethylene oxide methyl ether. ChemSusChem 2015;8(15):2503–13.

[34] Hagberg DP, Jiang X, Gabrielsson E, Linder M, Marinado T, Brinck T, et al. Symmetric and unsymmetric donor functionalization. comparing structural and spectral benefits of chromophores for dye-sensitized solar cells. J Mater Chem 2009;19(39):7232–8.

[35] Blouin N, Berny S, Jackson EA, Richter H, He F. Cyclohexadiene fullerene derivatives. 2014. US.

[36] Seo Y-H, Lee W-H, Park J-H, Bae C, Hong Y, Park J-W, et al. Side-chain effects on phenothiazine-based donor–acceptor copolymer properties in organic photovoltaic devices. J Polym Sci, Part A: Polym Chem 2012;50(4):649–58.

[37] Bejan A, Shova S, Damaceanu M-D, Simionescu BC, Marin L. Structure-directed functional properties of phenothiazine brominated dyes: morphology and photophysical and electrochemical properties. Cryst Growth Des 2016;16(7):3716–30.

[38] Billingsley KL, Buchwald SL. An improved system for the palladium-catalyzed borylation of aryl halides with pinacol borane. J Org Chem 2008;73(14):5589–91.

[39] Tian H, Yang X, Chen R, Zhang R, Hagfeldt A, Sun L. Effect of different dye baths and dye-structures on the performance of dye-sensitized solar cells based on triphenylamine dyes. J Phys Chem C 2008;112(29):11023–33.

[40] Dentani T, Kubota Y, Funabiki K, Jin J, Yoshida T, Minoura H, et al. Novel thiophene-conjugated indoline dyes for zinc oxide solar cells. New J Chem 2009;33(1):93–101.

[41] Pavlishchuk VV, Addison AW. Conversion constants for redox potentials measured versus different reference electrodes in acetonitrile solutions at 25°C. Inorg Chim Acta 2000;298(1):97–102.

[42] Kim SH, Kim HW, Sakong C, Namgoong J, Park SW, Ko MJ, et al. Effect of five-membered heteroaromatic linkers to the performance of phenothiazine-based dye-sensitized solar cells. Org Lett 2011;13(21):5784–7.

[43] Tian H, Yang X, Chen R, Pan Y, Li L, Hagfeldt A, et al. Phenothiazine derivatives for efficient organic dye-sensitized solar cells. Chem Commun 2007;(36):3741–3.

[44] Saygili Y, Söderberg M, Pellet N, Giordano F, Cao Y, Muñoz-García AB, et al. Copper bipyridyl redox mediators for dye-sensitized solar cells with high photovoltage. J Am Chem Soc 2016;138(45):15087–96.

[45] Frisch MJ, et al. Gaussian 09, revision b.01. Wallingford CT: Gaussian, Inc.; 2010.

[46] Christians JA, Manser JS, Kamat PV. Best practices in perovskite solar cell efficiency measurements. Avoiding the error of making bad cells look good. J Phys Chem Lett 2015;6(5):852–7.

[47] Buene AF, Boholm N, Hagfeldt A, Hoff B. Effect of furan π-spacer and triethylene oxide methyl ether substituents on performance of phenothiazine sensitizers in dye-sensitized solar cells. New J Chem 2019;43(24):9403–10.

[48] Pazoki M, Cappel UB, Johansson EMJ, Hagfeldt A, Boschloo G. Characterization techniques for dye-sensitized solar cells. Energy Environ Sci 2017;10(3):672–709.

[49] Fabregat-Santiago F, Bisquert J, Palomares E, Otero L, Kuang D, Zakeeruddin SM, et al. Correlation between photovoltaic performance and impedance spectroscopy of dye-sensitized solar cells based on ionic liquids. J Phys Chem C 2007;111(17):6550–60.

[50] Fabregat-Santiago F, Garcia-Belmonte G, Mora-Seró I, Bisquert J. Characterization of nanostructured hybrid and organic solar cells by impedance spectroscopy. Phys Chem Chem Phys 2011;13(20):9083–118.

[51] O'Boyle NM, Banck M, James CA, Morley C, Vandermeersch T, Hutchison GR. Open Babel: an open chemical toolbox. J Cheminf 2011;3(1):33.

[52] Stewart JJP. MOPAC2016. Colorado Springs, CO, USA: Stewart Computational Chemistry; 2016.

[53] Nazeeruddin MK, De Angelis F, Fantacci S, Selloni A, Viscardi G, Liska P, et al. Combined experimental and DFT-TDDFT computational study of photoelectrochemical cell ruthenium sensitizers. J Am Chem Soc 2005;127(48):16835–47.

Expanding the π-spacer of phenothiazine dyes for use in dye-sensitized solar cells.

David Moe Almenningen[a], Henrik Erring Hansen[b], Martin Furru Vold[a], Audun Formo Buene[a], Vishwesh Venkatraman[a], Svein Sunde[b], Bård Helge Hoff[a], Odd Reidar Gautun[a]*

a) Department of Chemistry, Norwegian University of Science and Technology, Høgskoleringen 5, NO-7491 Trondheim, Norway

b) Department of Materials Science and Engineering, Norwegian University of Science and Technology, Sem Sælands vei 12, NO-7491 Trondheim, Norway

* Corresponding author. Tel.: +47 73594101; E-mail address: odd.r.gautun@ntnu.no (O. R. Gautun).

List of contents

UV/Vis Absorption
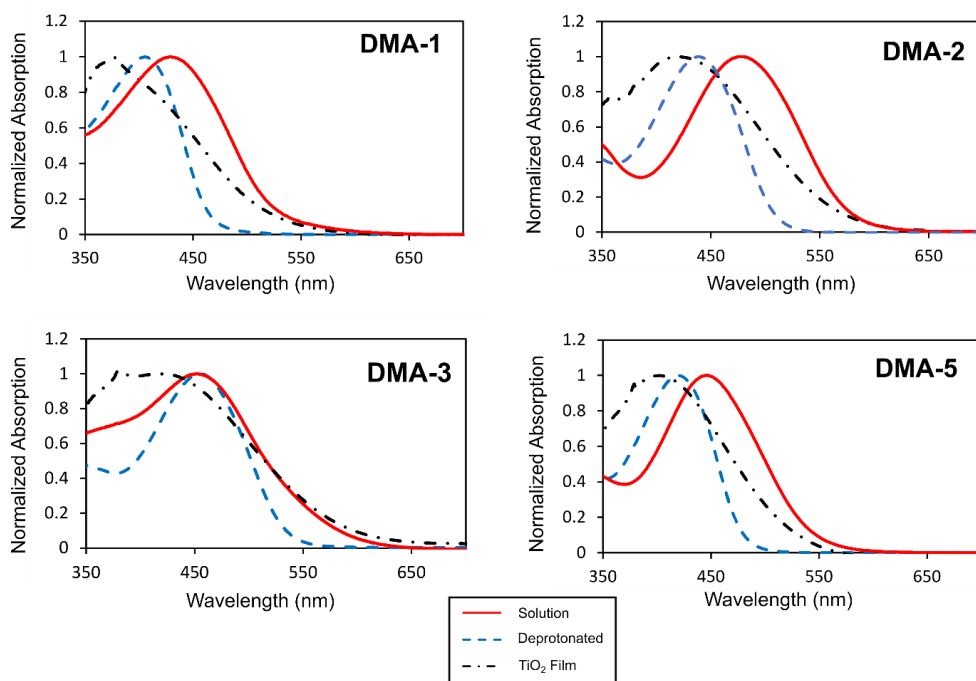
Figure S1. Absorption spectra of **DMA-1**, **DMA-2**, **DMA-3**, and **DMA-5** in solution (dichloromethane), deprotonated in solution, and sensitized on TiO$_2$ films. Deprotonation was done by adding a drop of triethylamine to the cuvette.
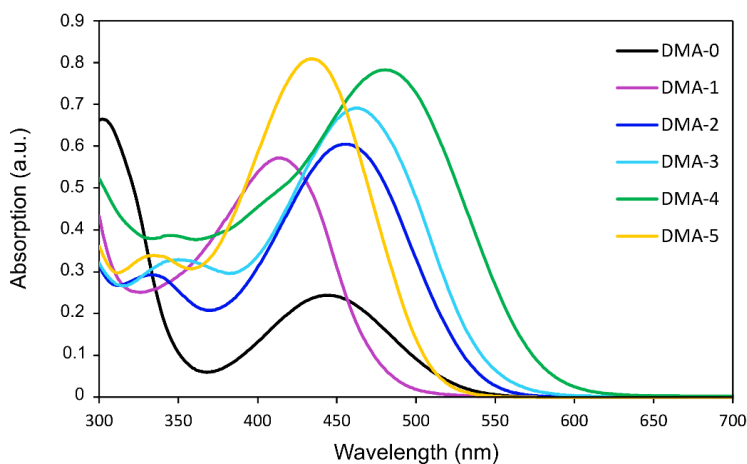
Figure S2. Absorption spectra of the dyes in THF-solution.

Cyclic voltammetry
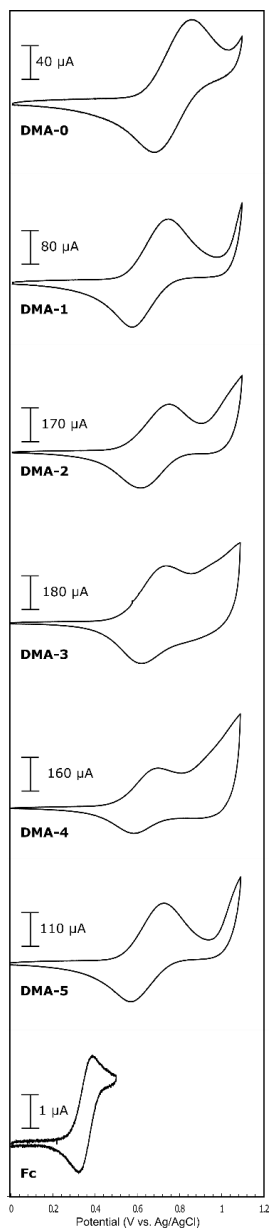
Figure S3. CVs of the dyes and ferrocene. Sensitizers measured on TiO$_2$ films (2.5 μm on FTO glass), carbon counter electrode, Ag/AgCl reference, 0.1 M LiTFSI supporting electrolyte. Ferrocene (Fc) was measured with a glassy carbon working electrode and used for calibration with a value of 0.624 V versus SHE.[2]

Theoretical calculations

HOMO   LUMO
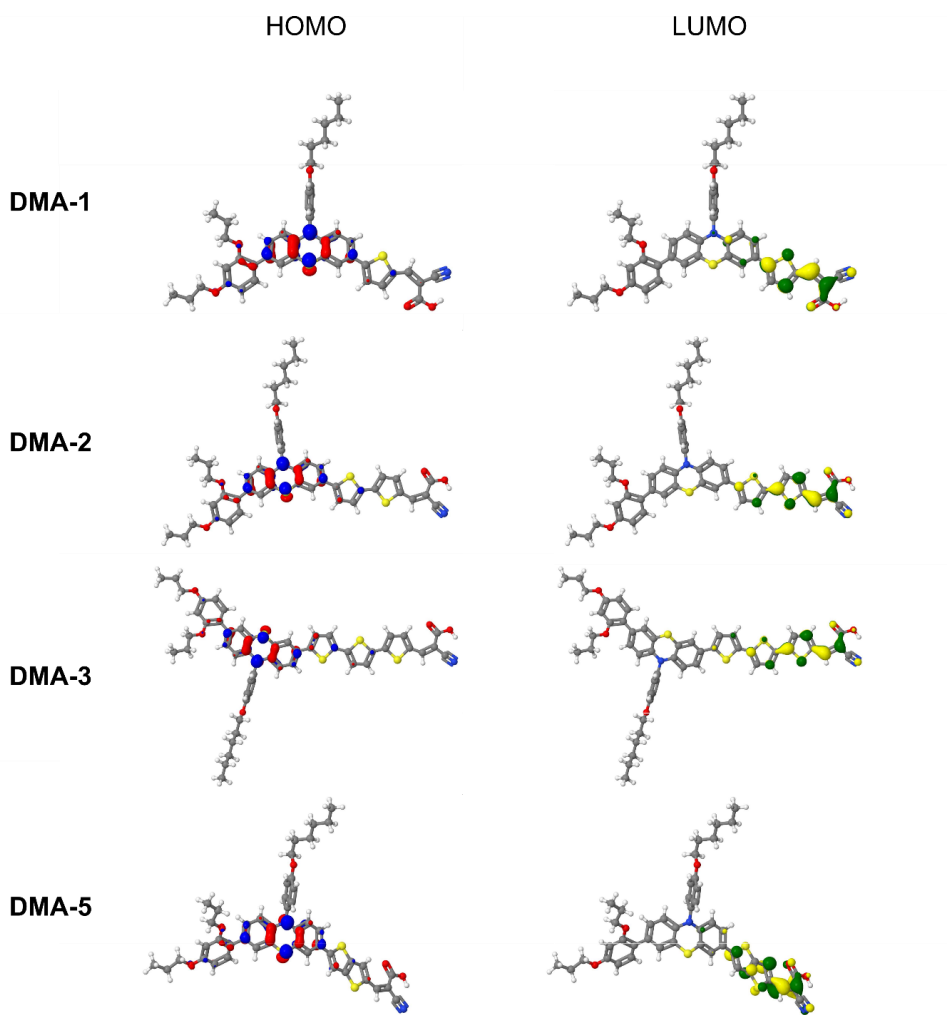
Figure S4. LUMOs and HOMOs for the dyes **DMA-1**, **DMA-2**, **DMA-3**, and **DMA-5** obtained at CAM-B3LYP/6-31G(d,p) level of theory.

Electrochemical impedance spectroscopy
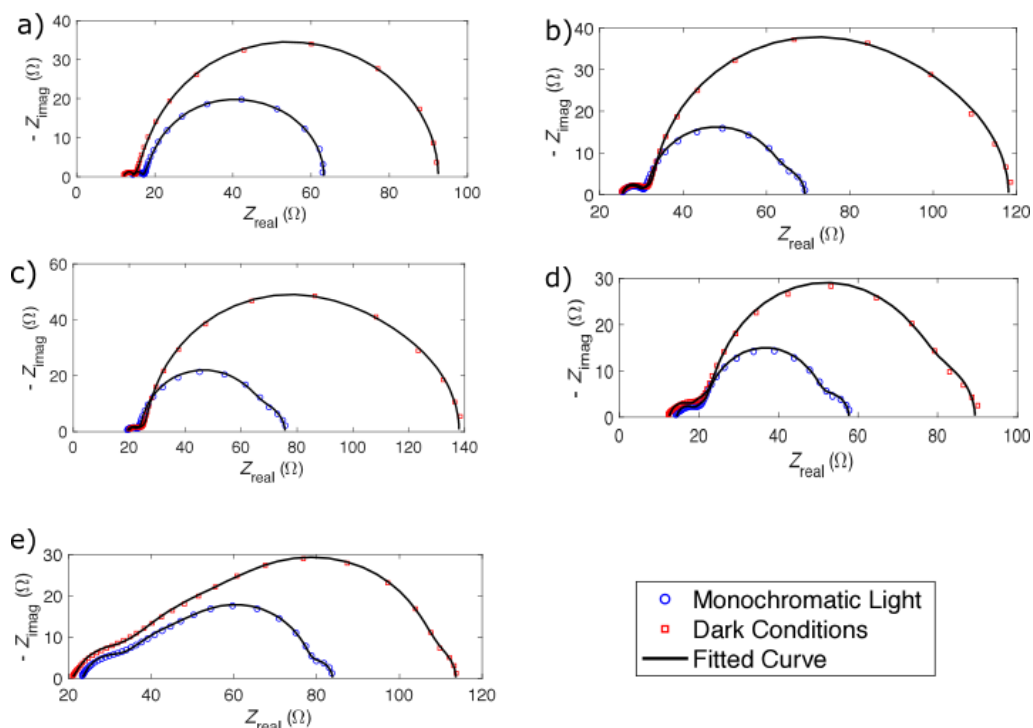
Figure S5. Complex plane diagrams obtained from electrochemical impedance spectroscopy under monochromatic light and dark conditions for a) **DMA-0**, b) **DMA-1**, c) **DMA-2** d) **DMA-3**, e) **DMA-4**.
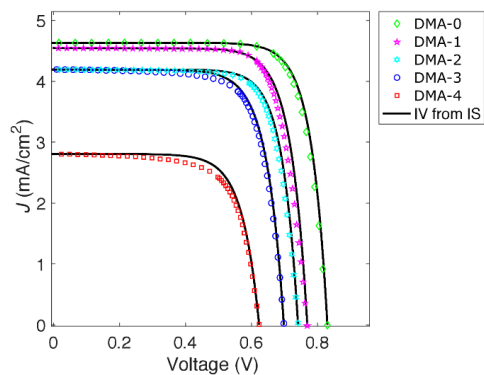
Figure S6. J-V curves of the dyes **DMA-0 – DMA-4** under monochromatic light of wavelength 479 nm, and J-V curves recreated from impedance data (-) using the model of Fabregat-Santiago et al.[1]

Table S1. *The initial guess of the parameters used in the fitting of the impedance data to the equivalent electrical circuit using the Levenberg-Marquardt method. R_0 is the series resistance, $\sqrt{R_{rec}R_{tr}}$ is the square root of the recombination resistance times the transport resistance, ω_{rec} is the characteristic frequency of the recombination, ω_{tr} is the characteristic frequency of the transport mechanisms, β is the deviation from ideality with 1 as the ideal value, R_{RC} is the resistance across the interface between the cathode and the electrolyte, ω_{RC} is the characteristic frequency for the parallel circuit across the interface between the cathode and the electrolyte, R_D is the diffusion resistance in the electrolyte, and ω_D is the characteristic frequency of the diffusion in the electrolyte.*

Dye	R_0	$\sqrt{R_{rec}R_{tr}}$	ω_{rec}	ω_{tr}	β	R_{RC}	ω_{RC}	R_D	ω_D
DMA-0	11	2	3	150	1	10	9000	10	1
DMA-1	14	10	10	150	1	3	10000	10	1
DMA-2	11	6	7.5	112	1	2	18000	10	1
DMA-3	14	20	80	150	1	10	9000	10	1
DMA-4	14	20	20	80	1	10	9000	10	1

Experimental

Materials and reagents

All reactions were carried out under nitrogen atmosphere, and all synthesis reagents were acquired from Sigma Aldrich unless specified otherwise.

Analytical instruments

NMR spectroscopy (^{1}H and ^{13}C) was recorded on 400 and 600 MHz Bruker instruments, and all chemical shifts are reported relative to the respective solvent signals. Mass determination was performed on a Waters "Synapt G2-S" QTOF instrument in positive mode. UV/Vis spectra were recorded on a Hitachi U-1900 instrument using quarts cuvettes for the solution samples, while fluorescence spectroscopy was recorded on a Cary Eclipse Fluorescence Spectrophotometer. Infrared spectroscopy was recorded on a BRUKER ALPHA ECO-ATR FTIR spectrometer.

Synthesis of 10-(4-(hexyloxy)phenyl)-10*H*-phenothiazine (1) [3]
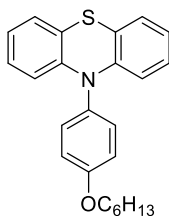
1-Bromo-4-(hexyloxy)benzene (12.13g, 47.2 mmol) was added along with 10*H*-phenothiazine (6.34 g, 31.8 mmol), Pd$_2$(dba)$_3$ (1.45 g, 1.6 mmol), PCy$_3$ (0.62 g, 2.2 mmol) and t-BuONa (7.66 g, 79.7 mmol), this was dissolved in degassed toluene (85 mL) in a N$_2$-atmosphere. The reaction mixture was stirred at 120 °C for 21 hours. The reaction mixture was cooled to rt, then water (100 mL) was added. The aqueous phase was extracted using CHCl$_3$ (3 x 100 mL), the combined organic phases were washed with water (100 mL) then dried with brine (100 mL) and Na$_2$SO$_4$. The solvents were removed in vacuo, the crude product was purified using column chromatography (SiO$_2$, toluene/n-pentane 1:6, R$_f$ 0.31). This yielded the product as an off-white solid (10.65 g, 28.3 mmol, 89%). m$_p$ 81.8-83.1 °C (Lit[3]: 89.1-94.1 °C) ¹H NMR (600 MHz, DMSO-d$_6$): δ 7.33-7.30 (m, 2H), 7.20-7.17 (m, 2H), 7.03 (dd, *J* = 7.6, 1.5 Hz, 2H), 6.90 (td, *J* = 7.3, 1.7 Hz, 2H), 6.83 (td, *J* = 7.6, 1.5 Hz, 2H), 6.14 (dd, *J* = 8.0, 1.0 Hz, 2H), 4.05 (t, *J* = 6.5 Hz, 2H), 1.76 (app. q, *J* = 6.7 Hz, 2H), 1.49-1.43 (m, 2H), 1.36-1.30 (m, 4H), 0.90 (tr, *J* = 7.1 Hz, 3H).

Synthesis of 10-(4-(hexyloxy)phenyl)-10*H*-phenothiazine-3-carbaldehyde (2) [3]
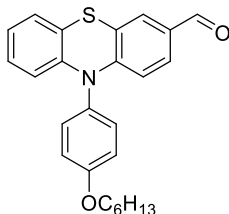
Anhydrous DMF (2.3 mL, 29.7 mmol) was cooled to 0 °C under N$_2$-atmosphere. POCl$_3$ (2.8 mL, 29.7 mmol) was added under constant stirring, the resulting Vilsmeier-Haack reagent was dissolved in 1.2-dichloroethane (30 mL) and stirred for 1 hour. A solution of **1** (1.88 g, 4.99 mmol) in anhydrous 1.2-dichloroethane (20 mL) was added before the reaction mixture was heated to 85 °C and left stirring overnight. The heat was removed, and the reaction mixture cooled to room temperature before it was poured to a flask containing water (200 mL). An aqueous solution of NaOH (1M, 100 mL) was added in portions until neutral pH. The organic phase was washed with water (3 x 100 mL) before the aqueous phase was extracted using DCM (3 x 150 mL). The combined organic phases were dried using Na$_2$SO$_4$. The solvents were removed under reduced pressure, the residue was purified using column chromatography (SiO$_2$, DCM/n-pentane 1:1, R$_f$ 0.12) before recrystallization (EtOH). This yielded **2** as a yellow solid (1.41 g, 3.50 mmol, 70%). ¹H NMR (400 MHz, DMSO-d$_6$): δ 9.69 (s, 1H), 7.50 (d, *J* = 1.5 Hz, 1H), 7.43 (dd, *J* = 8.8, 2.0 Hz, 1H), 7.36 (d, *J* = 8.8 Hz, 2H), 7.22 (d, *J* = 8.8 Hz, 2H), 7.06 (dd, *J* = 7.0, 2.0 Hz, 1H), 6.96-6.86 (m, 2H), 6.20 (d, *J* = 8.4 Hz, 1H), 6.11 (dd, *J* = 8.0, 1.5 Hz, 1H), 4.06 (t, *J* = 6.5 Hz, 2H), 1.76 (app. q, *J* = 6.3 Hz, 2H), 1.50-1.42 (m, 2H), 1.37-1.31 (m, 4H), 0.90 (t, *J* = 6.9 Hz, 3H).

Synthesis of 7-bromo-10-(4-(hexyloxy)phenyl)-10*H*-phenothiazine-3-carbaldehyde (3) [3]
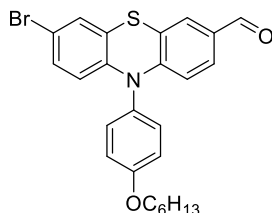
Compound **2** (1.40 g, 3.46 mmol) and NBS (0.62 g, 3.46 mmol) were added and dissolved in $CHCl_3$ (24 mL) and glacial acetic acid (16 mL) after establishing N_2-atmosphere. The reaction mixture was stirred at rt. for 24 hours, before an aqueous NaOH-solution (1 M, 200 mL) was added to neutralize the pH. $CHCl_3$ (3 x 50 mL) was used to extract the aqueous phase, the combined organic phases were washed with water (25 mL) then dried with brine (25 mL) and Na_2SO_4. The solvents were removed in vacuo, the crude product was purified using recrystallization (EtOAc). This afforded 9 as yellow crystals (1.27 g, 2.62 mmol, 76%). m_p 144.9-145.7 °C (Lit:[3] 147.1-150.9 °C). ^{1}H NMR (400 MHz, DMSO-d$_6$): δ 9.70 (s, 1H) 7.51 (d, J = 1.8 Hz, 1H), 7.43 (dd, J = 8.5, 2.0 Hz, 1H), 7.36 (d, J = 8.9 Hz, 2H), 7.29 (d, J = 2.2 Hz, 1H), 7.21 (d, J = 8.9 Hz, 2H), 7.10 (dd, J = 8.9, 2.2 Hz, 1H), 6.19 (d, J = 8.6 Hz, 1H), 6.00 (d, J = 8.6 Hz, 1H), 4.05 (t, J = 6.4 Hz, 2H), 1.76 (q, J = 6.8 Hz, 2H), 1.50-1.41 (m, 2H), 1.37-1.30 (m, 4H), 0.90 (t, J = 6.8 Hz, 3H).

Synthesis of 7-(2,4-dipropoxyphenyl)-10-(4-(hexyloxy)phenyl)-10*H*-phenothiazine-3-carbaldehyde (4)
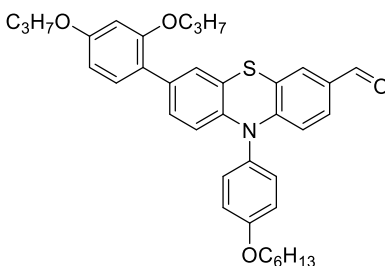
Compound **3** (601 mg, 1.24 mmol), (2,4-dipropoxyphenyl)boronic acid (448 mg, 1.88 mmol), Pd(OAc)$_2$ (14 mg, 0.06 mmol), SPhos (51 mg, 0.12 mmol) and K_3PO_4 (1.07 g, 5.04 mmol) were mixed. 1.4-Dioxane (24 mL) and water (24 mL) were degassed and added under nitrogen. The reaction mixture was heated to 80 °C and left stirring for 20 hours before cooling to room temperature. Water (50 mL) was added and the aqueous phase extracted by diethyl ether (3 × 60 mL). The combined organic phases were dried with brine (50 mL) and over anhydrous Na_2SO_4, filtered and the solvents were removed *in vacuo*. The crude product was purified by silica gel column chromatography (*n*-pentane/dichloromethane, 1:2, R_f = 0.55) to obtain compound **4** as a viscous dark orange liquid (593 mg, 0.99 mmol, 80%). ^{1}H NMR (400 MHz, CDCl$_3$): δ 9.68 (s, 1H), 7.45 (d, J = 2.0 Hz, 1H), 7.30-7.27 (m, 3H), 7.17 (d, J = 2.0 Hz, 1H), 7.15-7.11 (m, 3H), 7.00 (dd, J = 8.6, 2.0 Hz, 1H), 6.51-6.48 (m, 2H), 6.19 (d, J = 8.6 Hz, 1H), 6.15 (d, J = 8.6 Hz, 1H), 4.04 (*t, J* =

6.2 Hz, 2H), 3.96-3.87 (m, 4H), 1.89-1.83 (m, 2H), 1.80-1.77 (m, 4H), 1.55-1.48 (m, 2H), 1.40-1.36 (m, 4H), 1.04, (t, J = 7.4 Hz, 3H), 1.00 (t, J = 7.4 Hz, 3H), 0.92 (t, J = 6.6 Hz, 3H); ^{13}C NMR (100 MHz, CDCl$_3$): δ 189.9, 159.8, 159.3, 156.9, 149.6, 141.0, 134.1, 132.2 (2C), 131.7, 130.7, 130.4, 129.8, 127.9, 127.5, 121.7, 120.1, 118.1, 116.7 (2C), 116.0, 114.9, 105.3, 100.3, 69.9, 69.7, 68.4, 31.6, 29.2, 25.8, 22.6, 22.5, 14.1, 10.8, 10.6; IR (neat, cm^{-1}) ν: 2959 (m), 2931 (m), 2871 (m), 1685 (s), 1455 (s), 1244 (s), 1064 (s), 833 (m); HRMS (ASAP+, m/z): found 596.2828 (calcd. C$_{37}$H$_{42}$NO$_4$S 596.2835, [M+H]+).

Synthesis of 3-bromo-10-(4-(hexyloxy)phenyl)-10*H*-phenothiazine (5)[3]
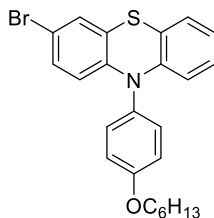
Compound **1** (4.05 g, 10.7 mmol) and NBS (1.91 g, 10.7 mmol) were added and N$_2$-atmosphere was established. Then CHCl$_3$ (21 mL) and glacial acetic acid (32 mL) were added. The reaction mixture was stirred at 0 °C for 3 hours, then allowed to reach room temperature overnight under continuous stirring. The reaction was quenched by adding a solution of NaOH (6.87 g, 171.7 mmol) in water (75 mL), the resulting mixture was stirred for 30 minutes. The aqueous phase was extracted using CHCl$_3$ (3 x 50 mL), the combined organic phases were dried using brine (50 mL) then Na$_2$SO$_4$. The solvents were removed in vacuo, the residue was purified using column chromatography (SiO2, dichloromethane/*n*-pentane 1:20). This yielded **5** as off-white crystals (3.63 g, 8.0 mmol, 75%). mp 69.9-70.2 °C (lit:[3] 73.5 °C). Rf 0.15 (SiO2, DCM/n-pentane 1:20). ^{1}H NMR (400 MHz, DMSO-d$_6$): δ 7.32 (d, J = 8.8 Hz, 2H), 7.26-7.23 (m, 1H), 7.18 (d, J = 8.8 Hz, 2H) 7.10-7.06 (m, 1H), 7.04 (dd, J = 7.5, 1.6 Hz, 1H), 6.94-6.89 (m, 1H), 6.84 (td, J = 7.4, 1.2 Hz, 1H), 6.15-6.10 (m, 1H), 6.04-5.99 (m, 1H), 4.04 (t, J = 6.6 Hz, 2H), 1.76 (app. q, J = 6.6 Hz, 2H), 1.49-1.41 (m, 2H), 1.37 1.30 (m, 4H), 0.89 (t, J = 6.6 Hz, 3H).

Synthesis of 3-(2,4-dipropoxyphenyl)-10-(4-(hexyloxy)phenyl)-10*H*-phenothiazine (6)
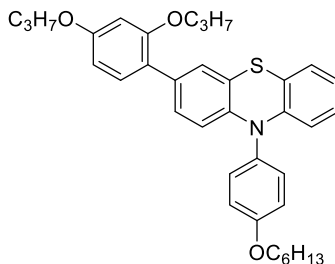
Compound **5** (1.99 g, 4.4 mmol), (2,4-dipropoxyphenyl)boronic acid (1.58 g, 6.6 mmol), Pd(OAc)$_2$ (53 mg, 0.24 mmol), SPhos (183 mg, 0.77 mmol) and K$_3$PO$_4$ (3.74 g, 17.6 mmol) were mixed. 1.4-Dioxane (84 mL) and water (84 mL) were degassed and added under nitrogen. The reaction mixture was heated to 80 °C and left stirring for 3 hours before cooling to room temperature. Water (170 mL) was added and the

aqueous phase extracted by diethyl ether (3 × 100 mL). The combined organic phases were dried with brine (100 mL) and over anhydrous Na$_2$SO$_4$, filtered and the solvents were removed *in vacuo*. The crude product was purified by silica gel column chromatography (*n*-pentane/toluene, 2:1, R_f = 0.16) to obtain compound **1** as a light-yellow oil (2.05 g, 3.6 mmol, 82%). ^{1}H NMR (400 MHz, DMSO-d$_6$): δ 7.33 (d, *J* = 8.4 Hz, 2H), 7.19 (d, *J* = 8.4 Hz, 2H), 7.17 (d, *J* = 2.1 Hz, 1H), 7.13 (d, *J* = 7.7 Hz, 1H), 7.03 (dd, *J* = 1.5, 6.0 Hz, 1H), 7.00 (dd, *J* = 2.1, 6.4 Hz, 1H), 6.90 (td, *J* = 1.7, 7.0 Hz, 1H), 6.80 (td, *J* = 1.1, 7.6 Hz, 1H), 6.57 (d, *J* = 1.9 Hz, 1H), 6.52 (dd, *J* = 2.5, 8.4 Hz, 1H), 6.12 (d, *J* = 8.6 Hz, 2H), 4.05 (t, *J* = 6.6 Hz, 2H), 3.90 (dt, *J* = 6.3, 11.5 Hz, 4H), 1.75 (app. sx, *J* = 6.4 Hz, 2H), 1.70 (app. q, *J* = 7.1 Hz, 2H), 1.69-1.63 (sx, *J* = 7.1 Hz, 2H), 1.48-1.44 (m, 2H), 1.37-1.34 (m, 4H), 0.99-0.94 (m, 6H), 0.89 (tr, *J* = 7.1 Hz, 3H); ^{13}C NMR (100 MHz, DMSO-d$_6$): δ 159.3, 158.5, 156.4, 143.9, 142.2, 132.4, 132.3 (2C), 131.9, 130.2, 127.6, 127.2, 126.8, 126.5, 122.4, 120.8, 118.6, 117.9, 116.6 (2C), 115.5, 115.1, 105.9, 100.0, 69.3, 69.1, 67.8, 31.1, 28.7, 25.3, 22.1 (2C), 22.0, 14.0, 10.7, 10.5; IR (neat, cm^{-1}) ν: 2931 (w), 2871 (w), 1607 (m), 1577 (w), 1460 (s), 1297 (m), 1180 (s), 1012 (m), 832 (m), 741 (s); HRMS (ASAP+, m/z): found 568.2887 (calcd. C$_{36}$H$_{42}$NO$_3$S 568.2887, [M+H]+).

Synthesis of [2,2':5',2''-terthiophene]-5-carbaldehyde (9a) [4]
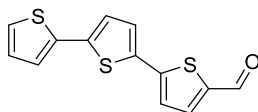
The commercially available 2,2':5',2''-terthiophene (abcr GmbH, 0.87 g, 3.5 mmol) was dissolved in anhydrous DCM (10 mL), this mixture was cooled to 0 °C. A mixture of POCl$_3$ (0.46 mL, 4.9 mmol) and dry DMF (0.39 mL, 4.9 mmol) in DCM (15 mL) was added dropwise over 20 min. to the reaction mixture. The reaction mixture was allowed to reach rt. and left stirring overnight. An aqueous solution of NaOAc (1 M, 30 mL) was added, this was stirred for 5 h. The aqueous phase was extracted with DCM (3 x 30 mL), the organic phases were combined and washed with water (30 mL), then dried with brine (30 mL) and over anhydrous MgSO$_4$. The solvents were removed under reduced pressure to yield a yellow solid crude product. This was purified by column chromatography (SiO2, 0-10% gradient DCM in pentane). This afforded the product **9a** as a yellow solid (0.38 g, 1.36 mmol, 39%). ^{1}H NMR (600 MHz, CDCl$_3$): δ 9.86 (s, 1H), 7.67 (d, *J* = 4.0 Hz, 1H), 7.28-7.27 (m, 2H), 7.25-7.23 (m, 2H), 7.13 (d, *J* = 4.0 Hz, 1H), 7.04 (app. dd, *J* = 1.2, 4.0 Hz, 1H).

Synthesis of [2,2':5',2'':5'',2'''-quaterthiophene]-5-carbaldehyde (10a) [5]
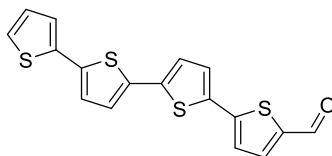
The commercially available 2,2':5',2'':5'',2'''-quaterthiophene (0.5 g, 1.5 mmol) was dissolved in dry 1.2-dichloroethane (10 mL). Dry DMF (0.13 mL, 1.7 mmol) was added, and the resultant solution cooled to 0 °C before addition of POCl3 (0.16 mL, 1.7 mmol). The reaction mixture was stirred while it was warmed to rt. The solution was then heated to reflux and left stirring overnight. An aqueous NaOAc-solution (1M, 30 mL) was added and the mixture was stirred for 5 hours at rt. The aqueous phase was extracted with DCM

(3x40 mL), the combined organic phases were washed with water (40 mL) then dried with brine (40 mL) and MgSO4. The solvents were removed in vacuo, the residue was a light orange solid, and was purified by column chromatography (SiO2, 1:1 pentane/DCM,). This yielded **10a** as a yellow solid (0.388 g, 1.08 mmol,72 %). ^{1}H NMR (600 MHz, CDCl$_3$): δ 9.87 (s, 1H), 7.67 (d, J = 3.7, 1H) 7.28 (d, J = 3.7 Hz, 1H), 7.26-7.24 (m, 2H), 7.20 (d, J = 3.7, 1H), 7.14-7.12 (dd, J = 1.1, 3.7 Hz, 2H), 7.10 (d, J = 3.7 Hz , 1H), 7.03 (dd, J = 1.1, 3.7 Hz, 1H).

Synthesis of 5''-bromo-[2,2':5',2''-terthiophene]-5-carbaldehyde (9b) [6]
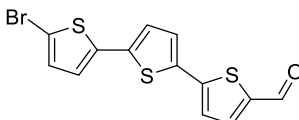
Compound **9a** (0.178 g, 0.64 mmol) was added along with NBS (0.139 g, 0.78 mmol) and cooled to 0 ° C, the compounds were dissolved in a mixture of CHCl$_3$ (2 mL) and glacial acetic acid (3 mL). The reaction mixture was left stirring overnight, before addition of an aqueous NaOH-solution (1M, 7 mL) followed by an additional 30 min. of stirring. The aqueous phase was extracted by CHCl$_3$ (3 x 20 mL), the combined organic phases were dried with brine (20 mL) and over MgSO$_4$. The solvents were removed in vacuo to yield the product **9b** as an orange solid (0.204 g, 0.57 mmol, 89%). ^{1}H NMR (600 MHz, acetone-d$_6$): δ 9.94 (s, 1H), 7.94 (d, J = 4.0 Hz, 1H), 7.50 (dd, J = 1.2, 4.0 Hz, 2H), 7.31 (d, J = 4.0 Hz, 1H), 7.21 (d, J = 4.0 Hz, 1H), 7.19 (d, J = 4.0 Hz, 1H).

Synthesis of 5'''-bromo-[2,2':5',2'':5'',2'''-quaterthiophene]-5-carbaldehyde (10b) [7]
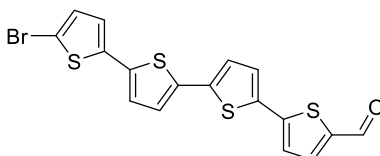
Compound **10a** (0.305 g, 0.8 mmol) was added along with NBS (0.155 g, 0.9 mmol) and cooled to 0 ° C, the compounds were dissolved in a mixture of CHCl$_3$ (10 mL) and glacial acetic acid (15 mL). The reaction mixture was left stirring overnight, before addition of an aqueous NaOH-solution (1M, 30 mL) followed by an additional 30 min. of stirring. The aqueous phase was extracted by CHCl$_3$ (3 x 50 mL), the combined organic phases were dried with brine (25 mL) and over MgSO$_4$. The solvents were removed in vacuo to yield the product **10b** as an orange solid (0.325 g, 0.7 mmol, 88%). ^{1}H NMR (400 MHz, DMSO-d$_6$): δ 9.89 (s, 1H), 8.01 (d, J = 4.0 Hz, 1H), 7.60 (d, J = 3.8 Hz, 1H), 7.57 (d, J = 3.8 Hz, 1H), 7.43 (d, J = 4.2 Hz, 1H), 7.42 (d, J = 4.2 Hz, 1H), 7.33 (d, J = 4.0 Hz 1H), 7.26-7.23 (dd, J = 7.6, 3.9 Hz, 2H).

Synthesis of 5-bromothieno[3,2-*b*]thiophene-2-carbaldehyde (11b) [8]
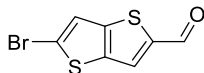
Commercially available thieno[3,2-b]thiophene-2-carbaldehyde (0.94 g, 5.6 mmol) was added along with NBS (1.35 g, 7.6 mmol) and cooled to 0 ° C, the compounds were dissolved in THF (110 mL). The reaction mixture was left stirring for 7 hours, before addition of water (55 mL). The aqueous phase was extracted by DCM (3 x 50 mL), the combined organic phases were dried with brine (50 mL) and over Na_2SO_4. The solvents were removed in vacuo, the resulting residue was purified by column chromatography (SiO_2, n-pentane/EtOAc 14:1) to yield the product **11b** as a yellow solid (0.99 g, 4.0 mmol, 72%). ^{1}H NMR (400 MHz, CDCl$_3$): δ_H 9.97 (s, 1H), 7.84 (s, 1H), 7.36 (s, 1H).

Synthesis of 5-(7-(2,4-dipropoxyphenyl)-10-(4-(hexyloxy)phenyl)-10*H*-phenothiazin-3-yl)thiophene-2-carbaldehyde (7)
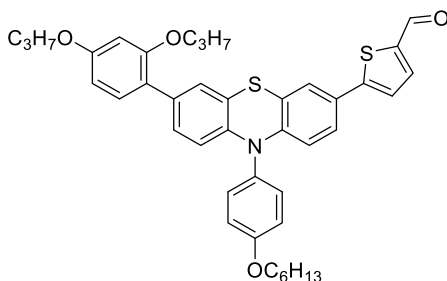

Compound **6** (220 mg, 0.39 mmol) was added along with NBS (196 mg, 0.93 mmol) and cooled to 0 ° C, the compounds were dissolved in a mixture of CHCl$_3$ (1 mL) and glacial acetic acid (2 mL). The reaction mixture was left stirring overnight, before addition of an aqueous NaOH-solution (1M, 5 mL) followed by an additional 30 min. of stirring. The aqueous phase was extracted by CHCl$_3$ (3 x 20 mL), the combined organic phases were dried with brine (20 mL) and over MgSO$_4$. The solvents were removed in vacuo to yield a light yellow oil. This crude mixture was used without further purification, it was added to a Schlenk tube along with PdCl$_2$(CH$_3$CN)$_2$ (4 mg, 16 µmol), SPhos (14 mg, 35 µmol). The compounds were dissolved in 1.4-dioxane (1 mL), then 4.4.5.5-tetramethyl-1.3.2-dioxaborolane (0.10 mL, 0.69 mmol) and NEt$_3$ (0.10 mL, 0.72 mmol) was added. The reaction mixture was heated to 110 °C and left stirring for 90 minutes before the reaction mixture was cooled to room temperature. The contents of the reaction were filtered through a Celite plug using EtOAc as eluent, the solvents were then removed in vacuo. The crude mixture was a brown viscous oil that was used without further purification.

The boronate crude product was added along with 5-bromothiophene-2-carbaldehyde (136 mg, 0.71 mmol), Pd(OAc)$_2$ (8 mg, 36 µmol), SPhos (21 mg, 51 µmol) and K$_3$PO$_4$ (400 mg, 1.9 mmol). 1.4-Dioxane (10 mL) and water (10 mL) were degassed and added under nitrogen. The reaction mixture was heated to 80 °C and left stirring for 22 hours before cooling to room temperature. Water (20 mL) was added and the aqueous phase extracted by diethyl ether (3 × 20 mL). The combined organic phases were dried with brine (30 mL)

and over anhydrous Na$_2$SO$_4$, filtered and the solvents were removed *in vacuo*. The crude product was purified by silica gel column chromatography (*n*-pentane/ethyl acetate, 12:1, R_f = 0.17) to obtain **7** as a red-orange wax (68 mg, 0.1 mmol, 26% over three steps from **6**).

^{1}H NMR (600 MHz, DMSO-d$_6$) : δ 9.87 (s, 1H), 7.94 (d, *J* = 4.1 Hz, 1H), 7.79 (d, *J* = 4.1 Hz, 1H), 7.74 (s, 1H), 7.36 (d, *J* = 8.9 Hz, 2H), 7.25 (d, *J* = 2.1 Hz, 1H), 7.21 (d, *J* = 8.9 Hz, 2H), 7.11 (dd, *J* = 8.4, 2.1 Hz, 1H), 7.05 (app. dd, *J* = 7.5, 1.4 Hz, 1H), 6.92 (app. td, *J* = 8.4, 1.5 Hz, 1H), 6.85-6.82 (m, 1H), 6.82 (s, 1H), 6.15 (d, *J* = 8.6 Hz, 2H), 4.22 (t, *J* = 6.5 Hz, 2H), 4.08-4.04 (m, 4H), 1.89 (sx, *J* = 6.8 Hz, 2H), 1.80-1.74 (m, 2H), 1.73-1.66 (m, 2H), 1.49-1.43 (m, 2H), 1.37-1.31 (m, 4H), 1.08 (t, *J* = 7.4 Hz, 3H), 0.97 (t, *J* = 7.2 Hz, 3H), 0.90 (t, *J* = 7.0 Hz, 3H); ^{13}C NMR (150 MHz, DMSO-d$_6$) : δ 184.0, 158.5, 157.5, 155.7, 148.4, 143.9, 142.6, 141.1, 137.7, 132.3, 132.0 (2C), 131.4 (2C), 129.1, 128.1, 127.2, 127.1, 126.5, 125.0, 122.4, 121.4, 118.5, 118.0, 116.6 (2C), 115.5, 115.1, 98.0, 70.7, 69.8, 67.8, 31.0, 28.7, 25.2, 22.1 (2C), 22.0, 13.9, 10.8, 10.7; IR (neat, cm^{-1}) ν: 2962 (w), 2857 (w), 1658 (s), 1605 (s), 1464 (m), 1439 (s), 1295 (m), 1225 (s), 1042 (m),741 (m); HRMS (ASAP+, *m/z*): found 678.2713 (calcd. C$_{41}$H$_{44}$NO$_4$S$_2$ 678.2712, [M+H]$^+$).

Synthesis of 5'-(7-(2,4-dipropoxyphenyl)-10-(4-(hexyloxy)phenyl)-10*H*-phenothiazin-3-yl)-[2,2'-bithiophene]-5-carbaldehyde (8)
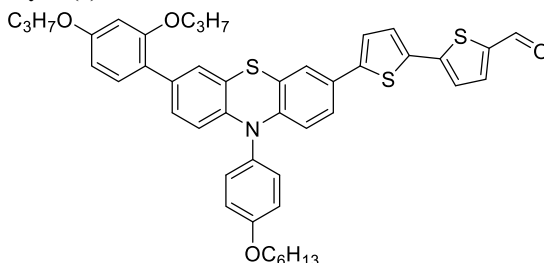
Compound **6** (393 mg, 0.69 mmol) was added along with NBS (137 mg, 0.76 mmol) and cooled 0 ° C, the compounds were dissolved in THF (14 mL). The reaction mixture was left stirring for 2.5 hours, before addition of water (10 mL). The aqueous phase was extracted by DCM (3 x 50 mL), the combined organic phases were dried with brine (25 mL) and over Na$_2$SO$_4$. The solvents were removed in vacuo to yield a light yellow oil. This crude mixture was used without further purification, it was added to a Schlenk tube along with PdCl$_2$(CH$_3$CN)$_2$ (7 mg, 28 μmol), SPhos (25 mg, 62 μmol). The compounds were dissolved in 1.4-dioxane (2 mL), then 4.4.5.5-tetramethyl-1.3.2-dioxaborolane (0.15 mL, 1.03 mmol) and NEt$_3$ (0.20 mL, 1.43 mmol) was added. The reaction mixture was heated to 110 °C and left stirring for 90 minutes before the reaction mixture was cooled to room temperature. The contents of the reaction were filtered through a Celite plug using EtOAc as eluent, the solvents were then removed in vacuo. The crude mixture was a brown viscous oil that was used without further purification.

The boronate crude product was added along with 5'-bromo-[2,2'-bithiophene]-5-carbaldehyde (260 mg, 0.96 mmol), Pd(OAc)$_2$ (6 mg, 27 μmol), SPhos (25 mg, 61 μmol) and K$_3$PO$_4$ (400 mg, 1.9 mmol). 1.4-Dioxane (10 mL) and water (10 mL) were degassed and added under nitrogen. The reaction mixture was heated to 80 °C and left stirring for 22 hours before cooling to room temperature. Water (20 mL) was added and the aqueous phase extracted by diethyl ether (3 × 20 mL). The combined organic phases were dried with brine (30 mL) and over anhydrous Na$_2$SO$_4$, filtered and the solvents were removed *in vacuo*. The crude

product was purified by silica gel column chromatography (*n*-pentane/ethyl acetate, 14:1, R_f = 0.05) to obtain compound **8** as a maroon wax (210 mg, 0.28 mmol, 39% over three steps from **6**).

^{1}H NMR (600 MHz, DMSO-d$_6$) : δ 9.87 (s, 1H), 7.98 (d, *J* = 3.7 Hz, 1H), 7.65 (s, 1H), 7.64 (d, *J* = 4.1 Hz, 1H), 7.56 (d, *J* = 4.1 Hz, 1H), 7.49 (d, *J* = 3.9 Hz, 1H), 7.36 (d, *J* = 8.8 Hz, 2H), 7.25 (d, *J* = 2.1 Hz, 1H), 7.21 (d, *J* = 8.8 Hz, 2H), 7.10 (dd, *J* = 8.5, 2.1 Hz, 1H), 7.05 (app. dd, *J* = 7.6, 1.5 Hz, 1H), 6.92 (app. td, *J* = 7.8, 1.5 Hz, 1H), 6.83 (app. td, *J* = 7.4, 1.2 Hz, 1H), 6.80 (s, 1H), 6.16-6.15 (m, 1H), 6.15-6.14 (m, 1H), 4.20 (t, *J* = 6.5 Hz, 2H), 4.07 (t, *J* = 6.5 Hz, 2H) 4.04 (t, *J* = 6.5 Hz, 2H), 1.92 (sx, *J* = 7.0 Hz, 2H), 1.80-1.74 (m, 2H), 1.71 (sx, *J* = 6.9 Hz, 2H), 1.50-1.44 (m, 2H), 1.38-1.30 (m, 4H), 1.11 (t, *J* = 7.4 Hz, 3H), 0.97 (t, *J* = 7.3 Hz, 3H), 0.90 (t, *J* = 7.0 Hz, 3H); ^{13}C NMR (150 MHz, DMSO-d$_6$) : δ 183.6, 158.5, 156.5, 154.9, 146.3, 143.9, 142.6, 140.5 (2C), 139.4, 133.4, 132.3, 131.9 (2C), 131.6, 128.2, 128.0, 127.2, 127.0, 126.5 (3C), 125.1, 124.3, 122.4, 121.3, 118.5, 118.0, 116.7 (2C), 115.5, 115.1, 98.1, 70.7, 69.7, 67.8, 31.0, 28.7, 25.2, 22.1 (2C), 22.0, 13.9, 10.9, 10.7; IR (neat, cm^{-1}) ν: 2925 (w), 2870 (w), 1658 (s), 1605 (s), 1507 (m), 1440 (s), 1284 (m), 1226 (s), 1044 (m), 741 (m); HRMS (ASAP+, *m/z*): found 760.2574 (calcd. C$_{45}$H$_{46}$NO$_4$S$_3$ 760.2589, [M+H]$^+$).

Synthesis of 5''-(7-(2,4-dipropoxyphenyl)-10-(4-(hexyloxy)phenyl)-10*H*-phenothiazin-3-yl)-[2,2':5',2''-terthiophene]-5-carbaldehyde (9)
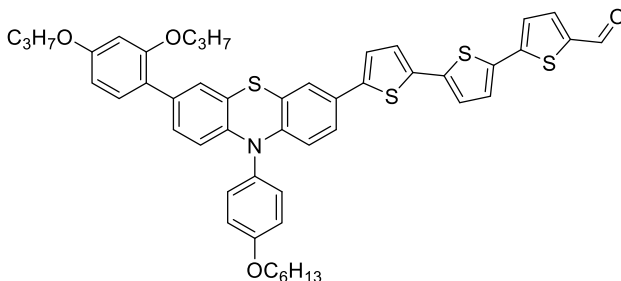
Compound **6** (371 mg, 0.65 mmol) was added along with NBS (120 mg, 0.67 mmol) and cooled 0 ° C, the compounds were dissolved in THF (14 mL). The reaction mixture was left stirring for 2.5 hours, before addition of water (10 mL). The aqueous phase was extracted by DCM (3 x 50 mL), the combined organic phases were dried with brine and over Na$_2$SO$_4$. The solvents were removed in vacuo to yield a light yellow oil. This crude mixture was used without further purification, it was added to a Schlenk tube along with PdCl$_2$(CH$_3$CN)$_2$ (7 mg, 28 µmol), SPhos (25 mg, 62 µmol). The compounds were dissolved in 1.4-dioxane (2 mL), then 4.4.5.5-tetramethyl-1.3.2-dioxaborolane (0.15 mL, 1.03 mmol) and NEt$_3$ (0.20 mL, 1.43 mmol) was added. The reaction mixture was heated to 110 °C and left stirring for 90 minutes before the reaction mixture was cooled to room temperature. The contents of the reaction were filtered through a Celite plug using EtOAc as eluent, the solvents were then removed in vacuo. The crude mixture was a brown viscous oil that was used without further purification.

The boronate crude product was added along with compound **9b** (185 mg, 0.52 mmol), Pd(OAc)$_2$ (6 mg, 27 µmol), SPhos (20 mg, 49 µmol) and K$_3$PO$_4$ (408 mg, 1.9 mmol). 1.4-Dioxane (9 mL) and water (9 mL) were degassed and added under nitrogen. The reaction mixture was heated to 80 °C and left stirring for 20

hours before cooling to room temperature. Water (50 mL) was added and the aqueous phase extracted by dichloromethane (3 × 40 mL). The combined organic phases were dried with brine (50 mL) and over anhydrous Na_2SO_4, filtered and the solvents were removed *in vacuo*. The crude product was purified by silica gel column chromatography (*n*-pentane/diethyl ether, 2:1, R_f = 0.14) to obtain compound **9** as a dark-red residue (98 mg, 0.12 mmol, 18% over three steps from **6**).

^{1}H NMR (600 MHz, CDCl$_3$) : δ 9.84 (s, 1H), 7.64 (d, *J* = 4.2 Hz, 1H), 7.52 (s, 1H), 7.34 (d, *J* = 3.8 Hz, 1H), 7.30 (d, *J* = 8.7 Hz, 2H), 7.25 (d, *J* = 3.5 Hz, 1H), 7.22 (d, *J* = 2.1 Hz, 1H), 7.21 (d, *J* = 4.0 Hz, 1H), 7.16 (d, *J* = 4.0 Hz, 1H), 7.11-7.09 (m, 3H), 7.02 (dd, *J* = 2.2, 8.5 Hz, 1H), 6.98 (dd, *J* = 1.5, 7.5 Hz, 1H), 6.81 (app. td, *J* = 1.5, 7.5 Hz, 1H), 6.76 (td, *J* = 1.2, 7.4 Hz, 1H), 6.55 (s, 1H), 6.21 (d, *J* = 8.7 Hz, 1H), 6.19 (dd, *J* = 1.0, 8.2 Hz, 1H), 4.08 (t, *J* = 6.4 Hz, 2H), 4.03 (t, *J* = 6.6 Hz, 2H), 3.93 (t, *J* = 6.4 Hz, 2H), 1.96 (sx, *J* = 6.7 Hz, 2H), 1.82 (app. sx, *J* = 8.1 Hz, 2H), 1.77 (sx, *J* = 8.1 Hz, 2H), 1.52-1.50 (m, 2H), 1.39-1.37(m, 4H), 1.15 (t, *J* = 8.1 Hz, 3H), 1.02 (t, *J* = 7.5 Hz, 3H), 0.95-0.92 (m, 3H); ^{13}C NMR (150 MHz, CDCl$_3$) : δ 182.4, 158.9, 156.5, 155.3, 147.2, 144.6, 143.2, 141.3, 140.1, 140.0, 137.4, 134.6, 133.7, 133.1, 132.2 (2C), 132.0, 129.2, 127.8, 127.4, 127.0, 126.8, 126.6, 124.6, 124.3, 123.82, 123.79, 122.4, 122.1, 119.6, 119.0, 116.4 (2C), 115.6, 115.4, 115.2, 97.8, 70.8, 70.3, 68.3, 31.6, 29.3, 25.8, 22.7, 22.63, 22.56, 14.1, 11.0, 10.8; IR (neat, cm^{-1}) ν: 2924 (m), 2869 (m), 1659 (s), 1446 (s), 1227 (s), 1063 (m), 787 (s); HRMS (ASAP+, *m/z*): found 842.2468 (calcd. $C_{49}H_{47}NO_4S_4$ 842.2466, [M+H]$^+$).

Synthesis of 5'''-(7-(2,4-dipropoxyphenyl)-10-(4-(hexyloxy)phenyl)-10H-phenothiazin-3-yl)-[2,2':5',2'':5'',2'''-quaterthiophene]-5-carbaldehyde (10)
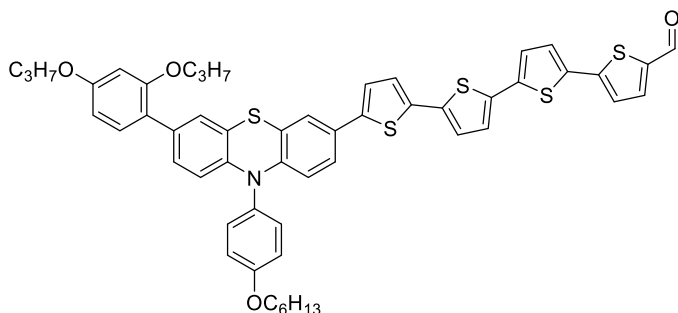
Compound **6** (458 mg, 0.81 mmol) was added along with NBS (152 mg, 0.85 mmol) and cooled 0 ° C, the compounds were dissolved in THF (14 mL). The reaction mixture was left stirring for 2.5 hours, before addition of water (10 mL). The aqueous phase was extracted by DCM (3 x 50 mL), the combined organic phases were dried with brine and over Na_2SO_4. The solvents were removed in vacuo to yield a light yellow oil. This crude mixture was used without further purification, it was added to a Schlenk tube along with PdCl$_2$(CH$_3$CN)$_2$ (7 mg, 28 μmol), SPhos (25 mg, 62 μmol). The compounds were dissolved in 1.4-dioxane (2 mL), then 4.4.5.5-tetramethyl-1.3.2-dioxaborolane (0.22 mL, 1.51 mmol) and NEt$_3$ (0.29 mL, 2.08 mmol) was added. The reaction mixture was heated to 110 °C and left stirring for 90 minutes before the reaction mixture was cooled to room temperature. The contents of the reaction were filtered through a Celite plug using EtOAc as eluent, the solvents were then removed in vacuo. The crude mixture was a brown viscous oil that was used without further purification.

The boronate crude product was added along with compound **10b** (264 mg, 0.6 mmol), Pd(OAc)$_2$ (7 mg, 31 µmol), SPhos (26 mg, 63 µmol) and K$_3$PO$_4$ (520 mg, 2.4 mmol). 1.4-Dioxane (12 mL) and water (12 mL) were degassed and added under nitrogen. The reaction mixture was heated to 80 °C and left stirring for 16 hours before cooling to room temperature. Water (60 mL) was added and the aqueous phase extracted by dichloromethane (3 × 50 mL). The combined organic phases were dried with brine (60 mL) and over anhydrous Na$_2$SO$_4$, filtered and the solvents were removed *in vacuo*. The crude product was purified by silica gel column chromatography (*n*-pentane/dichloromethane, 2:3, R_f = 0.11) to obtain compound **10** as a dark-red residue (122 mg, 0.13 mmol, 16% over three steps from **6**).

^{1}H NMR (600 MHz, CDCl$_3$) : δ 9.85 (s, 1H), 7.66 (d, J = 3.8 Hz, 1H), 7.52 (s, 1H), 7.33 (d, J = 3.7 Hz, 1H), 7.31 (d, J = 8.8 Hz, 2H) 7.27 (d, J = 3.5 Hz, 1H), 7.24-7.22 (m, 2H), 7.14 (d, J = 3.5 Hz, 1 H), 7.13-7.12 (m, 1H), 7.11 (d, J = 8.8 Hz, 2H), 7.11-7.10 (m, 1H), 7.08 (d, J = 3.6 Hz, 1H), 7.04-7.02 (m, 1H), 7.00-6.99 (m, 1H), 6.82 (app. t, J = 8.0 Hz, 1H), 6.77 (app. t, J = 7.7 Hz, 1H), 6.55 (s, 1H), 6.23-6.21 (m, 1H), 6.20-6.19 (m, 1H), 4.08 (t, J = 6.5 Hz, 2H), 4.03 (t, J = 6.3 Hz, 2H), 3.94 (t, J = 6.5 Hz, 2H), 1.97 (sx, J = 6.5 Hz, 2H), 1.82 (app. q, J = 6.3 Hz, 2H), 1.76 (app. sx, J = 6.5 Hz, 2H), 1.53-1.50 (m, 2H), 1.39-1.36 (m, 4H), 1.14 (t, J = 6.5 Hz, 3H), 1.01 (t, J = 6.5 Hz, 3H), 0.94-0.92 (m, 3H); ^{13}C NMR (150 MHz, CDCl$_3$) : δ 182.4, 158.9, 156.4, 155.3, 146.9, 144.6, 143.2, 141.5, 139.5, 139.2, 138.2, 137.4, 135.0, 134.4, 134.2, 133.1, 132.2 (2C), 132.1, 129.3, 127.8, 127.4, 127.0, 126.8, 126.6, 125.2, 124.6, 124.3, 124.0, 123.9, 123.7, 122.4, 122.1, 119.6, 119.0, 116.4 (2C), 115.59, 115.58, 115.2, 97.8, 70.8, 70.3, 68.3, 31.6, 29.3, 25.8, 22.7, 22.63, 22.57, 14.1, 11.0, 10.8; IR (neat, cm^{-1}) ν: 2922 (m), 2867 (m), 1659 (s), 1454 (s), 1436 (s), 1238 (s), 1171 (s), 787 (s); HRMS (ESI+, *m/z*): found 924.2338 (calcd. C$_{53}$H$_{49}$NO$_4$S$_5$ 924.2343, [M+H]$^+$).

Synthesis of 5-(7-(2,4-dipropoxyphenyl)-10-(4-(hexyloxy)phenyl)-10H-phenothiazin-3-yl)thieno[3,2-b]thiophene-2-carbaldehyde (11)

Compound **6** (393 mg, 0.69 mmol) was added along with NBS (137 mg, 0.76 mmol) and cooled 0 ° C, the compounds were dissolved in THF (14 mL). The reaction mixture was left stirring for 2.5 hours, before addition of water (10 mL). The aqueous phase was extracted by DCM (3 x 50 mL), the combined organic phases were dried with brine and over Na$_2$SO$_4$. The solvents were removed in vacuo to yield a light yellow oil. This crude mixture was used without further purification, it was added to a Schlenk tube along with PdCl$_2$(CH$_3$CN)$_2$ (7 mg, 28 µmol), SPhos (25 mg, 62 µmol). The compounds were dissolved in 1.4-dioxane (2 mL), then 4.4.5.5-tetramethyl-1.3.2-dioxaborolane (0.15 mL, 1.03 mmol) and NEt$_3$ (0.20 mL, 1.43 mmol) was added. The reaction mixture was heated to 110 °C and left stirring for 90 minutes before the reaction mixture was cooled to room temperature. The contents of the reaction were filtered through a Celite

plug using EtOAc as eluent, the solvents were then removed in vacuo. The crude mixture was a brown viscous oil that was used without further purification.

The boronate crude product was added along with compound **11b** (261 mg, 0.96 mmol), Pd(OAc)$_2$ (6 mg, 27 µmol), SPhos (21 mg, 51 µmol) and K$_3$PO$_4$ (400 mg, 1.9 mmol). 1.4-Dioxane (10 mL) and water (10 mL) were degassed and added under nitrogen. The reaction mixture was heated to 80 °C and left stirring for 28 hours before cooling to room temperature. Water (20 mL) was added and the aqueous phase extracted by diethyl ether (3 × 20 mL). The combined organic phases were dried with brine (30 mL) and over anhydrous Na$_2$SO$_4$, filtered and the solvents were removed *in vacuo*. The crude product was purified by silica gel column chromatography (*n*-pentane/ethyl acetate, 12:1, R_f = 0.16) to obtain compound **11** as a red wax (170 mg, 0.23 mmol, 32% over three steps from **6**).

^{1}H NMR (600 MHz, DMSO-d_6) : δ 9.94 (s, 1H), 8.36 (s, 1H), 8.04 (s, 1H), 7.72 (s, 1H), 7.36 (d, J = 8.8 Hz, 2H), 7.27 (d, J = 2.1 Hz, 1H), 7.22 (d, J = 8.8 Hz, 2H), 7.13 (dd, J = 8.6, 2.1 Hz, 1H), 7.06 (app. dd, J = 7.7, 1.3 Hz, 1H), 6.92 (app. td, J = 7.9, 1.5 Hz, 1H), 6.86-6.83 (m, 1H), 6.83-6.81 (m, 1H), 6.17-6.15 (m, 1H), 6.15-6.14 (m, 1H), 4.21 (t, J = 6.6 Hz, 2H), 4.06 (app. q, J = 6.4 Hz, 4H), 1.92 (sx, J = 7.1 Hz, 2H), 1.80-1.75 (m, 2H), 1.71 (sx, J = 7.4 Hz, 2H), 1.49-1.44 (m, 2H), 1.37-1.31 (m, 4H), 1.10 (t, J = 7.1 Hz, 3H), 0.98 (t, J = 7.1 Hz, 3H), 0.90 (t, J = 7.0 Hz, 3H); ^{13}C NMR (150 MHz, DMSO-d_6) : δ 184.3, 158.5, 157.1, 155.4, 148.2, 144,8, 143.9, 143.4, 142.6, 138.9, 132.3, 131.9 (2C), 131.5 (2C), 128.9, 128.0, 127.2, 127.0, 126.6, 122.5, 121.4, 118.5, 118.1, 116.7 (2C), 116.4, 115.5, 115.1, 114.4, 98.2, 70.7, 69.8, 67.8, 31.0, 28.7, 25.2, 22.1 (2C), 22.0 , 13.9, 10.9, 10.7; IR (neat, cm^{-1}) v: 2926 (w), 2855 (w), 1651 (s), 1605 (s), 1494 (m), 1457 (s), 1411 (m), 1297 (m), 1226 (s), 1122 (m), 970 (m), 741 (m); HRMS (ASAP+, *m/z*): found 734.2433 (calcd. C$_{43}$H$_{44}$NO$_4$S$_3$ 734.2432, [M+H]$^+$).

Synthesis of (E)-2-cyano-3-(7-(2,4-dipropoxyphenyl)-10-(4-(hexyloxy)phenyl)-10*H*-phenothiazin-3-yl)acrylic acid (DMA-0)
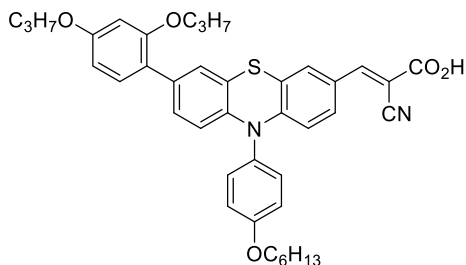
Compound **4** (148 mg, 0.25 mmol) and cyanoacetic acid (444 mg, 5.22 mmol) were dissolved in degassed acetonitrile (55 mL) under nitrogen atmosphere. Piperidine (0.32 mL, 276 mg, 3.2 mmol) was added and the reaction was heated to 80 °C for 2 hours before cooling to room temperature and quenched in HCl (4 M, 110 mL). Dichloromethane (3 × 80 mL) was used to extract the aqueous phase, and the combined organic phases were washed with water (4 × 100 mL), then dried over anhydrous Na$_2$SO$_4$, filtered and the solvents were removed *in vacuo*. The crude product was purified by silica gel column chromatography (gradient: 0-15% methanol in dichloromethane) to obtain sensitizer **DMA-0** as a dark-red solid (147 mg, 0.22 mmol, 88%), mp 237.2-240.0 °C.

^{1}H NMR (600 MHz, DMSO-d_6) : δ 7.83 (s, 1H), 7.52 (s, 1H), 7.33 (d, J = 8.3 Hz, 1H), 7.25 (d, J = 7.5 Hz, 2H), 7.15 (s, 1H), 7.14-7.10 (m, 3H), 6.98 (d, J = 10.8 Hz, 1H), 6.55 (s, 1H), 6.49 (d, J = 8.2 Hz, 1H), 6.07-6.04 (m, 2H), 3.98 (t, J = 5.8 Hz, 2H), 3.91-3.86 (m, 4H), 1.74-1.68 (m, 4H), 1.63 (hx, J = 5.9 Hz, 2H), 1.43-1.37 (m, 2H), 1.32-1.27 (m, 4H), 0.96 (t, J = 7.3 Hz, 3H), 0.92 (t, J = 7.3 Hz, 3H), 0.87 (t, J = 6.5 Hz, 3H); ^{13}C NMR (150 MHz, DMSO-d_6) : δ 165.3, 159.8, 159.1, 156.8, 147.8, 146.2, 141.2, 133.6, 132.0 (2C), 131.9, 130.6, 130.2, 128.2, 127.33, 127.30, 127.25, 121.0, 119.4, 119.1, 117.6, 117.2 (2C), 116.0, 115.5, 108.7, 106.2, 100.4, 69.7, 69.5, 68.3, 31.5, 29.1, 25.7, 22.6, 22.52, 22.48, 14.4, 11.1, 10.9; IR (neat, cm^{-1}) ν: 2959 (m), 2932 (m), 2872 (m), 2217 (w), 1607 (s), 1468 (s), 1245 (s), 1064 (s), 815 (m). HRMS (ASAP+, m/z): found 619.2994 (calcd. $C_{39}H_{43}N_2O_3S$ 619.2994, [M-CO$_2$+H]$^+$).

Synthesis of (E)-2-cyano-3-(5-(7-(2,4-dipropoxyphenyl)-10-(4-(hexyloxy)phenyl)-10H-phenothiazin-3-yl)thiophen-2-yl)acrylic acid (DMA-1)
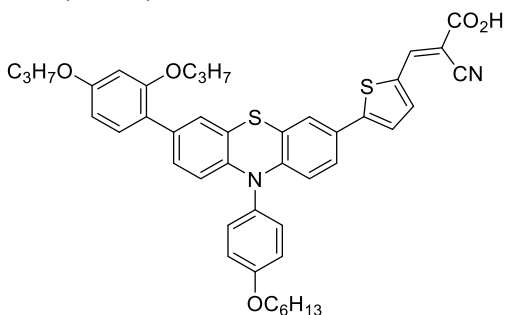
Compound **7** (40 mg, 59 μmol) and cyanoacetic acid (160 mg, 1.88 mmol) were dissolved in degassed acetonitrile (20 mL) under nitrogen atmosphere. Piperidine (0.12 mL, 103 mg, 1.2 mmol) was added and the reaction was heated to 80 °C for 2 hours before cooling to room temperature and quenched in HCl (4 M, 40 mL). Dichloromethane (3 × 70 mL) was used to extract the aqueous phase, and the combined organic phases were washed with water (4 × 100 mL), then dried over anhydrous Na$_2$SO$_4$, filtered and the solvents were removed *in vacuo*. The crude product was purified by silica gel column chromatography (gradient: 0-15% MeOH in CH$_2$Cl$_2$), to obtain sensitizer **DMA-1** as a dark solid (43 mg, 57 μmol, 97%), 223.7-225.0 °C (dec.).

^{1}H NMR (600 MHz, DMSO-d_6) : δ 8.17 (s, 1H), 7.77-7.65 (m, 3H), 7.35 (d, J = 8.7 Hz, 2H), 7.26-7.17 (m, 3H), 7.09 (d, J = 8.5 Hz, 1H), 7.05 (d, J = 7.2 Hz, 1H), 6.91 (t, J = 7.5 Hz, 1H), 6.86-6.76 (m, 2H), 6.18-6.10 (m, 2H), 4.17 (t, J = 5.7 Hz, 2H), 4.08-4.01 (m, 4H), 1.92 (hx, J = 6.5 Hz, 2H), 1.76 (q, J = 6.3 Hz, 2H), 1.70 (hx, J = 6.5 Hz, 2H), 1.49-1.42 (m, 2H), 1.37-1.29 (m, 4H), 1.08 (t, J = 6.5 Hz, 3H), 0.97 (t, J = 6.2 Hz, 3H), 0.89 (t, J = 6.5 Hz, 3H); ^{13}C NMR (150 MHz, DMSO-d_6) : δ 164.4, 158.4, 157.0, 155.4, 145.5, 143.9, 142.5, 135.6, 135.2, 132.3, 131.9 (2C), 131.5, 128.5, 128.0, 127.2, 127.0, 126.5, 124.3, 122.4, 121.4, 118.7, 118.5, 118.0, 116.6 (3C), 115.5, 115.1, 114.0, 101.4, 98.0, 70.7, 69.7, 67.8, 31.0, 28.7, 25.2, 22.1, 21.99, 21.96, 13.9, 11.0, 10.6; IR (neat, cm^{-1}) ν: 2926 (m), 2873 (m), 2215 (w), 1684 (m), 1563 (s), 1508, 1488 (m), 1409 (s), 1288 (m), 1192 (s), 1013 (m), 735(m); HRMS (ASAP+, m/z): found 701.2858 (calcd. $C_{43}H_{45}N_2O_3S_2$ 701.2872, [M-CO$_2$+H]$^+$).

Synthesis of (E)-2-cyano-3-(5'-(7-(2,4-dipropoxyphenyl)-10-(4-(hexyloxy)phenyl)-10H-phenothiazin-3-yl)-[2,2'-bithiophen]-5-yl)acrylic acid (DMA-2)
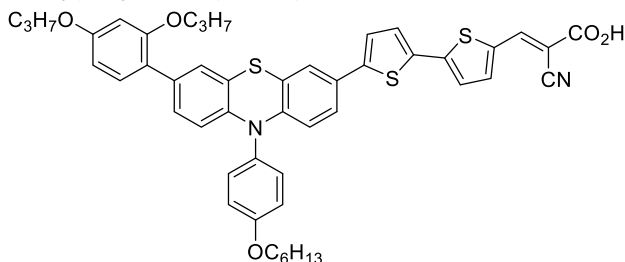
Compound **8** (150 mg, 0.197 mmol) and cyanoacetic acid (380 mg, 4.48 mmol) were dissolved in degassed acetonitrile (45 mL) under nitrogen atmosphere. Piperidine (0.30 mL, 259 mg, 3.0 mmol) was added and the reaction was heated to 80 °C for 2 hours before cooling to room temperature and quenched in HCl (4 M, 50 mL). Dichloromethane (3 × 70 mL) was used to extract the aqueous phase, and the combined organic phases were washed with water (4 × 100 mL), then dried over anhydrous Na_2SO_4, filtered and the solvents were removed *in vacuo*. The crude product was purified by silica gel column chromatography (gradient: 0-15% MeOH in CH_2Cl_2), to obtain sensitizer **DMA-2** as a dark solid (158 mg, 0.191 mmol, 97%), 228.9-230.5 °C (dec.).

^{1}H NMR (600 MHz, DMSO-d_6) : δ 8.46 (s, 1H), 7.96 (d, J = 4.2 Hz, 1H), 7.67-7.64 (m, 2H), 7.57 (d, J = 4.0 Hz, 1H), 7.52 (d, J = 4.0 Hz, 1H), 7.35 (d, J = 8.8 Hz, 2H), 7.25 (d, J = 2.0 Hz, 1H), 7.21 (d, J = 8.8 Hz, 2H), 7.10 (dd, J = 8.6, 2.1 Hz, 1H), 7.05 (dd, J = 7.5, 1.5 Hz, 1H), 6.92 (td, J = 7.5, 1.5 Hz, 1H), 6.83 (td, J = 7.4, 1.1 Hz, 1H), 6.80 (s, 1H), 6.15 (d, J = 3.3 Hz, 1H), 6.14 (d, J = 3.0 Hz, 1H), 4.20 (t, J = 6.5 Hz, 2H), 4.07-4.02 (m, 4H), 1.91 (hx, J = 7.2 Hz, 2H), 1.77 (q, J = 7.0 Hz, 2H), 1.70 (hx, J = 7.2 Hz, 2H), 1.49-1.43 (m, 2H), 1.37-1.30 (m, 4H), 7.11 (t, J = 7.2 Hz, 3H), 0.97 (t, J = 7.2 Hz, 3H), 0.89 (t, J = 7.0 Hz, 3H); ^{13}C NMR (150 MHz, DMSO-d_6) : δ 163.7, 158.4, 156.5, 154.9, 146.6, 146.3, 143.8, 142.5, 141.6, 141.0, 133.27, 133.26, 132.3, 131.9, 131.9 (2C), 131.6, 128.2, 128.0, 127.2, 127.0, 126.7, 126.5, 125.3, 124.1, 122.4, 121.3, 118.6, 118.0, 116.6 (3C), 115.5, 115.1, 114.1, 98.1, 97.3, 70.6, 69.7, 67.8, 31.0, 28.7, 25.2, 22.11, 22.08, 22.0, 13.9, 10.8, 10.6; IR (neat, cm^{-1}) ν: 2926 (m), 2855 (m), 2216 (w), 1682 (m), 1574 (s), 1465 (m), 1407 (s), 1052 (s), 971 (m), 739 (m); HRMS (ASAP+, *m/z*): found 783.2745 (calcd. $C_{47}H_{47}N_2O_3S_3$ 783.2749, [M-CO_2+H]$^+$).

Synthesis of (E)-2-cyano-3-(5''-(7-(2,4-dipropoxyphenyl)-10-(4-(hexyloxy)phenyl)-10*H*-phenothiazin-3-yl)-[2,2':5',2''-terthiophen]-5-yl)acrylic acid (DMA-3)
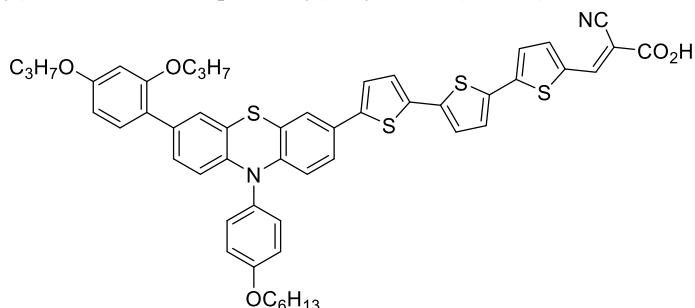
Compound **9** (96 mg, 0.11 mmol) and cyanoacetic acid (362 mg, 4.25 mmol) were dissolved in degassed acetonitrile (50 mL) under nitrogen atmosphere. Piperidine (0.26 mL, 259 mg, 3.0 mmol) was added and the reaction was heated to 80 °C for 2 hours before cooling to room temperature and quenched in HCl (4 M, 90 mL). Dichloromethane (3 × 70 mL) was used to extract the aqueous phase, and the combined organic phases were washed with water (4 × 100 mL), then dried over anhydrous Na_2SO_4, filtered and the solvents were removed *in vacuo*. The crude product was purified by silica gel column chromatography (gradient: 0-15% MeOH in CH_2Cl_2), to obtain sensitizer **DMA-3** as a dark solid (75 mg, 82 µmol, 73%), 244.7-246.4 °C (dec.).

^{1}H NMR (600 MHz, THF-d_8) : δ 8.36-8.04 (m, 1H), 7.77-7.51 (m, 2H), 7.41 (s, 1H), 7.37-7.25 (m, 3H), 7.24-7.19 (m, 2H), 7.18-7.12 (m, 3H), 7.03 (d, J = 7.9 Hz, 1H), 6.95 (d, J = 7.9 Hz, 1H), 6.80 (t, J = 7.9 Hz, 1H), 6.74 (t, J = 7.9 Hz, 1H), 6.67 (s, 1H), 6.21 (d, J = 8.5 Hz, 1H), 6.19 (d, J = 8.5 Hz, 1H), 4.16-4.09 (m, 2H), 4.06 (t, J = 6.7 Hz, 2H), 3.97 (t, J = 6.2 Hz, 2H), 2.00-1.91 (m, 2H), 1.83 (q, J = 7.4 Hz, 2H), 1.78-1.70 (overlapping signal, 2H), 1.57-1.50 (m, 2H), 1.42-1.36 (m, 4H), 1.13 (t, J = 6.9 Hz, 3H), 1.01 (t, J = 7.2 Hz, 3H), 0.94 (t, J = 6.9 Hz, 3H); ^{13}C NMR (150 MHz, THF-d_8) : δ 163.5, 160.3, 157.7, 156.4, 145.9, 145.0, 144.3, 141.0, 140.3, 136.4, 135.8, 135.0, 134.3, 133.5, 133.2 (2C), 133.1, 129.8, 128.7, 128.3, 127.6, 127.4, 125.6, 125.1, 124.8, 123.4, 123.0, 120.8, 120.0, 118.6, 117.7, 117.4 (3C), 116.61, 116.56, 116.1, 106.4, 101.2, 98.9, 71.7, 71.1, 69.1, 32.8, 30.4, 26.9, 23.74, 23.72, 23.66, 14.6, 11.4, 11.3; IR (neat, cm^{-1}) v: 2954 (m), 2851 (m), 2215 (w), 1573 (s), 1463 (s), 1374 (s), 1212 (s), 1159 (s); HRMS (ASAP+, *m/z*): found 865.2618 (calcd. $C_{51}H_{49}N_2O_3S_4$ 865.2626, [M-CO$_2$+H]$^+$).

Synthesis of (E)-2-cyano-3-(5'''-(7-(2,4-dipropoxyphenyl)-10-(4-(hexyloxy)phenyl)-10H-phenothiazin-3-yl)-[2,2':5',2'':5'',2'''-quaterthiophen]-5-yl)acrylic acid (DMA-4)
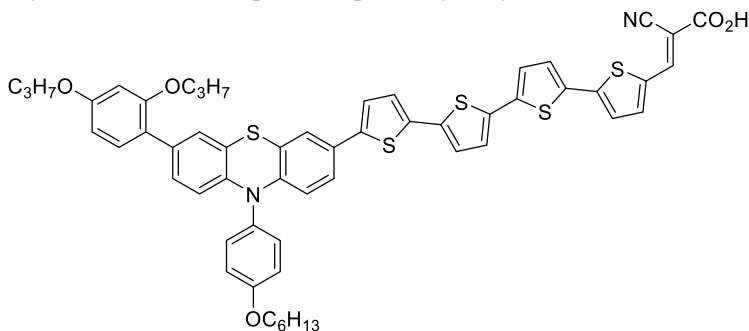
Compound **10** (104 mg, 0.12 mmol) and cyanoacetic acid (226 mg, 2.65 mmol) were dissolved in a mixture of degassed acetonitrile (60 mL) and 1.2-dichloroethane (8 mL) under nitrogen atmosphere. Piperidine (0.16 mL, 137 mg, 1.61 mmol) was added and the reaction was heated to 80 °C for 2 hours before cooling to room temperature and quenched in HCl (4 M, 60 mL). Dichloromethane (3 × 70 mL) was used to extract the aqueous phase, and the combined organic phases were washed with water (4 × 100 mL), then dried over anhydrous Na_2SO_4, filtered and the solvents were removed *in vacuo*. The crude product was purified by silica gel column chromatography (gradient: 0-15% MeOH in CH_2Cl_2), to obtain sensitizer **DMA-4** as a dark solid (84 mg, 84 µmol, 67%), 272.7-273.8 °C (dec.).

^{1}H NMR (600 MHz, THF-d_8) : δ 8.23 (br. s, 1H), 7.62 (br. s, 1H), 7.56 (s, 1H), 7.38 (s, 1H), 7.35-7.28 (m, 3H), 7.26 (s, 1H), 7.23 (d, J = 2.0 Hz, 1H), 7.19-7.11 (m, 5H), 7.09 (s, 1H), 7.03 (dd, J = 8.6, 1.9 Hz, 1H), 6.96 (dd, J = 7.4, 1.3 Hz, 1H), 6.80 (td, J = 7.4, 1.3 Hz, 1H), 6.74 (t, J = 7.3 Hz, 1H), 6.66 (s, 1H), 6.21 (d, J = 8.5 Hz, 1H), 6.19 (d, J = 8.5 Hz, 1H), 4.14-4.08 (m, 2H), 4.06 (t, J = 6.4 Hz, 2H), 3.96 (t, J = 6.1 Hz, 2H), 2.00-1.90 (m, 2H), 1.84 (q, J = 8.1 Hz, 2H), 1.78-1.70 (overlapping signal, 2H), 1.57-1.50 (m, 2H), 1.44-1.35 (m, 4H), 1.13 (t, J = 7.1 Hz, 3H), 1.01 (t, J = 7.5 Hz, 3H), 0.94 (t, J = 6.8 Hz, 3H); ^{13}C NMR (150 MHz, THF-d_8) : δ 168.9, 160.3, 157.6, 156.4, 145.8, 145.0, 144.2, 140.4, 139.3, 138.9, 136.6, 136.2, 136.0, 135.7, 135.6, 134.3, 133.5, 133.2 (2C), 129.8, 128.7, 128.3, 127.6, 127.5, 127.4, 126.2, 126.1, 125.5, 125.0, 124.6, 123.6, 123.3, 123.0, 122.6, 120.8, 120.0, 118.5, 117.4 (3C), 116.62, 116.59, 116.1, 98.9, 71.7, 71.0, 69.1, 32.8, 30.4, 26.9, 23.73, 23.71, 23.65, 14.6, 11.5, 11.3; IR (neat, cm^{-1}) ν: 2966 (m), 2865 (m), 2215 (w), 1574 (s), 1372 (s), 1238 (s), 1178 (s), 784 (s); HRMS (ESI+, *m/z*): found 947.2500 (calcd. $C_{55}H_{51}N_2O_3S_5$ 947.2503, [M-CO$_2$+H]$^+$).

Synthesis of (E)-2-cyano-3-(5-(7-(2,4-dipropoxyphenyl)-10-(4-(hexyloxy)phenyl)-10H-phenothiazin-3-yl)thieno[3,2-b]thiophen-2-yl)acrylic acid (DMA-5)
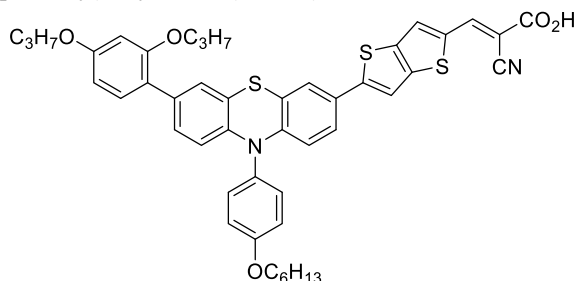
Compound **11** (160 mg, 0.22 mmol) and cyanoacetic acid (410 mg, 4.82 mmol) were dissolved in degassed acetonitrile (25 mL) under nitrogen atmosphere. Piperidine (0.30 mL, 259 mg, 3.0 mmol) was added and the reaction was heated to 80 °C for 2 hours before cooling to room temperature and quenched in HCl (4 M, 50 mL). Dichloromethane (3 × 70 mL) was used to extract the aqueous phase, and the combined organic phases were washed with water (4 × 100 mL), then dried over anhydrous Na_2SO_4, filtered and the solvents were removed *in vacuo*. The crude product was purified by silica gel column chromatography (gradient: 0-15% MeOH in CH_2Cl_2), to obtain sensitizer **DMA-5** as a dark solid (147 mg, 0.184 mmol, 84%), 248.3-250.2 °C (dec.).

^{1}H NMR (600 MHz, THF-d_8) : δ 8.38 (br. s, 1H), 8.25-7.98 (m, 1H), 7.93-7.78 (m, 1H), 7.72-7.56 (m, 1H), 7.33 (d, J = 9.3 Hz, 2H), 7.23 (d, J = 3.5 Hz, 1H), 7.17 (d, J = 9.3 Hz, 2H), 7.05 (d, J = 8.1 Hz, 1H), 6.95 (dd, J = 7.5, 1.5 Hz, 1H), 6.80 (td, J = 7.5, 1.5 Hz, 1H), 6.77-6.65 (m, 2H), 6.22 (d, J = 8.8 Hz, 1H), 6.19 (d, J = 8.8 Hz, 1H), 4.21-4.05 (m, 2H), 4.06 (t, J = 7.0 Hz, 2H), 4.04-3.96 (m, 2H), 2.02-1.92 (m, 2H), 1.84 (q, J = 7.0 Hz, 2H), 1.77 (hx, J = 7.0 Hz, 2H), 1.57-1.51 (m, 2H), 1.44-1.36 (m, 4H), 1.17-1.09 (m, 3H), 1.02 (t, J = 7.0 Hz, 3H), 0.94 (t, J = 7.0 Hz, 3H); ^{13}C NMR (150 MHz, THF-d_8) : δ 164.6, 160.3, 158.9, 157.1, 150.3, 149.3, 148.1, 147.5, 145.8, 144.4, 140.3, 137.9, 134.3, 133.2 (3C), 131.1, 130.5, 128.7, 128.2, 127.6, 127.4, 123.7, 123.0, 120.8, 120.1, 117.4 (3C), 117.2, 116.6, 116.4, 116.1, 98.8, 71.9, 71.1, 69.1, 32.8, 30.4, 26.9, 23.70, 23.67, 23.6, 14.6, 11.4, 11.3; IR (neat, cm^{-1}) ν: 2922 (m), 2869 (m), 2214 (w), 1682 (m), 1407 (s), 1130 (s), 1042 (m), 740 (m); HRMS (ASAP+, m/z): found 757.2600 (calcd. $C_{45}H_{45}N_2O_3S_3$ 757.2592, [M-CO$_2$+H]$^+$).

NMR
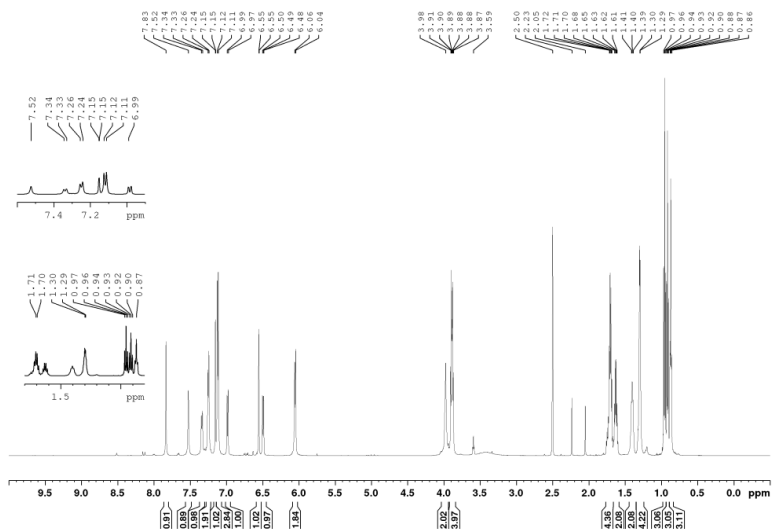
Figure S4. ^{1}H NMR (600 MHz, DMSO-d_6) for dye **DMA-0**.
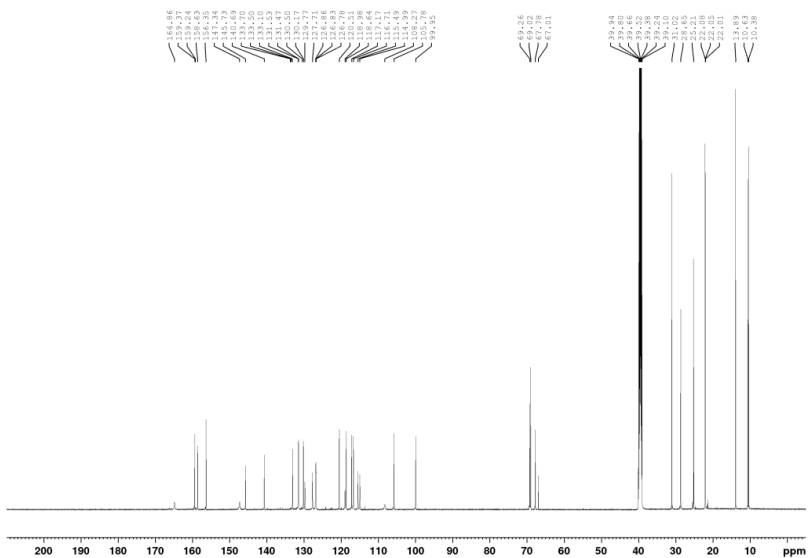
Figure S5. ^{13}C NMR (150 MHz, DMSO-d_6) for dye **DMA-0**.
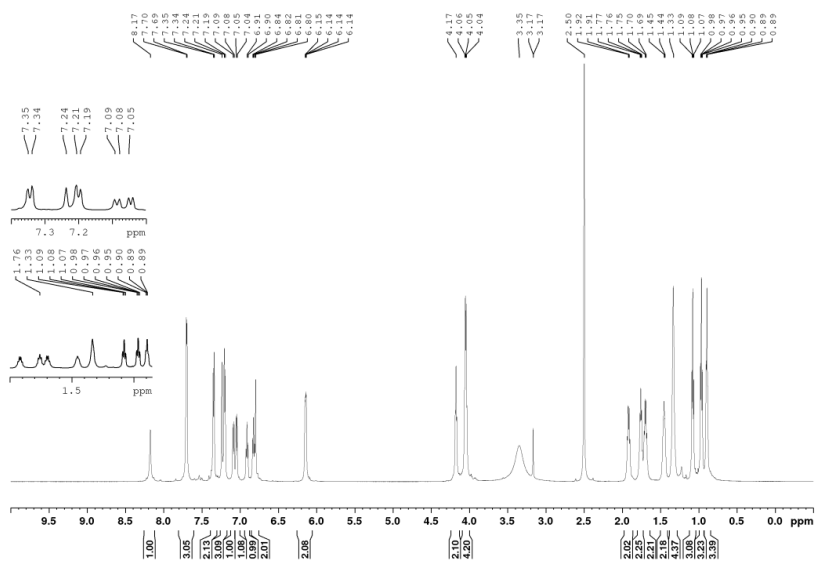
Figure S6. ^{1}H NMR (600 MHz, DMSO-d_6) for dye **DMA-1**.
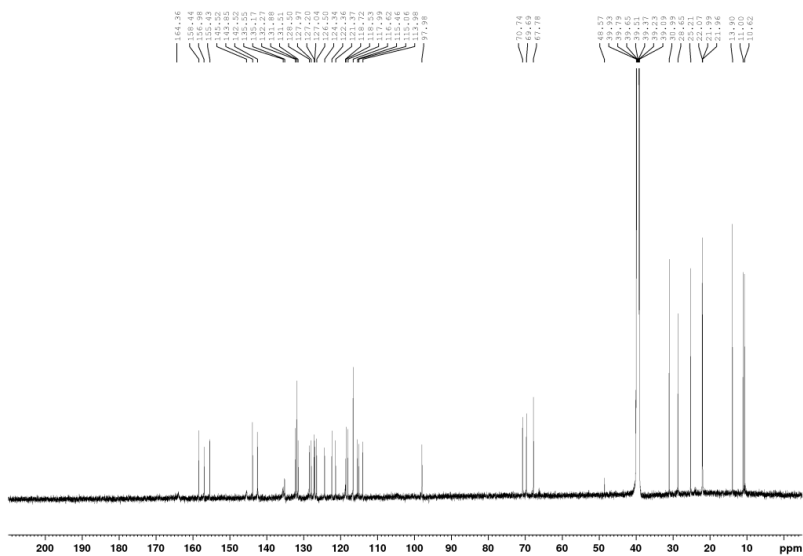
Figure S7. ^{13}C NMR (150 MHz, DMSO-d_6) for dye **DMA-1**.

Figure S8. ^{1}H NMR (600 MHz, DMSO-d_6) for dye **DMA-2**.

Figure S9. ^{13}C NMR (150 MHz, DMSO-d_6) for dye **DMA-2**.

Figure S10. ^{1}H NMR (600 MHz, THF-d_8) for dye **DMA-3**.

Figure S11. ^{13}C NMR (150 MHz, THF-d_8) for dye **DMA-3**.
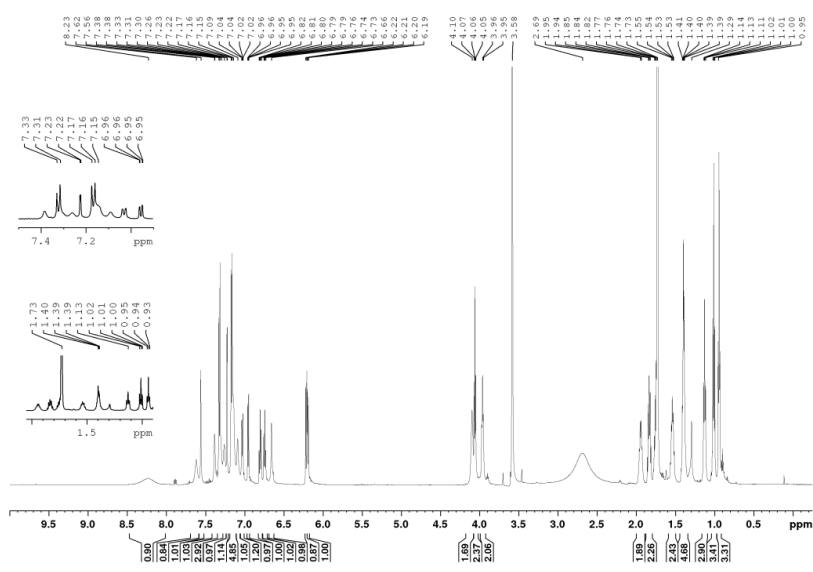
Figure S12. ^{1}H NMR (600 MHz, THF-d_8) for dye **DMA-4**.
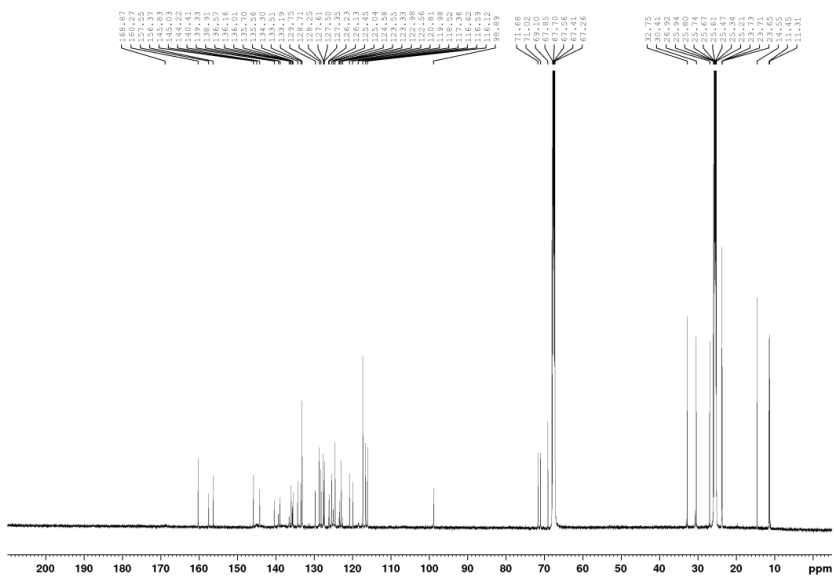
Figure S13. ^{13}C NMR (150 MHz, THF-d_8) for dye **DMA-4**.
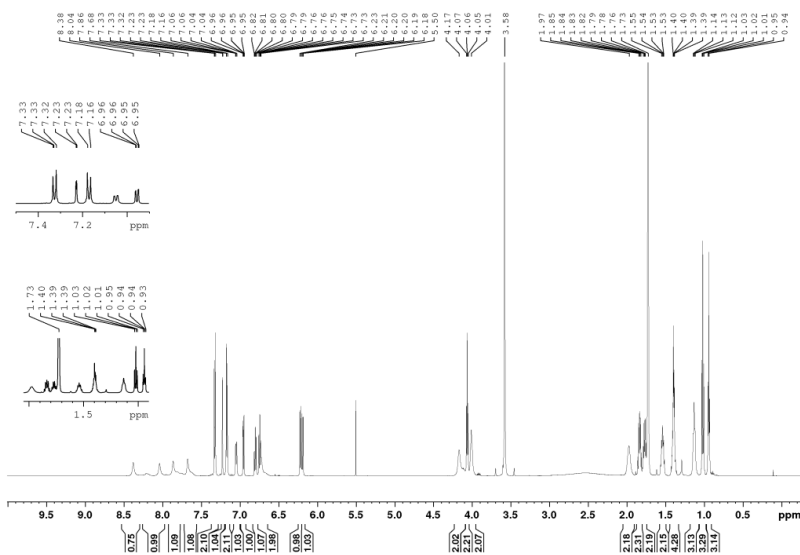
Figure S14. ^{1}H NMR (600 MHz, THF-d_8) for dye **DMA-5**.
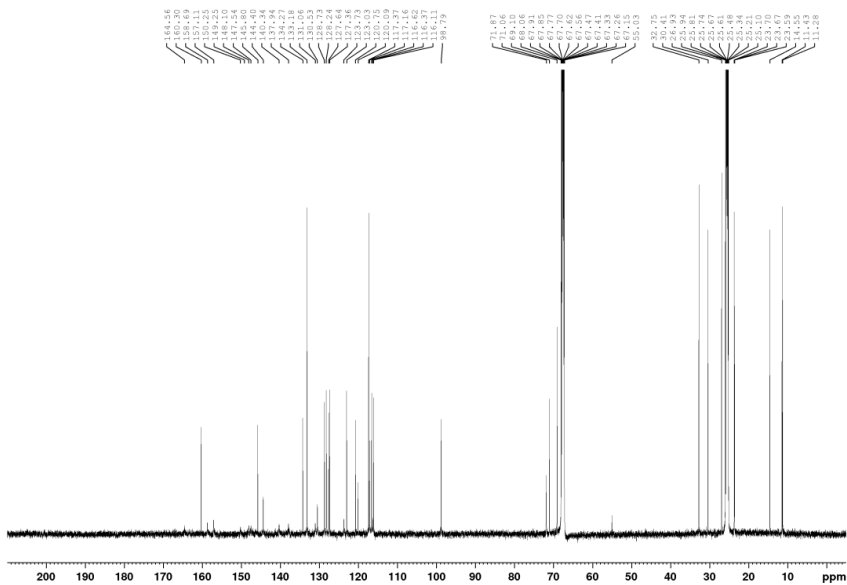
Figure S15. ^{13}C NMR (150 MHz, THF-d_8) for dye **DMA-5**.

References

[1] Fabregat-Santiago F, Bisquert J, Palomares E, Otero L, Kuang D, Zakeeruddin SM, et al. Correlation between Photovoltaic Performance and Impedance Spectroscopy of Dye-Sensitized Solar Cells Based on Ionic Liquids. The Journal of Physical Chemistry C. 2007;111(17):6550-60.

[2] Pavlishchuk VV, Addison AW. Conversion constants for redox potentials measured versus different reference electrodes in acetonitrile solutions at 25°C. Inorganica Chimica Acta. 2000;298(1):97-102.

[3] Bejan A, Shova S, Damaceanu M-D, Simionescu BC, Marin L. Structure-Directed Functional Properties of Phenothiazine Brominated Dyes: Morphology and Photophysical and Electrochemical Properties. Crystal Growth & Design. 2016;16(7):3716-30.

[4] Cheng J, Liang X, Cao Y, Guo K, Wong W-Y. Aldehyde end-capped terthiophene with aggregation-induced emission characteristics. Tetrahedron. 2015;71(34):5634-9.

[5] Yassar A, Videlot C, Jaafari A. Synthesis and photovoltaic properties of mono-substituted quaterthiophenes bearing strong electron-withdrawing group. Solar Energy Materials and Solar Cells. 2006;90(7):916-22.

[6] Chen R, Yang X, Tian H, Wang X, Hagfeldt A, Sun L. Effect of Tetrahydroquinoline Dyes Structure on the Performance of Organic Dye-Sensitized Solar Cells. Chemistry of Materials. 2007;19(16):4007-15.

[7] Liu J, Li R, Si X, Zhou D, Shi Y, Wang Y, et al. Oligothiophene dye-sensitized solar cells. Energy & Environmental Science. 2010;3(12):1924-8.

[8] Zhu S, An Z, Sun X, Wu Z, Chen X, Chen P. Synthesis and evaluation of simple molecule as a co-adsorbent dye for highly efficient co-sensitized solar cells. Dyes and Pigments. 2015;120:85-92.

Paper II

D. M. Almenningen, H. E. Hansen, A. F. Buene, B. H. Hoff and O. R. Gautun

Effect of seven different terthiophene π-spacers on dye performance in dye-sensitized solar cells,

Paper II

Paper II

Effect of seven different terthiophene π-spacers on dye performance in dye-sensitized solar cells

David Moe Almenningen[a], Henrik Erring Hansen[b], Audun Formo Buene[c], Bård Helge Hoff[a], Odd Reidar Gautun[a]*

[a] Department of Chemistry, Norwegian University of Science and Technology, Høgskoleringen 5, 7491 Trondheim, Norway

* Corresponding author. Tel.: +47 73594101; E-mail address: odd.r.gautun@ntnu.no (O. R. Gautun).

[b] Department of Materials Science and Engineering, Norwegian University of Science and Technology, Sem Sælands vei 12, 7491 Trondheim, Norway

[c] Department of Civil and Environmental Engineering, Norwegian University of Science and Technology, Høgskoleringen 7a, 7034 Trondheim, Norway.

Abstract

To ensure high photocurrents from dye-sensitized solar cells (DSSC), it is important that the dye absorbs as much of the energy from the sunlight as possible. To achieve a wide absorption and cover larger parts of the solar spectrum, dyes are frequently fitted with oligothiophene π-spacers. We wish to examine the terthiophene motif as π-spacers in triarylamine dyes and evaluate the suitability of using these in modern copper based DSSC devices. The foundation for this analysis will be the series of seven novel dyes (**DMA-6** – **DMA-12**) which all are fitted with the same donor and acceptor, but linked with seven different terthiophene motifs. The photovoltaic performance of the dyes show that the smallest π-spacer in the series, dithieno[3,2-b:2′,3′-d]thiophene, was the most efficient. The DSSC device sensitized by this dye achieved a power conversion efficiency of 4.4% (J_{sc} = 7.0 mA cm^{-2}, V_{oc} = 0.95 V, FF = 0.66). The photovoltaic performance of the dyes was tested in devices with two different TiO$_2$ thicknesses, and we established that the thinner TiO$_2$ yielded the best DSSC performance for all the dyes. Electrochemical impedance spectroscopy revealed that the thicker semiconductor layer resulted in a reduction of the effective electron diffusion length.

Keywords: Oligothiophene, triarylamine dye, dye-sensitized solar cells, terthiophene, Cu redox shuttle

1. Introduction

The dye-sensitized solar cell (DSSC), first reported by O'Regan and Grätzel back in 1991[1], is a photovoltaic technology with an impressive ability to tune properties such as color, transparency, and flexibility. The ability to tune color and transparency have made the DSSC a desirable technology for use in in building-integrated photovoltaics[2, 3]. While the tunable flexibility has been successfully utilized for integrating the DSSC in wearable devices[4]. More than 30 years of research and development on the DSSC technology have led to devices that vary greatly in materials and methods used in the fabrication of DSSC devices. It is however still possible to identify three key components present in a typical DSSC device, i) the semiconducting mesoporous metal oxide, commonly TiO_2 ii) the sensitizer coating the metal oxide responsible with light harvesting and electron injection into the TiO_2 iii) the redox shuttle responsible with regenerating the oxidized sensitizer[5]. Recent advances have been made on developing copper-based redox shuttles[6]. These severely reduced overpotential losses that previously plagued the DSSC devices operating with iodine redox shuttles. DSSCs utilizing the novel copper complexes have recently become the most efficient technology for ambient light photovoltaics[7, 8], making it a very promising energy source for electronics requiring low power.

To successfully take advantage of the novel copper electrolyte, there are certain requirements needed in the design of sensitizers. The redox potentials of the most common copper complexes are found in the range 0.87-0.97 V *vs.* standard hydrogen electrode (SHE)[6], significantly higher than that of the I^-/I_3^- redox shuttle at around 0.40 V *vs.* SHE[9]. This requires the design of dyes with oxidation potentials that are high enough to be regenerated by the copper complexes, and it has been shown that a 10 mV driving force for regeneration is sufficient[6]. Replacing the two-electron redox shuttle I^-/I_3^- with one-electron metal complexes led to a facilitation of the recombination of electrons in the TiO_2 with oxidants in the redox shuttle[10, 11]. This required dyes to be designed with alkyl chains that provide an insulating effect and prevents the redox complexes from approaching the TiO_2 surface. The tetra-alkoxy substituted triarylamine donor, referred to as the Hagfeldt donor, is a molecular motif that meets these two requirements expertly[12]. This donor provides excellent shielding of the TiO_2 surface and the reduction in electron recombination has allowed for devices with excellent photovoltages[8]. The downside of the triarylamine dyes is the limited light harvesting ability compared to other donors such as ullazine[13]. To improve the absorption properties of triarylamine dyes, they are frequently fitted with large π-spacers to improve the photocurrent[11, 14, 15].

In our previous study on π-spacers we found that the terthiophene π-spacer produced the highest photocurrent in dyes employing a phenothiazine donor[16]. Terthiophene is a simple oligothiophene unit comprised of three thiophenes, and over the years numerous variations of terthiophene motifs have been incorporated in dyes for DSSC[17-24]. To exploit the terthiophene light harvesting ability in a copper based DSSC device, we prepared a novel series of dyes with the Hagfeldt donor. Identifying important dye structure-performance relationships in the field of DSSC is difficult, since most studies

focus on only a few dyes, and there is significant variation in data for the same dye[25]. We have previously demonstrated the merit of synthesizing dye libraries to investigate various aspects of dye design such as π-spacers[26-29], auxiliary donors[30-32], or dye geometries[33, 34]. Therefore, we designed and synthesized seven novel dyes with different terthiophene motifs, and the structures of the dyes are shown in Figure 1. With dyes **DMA-6** – **DMA-12** we aimed to investigate the effect of the terthiophene structure on the optoelectronic properties of the sensitizers. We further wanted to identify traits of successful terthiophene π-spacers based on the photovoltaic performance of the dyes.
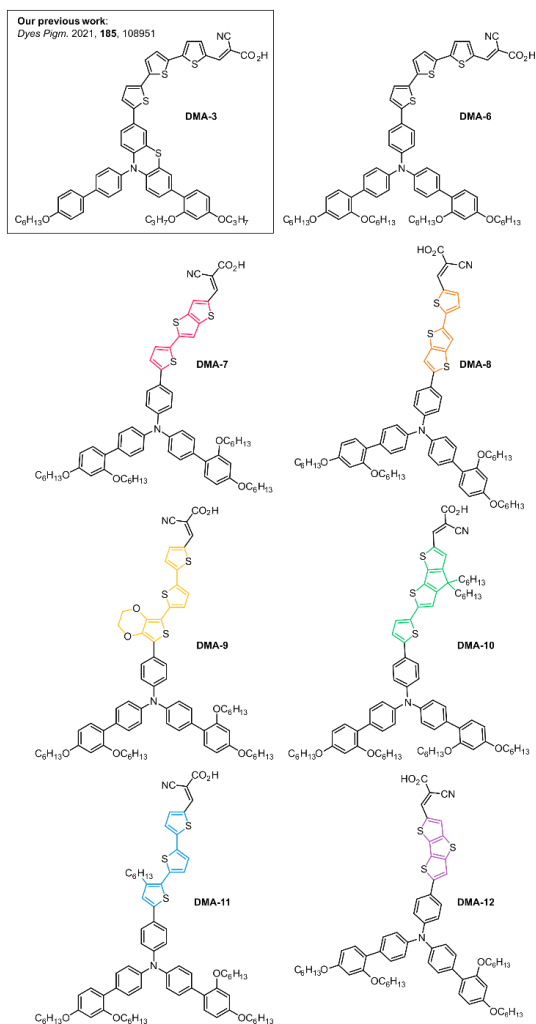
Figure 1. *The structure of the seven novel dyes* **DMA-6** *–* **DMA-12**, *and the previously investigated dye,* **DMA-3**.

2. Results and Discussion

2.1 Dye synthesis

The dyes reported herein was prepared following the two-step synthesis route shown in Scheme 1. The synthesis is based on the successful convergent/divergent synthesis approach reported by Gabrielsson et al[11]. A full synthetic account is given in the ESI. The advanced triarylamine donor fragment **1** was prepared as described in our previous report[35]. Compound **1** was coupled to the different π-spacer fragments, **2a-2g**, in a Suzuki-Miyaura cross-coupling. Excluding **2d**, all the π-spacer fragments underwent satisfactory reactions using Pd(OAc)$_2$/SPhos, and gave the corresponding dye precursors in yields of 22-55%. The brominated ethylenedioxythiophene **2d** decomposed under the initial reaction conditions, which led us to change the catalyst to PdCl$_2$(dppf) and we were able to produce and isolate enough of **3d** to prepare sufficient amounts of the resulting sensitizer **DMA-9**. Following the Knoevenagel condensation procedure reported by Iqbal et al.[36], the finished sensitizers, **DMA-6** – **DMA-12**, were prepared and isolated in yields of 63-99%.
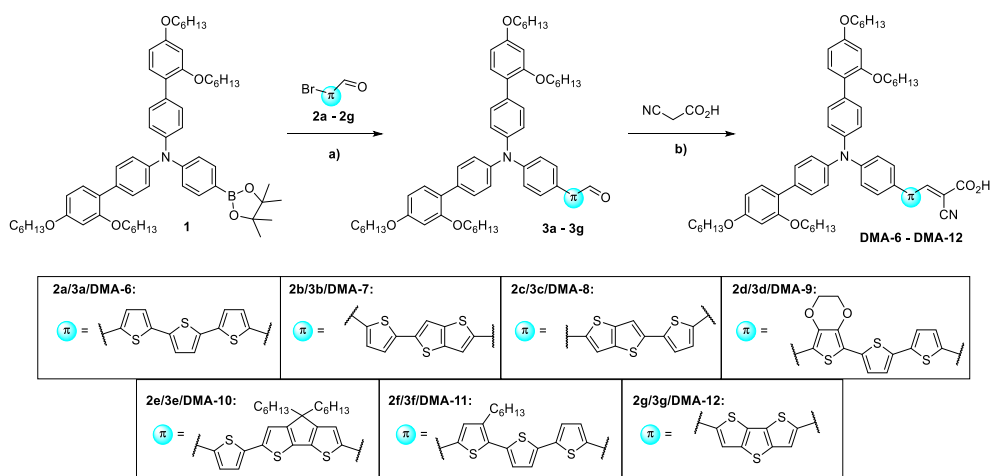
Scheme 1. *Our two-step synthesis route for the preparation of dyes **DMA-6** – **DMA-12**. a) Suzuki Miyaura cross-coupling catalyzed by either Pd(OAc)$_2$/SPhos or PdCl$_2$(dppf). b) Knoevenagel condensation mediated by piperidine.*

2.2 Photophysical properties

Altering the aromatic system of the π-spacer in D-π-A dyes is known to affect the optical properties of the resulting chromophores[37]. To measure the effect of the various π-spacers on the optical properties of the dyes, we performed UV/Vis spectroscopy on the dyes in a dichloromethane solution (2 · 10^{-5} M) and on dye-stained TiO$_2$ electrodes (2.5 μm, 18NR-T, Greatcell Solar). The results from these measurements are shown in Figure 2, and an overview of the obtained data is given in Table 1. In solution, the standard terthiophene-linked dye, **DMA-6**, display an absorption maximum of 481 nm. Remarkably, the absorption maxima of four of the other dyes (**DMA-7**, **DMA-8**, **DMA-11**, **DMA-12**) are found within 4 nm of the standard dye, **DMA-6**. This is surprising considering that the aromatic

system of **DMA-7** and **DMA-8** contains two fewer p-electrons and for **DMA-12** it contains four fewer p-electrons. The resulting aromatic system is more planar however, and this is likely the reason why the absorption is not blueshifted by the smaller π-spacers. Another striking effect of planarizing the aromatic system is seen for the dye **DMA-10**, where the absorption maxima of this dye is redshifted 61 nm compared to the standard terthiophene dye (**DMA-6**). The molar extinction coefficient of this dye (55900 M^{-1} cm^{-1}) is also significantly higher than the other dyes in this series, and comparable to that of the benchmark dye **Y123** (57300 M^{-1} cm^{-1}). We also see that substituting one thiophene for ethylenedioxythiophene is a successful strategy for redshifting absorption, as the absorption maxima of **DMA-9** is 22 nm redshifted compared to **DMA-6**. The redshift can be explained by the increased electron donating ability of the ethylenedioxythiophene compared to thiophene. It is also likely that there are non-covalent S-O interactions occurring between ethylenedioxythiophene and the neighboring thiophene. Such interactions have previously been shown to provide conformational locks and increase the planarity of the aromatic system[38, 39].

The absorption maxima were blueshifted for all the dyes when comparing the UV/Vis spectra of the stained TiO_2 electrodes to the spectra obtained in dichloromethane solution. Attaching dyes on TiO_2 is frequently associated with blueshifts of absorption, the deprotonation of the anchoring groups and the formation of H-aggregates are the likely causes for this behavior[17, 40]. The absorption maximum of the dye **DMA-10** was blueshifted the most upon being absorbed on TiO_2. Despite this, the absorption maximum of 498 nm was the highest of the dyes in this series, in addition it was also redshifted compared to the benchmark dye **Y123** (481 nm). The ethylenedioxythiophene unit is also highly successful in extending the light harvesting region of the dye, as demonstrated by the significantly redshifted absorption onset of **DMA-9** on TiO_2.

To further investigate the effect of the different π-spacers we calculated the optical band gaps, E_{0-0}, from the intersection between the normalized absorption and emission spectra shown in Figure S1. The unmodified terthiophene dye, **DMA-6**, display a band gap of 2.29 eV which is consistent with our previously reported terthiophene dye (**DMA-3**) with a band gap of 2.38 eV[16]. We also see that all the other terthiophene motifs reported in this paper produce smaller optical band gaps than the reference dye **DMA-6**. The two structural isomers **DMA-7** and **DMA-8** display similar optical band gaps, showing that the position of the fused bithiophene unit does not affect the band gap of the chromophore. By employing a fully fused terthiophene π-spacer, as seen for **DMA-12**, the band gap is reduced further to 2.17 eV. The most pronounced effect is seen for the cyclopentadithiophene modified dye, **DMA-10**, where the optical band gap is 0.21 eV smaller than the reference dye **DMA-6**.
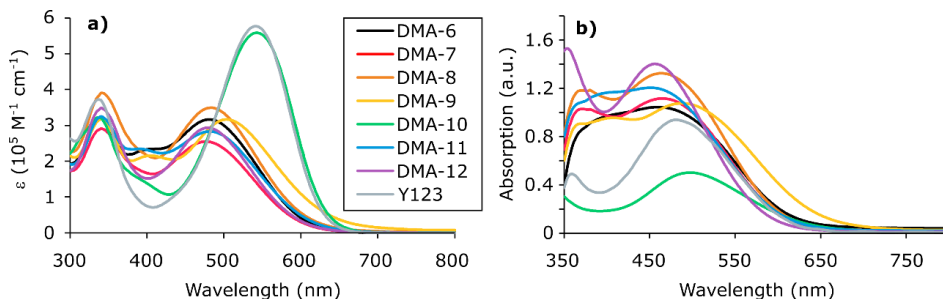
Figure 2. *Absorption spectra of all dyes a) in dichloromethane solution, b) on TiO$_2$ films (2.5 µm, 18NR-T, Greatcell Solar).*

Table 1. *Photophysical and electrochemical properties of dyes in the series.*

Dye	λ_{abs}[a] (nm)	ε (M^{-1}cm^{-1})	Em.[b] (nm)	λ_{abs}[c] on TiO$_2$ (nm)	E_{0-0}[d] (eV)	E_{ox}[e] (V vs. SHE)	E_{LUMO}[f] (V vs. SHE)
DMA-6	481	31700	600	459	2.29	1.09	-1.20
DMA-7	477	25500	614	465	2.25	1.10	-1.15
DMA-8	483	35000	618	464	2.24	1.10	-1.14
DMA-9	503	31700	632	488	2.16	0.96	-1.20
DMA-10	542	55900	691	498	2.08	1.01	-1.07
DMA-11	481	28300	635	451	2.25	1.05	-1.20
DMA-12	479	29400	705	456	2.17	1.11	-1.06

[a] *Maximum of most redshifted peak.* [b] *Emission when ICT band is excited, in DCM solution.* [c] *Maximum of most redshifted peak on TiO$_2$ (2.5 µm, GreatcellSolar 18NR-T).* [d] *Calculated from the intersection of the absorption and normalized emission spectra.* [e] *Measured vs. Fc$^+$/Fc on stained TiO$_2$ electrodes in acetonitrile with 0.1 M LiTFSI, converted to V vs. SHE by 0.624 V. Scan rate 10 mV s^{-1}.* [f] *Calculated from E$_{ox}$-E$_{0-0}$.*

2.3 Electrochemical properties

Alterations of the aromatic system of D-π-A dyes are likely to affect the electronic properties as well as the optical properties. To quantify this effect, we carried out cyclic voltammetry (CV) experiments on stained TiO$_2$ electrodes for all the dyes in the series. The obtained voltammograms are shown in Figure S2, and the energy levels of the frontier orbitals are found in Table 1. The oxidation potential of the reference dye, **DMA-6**, was found at 1.09 V *vs.* SHE. This demonstrates the benefit of switching from a phenothiazine donor to a triarylamine donor, as our previously reported terthiophene dye displayed a 13 mV lower oxidation potential[16]. Four other dyes (**DMA-7**, **DMA-8**, **DMA-11**, **DMA-12**) were all found within 4 mV of the reference dye and with sufficient driving force for regeneration with a Cu(dmp)$_2$$^{1+/2+}$ based redox shuttle (redox potential of 0.93 V *vs.* SHE)[6]. The dye **DMA-10**, with its oxidation potential of 1.01 V *vs.* SHE, is narrowly outside of the 10 mV driving force potential that has been shown previously to be sufficient[6]. While the dye **DMA-9** has an oxidation potential

(0.96 V *vs*. SHE) that is expected to be too low to be effectively regenerated by $Cu(dmp)_2^{1+/2+}$. By employing these dyes in DSSCs with a $Cu(dmp)_2^{1+/2+}$ based redox shuttle we will further investigate the driving force requirements for this electrolyte.

Figure 3. *Energy levels of the frontier orbitals for the sensitizers in this study, R = C_6H_{13}.*

2.4 Photovoltaic properties

The photovoltaic performance of the different sensitizers in this study was measured by preparing DSSC devices sensitized by each dye. The results from these measurements are given as averages of three devices in Table 2, and the *J-V* curve of the best performing device for each dye is shown in Figure 4. We have previously demonstrated the benefit of increasing the thickness of the active TiO_2 layers in DSSCs employing copper redox shuttles[35]. Based on this, we set out to prepare devices with varying film thickness of the active 30NR-D TiO_2 layer (4.5 μm and 9.0 μm) while keeping the thickness of the scattering WER2-O TiO_2 layer fixed (4.5 μm).

Based on the series of dyes **DMA-6** – **DMA-12**, we can identify certain successful traits in the various terthiophene designs. There is a massive benefit in putting the thieno[3,2-b]thiophene unit on the donor side of the π-spacer, as demonstrated by comparing the photovoltaic performance of the structural isomers **DMA-7** and **DMA-8**. When we examine the incident photon-to-current efficiency (IPCE) spectra, shown in Figure 5, we see that the dye **DMA-8** outperforms its analog throughout the entire range of wavelengths. This translates to an improvement in J_{sc} from 5.1 to 6.4 mA cm^{-2} (25% improvement) in the thin TiO_2 devices, and an improvement from 4.3 to 5.7 mA cm-2 (33% improvement) in the thicker TiO_2. Under the optimal thin TiO_2 conditions, the hexyl substituted terthiophene (**DMA-11**) yielded an 24% increase in PCE compared to the non-modified terthiophene

(**DMA-6**). Under the same conditions, the fully fused terthiophene of **DMA-12** improved the PCE by 33% compared to the standard terthiophene of **DMA-6**. The dye **DMA-12** under thin film conditions proved to be the most efficient device in the series, delivering a PCE of 4.4% (J_{sc} = 7.0 mA cm^{-2}, V_{oc} = 0.95 V, FF = 0.66).

Conversely, the PCE data of this series of dyes also highlights terthiophene design concepts to avoid in the future. This is perhaps most striking when we consider that the performance of the dyes in this series was also compared to the known benchmark dye **Y123,** which in molecular structure closely resembles the dye **DMA-10**. The only difference between these two dyes is that **Y123** has one thiophene less in the π-spacer. Although the absorption properties of **DMA-10** are similar to that of **Y123** in solution, this does not translate into improved short-circuit current (J_{sc}) for the larger dye. The larger π-spacer of **DMA-10** leaves it more susceptible to aggregate than the more concise dye **Y123.** This could be part of the reason why the photovoltaic performance drops so severely by the introduction of an additional thiophene in the π-spacer of **DMA-10**. The formation of H-aggregates when dyes are sensitized on TiO$_2$ is known to blueshift absorption and also promote excited state quenching[41], both of which are deleterious for solar cell performance. The extra thiophene unit also lowered the oxidation potential from 1.07 V *vs*. SHE for **Y123** to 1.01 V vs. SHE for **DMA-10**, which leaves the driving force for regeneration of the latter dye at only 8 mV in the redox shuttle employed in this study. A large number of oxidized dye molecules not being effectively regenerated, is expected to contribute to the low J_{sc} produced by a dye with such a wide range of absorption as **DMA-10**. The effect of low oxidation potentials is even more apparent when we consider the photovoltaic performance of the dye **DMA-9**, which has a mere 3 mV driving force for regeneration. Despite possessing improved absorption properties in solution and while sensitized on TiO$_2$ compared to the other dyes in the series, the dye **DMA-9** produces the lowest J_{sc}-values of all the dyes reported herein. As a result, the photovoltaic performance of the dye **DMA-9** is by far the worst, and highlights the importance of dyes having oxidation potentials that matches the redox shuttle.

In a recent paper by Velore et al.[42] they highlight the potential pitfalls of using thicker TiO$_2$ layers and copper redox shuttles together, under 1 sun illumination this strategy can lead to devices suffering from mass transport issues. The results obtained herein support this finding, as all the dyes perform better in the thin TiO$_2$ devices. The two most efficient dyes, **DMA-11** and **DMA-12**, were also the dyes that displayed the most drastic decrease in performance when going from a thinner active TiO$_2$ layer to a thicker one. This suggest that these two dyes suffer the most from mass transport issues in a 9 μm TiO$_2$ device, which could indicate that they form the most closely packed dye layers and limit the movement of the redox shuttle the most.

Table 2. *Photovoltaic performance of all dyes under 1 sun AM 1.5G illumination, given as averages of three separate DSSC devices. Along with the integrated current density from IPCE measurements. Results from dye loading experiments is also included.*

Dye	TiO$_2$ (µm)[a]	IPCE J_{sc} (mA cm^{-2})[b]	J_{sc} (mA cm^{-2})	V_{oc} (V)	FF	PCE (%)	Dye loading (10^{-8} mol cm^{-2})[c]
DMA-6	4.5	7.54	6.1 ± 0.2	0.89 ± 0.01	0.61 ± 0.05	3.3 ± 0.2	8.4 ± 0.4
	9	6.74	5.0 ± 0.3	0.85 ± 0.00	0.66 ± 0.00	2.8 ± 0.2	17.5 ± 0.3
DMA-7	4.5	5.58	5.1 ± 0.2	0.87 ± 0.00	0.63 ± 0.05	2.8 ± 0.3	8.9 ± 0.9
	9	5.82	4.3 ± 0.2	0.84 ± 0.00	0.65 ± 0.05	2.4 ± 0.2	11.5 ± 0.3
DMA-8	4.5	7.25	6.4 ± 0.3	0.91 ± 0.00	0.59 ± 0.02	3.4 ± 0.2	10.5 ± 1.1
	9	7.75	5.7 ± 0.2	0.86 ± 0.01	0.64 ± 0.02	3.1 ± 0.1	13.1 ± 1.7
DMA-9	4.5	4.50	3.1 ± 0.4	0.78 ± 0.01	0.55 ± 0.04	1.3 ± 0.2	7.3 ± 0.4
	9	2.84	2.3 ± 0.0[d]	0.75 ± 0.01[d]	0.48 ± 0.01[d]	0.8 ± 0.0[d]	22.2 ± 0.5
DMA-10	4.5	6.84	5.9 ± 0.2	0.83 ± 0.00	0.68 ± 0.00	3.3 ± 0.1	12.5 ± 1.6
	9	7.00	5.7 ± 0.1	0.81 ± 0.00	0.65 ± 0.01	3.0 ± 0.0	17.4 ± 0.3
DMA-11	4.5	8.77	7.0 ± 0.0	0.94 ± 0.00	0.62 ± 0.01	4.1 ± 0.1	11.3 ± 0.5
	9	7.12	5.5 ± 0.5	0.86 ± 0.01	0.52 ± 0.01	2.5 ± 0.3	23.2 ± 0.1
DMA-12	4.5	8.32	7.0 ± 0.2	0.95 ± 0.02	0.66 ± 0.01	4.4 ± 0.2	12.2 ± 0.6
	9	6.11	4.1 ± 0.3	0.83 ± 0.01	0.41 ± 0.02	1.4 ± 0.1	14.1 ± 1.2
Y123[e]	4.5	11.30	9.9	0.95	0.68	6.4	13.8 ± 0.9
	9	11.30	8.8	0.93	0.58	4.7	18.6 ± 0.2

[a] Thickness of active 30 NR-D layer, the scattering WER2-O layer was fixed at 4.5 µm [b] Obtained by integration of the IPCE spectrum over the 1 sun AM 1.5 G spectrum. [c] Values averaged of two desorbed TiO$_2$-electrodes. [d] Average values of two cells. [e] Values from best-performing device.

Figure 4. *J-V curves for the best parallel of each dye, obtained under 1 sun AM 1.5G illumination a) 4.5 µm TiO$_2$ devices b) 9 µm TiO$_2$ devices.*

Figure5. *IPCE spectra of the best performing parallel for each dye a) 4.5 μm TiO₂ devices b) 9 μm TiO₂ devices.*

2.5 Electrochemical impedance spectroscopy

To evaluate the influence of TiO$_2$ thickness on the electron transport properties of the dyes we examined the effective electron diffusion length (L_n), and the results are shown in Figure 6. The effective electron diffusion length is a measure of the competition between charge collection and charge recombination[43], and is given by

$$L_n = L \sqrt{\frac{R_{rec}}{R_{tr}}} \tag{1}$$
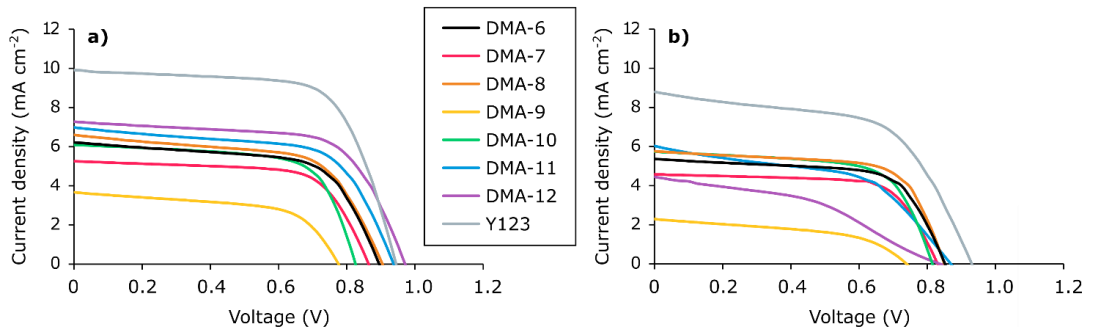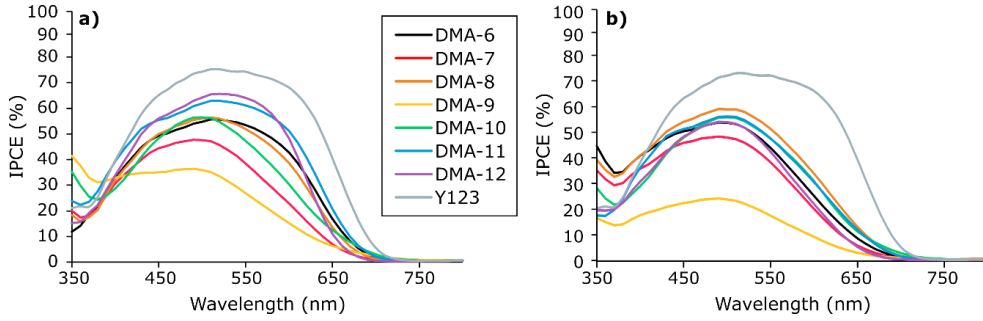
where L is the film thickness, R_{rec} is the recombination resistance and R_{tr} is the transport resistance. The two resistances were obtained from electrochemical impedance spectroscopy (EIS), and the complex plane plots and resistance data extracted from the EIS measurements are shown in Figure S3-S6 in the ESI. We see that the dye **DMA-12** in the 4.5 μm TiO$_2$ devices provide by far the best L_n values of the dyes in this series, which is largely owed to the significantly lower transport resistance in this DSSC device. This could indicate that the smallest π-spacer ensures the highest electron density in the TiO$_2$, possibly from an increased electron injection efficiency. When considering the effective electron diffusion length of the devices with different TiO$_2$ film thickness, we see a detrimental effect from the thicker metal oxide layers. Excluding **DMA-9**, all the dyes have reduced L_n values in the thicker TiO$_2$ devices. The effective electron diffusion lengths displayed in Figure 6 b) show that these devices are described by Gerischer impedance[44], where the transport resistance is larger than the recombination resistance. This highlights and confirms the need for thinner TiO$_2$ layers in devices employing copper complex redox shuttles.
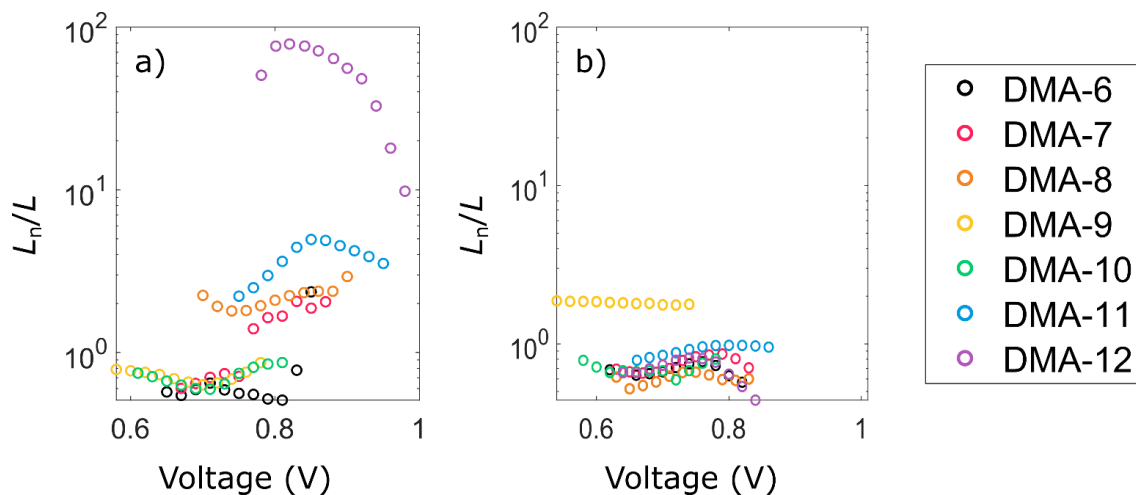
Figure 6. The ratio of effective electron diffusion length and TiO₂ film thickness a) for 4.5 µm active TiO₂ devices b) for 9 µm active TiO₂ devices.

3. Conclusion

We have successfully synthesized a series of seven novel dyes with varying terthiophene π-spacer motifs and shown the merit of the convergent/divergent synthesis approach to prepare libraries of dyes. We have demonstrated that reducing the size of the terthiophene aromatic system through fused bithiophenes (**DMA-7** and **DMA-8**) or fused terthiophene (**DMA-12**) does not blueshift the absorption maximum. In addition, all modifications to the terthiophene unit reported herein resulted in a smaller optical band gap compared to the reference sensitizer **DMA-6**. Through photovoltaic characterization, we were able to identify the hexyl-substituted terthiophene (**DMA-11**) and the fully fused terthiophene (**DMA-12**) as the most successful π-spacer motifs. Alas, the dyes displaying the best absorption properties (**DMA-9** and **DMA-10**) had their HOMO energy levels lowered too much to be used effectively in the copper redox shuttle. It is however an exciting prospect to take advantage of the improved absorption of these dyes in devices with redox shuttles that are more compatible such as cobalt complexes. Through EIS experiments we also confirmed the deleterious effect of using thick TiO₂ layers in copper regenerated devices, as all the 9 µm TiO₂ devices showed a Gerischer behavior.

4. Experimental

4.1 Materials and reagents

The donor moiety was prepared following our previously reported procedure[35]. The π-spacers, 5″-bromo[2,2′:5′,2″-terthiophene]-5-carboxaldehyde (**2a**)[16], 5-(5-bromothiophen-2-yl)thieno[3,2-b]thiophene-2-carbaldehyde (**2b**)[45], 5-(5-bromothieno[3,2-b]thiophen-2-yl)thiophene-2-carbaldehyde (**2c**)[46], 5″-bromo-3″-hexyl-[2,2′:5′,2″-terthiophene]-5-carbaldehyde (**2f**)[47], 6-bromodithieno[3,2-b:2′,3′-d]thiophene-2-carboxaldehyde (**2g**)[48], were prepared from literature procedures. The starting material, 6-bromo-4,4-dihexyl-4H-cyclopenta[2,1-b:3,4-b′]dithiophene-2-carbaldehyde, for the synthesis of π-spacer fragment **2e** was prepared according to a literature procedure[49].

The benchmark dye **Y123**, and the copper complexes $Cu^{(I)}(dmp)_2(TFSI)$ and $Cu^{(II)}(dmp)_2(TFSI)_2$ were purchased from Dyenamo AB (Sweden). The remaining chemicals were purchased from Merck (Germany) unless specified otherwise.

4.2 Fabrication of dye-sensitized solar cells

The anodes were prepared from FTO glass (NSG10, Nippon Sheet Glass), which was first cleaned in a Deconex 21-solution (2 g/L) under sonication for 45 minutes. Next the FTO was treated with UV/O_3 (Novascan PSD PRO-UV T6) for 15 minutes. Immersion of the glass in aqueous $TiCl_4$-solution (40 mM) at 70 °C for 2 × 45 minutes followed by rinsing with deionized water and ethanol was carried out to deposit a blocking layer on the FTO-sample. Pastes of TiO_2 were screen printed onto the FTO (mesh count 54, thread diameter 64 mm, area 0.2826 cm^2), for the 4.5 μm devices one active layer (30NR-D, Dyesol) was printed. For the 9 μm devices two active layers were printed with 5 minutes heating on a hotplate at 125 °C after each layer. A scattering layer (WER2-O, Dyesol) was ultimately printed, and the TiO_2 was sintered in a programmable furnace (Nabertherm LT 9/12) at set temperatures of 125, 250, 325, 450, and 500 °C for 5, 5, 5, 15, and 15 minutes with a ramping time of 10 minutes. The thickness of the TiO_2 layers were measured with a Veeco Dektak 150 profilometer. Before staining, the electrodes were annealed at 500 °C for 30 minutes using a hotplate.

The counter electrodes were prepared from TEC10 FTO glass supplied by Sigma Aldrich. Holes were drilled into the electrodes from the FTO-side using a diamond drill bit, this procedure was carried out under water. The glass plates were then cleaned using Deconex 21 (aq., 2 g/L), deionized water, ethanol, and acetone, in a ultrasonic bath for 15 minutes for each. A catalytic layer of PEDOT was formed following the electrochemical deposition procedure reported by Ellis et al[50].

The photoanodes were placed in the dye bath while still holding ~ 80 °C from the annealing procedure and stored in an oven at 30 °C overnight. The dye baths were prepared using a mixture of *t*-BuOH, MeCN and THF (1:1:1, v/v) to make a solution of dye and co-adsorbent CDCA, at concentrations of 0.1 mM and 1 mM respectively. The staining of the benchmark dye **Y123** was done similarly, but the solvents used was in this case *t*-BuOH and MeCN (1:1, v/v). Following 15 hours of staining the electrodes were rinsed in acetonitrile for 2 minutes, then sealed to the counter electrode using Surlyn (25 μm, Solaronix) in a drybox. A 4×20 second treatment of the cell using a 50 W PTC heat element was sufficient to seal the cells. The electrolyte was vacuum backfilled into the device, the filling-hole was sealed with Surlyn and a glass cover disk, then to complete the devices the electrodes were painted with silver conducting paint (Electrolube, SCP). The electrolyte employed consisted of [Cu(I)(dmp)$_2$]TFSI (0.20 M), [Cu(II)(dmp)$_2$](TFSI)$_2$ (0.10 M), LiTFSI (0.10 M), and *N*-methylbenzimidazole (0.60 M) dissolved in dry acetonitrile.

4.3 Device characterization

J-V curves were obtained under 1 sun illumination AM 1.5G illumination provided by a Sciencetech SP300B solar simulator, calibrated with a Newport Reference Cell (91150V), connected to a Keithley 2450 SourceMeter. A mask with an active area of 0.238 cm^2 was used on all the J-V measurements. IPCE measurements were carried out using a halogen lamp (Ocean Optics HL-2000) and a monochromator (Spectral Products CM110) connected to the Keithley 2450. The devices and the reference photodiode (Thorlabs, FDS100-CAL) were covered with a mask with a size of 0.049 cm^2.

The electrochemical impedance properties were measured in a light-exclusion box containing a Zahner CIMPS QE/IPCE TLS03 tunable light source under constant illumination at wavelength 479 nm with an intensity of 12.6 mW/cm^2. The procedure for these measurements is identical to our previous study[16].

CRediT authorship contribution statement

David Moe Almenningen: Investigation, Methodology, Conceptualization, Writing – Original Draft, Writing – Review & Editing, Visualization. **Henrik Erring Hansen:** Investigation, Writing – Review & Editing, Visualization. **Audun Formo Buene:** Methodology, Writing – Review & Editing, Visualization. **Bård Helge Hoff:** Supervision, Writing – Review & Editing. **Odd Reidar Gautun:** Supervision, Conceptualization, Writing – Review & Editing.

References

[1] O'Regan B, Grätzel M. A low-cost, high-efficiency solar cell based on dye-sensitized colloidal TiO2 films. Nature. 1991;353(6346):737-40.

[2] Yoon S, Tak S, Kim J, Jun Y, Kang K, Park J. Application of transparent dye-sensitized solar cells to building integrated photovoltaic systems. Build. Environ. 2011;46(10):1899-904.

[3] Grifoni F, Bonomo M, Naim W, Barbero N, Alnasser T, Dzeba I, et al. Toward Sustainable, Colorless, and Transparent Photovoltaics: State of the Art and Perspectives for the Development of Selective Near-Infrared Dye-Sensitized Solar Cells. Adv. Energy Mater. 2021;11(43):2101598.

[4] Yun MJ, Cha SI, Seo SH, Lee DY. Highly Flexible Dye-sensitized Solar Cells Produced by Sewing Textile Electrodes on Cloth. Sci Rep. 2014;4:5322.

[5] Hagfeldt A, Boschloo G, Sun L, Kloo L, Pettersson H. Dye-Sensitized Solar Cells. Chem Rev. 2010;110(11):6595-663.

[6] Saygili Y, Söderberg M, Pellet N, Giordano F, Cao Y, Muñoz-García AB, et al. Copper Bipyridyl Redox Mediators for Dye-Sensitized Solar Cells with High Photovoltage. J. Am. Chem. Soc. 2016;138(45):15087-96.

[7] Cao Y, Liu Y, Zakeeruddin SM, Hagfeldt A, Grätzel M. Direct Contact of Selective Charge Extraction Layers Enables High-Efficiency Molecular Photovoltaics. Joule. 2018;2(6):1108-17.

[8] Zhang D, Stojanovic M, Ren Y, Cao Y, Eickemeyer FT, Socie E, et al. A molecular photosensitizer achieves a Voc of 1.24 V enabling highly efficient and stable dye-sensitized solar cells with copper(II/I)-based electrolyte. Nat. Commun. 2021;12(1):1777.

[9] Kay A, Humphry-Baker R, Graetzel M. Artificial Photosynthesis. 2. Investigations on the Mechanism of Photosensitization of Nanocrystalline TiO2 Solar Cells by Chlorophyll Derivatives. J. Phys. Chem. 1994;98(3):952-9.

[10] Feldt SM, Gibson EA, Gabrielsson E, Sun L, Boschloo G, Hagfeldt A. Design of Organic Dyes and Cobalt Polypyridine Redox Mediators for High-Efficiency Dye-Sensitized Solar Cells. J. Am. Chem. Soc. 2010;132(46):16714-24.

[11] Gabrielsson E, Ellis H, Feldt S, Tian H, Boschloo G, Hagfeldt A, et al. Convergent/Divergent Synthesis of a Linker-Varied Series of Dyes for Dye-Sensitized Solar Cells Based on the D35 Donor. Adv. Energy Mater. 2013;3(12):1647-56.

[12] Baumann A, Curiac C, Delcamp JH. The Hagfeldt Donor and Use of Next-Generation Bulky Donor Designs in Dye-Sensitized Solar Cells. ChemSusChem. 2020;13(10):2503-12.

[13] Delcamp JH, Yella A, Holcombe TW, Nazeeruddin MK, Grätzel M. The Molecular Engineering of Organic Sensitizers for Solar-Cell Applications. Angew. Chem. Int. Ed. 2013;52(1):376-80.

[14] Zhang X, Xu Y, Giordano F, Schreier M, Pellet N, Hu Y, et al. Molecular Engineering of Potent Sensitizers for Very Efficient Light Harvesting in Thin-Film Solid-State Dye-Sensitized Solar Cells. J. Am. Chem. Soc. 2016;138(34):10742-5.

[15] Eom YK, Kang SH, Choi IT, Yoo Y, Kim J, Kim HK. Significant light absorption enhancement by a single heterocyclic unit change in the π-bridge moiety from thieno[3,2-b]benzothiophene to thieno[3,2-b]indole for high performance dye-sensitized and tandem solar cells. J. Mater. Chem. A. 2017;5(5):2297-308.

[16] Almenningen DM, Hansen HE, Vold MF, Buene AF, Venkatraman V, Sunde S, et al. Effect of thiophene-based π-spacers on N-arylphenothiazine dyes for dye-sensitized solar cells. Dyes Pigm. 2021;185:108951.

[17] Tian H, Yang X, Chen R, Zhang R, Hagfeldt A, Sun L. Effect of Different Dye Baths and Dye-Structures on the Performance of Dye-Sensitized Solar Cells Based on Triphenylamine Dyes. J. Phys. Chem. C. 2008;112(29):11023-33.

[18] Fischer MKR, Wenger S, Wang M, Mishra A, Zakeeruddin SM, Grätzel M, et al. D-π-A Sensitizers for Dye-Sensitized Solar Cells: Linear vs Branched Oligothiophenes. Chem. Mater. 2010;22(5):1836-45.

[19] Won YS, Yang YS, Kim JH, Ryu J-H, Kim KK, Park SS. Organic Photosensitizers Based on Terthiophene with Alkyl Chain and Double Acceptors for Application in Dye-Sensitized Solar Cells. Energy Fuels. 2010;24(6):3676-81.

[20] Feng Q, Zhang Q, Lu X, Wang H, Zhou G, Wang Z-S. Facile and Selective Synthesis of Oligothiophene-Based Sensitizer Isomers: An Approach toward Efficient Dye-Sensitized Solar Cells. ACS Appl. Mater. Interfaces. 2013;5(18):8982-90.

[21] Feng Q, Zhou G, Wang Z-S. Varied alkyl chain functionalized organic dyes for efficient dye-sensitized solar cells: Influence of alkyl substituent type on photovoltaic properties. J. Power Sources. 2013;239:16-23.

[22] Elmorsy MR, Su R, Fadda AA, Etman HA, Tawfik EH, El-Shafei A. Effect of terthiophene spacer position in Ru(II) bipyridyl complexes on the photocurrent and photovoltage for high efficiency dye-sensitized solar cells. Dyes Pigm. 2018;156:348-56.

[23] Elmorsy MR, Su R, Fadda AA, Etman HA, Tawfik EH, El-Shafei A. Co-sensitization of Ru(ii) complex with terthiophene-based D–π–π–A metal-free organic dyes for highly efficient dye-sensitized solar cells: influence of anchoring group on molecular geometry and photovoltaic performance. New J. Chem. 2018;42(14):11430-7.

[24] Wu Z-S, Song X-C, Liu Y-D, Zhang J, Wang H-S, Chen Z-J, et al. New organic dyes with varied arylamine donors as effective co-sensitizers for ruthenium complex N719 in dye sensitized solar cells. J. Power Sources. 2020;451:227776.

[25] Buene AF, Almenningen DM. Phenothiazine and phenoxazine sensitizers for dye-sensitized solar cells – an investigative review of two complete dye classes. J. Mater. Chem. C. 2021;9(36):11974-94.

[26] Buene AF, Boholm N, Hagfeldt A, Hoff B. Effect of furan π-spacer and triethylene oxide methyl ether substituents on performance of phenothiazine sensitizers in dye-sensitized solar cells. New J. Chem. 2019.

[27] Buene AF, Uggerud N, Economopoulos SP, Gautun OR, Hoff BH. Effect of π-linkers on phenothiazine sensitizers for dye-sensitized solar cells. Dyes Pigm. 2018;151:263-71.

[28] Gudim NS, Mikhailov MS, Knyazeva EA, Almenningen DM, Mikhalchenko LV, Economopoulos SP, et al. Monitoring the dependence of the photovoltaic properties of dye-sensitized solar cells from the structure of D–A–π–A-type sensitizers with a 9-(p-tolyl)-2,3,4,4a,9,9a-hexahydro-1H-1,4-methanocarbazole donor building block. Mol. Syst. Des. Eng. 2022.

[29] Yemene AE, Venkatraman V, Moe Almenningen D, Hoff BH, Gautun OR. Synthesis of Novel 3,6-Dithienyl Diketopyrrolopyrrole Dyes by Direct C-H Arylation. Molecules. 2020;25(10):2349.

[30] Buene AF, Christensen M, Hoff BH. Effect of Auxiliary Donors on 3,8-Phenothiazine Dyes for Dye-Sensitized Solar Cells. Molecules. 2019;24(24):4485.

[31] Buene AF, Ose EE, Zakariassen A, Hagfeldt A, Hoff B. Auxiliary donors for phenothiazine sensitizers for dye-sensitized solar cells – How important are they really? J. Mater. Chem. A. 2019.

[32] Almenningen DM, Haga BS, Hansen HE, Buene AF, Hoff BH, Gautun OR. Adamantyl Side-Chains as Anti-aggregating Moieties in Dyes for Dye-Sensitized Solar Cells. Chem. Eur. J. 2022;Accepted Article.

[33] Buene AF, Hagfeldt A, Hoff BH. A comprehensive experimental study of five fundamental phenothiazine geometries increasing the diversity of the phenothiazine dye class for dye-sensitized solar cells. Dyes Pigm. 2019;169:66-72.

[34] Almenningen DM, Engh VM, Strømsodd EA, Hansen HE, Buene AF, Hoff BH, et al. Synthetic Efforts to Investigate the Effect of Planarizing the Triarylamine Geometry in Dyes for Dye-Sensitized Solar Cells. ACS Omega. 2022;7(25):22046-57.

[35] Buene AF, Almenningen DM, Hagfeldt A, Gautun OR, Hoff BH. First Report of Chenodeoxycholic Acid–Substituted Dyes Improving the Dye Monolayer Quality in Dye-Sensitized Solar Cells. Sol. RRL. 2020;4(4):1900569.

[36] Iqbal Z, Wu W-Q, Huang Z-S, Wang L, Kuang D-B, Meier H, et al. Trilateral π-conjugation extensions of phenothiazine-based dyes enhance the photovoltaic performance of the dye-sensitized solar cells. Dyes Pigm. 2016;124:63-71.

[37] Bureš F. Fundamental aspects of property tuning in push–pull molecules. RSC Adv. 2014;4(102):58826-51.

[38] Lang Y, Chen H, Lai H, Lu Y, Zhu Y, Yu P, et al. Isomeric Nonfullerene Acceptors: Planar Conformation Leading to a Higher Efficiency. ACS Appl. Energy Mater. 2022.

[39] Zhong J, Cui Y, Zhu P, Zhang M, Xie W, Liu H, et al. Nonfused Ring Electron Acceptors for Efficient Organic Solar Cells Enabled by Multiple Intramolecular Conformational Locks. ACS Appl. Energy Mater. 2022.

[40] Dentani T, Kubota Y, Funabiki K, Jin J, Yoshida T, Minoura H, et al. Novel thiophene-conjugated indoline dyes for zinc oxide solar cells. New J. Chem. 2009;33(1):93-101.

[41] Zhang L, Cole JM. Dye aggregation in dye-sensitized solar cells. J. Mater. Chem. A. 2017;5(37):19541-59.

[42] Velore J, Chandra Pradhan S, Hamann TW, Hagfeldt A, Unni KNN, Soman S. Understanding Mass Transport in Copper Electrolyte-Based Dye-Sensitized Solar Cells. ACS Appl. Energy Mater. 2022;5(3):2647-54.

[43] Wang Q, Ito S, Grätzel M, Fabregat-Santiago F, Mora-Seró I, Bisquert J, et al. Characteristics of High Efficiency Dye-Sensitized Solar Cells. J. Phys. Chem. B. 2006;110(50):25210-21.

[44] Wang Q, Moser J-E, Grätzel M. Electrochemical Impedance Spectroscopic Analysis of Dye-Sensitized Solar Cells. J. Phys. Chem. B. 2005;109(31):14945-53.

[45] Cai S, Tian G, Li X, Su J, Tian H. Efficient and stable DSSC sensitizers based on substituted dihydroindolo[2,3-b]carbazole donors with high molar extinction coefficients. J. Mater. Chem. A. 2013;1(37):11295-305.

[46] Zhu S, An Z, Chen X, Chen P, Liu Q. Cyclic thiourea functionalized dyes with binary π-linkers: Influence of different π-conjugation segments on the performance of dye-sensitized solar cells. Dyes Pigm. 2015;116:146-54.

[47] Yang J, He W, Denman K, Jiang Y-B, Qin Y. A molecular breakwater-like tetrapod for organic solar cells. J. Mater. Chem. A. 2015;3(5):2108-19.

[48] Chen R, Yang X, Tian H, Wang X, Hagfeldt A, Sun L. Effect of Tetrahydroquinoline Dyes Structure on the Performance of Organic Dye-Sensitized Solar Cells. Chem. Mater. 2007;19(16):4007-15.

[49] Li R, Liu J, Cai N, Zhang M, Wang P. Synchronously Reduced Surface States, Charge Recombination, and Light Absorption Length for High-Performance Organic Dye-Sensitized Solar Cells. J. Phys. Chem. B. 2010;114(13):4461-4.

[50] Ellis H, Vlachopoulos N, Häggman L, Perruchot C, Jouini M, Boschloo G, et al. PEDOT counter electrodes for dye-sensitized solar cells prepared by aqueous micellar electrodeposition. Electrochim. Acta. 2013;107:45-51.

Effect of seven different terthiophene π-spacers on dye performance in dye-sensitized solar cells

David Moe Almenningen[a], Henrik Erring Hansen[b], Audun Formo Buene[c], Bård Helge Hoff[a], Odd Reidar Gautun[a] *

[a] Department of Chemistry, Norwegian University of Science and Technology, Høgskoleringen 5, 7491 Trondheim, Norway

* Corresponding author. Tel.: +47 73594101; E-mail address: odd.r.gautun@ntnu.no (O. R. Gautun).

[b] Department of Materials Science and Engineering, Norwegian University of Science and Technology, Sem Sælands vei 12, 7491 Trondheim, Norway

[c] Department of Civil and Environmental Engineering, Norwegian University of Science and Technology, Høgskoleringen 7a, 7034 Trondheim, Norway.

List of contents

Absorption and emission

Figure S1. Normalized absorption (-) and emission (--) spectra of the dyes in DCM solution.

Cyclic voltammetry

Figure S2 CVs of the dye in the series. The low signal/noise ratio for **DMA-10** could suggest that the two hexyl-substituents on the cyclopentadiothiophene unit slows down the hole hopping responsible for carrying the current.

Electrochemical impedance spectroscopy
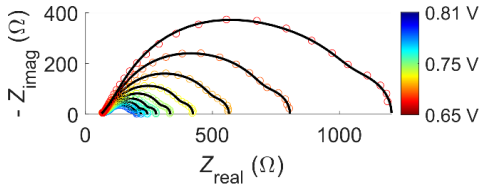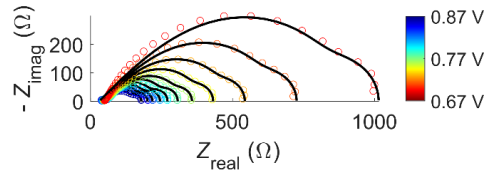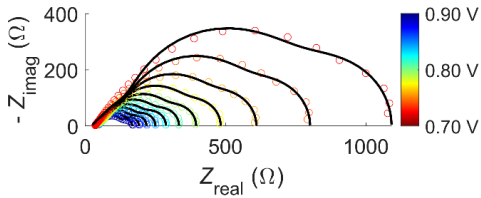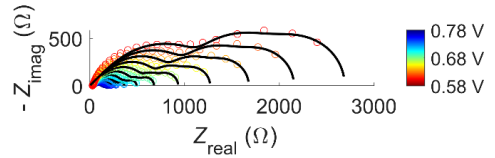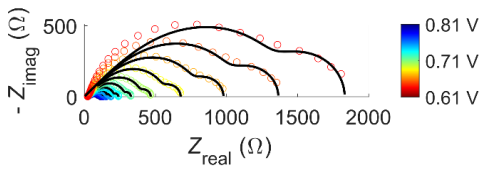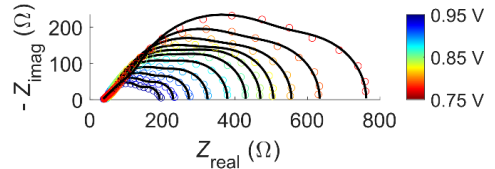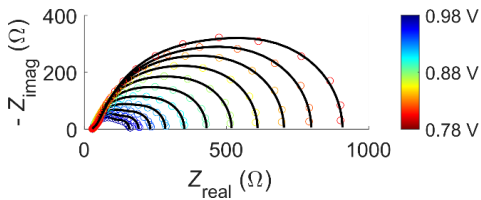
Figure S3 Complex plane diagrams obtained at different applied voltages for the 4.5 µm TiO$_2$ devices.
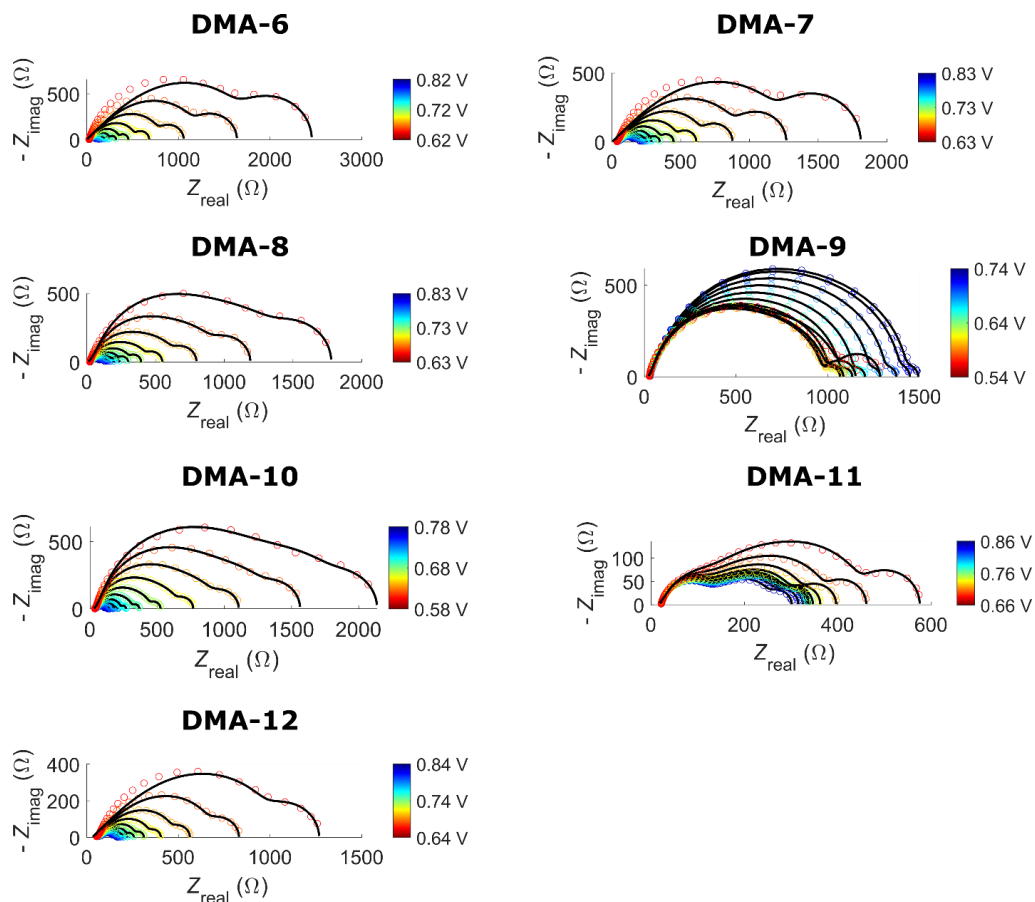
Figure S4 Complex plane diagrams obtained at different applied voltages 9 µm TiO_2 devices.
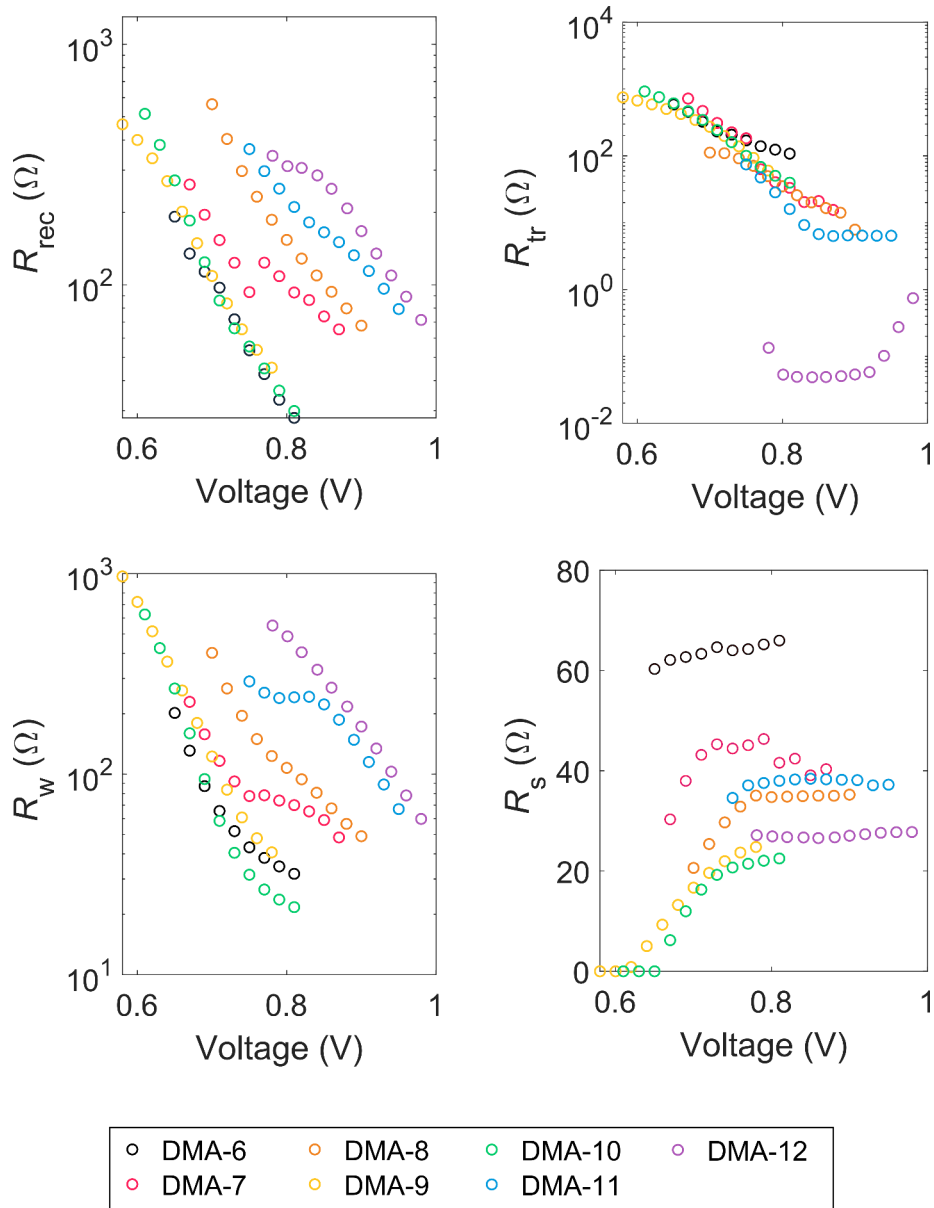
Figure S5 Resistances extracted from EIS measurements of 4.5 μm TiO₂ devices a) Recombination resistance as a function of applied voltage b) Transport resistance as a function of applied voltage c) Warburg-Impedance as a function of applied voltage. d) Series resistance as a function of applied voltage.
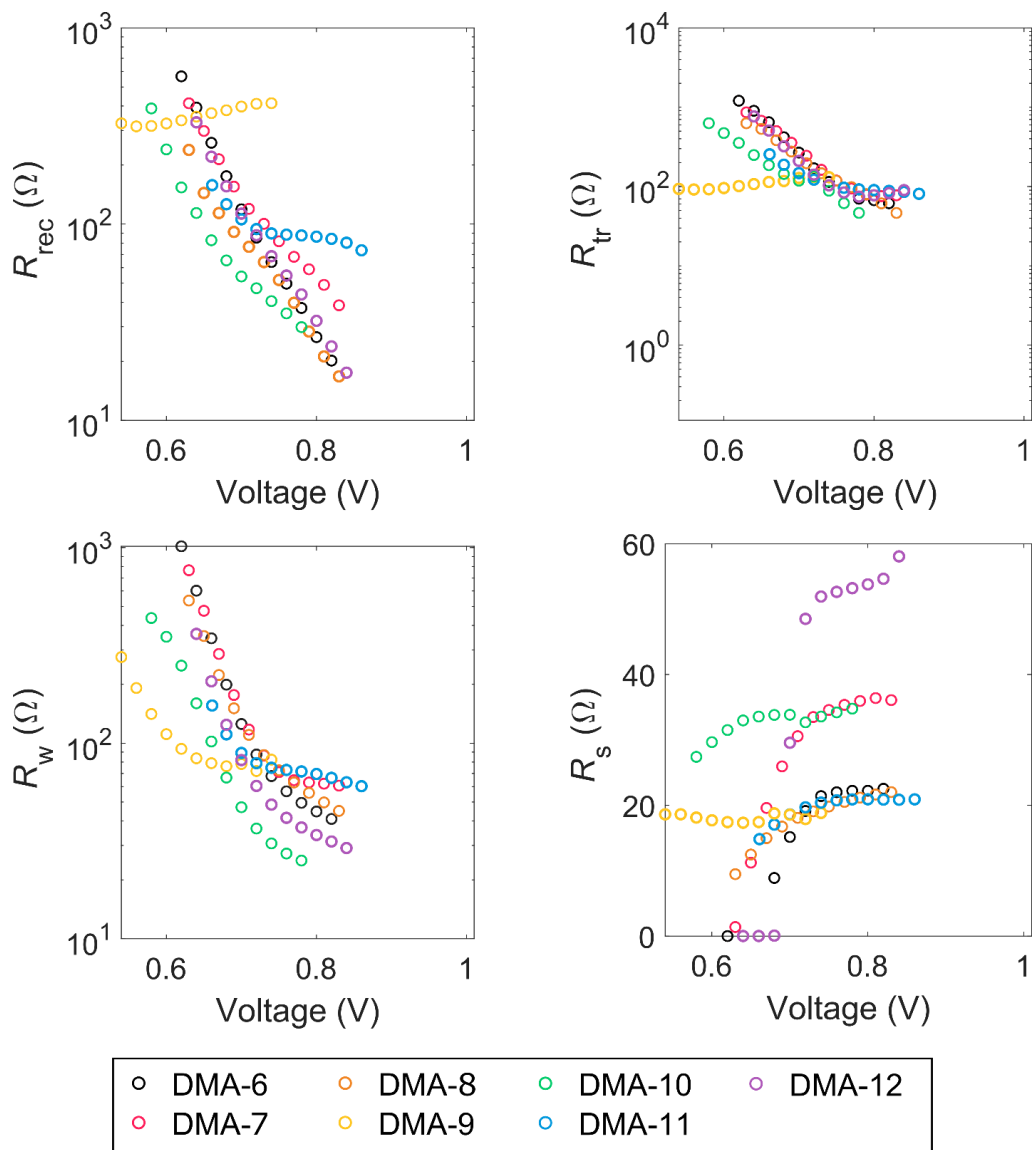
Figure S6 Resistances extracted from EIS measurements of 9 μm TiO$_2$ devices a) Recombination resistance as a function of applied voltage b) Transport resistance as a function of applied voltage c) Warburg-Impedance as a function of applied voltage. d) Series resistance as a function of applied voltage.

Experimental

All reactions were carried out under nitrogen atmosphere.

Analytical instruments

NMR spectroscopy (^{1}H and ^{13}C) was recorded on 400 and 600 MHz Bruker instruments, and all chemical shifts are reported relative to the respective solvent signals. Mass determination was performed on a Waters "Synapt G2-S" QTOF instrument in positive and negative modes. UV/Vis spectra were recorded on a Hitachi U-1900 instrument using quarts cuvettes for the solution samples, while fluorescence spectroscopy was recorded on a Cary Eclipse Fluorescence Spectrophotometer. Infrared spectroscopy was recorded on an FTIR Thermo Nicolet Nexus FT-IR spectrophotometer.

5'-(2,3-dihydrothieno[3,4-*b*][1,4]dioxin-5-yl)-[2,2'-bithiophene]-5-carbaldehyde (2d')
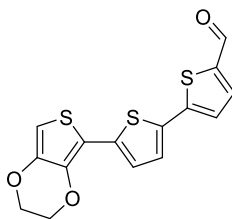
The commercially available 2-(2,3-dihydrothieno[3,4-*b*][1,4]dioxin-5-yl)-4,4,5,5-tetramethyl-1,3,2-dioxaborolane (236 mg, 0.88 mmol), and commercially available 5'-bromo-[2,2'-bithiophene]-5-carbaldehyde (200 mg, 0.73 mmol), K_3PO_4 (311 mg, 1.46 mmol), and XPhos Pd G3 (12 mg, 0.014 mmol) were added to a Schlenk tube. A mixture of water and tetrahydrofuran (2:1, v/v, 4.5 mL) was degassed and added under nitrogen to dissolve the compounds. The reaction mixture was left stirring for 90 minutes at room temperature, after which water (20 mL) was added to the reaction mixture. The aqueous phase was extracted using dichloromethane (3 x 30 mL), and the organic phase was dried over Na_2SO_4. The organic phase was the filtered and concentrated under reduced pressure. The crude product was purified by silica gel column chromatography (*n*-pentane/dichloromethane, 1:1, R_f = 0.43). The product **2d'** was isolated as an orange wax (60.3 mg, 0.18 mmol, 25%). ^{1}H NMR (400 MHz, CDCl₃) δ: 9.84 (s, 1H), 7.65 (d, *J* = 4.0 Hz, 1H), 7.27 (d, *J* = 4.0 Hz, 1H), 7.22 (d, *J* = 3.6 Hz, 1H), 7.14 (d, *J* = 3.6 Hz, 1H), 6.29 (s, 1H), 4.40-4.35 (m, 2H), 4.29-4.24 (m, 2H); ^{13}C NMR (100 MHz, CDCl₃) δ: 182.4, 147.4, 141.9, 141.2, 138.4, 137.5, 136.9, 133.7, 126.4, 123.6, 123.5, 111.6, 98.2, 65.2, 64.6.

5'-(7-bromo-2,3-dihydrothieno[3,4-*b*][1,4]dioxin-5-yl)-[2,2'-bithiophene]-5-carbaldehyde (2d)
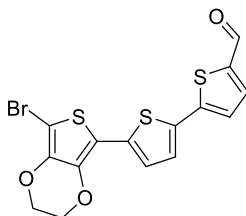
Compound **2d'** (60 mg, 0.18 mmol) and NBS (32 mg, 0.18 mmol) were added under dark conditions along with degassed dichloromethane (8 mL) under nitrogen at 0 °C. The reaction mixture was then allowed to warm to room temperature while stirring for 15 hours. Water (20 mL) was added and the aqueous phase was extracted using dichloromethane (3 × 15 mL). The combined organic phases were dried over anhydrous Na_2SO_4, filtered and the solvents were removed *in vacuo*. The crude product was purified by a short silica

gel plug (dichloromethane, R_f = 0.5). The crude product **2d** was used immediately in the next step to prevent it from decomposing.

4,4-dihexyl-6-(thiophen-2-yl)-4*H*-cyclopenta[2,1-*b*:3,4-*b′*]dithiophene-2-carbaldehyde (2e')
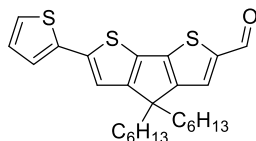
The commercially available thiophen-2-yl boronic acid (212 mg, 1.65 mmol), 6-bromo-4,4-dihexyl-4*H*-cyclopenta[2,1-*b*:3,4-*b′*]dithiophene-2-carbaldehyde (500 mg, 1.10 mmol), K_3PO_4 (468 mg, 2.21 mmol), and XPhos Pd G3 (19 mg, 0.022 mmol) were added to a Schlenk tube. A mixture of water and tetrahydrofuran (2:1, v/v, 6 mL) was degassed and added under nitrogen to dissolve the compounds. The reaction mixture was warmed to 40 °C and left stirring for 90 minutes. Upon being cooled to room temperature, water (20 mL) was added to the reaction mixture. The aqueous phase was extracted using dichloromethane (3 x 50 mL), and the organic phase was dried over Na_2SO_4. The organic phase was the filtered and concentrated under reduced pressure. The crude product was purified by silica gel column chromatography (*n*-pentane/dichloromethane, 1:1, R_f = 0.43). The product **2e'** was isolated as an orange oil (335 mg, 0.73 mmol, 66%). ^{1}H NMR (600 MHz, CDCl₃) δ: 9.83 (s, 1H), 7.55 (s, 1H), 7.26 (dd, *J* = 1.2 Hz, 5.0 Hz, 1H), 7.24 (d, *J* = 1.2 Hz, 3.8 Hz, 1H), 7.06-7.04 (m, 2H), 1.94-1.82 (m, 4H), 1.24-1.10 (m, 12H), 1.02-0.92 (m, 4H), 0.82 (t, *J* = 7.2 Hz, 6H); ^{13}C NMR (150 MHz, CDCl₃) δ: 182.5, 163.1, 157.7, 147.6, 143.3, 142.1, 137.6, 134.2, 129.9, 128.1, 125.0, 124.0, 118.2, 54.2, 37.7 (2C), 31.6 (2C), 29.6 (2C), 24.6 (2C), 22.6 (2C), 14.0 (2C).

6-(5-bromothiophen-2-yl)-4,4-dihexyl-4H-cyclopenta[2,1-b:3,4-b']dithiophene-2-carbaldehyde (2e)
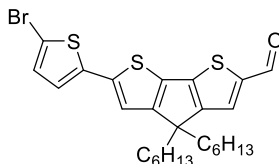
Compound **2e'** (300 mg, 0.66 mmol) and NBS (123 mg, 0.69 mmol) were added under dark conditions along with degassed dichloromethane (8 mL) under nitrogen at 0 °C. The reaction mixture was then allowed to warm to room temperature while stirring for 15 hours. Water (20 mL) was added, and the aqueous phase was extracted using dichloromethane (3 × 30 mL). The combined organic phases were dried over anhydrous Na_2SO_4, filtered and the solvents were removed *in vacuo*. The crude product was purified by a short silica gel plug (dichloromethane, R_f = 0.57sc). The crude product was purified by a short silica gel column plug (dichloromethane, R_f = 0.8). The crude product **2e** was used immediately in the next step to prevent it from decomposing.

General Suzuki-Miyaura procedure A.

The brominated terthiophene carboxaldehyde compound **2** (1 eq., 130-190 µmol), the triarylamine boronic ester **1** (1.3 eq.), K_3PO_4 (4 eq.), Pd(OAc)₂ (5 mol%), and SPhos (10 mol%) was added to a Schlenk tube and a N₂-atmosphere was established. A mixture of 1,4-dioxane and water (1:1, 0.07 mL/mg terthiophene) was degassed and used to dissolve the reaction mixture. The reaction mixture was then heated to 80 °C, and left stirring for 1-4 hours before being cooled down. Upon reaching room temperature, the reaction mixture was added water (20 mL) and the aqueous phase was extracted using dichloromethane (3 x 30 mL). The

combined organic phases were dried over Na$_2$SO$_4$ and filtered, and then the solvents were removed *in vacuo*. The crude residue was purified by silica gel column chromatography.

General Suzuki-Miyaura procedure B.

The brominated terthiophene carboxaldehyde compound **2** (1 eq., 130-190 µmol), the triarylamine boronic ester **1** (1.3 eq.), K$_2$CO$_3$ (4 eq.) and PdCl$_2$(dppf) (5 mol%) were added to a Schlenk tube and a N$_2$-atmosphere was established. A mixture of 1,4-dioxane and water (1:1, 0.04 mL/mg terthiophene) was degassed and used to dissolve the reaction mixture. The reaction mixture was then heated to 80 °C, and left stirring for 2 hours before being cooled down. Upon reaching room temperature, the reaction mixture was added water (20 mL) and the aqueous phase was extracted using dichloromethane (3 x 30 mL). The combined organic phases were dried over Na$_2$SO$_4$ and filtered, and then the solvents were removed *in vacuo*. The crude residue was purified by silica gel column chromatography.

5''-(4-(bis(2',4'-bis(hexyloxy)-[1,1'-biphenyl]-4-yl)amino)phenyl)-[2,2':5',2''-terthiophene]-5-carbaldehyde (3a)
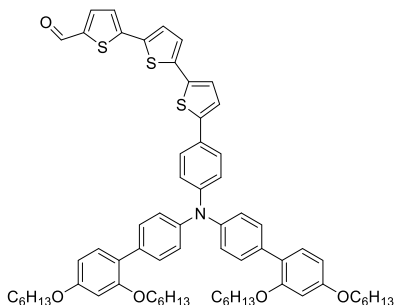
The synthesis of **3a** was performed as described in the general Suzuki coupling procedure A. The crude product was purified by silica gel column chromatography (dichloromethane, R_f = 0.51). This produced **3a** (63.2 mg, 63 µmol, 35%) as a red wax.

^{1}H NMR (600 MHz, CD$_2$Cl$_2$) δ: 9.85 (s, 1H), 7.70 (d, *J* = 3.2 Hz, 1H), 7.51 (d, *J* = 8.1 Hz, 2H), 7.47 (d, *J* = 9.3 Hz, 4H), 7.32 (d, *J* = 3.4 Hz, 1H), 7.28 (d, *J* = 4.2 Hz, 1H), 7.25 (d, *J* = 8.9 Hz, 2H), 7.22 (d, *J* = 3.4 Hz, 1H), 7.20 (d, *J* = 4.2 Hz, 1H), 7.18-7.14 (m, 7H), 6.56-6.52 (m, 4H), 4.01-3.95 (m, 8H), 1.82-1.71 (m, 8H), 1.51-1.40 (m, 8H), 1.39-1.34 (m, 8H), 1.34-1.29 (m, 8H), 0.92 (t, *J* = 7.1 Hz, 6H), 0.88 (t, *J* = 6.9 Hz, 6H); ^{13}C NMR (150 MHz, CD$_2$Cl$_2$) δ: 182.8, 160.2 (2C), 157.4 (2C), 148.3, 146.9, 145.9 (2C), 144.8, 142.1, 139.7, 137.9, 134.9, 134.6, 134.1 (2C), 131.2 (2C), 130.7 (4C), 127.7, 127.5, 126.8 (2C), 125.9, 124.7, 124.6, 124.5 (4C), 123.6 (2C), 123.4, 123.0 (2C), 105.9 (2C), 100.6 (2C), 68.8 (2C), 68.6 (2C), 32.0 (2C), 31.9 (2C), 29.7 (2C), 29.5 (2C), 26.2 (2C), 26.1 (2C), 23.1 (2C), 23.0 (2C), 14.24 (2C), 14.23 (2C); HRMS (ASAP+, *m/z*): found 1071.4971 (calcd. C$_{67}$H$_{77}$NO$_5$S$_3$ 1071.4964, [M*]$^+$).

5-(5-(4-(bis(2',4'-bis(hexyloxy)-[1,1'-biphenyl]-4-yl)amino)phenyl)thiophen-2-yl)thieno[3,2-b]thiophene-2-carbaldehyde (3b)
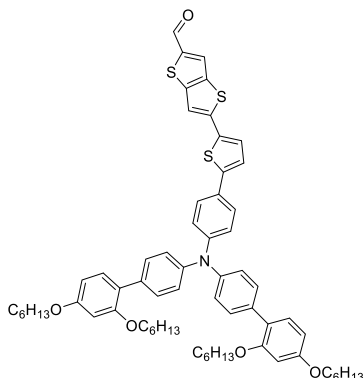
The synthesis of **3b** was performed as described in the general Suzuki coupling procedure A. The crude product was purified by silica gel column chromatography (*n*-pentane/dichloromethane 1:1, R_f = 0.22). This produced **3b** (44.6 mg, 43 µmol, 28%) as a red wax.

^{1}H NMR (600 MHz, CD$_2$Cl$_2$) δ: 9.84 (s, 1H), 7.68 (d, *J* = 4.3 Hz, 1H), 7.55-7.51 (m, 3H), 7.48 (d, *J* = 8.5 Hz, 4H), 7.40 (s, 1H), 7.29 (d, *J* = 4.3 Hz, 1H), 7.25 (d, *J* = 7.3 Hz, 2H), 7.19-7.14 (m, 6H), 6.58-6.52 (m, 4H), 4.01-3.95 (m, 8H), 1.84-1.72 (m, 8H), 1.52-1.40 (m, 8H), 1.40-1.28 (m, 16H), 0.93 (t, *J* = 6.9 Hz, 6H), 0.89 (t, *J* = 7.1 Hz, 6H); ^{13}C NMR (150 MHz, CD$_2$Cl$_2$) δ: 182.7, 160.2 (2C), 157.4 (2C), 148.7, 148.6, 147.5, 145.7 (2C), 142.1, 141.5, 138.9, 137.8, 136.8, 134.2 (2C), 131.2 (2C), 130.7 (4C), 127.9, 127.0 (2C), 124.6 (4C), 124.5, 123.4, 123.0, 118.9 (2C), 114.5 (2C), 105.9 (2C), 100.6 (2C), 68.8 (2C), 68.6 (2C), 32.1 (2C), 31.9 (2C), 29.7 (2C), 29.5 (2C), 26.20 (2C), 26.15 (2C), 23.1 (2C), 23.0 (2C), 14.26 (2C), 14.25 (2C); HRMS (ASAP+, *m/z*): found 1045.4802 (calcd. C$_{65}$H$_{75}$NO$_5$S$_3$ 1045.4807, [M*]$^+$).

5-(5-(4-(bis(2',4'-bis(hexyloxy)-[1,1'-biphenyl]-4-yl)amino)phenyl)thieno[3,2-b]thiophen-2-yl)thiophene-2-carbaldehyde (3c)
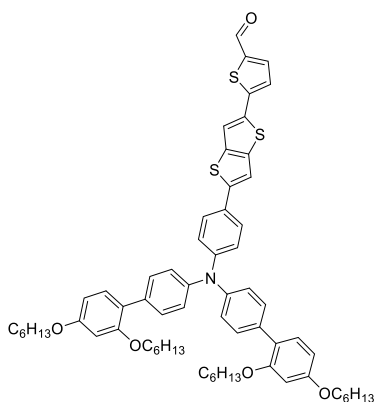
The synthesis of **3c** was performed as described in the general Suzuki coupling procedure A. The crude product was purified by silica gel column chromatography (*n*-pentane/dichloromethane 3:1, R_f = 0.23). This produced **3c** (61.7 mg, 59 µmol, 43%) as a red wax.

^{1}H NMR (600 MHz, CD_2Cl_2) δ: 9.85 (s, 1H), 7.69 (d, *J* = 4.1 Hz, 1H), 7.54-7.51 (m, 3H), 7.48 (d, *J* = 8.5 Hz, 4H), 7.40 (s, 1H), 7.30 (d, *J* = 4.1 Hz, 1H), 7.25 (d, *J* = 7.7 Hz, 2H), 7.18-7.14 (m, 6H), 6.56-6.52 (m, 4H), 4.01-3.94 (m, 8H), 1.82-1.72 (m, 8H), 1.51-1.39 (m, 8H), 1.39-1.34 (m, 8H), 1.34-1.29 (m, 8H), 0.93 (t, *J* = 7.2 Hz, 6H), 0.88 (t, *J* = 7.1 Hz, 6H); ^{13}C NMR (150 MHz, CD_2Cl_2) δ: 182.7, 160.2 (2C), 157.4 (2C), 148.7, 148.6, 147.6, 145.8 (2C), 142.1, 141.5, 138.9, 137.8, 136.8, 134.2 (2C), 131.2 (2C), 130.7 (4C), 128.0, 127.0 (2C), 124.6 (4C), 124.5, 123.4, 123.0, 118.9 (2C), 114.5 (2C), 105.9 (2C), 100.6 (2C), 68.8 (2C), 68.6 (2C), 32.0 (2C), 31.9 (2C), 29.7 (4C), 26.20 (2C), 26.15 (2C), 23.1 (2C), 23.0 (2C), 14.25 (2C), 14.24 (2C); HRMS (ASAP+, *m/z*): found 1046.4868 (calcd. $C_{65}H_{76}NO_5S_3$ 1046.4886, [M+H]$^+$).

5'-(7-(4-(bis(2',4'-bis(hexyloxy)-[1,1'-biphenyl]-4-yl)amino)phenyl)-2,3-dihydrothieno[3,4-*b*][1,4]dioxin-5-yl)-[2,2'-bithiophene]-5-carbaldehyde (3d)
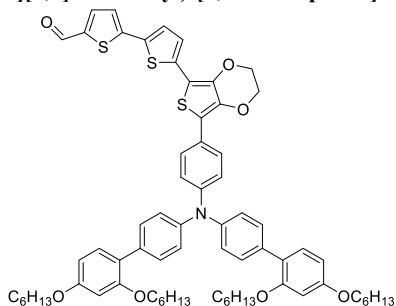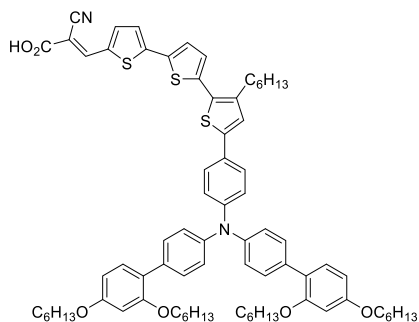

The synthesis of **3d** was performed as described in the general Suzuki coupling procedure B. The crude product was purified by silica gel column chromatography (*n*-pentane/dichloromethane 1:1, R_f = 0.19). This produced **3d** (25.4 mg, 23 µmol, 17% over two steps from **2d'**) as a dark red wax.

^{1}H NMR (600 MHz, CD_2Cl_2) δ: 9.83 (s, 1H), 7.68 (d, *J* = 4.8 Hz, 1H), 7.63 (d, *J* = 8.5 Hz, 2H), 7.46 (d, *J* = 8.2 Hz, 4H), 7.32 (d, *J* = 3.8 Hz, 1H), 7.28-7.22 (m, 3H), 7.20-7.12 (m, 7H), 6.56-6.52 (m, 4H), 4.45-4.42 (m, 2H), 4.39-4.36 (m, 2H), 4.01-3.95 (m, 8H), 1.82-1.72 (m, 8H), 1.51-1.40 (m, 8H), 1.39-1.28 (m, 16H), 0.92 (t, *J* = 7.2 Hz, 6H), 0.88 (t, *J* = 7.1 Hz, 6H); ^{13}C NMR (150 MHz, CD_2Cl_2) δ: 182.7, 160.1 (2C), 157.4 (2C), 147.4, 147.2, 145.9, 141.7, 138.2, 138.0 (2C), 133.9 (3C), 131.1 (2C), 130.6 (4C), 127.2 (2C), 126.9, 124.3 (4C), 124.1, 123.7 (2C), 123.6, 123.1 (2C), 116.5 (2C), 108.7, 105.8 (2C), 100.6 (2C), 68.8 (2C), 68.6 (2C), 65.6, 65.2, 32.0 (2C), 31.9 (2C), 29.7 (2C), 29.5 (2C), 26.2 (2C), 26.1 (2C), 23.04 (2C), 23.01 (2C), 14.24 (2C), 14.22 (2C).

6-(5-(4-(bis(2',4'-bis(hexyloxy)-[1,1'-biphenyl]-4-yl)amino)phenyl)thiophen-2-yl)-4,4-dihexyl-4H-cyclopenta[2,1-*b*:3,4-*b'*]dithiophene-2-carbaldehyde (3e)
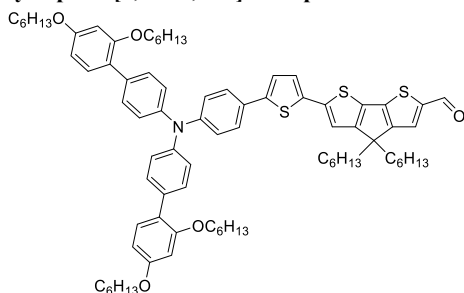
The synthesis of **3e** was performed as described in the general Suzuki coupling procedure A. The crude product was purified by silica gel column chromatography (*n*-pentane/diethyl ether 3:1, R_f = 0.42). This produced **3e** (129.5 mg, 103 µmol, 55% over two steps from **2e'**) as a red wax.

^{1}H NMR (600 MHz, CD$_2$Cl$_2$) δ: 9.82 (s, 1H), 7.55 (s, 1H), 7.55-7.44 (m, 6H), 7.28-7.25 (m, 2H), 7.21-7.09 (m, 8H), 7.06 (s, 1H), 6.57-6.52 (m, 4H), 4.02-3.93 (m, 8H), 1.94-1.71 (m, 12H), 1.52-1.38 (m, 8H), 1.38-1.27 (m, 16H), 1.23-1.10 (m, 12H), 1.03-0.93 (m, 4H), 0.92 (t, J = 7.0 Hz, 6H), 0.88 (t, J = 6.7 Hz, 6H), 0.82 (t, J = 6.7 Hz, 6H); ^{13}C NMR (150 MHz, CD$_2$Cl$_2$) δ: 182.4, 163.3, 159.6 (2C), 157.7, 157.0 (2C), 147.8, 147.7, 145.4 (2C), 144.1, 143.1, 142.5, 135.6, 134.0, 133.5 (2C), 130.9 (2C), 130.3 (4C), 127.3, 126.3 (2C), 124.9, 124.0 (4C), 123.3 (2C), 122.92 (2C), 122.86 (2C), 117.6 (2C), 105.4 (2C), 100.4 (2C), 68.4 (2C), 68.1 (2C), 54.2, 37.7 (2C), 31.62 (2C), 31.57 (2C), 31.5 (2C), 29.6 (2C), 29.3 (2C), 29.1 (2C), 25.8 (4C), 24.6 (2C), 22.63 (2C), 22.61 (2C), 22.59 (2C), 14.05 (4C), 14.01 (2C); HRMS (ASAP+, *m/z*): found 1251.6830 (calcd. C$_{80}$H$_{101}$NO$_5$S$_3$ 1251.6842, [M*]$^+$).

5''-(4-(bis(2',4'-bis(hexyloxy)-[1,1'-biphenyl]-4-yl)amino)phenyl)-3''-hexyl-[2,2':5',2''-terthiophene]-5-carbaldehyde (3f)
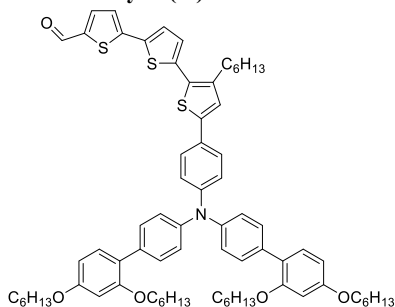
The synthesis of **3f** was performed as described in the general Suzuki coupling procedure A. The crude product was purified by silica gel column chromatography (dichloromethane, R_f = 0.56). This produced **3f** (85.6 mg, 74 µmol, 47%) as a red wax.

^{1}H NMR (600 MHz, CD$_2$Cl$_2$) δ: 9.85 (s, 1H), 7.70 (d, J = 4.1 Hz, 1H), 7.50 (d, J = 8.8 Hz, 2H), 7.47 (d, J = 8.3 Hz, 4H), 7.36 (d, J = 4.2 Hz, 1H), 7.29 (d, J = 4.1 Hz, 1H), 7.25 (d, J = 8.6 Hz, 2H), 7.17-7.11 (m, 8H), 6.56-6.52 (m, 4H), 4.01-3.95 (m, 8H), 2.81 (t, J = 8.6 Hz, 2H), 1.82-1.67 (m, 10H), 1.52-1.40 (m, 10H), 1.39-1.28 (m, 20H), 0.95-0.84 (m, 15H); ^{13}C NMR (150 MHz, CD$_2$Cl$_2$) δ: 182.8, 160.2 (2C), 157.4 (2C), 148.1, 147.0, 145.9 (2C), 143.1, 142.2, 142.1, 138.9, 137.9, 135.3, 134.0 (2C), 131.2 (2C), 130.7

(4C), 128.6, 127.8, 127.0 (2C), 126.7 (2C), 125.9, 125.1, 124.5, 124.4 (4C), 123.7, 123.1 (2C), 105.9 (2C), 100.6 (2C), 68.8 (2C), 68.6 (2C), 32.1, 32.0 (2C), 31.9 (2C), 30.8, 30.1, 29.7 (2C), 29.6, 29.5 (2C), 26.21 (2C), 26.15 (2C), 23.05 (2C), 23.04, 23.02 (2C), 14.28, 14.25 (2C), 14.2 (2C); HRMS (ASAP+, *m/z*): found 1155.5922 (calcd. $C_{73}H_{89}NO_5S_3$ 1155.5903, [M*]$^+$).

6-(4-(bis(2',4'-bis(hexyloxy)-[1,1'-biphenyl]-4-yl)amino)phenyl)dithieno[3,2-*b*:2',3'-*d*]thiophene-2-carbaldehyde (3g)
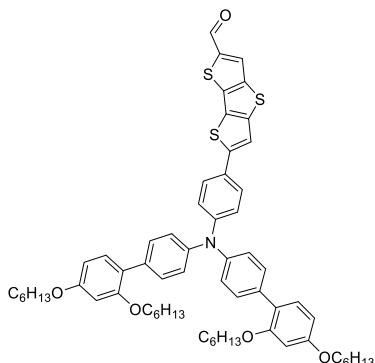
The synthesis of **3g** was performed as described in the general Suzuki coupling procedure A. The crude product was purified by silica gel column chromatography (*n*-pentane/dichloromethane 1:2, R_f = 0.42). This produced **3g** (36.6 mg, 36 µmol, 22%) as a red wax.

^{1}H NMR (600 MHz, CD_2Cl_2) δ: 9.93 (s, 1H), 7.97 (s, 1H), 7.56 (d, *J* = 8.6 Hz, 2H), 7.51-7.47 (m, 5H), 7.25 (d, *J* = 8.8 Hz, 2H), 7.19-7.15 (m, 6H), 6.57-6.52 (m, 4H), 4.02-3.94 (m, 8H), 1.83-1.72 (m, 8H), 1.51-1.40 (m, 8H), 1.39-1.27 (m, 16H), 0.92 (t, *J* = 7.0 Hz, 6H), 0.88 (t, *J* = 7.2 Hz, 6H); ^{13}C NMR (150 MHz, CD_2Cl_2) δ: 183.1, 160.2 (2C), 157.4 (2C), 149.7, 149.0, 147.6, 145.7 (2C), 143.8, 141.0, 138.4, 134.4 (2C), 131.2 (2C), 130.8 (4C), 129.3, 127.4, 127.1 (2C), 124.7 (4C), 123.2 (2C), 123.0, 115.8 (2C), 105.9 (2C), 100.6 (2C), 68.8 (2C), 68.6 (2C), 32.0 (2C), 31.9 (2C), 29.7 (2C), 29.5 (2C), 26.2 (2C), 26.1 (2C), 23.1 (2C), 23.0 (2C), 14.24 (2C), 14.23 (2C); HRMS (ASAP+, *m/z*): found 1019.4666 (calcd. $C_{63}H_{73}NO_5S_3$ 1019.4651, [M*]$^+$).

General Knoevenagel condensation procedure

The triarylamine carboxaldehydes **3** (1 eq., 20-80 µmol) and cyanoacetic acid (21 eq.) was added along with degassed acetonitrile (10 mL). The reaction mixture was then heated to 80 °C, and added tetrahydrofuran (1 mL) if the starting material proved difficult to dissolve. Upon full solvation, piperidine (13 eq.) was added and the reaction mixture was then stirred for 1 hour before being cooled to room temperature. An aqueous HCl solution (4 M, 450 mL/mmol substrate) was then added, and the aqueous phase was extracted with dichloromethane (3 x 30 mL). The organic phase was then washed with water (4 x 50 mL) and then dried over Na_2SO_4. The organic phase was then filtered and concentrated under reduced pressure. The crude product was purified by silica gel column chromatography.

(*E*)-3-(5''-(4-(bis(2',4'-bis(hexyloxy)-[1,1'-biphenyl]-4-yl)amino)phenyl)-[2,2':5',2''-terthiophen]-5-yl)-2-cyanoacrylic acid (DMA-6)
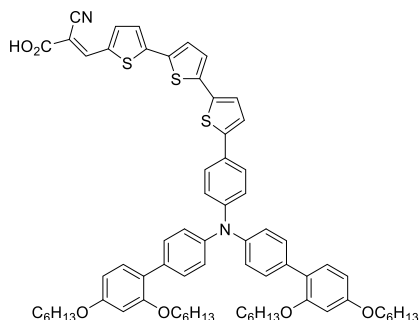
The synthesis of **DMA-6** was performed as described in the general Knoevenagel condensation procedure. The crude product was purified by silica gel column chromatography (gradient: 0-15% methanol in dichloromethane), to obtain sensitizer **DMA-6** as a dark solid (44.4 mg, 39 µmol, 84%).

^{1}H NMR (600 MHz, acetone-d_6) δ: 8.45 (s, 1H), 7.95 (d, *J* = 4.4 Hz, 1H), 7.62 (d, *J* = 9.0 Hz, 2H), 7.56 (d, *J* = 4.0 Hz, 1H), 7.55-7.50 (m, 5H), 7.40 (d, *J* = 3.5 Hz, 1H), 7.39 (d, *J* = 3.5 Hz, 1H), 7.35 (d, *J* = 4.0 Hz, 1H), 7.27 (d, *J* = 8.3 Hz, 2H), 7.18-7.11 (m, 6H), 6.64 (d, *J* = 2.5 Hz, 2H), 6.59 (dd, *J* = 2.5 Hz, 8.3 Hz, 2H), 4.05-4.00 (m, 8H), 1.82-1.71 (m, 8H), 1.53-1.42 (m, 8H), 1.39-1.35 (m, 8H), 1.33-1.27 (m, 8H), 0.91 (t, *J* = 7.4 Hz, 6H), 0.87 (t, *J* = 6.7 Hz, 6H); ^{13}C NMR (150 MHz, acetone-d_6) δ: 163.9, 160.8 (2C), 158.0 (2C), 148.8, 147.2, 147.1, 146.3, 145.2, 141.6, 140.2, 135.4, 135.2 (2C), 135.0, 134.8, 131.6 (2C), 131.3 (4C), 130.4, 128.7, 128.1, 127.3 (2C), 127.0, 125.8 (2C), 125.6 (2C), 124.9 (4C), 124.4, 123.9 (2C), 123.4 (2C), 116.9, 106.7 (2C), 101.1 (2C), 98.9, 69.0 (2C), 68.7 (2C), 32.4 (2C), 32.3 (2C), 30.4 (4C), 26.6 (2C), 26.5 (2C), 23.3 (4C), 14.4 (2C), 14.3 (2C); IR (neat, cm^{-1}) ν: 2929 (s), 2858 (m), 2218 (w), 1601 (s), 1492 (s), 1393 (m), 1136 (m), 1048 (m); HRMS (ASAP+, *m/z*): found 1095.5190 (calcd. $C_{69}H_{79}N_2O_4S_3$ 1095.5202, [M-CO$_2$+H]$^+$).

(*E*)-3-(5-(5-(4-(bis(2',4'-bis(hexyloxy)-[1,1'-biphenyl]-4-yl)amino)phenyl)thiophen-2-yl)thieno[3,2-*b*]thiophen-2-yl)-2-cyanoacrylic acid (DMA-7)
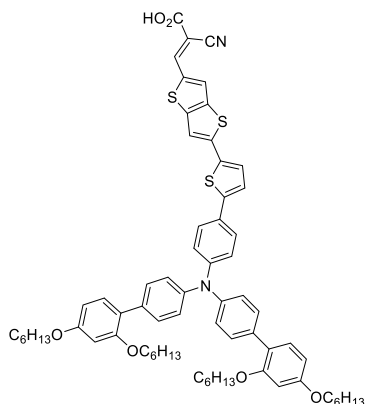
The synthesis of **DMA-7** was performed as described in the general Knoevenagel condensation procedure. The crude product was purified by silica gel column chromatography (gradient: 0-15% methanol in dichloromethane), to obtain sensitizer **DMA-7** as a dark solid (26.9 mg, 24 µmol, 63%).

^{1}H NMR (600 MHz, acetone-d$_6$) δ: 8.42 (s, 1H), 7.92 (d, *J* = 3.8 Hz, 1H), 7.82 (s, 1H), 7.63 (s, 1H), 7.59 (d, *J* = 9.1 Hz, 2H), 7.52-7.48 (m, 5H), 7.24 (d, *J* = 9.6 Hz, 2H), 7.13 (d, *J* = 7.7 Hz, 4H), 7.10 (d, *J* = 9.1 Hz, 2H), 6.62 (d, *J* = 2.4 Hz, 2H), 6.56 (dd, *J* = 2.4 Hz, 9.6 Hz, 2H), 4.04-3.97 (m, 8H), 1.81-1.69 (m, 8H), 1.52-1.40 (m, 8H), 1.38-1.28 (m, 16H), 0.91 (t, *J* = 7.2 Hz, 6H), 0.85 (t, *J* = 7.3 Hz, 6H); ^{13}C NMR (150 MHz, acetone-d$_6$) δ: 163.9, 160.8 (2C), 158.0 (2C), 149.3, 149.1, 148.0, 147.2, 146.1 (2C), 142.3, 141.5, 139.7, 137.0, 135.3, 135.0 (2C), 131.6 (2C), 131.3 (4C), 128.5, 127.4 (2C), 125.4, 125.0 (4C), 123.6 (2C), 123.4 (2C), 120.1, 116.9, 115.5, 106.7 (2C), 101.1 (2C), 98.7, 69.0 (2C), 68.6 (2C), 32.4 (2C), 32.3 (2C), 29.2 (4C)*, 26.58 (2C), 26.54 (2C), 23.32 (4C), 14.4 (2C), 14.3 (2C); IR (neat, cm^{-1}) ν: 2928 (s), 2857 (m), 2216 (w), 1685 (m), 1599 (s), 1492 (s), 1405 (s), 1323 (m), 1136 (m), 1058 (m); HRMS (ASAP+, *m/z*): found 1112.4868 (calcd. C$_{68}$H$_{76}$N$_2$O$_6$S$_3$ 1112.4866, [M*]$^+$). *Signal found using ^{1}H-^{13}C HSQC spectroscopy due to overlapping residual solvent signal.

(*E*)-3-(5-(5-(4-(bis(2',4'-bis(hexyloxy)-[1,1'-biphenyl]-4-yl)amino)phenyl)thieno[3,2-*b*]thiophen-2-yl)thiophen-2-yl)-2-cyanoacrylic acid (DMA-8)
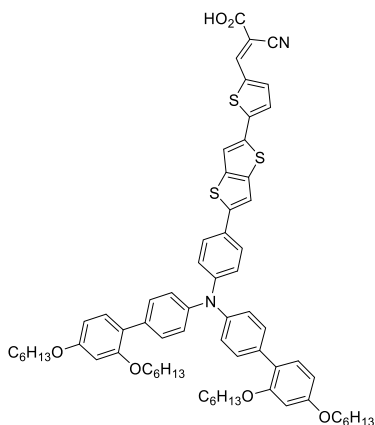
The synthesis of **DMA-8** was performed as described in the general Knoevenagel condensation procedure. The crude product was purified by silica gel column chromatography (gradient: 0-15% methanol in dichloromethane), to obtain sensitizer **DMA-8** as a dark solid (39.9 mg, 36 µmol, 94%).

^{1}H NMR (600 MHz, acetone-d_6) δ: 8.45 (s, 1H), 7.97 (d, *J* = 5.1 Hz, 1H), 7.92 (s, 1H), 7.73 (s, 1H), 7.66 (d, *J* = 8.5 Hz, 2H), 7.56 (d, *J* = 5.1 Hz, 1H), 7.54 (d, *J* = 9.3 Hz, 4H), 7.28 (d, *J* = 8.1 Hz, 2H), 7.17 (d, *J* = 9.3 Hz, 4H), 7.15 (d, *J* = 8.5 Hz, 2H), 6.65 (d, *J* = 2.4 Hz, 2H), 6.60 (dd, *J* = 2.4 Hz, 8.1 Hz, 2H), 4.06-3.99 (m, 8H), 1.83-1.71 (m, 8H), 1.54-1.42 (m, 8H), 1.40-1.26 (m, 16H), 0.92 (t, *J* = 7.1 Hz, 6H), 0.87 (t, *J* = 6.9 Hz, 6H); ^{13}C NMR (150 MHz, acetone-d_6) δ: 163.8, 160.9 (2C), 158.0 (2C), 149.3, 149.2, 148.0, 147.2, 146.2 (2C), 142.3, 141.6, 139.7, 137.0, 135.3, 135.1 (2C), 131.6 (2C), 131.3 (4C), 128.5, 127.5 (2C), 125.5, 125.0 (4C), 123.7 (2C), 123.4 (2C), 120.2, 116.9, 115.6, 106.8 (2C), 101.1 (2C), 98.8, 69.0 (2C), 68.7 (2C), 32.4 (2C), 32.3 (2C), 29.1 (4C)*, 26.6 (2C), 26.5 (2C), 23.3 (4C), 14.4 (2C), 14.3 (2C); IR (neat, cm[-1]) ν: 2926 (s), 2857 (m), 2216 (w), 1685 (m), 1598 (s), 1490 (s), 1390 (s), 1136 (m), 1032 (m); HRMS (ASAP+, *m/z*): found 1113.4922 (calcd. $C_{68}H_{77}N_2O_6S_3$ 1113.4944, [M+H]$^+$). *Signal found using ^{1}H-^{13}C HSQC spectroscopy due to overlapping residual solvent signal.

(*E*)-3-(5'-(7-(4-(bis(2',4'-bis(hexyloxy)-[1,1'-biphenyl]-4-yl)amino)phenyl)-2,3-dihydrothieno[3,4-*b*][1,4]dioxin-5-yl)-[2,2'-bithiophen]-5-yl)-2-cyanoacrylic acid (DMA-9)
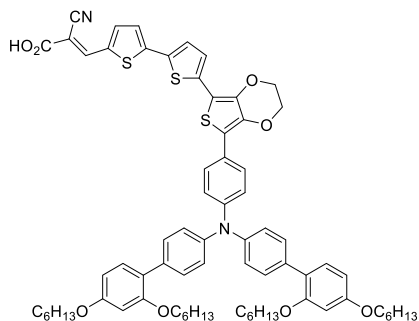
The synthesis of **DMA-9** was performed as described in the general Knoevenagel condensation procedure. The crude product was purified by silica gel column chromatography (gradient: 0-15% methanol in dichloromethane), to obtain sensitizer **DMA-9** as a dark solid (21.1 mg, 18 µmol, 99%).

^{1}H NMR (600 MHz, acetone-d_6) δ: 8.42 (s, 1H), 7.93 (d, J = 3.9 Hz, 1H), 7.66 (d, J = 9.2 Hz, 2H), 7.54 (d, J = 5.3 Hz, 1H), 7.53-7.48 (m, 5H), 7.29-7.24 (m, 3H), 7.16-7.08 (m, 6H), 6.63 (d, J = 2.4 Hz, 2H), 6.58 (dd, J = 2.4 Hz, 8.3 Hz, 2H), 4.55-4.51 (m, 2H), 4.48-4.43 (m, 2H), 4.06-3.99 (m, 8H), 1.82-1.70 (m, 8H), 1.53-1.41 (m, 8H), 1.40-1.26 (m, 16H), 0.91 (t, J = 7.0 Hz, 6H), 0.87 (t, J = 6.9 Hz, 6H); ^{13}C NMR (150 MHz, acetone-d_6) δ: 164.0, 160.8 (2C), 158.0 (2C), 147.8, 147.2 (2C), 146.3, 141.8, 140.7, 139.1, 138.0, 134.9, 134.8 (2C), 134.0, 131.5 (2C), 131.2 (4C), 128.0, 127.7 (2C), 127.2, 125.8, 125.0, 124.7 (4C), 124.4, 123.9 (2C), 123.5 (2C), 117.0, 116.8, 108.9, 106.7 (2C), 101.1 (2C), 98.2, 69.0 (2C), 68.6 (2C), 66.2, 65.7, 32.4 (2C), 32.3 (2C), 29.1 (4C)*, 26.6 (2C), 26.5 (2C), 23.3 (4C), 14.4 (2C), 14.3 (2C); IR (neat, cm^{-1}) ν: 2925 (s), 2854 (m), 2216 (w), 1682 (m), 1603 (m), 1493 (s), 1322 (m), 1183 (s), 1053 (s); HRMS (ASAP+, *m/z*): found 1196.5079 (calcd. $C_{72}H_{80}N_2O_8S_3$ 1196.5077, [M*]$^+$). *Signal found using ^{1}H-^{13}C HSQC spectroscopy due to overlapping residual solvent signal.

(*E*)-3-(6-(5-(4-(bis(2',4'-bis(hexyloxy)-[1,1'-biphenyl]-4-yl)amino)phenyl)thiophen-2-yl)-4,4-dihexyl-4*H*-cyclopenta[2,1-*b*:3,4-*b'*]dithiophen-2-yl)-2-cyanoacrylic acid (DMA-10)
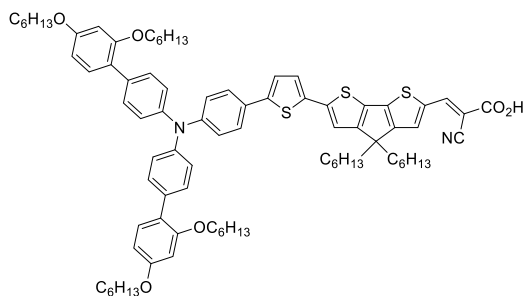
The synthesis of **DMA-10** was performed as described in the general Knoevenagel condensation procedure. The crude product was purified by silica gel column chromatography (gradient: 0-15% methanol in dichloromethane), to obtain sensitizer **DMA-10** as a dark solid (89.5 mg, 68 µmol, 85%).

^{1}H NMR (600 MHz, acetone-d_6) δ: 8.33 (s, 1H), 7.74 (s, 1H), 7.53 (d, J = 9.4 Hz, 2H), 7.46 (d, J = 8.6 Hz, 4H), 7.31-7.27 (m, 3H), 7.22 (d, J = 8.7 Hz, 2H), 7.15-7.11 (m, 6H), 6.58 (d, J = 2.4 Hz, 2H), 6.53 (dd, J = 2.4 Hz, 8.7 Hz, 2H), 4.00-3.94 (m, 8H), 2.02-1.90 (m, 4H), 1.81-1.69 (m, 8H), 1.53-1.40 (m, 8H), 1.39-

1.27 (m, 16H), 1.23-1.11 (m, 12H), 1.06-0.96 (m, 4H), 0.92 (t, J = 7.2 Hz, 6H), 0.88 (t, J = 7.0 Hz, 6H), 0.81 (t, J = 6.9 Hz, 6H); ^{13}C NMR (150 MHz, acetone-d$_6$) δ: 165.6, 164.4, 160.8 (2C), 158.8, 158.0 (2C), 149.2, 148.9, 147.4, 146.4 (2C), 144.9, 144.0, 137.9, 136.5, 135.2, 135.0 (2C), 131.4 (2C), 131.1 (4C), 128.4, 127.1 (2C), 126.0, 124.7 (4C), 124.1 (2C), 124.0, 123.7 (2C), 118.7, 117.3, 114.6, 106.3 (2C), 101.1 (2C), 96.0, 69.0 (2C), 68.6 (2C), 55.0, 38.6 (2C), 32.6 (2C), 32.5 (2C), 32.4 (2C), 30.6 (2C), 30.3 (2C), 30.1 (2C), 26.7 (2C), 25.8 (2C), 24.2 (2C), 23.54 (2C), 23.49 (2C), 23.48 (2C), 14.43 (2C), 14.38 (2C), 14.3 (2C); IR (neat, cm^{-1}) ν: 2929 (s), 2857 (m), 2214 (w), 1734 (s), 1601 (m), 1492 (s), 1408 (s), 1182 (s), 1046 (w); HRMS (ASAP+, m/z): found 1318.6893 (calcd. $C_{83}H_{102}N_2O_6S_3$ 1318.6900, [M*]$^+$). *Signal found using ^{1}H-^{13}C HSQC spectroscopy due to overlapping residual solvent signal.

(*E*)-3-(5''-(4-(bis(2',4'-bis(hexyloxy)-[1,1'-biphenyl]-4-yl)amino)phenyl)-3''-hexyl-[2,2':5',2''-terthiophen]-5-yl)-2-cyanoacrylic acid (DMA-11)

The synthesis of **DMA-11** was performed as described in the general Knoevenagel condensation procedure. The crude product was purified by silica gel column chromatography (gradient: 0-15% methanol in dichloromethane), to obtain sensitizer **DMA-11** as a dark solid (62.0 mg, 51 μmol, 98%).

^{1}H NMR (600 MHz, acetone-d$_6$) δ: 8.43 (s, 1H), 7.93 (d, J = 4.1 Hz, 1H), 7.58-7.54 (m, 3H), 7.52-7.47 (m, 5H), 7.31 (s, 1H), 7.26-7.21 (m, 3H), 7.12 (d, J = 8.6 Hz, 4H), 7.09 (d, J = 8.1 Hz, 2H), 6.62 (d, J = 2.4 Hz, 2H), 6.56 (dd, J = 2.4 Hz, 8.8 Hz, 2H), 4.04-3.97 (m, 8H), 2.83 (t, J = 7.8 Hz, 2H), 1.81-1.68 (m, 10H), 1.52-1.40 (m, 10H), 1.38-1.27 (m, 20H), 0.91 (t, J = 7.1 Hz, 6H), 0.89-0.82 (m, 9H); ^{13}C NMR (150 MHz, acetone-d$_6$) δ: 163.9, 160.8 (2C), 158.0 (2C), 148.7, 147.21, 147.19, 146.3 (2C), 143.6, 142.7, 141.5, 139.4, 135.5, 135.3, 134.8 (2C), 131.6 (2C), 131.2 (4C), 129.0, 128.24, 128.17, 127.6, 127.2 (2C), 126.7, 125.5, 124.8 (4C), 124.0 (2C), 123.4 (2C), 116.8, 106.7 (2C), 101.1 (2C), 98.7, 69.0 (2C), 68.6 (2C), 32.41, 32.39 (2C), 32.3 (2C), 31.1, 30.38, 30.35, 29.6 (4C)*, 26.6 (2C), 26.5 (2C), 23.33 (4C), 23.30, 14.41 (2C), 14.39, 14.3 (2C); IR (neat, cm^{-1}) ν: 2928 (s), 2857 (m), 2217 (w), 1688 (m), 1601 (s), 1493 (s), 1322 (m), 1182 (s), 1053 (m); HRMS (ASAP+, m/z): found 1222.5961 (calcd. $C_{76}H_{90}N_2O_6S_3$ 1222.5961, [M*]$^+$). *Signal found using ^{1}H-^{13}C HSQC spectroscopy due to overlapping residual solvent signal.

(*E*)-3-(6-(4-(bis(2',4'-bis(hexyloxy)-[1,1'-biphenyl]-4-yl)amino)phenyl)dithieno[3,2-*b*:2',3'-*d*]thiophen-2-yl)-2-cyanoacrylic acid (DMA-12)
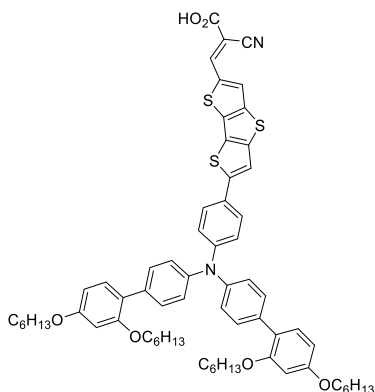
The synthesis of **DMA-12** was performed as described in the general Knoevenagel condensation procedure. The crude product was purified by silica gel column chromatography (gradient: 0-15% methanol in dichloromethane), to obtain sensitizer **DMA-12** as a dark solid (32.9 mg, 30 μmol, 77%).

^{1}H NMR (600 MHz, acetone-d_6) δ: 8.49 (s, 1H), 8.28 (s, 1H), 7.75 (s, 1H), 7.62 (d, J = 8.1 Hz, 2H), 7.51 (d, J = 8.1 Hz, 4H), 7.23 (d, J = 8.1 Hz, 2H), 7.14 (d, J = 8.1 Hz, 4H), 7.11 (d, J = 8.1 Hz, 2H), 6.62 (d, J = 2.4 Hz, 2H), 6.56 (dd, J = 2.4 Hz, 8.1 Hz, 2H), 4.04-3.97 (m, 8H), 1.81-1.69 (m, 8H), 1.52-1.41 (m, 8H), 1.38-1.25 (m, 16H), 0.91 (t, J = 7.2 Hz, 6H), 0.85 (t, J = 7.2 Hz, 6H); ^{13}C NMR (150 MHz, acetone-d_6) δ: 163.9, 160.8 (2C), 158.0 (2C), 150.5, 149.5, 148.8, 148.0, 146.0 (2C), 142.2, 139.3, 137.0, 135.2 (2C), 133.4, 131.6 (2C), 131.3 (4C), 129.3, 127.8, 127.6 (2C), 125.2 (4C), 123.34 (2C), 123.27 (2C), 116.94, 116.90, 106.7 (2C), 101.1 (2C), 98.04, 69.0 (2C), 68.6 (2C), 32.4 (2C), 32.3 (2C), 29.1 (4C)*, 26.6 (2C), 26.5 (2C), 23.3 (4C), 14.4 (2C), 14.3 (2C); IR (neat, cm^{-1}) ν: 2926 (s), 2857 (m), 2218 (w), 1687 (m), 1600 (m), 1470 (s), 1261 (s), 1182 (s), 1046 (m); HRMS (ASAP+, *m/z*): found 1086.4727 (calcd. $C_{66}H_{74}N_2O_6S_3$ 1086.4709, [M*]$^+$). *Signal found using ^{1}H-^{13}C HSQC spectroscopy due to overlapping residual solvent signal.

NMR
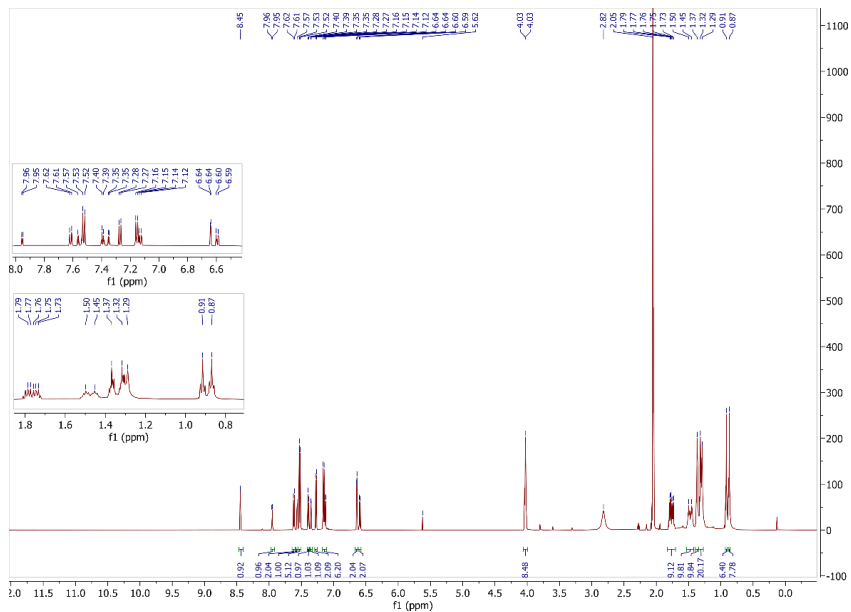
Figure S7. ^{1}H NMR (600 MHz, Acetone-d_6) spectrum for dye **DMA-6**.
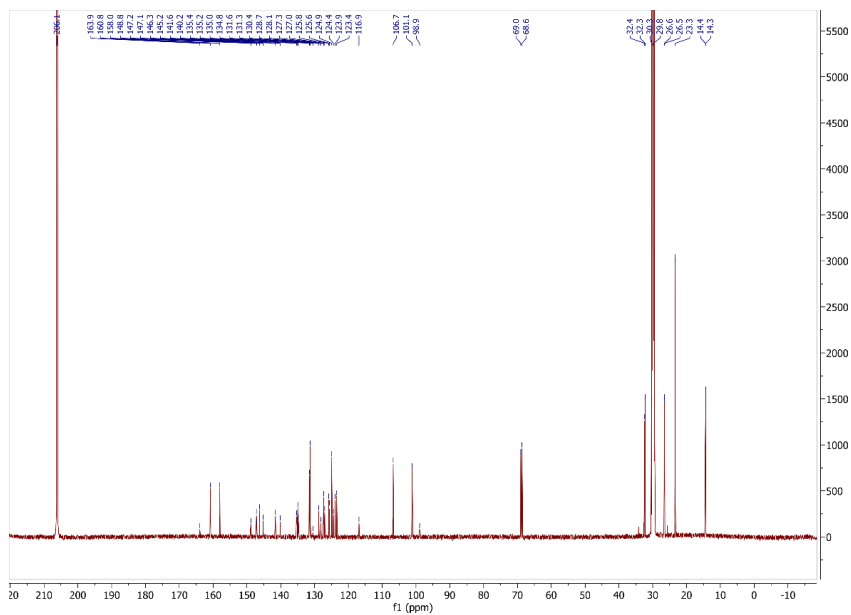
Figure S8. ^{13}C NMR (150 MHz, Acetone-d_6) spectrum for dye **DMA-6**.
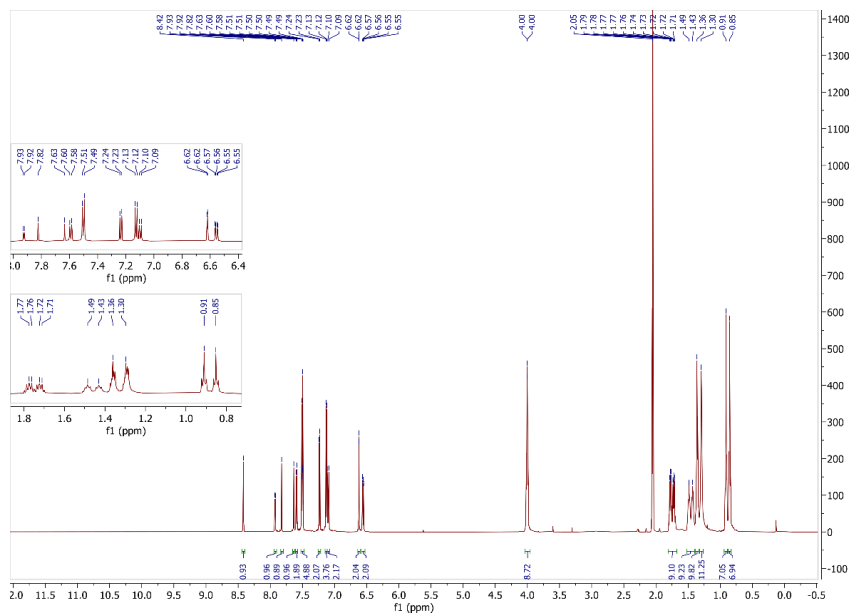
Figure S9. ^{1}H NMR (600 MHz, Acetone-d_6) spectrum for dye **DMA-7**.
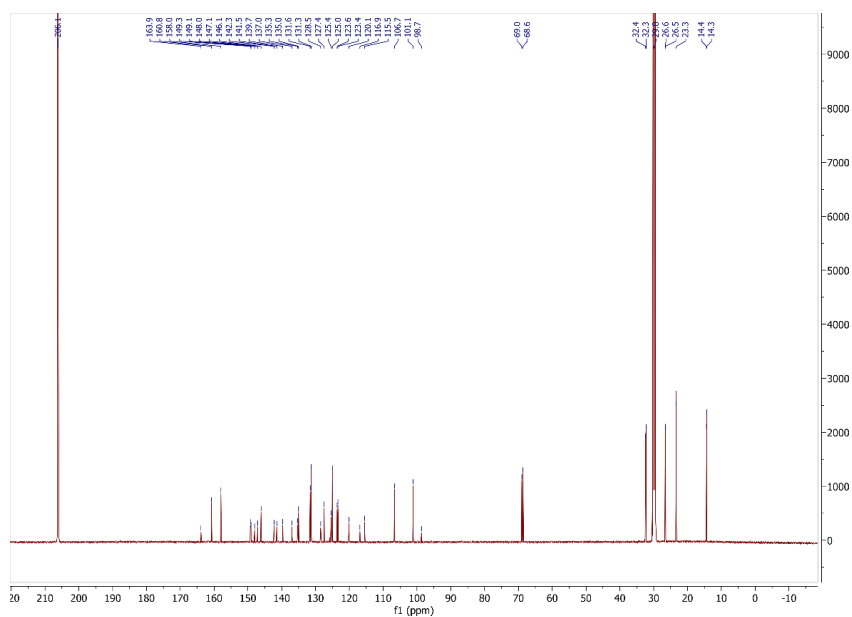
Figure S10. ^{13}C NMR (150 MHz, Acetone-d_6) spectrum for dye **DMA-7**.
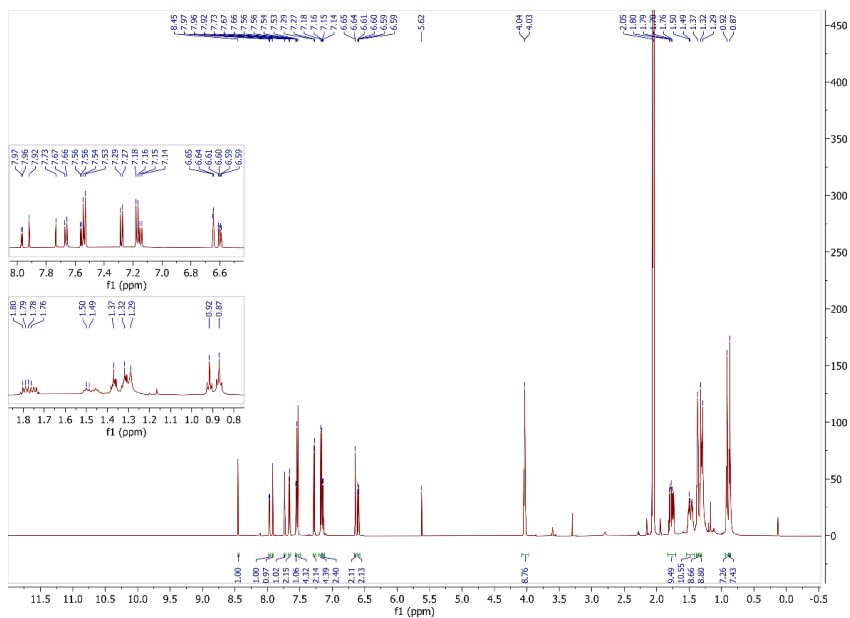
Figure S11. ^{1}H NMR (600 MHz, Acetone-d_6) spectrum for dye **DMA-8**.
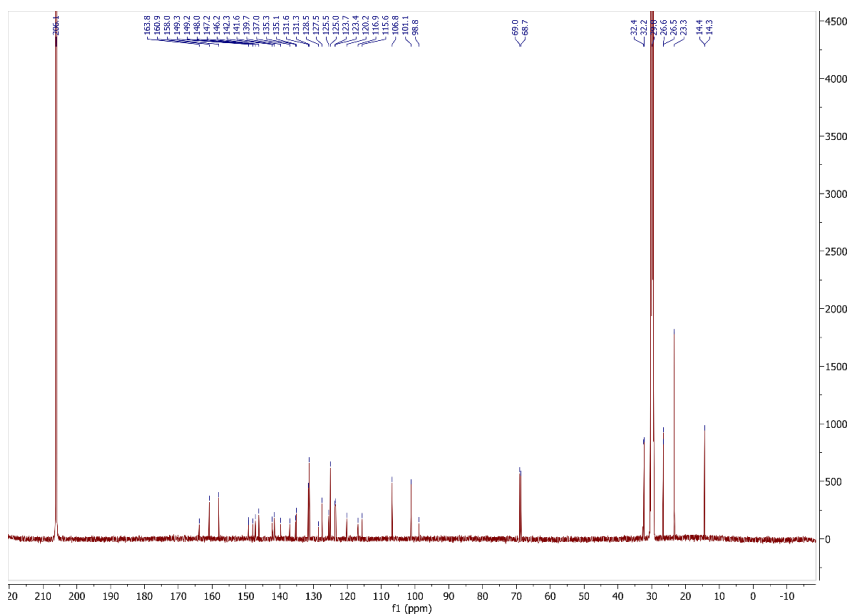
Figure S12. ^{13}C NMR (150 MHz, Acetone-d_6) spectrum for dye **DMA-8**.
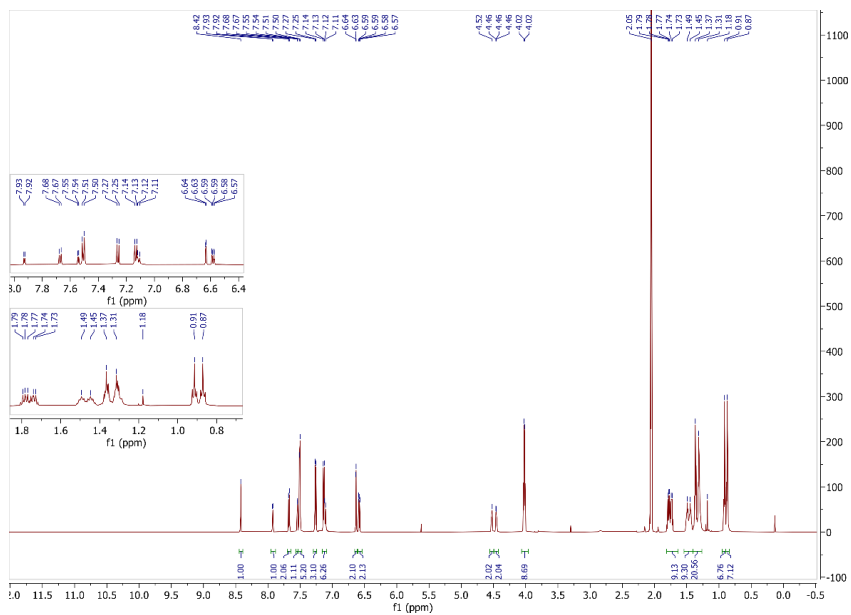
Figure S13. ^{1}H NMR (600 MHz, Acetone-d_6) spectrum for dye **DMA-9**.
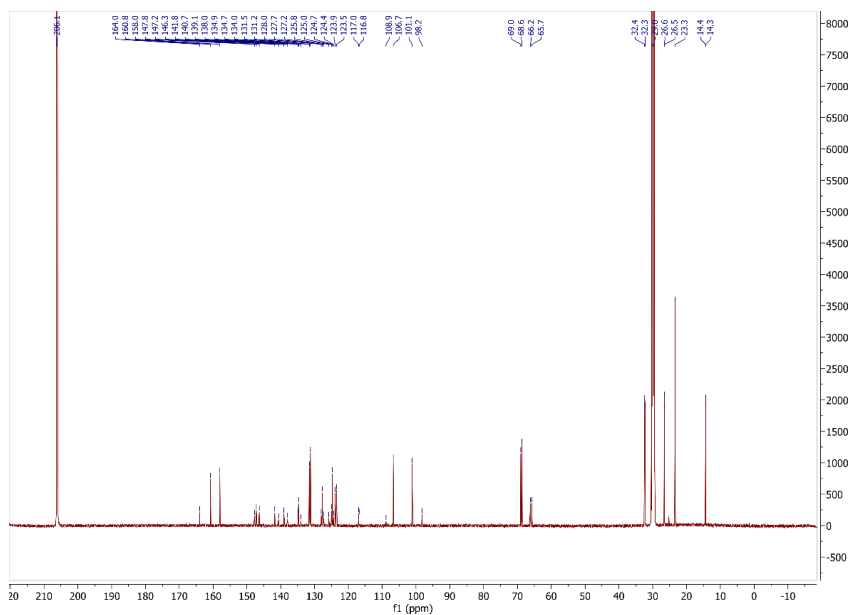
Figure S14. ^{13}C NMR (150 MHz, Acetone-d_6) spectrum for dye **DMA-9**.
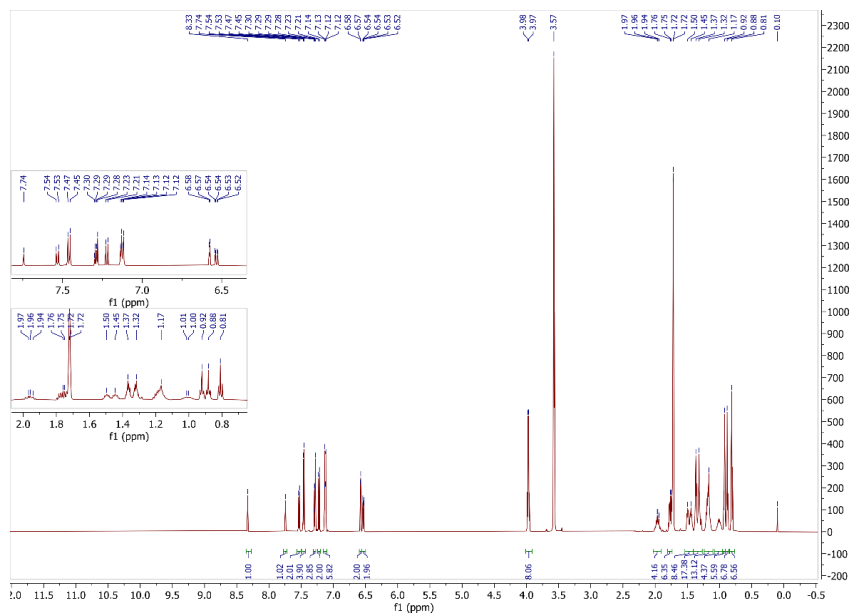
Figure S15. ^{1}H NMR (600 MHz, THF-d_8) spectrum for dye **DMA-10**.
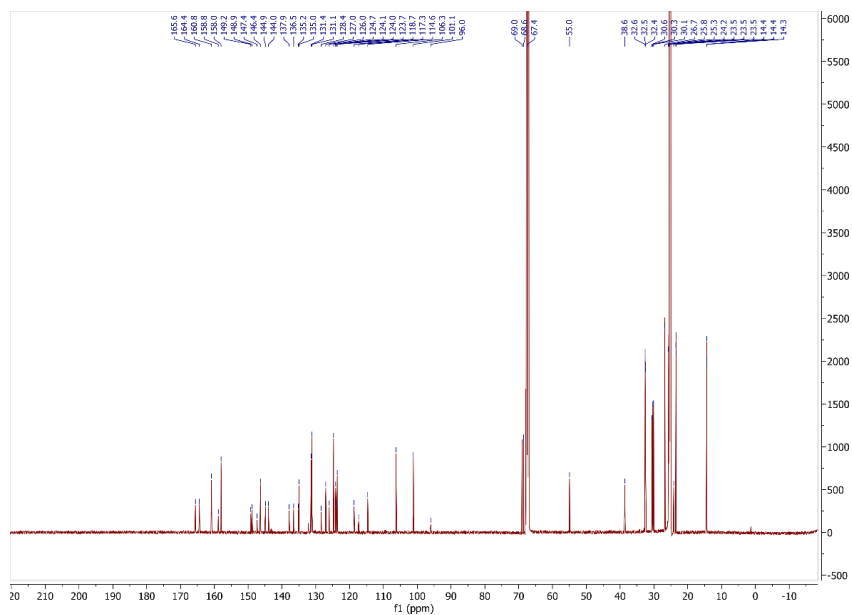
Figure S16. ^{13}C NMR (150 MHz, THF-d_8) spectrum for dye **DMA-10**.
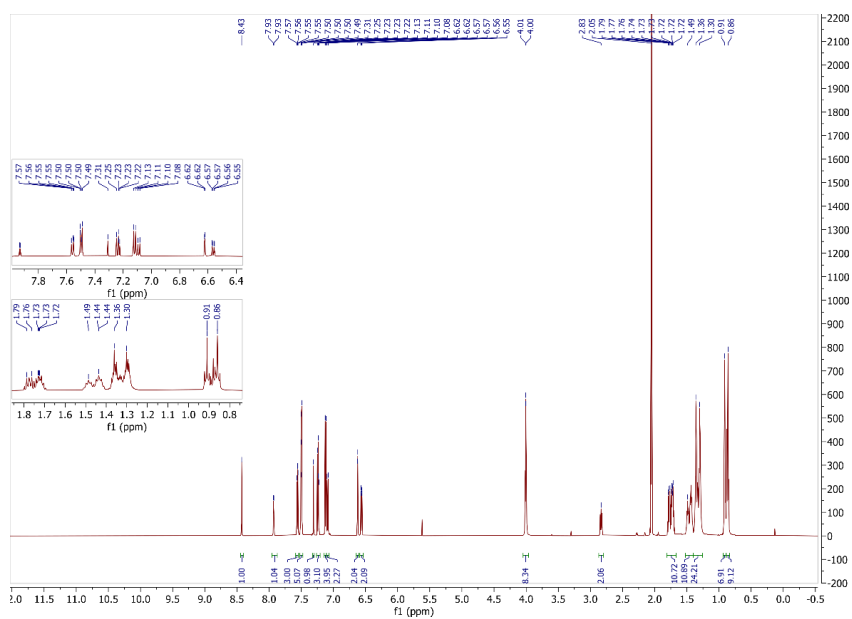
Figure S17. ^{1}H NMR (600 MHz, Acetone-d_6) spectrum for dye **DMA-11**.
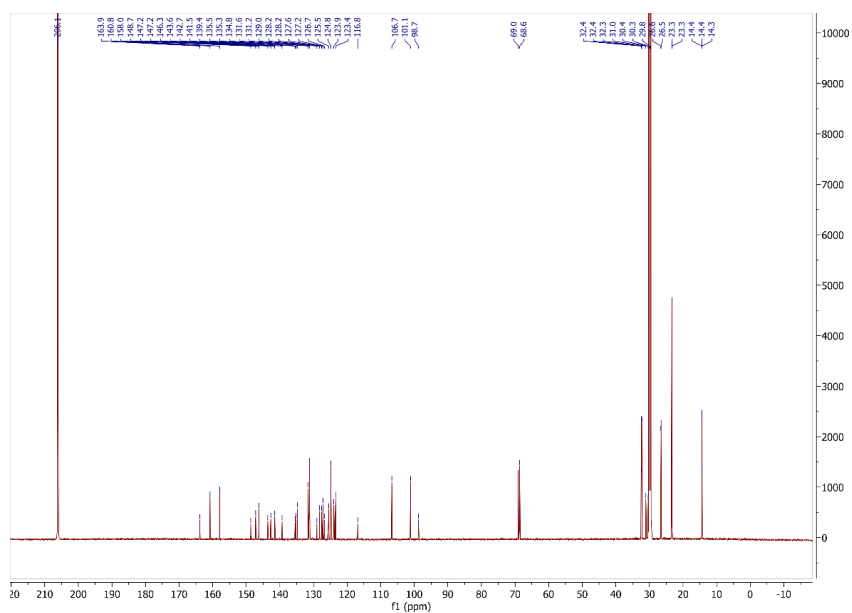
Figure S18. ^{13}C NMR (150 MHz, Acetone-d_6) spectrum for dye **DMA-11**.
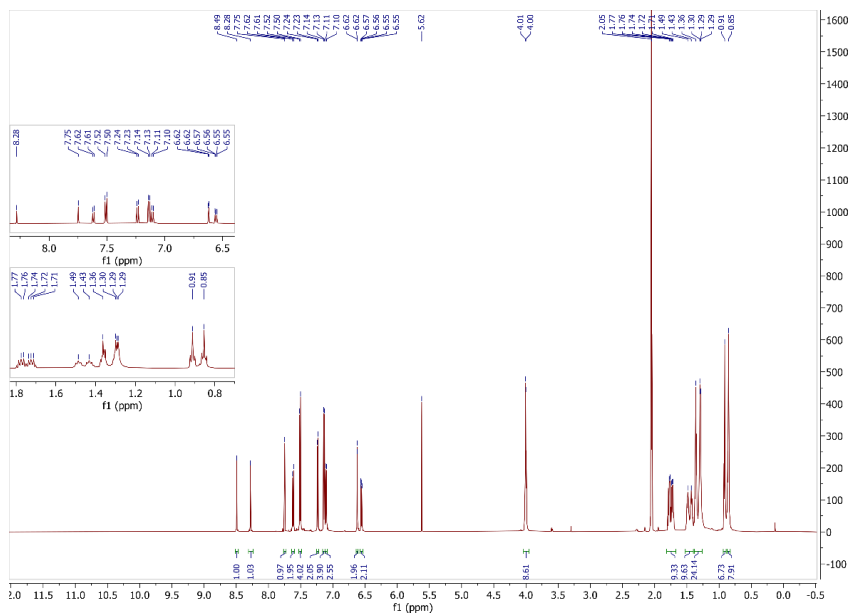
Figure S19. ^{1}H NMR (600 MHz, Acetone-d_6) spectrum for dye **DMA-12**.
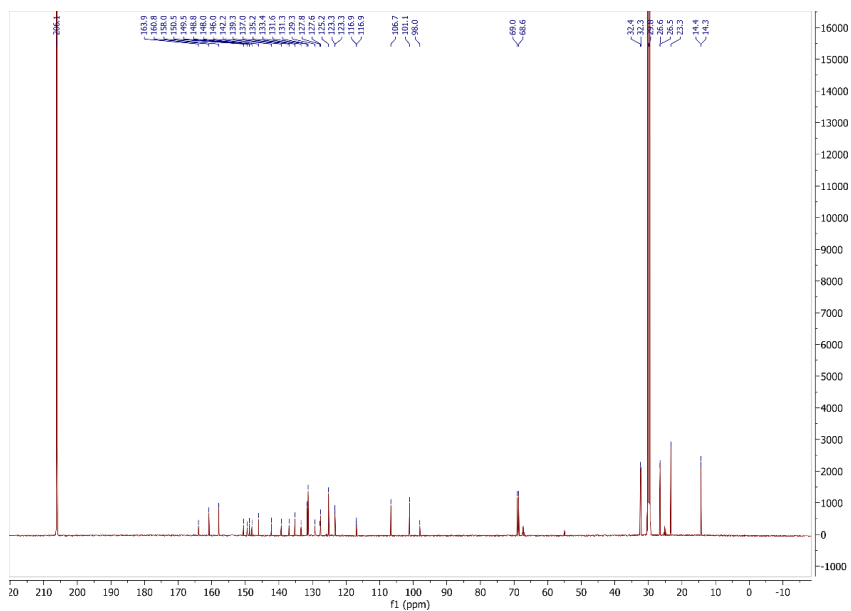
Figure S9. ^{13}C NMR (150 MHz, Acetone-d_6) spectrum for dye **DMA-12**.

Paper III

D. M. Almenningen, V. M. Engh, E. A. Strømsodd, H. E. Hansen, A. F. Buene,
O. R. Gautun and B. H. Hoff

*Synthetic Efforts to Investigate the Effect of Planarizing the Triarylamine
Geometry in Dyes for Dye-Sensitized Solar Cells*,

Paper III

Article

Synthetic Efforts to Investigate the Effect of Planarizing the Triarylamine Geometry in Dyes for Dye-Sensitized Solar Cells

David Moe Almenningen, Veslemøy Minge Engh, Eivind Andreas Strømsodd, Henrik Erring Hansen, Audun Formo Buene, Bård Helge Hoff,* and Odd Reidar Gautun*

Read Online

ACCESS | Metrics & More | Article Recommendations | Supporting Information

ABSTRACT: The geometry of a dye for dye-sensitized solar cells (DSSCs) has a major impact on its optical and electronic properties. The dye structure also dictates the packing properties and how well the dye insulates the metal−oxide surface from oxidants in the electrolyte. The aim of this work is to investigate the effect of planarizing the geometry of the common triarylamine donor, frequently used in dyes for DSSC. Five novel dyes were designed and prepared; two employ conventional triarylamine donors with thiophene and furan π-spacers, two dyes have had their donors planarized through one sulfur bridge (making two distinct phenothiazine motifs), and the final dye has been planarized by forming a double phenoxazine. The synthesis of these model dyes proved to be quite challenging, and each required specially designed total syntheses. We demonstrate that the planarization of the triarylamine donor can have different effects. When planarization was achieved by a 3,7-phenothiazine and double phenoxazine structures, improved absorption properties were noted, and a panchromatic absorption was achieved by the latter. However, an incorrect linking of donor and acceptor moieties has the opposite effect. Further, electrochemical impedance spectroscopy revealed clear differences in charge recombination depending on the structure of the dye. A drawback of planarized dyes in relation to DSSC is their low oxidation potentials. The best photovoltaic performance was achieved by 3,7-phenothazine with furan as a π-spacer, which produces a power conversion efficiency of 5.2% (J_{sc} = 8.8 mA cm^{-2}, V_{oc} = 838 mV, FF = 0.70).
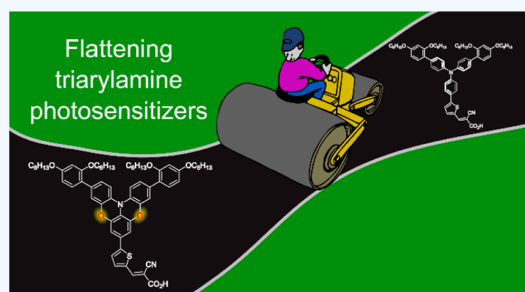
INTRODUCTION

Ever since its original report in 1991,[1] the dye-sensitized solar cell (DSSC) has been a keen object to study for many researchers worldwide. The DSSC enjoys a relatively simple structure with three key components, the mesoporous semiconducting metal oxide (most commonly TiO_2), the dye which is adsorbed on the metal oxide, and the redox shuttle responsible for regenerating the dye with electrons from the counter electrode.[2] After more than 30 years of constant research trying to improve the power conversion efficiency (PCE) of the DSSC, a laboratory-scale cell with a PCE of 14.3% has been reported.[3] This is obviously a lot lower than that of the conventional silicon-based solar cells, but recent developments in redox shuttles and dye design have made the DSSC the most efficient technology for ambient light photovoltaics.[4,5] Excellent indoor lighting PCE achieved by DSSCs lends itself nicely to be used to power the ever-increasing internet-of-things applications.[6−8] The aesthetically pleasing aspect of the DSSC is another inherent strength of this technology, which could be exploited by the use of DSSC in building-integrated photovoltaics (BIPVs).[9,10] The recent development of near-infrared absorbing dyes[11] and photo-

chromic dyes[12] will even allow for transparent devices that could be used in BIPV as power-generating windows.[13]

A marked improvement in DSSC performance was seen when one-electron metal complex redox shuttles were employed in place of the I^-/I_3^- redox shuttle.[14] These metal complexes, mainly based on Co and Cu, display redox potentials that are more closely matched to the oxidation potential of the dyes in the cell. Although this feature effectively reduced the overpotential losses in the DSSC, there were some initial problems with the fact that these complexes are easily reduced by electrons in TiO_2.[15] To combat this phenomenon, it became important to find a way to passivate the surface of TiO_2, for instance, through the use of alkoxysilanes as a coating material for the mesoporous electrode.[16] A more efficient strategy was the use of bulky
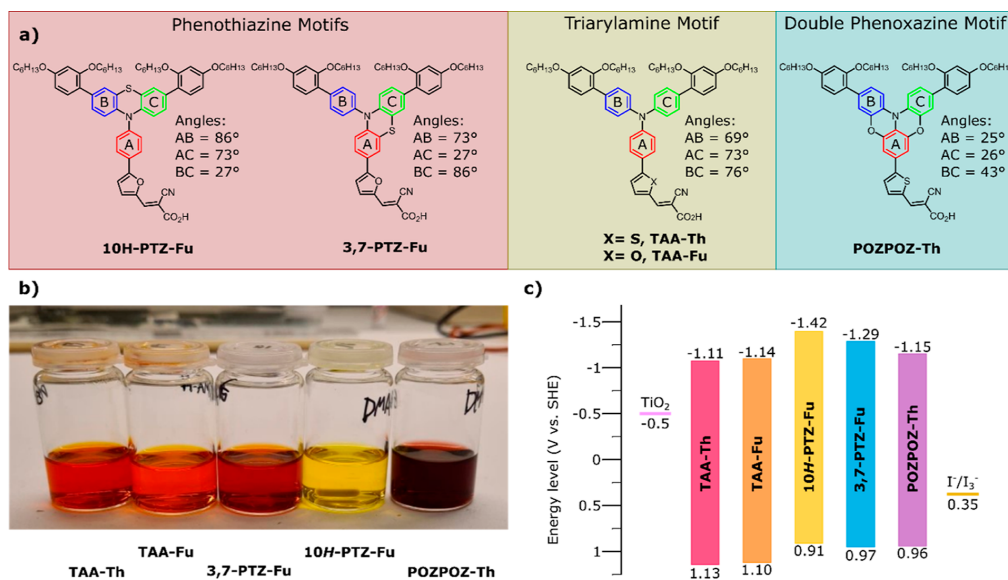
Figure 1. (a) Molecular structures and design concepts of the five different dyes reported in this paper. The degree of planarization is postulated from the out-of-plane angle between the three central phenyl rings based on crystallographic data of 2-chloro-10-phenylphenothiazine,[31] triphenylamine,[32] and benzo[5,6][1,4]oxazino[2,3,4-*kl*]phenoxazine.[33] (b) Staining solutions of the dyes; the concentration of each dye is 0.5 mM in a mixture of acetonitrile and THF (43:57, v/v). (c) Energy levels of the frontier orbitals of the dyes, TiO_2, and the I^-/I_3^- redox shuttle.

organic dyes, such as the tetra-alkoxy-substituted triarylamine motif, commonly referred to as the Hagfeldt donor, that has been used in several highly successful dyes.[3,5,17−20] The triarylamine scaffold holds a three-dimensional propeller shape that provides an umbrella effect for the surface of TiO_2, where it prevents the electrolyte from approaching the semiconductor and recombining with the electrons there.[21]

A possible downside of this out-of-plane geometry is that the aromatic system suffers from a sub-optimal overlap between the molecular orbitals. This is detrimental to the absorption properties of the dyes and in turn the possible photocurrent that it is possible to extract from them. As a result of this, triarylamine dyes are frequently extended with large π-spacers to improve their absorption properties[19,22,23] at the expense of complicating synthesis and increasing the cost of production. Planarization of the donor has previously been a successful design concept to improve absorption properties, most notably perhaps is the wide absorption spectra of ullazine-based dyes without any π-spacers.[24] Planarization of the donor has also shown to boost the intramolecular charge transfer (ICT) of dyes[25] and improve the interfacial charge-transfer processes of indoline and carbazole dyes.[26,27]

There are studies on planarizing the triarylamine donor through bridging with methylene[28] and diarylmethylene[29] compared to the "free" triarylamine. Planarizing the triarylamine donor through two sulfur bridges reported worse photovoltaic performance compared to a "free" triarylamine reference dye.[30] To study the effect of planarizing the triarylamine donor with heteroatom bridges, we report herein five novel dyes with moderately sized π-spacers based on the common triarylamine donor motif, see Figure 1a. The degree of planarization on these donors varies from the "free" triarylamine motif to the single planarization of the phenothiazine motifs and all the way to the double

phenoxazine motif. We demonstrate the possibility of tuning absorption through planarizing of the triarylamine donor, and the impact of these alterations on the color of the dyes is shown in Figure 1b. By comparing the photovoltaic performance of the "free" triarylamine dyes to the planarized ones, we aim to investigate the importance of the three-dimensional structure on solar cell performance.

■ EXPERIMENTAL SECTION

Materials. The reference dye **N719** was purchased from Dyenamo AB (Sweden), 2-bromo-5-iodophenol (**25**) was purchased from Apollo Scientific (UK), and 5-bromo-1,3-difluoro-2-nitrobenzene was purchased from abcr (Germany). The remaining chemicals and solvents used were all purchased from Merck. A full account of the synthetic procedures is given in the ESI.

Electrochemical Characterization. Cyclic voltammetry (CV) experiments were carried out using a Versastat 3 Potentiostat; the data were acquired using the Versastudio software. A stained TiO_2 photoanode as the working electrode, a graphite carbon counter electrode, and a Ag/AgCl reference were the components of the three-electrode system. The scan speed was 10 mV s^{-1}, and the supporting electrolyte was 0.1 M LiTFSI in dry acetonitrile.

Fabrication of DSSCs. The anodes were prepared from FTO glass (NSG10, Nippon Sheet Glass), which was cleaned in a KOH solution (150 g/L) in 70 w % ethanol under sonication for 45 min. Immersion of the glass in aqueous $TiCl_4$ solution (40 mM) at 70 °C for 2 × 45 min, followed by rinsing with deionized water and ethanol, was carried out before sintering TiO_2 for 1 h at 500 °C on a hotplate to deposit a blocking layer on the FTO sample. Pastes of TiO_2 were screen-printed onto FTO (53 T mesh, area 0.238 cm^2, Seritec Services S.A.); the first two active layers (18NR-T, Dyesol) were

Scheme 1. Synthesis of TAA-Th and TAA-Fu
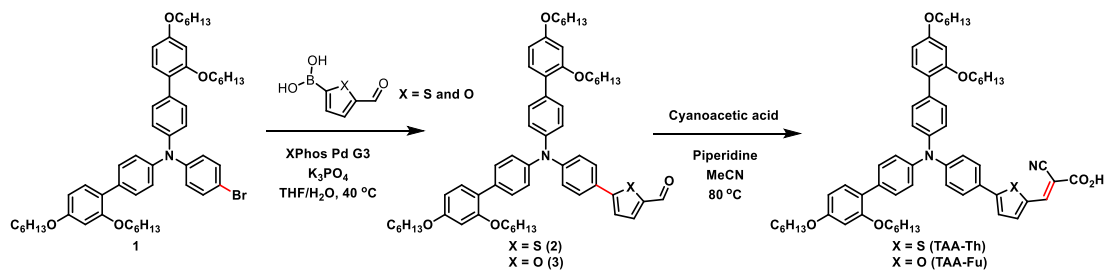
printed with 10 min heating on a hotplate at 125 °C after each layer. A scattering layer (WER2-O, Dyesol) was ultimately printed, and TiO$_2$ was sintered using a programmable furnace at set temperatures of 125, 250, 375, 450, and 500 °C for 5, 5, 5, 15, and 15 min with a ramping time of 10 min. Before staining, the electrodes were annealed at 500 °C for 30 min using a hotplate. The thicknesses of the TiO$_2$ layers were measured using a Veeco Dektak 150 profilometer and found to be 2 × 6 μm 18NR-T + 6 μm WER2-O.

The counter electrodes were prepared from TEC10 FTO glass supplied by Sigma-Aldrich. Holes were drilled into the electrodes from the FTO side using a diamond drill bit; this procedure was carried out under water. The glass plates were then cleaned using Deconex 21 (aq, 2 g/L), deionized water, ethanol, and acetone in an ultrasonic bath for 15 min for each. A solution of H$_2$PtCl$_6$ (10 mM) in 2-propanol was dropcast on FTO before heating at 400 °C for 15 min with a hot air gun, forming the catalytic layer of Pt.

The photoanodes were placed in the dye bath while still holding ∼80 °C from the annealing procedure and stored in a chamber at 30 °C overnight. The dye baths were prepared using a mixture of acetonitrile and tetrahydrofuran (THF) (43:57, v/v) to make a solution of the dye (0.5 mM) and co-adsorbent CDCA (5 mM). The staining of the reference N719 was done similarly, but the solvent mixture used was in this case t-butanol and acetonitrile (1:1, v/v). Following 15 h of staining, the electrodes were rinsed in acetonitrile for 2 min and then sealed to the counter electrode using Surlyn (25 μm, Solaronix) in a drybox. A 4 × 20 s treatment of the cell using a 50 W PTC heat element was sufficient to seal the cells. The electrolyte was vacuum-backfilled into the device; the filling hole was sealed with Surlyn and a glass cover disk. To complete the devices, the electrodes were painted with silver conducting paint (Electrolube, SCP). The electrolyte employed was a previously reported electrolyte A6141, consisting of butylmethylimidazolium iodide (0.60 M), I$_2$ (0.03 M), guanidinium thiocyanate (0.10 M), and 4-t-butylpyridine (0.60 M) dissolved in a mixture of acetonitrile and valeronitrile (85:15, v/v).[34]

Device Characterization. J−V curves were obtained under 1 sun illumination AM 1.5G illumination provided by a Sciencetech SP300B solar simulator, calibrated with a Newport Reference Cell (91150V), connected to a Keithley 2450 SourceMeter. A mask with an active area of 0.159 cm^2 was used on all the J−V measurements. IPCE measurements were carried out using a halogen lamp (Ocean Optics HL-2000) and a monochromator (Spectral Products CM110) connected to a Keithley 2450. The devices and the reference photodiode (Thorlabs, FDS100-CAL) were covered with a mask with a size of 0.049 cm^2. The electrochemical impedance properties were measured under constant illumination at 479 nm (12.6 mW cm^{-2}) and following the procedure we reported in our previous publication.[35]

■ RESULTS AND DISCUSSION

Dye Design. TAA-Th (thieno-linker) and TAA-Fu (furo-linker) are novel dyes, closely related to the dye D35 described by Hagberg et al., reaching a PCE of 6% in the initial study.[36] The dye D35 was one of the first dyes to demonstrate the usefulness of the alkoxy-substituted triarylamine donor to provide surface protection for the novel one-electron Co$^{2+/3+}$ redox shuttle.[37] It has since proven to be compatible with Cu electrolytes allowing for even higher voltages in DSSC.[38] It is expected that some increase in recombination resistance could be achieved by changing to hexyl side chains as presented in TAA-Th and TAA-Fu. In our previous study on phenothiazine, we found that dyes with a furan π-spacer perform slightly better than the corresponding thiophene analogue.[39] By comparing these two new triarylamine dyes, we will determine whether this holds for this dye class as well.

The dyes 10H-PTZ-Fu and 3,7-PTZ-Fu are designed in such a way that rotation and twisting of the aryl amine units are partially hindered by a covalent carbon−sulfur bond, placed symmetrically and asymmetrically respectively. The geometry of 10H-PTZ-Fu is atypical for phenothiazine dyes as our recent review of the entire class of phenothiazine dyes found this motif in only 4% of all dyes reported.[40] The molecular geometry of 3,7-PTZ-Fu follows the most conventional of phenothiazine dye designs, where dyes decorated with the auxiliary donor and π-spacer in positions 3 and 7 on phenothiazine make up 24% of all dyes.[40] The fully planarized double phenoxazine donor, seen for POZPOZ-Th, has not previously been reported. However, some double phenothiazine helicene analogues have been used in dyes for DSSC by Kim et al.[30]

To assess the planarity of the different donors reported herein, we use previously reported crystallographic data of the simpler compounds triphenylamine,[32] 2-chloro-10-phenyl-phenothiazine,[31] and benzo[5,6][1,4]oxazino[2,3,4-kl]-phenoxazine.[33] The three central rings of the "free" triarylamine donor (TAA-Th and TAA-Fu) are all expected to be 69−76° out of plane with each other. The sulfur-bridged compounds (10H-PTZ-Fu and 3,7-PTZ-Fu) have the angle between two of their three central rings reduced to 27°. The double phenoxazine motif (POZPOZ-Th) has through the two oxygen bridges reduced the angle between the three central rings to 25 and 26°.

Scheme 2. Synthesis of 10H-PTZ-Fu
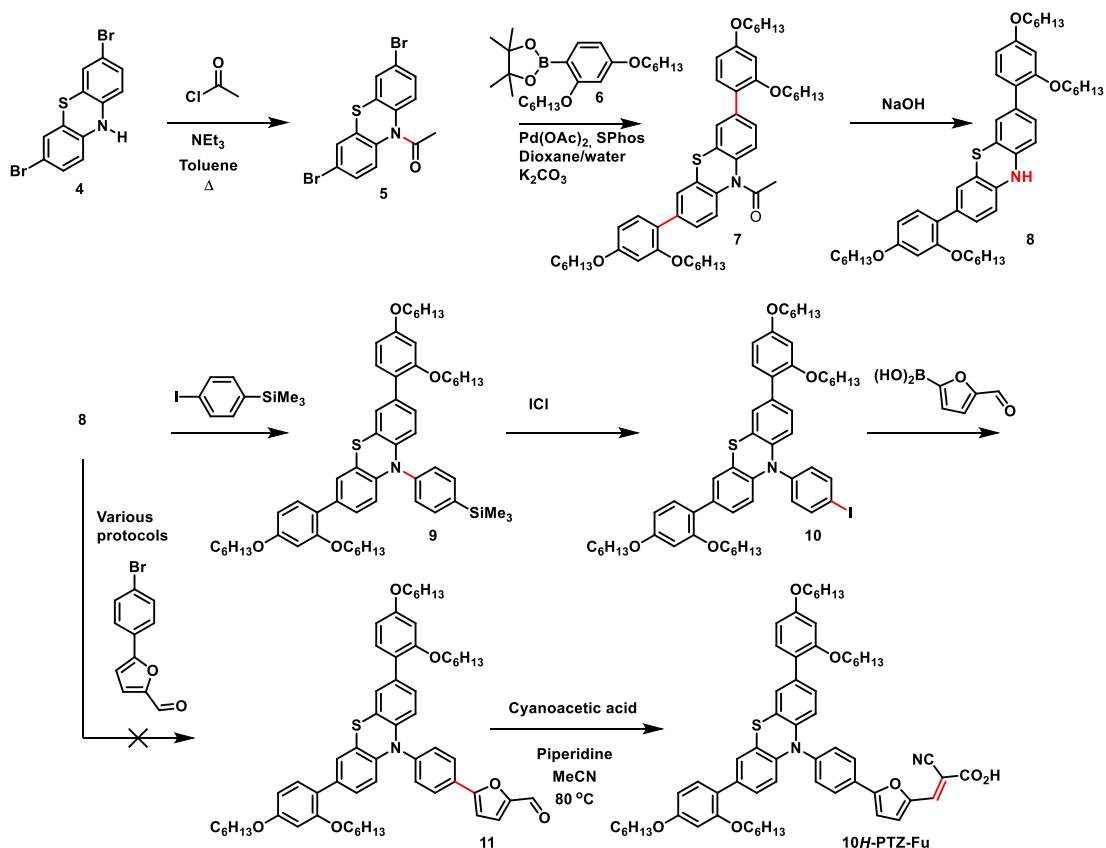
Synthesis. The synthesis route of **TAA-Th** and **TAA-Fu** is shown in Scheme 1. The advanced triarylamine fragment **1** was prepared as previously described by our group.[41] Then, a Suzuki cross-coupling with (5-formylthiophen-2-yl)boronic acid and (5-formylfuran-2-yl)boronic acid was carried out. These boronic acids are rather unstable,[42] so we selected the very active XPhos palladium third-generation precatalyst for the transformation.[43] Fortunately, when performed at 40 °C, the reaction gave the thiophene-containing aldehyde **2** in 40% yield and furan analogue **3** in 56% yield. Finally, a Knoevenagel condensation installed the cyanoacrylic acid anchoring group, giving **TAA-Th** and **TAA-Fu** in yields of 95 and 75%, respectively.

Synthesis of **10H-PTZ-Fu** was more cumbersome. We planned to employ 3,7-diarylated phenothiazine **8** in a Buchwald−Hartwig amination, see Scheme 2. To reach this critical intermediate, a direct double Suzuki coupling on 3,7-dibromo-10H-phenothiazine (**4**) was attempted, but purification of the material proved very difficult. To ensure sufficient amounts of the target dye to work with, we set out to improve the first step of the synthesis route. This was done by protecting the N-10 position of **4** as N-acetyl, allowing for a decent Suzuki cross-coupling between phenothiazine **5** and pinacol boronate ester **6**,[41] giving **7** in 65% yield. A facile deprotection then gave the key intermediate **8** (Scheme 2).

The Buchwald−Hartwig amination of **8** was first evaluated in a model reaction using 4-bromoanisole, which worked satisfactorily. However, the corresponding reaction with 5-(4-bromophenyl)furan-2-carbaldehyde, intended to give compound **11** directly, failed to convert the starting material under a number of reaction conditions.[44−48] Instead of tuning this reaction, we went for the longer route via silylated **9**. The Buchwald−Hartwig amination utilizing 1-bromo-4-(trimethylsilyl)benzene proceeded well, giving **9** in 91% yield. Conversion of trimetylsilyl groups to the corresponding iodide has previously been performed on simpler phenothiazines in high yields.[49,50] However, compound **9** is fairly electron-rich and we experienced the formation of byproducts, causing a difficult purification. This limited the isolated yield to 19%. The identities of the byproducts were indicated by mass spectroscopy to be the protodesilylated derivative, a di-iodinated product, and a tri-iodinated derivative. The structure of the latter compound was confirmed by NMR spectroscopic studies of a purified sample; the identity and the corresponding NMR spectra are shown in the Supporting Information. The iodinated derivative **10** was then subjected to Suzuki cross-coupling with 2-formylfuran-5-boronic acid. When employing the PdCl2(dppf) catalyst at 80 °C, no consumption of the starting material was observed. However, upon changing the catalyst to XPhos Pd G3 at 40 °C and using 1.6 equivalents of

Scheme 3. Synthesis of 3,7-PTZ-Fu
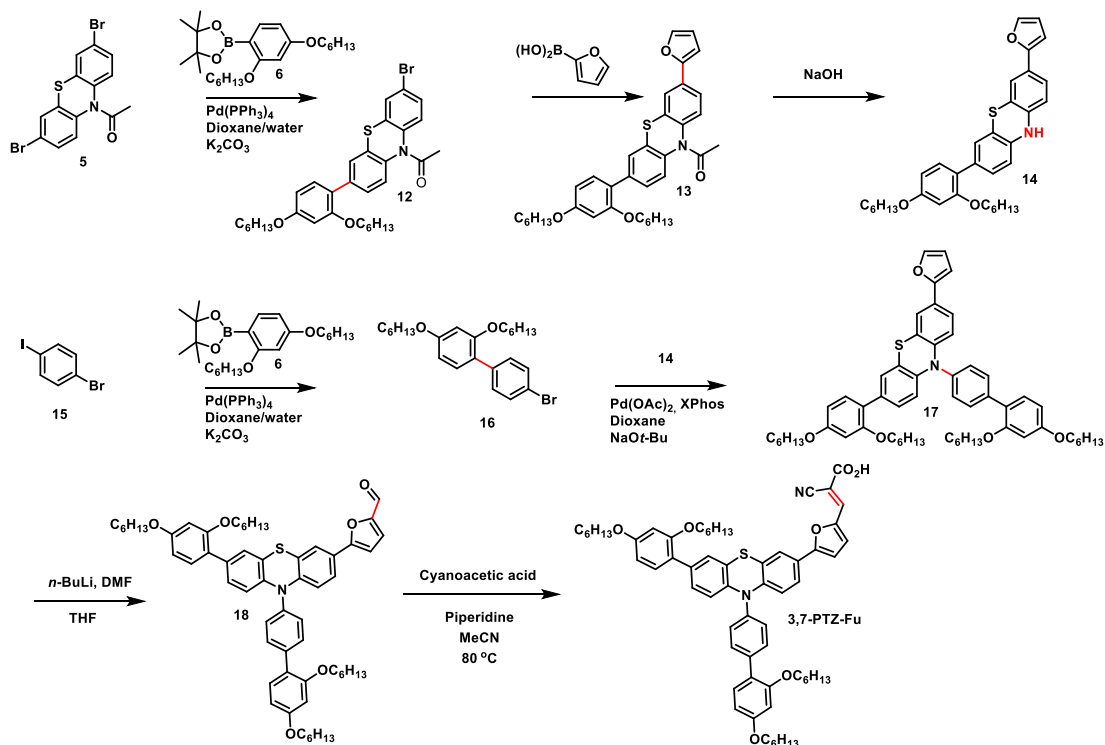
Scheme 4. Our Original Synthesis of Key Intermediate 24
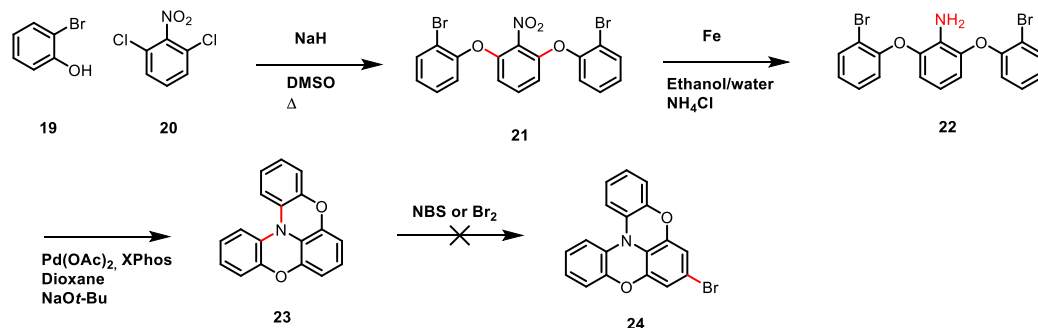
boronic acid allowed for isolation of the furan-functionalized **11** in 43% yield after purification. A Knoevenagel condensation concluded the synthesis and gave **10H-PTZ-Fu** in a yield of 85%.

The synthesis of **3,7-PTZ-Fu** borrowed several of the successful concepts from the synthesis route of **10H-PTZ-Fu**; however, special precautions were taken to ensure the asymmetric substitution on the phenothiazine donor. Starting with the *N*-acetyl-protected building block **5** (Scheme 3), we coupled it with 1.2 equivalents of pinacol boronate ester **6** in a Suzuki−Miyaura reaction. We have demonstrated on another set of phenothiazine sensitizers that these reaction conditions give an approximate 1:2:1 distribution of the starting material,

monocoupled product, and dicoupled product.[39] Following purification by column chromatography, intermediate **12** was isolated in a yield of 45%. The furanyl π-spacer was introduced through a subsequent Suzuki reaction catalyzed by PdCl$_2$(dppf), and compound **13** was obtained in a yield of 64%. Compound **14** was obtained from a simple hydrolysis of the protection group, and the coupling partner, **16**, was prepared from a Suzuki coupling on the iodide of 1-bromo-4-iodobenzene with pinacol boronate ester **6**. A Buchwald−Hartwig reaction between **14** and **16** produced the donor part of the dye, and intermediate **17** was obtained in a yield of 65%. To introduce the aldehyde functionality, the furan moiety was lithiated using *n*-BuLi and then quenched with DMF to

Scheme 5. Synthesis of POZPOZ-Th
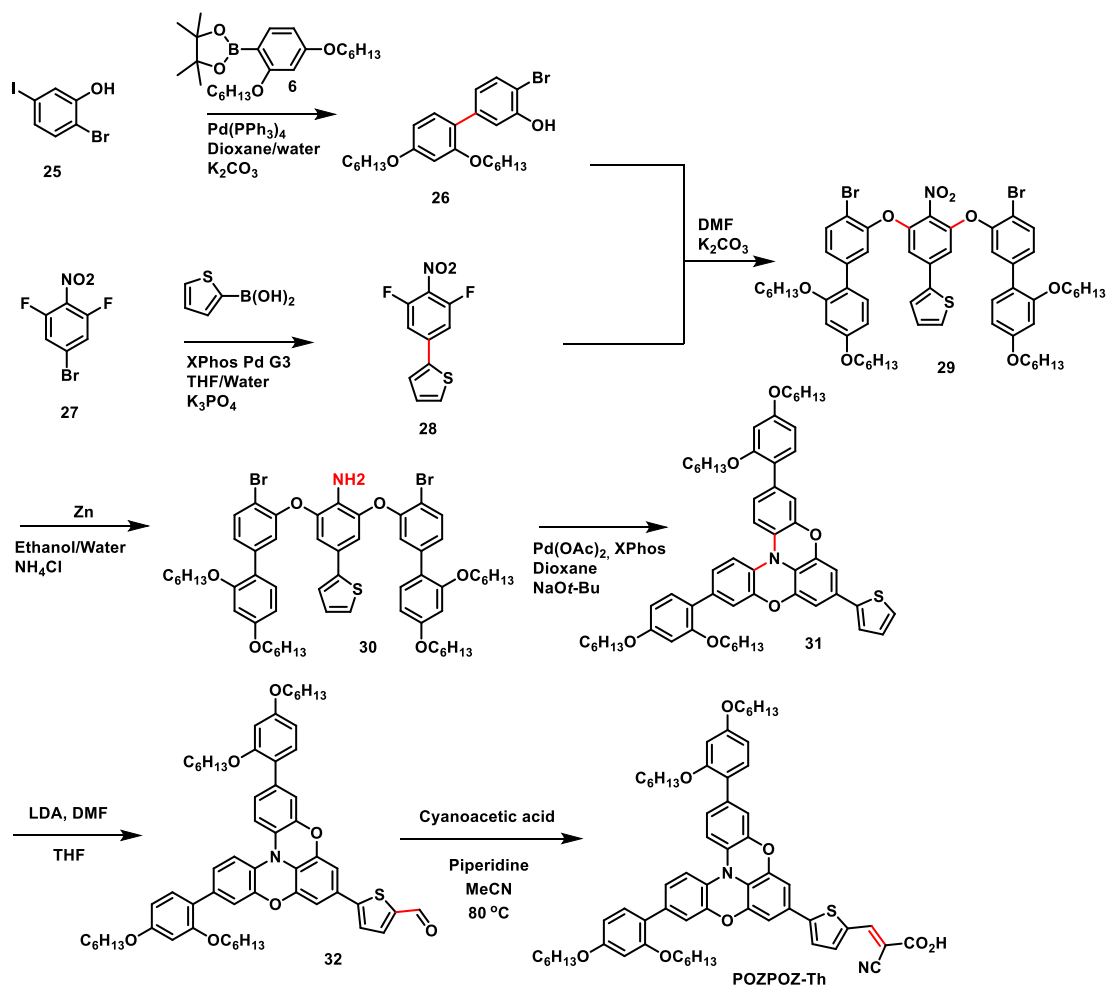
produce the advanced intermediate **18** in a yield of 34%. A Knoevenagel reaction was again used to complete the finished dye, giving **3,7-PTZ-Fu** in a yield of 65%.

The synthesis of **POZPOZ-Th** proved to be the most laborious of the dyes in this series as our original strategy, shown in Scheme 4, was unsuccessful. This synthesis is based on the route reported by Kuratsu et al.[33] for the synthesis of **23**. The first step is a nucleophilic aromatic substitution using the dimsyl anion as a base, which afforded **21** in a yield of 56%. We chose a Fe/NH₄Cl reduction procedure instead of using the hydrazine and Pd/C conditions reported in the original synthesis to avoid reducing the aromatic bromide. This approach worked as intended with no signs of a competing reduction of the bromides. Aniline **22** was used in the next step without the need for any purification beyond removing the inorganic solids. The final step in preparing helicene **23** involved a double intramolecular Buchwald−Hartwig amination catalyzed by Pd(OAc)₂ and XPhos, and **23** was isolated in a yield of 50% over two steps from **21**. Unfortunately, we were unsuccessful in selectively brominating **23**, even though two patents report the preparation of **24** by bromination.[51,52] This led us to devise a synthesis strategy which would not rely on a selective electrophilic aromatic substitution (EAS).

The final synthesis route for the successful preparation of **POZPOZ-Th** is shown in Scheme 5. First, phenol **26** was prepared in a similar manner to the previously mentioned intermediate **16**. In parallel, biaryl **28** was prepared in 74% yield using once more the conditions and precatalyst reported by Bruno et al.[43] Phenol **26** was then coupled to the central ring fragment **28** in a nucleophilic aromatic substitution reaction and afforded intermediate **29** in a yield of 59%. o-Fluoro-nitrophenyl is a common motif for directing nucleophilic aromatic substitutions, as exemplified by the total synthesis of vancomycin recently reported by Moore et al.,[53] where this motif is present on multiple occasions in the complex synthesis. The reduction of **29** to **30** went smoothly using Zn, and the only purification needed was the removal of inorganic solids. Using the previous conditions for intramolecular Buchwald−Hartwig coupling, we prepared the cyclized intermediate **31** in a yield of 39% over two steps
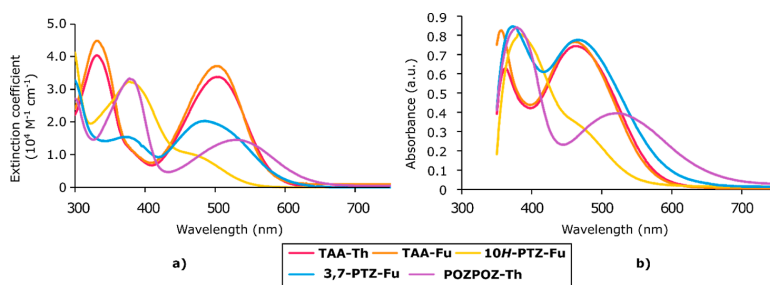
Figure 2. (a) UV/vis spectra of the dyes in dichloromethane (2×10^{-5} M). (b) UV/vis spectra of the dyes sensitized on a TiO_2 film (2.5 μm, GreatcellSolar, 18NR-T).

Table 1. Photophysical and Electrochemical Properties of Dyes in the Series

dye	$\lambda_{abs}{}^a$ (nm)	ε (M^{-1} cm^{-1})	Em[b] (nm)	$\lambda_{abs}{}^c$ on TiO_2 (nm)	$E_{0-0}{}^d$ (eV)	$E_{ox}{}^e$ (V vs SHE)	$E_{LUMO}{}^f$ (V vs SHE)
TAA-Th	504	33,800	639	464	2.24	1.13	−1.11
TAA-Fu	503	37,100	638	462	2.24	1.10	−1.14
10H-PTZ-Fu	461[g]	10,500[g]	591	461[g]	2.33	0.91	−1.42
3,7-PTZ-Fu	485	20,300	591	466	2.26	0.97	−1.29
POZPOZ-Th	530	14,500	639	522	2.11	0.96	−1.15

[a]Maximum of the most red-shifted peak. [b]Emission when the ICT band is excited in DCM solution. [c]Maximum of the most red-shifted peak on TiO_2 (2.5 μm, GreatcellSolar 18NR-T). [d]Calculated from the intersection of the absorption and normalized emission spectra. [e]Measured vs $F_c{}^+/F_c$ on stained TiO_2 electrodes in acetonitrile with 0.1 M LiTFSI, converted to V vs SHE by 0.624 V. Scan rate 10 mV s^{-1}. [f]Calculated from $E_{ox} - E_{0-0}$. [g]Shoulder.

from **29**. Because we chose a thiophene π-spacer for **POZPOZ-Th**, which is slightly more acidic than furan, we were able to generate the lithiated thiophene using LDA instead of *n*-BuLi. The lithiated intermediate of **31** was quenched with DMF, affording aldehyde **32** in a yield of 48%. To complete the synthesis of the double phenoxazine dye, we carried out a Knoevenagel condensation, isolating **POZPOZ-Th** in a yield of 84%.

Photophysical Properties. The planarization of the triarylamine donor has a profound effect on the absorption properties of the dyes. To quantify this effect, we performed UV/vis measurements on the dyes in a solution of dichloromethane (2×10^{-5} M) and while adsorbed on a TiO_2-film (2.5 μm). The results from these measurements are shown in Figure 2 and summarized in Table 1. The two triarylamine sensitizers, **TAA-Th** and **TAA-Fu**, display similar absorption properties in solution, albeit with a slightly higher molar extinction coefficient for the furan-linked dye. Comparing the absorption properties of the furan-linked dyes, we see that the absorption properties are adversely affected by the introduction of a sulfur bridge. The standard phenothiazine dye **3,7-PTZ-Fu**, is blue-shifted by 18 nm compared to **TAA-Fu**. For the symmetric phenothiazine dye, **10H-PTZ-Fu**, we assign the shoulder at ~460 nm to stem from the charge-transfer absorption and a 42 nm blue shift, and a drastic reduction in molar extinction coefficient is observed. This blue shift is noted in several studies comparing 10*H*-phenothiazine dyes to conventional phenothiazine dyes[54] and to triarylamine dyes.[55,56] The absorption properties of dyes that adopt this configuration suffer from a poor orbital mixing between the donor and acceptor since the acceptor part of the conjugated system sits perpendicular to the phenothiazine donor.[56] An example of the opposite is seen for the double phenoxazine dye, **POZPOZ-Th**, where more of the aromatic system of the donor is brought into the plane of the acceptor. The

absorption maximum of this dye is red-shifted by 26 nm compared to its "free" triarylamine analogue, **TAA-Th**, proving that the double planarization of the triphenylamine donor is a suitable strategy for improving absorption properties, although the molar extinction coefficient is more than halved compared to the triarylamine analogue, **TAA-Th**.

The absorption properties of the dyes on TiO_2 revealed that all the dyes except **10H-PTZ-Fu** were blue-shifted upon absorption to TiO_2. This blue-shift phenomenon is reported in the literature to be caused by a combination of deprotonation of the dye anchoring group upon attachment to the semiconductor and the formation of H-aggregated dye clusters on the surface of TiO_2.[57,58] To investigate this further, we obtained the absorption spectra of the dyes with 10 equiv anti-aggregation additive CDCA; the spectra are shown in Figure S1 in the Supporting Information. The spectra of the dyes with CDCA were fairly similar to the ones without CDCA but at a slightly lower intensity of absorption, which is likely attributed to a lower dye loading. The **10H-PTZ-Fu** dye displayed a similar absorption shoulder at the same wavelengths when adsorbed on TiO_2 as when measured in solution. This is in accordance with the trend seen for the class of 10*H*-phenothiazine dyes,[40] where this geometry is the only phenothiazine motif frequently associated with red shifts of absorption on TiO_2 and the only geometry where the phenothiazine moieties can align to form *J*-aggregates when anchored on the surface. We also see that the conventional 3,7-phenothiazine geometry is less blue-shifted upon absorption on TiO_2 than the triarylamine dyes, and in fact, it displays a slightly higher absorption maximum than the **TAA** dyes on TiO_2. This could suggest that the 3,7-phenothiazine scaffold is less susceptible to form H-aggregates than triarylamines on the surface of titania.

Electrochemical Properties. CV on stained TiO_2 electrodes was performed for each dye in the series. The obtained

Table 2. Photovoltaic Performance of all Dyes under 1 sun AM 1.5G Illumination and from IPCE Measurements[a]

dye	IPCE J_{SC} (mA cm^{-2})[b]	J_{SC} (mA cm^{-2})[c]	V_{OC} (mV)[c]	FF[c]	PCE (%)[c]	dye loading (10^{-8} mol cm^{-2})[d]
TAA-Th	9.05	7.5 ± 0.2	829 ± 4	0.66 ± 0.01	4.1 ± 0.1	22 ± 1.4
TAA-Fu	8.43	7.7 ± 0.0	869 ± 4	0.70 ± 0.02	4.7 ± 0.1	31 ± 0.4
10H-PTZ-Fu	5.25	4.9 ± 0.0	839 ± 9	0.77 ± 0.01	3.1 ± 0.1	25 ± 0.4
3,7-PTZ-Fu	10.82	8.8 ± 0.2	838 ± 10	0.70 ± 0.00	5.2 ± 0.1	29 ± 0.5
POZPOZ-Th	7.56	5.8 ± 0.2	673 ± 0	0.59 ± 0.03	2.3 ± 0.1	33 ± 0.5
N719[e]	13.61	11.8	742	0.72	6.3	

[a]Results from dye loading experiments are also included. [b]Otained by integration of the IPCE spectrum over the 1 sun AM 1.5 G spectrum. [c]Average values of three separate devices. [d]Values averaged of two desorbed TiO$_2$ electrodes. [e]Values from the best-performing device.

voltammograms are displayed in Figure S2, and the energy levels of the frontier orbitals are shown in Figure 1c and Table 1. The properties of the two triarylamine dyes are nearly identical, and their oxidation potentials are found at 1.10−1.13 V versus SHE. Incorporating a sulfur bridge in a symmetrical manner (**10H-PTZ-Fu**) lowers the oxidation potential by 19 mV, and in an asymmetrical manner (**3,7-PTZ-Fu**), it is lowered by 13 mV compared to their reference dye **TAA-Fu**. The double phenoxazine dye (**POZPOZ-Th**) has a 17 mV lower oxidation potential than its triarylamine analogue, **TAA-Th**. Unfortunately, the planarization of the triarylamine donor renders the dyes incompatible with the V_{OC}-enhancing copper-based electrolytes due to an insufficient driving force for the regeneration of the dye cations. A range of cobalt complexes has been reported with redox potentials of 0.43−0.85 V versus NHE,[37] suggesting that a cobalt-based electrolyte could be used for the planarized dyes. However, the low molar extinction coefficients of **10H-PTZ-Fu**, **3,7-PTZ-Fu**, and **POZPOZ-Th** would not be optimal for the thin TiO$_2$ layers required for the diffusion-limited cobalt redox shuttles. Hence, we opted for the traditional I$^-$/I$_3^-$ redox shuttle for our photovoltaic evaluation of the sensitizers reported herein.

Photovoltaic Properties. To evaluate the photovoltaic performance of the sensitizers, we prepared three DSSC devices for each dye, and the average photovoltaic parameters are presented in Table 2. The J−V curves of the best device for each dye are shown in Figure 3, and the obtained IPCE spectra

Figure 4. IPCE spectra of the best performing DSSC device for each dye and the reference sensitizer **N719**.

study on π-spacers for phenothiazine dyes in the I$^-$/I$_3^-$ electrolyte.[39] The drop in photovoltage seen for dyes with thiophene linkers could be caused by the facilitation of recombination stemming from iodine−sulfur interactions occurring near the surface of TiO$_2$.[59] The significantly higher dye loading of **TAA-Fu** compared to **TAA-Th** could also provide better surface protection of TiO$_2$, which would also retard recombination between electrons in the semiconductor and oxidants in the electrolyte. The IPCE spectrum of **TAA-Th** is in fact slightly wider than its furan counterpart and would therefore be expected to produce a larger photocurrent. Inconsistencies between IPCE and J−V measurements can be expected due to the IPCE measurements being carried out at lower intensities of irradiation and at single wavelengths.[60]

The effect of the sulfur bridge on photovoltaic performance is apparent when comparing the phenothiazine dyes and the furan-linked triarylamine dye. Although the **10H-PTZ-Fu** dye consistently produced the highest fill factors of this series, the severely reduced light harvesting ability of this dye meant that the overall performance was significantly reduced compared to the non-planarized triarylamine analogue. The sub-optimal performance of this dye was expected as this type of phenothiazine motif is associated with the worst overall performance of phenothiazine dyes.[40] The conventional **3,7-PTZ-Fu** dye displayed improved light harvesting abilities compared to the triarylamine reference dye, **TAA-Fu**. As a result of this, the J_{sc} of **3,7-PTZ-Fu** was increased by 14% by planarizing the triarylamine dye with a sulfur bridge in an asymmetrical manner. Although the phenothiazine dye produced higher photocurrents, a 30 mV reduction in V_{oc} was also seen for the 3,7-phenothiazine dye. Still, the photovoltage of 3,7-PTZ-Fu was remarkably high for an I$^-$/I$_3^-$ electrolyte and consistent with our previous report on the *N*-arylphenothiazine dye **DMA-0** achieving a similar photovoltage.[35] The best photovoltaic performance of this series of dyes was in fact found for the conventional phenothiazine dye. This demonstrates that there is some merit to the

Figure 3. J−V curves of the best performing DSSC device for each dye and the reference sensitizer **N719**.

from these devices are shown in Figure 4. The integrated IPCE spectra show consistently higher short-circuit currents than what was measured under 1 sun AM 1.5G illumination, meaning that the reported efficiencies do not fail our previously reported data credibility assessment.[40] The triarylamine dyes revealed that the furan π-spacer is beneficial for boosting photovoltaic performance compared to a thiophene π-spacer. The V_{oc} of **TAA-Fu** was 40 mV larger than that of **TAA-Th**; this is consistent with the results from our previous

Figure 5. (a) Recombination resistance of the DSSC devices as a function of applied voltage. (b) Ratio of effective electron diffusion length to TiO$_2$ film thickness as a function of applied voltage.

phenothiazine donor over the triarylamine donor because of an increased light harvesting ability. It should be noted that this only holds when employing a traditional I$^-$/I$_3^-$ electrolyte.

When considering the IPCE spectra shown in Figure 4, we see that the double oxygen bridge planarization of **POZPOZ-Th** leads to a panchromatic IPCE response. This dye produced an IPCE spectrum with absorption as wide as the reference sensitizer, **N719**, albeit at approximately halved intensity. The IPCE of a DSSC is a product of light harvesting efficiency, charge injection efficiency, and charge collection efficiency.[61] Considering that the dye loading of **POZPOZ-Th** is the highest in this series and the molar extinction coefficient is superior to that of **N719** (1.3×10^4 M^{-1} cm^{-1}),[62] it is likely that the fully planar dye suffers from poor charge injection or charge collection. The planar design should leave the dyes more susceptible to aggregate, which often promotes excited-state quenching and impaired charge injection.[63] The less bulky design of **POZPOZ-Th** could also promote recombination of electrons in TiO$_2$ with oxidants in the electrolyte, adversely affecting the charge collection efficiency. In any case, the fully planarized dye displayed the worst photovoltaic performance in the series, despite its excellent spectral coverage. Also worth noting is the strange behavior of the J–V curve of **POZPOZ-Th** where the slope changes around 550 mV.

Electrochemical Impedance Spectroscopy. To examine the effect the planarization has on the surface passivation ability of the dyes, we performed electrochemical impedance spectroscopy (EIS) on the best-performing device fabricated for each dye. The obtained complex plane plots are shown in the Supporting Information, Figure S3, and from these, we extracted the recombination resistance, R_{rec}, and plotted these versus applied voltage, as shown in Figure 5a. We also extracted the series resistance, R_s, and the transport resistance, R_{tr}; the plot of these as a function of applied voltage is shown in the Supporting Information, Figure S4. The recombination resistance plot, Figure 5a, shows that the lowest charge recombination is achieved by the symmetrical sulfur-bridged dye, **10H-PTZ-Fu**. This suggests that this geometry in fact produces a superior surface passivation compared to the triarylamine dyes. As the triarylamine class of dyes has gained much of its success from being superb blockers of electron recombination,[21] the improved blocking ability of **10H-PTZ-Fu** is an impressive feature of this dye. The surface passivation properties of the 3,7-phenothiazine dye were also comparable to that of the triarylamine dyes. Meanwhile, the fully planarized

double phenoxazine dye displayed an irregular and unexpected behavior, where the recombination resistance increased with increasing voltage from 0.55 V. This behavior is however in line with what we expect from the change of slope seen in the J–V curve of **POZPOZ-Th**. The relationship between recombination resistance and voltage is

$$R_{rec}(V) = \left(\frac{dJ}{dV}\right)^{-1} \tag{1}$$

where V is the voltage and J is the current density. The less steep slope of the J–V curve after 0.55 V is expected to affect the recombination resistance, as seen in Figure 5a. We attribute the irregular behavior and lower recombination resistance of **POZPOZ-Th** at voltages lower than V_{OC} to the more planar structure of this dye compared to the other dyes in the series. To further investigate the strange behavior of **POZPOZ-Th**, we looked at the effective electron diffusion length, L_n, which is a measure of the competition between recombination and charge collection.[64] The effective diffusion length is obtained readily from EIS measurements and is

$$L_n = L\sqrt{\frac{R_{rec}}{R_{tr}}} \tag{2}$$

where L is the film thickness, R_{rec} is the recombination resistance, and R_{tr} is the transport resistance. When considering the plot of the effective electron diffusion length in Figure 5b, we see that for all dyes except **POZPOZ-Th**, it decreases with increasing applied potential. In fact, the effective electron diffusion length of **POZPOZ-Th** approaches 1 at lower voltages, suggesting that we are approaching a device described by Gerischer impedance.[65] This shows that for the fully planar dye, **POZPOZ-Th**, there is an unfavorable competition between charge collection and charge recombination. The incomplete electron collection likely contributes to the reduced IPCE intensity and in turn the low photocurrent produced by **POZPOZ-Th**. This is supported by the absorption intensity of the charge-transfer absorption of **POZPOZ-Th**, which is found to be slightly bigger than that of **10H-PTZ-Fu** when measured on TiO$_2$, and the latter displays a considerably bigger IPCE intensity. Interestingly, Figure 5b also shows that both the phenothiazine dyes display longer effective electron diffusion lengths than the triarylamine analogues, showing that the sulfur bridges are useful for steering electrons toward collection instead of recombination with the redox shuttle.

■ CONCLUSIONS

We have successfully demonstrated the synthesis of five novel triarylamine dyes with varying degrees of planarization in the donor moiety. We have shown that the planarization of the triarylamine donor has a profound effect on the electronic properties of the dyes, in addition to the geometrical and conformational effects of a more planar donor. A downside of this is the ambiguity when it comes to tracing changes in photovoltaic performance back to an electronic effect or a conformational effect or even a combination of the two. In any case, with evaluation of the "free" triarylamine dyes, **TAA-Th** and **TAA-Fu**, a clear performance advantage from using a furan π-spacer was noted. The furan-linked dye, **TAA-Fu**, produced an excellent photovoltage of 869 mV in an I^-/I_3^- electrolyte. When considering the sulfur-bridged dyes, **10H-PTZ-Fu** and **3,7-PTZ-Fu**, we saw some advantages associated with this type of planarization. Most notably, the dye **3,7-PTZ-Fu** displayed improved light harvesting ability and J_{sc} compared to its triarylamine analogue. The DSSC devices sensitized by this dye were the most efficient in this series of dyes at 5.2% (J_{sc} = 8.8 mA cm^{-2}, V_{oc} = 838 mV, FF = 0.70). Moreover, EIS revealed that the symmetrical phenothiazine donor of **10H-PTZ-Fu** provided the highest recombination resistances and the longest effective diffusion lengths, which suggests that the geometry of this donor provides a better surface passivation than the propeller shape of triarylamines. Going to a fully planarized donor as in **POZPOZ-Th**, we show that this planarization produced a panchromatic IPCE spectrum. Alas, this planar donor provided a considerably worse charge collection than the other dyes in this series, as shown by the effective electron diffusion length measured by EIS. This has severe consequences for the photovoltaic performance of the dye **POZPOZ-Th**, and it proved to be the worst-performing dye in this series. Overall, we conclude that the out-of-plane geometry of "free" triarylamine is sub-optimal for light harvesting and that it is possible to improve this through planarization.

■ ASSOCIATED CONTENT

ⓈⒾ Supporting Information

The Supporting Information is available free of charge at https://pubs.acs.org/doi/10.1021/acsomega.2c03163.

> Cyclic voltammograms, complex plane plots from EIS, extracted transport resistance and series resistance data, experimental details related to the organic synthesis, and 1H and 13C NMR spectra of the reported compounds (PDF)

■ AUTHOR INFORMATION

Corresponding Authors

Bård Helge Hoff − *Department of Chemistry, Norwegian University of Science and Technology, 7491 Trondheim, Norway*; Email: bard.h.hoff@ntnu.no

Odd Reidar Gautun − *Department of Chemistry, Norwegian University of Science and Technology, 7491 Trondheim, Norway*; ⓞ orcid.org/0000-0001-9810-8682; Email: odd.r.gautun@ntnu.no

Authors

David Moe Almenningen − *Department of Chemistry, Norwegian University of Science and Technology, 7491 Trondheim, Norway*

Veslemøy Minge Engh − *Department of Chemistry, Norwegian University of Science and Technology, 7491 Trondheim, Norway*

Eivind Andreas Strømsodd − *Department of Chemistry, Norwegian University of Science and Technology, 7491 Trondheim, Norway*

Henrik Erring Hansen − *Department of Materials Science and Engineering, Norwegian University of Science and Technology, 7491 Trondheim, Norway*

Audun Formo Buene − *Department of Civil and Environmental Engineering, Norwegian University of Science and Technology, 7034 Trondheim, Norway*

Complete contact information is available at:
https://pubs.acs.org/10.1021/acsomega.2c03163

Author Contributions

The manuscript was written through contributions of all authors. All authors have given approval to the final version of the manuscript.

Notes

The authors declare no competing financial interest.

■ ACKNOWLEDGMENTS

■ REFERENCES

(1) O'Regan, B.; Grätzel, M. A low-cost, high-efficiency solar cell based on dye-sensitized colloidal TiO2 films. *Nature* **1991**, *353*, 737−740.

(2) Hagfeldt, A.; Boschloo, G.; Sun, L.; Kloo, L.; Pettersson, H. Dye-Sensitized Solar Cells. *Chem. Rev.* **2010**, *110*, 6595−6663.

(3) Kakiage, K.; Aoyama, Y.; Yano, T.; Oya, K.; Fujisawa, J.-i.; Hanaya, M. Highly-efficient dye-sensitized solar cells with collaborative sensitization by silyl-anchor and carboxy-anchor dyes. *Chem. Commun.* **2015**, *51*, 15894−15897.

(4) Saygili, Y.; Söderberg, M.; Pellet, N.; Giordano, F.; Cao, Y.; Muñoz-García, A. B.; Zakeeruddin, S. M.; Vlachopoulos, N.; Pavone, M.; Boschloo, G.; Kavan, L.; Moser, J.-E.; Grätzel, M.; Hagfeldt, A.; Freitag, M. Copper Bipyridyl Redox Mediators for Dye-Sensitized Solar Cells with High Photovoltage. *J. Am. Chem. Soc.* **2016**, *138*, 15087−15096.

(5) Zhang, D.; Stojanovic, M.; Ren, Y.; Cao, Y.; Eickemeyer, F. T.; Socie, E.; Vlachopoulos, N.; Moser, J.-E.; Zakeeruddin, S. M.; Hagfeldt, A.; Grätzel, M. A molecular photosensitizer achieves a Voc of 1.24 V enabling highly efficient and stable dye-sensitized solar cells with copper(II/I)-based electrolyte. *Nat. Commun.* **2021**, *12*, 1777.

(6) Aslam, A.; Mehmood, U.; Arshad, M. H.; Ishfaq, A.; Zaheer, J.; Ul Haq Khan, A.; Sufyan, M. Dye-sensitized solar cells (DSSCs) as a potential photovoltaic technology for the self-powered internet of things (IoTs) applications. *Sol. Energy* **2020**, *207*, 874−892.

(7) Michaels, H.; Benesperi, I.; Freitag, M. Challenges and prospects of ambient hybrid solar cell applications. *Chem. Sci.* **2021**, *12*, 5002−5015.

(8) Pecunia, V.; Occhipinti, L. G.; Hoye, R. L. Z. Emerging Indoor Photovoltaic Technologies for Sustainable Internet of Things. *Adv. Energy Mater.* **2021**, *11*, 2100698.

(9) Yoon, S.; Tak, S.; Kim, J.; Jun, Y.; Kang, K.; Park, J. Application of transparent dye-sensitized solar cells to building integrated photovoltaic systems. *Build. Environ.* **2011**, *46*, 1899−1904.

(10) Roy, A.; Ghosh, A.; Bhandari, S.; Selvaraj, P.; Sundaram, S.; Mallick, T. K. Color Comfort Evaluation of Dye-Sensitized Solar Cell (DSSC) Based Building-Integrated Photovoltaic (BIPV) Glazing after 2 Years of Ambient Exposure. *J. Phys. Chem. C* **2019**, *123*, 23834−23837.

(11) Naim, W.; Novelli, V.; Nikolinakos, I.; Barbero, N.; Dzeba, I.; Grifoni, F.; Ren, Y.; Alnasser, T.; Velardo, A.; Borrelli, R.; Haacke, S.; Zakeeruddin, S. M.; Graetzel, M.; Barolo, C.; Sauvage, F. Transparent and Colorless Dye-Sensitized Solar Cells Exceeding 75% Average Visible Transmittance. *JACS Au* **2021**, *1*, 409−426.

(12) Huaulmé, Q.; Mwalukuku, V. M.; Joly, D.; Liotier, J.; Kervella, Y.; Maldivi, P.; Narbey, S.; Oswald, F.; Riquelme, A. J.; Anta, J. A.; Demadrille, R. Photochromic dye-sensitized solar cells with light-driven adjustable optical transmission and power conversion efficiency. *Nat. Energy* **2020**, *5*, 468−477.

(13) Grifoni, F.; Bonomo, M.; Naim, W.; Barbero, N.; Alnasser, T.; Dzeba, I.; Giordano, M.; Tsaturyan, A.; Urbani, M.; Torres, T.; Barolo, C.; Sauvage, F. Toward Sustainable, Colorless, and Transparent Photovoltaics: State of the Art and Perspectives for the Development of Selective Near-Infrared Dye-Sensitized Solar Cells. *Adv. Energy Mater.* **2021**, *11*, 2101598.

(14) Velore, J.; Chandra Pradhan, S.; Hamann, T. W.; Hagfeldt, A.; Unni, K. N. N.; Soman, S. Understanding Mass Transport in Copper Electrolyte-Based Dye-Sensitized Solar Cells. *ACS Appl. Energy Mater.* **2022**, *5*, 2647−2654.

(15) Feldt, S. M.; Gibson, E. A.; Gabrielsson, E.; Sun, L.; Boschloo, G.; Hagfeldt, A. Design of Organic Dyes and Cobalt Polypyridine Redox Mediators for High-Efficiency Dye-Sensitized Solar Cells. *J. Am. Chem. Soc.* **2010**, *132*, 16714−16724.

(16) Carli, S.; Casarin, L.; Caramori, S.; Boaretto, R.; Busatto, E.; Argazzi, R.; Bignozzi, C. A. A viable surface passivation approach to improve efficiency in cobalt based dye sensitized solar cells. *Polyhedron* **2014**, *82*, 173−180.

(17) Zhang, W.; Wu, Y.; Bahng, H. W.; Cao, Y.; Yi, C.; Saygili, Y.; Luo, J.; Liu, Y.; Kavan, L.; Moser, J.-E.; Hagfeldt, A.; Tian, H.; Zakeeruddin, S. M.; Zhu, W.-H.; Grätzel, M. Comprehensive control of voltage loss enables 11.7% efficient solid-state dye-sensitized solar cells. *Energy Environ. Sci.* **2018**, *11*, 1779−1787.

(18) Freitag, M.; Teuscher, J.; Saygili, Y.; Zhang, X.; Giordano, F.; Liska, P.; Hua, J.; Zakeeruddin, S. M.; Moser, J.-E.; Grätzel, M.; Hagfeldt, A. Dye-sensitized solar cells for efficient power generation under ambient lighting. *Nat. Photonics* **2017**, *11*, 372−378.

(19) Eom, Y. K.; Kang, S. H.; Choi, I. T.; Yoo, Y.; Kim, J.; Kim, H. K. Significant light absorption enhancement by a single heterocyclic unit change in the π-bridge moiety from thieno[3,2-b]-benzothiophene to thieno[3,2-b]indole for high performance dye-sensitized and tandem solar cells. *J. Mater. Chem. A* **2017**, *5*, 2297−2308.

(20) Tsao, H. N.; Yi, C.; Moehl, T.; Yum, J.-H.; Zakeeruddin, S. M.; Nazeeruddin, M. K.; Grätzel, M. Cyclopentadithiophene Bridged Donor−Acceptor Dyes Achieve High Power Conversion Efficiencies in Dye-Sensitized Solar Cells Based on the tris-Cobalt Bipyridine Redox Couple. *ChemSusChem* **2011**, *4*, 591−594.

(21) Baumann, A.; Curiac, C.; Delcamp, J. H. The Hagfeldt Donor and Use of Next-Generation Bulky Donor Designs in Dye-Sensitized Solar Cells. *ChemSusChem* **2020**, *13*, 2503−2512.

(22) Gabrielsson, E.; Ellis, H.; Feldt, S.; Tian, H.; Boschloo, G.; Hagfeldt, A.; Sun, L. Convergent/Divergent Synthesis of a Linker-Varied Series of Dyes for Dye-Sensitized Solar Cells Based on the D35 Donor. *Adv. Energy Mater.* **2013**, *3*, 1647−1656.

(23) Zhang, X.; Xu, Y.; Giordano, F.; Schreier, M.; Pellet, N.; Hu, Y.; Yi, C.; Robertson, N.; Hua, J.; Zakeeruddin, S. M.; Tian, H.; Grätzel, M. Molecular Engineering of Potent Sensitizers for Very Efficient Light Harvesting in Thin-Film Solid-State Dye-Sensitized Solar Cells. *J. Am. Chem. Soc.* **2016**, *138*, 10742−10745.

(24) Delcamp, J. H.; Yella, A.; Holcombe, T. W.; Nazeeruddin, M. K.; Grätzel, M. The Molecular Engineering of Organic Sensitizers for Solar-Cell Applications. *Angew. Chem., Int. Ed.* **2013**, *52*, 376−380.

(25) Park, J.-H.; Nam, D. G.; Kim, B.-M.; Jin, M. Y.; Roh, D.-H.; Jung, H. S.; Ryu, D. H.; Kwon, T.-H. Planar D−D−π-A Organic Sensitizers for Thin-Film Photoanodes. *ACS Energy Lett.* **2017**, *2*, 1810−1817.

(26) Tian, L.; Wang, Y.; Zhang, Y.; Li, X.; Wu, W.; Liu, B. Molecular Engineering of Indoline Dyes and Their Application in Dye-Sensitized Solar Cells: Effect of Planarity and Side Chain on Interfacial Charge-Transfer Processes. *ACS Appl. Energy Mater.* **2021**, *4*, 242−248.

(27) Liu, Y.; Zhang, X.; Li, C.; Tian, Y.; Zhang, F.; Wang, Y.; Wu, W.; Liu, B. Energy-Level Control via Molecular Planarization and Its Effect on Interfacial Charge-Transfer Processes in Dye-Sensitized Solar Cells. *J. Phys. Chem. C* **2019**, *123*, 13531−13537.

(28) Do, K.; Kim, D.; Cho, N.; Paek, S.; Song, K.; Ko, J. New Type of Organic Sensitizers with a Planar Amine Unit for Efficient Dye-Sensitized Solar Cells. *Org. Lett.* **2012**, *14*, 222−225.

(29) Wu, F.; Zhao, S.; Lee, L. T. L.; Wang, M.; Chen, T.; Zhu, L. Novel D-π-A organic sensitizers containing diarylmethylene-bridged triphenylamine and different spacers for solar cell application. *Tetrahedron Lett.* **2015**, *56*, 1233−1238.

(30) Kim, C.; Choi, H.; Paek, S.; Kim, J.-J.; Song, K.; Kang, M.-S.; Ko, J. Molecular engineering of thia-bridged triphenylamine heterohelicenes as novel organic dyes for dye-sensitized solar cells. *J. Photochem. Photobiol., A* **2011**, *225*, 17−25.

(31) de Meester, P.; Chu, S. S. C.; Jovanovic, M. V.; Biehl, E. R. Structure of 2-chloro-10-phenylphenothiazine. *Acta Crystallogr., Sect. C: Cryst. Struct. Commun.* **1986**, *42*, 750−753.

(32) Sobolev, A. N.; Belsky, V. K.; Romm, I. P.; Chernikova, N. Y.; Guryanova, E. N. Structural investigation of the triaryl derivatives of the Group V elements. IX. Structure of triphenylamine, C18H15N. *Acta Crystallogr., Sect. C: Cryst. Struct. Commun.* **1985**, *41*, 967−971.

(33) Kuratsu, M.; Kozaki, M.; Okada, K. Synthesis, Structure, and Electron-Donating Ability of 2,2′:6′,2″-Dioxatriphenylamine and Its Sulfur Analogue. *Chem. Lett.* **2004**, *33*, 1174−1175.

(34) Nazeeruddin, M. K.; De Angelis, F.; Fantacci, S.; Selloni, A.; Viscardi, G.; Liska, P.; Ito, S.; Takeru, B.; Grätzel, M. Combined Experimental and DFT-TDDFT Computational Study of Photo-electrochemical Cell Ruthenium Sensitizers. *J. Am. Chem. Soc.* **2005**, *127*, 16835−16847.

(35) Almenningen, D. M.; Hansen, H. E.; Vold, M. F.; Buene, A. F.; Venkatraman, V.; Sunde, S.; Hoff, B. H.; Gautun, O. R. Effect of thiophene-based π-spacers on N-arylphenothiazine dyes for dye-sensitized solar cells. *Dyes Pigm.* **2021**, *185*, 108951.

(36) Hagberg, D. P.; Jiang, X.; Gabrielsson, E.; Linder, M.; Marinado, T.; Brinck, T.; Hagfeldt, A.; Sun, L. Symmetric and unsymmetric donor functionalization. comparing structural and spectral benefits of chromophores for dye-sensitized solar cells. *J. Mater. Chem.* **2009**, *19*, 7232−7238.

(37) Feldt, S. M.; Wang, G.; Boschloo, G.; Hagfeldt, A. Effects of Driving Forces for Recombination and Regeneration on the Photovoltaic Performance of Dye-Sensitized Solar Cells using Cobalt Polypyridine Redox Couples. *J. Phys. Chem. C* **2011**, *115*, 21500−21507.

(38) Saygili, Y.; Stojanovic, M.; Michaels, H.; Tiepelt, J.; Teuscher, J.; Massaro, A.; Pavone, M.; Giordano, F.; Zakeeruddin, S. M.; Boschloo, G.; Moser, J.-E.; Grätzel, M.; Muñoz-García, A. B.; Hagfeldt, A.; Freitag, M. Effect of Coordination Sphere Geometry of Copper Redox Mediators on Regeneration and Recombination Behavior in Dye-Sensitized Solar Cell Applications. *ACS Appl. Energy Mater.* **2018**, *1*, 4950−4962.

(39) Buene, A. F.; Uggerud, N.; Economopoulos, S. P.; Gautun, O. R.; Hoff, B. H. Effect of π-linkers on phenothiazine sensitizers for dye-sensitized solar cells. *Dyes Pigm.* **2018**, *151*, 263−271.

(40) Buene, A. F.; Almenningen, D. M. Phenothiazine and phenoxazine sensitizers for dye-sensitized solar cells − an investigative review of two complete dye classes. *J. Mater. Chem. C* **2021**, *9*, 11974−11994.

(41) Buene, A. F.; Almenningen, D. M.; Hagfeldt, A.; Gautun, O. R.; Hoff, B. H. First Report of Chenodeoxycholic Acid−Substituted Dyes Improving the Dye Monolayer Quality in Dye-Sensitized Solar Cells. *Sol. RRL* **2020**, *4*, 1900569.

(42) Cox, P. A.; Leach, A. G.; Campbell, A. D.; Lloyd-Jones, G. C. Protodeboronation of Heteroaromatic, Vinyl, and Cyclopropyl Boronic Acids: pH−Rate Profiles, Autocatalysis, and Disproportionation. *J. Am. Chem. Soc.* **2016**, *138*, 9145−9157.

(43) Bruno, N. C.; Tudge, M. T.; Buchwald, S. L. Design and preparation of new palladium precatalysts for C−C and C−N cross-coupling reactions. *Chem. Sci.* **2013**, *4*, 916−920.

(44) Xiang, S.; Huang, Z.; Sun, S.; Lv, X.; Fan, L.; Ye, S.; Chen, H.; Guo, R.; Wang, L. Highly efficient non-doped OLEDs using aggregation-induced delayed fluorescence materials based on 10-phenyl-10H-phenothiazine 5,5-dioxide derivatives. *J. Mater. Chem. C* **2018**, *6*, 11436−11443.

(45) Buene, A. F.; Boholm, N.; Hagfeldt, A.; Hoff, B. H. Effect of furan π-spacer and triethylene oxide methyl ether substituents on performance of phenothiazine sensitizers in dye-sensitized solar cells. *New J. Chem.* **2019**, *43*, 9403.

(46) Henderson, J. L.; Buchwald, S. L. Efficient Pd-Catalyzed Amination Reactions for Heterocycle Functionalization. *Org. Lett.* **2010**, *12*, 4442−4445.

(47) Kurata, R.; Sakamaki, D.; Uebe, M.; Kinoshita, M.; Iwanaga, T.; Matsumoto, T.; Ito, A. Isolable Triradical Trication of Hexaaza[16]-paracyclophane with Embedded 9,10-Anthrylenes: A Frustrated Three-Spin System. *Org. Lett.* **2017**, *19*, 4371−4374.

(48) Gong, H.; Zhao, Y.; Shen, X.; Lin, J.; Chen, M. Organo-catalyzed Photocontrolled Radical Polymerization of Semifluorinated (Meth)acrylates Driven by Visible Light. *Angew. Chem., Int. Ed.* **2018**, *57*, 333−337.

(49) Hanss, D.; Wenger, O. S. Electron Tunneling through Oligo-p-xylene Bridges. *Inorg. Chem.* **2008**, *47*, 9081−9084.

(50) Hanss, D.; Wenger, O. S. Tunneling Barrier Effects on Photoinduced Charge Transfer through Covalent Rigid Rod-Like Bridges. *Inorg. Chem.* **2009**, *48*, 671−680.

(51) Brocke, C.; Plumm, C.; Parham, H. A.; Fortte, R. Heteroaromatic Compounds and Their Preparation and Use in Electronic Devices. WO 2011107186 A2, 2011.

(52) Parham, A.; Kroeber, J.; Joosten, D.; Ludemann, A.; Grossmann, T. Bridged Triarylamine Derivatives, Their Preparation, Use in Electronic Devices, and the Devices. WO 2018095839 A1, 2018.

(53) Moore, M. J.; Qu, S.; Tan, C.; Cai, Y.; Mogi, Y.; Jamin Keith, D.; Boger, D. L. Next-Generation Total Synthesis of Vancomycin. *J. Am. Chem. Soc.* **2020**, *142*, 16039−16050.

(54) Hart, A. S.; K C, C. B.; Subbaiyan, N. K.; Karr, P. A.; D'Souza, F. Phenothiazine-Sensitized Organic Solar Cells: Effect of Dye Anchor Group Positioning on the Cell Performance. *ACS Appl. Mater. Interfaces* **2012**, *4*, 5813−5820.

(55) Wan, Z.; Jia, C.; Zhou, L.; Huo, W.; Yao, X.; Shi, Y. Influence of different arylamine electron donors in organic sensitizers for dye-sensitized solar cells. *Dyes Pigm.* **2012**, *95*, 41−46.

(56) Chiykowski, V. A.; Lam, B.; Du, C.; Berlinguette, C. P. Comparative analysis of triarylamine and phenothiazine sensitizer donor units in dye-sensitized solar cells. *Chem. Commun.* **2017**, *53*, 2367−2370.

(57) Tian, H.; Yang, X.; Chen, R.; Zhang, R.; Hagfeldt, A.; Sun, L. Effect of Different Dye Baths and Dye-Structures on the Performance of Dye-Sensitized Solar Cells Based on Triphenylamine Dyes. *J. Phys. Chem. C* **2008**, *112*, 11023−11033.

(58) Dentani, T.; Kubota, Y.; Funabiki, K.; Jin, J.; Yoshida, T.; Minoura, H.; Miura, H.; Matsui, M. Novel thiophene-conjugated indoline dyes for zinc oxide solar cells. *New J. Chem.* **2009**, *33*, 93−101.

(59) Zhang, M.; Liu, J.; Wang, Y.; Zhou, D.; Wang, P. Redox couple related influences of π-conjugation extension in organic dye-sensitized mesoscopic solar cells. *Chem. Sci.* **2011**, *2*, 1401−1406.

(60) Christians, J. A.; Manser, J. S.; Kamat, P. V. Best Practices in Perovskite Solar Cell Efficiency Measurements. Avoiding the Error of Making Bad Cells Look Good. *J. Phys. Chem. Lett.* **2015**, *6*, 852−857.

(61) Pazoki, M.; Cappel, U. B.; Johansson, E. M. J.; Hagfeldt, A.; Boschloo, G. Characterization techniques for dye-sensitized solar cells. *Energy Environ. Sci.* **2017**, *10*, 672−709.

(62) Sun, Y.; Onicha, A. C.; Myahkostupov, M.; Castellano, F. N. Viable Alternative to N719 for Dye-Sensitized Solar Cells. *ACS Appl. Mater. Interfaces* **2010**, *2*, 2039−2045.

(63) Zhang, L.; Cole, J. M. Dye aggregation in dye-sensitized solar cells. *J. Mater. Chem. A* **2017**, *5*, 19541−19559.

(64) Wang, Q.; Ito, S.; Grätzel, M.; Fabregat-Santiago, F.; Mora-Seró, I.; Bisquert, J.; Bessho, T.; Imai, H. Characteristics of High Efficiency Dye-Sensitized Solar Cells. *J. Phys. Chem. B* **2006**, *110*, 25210−25221.

(65) Wang, Q.; Moser, J.-E.; Grätzel, M. Electrochemical Impedance Spectroscopic Analysis of Dye-Sensitized Solar Cells. *J. Phys. Chem. B* **2005**, *109*, 14945−14953.

Synthetic efforts to investigate the effect of planarizing the triarylamine geometry in dyes for dye-sensitized solar cells.

David Moe Almenningen [a], Veslemøy Minge Engh [a], Eivind Andreas Strømsodd [a], Henrik Erring Hansen [b], Audun Formo Buene [c], Bård Helge Hoff* [a], Odd Reidar Gautun* [a]

[a] Department of Chemistry, Norwegian University of Science and Technology, Høgskoleringen 5, 7491 Trondheim, Norway

* Corresponding author. E-mail address: bard.h.hoff@ntnu.no (B. H. Hoff).

* Corresponding author. E-mail address: odd.r.gautun@ntnu.no (O. R. Gautun).

[b] Department of Materials Science and Engineering, Norwegian University of Science and Technology, Sem Sælands vei 12, 7034 Trondheim, Norway

[c] Department of Civil and Environmental Engineering, Norwegian University of Science and Technology, Høgskoleringen 7a, 7491 Trondheim, Norway

List of contents
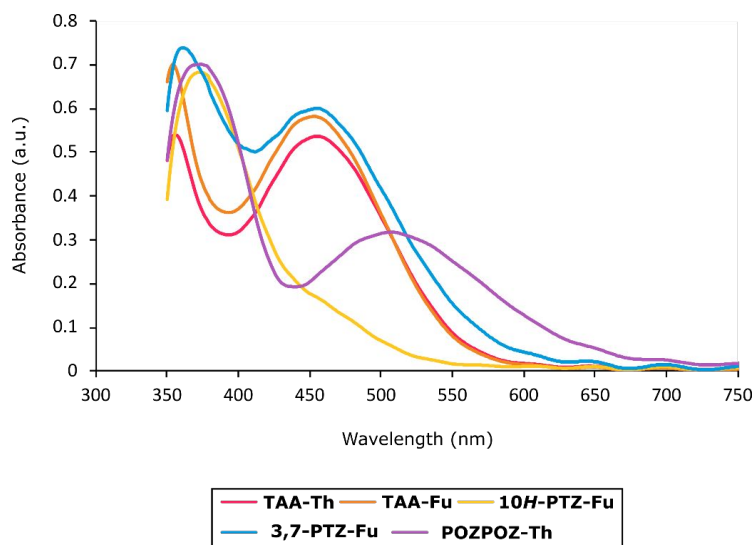
UV/Vis

Figure S1 UV/Vis spectra of the dyes sensitized on a TiO$_2$ film with 10 eq. CDCA in the staining solution (2.5 μm, GreatcellSolar, 18NR-T).

Cyclic voltammetry
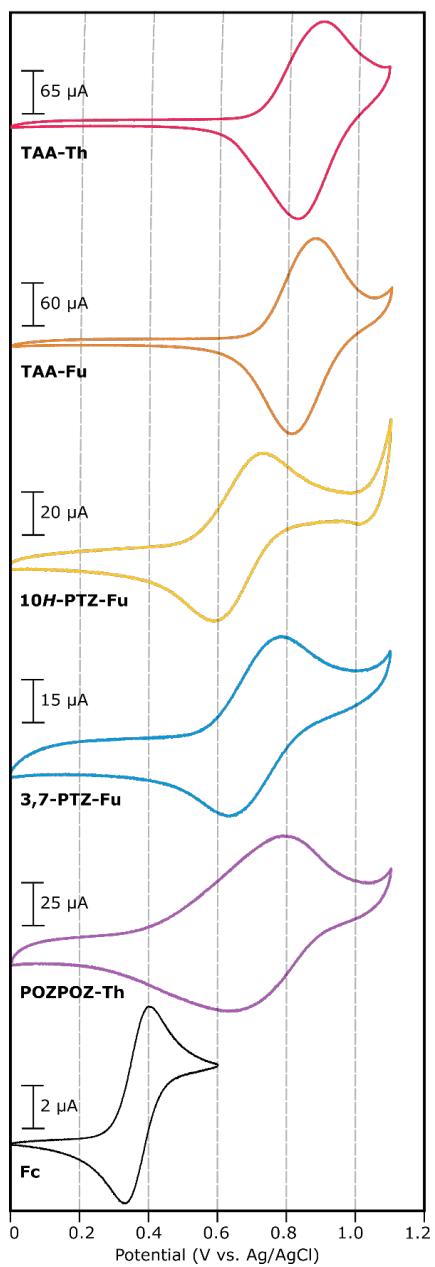
Figure S2 Cyclic voltammograms of the different dyes sensitized on TiO$_2$ electrodes.

Electrochemical impedance spectroscopy
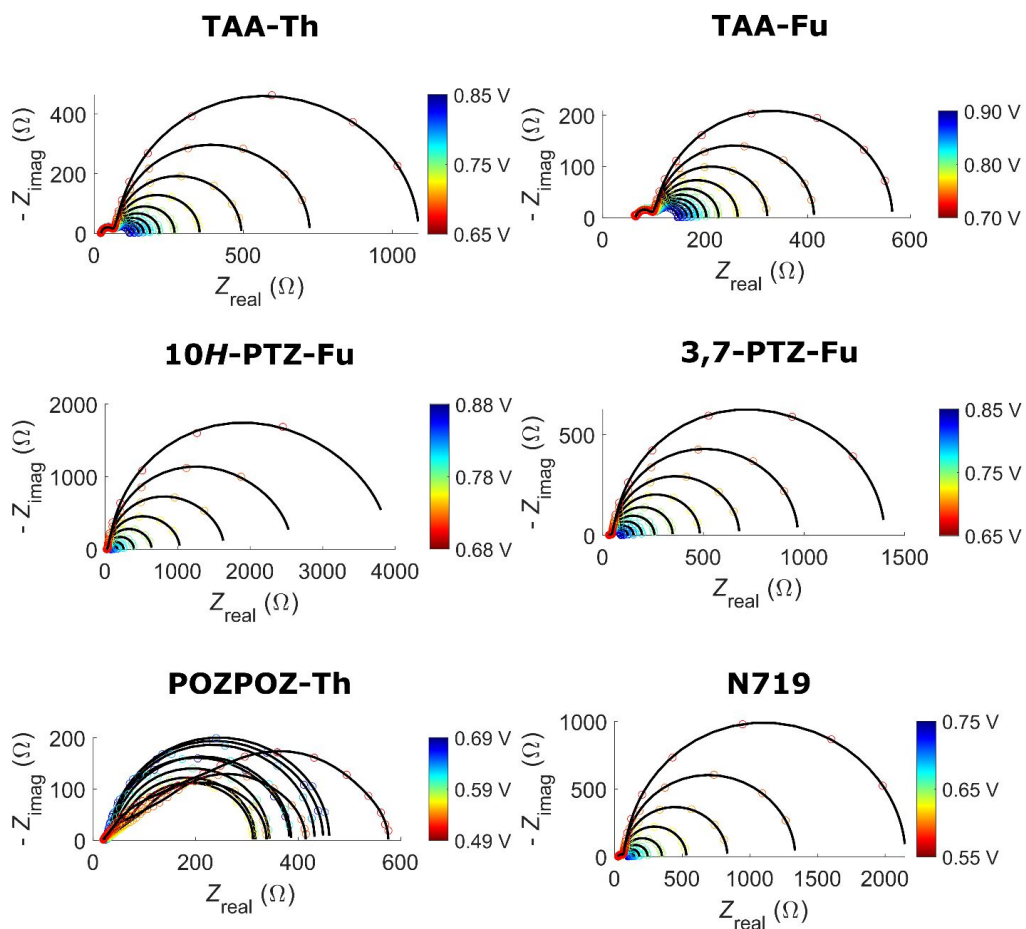
Figure S3 Complex plane diagrams obtained at different applied voltages.
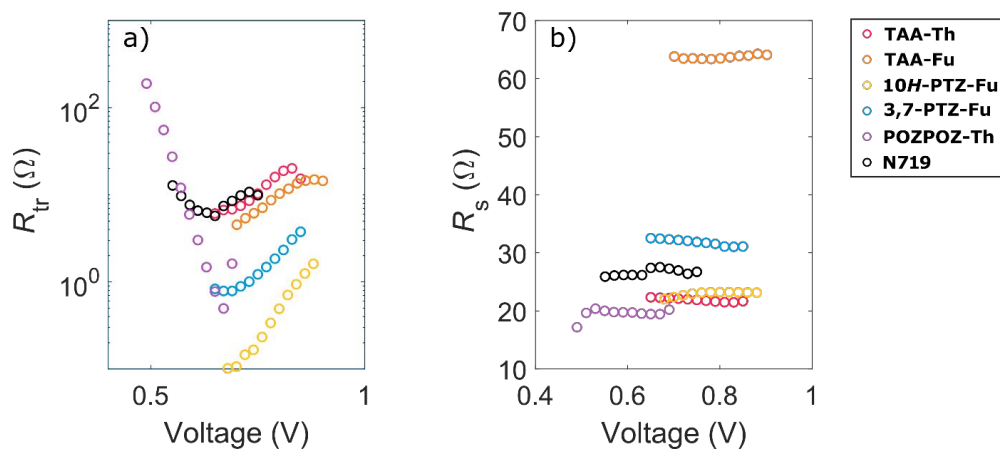
Figure S4 a) Transport resistance as a function of applied voltage. b) Series resistance as a function of applied voltage.

Experimental

Synthesis. All reactions were performed under inert N_2-atmosphere.

Analytical instruments. ^{1}H and ^{13}C NMR was performed using either a BRUKER 400 MHz or 600 MHz magnet, the spectra obtained are calibrated against residual solvent peak of CDCl$_3$ (7.26/77.16 ppm), CD$_2$Cl$_2$ (5.32/53.84 ppm), DMSO-d_6 (2.50/39.52 ppm), Acetone-d_6 (2.05/29.84 ppm) or THF-d_8 (1.72/25.31 ppm). The IR-spectra are obtained using a BRUKER Alpha Eco-ATR FTIR spectrometer, the data is reported with wavenumber and intensity of the signal. Mass determination was performed by MS-analysis in positive ionization mode on a Synapt G2-S Q-TOF-instrument for Waters, the samples were ionized by an ASAP-probe (APCI) without prior chromatographic separation. UV-Vis spectroscopy was performed using a Hitachi U-1900 spectrometer, and photoluminescence characterization was carried out on an Edinburgh Instruments FS5-spectrofluorometer.

5-(4-(bis(2',4'-bis(hexyloxy)-[1,1'-biphenyl]-4-yl)amino)phenyl)thiophene-2-carbaldehyde (2)
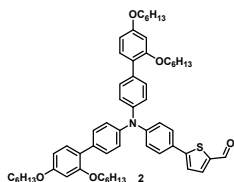
The triaryl bromide **1** (101 mg, 0.115 mmol), 5-formylthiophen-2-yl-boronic acid (28.9 mg, 0.185 mmol), XPhos Pd G3 (7.0 mg, 8.27 × 10^{-3} mmol) and K$_3$PO$_4$ (85.5 mg, 0.403 mmol) were mixed in a Schlenk-tube, before the reaction system was evacuated and filled with dry nitrogen gas. THF (2 mL) and water (4 mL) were degassed and added to the mixture. The reaction mixture was stirred at 40 °C for 4 h before cooling to 22 °C. Water (10 mL) and Et$_2$O (10 mL) were then added, and the aqueous and organic phases were separated. The aqueous phase was extracted with more Et$_2$O (3 × 10 mL). The combined organic phases were dried with anhydrous Na$_2$SO$_4$, filtered and the solvents removed in vacuo. The crude product (59.9 mg) was purified by silica-gel column chromatography (gradient: start: CH$_2$Cl$_2$/n-pentane, 1:3, R$_f$= 0.29, end: CH$_2$Cl$_2$) to yield **2** as yellow resin (41.8 mg, 0.0460 mmol, 40%). ^{1}H NMR (600 MHz, CDCl$_3$) δ: 9.85 (s, 1H), 7.70 (d, J = 3.9 Hz, 1H), 7.54-7.51 (m, 2H), 7.49-7.46 (m, 4H), 7.30 (d, J = 3.9 Hz, 1H), 7.27-7.25 (m,

2H), 7.19-7.14 (m, 6H), 6.56-6.52 (m, 4H), 3.99 (t, J = 6.6 Hz, 4H), 3.96 (t, J = 6.5 Hz, 4H), 1.83-1.71 (m, 8H), 1.52-1.23 (m, 24H), 0.92 (t, J = 7.0 Hz, 6H), 0.87 (t, J = 7.0 Hz, 6H); ^{13}C NMR (150 MHz, CDCl$_3$) δ: 182.6, 159.7 (2C), 157.0 (2C), 154.8, 149.3, 145.0 (2C), 141.2, 137.7, 134.1 (2C), 130.9 (2C),130.4 (4C), 127.2 (2C), 125.8, 124.5 (4C), 122.8 (2C), 122.7, 122.3 (2C), 105.4 (2C), 100.4 (2C), 68.4 (2C), 68.1 (2C), 31.6 (2C), 31.5 (2C), 29.3 (2C), 29.1 (2C), 25.78 (2C), 25.76 (2C), 22.63 (2C), 22.58 (2C), 14.1 (2C), 14.0 (2C); IR (EtOAc, cm^{-1}): 3354 (w), 3313 (w), 2924 (s), 2854 (s), 2655 (m), 2325 (m), 2051 (m), 1665 (s), 1597 (s), 1444 (s), 1291 (m), 1271 (m), 1181 (s), 1051 (s), 828 (m), 612 (s), 530 (s), 505 (s); HRMS (ASAP+, m/z): found 907.5206, calcd. for C$_{59}$H$_{73}$NO$_5$S [M*]$^+$ 907.5209.

5-(4-(bis(2',4'-bis(hexyloxy)-[1,1'-biphenyl]-4-yl)amino)phenyl)furan-2-carbaldehyde (3)
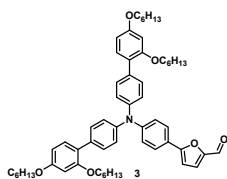
The synthesis of **3** was performed as described for compound **2** using 5-formylfuran-2-yl-boronic acid (27.7 mg, 0.198 mmol). Silica-gel column chromatography (gradient: start: CH$_2$Cl$_2$/n-pentane, 1:3, R$_f$ = 0.26, end: CH$_2$Cl$_2$) gave (57.0 mg, 0.0639 mmol, 56%) of **3** as a yellow resin. ^{1}H NMR (600 MHz, CDCl$_3$) δ: 9.59 (s, 1H), 7.69-7.65 (m, 2H), 7.51-7.45 (m, 4H), 7.30 (d, J = 3.7 Hz, 1H), 7.27-7.25 (m, 2H), 7.17 (d, J = 8.6 Hz, 6H), 6.70 (d, J = 3.7 Hz, 1H), 6.56-6.52 (m, 4H), 3.99 (t, J = 6.6 Hz , 4H), 3.96 (t, J = 6.4 Hz, 4H), 1.84-1.71 (m, 8H), 1.51-1.22 (m, 24H), 0.92 (t, J = 7.0 Hz, 6H), 0.87 (t, J = 7.0 Hz, 6H); ^{13}C NMR (150 MHz, CDCl$_3$) δ: 176.7, 160.1, 159.7 (2C), 157.0 (3C), 151.6, 149.5, 145.0 (2C), 134.1 (2C), 130.9 (2C), 130.4 (4C), 126.3 (2C), 124.6 (4C), 122.8 (2C), 122.1 (2C), 121.7, 106.3, 105.4 (2C), 100.4 (2C), 68.4 (2C), 68.1 (2C), 31.6 (2C), 31.5 (2C), 29.3 (2C), 29.1 (2C), 25.8 (4C), 22.63 (2C), 22.59 (2C), 14.1 (2C), 14.0 (2C); IR (EtOAc, cm^{-1}): 2954 (s), 2926 (s), 2857 (s), 2662 (m), 1674 (s), 1601 (s), 1474 (s), 1323 (m), 1271 (m), 1182 (s), 1027 (m), 1003 (m), 835 (m), 518 (m); HRMS (ASAP+, m/z): found 892.5507, calcd. for C$_{59}$H$_{74}$NO$_6$ [M+H]$^+$ 892.5516.

(E)-3-(5-(4-(bis(2',4'-bis(hexyloxy)-[1,1'-biphenyl]-4-yl)amino)phenyl)thiophen-2-yl)-2-cyanoacrylic acid (TAA-Th)
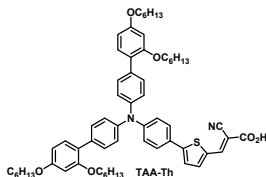
Compound **2** (36 mg, 0.0396 mmol) and cyanoacetic acid (79 mg, 0.926 mmol) were dissolved in degassed MeCN (15 mL) under nitrogen atmosphere. Piperidine (60.0 μL, 51.7 mg, 0.607 mmol) was added to the mixture, and the reaction was stirred at 80 °C for 1.5 h before cooling to 22 °C. The reaction mixture was then quenched in aqueous HCl (4M, 25 mL). CH_2Cl_2 (100 mL) was added and the organic phase was washed with water (6 × 100 mL), then dried over anhydrous Na_2SO_4, filtered and the solvents were removed in vacuo. The crude product (44.8 mg) was purified by silica-gel column chromatography (gradient: 0-20% MeOH in CH_2Cl_2, R_f = 0.00 in CH_2Cl_2). The dye-containing fractions were washed with HCl (1M, 2 × 20 mL), dried over anhydrous Na_2SO_4 and filtered to obtain (37 mg, 0.0383 mmol, 95%) of **TAA-Th** as a dark purple solid, mp. 62.1-67.5 °C. ^1H NMR (600 MHz, $CDCl_3$) δ: 8.32 (s, 1H), 7.78 (d, J = 4.0 Hz, 1H), 7.56 (d, J = 8.5 Hz, 2H), 7.49 (d, J = 8.6 Hz, 4H), 7.34 (d, J = 4.0 Hz, 1H), 7.28-7.24 (m, 2H), 7.18 (d, J = 8.6 Hz, 4H), 7.15 (d, J = 8.8 Hz, 2H), 6.57-6.52 (m, 4H), 3.99 (t, J = 6.5 Hz, 4H), 3.97 (t, J = 6.4 Hz, 4H), 1.84-1.71 (m, 8H), 1.52-1.22 (m, 24H), 0.92 (t, J = 7.0 Hz, 6H), 0.87 (t, J = 7.0 Hz, 6H); ^{13}C NMR (150 MHz, $CDCl_3$) δ: 168.1, 159.7 (2C), 157.0 (2C), 156.9, 149.8, 147.9, 144.8 (2C), 140.5, 134.3 (2C), 133.5, 130.9 (2C), 130.4 (4C), 127.4 (2C), 125.1, 124.7 (4C), 123.3, 122.7 (2C), 121.9 (2C), 115.9, 105.4 (2C), 100.4 (2C), 95.2, 68.4 (2C), 68.1 (2C), 31.6 (2C), 31.5 (2C), 29.3 (2C), 29.1 (2C), 25.78 (2C), 25.76 (2C), 22.62 (2C), 22.59 (2C), 14.0 (4C); IR (EtOAc, cm^{-1}): 2954 (m), 2928 (s), 2857 (m), 2321 (w), 2217 (w), 2069 (w), 1686 (m), 1576 (s), 1493 (s), 1412 (s), 1323 (m), 1281 (s), 1222 (m), 1183 (s), 1063 (m), 599 (m), 480 (m); HRMS (ASAP+, m/z): found 975.5330, calcd. for $C_{62}H_{75}N_2O_6S$ [M+H]$^+$ 975.5346.

(E)-3-(5-(4-(bis(2',4'-bis(hexyloxy)-[1,1'-biphenyl]-4-yl)amino)phenyl)furan-2-yl)-2-cyanoacrylic acid (TAA-Fu)
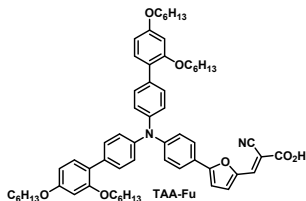
Synthesis and purification of **TAA-Fu** were performed as described for **TAA-Th** starting with intermediate **3** (52.6 mg, 0.059 mmol). This gave 42.3 mg (0.0441 mmol, 75%), of a dark purple solid, mp. 62.4-68.9 °C. ^{1}H NMR (600 MHz, CDCl$_3$) δ: 7.95 (s, 1H), 7.73 (d, J = 8.9 Hz, 2H), 7.51-7.47 (m, 4H), 7.28-7.24 (m, 2H), 7.21-7.16 (m, 6H), 6.81 (d, J = 3.9 Hz, 1H), 6.57-6.52 (m, 4H), 3.99 (t, J = 6.7, 4H), 3.97 (t, J = 6.6 Hz, 4H), 1.82-1.71 (m, 8H), 1.52-1.22 (m, 24H), 0.92 (t, J = 7.0 Hz, 6H), 0.86 (t, J = 7.0 Hz, 6H); ^{13}C NMR (150 MHz, CDCl$_3$) δ: 168.5, 161.8, 159.7 (2C), 157.0 (2C), 150.0, 147.2, 144.7 (2C), 138.6, 134.4 (2C), 130.9 (2C), 130.5 (4C), 126.8 (2C), 124.9 (4C), 122.8 (2C), 121.6 (2C), 120.8 (2C), 115.9, 108.2, 105.4 (2C), 100.4 (2C), 93.6, 68.4 (2C), 68.1 (2C), 31.6 (2C), 31.4 (2C), 29.3 (2C), 29.1 (2C), 25.77 (2C), 25.75 (2C), 22.62 (2C), 22.58 (2C), 14.1 (2C), 14.0 (2C); IR (EtOAc, cm^{-1}): 3270 (w), 3239 (w), 3087 (w), 2956 (s), 2930 (s), 2860 (m), 1591 (s), 1494 (s), 1470 (s), 1268 (m), 1182 (m), 824 (m), 792 (m); HRMS (ASAP+, m/z): found 957.5399, calcd. for C$_{62}$H$_{73}$N$_2$O$_7$ [M-H]$^+$ 957.5418.

1-(3,7-dibromo-10H-phenothiazin-10-yl)ethan-1-one (5)
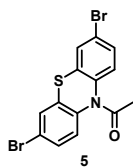
3,7-Dibromo-10H-phenothiazine (**4**) (1.05 g, 2.94 mmol) was suspended in dry toluene (30 mL). Acetyl chloride (0.461 g, 5.88 mmol) was added under a nitrogen atmosphere and the reaction mixture was then stirred for 3 h at reflux. The solvent was removed and the crude product washed with cold hexane to give **5** as a green powder (1.01 g, 2.52 mmol, 83%), mp. 138.5 °C. ^{1}H NMR (400 MHz, DMSO-d_6) δ: 7.83 (d, J = 2.0 Hz, 2H), 7.60 (dd, J = 8.5, 2.1 Hz, 2H), 7.56 (d, J = 8.5

Hz, 2H), 2.13 (s, 3H); ^{13}C NMR (100 MHz, DMSO-d_6) δz: 168.8, 138.2 (2C), 134.4 (2C), 130.2 (2C), 139.6 (2C), 129.5 (2C), 119.9 (2C), 23.1; IR (neat, cm^{-1}): 3026, 1683, 1568, 1459, 1356, 1301, 1253, 1018 and 818; HRMS (ASAP+, m/z): found 399.8834, calcd. for $C_{14}H_{10}NOS^{81}Br_2$ [M+H]$^+$ 399.8829.

1-(3,7-bis(2,4-bis(hexyloxy)phenyl)-10*H*-phenothiazin-10-yl)ethan-1-one (7)
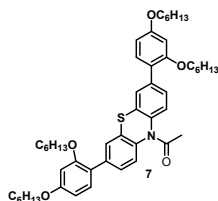
Formation of pinacol borane: A mixture of 1-bromo-2,4-bis(hexyloxy)benzene (2.67 mg, 7.52 mmol mmol), PdCl$_2$(CH$_3$CN)$_2$ (67.3 mg, 259 μmol) and SPhos (199 mg, 485 μmol) was evacuated before a nitrogen atmosphere was established. Degassed and dry 1,4-dioxane (23 mL) was then added and the reaction mixture was stirred for 20 min. Then dry triethylamine (2.46 g, 24.4 mmol) and 4,4,5,5-tetramethyl-1,3,2-dioxoborolane (1.92 mg, 15.0 mmol were added and the reaction mixture stirred at 105 °C for 90 min. The reaction mixture was then cooled down and filtered through Celite, before the solvents were removed *in vacuo* to give crude 2-(2,4-bis(hexyloxy)phenyl)-4,4,5,5-tetramethyl-1,3,2-dioxaborolane as a yellow oil, which was then used directly in the Suzuki cross-coupling reaction.

Suzuki cross-coupling: Crude **6** (1.19 g, 2.98 mmol), Pd(OAc)$_2$ (35.0 mg, 160 μmol), SPhos (126 mg, 307 μmol) and K$_2$CO$_3$ (2.06 g, 14.9 mmol) were mixed with 2-(2,4-bis(hexyloxy)phenyl)-4,4,5,5-tetramethyl-1,3,2-dioxaborolane from above, before the mixture was evacuated and a nitrogen atmosphere established. Degassed H$_2$O (20 mL) and 1,4-dioxane (20 mL) were added under a nitrogen atmosphere. This mixture was stirred at 80 °C for 6 h. After the mixture was cooled down to rt, H$_2$O (75 mL) was added and the aqueous phase extracted with CH$_2$Cl$_2$ (4 × 75 mL). The combined organic phase was washed with H$_2$O (2 × 50 mL), dried over Na$_2$SO$_4$ before the solvents were removed in vacuo. The crude product was purified twice with column chromatography (*n*-pentane/EtOAc, 17:3, R$_f$ = 0.25) to yield **7** (1.54 g, 1.93 mmol, 65%) as an orange oil. ^{1}H NMR (600 MHz, DMSO-d_6, 80 °C) δ: 7.65-7.59 (m, 4H), 7.45 (dd, J = 2.0, 8.4 Hz, 2H), 7.26 (d, J = 8.4 Hz, 2H), 6.62 (d, J = 2.4 Hz, 2H), 6.60 (dd, J = 8.5, 2.3 Hz, 2H), 4.02-3.94

(m, 8H), 2.19 (s, 3H), 1.77-1.70 (m, 4H), 1.67-1.61 (m, 4H), 1.47-1.39 (m, 4H), 1.39-1.27 (m, 12H), 1.27-1.18 (m, 8H), 0.88 (t, J = 6.7 Hz, 6H), 0.77 (t, J = 6.7 Hz, 6H); ^{13}C NMR (150 MHz, DMSO-d_6, 80 °C) δ: 168.0, 159.6 (2C), 156.4 (2C), 136.6 (2C), 136.5 (2C), 131.1 (2C), 130.3 (2C), 127.6 (2C), 127.3 (2C), 126.2 (2C), 120.8 (2C), 106.3 (2C), 100.4 (2C), 68.0 (2C), 67.5 (2C), 30.50 (2C), 30.45 (2C), 28.29 (2C), 28.20 (2C), 24.9 (2C), 24.7 (2C), 22.1, 21.49 (2C), 21.45 (2C), 13.2 (2C), 13.1 (2C); IR (CH$_2$Cl$_2$, cm^{-1}): 2928, 2857, 1682, 1608, 1499, 1301, 1277, 1181; HRMS (ASAP+, m/z): found 794.4808, calcd. for C$_{50}$H$_{68}$NO$_5$S [M+H]$^+$ 794.4818.

3,7-bis(2,4-bis(hexyloxy)phenyl)-10H-phenothiazine (8)
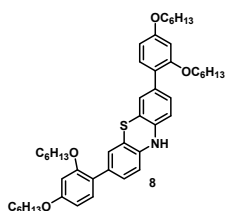
Compound **7** (1.52 g, 1.91 mmol) was dissolved in THF (8 mL) and MeOH (20 mL), before this solution was degassed and added under a nitrogen atmosphere to a flask containing NaOH (319 mg, 7.98 mmol). This mixture was then stirred for 2 h at 60 °C, before being cooled down to 22 °C. Water (50 mL) was added and the aqueous phase extracted with CH$_2$Cl$_2$ (4 × 50 mL). The organic phases were combined and washed with saturated NaHCO$_3$ (3 × 50 mL) and H$_2$O (4 × 50 mL) before being dried over Na$_2$SO$_4$. The solvents were removed in vacuo to give **8** (1.34 g, 1.78 mmol, 93%) as a green solid; mp. 85-89 °C. ^{1}H NMR (600 MHz, DMSO-d_6) δ: 8.62 (s, 1H), 7.13 (d, J = 8.2 Hz, 2H), 7.08-7.05 (m, 2H), 7.05-7.01 (m, 2H), 6.69 (d, J = 8.2 Hz, 2H), 6.58-6.54 (m, 2H), 6.54-6.49 (m, 2H), 4.00-3.88 (m, 8H), 1.73-1.66 (m, 4H), 1.66-1.58 (m, 4H), 1.46-1.34 (m, 8H), 1.34-1.20 (m, 16H), 0.88 (t, J = 6.7 Hz, 6H), 0.84 (t, J = 6.7 Hz, 6H); ^{13}C NMR (150 MHz, DMSO-d_6) δ: 159.0 (2C), 156.3 (2C), 140.2 (2C), 131.5 (2C), 130.0 (2C), 128.0 (2C), 126.7 (2C), 121.4 (2C), 115.6 (2C), 113.9 (2C), 105.8 (2C), 100.1 (2C), 67.7 (2C), 67.5 (2C), 31.00 (2C), 30.97 (2C), 28.7 (2C), 28.6 (2C), 25.4 (2C), 25.2 (2C), 22.10 (2C), 22.06 (2C), 13.88 (2C), 13.86 (2C); IR (CH$_2$Cl$_2$, cm^{-1}): 3374 (w), 2954 (m), 2931 (m), 2867 (m), 1604 (m), 1576 (w), 1487 (m), 1287 (m), 1269 (m), 1257 (m), 1184 (m), 1040 (w), 1019 (w), 819 (m); HRMS (ASAP+, m/z): found 752.4700, calcd. for C$_{48}$H$_{66}$NO$_4$S, [M+H]$^+$, 752.4713.

3,7-bis(2,4-bis(hexyloxy)phenyl)-10-(4-(trimethylsilyl)phenyl)-10*H*-phenothiazine (9)
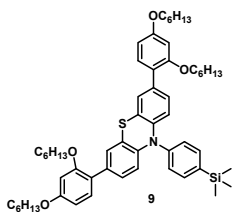
Compound **8** (764 mg, 1.06 mmol), NaO-*t*Bu (137 mg, 1.42 mmol), XPhos (48.4 mg, 102 mmol) and Pd(OAc)$_2$ (11.4 mg, 50.8 mmol) were mixed and degassed 1,4-dioxane (5 mL) was added under nitrogen atmosphere, before this mixture was left for stirring at rt for a couple of minutes. 1-Bromo-4(trimethylsilyl)benzene (704 mg, 3.07 mmol) was then added, and the reaction mixture was heated to 110 °C and left stirring for 15 h. The reaction mixture was then cooled down to rt, H$_2$O (100 mL) was added and the crude product extracted with CH$_2$Cl2 (4 × 75 mL). The organic phases were combined, washed with H$_2$O (2 × 100 mL), dried over Na2SO4 and filtrated before the solvents were removed *in vacuo*. Purification by silica-gel column chromatography (*n*-pentane/CH$_2$Cl$_2$, 1:3, R*f* = 0.20) gave **9** (828 mg, 0.920 mmol, 87%) as a green oil. ^{1}H NMR (600 MHz, CD$_2$Cl$_2$) δ: 7.78 (d, *J* = 8.0 Hz, 2H), 7.40 (d, *J* = 8.1 Hz, 2H), 7.22 (d, *J* = 1.9 Hz, 2H), 7.15 (d, *J* = 8.1 Hz, 2H), 7.02 (dd, *J* = 8.4, 1.9 Hz, 2H), 6.52-6.48 (m, 4H), 6.24 (d, *J* = 8.6 Hz, 2H), 3.96 (t, *J* = 6.7 Hz, 4H), 3.93 (t, *J* = 6.4 Hz, 4H), 1.81-1.69 (m, 8H), 1.50-1.40 (m, 8H), 1.40-1.28 (m, 16H), 0.93 (t, *J* = 6.9 Hz, 6H), 0.88 (t, *J* = 6.8 Hz, 6H), 0.36 (s, 9H); ^{13}C NMR (150 MHz, CD$_2$Cl$_2$) δ: 160.1 (2C), 157.3 (2C), 142.8 (2C), 142.2, 141.0, 136.1 (2C), 133.3 (2C), 130.8 (2C), 129.8 (2C), 128.1 (2C), 127.8 (2C), 122.3 (2C), 120.2 (2C), 116.2 (2C), 105.8 (2C), 100.5 (2C), 68.8 (2C), 68.6 (2C), 32.03 (2C), 31.97 (2C), 29.7 (2C), 29.6 (2C), 26.3 (2C), 26.1 (2C), 23.0 (4C), 14.3 (2C), 14.2 (2C), -1.0 (3C); IR (CH$_2$Cl$_2$, cm^{-1}): 2954, 2930, 2859, 1608, 1466, 1297, 1248, 1179, 1135, 1077, 1017, 832, 662, 602, 537; HRMS (ASAP+, m/z): found 899.5332, calcd. for C$_{57}$H$_{77}$NO$_4$SiS, [M*]$^+$ 899.5343

3,7-bis(2,4-bis(hexyloxy)phenyl)-10-(4-iodophenyl)-10*H*-phenothiazine (10)
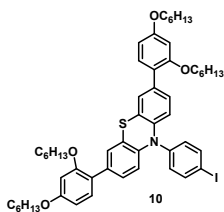
Compound **9** (693 mg, 0.770 mmol) was dissolved in dry CH_2Cl_2 (16 mL) and dry acetonitrile (16 mL) and left stirring at 0 °C for 5 min. Then a solution of ICl in CH_2Cl_2 (1.88 mL, 0.6 M) was added at 0 °C and the reaction was left stirring at 22°C for 20 h. The reaction was then quenched with an aqueous solution of $Na_2S_2O_3$ (5 wt%, 40 mL) and the mixture was extracted with CH_2Cl_2 (2 × 60 mL). The combined organic phases were washed with H_2O (30 mL) , dried over Na_2SO_4, filtered and the solvents removed *in vacuo*. The product was purified by silica-gel column chromatography (*n*-pentane/acetone, 20:1, R_f = 0.15) to yield **10** (137 mg, 0.144 mmol, 19%) as a yellow oil. ^{1}H NMR (600 MHz, acetone-d_6) δ: 8.01 (d, *J* = 8.6 Hz, 2H), 7.30 (d, *J* = 2.0 Hz, 2H), 7.26 (d, *J* = 8.5 Hz, 2H), 7.18 (d, *J* = 8.4 Hz, 2H), 7.10 (dd, *J* = 8.5, 2.0 Hz, 2H), 6.59 (d, *J* = 2.2 Hz, 2H), 6.54 (dd, *J* = 8.5, 2.3 Hz, 2H), 6.33 (d, *J* = 8.5 Hz, 2H), 4.02-3.96 (m, 8H), 1.81-1.67 (m, 8H), 1.52-1.42 (m, 8H), 1.40-1.27 (m, 16H), 0.90 (t, *J* = 7.1 Hz, 6H), 0.87 (t, *J* = 6.9 Hz, 6H); ^{13}C NMR (150 MHz, acetone-d_6) δ: 160.9 (2C), 157.8 (2C), 142.7 (2C), 142.5, 140.9 (2C), 134.5 (2C), 132.9 (2C), 131.2 (2C), 128.7 (2C), 128.5 (2C), 122.5 (2C), 121.4 (2C), 117.4 (2C), 106.7 (2C), 101.0 (2C), 93.2, 69.0 (2C), 68.6 (2C), 32.4 (4C), 30.04 (2C), 30.00 (2C), 26.8 (2C), 26.5 (2C), 23.4 (2C), 23.3 (2C), 14.4 (2C), 14.3 (2C); IR (CH_2Cl_2, cm^{-1}): 2953, 2929, 2868, 2858, 1608, 1455, 1388, 1298, 1181, 1135, 1053, 1010, 833, 816, 602, 532; HRMS (ASAP+, m/z): found 953.3906, calcd. for $C_{54}H_{68}NO_4SI$, [M*]$^+$ 953.3914.

3,7-bis(2,4-bis(hexyloxy)-5-iodophenyl)-10-(4-iodophenyl)-10H-phenothiazine (10-by)
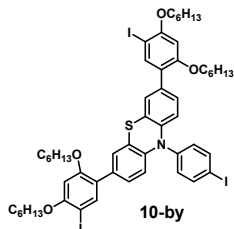
The tri-iodinated by-product **10-by** was isolated in a synthesis as described for compound **10**, but starting with **9** (897 mg, 0.996 mmol) and more ICl (485 mg, 2.99 mmol). Two purifications using silica-gel column chromatography (*n*-pentane/ CH_2Cl_2, 1:2, R_f = 0.35) gave **10-by** (193 mg, 0.160 mmol, 16%) as a yellow solid, mp. 145 °C. ^{1}H NMR (600 MHz, CD_2Cl_2) δ: 7.95 (d, *J* = 8.5 Hz, 2H), 7.60 (s, 2H), 7.23-7.16 (m, 4H), 7.00 (br.d, *J* = 5.2 Hz, 2H), 6.47 (s, 2H), 6.25 (br.d, *J* = 5.8 Hz, 2H), 4.03 (t, *J* = 6.5 Hz, 4H), 3.95 (t, *J* = 6.4 Hz, 4H), 1.87-1.79 (m, 4H), 1.76-1.68 (m, 4H), 1.58-1.50 (m, 4H), 1.46-1.28 (m, 20H), 0.92 (t, *J* = 7.2 Hz, 6H), 0.88 (t, *J* = 7.0 Hz, 6H); ^{13}C NMR (150 MHz, CD_2Cl_2) δ: 158.3 (2C), 157.8 (2C), 140.5 (2C), 139.59 (2C), 139.57, 132.6 (2C), 128.1 (2C), 127.8 (2C), 124.3 (2C), 116.4 (2C), 115.8 (2C), 98.7 (2C), 93.3, 75.3 (2C), 70.0 (2C), 69.2 (2C), 31.92 (2C), 31.90 (2C), 29.51 (2C), 29.50 (2C), 26.23 (2C), 26.13 (2C), 14.25 (2C), 14.22 (2C); IR (CH_2Cl_2, cm^{-1}): 2950, 2925, 2867, 2856, 1590, 1460, 1359, 1302, 1244, 1187, 1040, 1009, 814, 538; HRMS (ASAP+, m/z): found 1205.1830 calc for $C_{54}H_{66}I_3NO_4S$, [M*]$^+$ 1205.1847.

5-(4-(3,7-bis(2,4-bis(hexyloxy)phenyl)-10*H*-phenothiazin-10-yl)phenyl)furan-2-carbaldehyde (11)
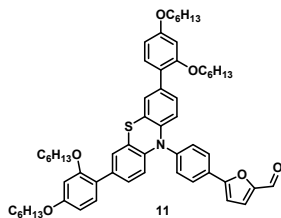
(5-Formylfuran-2-yl)boronic acid (31.0 mg, 0.221 mmol, 1.6 equiv), K_3PO_4 (59.0 mg, 0.278 mmol), and XPhos Pd G3 (2.30 mg, 2.73 µmol) were mixed in a Schlenk tube. Then compound **10** (132 mg, 0.138 mmol) was dissolved in degassed THF (2.5 mL) and added to the mixture, followed by degassed H_2O (5 mL). The reaction mixture was stirred at 40 °C for 23 h before being cooled down to rt, followed by addition of H_2O (20 mL).The mixture was then extracted using CH_2Cl_2 (4 × 20 mL), and the organic phases washed with H_2O (40 mL). After drying over Na_2SO_4, and concentration in vacuo, the material was purified by silica-gel column chromotography (n-pentane/acetone, 1:8, R_f = 0.15) to yield **11** (55.0 mg, 0.0596 mmol, 43%) as a yellow oil. ^{1}H NMR (600 MHz, acetone-d_6) δ: 9.70 (s, 1H), 8.13-8.11 (m, 2H), 7.56 (d, *J* = 3.7 Hz, 1H), 7.56-7.53 (m, 2H), 7.37 (d, *J* = 2.1 Hz, 2H), 7.24 (d, *J* = 3.8 Hz, 1H), 7.20 (d, *J* = 8.4 Hz, 2H), 7.16 (dd, *J* = 8.5, 2.1 Hz, 2H), 6.61 (d, *J* = 2.2 Hz, 2H), 6.57-6.52 (m, 4H), 4.03-3.98 (m, 8H), 1.80-1.68 (m, 8H),

1.57-1.43 (m, 8H), 1.38-1.27 (m, 16H), 0.90 (t, J = 7.1 Hz, 6H), 0.86 (t, J = 7.0 Hz, 6H); ^{13}C NMR (150 MHz, acetone-d_6) δ: 178.0, 160.9 (2C), 158.9, 157.9 (2C), 153.5, 144.1, 142.5 (2C), 134.9 (2C), 131.3 (2C), 129.5 (2C), 128.76 (2C), 128.71, 128.60 (2C), 128.23 (2C), 124.8, 122.94 (2C), 122.45 (2C), 118.6 (2C), 109.3, 106.7 (2C), 101.0 (2C), 69.0 (2C), 68.6 (2C), 32.4 (4C), 30.0 (4C)*, 26.8 (2C), 26.5 (2C), 23.35 (2C), 23.30 (2C), 14.40 (2C), 14.32 (2C); IR (CH$_2$Cl$_2$, cm^{-1}): 2954, 2930, 2867, 2856, 1679, 1608, 1467, 1158, 1137, 1121, 1077, 1016, 822, 625, 603, 512; HRMS (ASAP+, m/z): found 921.4983, calcd. for C$_{59}$H$_{71}$NO$_6$S, [M*]$^+$) 921.5002. *Signal found using ^{1}H-^{13}C HSQC NMR due to overlap with solvent residual signal.

(*E*)-3-(5-(4-(3,7-bis(2,4-bis(hexyloxy)phenyl)-10*H*-phenothiazin-10-yl)phenyl)furan-2-yl)-2-cyanoacrylic acid (10*H*-PTZ-Fu)
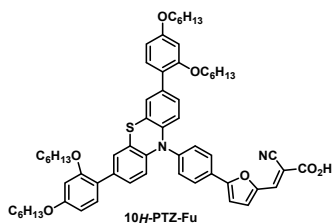
10*H*-PTZ-Fu was prepared as described for **TAA-Th** starting with the aldehyde **11** (54.0 mg, 58.6 μmol) and reacting for 1.5 h. Purification by silica-gel column chromatography (0-10% MeOH in CH$_2$Cl$_2$) gave **10*H*-PTZ-Fu** (49.5 mg, 50.0 μmol, 85%) as a red solid, mp. 173-178 °C. ^{1}H NMR (600 MHz, CDCl$_3$) δ: 11.11 (s, 1H), 8.03 (s, 1H), 7.95 (br.d, J = 6.3 Hz, 2H), 7.46-7.35 (m, 5H), 7.23-7.15 (m, 4H), 6.90 (s, 1H), 6.68 (d, J = 8.1 Hz, 2H), 6.53-6.49 (m, 4H), 4.00-3.90 (m, 8H), 1.83-1.68 (m, 8H), 1.52-1.23 (m, 24H), 0.92 (t, J = 7.0 Hz, 6H), 0.86 (t, J = 6.7 Hz, 6H); ^{13}C NMR (150 MHz, CDCl3) δ: 168.3, 160.7, 159.9 (2C), 157.1 (2C), 147.9, 144.9, 141.2 (2C), 140.2, 139.1, 134.5 (2C), 130.8 (2C), 128.6 (2C), 128.1 (2C), 127.6 (2C), 126.7, 125.8 (2C), 125.5, 125.2 (2C), 122.2 (2C), 119.6 (2C), 115.9, 109.3, 105.4 (2C), 100.5 (2C), 68.5 (2C), 68.3 (2C), 31.74 (2C), 31.64 (2C), 29.4 (2C), 29.2 (2C), 26.0 (2C), 25.9 (2C), 22.8 (4C), 14.2 (4C); IR (CH$_2$Cl$_2$, cm^{-1}): 2954, 2926, 2855, 1609, 1579, 1467, 1390, 1297, 1260, 1248, 1182, 1135, 1030, 797; HRMS (ASAP+, m/z): found 989.5113, calcd. for C$_{62}$H$_{72}$N$_2$O$_7$S, [M*]$^+$ 989.5138.

1-(3-(2,4-bis(hexyloxy)phenyl)-7-bromo-10*H*-phenothiazin-10-yl)ethan-1-one (12)
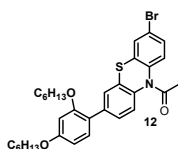
The compound **12** was prepared as described for compound **7** starting with the building block **5** (1.20 g, 3.01 mmol), except this time with a halved amount of 1-bromo-2,4-bis(hexyloxy)benzene (682 mg, 3.61 mmol) was used. The crude product was purified with column chromatography (*n*-pentane/EtOAc, 6:1, R_f = 0.26) to yield **12** as a colorless oil (800 mg, 1.34 mmol, 45%). ^{1}H NMR (600 MHz, DMSO-d_6) δ: 7.80 (d, *J* = 1.8 Hz, 1H), 7.65-7.54 (m, 4H), 7.46 (dd, *J* = 2.0 Hz, 8.3 Hz, 1H), 7.26 (d, *J* = 8.5 Hz, 1H), 6.63 (d, *J* = 2.4 Hz, 1H), 6.59 (dd, *J* = 2.0 Hz, 8.3 Hz, 1H), 4.03-3.94 (m, 4H), 2.16 (s, 3H), 1.71 (q, *J* = 7.7 Hz, 2H), 1.65-1.58 (m, 2H), 1.46-1.39 (m, 2H), 1.36-1.28 (m, 6H), 1.25-1.17 (m, 4H), 0.88 (t, *J* = 7.7 Hz, 3H), 0.79 (t, *J* = 7.7 Hz, 3H); ^{13}C NMR (150 MHz, DMSO-d_6) δ: 168.4, 159.9, 156.5, 138.0, 137.0, 136.5, 134.6, 130.9, 130.6, 130.0 (2C), 129.0, 128.2, 128.1, 126.7, 120.5, 119.1, 106.1, 100.1, 67.9, 67.6, 31.0, 30.9, 28.6, 28.5, 25.4, 25.2, 22.6, 22.07, 22.05, 13.9, 13.8; IR (CH$_2$Cl$_2$, cm^{-1}): 2927 (m), 2856 (m), 1684 (s), 1607 (s), 1480 (m), 1300 (m), 1269 (s), 1180 (m), 1012 (m); HRMS (ASAP+, m/z): found 596.1836, calcd. for C$_{32}$H$_{39}$NO$_3$SBr [M+H]$^+$ 596.1834.

1-(3-(2,4-bis(hexyloxy)phenyl)-7-(furan-2-yl)-10*H*-phenothiazin-10-yl)ethan-1-one (13)
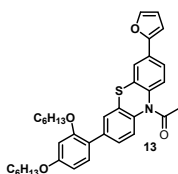
Compound **12** (475 mg, 0.80 mmol), PdCl$_2$(dppf) (30.7 mg, 42 μmol), and K$_2$CO$_3$ (463 mg, 3.35 mmol) were mixed with 2-furanylboronic acid (141 mg, 1.26 mmol), before the mixture was evacuated and a nitrogen atmosphere established. Degassed H$_2$O (7 mL) and 1,4-dioxane (7 mL) were added under a nitrogen atmosphere. This mixture was stirred at 80 °C for 1.5 h. After the mixture was cooled down to rt, H$_2$O (75 mL) was added, and the aqueous phase extracted with ethyl acetate (3 × 50 mL). The combined organic phase was washed with H$_2$O (2 × 50 mL), dried over Na$_2$SO$_4$ before the solvents were removed in vacuo. The crude product was purified with

column chromatography (CH$_2$Cl$_2$, R$_f$ = 0.16) to yield **13** as a light-orange oil (298 mg, 0.51 mmol, 64%). ^{1}H NMR (400 MHz, DMSO-d_6) δ: 7.85 (d, J = 2.0 Hz, 1H), 7.78 (d, J = 2.0 Hz, 1H), 7.74-7.65 (m, 2H), 7.65-7.59 (m, 2H), 7.45 (dd, J = 2.0 Hz, 8.3 Hz, 1H), 7.26 (d, J = 8.6 Hz, 1H), 7.06 (d, J = 3.3 Hz, 1H), 6.65-6.56 (m, 3H), 4.03-3.94 (m, 4H), 2.18 (s, 3H), 1.76-1.67 (m, 2H), 1.66-1.57 (m, 2H), 1.47-1.38 (m, 2H), 1.37-1.27 (m, 6H), 1.26-1.19 (m, 4H), 0.88 (t, J = 6.5 Hz, 3H), 0.78 (t, J = 6.7 Hz, 3H); ^{13}C NMR (150 MHz, DMSO-d_6) δ: 168.5, 159.8, 156.5, 151.6, 143.5, 137.5, 136.8, 136.6, 130.9 (2C), 128.9, 128.1, 127.7 (2C), 126.7, 122.3, 122.1, 120.6, 112.3, 107.1, 106.1, 100.1, 97.2, 67.9, 67.6, 30.99, 30.95, 28.7, 28.5, 25.4, 25.2, 25.1, 22.07, 22.05, 13.9, 13.8; IR (CH$_2$Cl$_2$, cm^{-1}): 2928 (m), 2857 (m), 1682 (s), 1607 (s), 1464 (s), 1302 (s), 1274 (s), 1180 (m) 1101 (m); HRMS (ASAP+, m/z): found 584.2830, calcd. for C$_{36}$H$_{42}$NO$_4$S [M+H]$^+$ 584.2835.

3-(2,4-bis(hexyloxy)phenyl)-7-(furan-2-yl)-10*H*-phenothiazine (14)
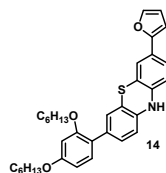
The compound **14** was prepared as described for compound **8** starting with the compound **13** (260 mg, 0.45 mmol). This produced **14** as a red resin (205 mg, 0.38 mmol, 85%). ^{1}H NMR (600 MHz, DMSO-d_6) δ: 8.76 (s, 1H), 7.65 (d, J = 1.3 Hz, 1H), 7.32 (dd, J = 2.1 Hz, 8.5 Hz, 1H), 7.23 (d, J = 2.1 Hz, 1H), 7.14 (d, J = 8.5 Hz, 1H), 7.07 (dd, J = 2.0 Hz, 8.2 Hz, 1H), 7.04 (d, J = 2.0 Hz, 1H), 6.74 (dd, J = 0.8 Hz, 3.4 Hz, 1H), 6.71 (d, J = 8.4 Hz, 1H), 6.68 (d, J = 8.2 Hz, 1H), 6.57 (d, J = 2.4 Hz, 1H), 6.55-6.51 (m, 2H), 4.00-3.91 (m, 4H), 1.70 (q, J = 8.0 Hz, 2H), 1.64 (q, J = 8.5 Hz, 2H), 1.46-1.35 (m, 4H), 1.35-1.21 (m, 8H), 0.91-0.83 (m, 6H); ^{13}C NMR (150 MHz, DMSO-d_6) δ: 159.1, 156.3, 152.5, 142.0, 141.1, 139.6, 131.8, 130.0, 128.2, 126.7, 124.3, 122.9, 121.4, 121.2, 116.9, 115.2, 114.5, 114.0, 111.9, 105.8, 104.0, 100.1, 67.7, 67.5, 31.00, 30.98, 28.7, 28.6, 25.4, 25.2, 22.12, 22.07, 13.91 (2C); IR (CH$_2$Cl$_2$, cm^{-1}): 3399 (w), 2954 (m), 2927 (m), 2857 (m), 1607 (m), 1488 (s), 1296 (m), 1271 (m), 1177 (m), 1010(m); HRMS (ASAP+, m/z): found 541.2644, calcd. for C$_{34}$H$_{39}$NO$_3$S [M+H]$^+$ 541.2651.

4'-bromo-2,4-bis(hexyloxy)-1,1'-biphenyl (16)
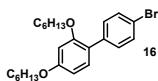
Compound 16 was prepared following a modified procedure reported by Seo et al.[1] 1-Bromo-4-iodobenzene **15** (200 mg, 0.71 mmol), Pd(PPh$_3$)$_4$ (40.9 mg, 35 μmol), and K$_2$CO$_3$ (391 mg, 2.83 mmol) were mixed with crude 2-(2,4-bis(hexyloxy)phenyl)-4,4,5,5-tetramethyl-1,3,2-dioxaborolane **6** (343 mg, 0.85 mmol), before the mixture was evacuated and a nitrogen atmosphere established. Degassed H$_2$O (7 mL) and 1,4-dioxane (7 mL) were added under a nitrogen atmosphere. This mixture was stirred at 80 °C for 1 h. After the mixture was cooled down to rt, H$_2$O (75 mL) was added and the aqueous phase extracted with ethyl acetate (3 × 50 mL). The combined organic phase was washed with H$_2$O (50 mL), dried over Na$_2$SO$_4$ before the solvents were removed in vacuo. The crude product was purified with column chromatography (*n*-pentane/CH$_2$Cl$_2$, 5:1, R$_f$ = 0.16) to yield **16** as a yellow oil (189 mg, 0.44 mmol, 62%). ^{1}H NMR (400 MHz, DMSO-d_6) δ: 7.53 (d, J = 9.0 Hz, 2H), 7.39 (d, J = 9.0 Hz, 2H), 7.19, (d, J = 8.0 Hz, 1H), 6.62 (d, J = 2.5 Hz, 1H), 6.57 (dd, J = 2.5 Hz, 8.0 Hz, 1H), 4.02-3.92 (m, 4H), 1.71 (q, J = 7.7 Hz, 2H), 1.62 (q, J = 7.8 Hz, 2H), 1.47-1.37 (m, 2H), 1.37-1.27 (m, 6H) 1.27-1.18 (m, 4H), 0.88 (t, J = 7.8 Hz, 3H), 0.83 (t, J = 7.7 Hz, 3H); ^{13}C NMR (100 MHz, DMSO-d_6) δ: 159.7, 156.4, 137.3, 131.1 (2C), 130.68, 130.66 (2C), 121.0, 119.4, 106.0, 100.1, 67.9, 67.5, 31.0, 30.8, 28.7, 28.5, 25.20, 25.16, 22.1, 22.0, 13.9, 13.8.

10-(2',4'-bis(hexyloxy)-[1,1'-biphenyl]-4-yl)-3-(2,4-bis(hexyloxy)phenyl)-7-(furan-2-yl)-10*H*-phenothiazine (17)
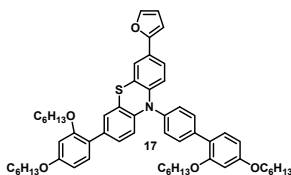
The compound **17** was prepared as described for compound **9** starting with the compound **14** (140 mg, 0.26 mmol) and compound **16** (135 mg, 0.31 mmol). The crude product was purified with column chromatography (*n*-pentane/CH$_2$Cl$_2$, 2:1, R$_f$ = 0.68) to yield **17** as an orange wax (154 mg, 0.17 mmol, 65%). ^{1}H NMR (600 MHz, DMSO-d_6) δ: 7.77 (d, J = 8.6 Hz, 2H), 7.68 (d, J = 1.7 Hz,

1H), 7.44 (d, J = 8.6 Hz, 2H), 7.41 (d, J = 2.1 Hz, 1H), 7.36 (d, J = 8.6 Hz, 1H), 7.26 (dd, J = 2.2 Hz, 8.7 Hz, 1H), 7.22 (d, J = 2.1 Hz, 1H), 7.15 (d, J = 8.5 Hz, 1H), 7.03 (dd, J = 2.1 Hz, 8.6 Hz, 1H), 6.81 (d, J = 3.3 Hz, 1H), 6.68 (d, J = 2.3 Hz, 1H), 6.64 (dd, 2.3 Hz, 8.5 Hz, 1H), 6.59 (d, J = 2.2 Hz, 1H), 6.56-6.53 (m, 2H), 6.25 (d, J = 8.7 Hz, 1H), 6.21 (d, J = 8.5 Hz, 1H), 4.06-3.99 (m, 4H), 3.99-3.91 (m, 4H), 1.78-1.60 (m, 8H), 1.48-1.19 (m, 24H), 0.93-0.85 (m, 6H), 0.85-0.76 (m, 6H); ^{13}C NMR (150 MHz, DMSO-d_6) δ: 159.8, 159.3, 156.6, 156.4, 152.0, 142.7, 142.4, 141.5, 138.4, 138.0, 132.7, 131.6 (2C), 130.9, 130.1 (2C), 129.7, 129.1, 127.7, 127.0, 125.1, 122.3, 121.3, 120.8, 119.8, 117.9, 115.9, 115.5, 112.0, 106.1, 105.9, 104.8, 100.2, 100.1, 67.9, 67.8, 67.6, 67.5, 31.01, 30.99 (2C), 30.8, 28.69, 28.65, 28.6, 28.5, 25.4, 25.22 (2C), 25.19, 22.09 (2C), 22.07, 22.0, 13.92, 13.90, 13.85, 13.8; IR (CH$_2$Cl$_2$, cm^{-1}): 2926 (m), 2857 (m), 1607 (m), 1492 (s), 1296 (s), 1274 (s), 1178 (s), 1011 (m); HRMS (ASAP+, m/z): found 893.5048, calcd. for C$_{58}$H$_{71}$NO$_5$S [M*]$^+$ 893.5053.

5-(10-(2',4'-bis(hexyloxy)-[1,1'-biphenyl]-4-yl)-7-(2,4-bis(hexyloxy)phenyl)-10*H*-phenothiazin-3-yl)furan-2-carbaldehyde (18)
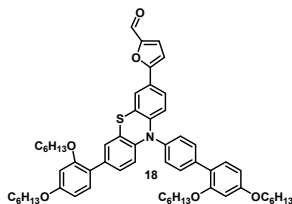
Compound **17** (130 mg, 0.15 mmol) was dissolved in anhydrous THF (4 mL) and cooled to -78 °C, a solution of *n*-BuLi in hexanes (1.4 M, 160 µL, 0.22 mmol) was added to this over 5 minutes. The reaction mixture was then stirred for 15 minutes before DMF (40 µL, 0.51 mmol) was added. After 15 more minutes of stirring, the reaction vessel was removed from the cooling mixture and left to reach r.t over 45 minutes. The reaction was quenched by addition of aqueous HCl (2 M, 4 mL), the aqueous phase was extracted with ethyl acetate (3 x 15 mL). The combined organic phase was washed with H$_2$O (15 mL), dried over Na$_2$SO$_4$ before the solvents were removed in vacuo. The crude product was purified with column chromatography (CH$_2$Cl$_2$, R$_f$ = 0.58) to yield **18** as a red wax (46 mg, 50 µmol, 34%). ^{1}H NMR (600 MHz, CD$_2$Cl$_2$) δ: 9.55 (s, 1H), 7.81 (d, J = 8.8 Hz, 2H), 7.46 (d, J = 2.0 Hz, 1H), 7.41 (d, J = 8.8 Hz, 2H), 7.35, (d, J = 9.0 Hz, 1H), 7.30-7.26 (m, 2H), 7.22 (d, J = 2.0 Hz, 1H), 7.14 (d, J = 8.1 Hz, 1H), 7.02 (dd, J = 1.9 Hz, 8.7 Hz, 1H), 6.69 (d,

J = 4.1 Hz, 1H), 6.62-6.59 (m, 2H), 6.52-6.48 (m, 2H), 6.32 (d, *J* = 9.0 Hz, 1H), 6.27 (d, *J* = 9.0 Hz, 1H), 4.02 (app. t, *J* = 6.2 Hz, 4H), 3.96 (t, *J* = 6.7 Hz, 2H), 3.94 (t, *J* = 6.7 Hz, 2H), 1.84-1.69 (m, 8H), 1.52-1.41 (m, 8H), 1.40-1.28 (m, 16H), 0.96-0.84 (m, 12H); ^{13}C NMR (150 MHz, CD$_2$Cl$_2$) δ: 177.0, 160.8, 160.3, 159.2, 157.5, 157.3, 152.2, 145.9, 142.1, 139.6, 138.7, 133.9, 132.3 (3C), 131.5 (2C), 130.7, 130.5, 128.3, 127.8, 124.5, 123.5, 123.5, 122.4, 122.1, 121.0, 118.7, 116.2 (2C), 106.9, 106.0, 105.8, 100.64, 100.55, 68.9, 68.8, 68.64, 68.57, 32.04, 32.02, 31.99, 31.9, 29.71, 29.69, 29.6, 29.5, 26.3, 26.21, 26.15, 26.1, 23.1 (2C), 23.04, 23.02, 14.3, 14.24, 14.22 (2C); IR (CH$_2$Cl$_2$, cm^{-1}): 2953 (m), 2929 (m), 2858 (m), 1675 (m), 1609 (m), 1460 (s), 1298 (m), 1265 (m), 1182 (m); HRMS (ASAP+, m/z): found 921.4994, calcd. for C$_{59}$H$_{71}$NO$_6$S [M*]$^+$ 921.5002.

(*E*)-3-(5-(10-(2',4'-bis(hexyloxy)-[1,1'-biphenyl]-4-yl)-7-(2,4-bis(hexyloxy)phenyl)-10*H*-phenothiazin-3-yl)furan-2-yl)-2-cyanoacrylic acid (3,7-PTZ-Fu)
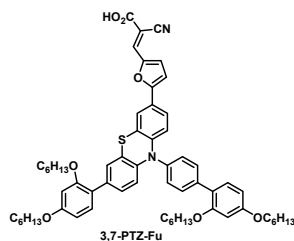
3,7-PTZ-Fu was prepared as described for **TAA-Th** starting with the aldehyde **18** (45.0 mg, 48.8 *μ*mol) and reacting for 1.5 h. Purification by silica-gel column chromatography (0-10% MeOH in CH2Cl2) gave **3,7-PTZ-Fu** as a red solid (31.2 mg, 31.5 μmol, 65%), mp. 74.1-75.8 °C. ^{1}H NMR (600 MHz, acetone-*d$_6$*) δ: 8.01 (s, 1H), 7.86 (d, *J* = 8.3 Hz, 2H), 7.64 (d, *J* = 2.1 Hz, 1H), 7.51 (dd, *J* = 2.1 Hz, 8.9 Hz, 1H), 7.49 (d, *J* = 4.2 Hz, 1H), 7.46 (d, *J* = 8.3 Hz, 2H), 7.38 (d, *J* = 8.5 Hz, 1H), 7.26 (d, *J* = 2.1 Hz, 1H), 7.18 (d, *J* = 8.5 Hz, 1H), 7.10 (d, *J* = 3.6 Hz, 1H), 7.05 (dd, *J* = 2.1 Hz, 8.9 Hz, 1H), 6.69 (d, *J* = 2.5 Hz, 1H), 6.64 (dd, *J* = 2.5 Hz, 8.4 Hz, 1H), 6.60 (d, *J* = 2.5 Hz, 1H), 6.54 (dd, *J* = 2.5 Hz, 8.2 Hz, 1H), 6.33 (d, *J* = 8.7 Hz, 1H), 6.27 (d, *J* = 8.7 Hz, 1H), 4.09-4.04 (m, 4H), 4.02-3.97 (m, 4H), 1.84-1.68 (m, 8H), 1.54-1.43 (m, 8H), 1.41-1.24 (m, 16H), 0.95-0.81 (m, 12H); ^{13}C NMR (150 MHz, Acetone-*d$_6$*) δ: 164.3, 161.4, 160.9, 159.9, 158.1, 157.9, 148.5, 146.3, 142.3, 140.4, 139.1, 138.5, 134.7, 132.9 (2C), 132.0, 131.2, 130.9 (2C), 128.8, 128.2, 127.0, 125.3, 124.02 (2C), 122.8, 122.3, 121.4, 118.9, 117.0, 116.7, 116.7, 109.3, 106.9, 106.7, 101.1, 101.0, 97.1, 69.1, 69.0, 68.7, 68.6, 32.38, 32.36 (2C), 32.2, 29.9 (4C)*, 26.7, 26.6, 26.53,

26.51, 23.4, 23.33, 23.30 (2C), 14.43, 14.37, 14.34, 14.32; IR (CH$_2$Cl$_2$, cm^{-1}): 2953 (m), 2937 (m), 2869 (m), 2337 (w), 1686 (m), 1608 (m), 1493 (s), 1299 (m), 1263 (m), 1182 (m); HRMS (ASAP+, m/z): found 988.5042, calcd. for C$_{62}$H$_{72}$N$_2$O$_7$S [M*]$^+$ 988.5060. *Signal found using ^{1}H-^{13}C HSQC NMR due to overlap with solvent residual signal.

2,2'-((2-nitro-1,3-phenylene)bis(oxy))bis(bromobenzene) (21)
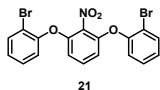
Sodium hydride (103 mg, 4.30 mmol) and 2-bromophenol **19** (0.3 mL, 2.60 mmol) was dissolved in DMSO (2 mL) before being heated to 50 °C. The reaction mixture was stirred for 15 minutes before 1,3-dichloro-2-nitrobenzene (100 mg, 0.52 mmol) was added, then the reaction was left stirring for 24 hours. Upon cooling to room temperature H$_2$O (10 mL) was added, and the aqueous phase was extracted using diethyl ether (3 x 25 mL). The combined organic phases were washed with water (3 x 25 mL), before being dried with brine and over Na$_2$SO$_4$. The crude product was concentrated in vacuo and purified by silica gel column chromatography (*n*-pentane/CH$_2$Cl$_2$, 10:1, R$_f$ = 0.08) to give compound **21** as a yellow solid (136 mg, 0.29 mmol, 56%), mp. 128.4-129.6 °C. ^{1}H NMR (600 MHz, DMSO-d_6) δ: 7.81 (dd, J = 1.7 Hz, 8.1 Hz, 2H), 7.51 (td, J = 1.7 Hz, 8.2 Hz, 2H), 7.44 (t, J = 8.7 Hz, 1H), 7.35 (dd, J = 1.4 Hz, 8.2 Hz, 2H), 7.28 (td, J = 1.4 Hz, 7.9 Hz, 2H), 6.60 (d, J = 8.7 Hz, 2H); ^{13}C NMR (150 MHz, DMSO-d_6) δ: 150.7, 148.9, 134.1, 132.8, 132.6, 129.9, 127.7, 122.2, 114.5, 111.3; IR (CH$_2$Cl$_2$, cm^{-1}): 2895 (w), 1608 (m), 1464 (s), 1307 (m), 1244 (s), 1121 (s); HRMS (ASAP+, m/z): found 463.9138, calcd. for C$_{18}$H$_{12}$NO$_4$Br$_2$ [M+H]$^+$ 463.9133.

2,6-bis(2-bromophenoxy)aniline (22)
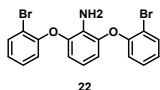
Compound **21** (100 mg, 0.22 mmol) was mixed with NH$_4$Cl (104 g, 1.94 mmol) and iron powder (36 mg, 0.65 mmol), before EtOH (2 mL) and water (0.5 mL) were added under nitrogen atmosphere. The reaction mixture was stirred at 78 °C for 4 h, cooled to rt, filtered through celite using ethyl acetate as eluent, and concentrated. This provided **22** as a colorless wax that was carried forward without further purification.

benzo[5,6][1,4]oxazino[2,3,4-*kl*]phenoxazine (23)
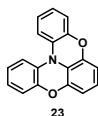
Compound **22** (94 mg, 0.22 mmol), Pd(OAc)2 (2.4 mg, 11 μmol), XPhos (10 mg, 22 μmol), and sodium tert-butoxide (42 mg, 0.43 mmol) was added to a Schlenk tube, and nitrogen atmosphere was established. Dry 1,4-dioxane (2 mL) was added under nitrogen and the reaction mixture was heated to 110 °C, the reaction was stirred for 18 hours. Upon cooling down to room temperature, an aqueous solution of NH$_4$Cl was added (saturated, 5 mL). The aqueous phase was extracted with ethyl acetate (3 x 25 mL), and the combined organic phase was dried with brine and over Na$_2$SO$_4$. The solvents were removed in vacuo, and the crude product was purified by silica gel column chromatography (*n*-pentane/CH$_2$Cl$_2$, 1:1, R$_f$ = 0.66) to give compound **23** as a white solid (26 mg, 0.11 mmol, 50% over two steps from **21**), mp. 163.7-164.8 °C (lit. 165 °C).[2] ^{1}H NMR (600 MHz, DMSO-d_6) δ: 7.37 (d, J = 8.2 Hz, 2H), 7.08-6.95 (m, 6H), 6.87 (t, J = 8.3 Hz, 1H), 6.64 (d, J = 8.3 Hz, 2H); ^{13}C NMR (150 MHz, DMSO-d_6) δ: 146.0, 144.6, 128.3, 124.3, 124.2, 123.9, 120.2, 117.3, 114.8, 111.2; IR (CH$_2$Cl$_2$, cm^{-1}): 3425 (w), 2922 (w), 2850 (w), 1618 (m), 1468 (s), 1306 (m), 1281 (s), 1112 (m), 738 (s); HRMS (ASAP+, m/z): found 274.0867, calcd. for C$_{18}$H$_{12}$NO$_2$ [M+H]$^+$ 274.0868. ^{1}H NMR spectrum is accordance with previously reported data.[2]

7-bromobenzo[5,6][1,4]oxazino[2,3,4-kl]phenoxazine (24)
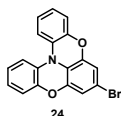
The synthesis of 7-bromobenzo[5,6][1,4]oxazino[2,3,4-kl]phenoxazine, **24**, was attempted through the following two procedures [3,4] with slight modifications. In our hands the resulting product mixture proved impossible to purify by column chromatography or recrystallization.

NBS-procedure: A solution of compound **23** (20 mg, 0.073 mmol) in chloroform (4 mL) is mixed with N-bromosuccinimide (11.7 g, 0.066 mmol) at 0 °C under exclusion of light, and the mixture was stirred at this temperature for 2 h. The reaction was quenched by addition of sodium sulfite solution (5w%, 10 mL), and the mixture was stirred at room temperature for a further 30 min. After phase separation, the organic phase was washed with water (20 mL), and the aqueous phase was extracted with dichloromethane (3 x 20 mL).

The combined organic phases were dried over sodium sulfate and concentrated in vacuum. The residue was dissolved in ethyl acetate and filtered over silica gel. The crude product was subsequently recrystallized from hexane.

Br$_2$-Procedure:

A stirred solution of compound **23** (50 mg, 0.18 mmol) in acetic acid (2 mL) was flushed with nitrogen then a solution of bromine (1 M, 0.20 mL, 1 mmol) in acetic acid was added dropwise, and stirring was continued overnight. The reaction was quenched by addition of sodium sulfite (5w%, 20 mL) solution, and the mixture was stirred at room temperature for a further 30 min. After phase separation, the organic phase was washed with water (20 mL), and the aqueous phase was extracted with dichloromethane (3 x 20 mL). The combined organic phases were dried over sodium sulfate and concentrated in vacuum. The crude product was subjected to silica gel column chromatography (*n*-pentane/CH$_2$Cl$_2$, 1:3, R$_f$ = 0.30).

4-bromo-2',4'-bis(hexyloxy)-[1,1'-biphenyl]-3-ol (26)
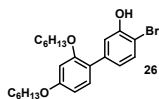
The compound **26** was prepared as described for compound **16** starting with the building block **6** (1.40 g, 3.45 mmol), except this time with it was coupled with 2-bromo-5-iodophenol **25** (860 mg, 2.88 mmol) in a 3 hour reaction. The crude product was purified with column chromatography (*n*-pentane/EtOAc, 10:1, R$_f$ = 0.37) to yield **26** as a colorless oil (663 mg, 1.58 mmol, 51%). ^{1}H NMR (400 MHz, DMSO-d_6) δ: 10.09 (s, 1H), 7.41 (d, *J* = 8.9 Hz, 1H), 7.14 (d, *J* = 8.2 Hz, 1H), 7.06 (d, *J* = 2.0 Hz, 1H), 6.80 (dd, *J* = 2.0 Hz, 8.9 Hz, 1H), 6.60 (d, *J* = 2.5 Hz, 1H), 6.56 (dd, *J* = 2.5 Hz, 8.2Hz, 1H), 3.98 (t, *J* = 6.6 Hz, 2H), 3.94 (t, *J* = 6.1 Hz, 2H), 1.71 (q, *J* = 6.6 Hz, 2H), 1.63 (q, *J* = 6.1 Hz, 2H), 1.45-1.38 (m, 2H), 1.36-1.28 (m, 6H), 1.28-1.20 (m, 4H), 0.88 (t, *J* = 6.6 Hz, 3H), 0.83 (t, *J* = 6.1 Hz, 3H); ^{13}C NMR (100 MHz, DMSO-d_6) δ:159.6, 156.4, 153.5, 138.7, 131.9, 130.5, 121.5, 121.4, 117.1, 107.1, 105.9, 100.2, 68.0, 67.5, 31.0, 30.9, 28.7, 28.5, 25.2, 25.1, 22.1, 22.0, 13.9, 13.8; IR (CH$_2$Cl$_2$, cm^{-1}): 2928, 2857, 1682, 1608, 1499, 1301, 1277, 1181; HRMS (ASAP+, m/z): found 449.1657, calcd. for C$_{24}$H$_{34}$BrO$_3$ [M+H]$^+$ 449.1691.

2-(3,5-difluoro-4-nitrophenyl)thiophene (28)
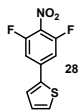
The compound **28** was prepared as described for compound **2** starting with the building block 5-bromo-1,3-difluoro-2-nitrobenzene **27** (250 mg, 1.05 mmol) and thiophen-2-ylboronic acid (202 mg, 1.58 mmol) The crude product was purified with column chromatography (*n*-pentane/toluene, 3:1, R_f = 0.28) to yield **28** as a green solid (188 mg, 0.78 mmol, 74%), mp. 96.3-97.1 °C. ^{1}H NMR (600 MHz, DMSO-d_6) δ: 7.91 (d, *J* = 4.0 Hz, 1H), 7.86-7.80 (m, 3H), 7.25 (dd, *J* = 4.0 Hz, 5.0 Hz, 1H); ^{13}C NMR (150 MHz, DMSO-d_6) δ: 154.8 (dd, *J* = 2.2 Hz, 258.7 Hz), 140.1 (t, *J* = 11.0 Hz), 138.9 (t, *J* = 2.6 Hz), 130.3 (s), 129.2 (s), 128.5 (s), 126.6 (t, *J* = 14.2 Hz), 109.7 (dd, *J* = 3.3 Hz, 21.9 Hz); IR (CH_2Cl_2, cm^{-1}): 3110 (w), 1610 (m), 1478 (m), 1369 (m), 1233 (m), 1083 (m); HRMS (ASAP+, m/z): found 241.0013, calcd. for $C_{10}H_5NO_2F_2S$ [M+H]$^+$ 241.0009.

2-(3,5-bis((4-bromo-2',4'-bis(hexyloxy)-[1,1'-biphenyl]-3-yl)oxy)-4-nitrophenyl)thiophene (29)
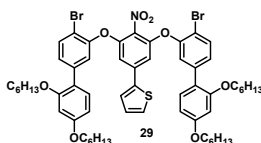
Compound **26** (407 mg, 0.91 mmol) and compound **28** (100 mg, 0.41 mmol) were dissolved in DMF (3 mL). K_2CO_3 (378 mg, 2.74 mmol) was added and the mixture was stirred at 100 °C for 4 h. After addition of 1 M HCl aq. (5 mL), the products were extracted with CH_2Cl_2 (3 × 25 mL). The organic phase was dried over Na_2SO_4, filtered off, and concentrated under reduced pressure. The obtained crude product was purified by silica gel column chromatography (CH_2Cl_2, R_f = 0.59) to give compound **29** as a yellow wax (269 mg, 0.24 mmol, 59%). ^{1}H NMR (400 MHz, DMSO-d_6) δ: 7.80 (d, *J* = 8.6 Hz, 2H), 7.61 (dd, *J* = 1.3 Hz, 5.0 Hz, 1H), 7.48 (d, *J* = 2.0 Hz, 2H), 7.46 (dd, *J* = 1.2 Hz, 3.8 Hz, 1H), 7.34 (dd, *J* = 2.3 Hz, 8.6 Hz, 2H), 7.30 (app. d, *J* = 9.4 Hz, 2H), 7.08 (dd, *J* = 3.8 Hz, 5.0 Hz, 1H), 6.91 (s, 2H), 6.61-6.57 (m, 4H), 3.99 (t, *J* = 6.6 Hz, 4H), 3.86 (t, *J* = 6.6 Hz, 4H), 1.70 (q, *J* = 7.7 Hz, 4H), 1.46-1.37 (m, 8H), 1.34-1.27 (m, 8H), 1.15-1.09 (m, 4H), 1.07-0.95 (m, 8H), 0.87 (t, *J* = 7.0 Hz, 6H), 0.67 (t, *J* = 7.7 Hz, 6H); ^{13}C NMR (150 MHz, DMSO-

d_6) δ: 160.1 (2C), 156.4 (2C), 150.4 (2C), 149.5 (2C), 139.7 (3C), 138.0, 133.5 (2C), 132.3, 130.8 (2C), 129.0, 128.6 (2C), 127.6, 126.9, 121.7 (2C), 119.6 (2C), 111.4 (2C), 108.7 (2C), 106.2 (2C), 100.0 (2C), 67.9 (2C), 67.6 (2C), 31.0 (2C), 30.7 (2C), 28.6 (2C), 28.4 (2C), 25.2 (2C), 25.0 (2C), 22.1 (2C), 21.9 (2C), 13.9 (2C), 13.7 (2C); IR (CH_2Cl_2, cm^{-1}): 2928 (m), 2857 (m), 1604 (m), 1509 (m), 1299 (m), 1244 (s), 1180 (s), 700 (m); HRMS (ASAP+, m/z): found 1097.3098, calcd. for $C_{58}H_{69}NO_8SBr_2$ [M*]$^+$ 1097.3111.

2,6-bis((4-bromo-2',4'-bis(hexyloxy)-[1,1'-biphenyl]-3-yl)oxy)-4-(thiophen-2-yl)aniline (30)
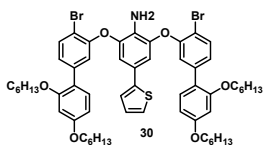
A solution of **29** (250 mg, 0.23 mmol) in acetone (20 mL) was treated with saturated aqueous NH$_4$Cl (5 mL), followed by Zn^0 (297 mg, 4.5 mmol). The reaction mixture was stirred at room temperature for 3 h before the reaction mixture was filtered through a plug of Celite (EtOAc). Removal of solvents in vacuo provided **30** as a colorless wax that was carried forward without further purification.

3,11-bis(2,4-bis(hexyloxy)phenyl)-7-(thiophen-2-yl)benzo[5,6][1,4]oxazino[2,3,4-*kl*]phenoxazine (31)
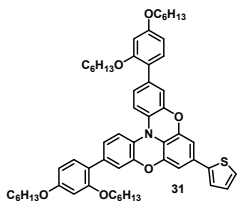
The compound **31** was prepared as described for compound **23** starting with the crude **30** (243 mg, 0.23 mmol). The crude **31** was purified with column chromatography (*n*-pentane/CH$_2$Cl$_2$, 10:1, R$_f$ = 0.43) to yield **31** as a slight green oil (80 mg, 0.09 mmol, 39% over two steps from **29**). ^{1}H NMR (600 MHz, CD$_2$Cl$_2$) δ:7.38 (d, *J* = 7.8 Hz, 2H), 7.27-7.21 (m, 4H), 7.17-7.12 (m, 4H), 7.05 (dd, *J* = 3.6 Hz, 5.0 Hz, 1H), 6.80 (s, 2H), 6.57-6.51 (m, 4H), 4.03-3.95 (m, 8H), 1.84-1.74 (m, 8H), 1.53-1.44 (m, 8H), 1.42-1.32 (m, 16H), 0.98-0.88 (m, 12H); ^{13}C NMR (150 MHz, CD$_2$Cl$_2$) δ: 160.4 (2C), 157.4 (2C), 146.4 (2C), 145.8 (2C), 143.5, 134.5 (2C), 130.9 (2C), 130.7, 128.4, 127.3 (2C), 124.9 (2C), 124.8, 123.2, 122.2 (2C), 120.6, 118.7 (2C), 114.5 (2C), 108.8 (2C), 105.9 (2C), 100.6

(2C), 68.9 (2C), 68.6 (2C), 32.1 (2C), 32.0 (2C), 29.7 (2C), 29.6 (2C), 26.3 (2C), 26.2 (2C), 23.1 (4C), 14.28 (2C), 14.26 (2C); IR (CH$_2$Cl$_2$, cm^{-1}): 2928, 2857, 1682, 1608, 1499, 1301, 1277, 1181; HRMS (ASAP+, m/z): found 907.3835, calcd. for C$_{58}$H$_{69}$NO$_6$S [M*]$^+$ 907.3846.

5-(3,11-bis(2,4-bis(hexyloxy)phenyl)benzo[5,6][1,4]oxazino[2,3,4-*kl*]phenoxazin-7-yl)thiophene-2-carbaldehyde (32)
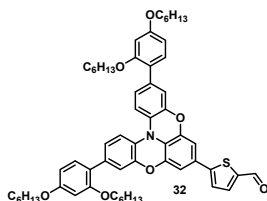
Compound **31** (80 mg, 0.09 mmol) was dissolved in anhydrous THF (2 mL) and cooled to -78 °C, a solution of lithium diisopropylamide in THF (2.0 M, 66 µL, 0.13 mmol) was added to this over 5 minutes. The reaction mixture was then stirred for 15 minutes before DMF (20 µL, 0.26 mmol) was added. After 15 more minutes of stirring, the reaction vessel was removed from the cooling bath and left to reach r.t over 45 minutes. The reaction was quenched by addition of aqueous HCl (2 M, 3 mL), the aqueous phase was extracted with ethyl acetate (3 x 15 mL). The combined organic phase was washed with H$_2$O (15 mL), dried over Na$_2$SO$_4$ before the solvents were removed in vacuo. The crude product was purified with column chromatography (CH$_2$Cl$_2$, R$_f$ = 0.44) to yield **32** as a red wax (40 mg, 43 µmol, 48%). ^{1}H NMR (600 MHz, CD$_2$Cl$_2$) δ: 9.83 (s, 1H), 7.69 (d, J = 4.2 Hz, 1H), 7.37 (d, J = 8.9 Hz, 2H), 7.30 (d, J = 4.2 Hz, 1H), 7.22 (d, J = 7.4 Hz, 2H), 7.17-7.12 (m, 4H), 6.84 (s, 2H), 6.56-6.51 (m, 4H), 4.01-3.95 (m, 8H), 1.83-1.73 (m, 8H), 1.52-1.44 (m, 8H), 1.41-1.30 (m, 16H), 0.96-0.87 (m, 12H); ^{13}C NMR (150 MHz, CD$_2$Cl$_2$) δ: 182.9, 160.4 (2C), 157.4 (2C), 153.0, 146.3 (2C), 145.9 (2C), 142.3 (2C), 137.8, 134.9 (2C), 130.9 (2C), 129.1, 126.9, 125.0 (2C), 124.1, 122.7, 122.1 (2C), 118.7 (2C), 114.6 (2C), 109.5 (2C), 105.9 (2C), 100.6 (2C), 68.9 (2C), 68.6 (2C), 32.1 (2C), 32.0 (2C), 29.7 (2C), 29.6 (2C), 26.3 (2C), 26.2 (2C), 23.07 (2C), 23.06 (2C), 14.3 (2C), 14.2 (2C); IR (CH$_2$Cl$_2$, cm^{-1}): 2926 (m), 2857 (m), 1667 (s), 1608 (s), 1491 (s), 1299 (s), 1282 (s), 1179 (m), 797 (m); HRMS (ASAP+, m/z): found 935.4779, calcd. for C$_{59}$H$_{69}$NO$_7$S [M*]$^+$ 935.4795.

(*E*)-3-(5-(3,11-bis(2,4-bis(hexyloxy)phenyl)benzo[5,6][1,4]oxazino[2,3,4-*kl*]phenoxazin-7-yl)thiophen-2-yl)-2-cyanoacrylic acid (POZPOZ-Th)
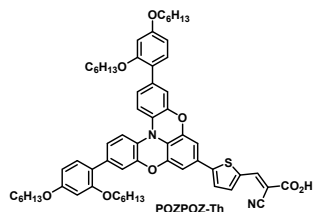
POZPOZ-Th was prepared as described for **TAA-Th** starting with the aldehyde **32** (40.0 mg, 42.7 μmol) and reacting for 2.5 h. Purification by silica-gel column chromatography (0-10% MeOH in CH2Cl2) gave **POZPOZ-Th** as a dark purple solid (36.2 mg, 36.0 μmol, 84%); mp. 82.4-84.1 °C. ^{1}H NMR (600 MHz, DMSO-d_6) δ: 8.35 (s, 1H), 7.86 (d, J = 4.2 Hz, 1H), 7.60 (d, J = 4.2 Hz, 1H), 7.23 (d, J = 8.6 Hz, 2H), 7.12 (d, J = 8.4 Hz, 2H), 7.07-7.00 (m, 4H), 6.89 (s, 2H), 6.55 (s, 2H), 6.47 (d, J = 8.4 Hz, 2H), 3.98-3.88 (m, 8H), 1.74-1.61 (m, 8H), 1.43-1.35 (m, 8H), 1.34-1.23 (m, 16H), 0.88 (t, J = 6.9 Hz, 6H), 0.83 (t, J = 6.7 Hz, 6H); ^{13}C NMR (150 MHz, DMSO-d_6) δ: 163.6, 159.4 (2C), 156.4 (2C), 150.6, 145.6, 144.9 (2C), 144.7 (2C), 140.5, 134.3, 134.0 (2C), 130.2 (2C), 128.2, 125.5 (2C), 124.8, 124.3, 121.2 (2C), 120.6 (3C), 117.7 (2C), 116.7, 114.1 (2C), 108.6 (2C), 105.7 (2C), 100.0 (2C), 67.8 (2C), 67.5(2C), 31.04 (2C), 30.98 (2C), 28.7 (2C), 28.6 (2C), 25.4 (2C), 25.2 (2C), 22.1 (4C), 13.9 (2C), 13.8 (2C); IR (CH$_2$Cl$_2$, cm^{-1}): 3064 (m), 3041(m), 2928 (m), 2859 (m), 2220 (w), 1692 (m), 1609 (m), 1494 (s), 1300 (m), 1282 (m), 1182 (m); HRMS (ASAP+, m/z): found 1002.4837, calcd. for C$_{62}$H$_{70}$N$_2$O$_8$S [M*]$^+$ 1002.4853.

References

1.   Seo, K. D.; Choi, I. T.; Kim, H. K., D–π–A organic dyes with various bulky amine-typed donor moieties for dye-sensitized solar cells employing the cobalt electrolyte. *Org. Electron.* **2015,** *25*, 1-5. DOI:10.1016/j.orgel.2015.06.011

2.   Kuratsu, M.; Kozaki, M.; Okada, K., Synthesis, Structure, and Electron-Donating Ability of 2,2':6',2''-Dioxatriphenylamine and Its Sulfur Analogue. *Chem. Lett.* **2004,** *33* (9), 1174-1175. DOI:10.1246/cl.2004.1174

3.   Brocke, C.; Plumm, C.; Parham, H.A.; Fortte, R., Heteroaromatic compounds and their preparation and use in electronic devices. WO2011107186A2. **2011**.

4.   Parham, A.; Kroeber, J.; Joosten, D.; Ludemann, A.; Grossmann, T., Bridged triarylamine derivatives, their preparation, use in electronic devices, and the devices. WO2018095839A1. **2018**.

NMR
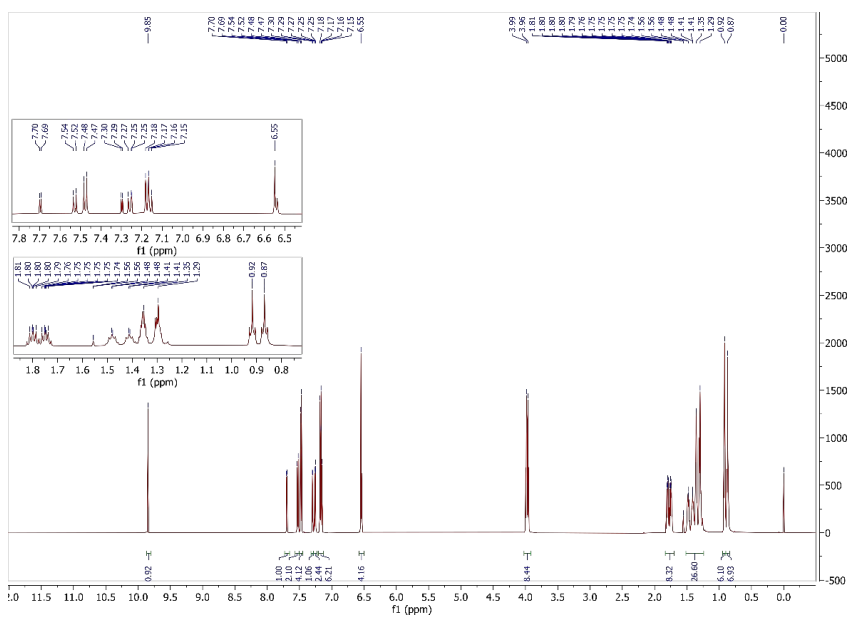
Figure S5 ¹H NMR (600 MHz, CDCl₃) of compound **2**.
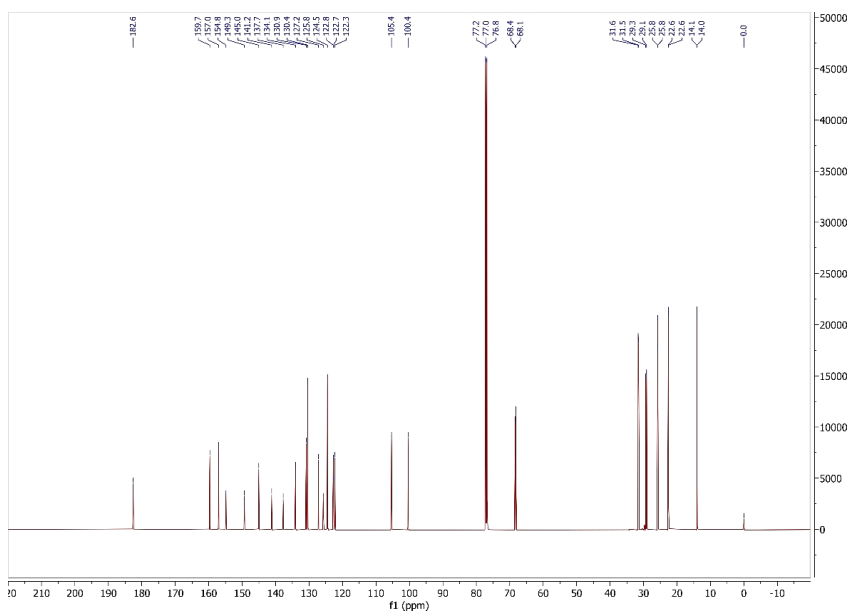
Figure S6 ¹³C NMR (150 MHz, CDCl₃) of compound **2**.
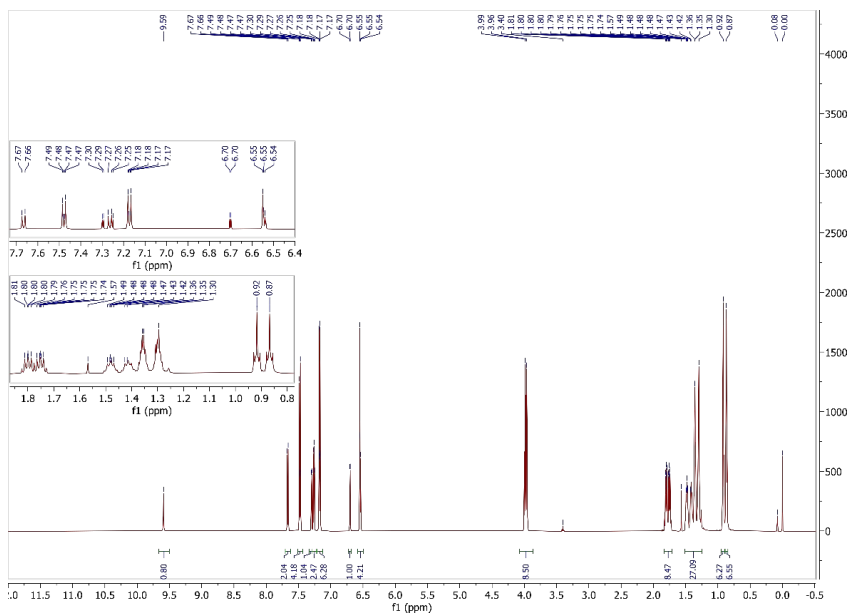
Figure S7 ^{1}H NMR (600 MHz, CDCl$_3$) of compound **3**.
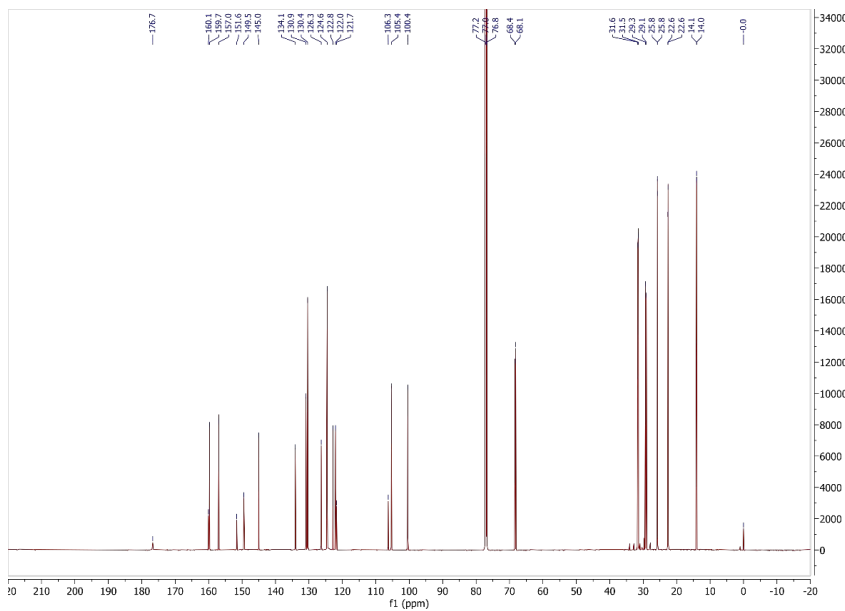
Figure S8 ^{13}C NMR (150 MHz, CDCl$_3$) of compound **3**.
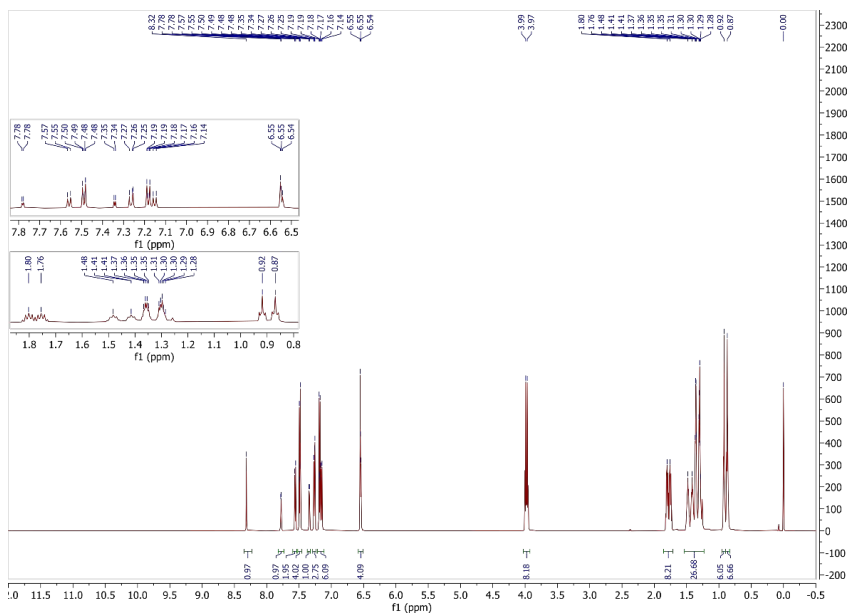
Figure S9 ^{1}H NMR (600 MHz, CDCl$_3$) of dye **TAA-Th**.
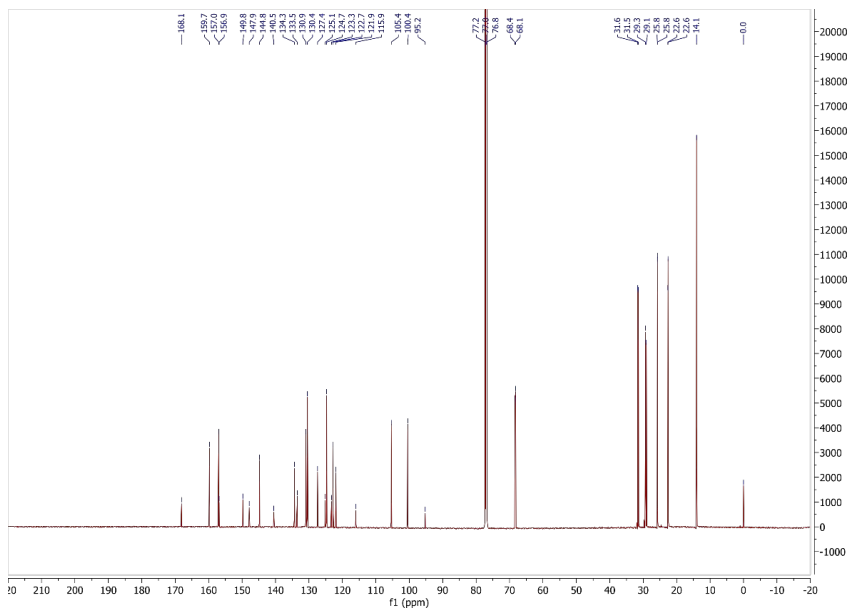
Figure S10 ^{13}C NMR (150 MHz, CDCl$_3$) of dye **TAA-Th**.
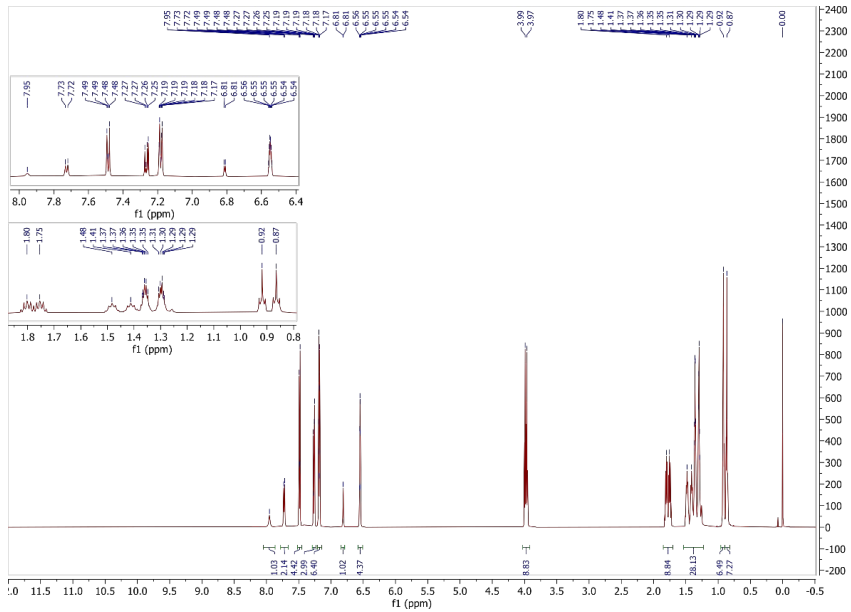
Figure S11 ^{1}H NMR (600 MHz, CDCl$_3$) of dye **TAA-Fu**.
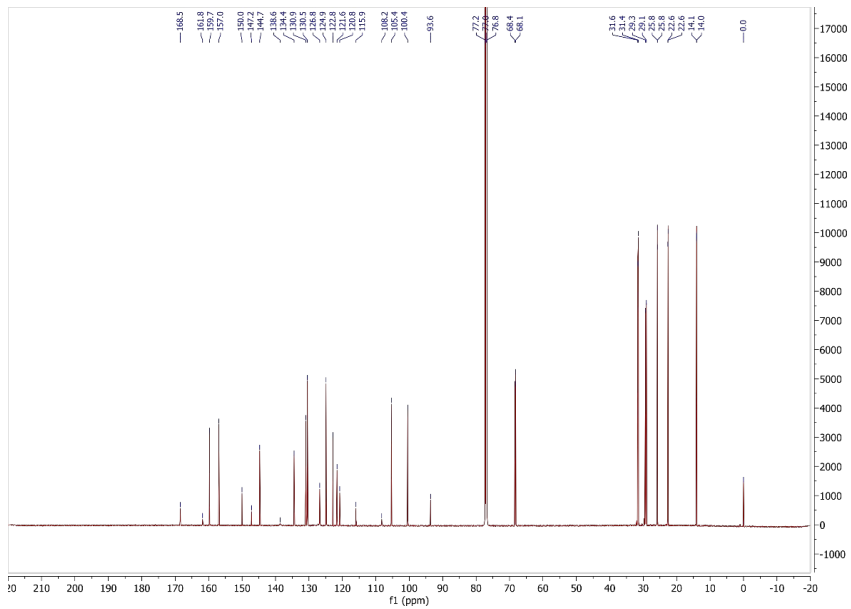
Figure S12 ^{13}C NMR (150 MHz, CDCl$_3$) of dye **TAA-Fu**.
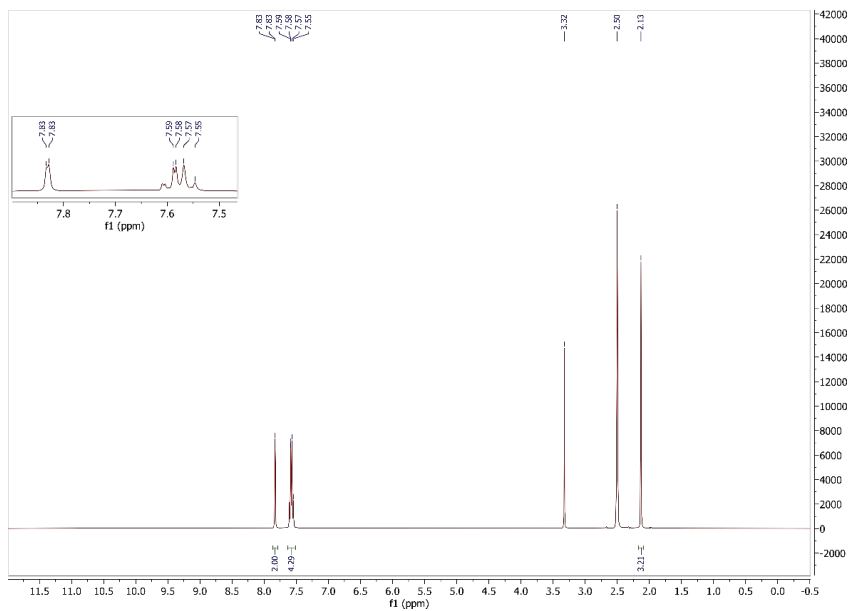
Figure S13 ^{1}H NMR (600 MHz, DMSO-d_6) of compound **5**.
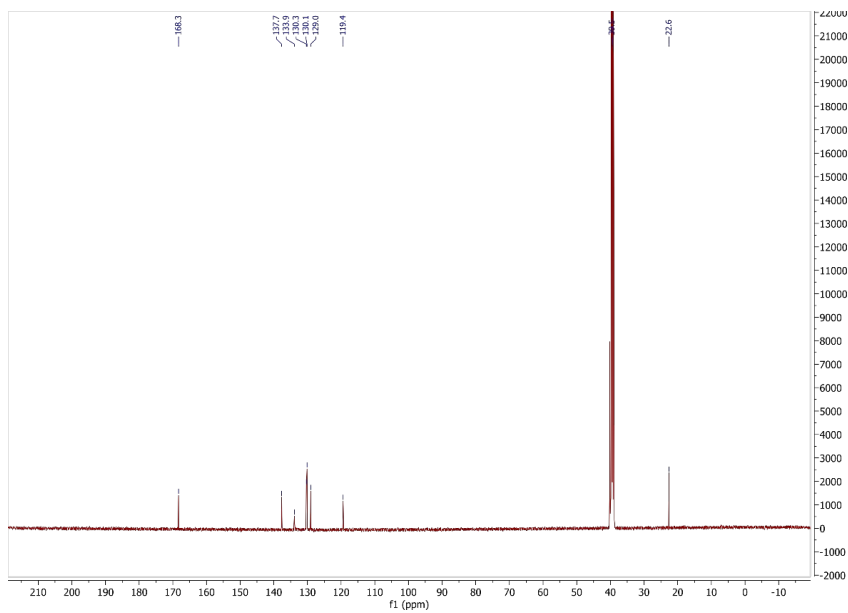
Figure S14 ^{13}C NMR (150 MHz, DMSO-d_6) of compound **5**.
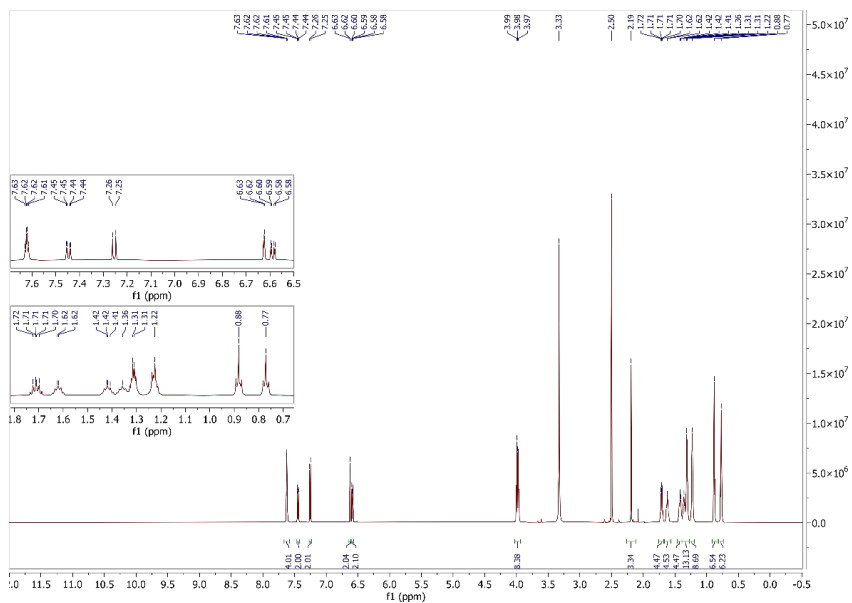
Figure S15 ^{1}H NMR (600 MHz, DMSO-d_6) of compound **7**.
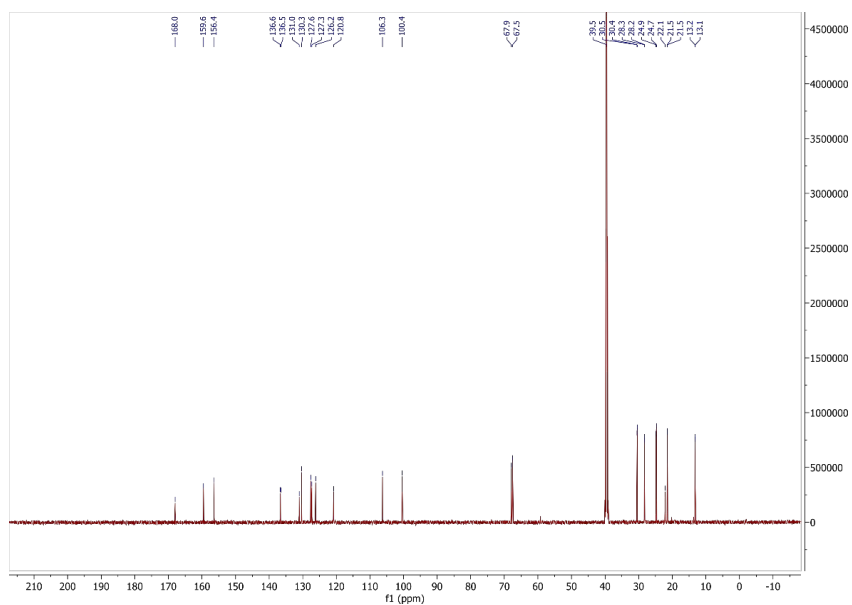
Figure S16 ^{13}C NMR (150 MHz, DMSO-d_6) of compound **7**.
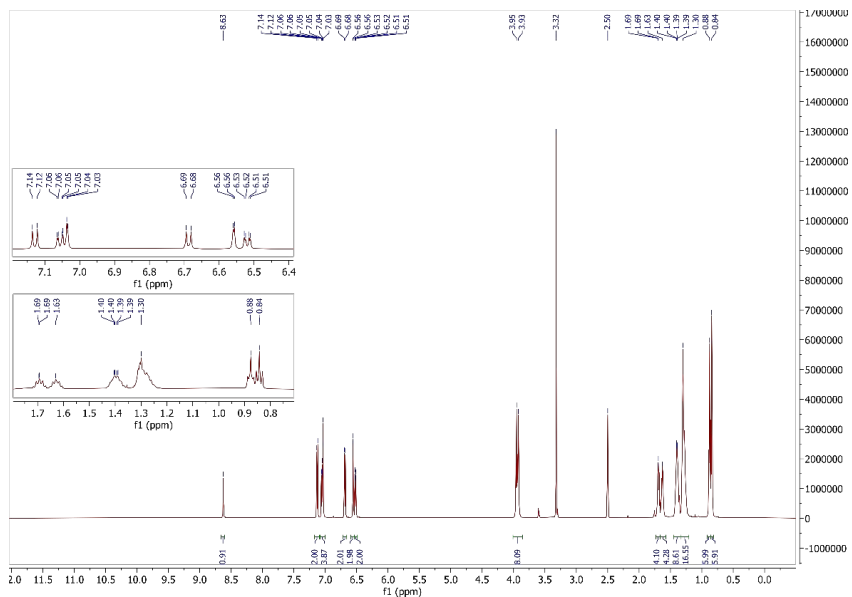
Figure S17 ^{1}H NMR (600 MHz, DMSO-d_6) of compound **8**.
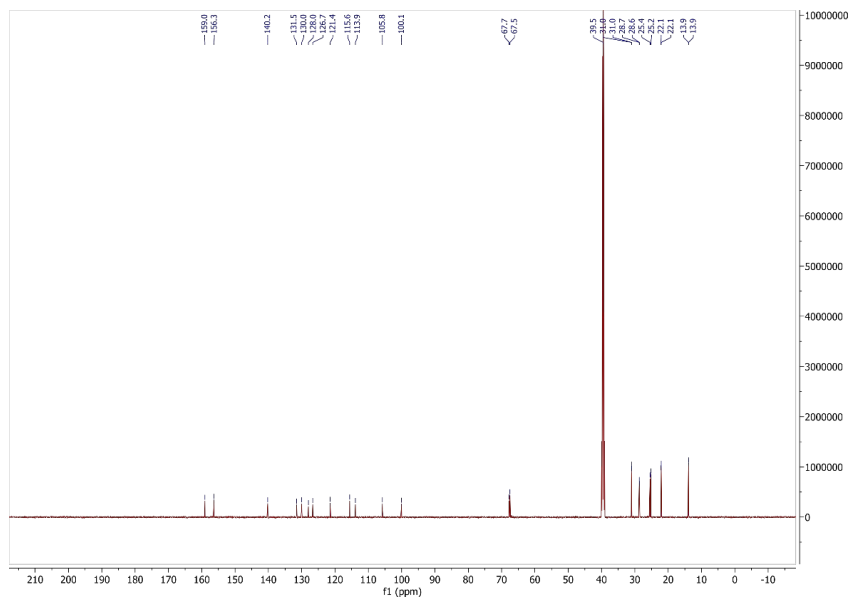
Figure S18 ^{13}C NMR (150 MHz, DMSO-d_6) of compound **8**.
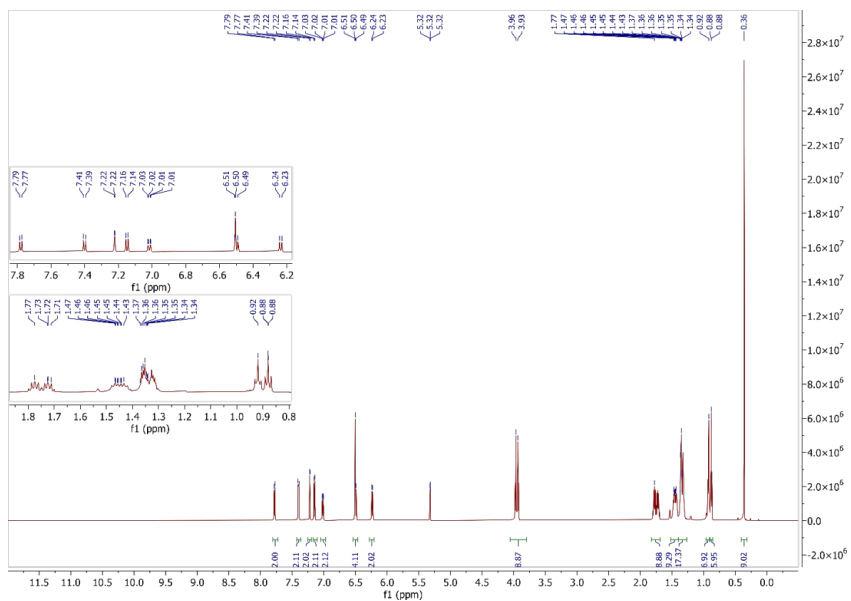
Figure S19 ^{1}H NMR (600 MHz, CD$_2$Cl$_2$) of compound **9**.
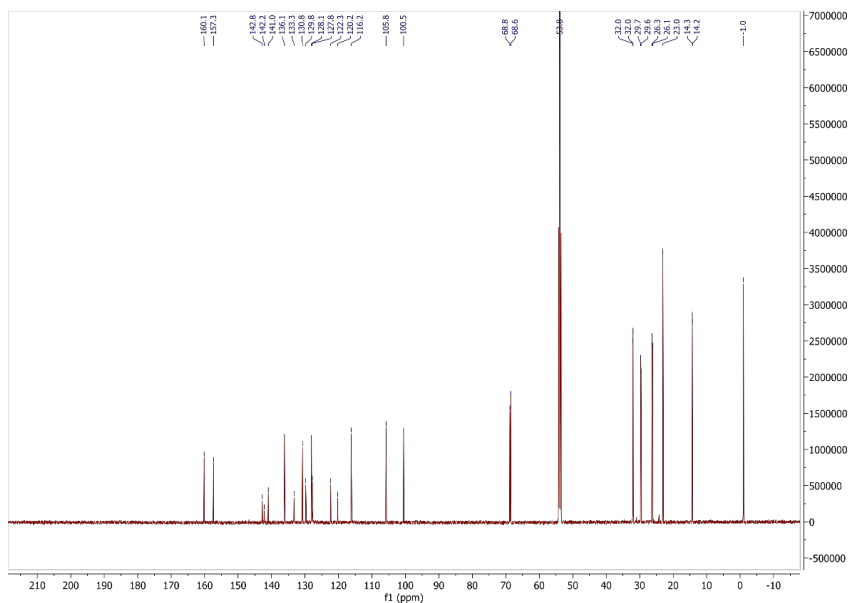
Figure S20 ^{13}C NMR (150 MHz, CD$_2$Cl$_2$) of compound **9**.
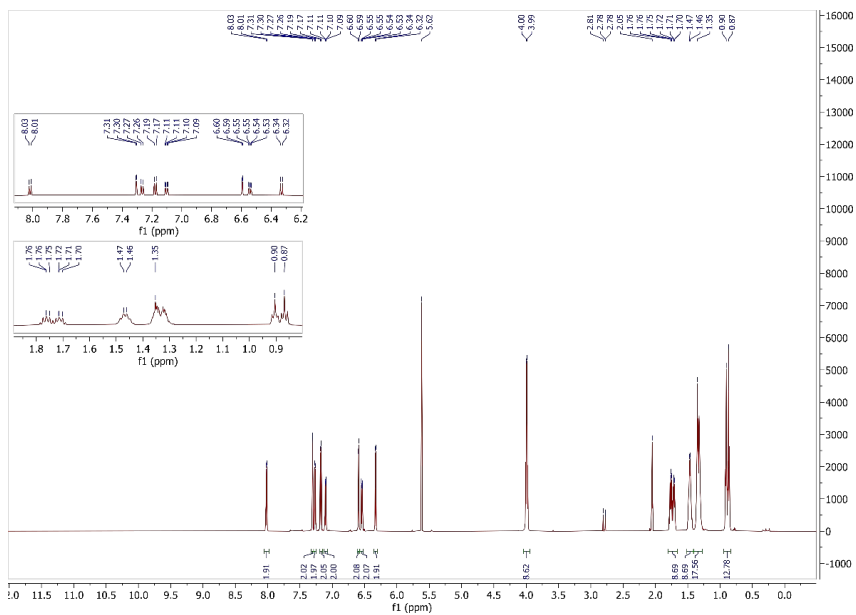
Figure S21 ^{1}H NMR (600 MHz, acetone-d_6) of compound **10**.
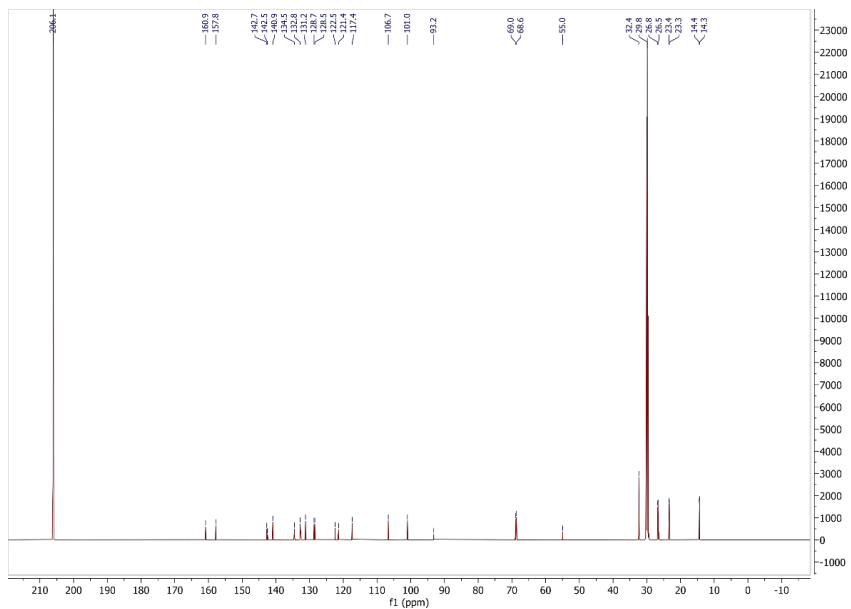
Figure S22 ^{13}C NMR (150 MHz, acetone-d_6) of compound **10**.
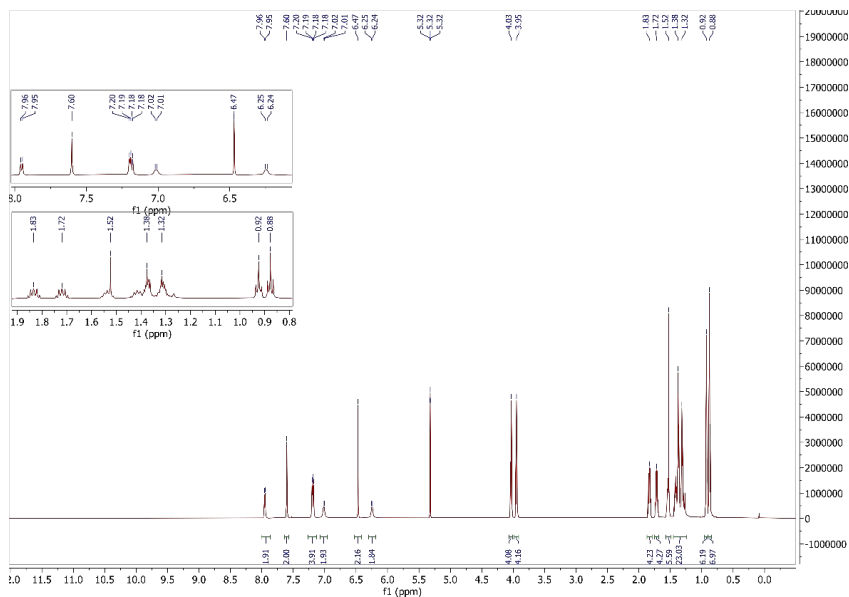
Figure S23 ^{1}H NMR (600 MHz, CD$_2$Cl$_2$) of compound **10-by**.
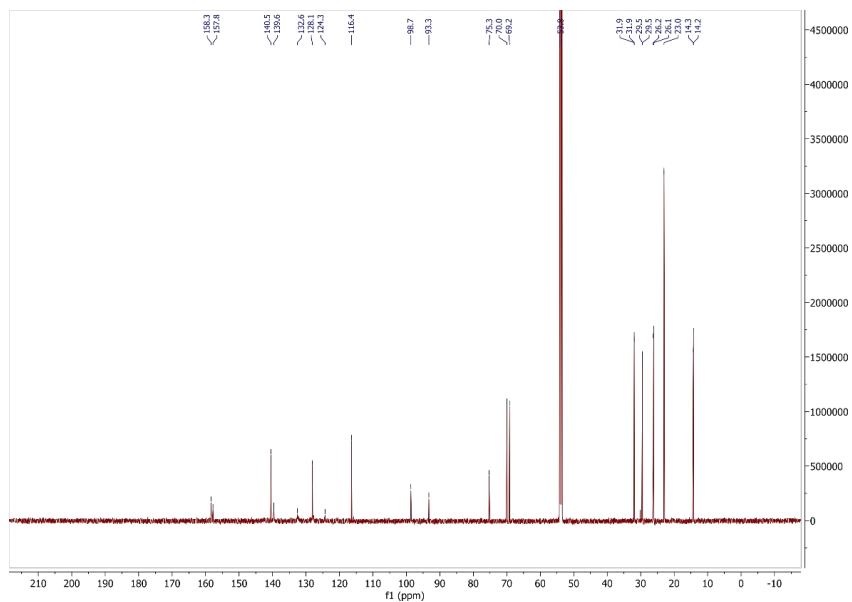
Figure S24 ^{13}C NMR (150 MHz, CD$_2$Cl$_2$) of compound **10-by**.
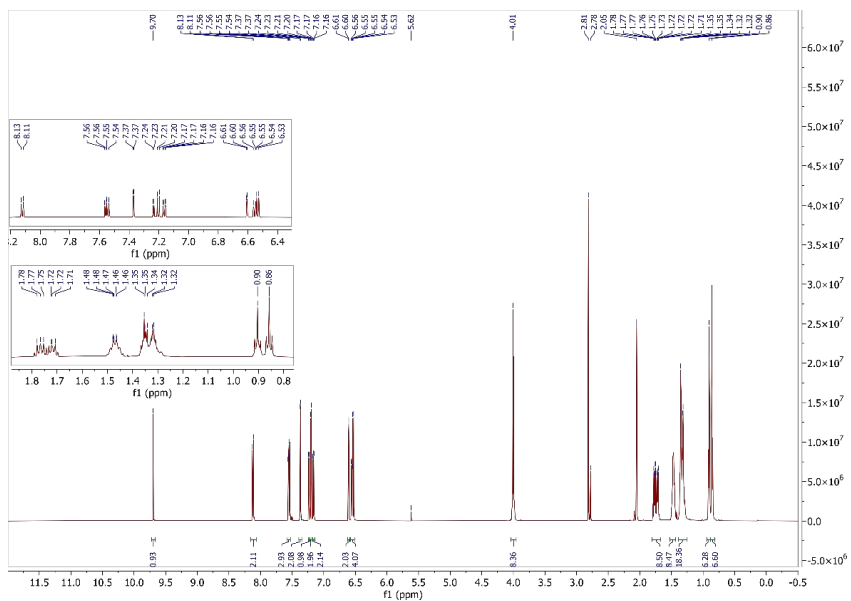
Figure S25 ^{1}H NMR (600 MHz, acetone-d_6) of compound **11**.
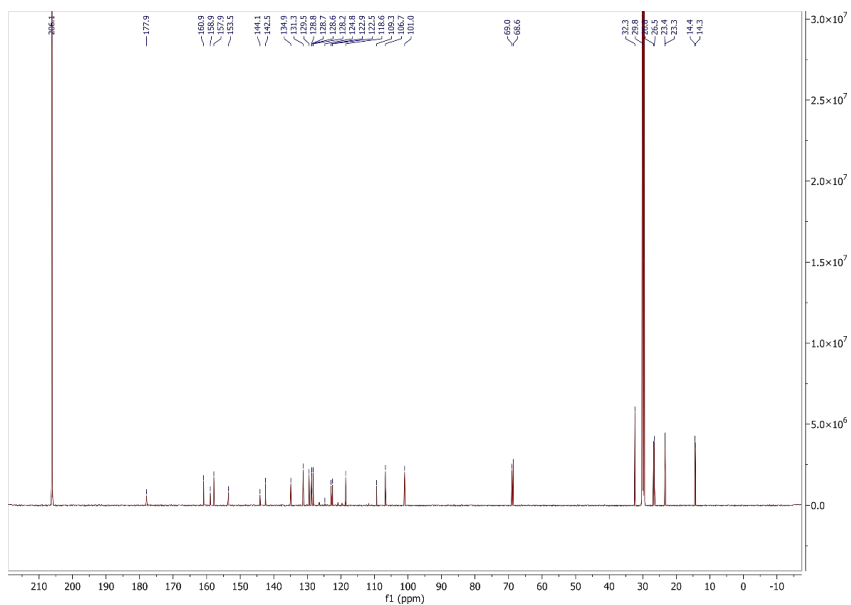
Figure S26 ^{13}C NMR (150 MHz, acetone-d_6) of compound **11**.
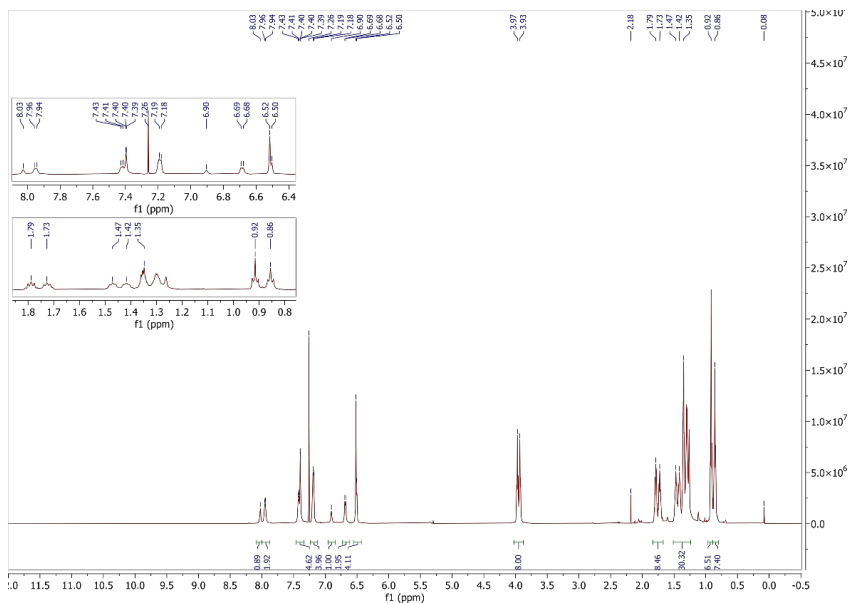
Figure S27 ^{1}H NMR (600 MHz, CDCl$_3$) of dye **10H-PTZ-Fu**.
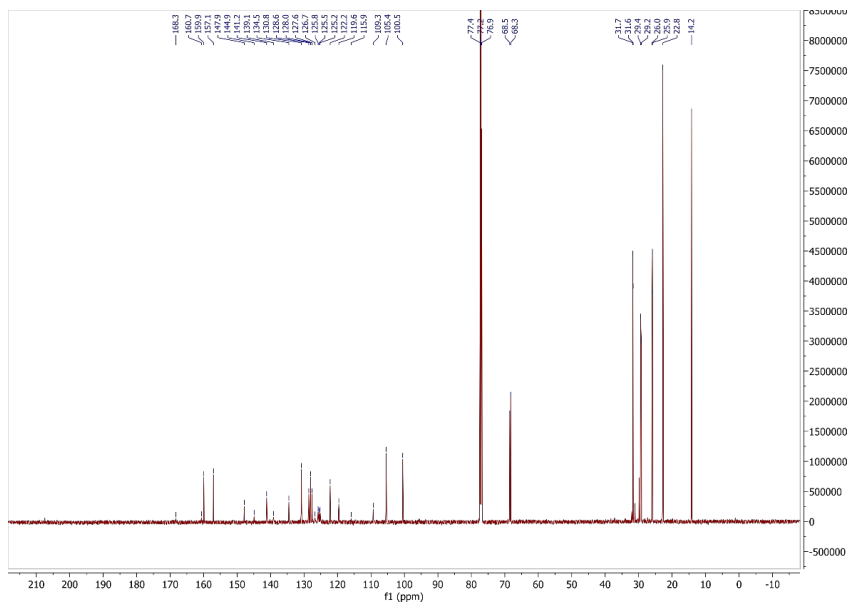
Figure S28 ^{13}C NMR (150 MHz, CDCl$_3$) of dye **10H-PTZ-Fu**.
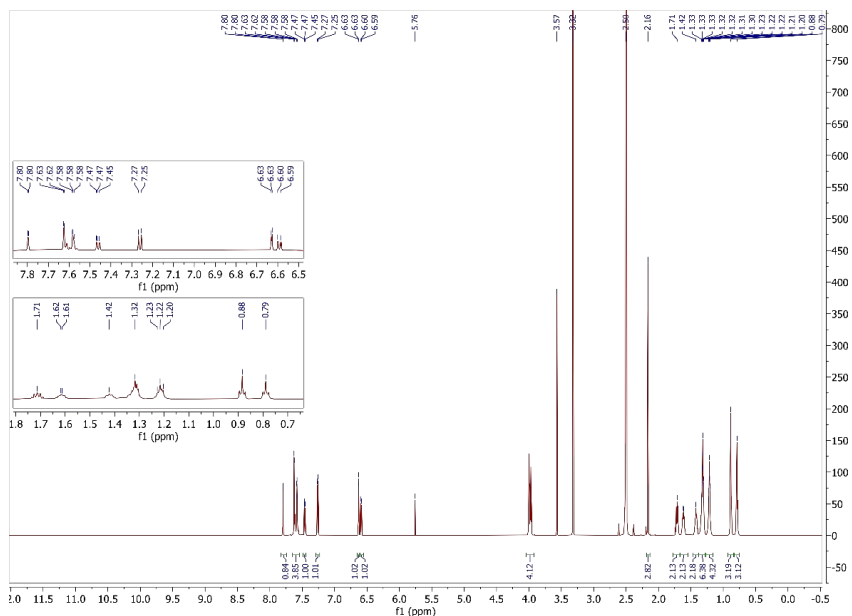
Figure S29 ¹H NMR (600 MHz, DMSO-d_6) of compound **12**.
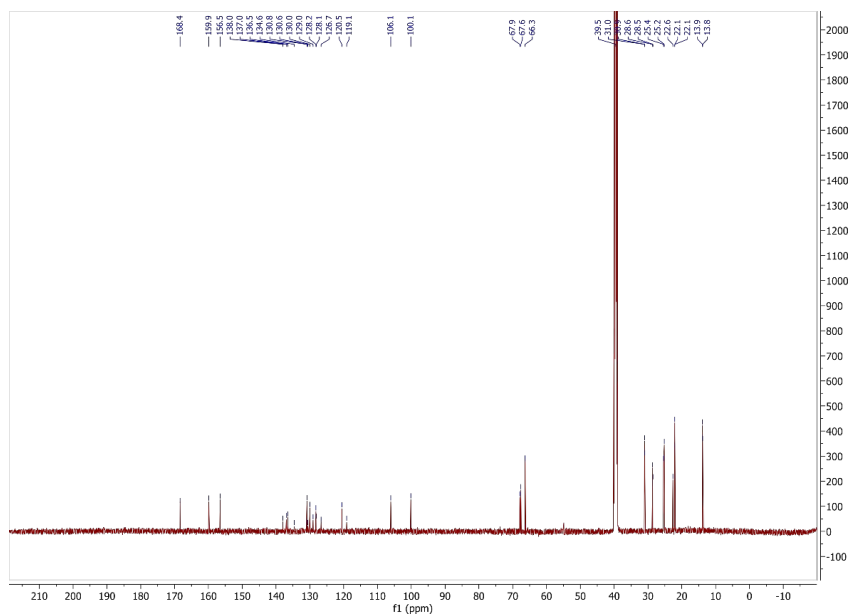
Figure S30 ¹³C NMR (150 MHz, DMSO-d_6) of compound **12**.
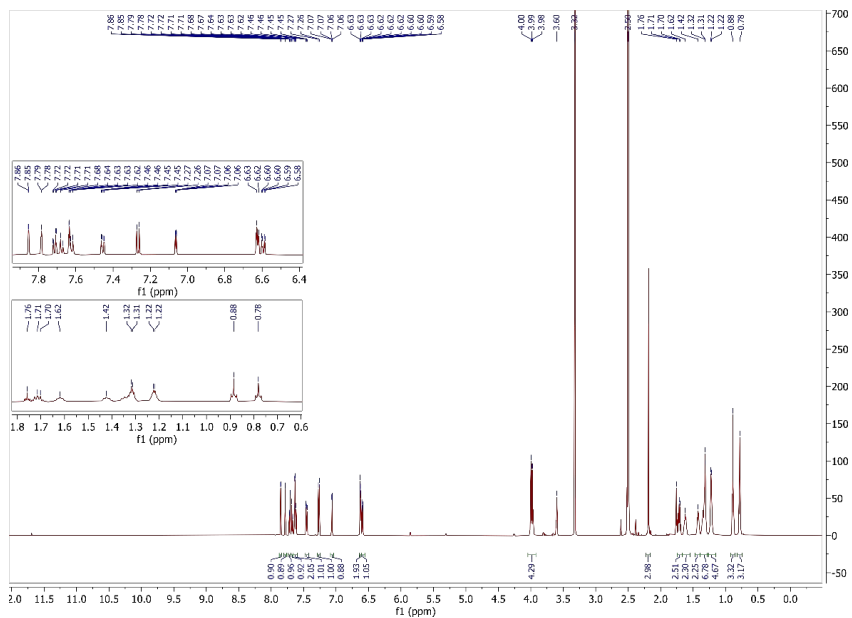
Figure S31 ^{1}H NMR (600 MHz, DMSO-d_6) of compound **13**.
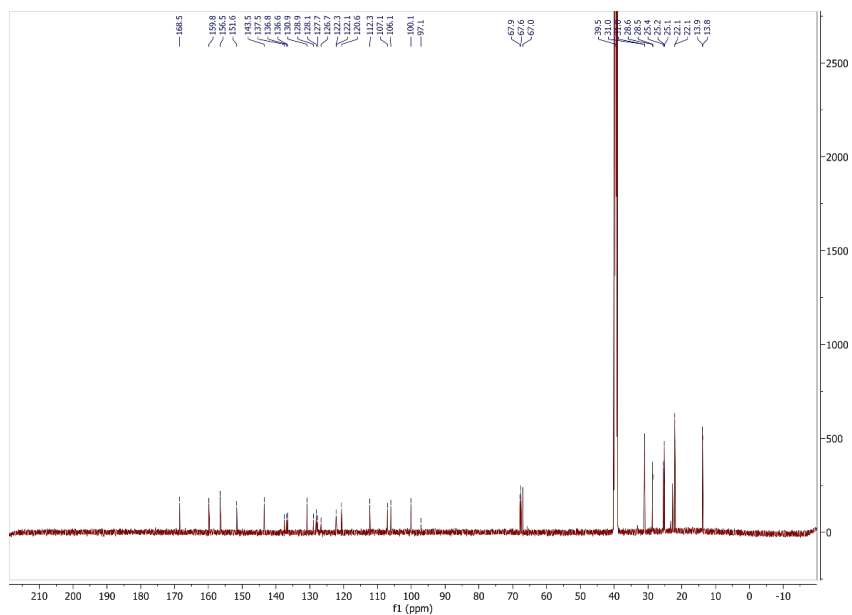
Figure S32 ^{13}C NMR (150 MHz, DMSO-d_6) of compound **13**.
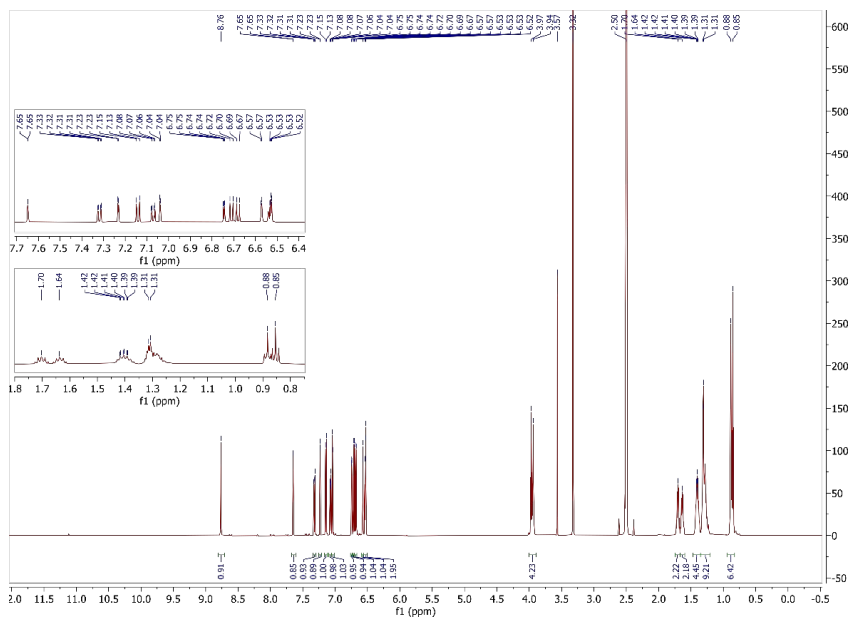
Figure S33 ^{1}H NMR (600 MHz, DMSO-d_6) of compound **14**.
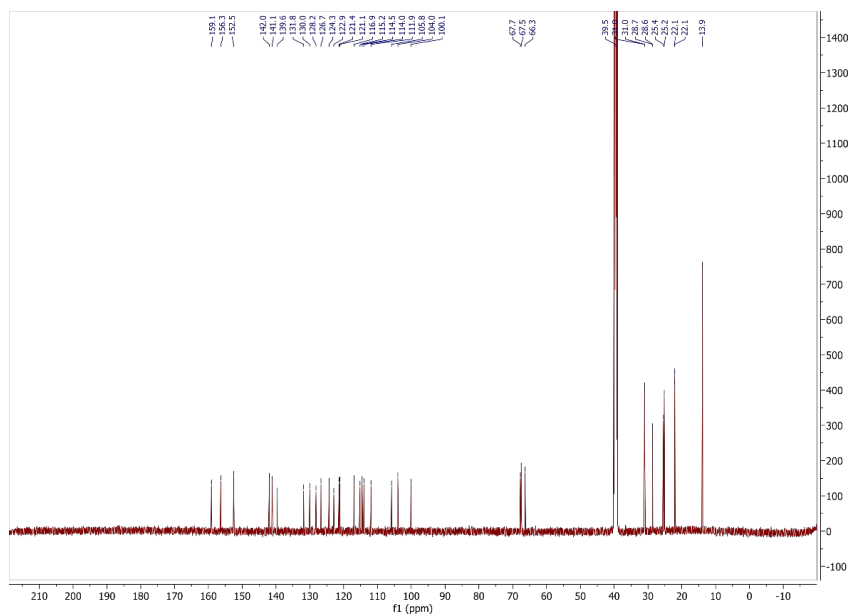
Figure S34 ^{13}C NMR (150 MHz, DMSO-d_6) of compound **14**.
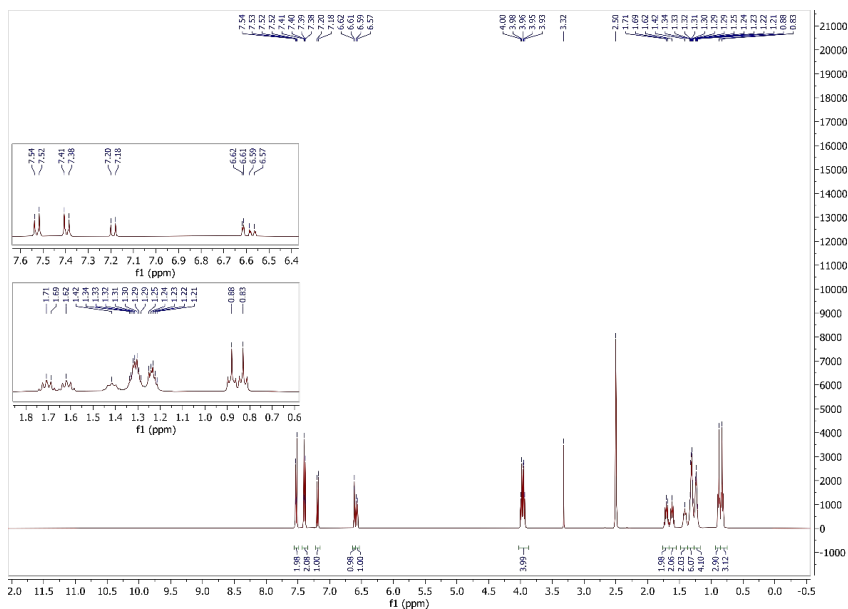
Figure S35 ^{1}H NMR (600 MHz, DMSO-d_6) of compound **16**.
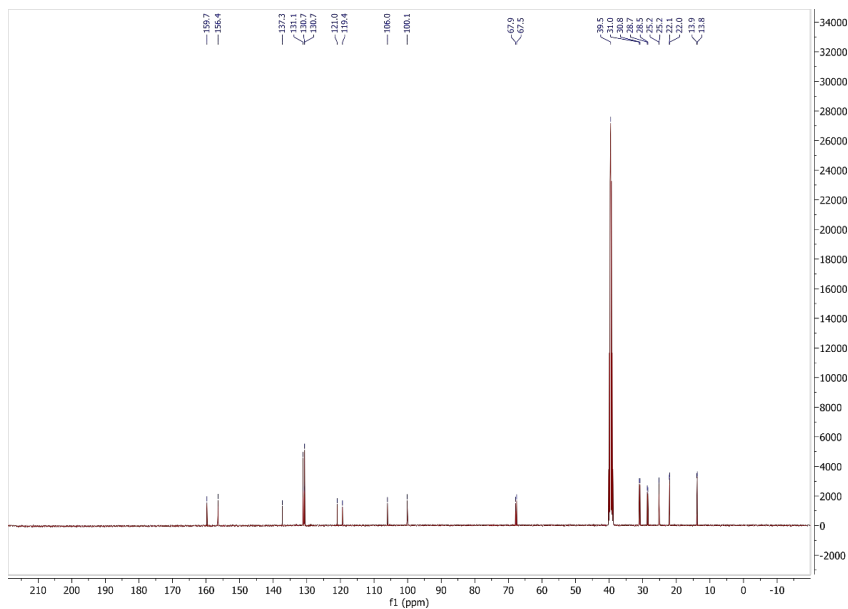
Figure S36 ^{13}C NMR (150 MHz, DMSO-d_6) of compound **16**.

Figure S37 ^{1}H NMR (600 MHz, DMSO-d_6) of compound **17**.

Figure S38 ^{13}C NMR (150 MHz, DMSO-d_6) of compound **17**.

Figure S39 ^{1}H NMR (600 MHz, CD$_2$Cl$_2$) of compound **18**.

Figure S40 ^{13}C NMR (150 MHz, CD$_2$Cl$_2$) of compound **18**.
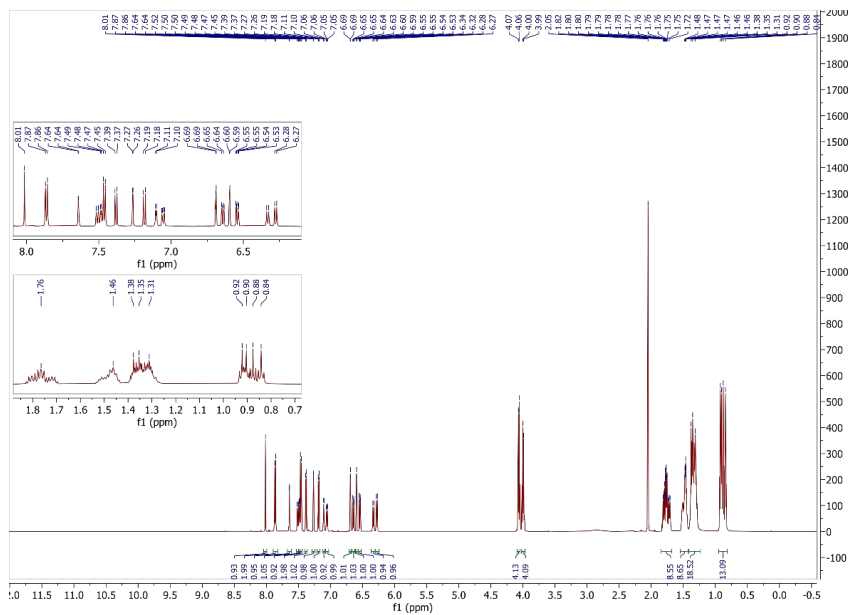
Figure S41 ^{1}H NMR (600 MHz, acetone-d_6) of dye **3,7-PTZ-Fu**.
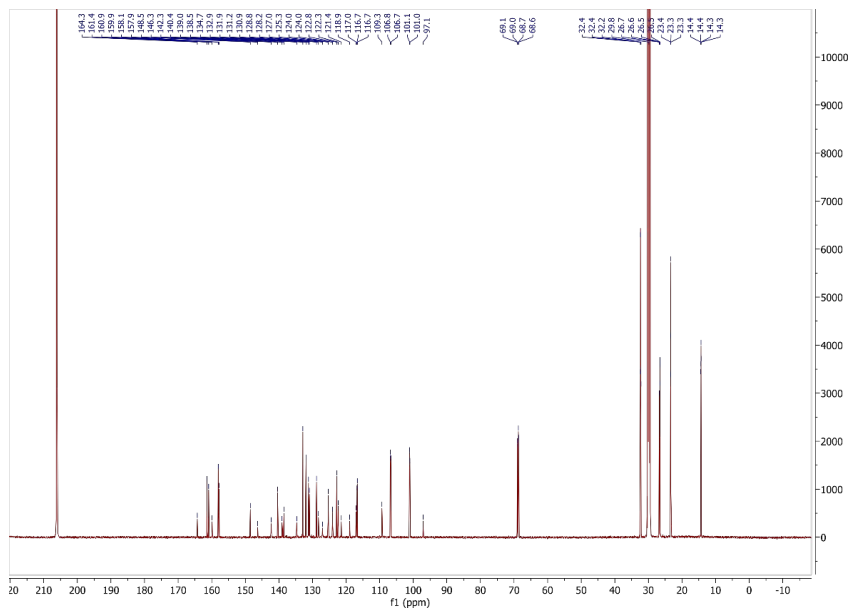
Figure S42 ^{13}C NMR (150 MHz, acetone-d_6) of dye **3,7-PTZ-Fu**.
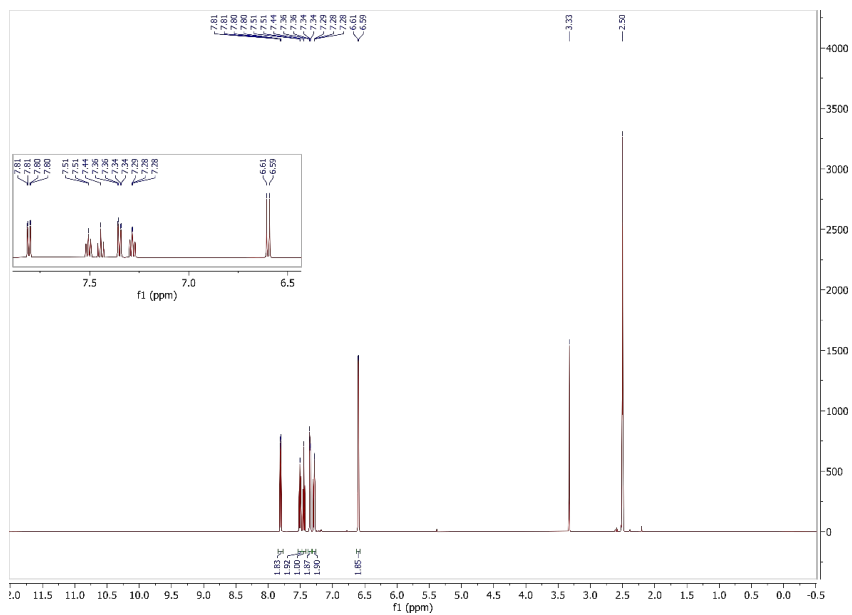
Figure S43 ¹H NMR (600 MHz, DMSO-d_6) of compound **21**.
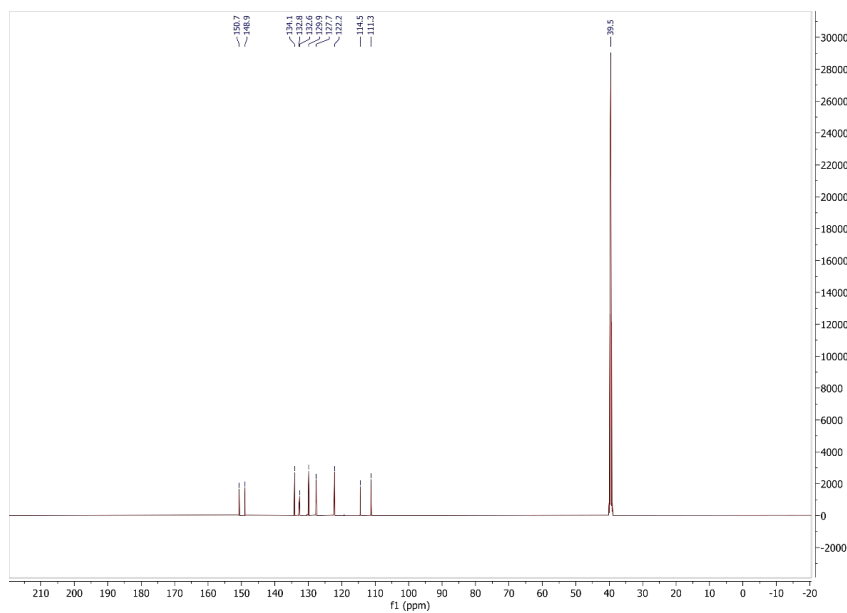
Figure S44 ¹³C NMR (150 MHz, DMSO-d_6) of compound **21**.
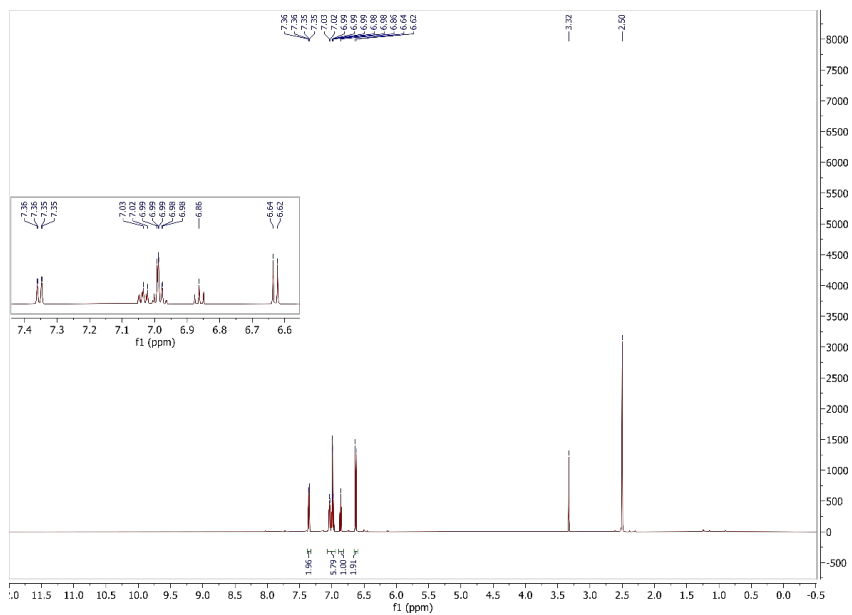
Figure S45 ^{1}H NMR (600 MHz, DMSO-d_6) of compound **23**.
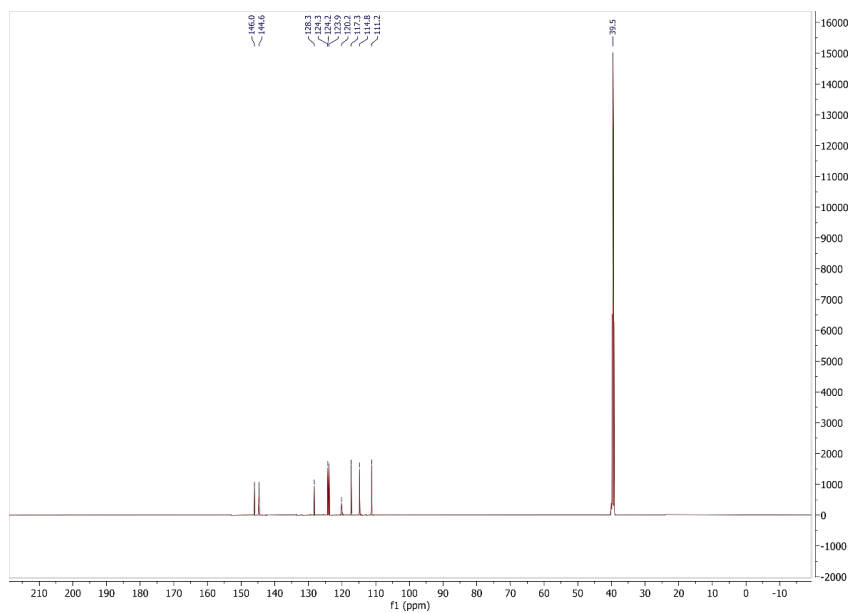
Figure S46 ^{13}C NMR (150 MHz, DMSO-d_6) of compound **23**.
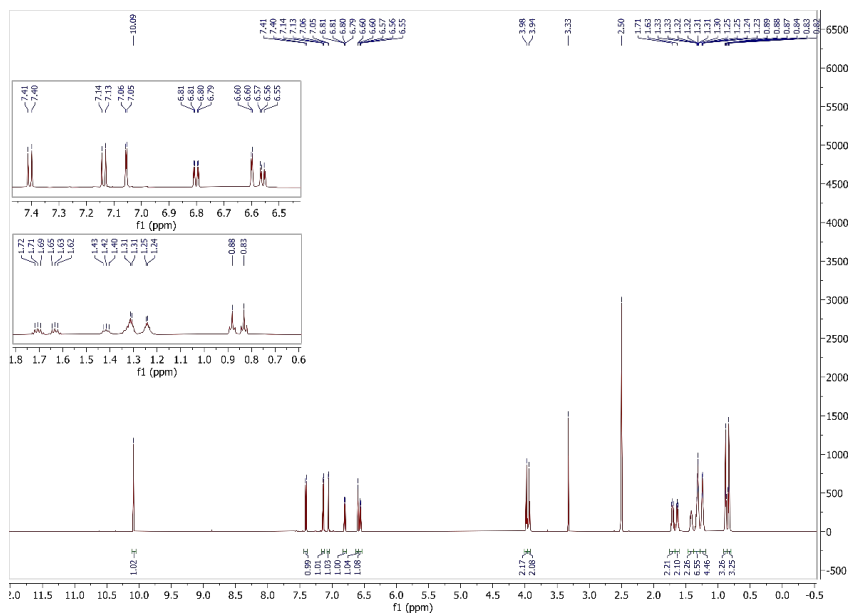
Figure S47 ¹H NMR (600 MHz, DMSO-d_6) of compound **26**.
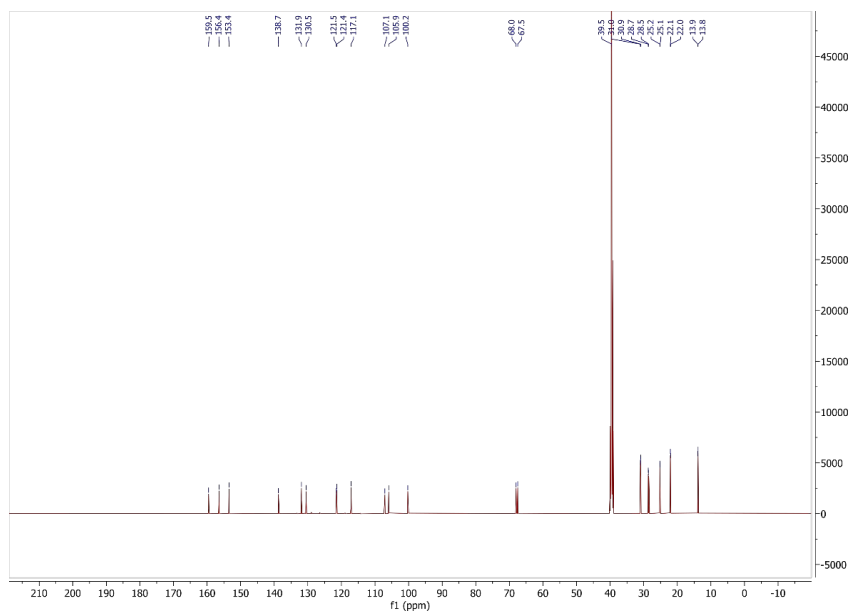
Figure S48 ¹³C NMR (150 MHz, DMSO-d_6) of compound **26**.
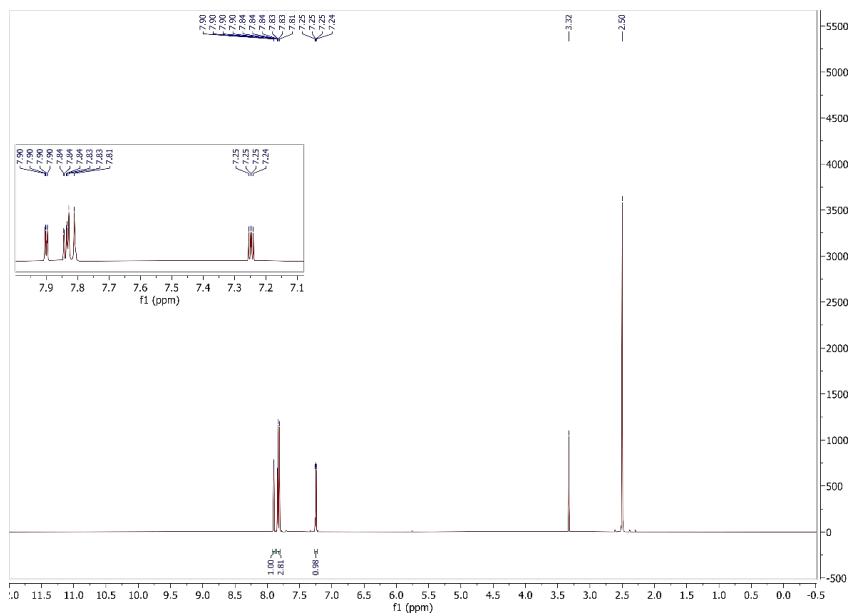
Figure S49 ^{1}H NMR (600 MHz, DMSO-d_6) of compound **28**.
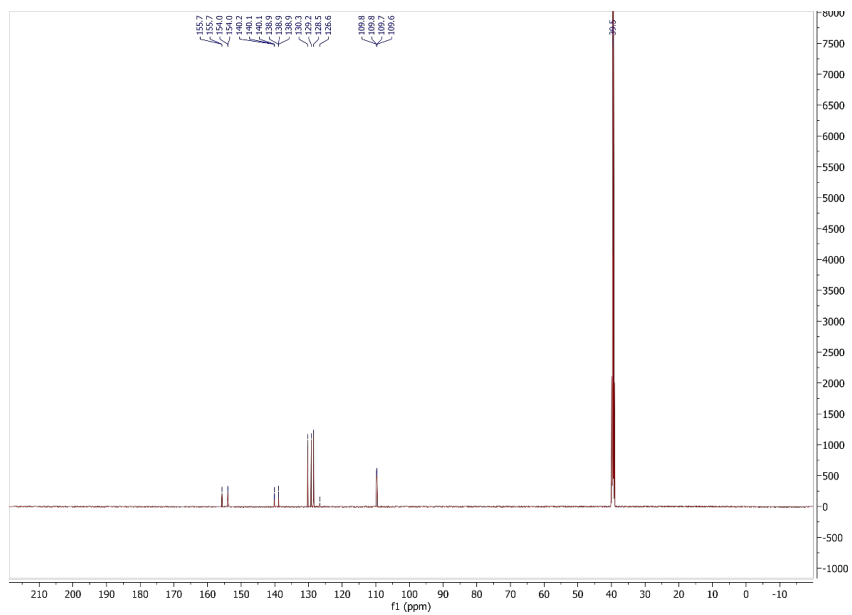
Figure S50 ^{13}C NMR (150 MHz, DMSO-d_6) of compound **28**.

Figure S51 ^{1}H NMR (600 MHz, DMSO-d_6) of compound **29**.

Figure S52 ^{13}C NMR (150 MHz, DMSO-d_6) of compound **29**.

Figure S53 ^{1}H NMR (600 MHz, CD$_2$Cl$_2$) of compound **31**.

Figure S54 ^{13}C NMR (150 MHz, CD$_2$Cl$_2$) of compound **31**.

Figure S55 ^{1}H NMR (600 MHz, CD$_2$Cl$_2$) of compound **32**.
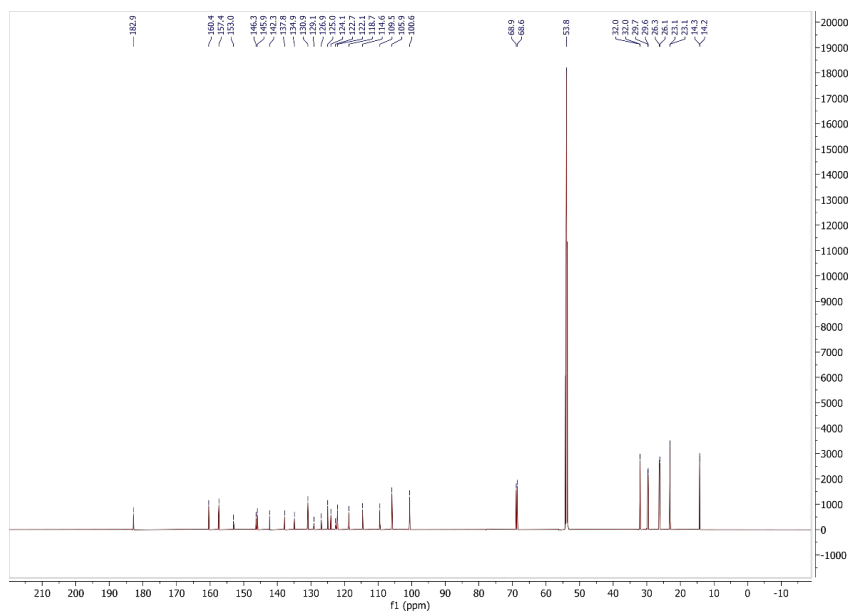
Figure S56 ^{13}C NMR (150 MHz, CD$_2$Cl$_2$) of compound **32**.

Figure S57 ^{1}H NMR (600 MHz, DMSO-d_6) of compound **POZPOZ-Th**.

Figure S58 ^{13}C NMR (150 MHz, DMSO-d_6) of compound **POZPOZ-Th**.

Paper IV

A. F. Buene, D. M. Almenningen, A. Hagfeldt, O. R. Gautun and B. H. Hoff

First Report of Chenodeoxycholic Acid–Substituted Dyes Improving the Dye Monolayer Quality in Dye-Sensitized Solar Cells,

Paper IV

Paper IV

First Report of Chenodeoxycholic Acid–Substituted Dyes Improving the Dye Monolayer Quality in Dye-Sensitized Solar Cells

Audun F. Buene, David M. Almenningen, Anders Hagfeldt, Odd R. Gautun, and Bård H. Hoff*

Chenodeoxycholic acid (CDCA) is the most used antiaggregation additive in dye-sensitized solar cells since its introduction to the field in 1993. However, effective suppression of dye aggregation comes at the cost of reduced dye loading, a lower open-circuit voltage, and limited control of dye/additive distribution when cosensitizing with free CDCA. To combat this, herein, a novel dye design concept that uses the covalent attachment of a CDCA moiety to triarylamine sensitizers is reported. The CDCA substituents do not affect the photophysical or electrochemical properties of the sensitizers but have a positive effect on the photovoltaic performance with $[Cu^{+/2+}(tmby)_2](TFSI)_{1/2}$ electrolyte (tmby = 4,4′,6,6′-tetramethyl-2,2′-bipyridine, TFSI = bis(trifluoromethanesulfonyl)imide). By ensuring a one-to-one ratio of dye and CDCA, paired with isotropic distributions of each component, this approach results in a higher-quality dye monolayer. Compared with the reference system, the novel approach reported herein gives a higher open-circuit voltage and power conversion efficiency (PCE). The best device is fabricated with the dye C_6–CDCA, delivering a PCE of 6.84% (8 μm TiO_2, 1 mM CDCA, $J_{SC} = 8.64$ mA cm^{-2}, $V_{OC} = 1007$ mV, and FF = 0.77).

1. Introduction

Dye-sensitized solar cells (DSSCs) is a photovoltaic technology based on sensitized mesoscopic nanoparticles of a wide-bandgap semiconductor such as TiO_2.[1,2] Coupled with a counter electrode and an electrolyte, the complete photoelectrochemical cell

Dr. A. F. Buene, D. M. Almenningen, Prof. O. R. Gautun, Prof. B. H. Hoff
Department of Chemistry
Norwegian University of Science and Technology
Høgskoleringen 5, NO-7491 Trondheim, Norway
E-mail: bard.h.hoff@ntnu.no

Prof. A. Hagfeldt
Laboratory of Photomolecular Science
Institute of Chemical Sciences and Engineering
École Polytechnique Fédérale de Lausanne (EPFL)
Chemin des Alambics, Station 6, CH-1015 Lausanne, Switzerland

The ORCID identification number(s) for the author(s) of this article can be found under https://doi.org/10.1002/solr.201900569.

is remarkably efficient compared with other long-established technologies such as GaAs solar cells, particularly under low-light conditions.[3] Flexible, semitransparent, and aesthetically decorative devices can be manufactured from low-cost materials.[4] As the most important components within DSSCs, the dyes themselves are currently the subject of extensive development and optimization.[5,6] Improvements in device architecture or electrolyte composition often spark the development of new dyes, which are more compatible with the new components.[7,8] Improving the efficiency of DSSCs through dye development is largely focused on enhancing the overall absorption properties, and increasing the size of the conjugated system is a popular method of achieving this. There is a drawback to the extensive conjugation, namely undesirable π–π interactions. Intermolecular aggregation between dye molecules will increase charge recombination and can be detrimental to device performance.[9]

A common strategy for reducing aggregation for both metal-complex dyes and organic sensitizers is the use of alkyl or alkoxy chains, present in just about all of the highest-performing sensitizers.[8,10–15] One of the more exciting examples of a novel antiaggregation unit was the use of a glucose derivative attached by click chemistry to a dianchoring phenothiazine sensitizer, reported by Manfredi et al. and demonstrated for dye-sensitized photocatalytic hydrogen production.[16]

Another antiaggregation approach was presented as early as 1993, by Kay and Grätzel.[17] Bile acids are compounds based on a steroid scaffold with one to three hydroxyl groups, in addition to a flexible chain with a carboxylic acid. Consequently, they are amphiphilic and chiral compounds. In biology they are well known to facilitate fat absorption; they are signaling molecules, affecting both nuclear and membrane receptors,[18] and are useful in various applications due to their tendency to form micelles.[19] Originally, bile acids were intended as additives for staining solutions, suppressing the formation of dye aggregates. These additives, such as chenodeoxycholic acid (CDCA), were later also found to anchor on the TiO_2 surface. By suppressing unfavorable dye–dye interactions, CDCA has become the most widely used additive in DSSCs.

For steric reasons, cosensitization with CDCA leads to a reduction in dye loading. Furthermore, the additional carboxylic acids in the staining solution increase the degree of protonation of TiO_2. The expected effect is a lowering of the conduction band edge of titania, which in most cases leads to a reduction in V_{OC}. Maximizing the positive effects of CDCA is a careful balancing act in most scenarios, and the only real measure available to the researcher is to vary the concentration of CDCA. It was early established that quite large CDCA concentrations were necessary to compete with dye molecules for adsorption onto the TiO_2 surface.[17] The exact ratio of dye to additive will vary between dyes and solvent systems, but additive concentrations 10–100 times higher than those of the dye are frequently reported in the literature.[20–23] Screening a range of CDCA concentrations is a common strategy. Despite optimizing the amount of coadsorbent, the researcher still has little control over the distribution of dye and additive with the conventional approach, as shown in **Figure 1**.

Herein we report the first examples of sensitizers with chenodeoxycholic substituents. The dyes differ by the length of the alkoxy chains on the donor moiety (C_3H_7 vs C_6H_{13}), which

is likely to affect the antiaggregation properties of dyes. With this approach, we improve the distribution of CDCA moieties, achieving a higher-quality self-assembled monolayer (SAM). Simultaneously, this reduces the total number of carboxylate anchoring groups on TiO_2, increasing V_{OC}. Two control sensitizers without CDCA substituents, but otherwise identical, were also prepared for the effects of the CDCA substituents to be measured. The choice of triarylamine as dye scaffold enables the use of novel copper electrolytes in the DSSC devices. With copper electrolytes, the energy loss in dye regeneration is significantly reduced compared with conventional I^-/I_3^- electrolytes.[24,25] The thiophene–furan π-spacer has recently been successfully used in a number of DSSC studies.[26–30] More importantly, this π-spacer proved suitable as a point of attachment for the very large CDCA substituent without inducing excessive ring twisting and was therefore selected for this study. In addition, this point of attachment places the CDCA substituent in a position comparable with that of free CDCA when anchored on the TiO_2 surface.
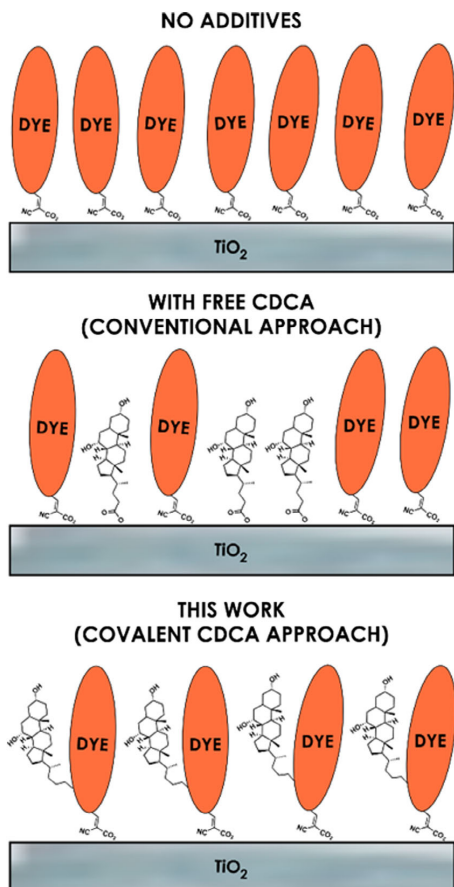
2. Results and Discussion

The aim for this work was to improve the SAM quality by the covalent attachment of CDCA to the dye structure. This design was chosen to improve the distribution of dyes and additives in the SAM and reduce the total number of molecules anchored on the TiO_2 surface, with the intention of achieving an overall higher power conversion efficiency (PCE) and increased V_{OC}. Recently, triarylamine-based sensitizers have achieved outstanding results in DSSCs, using novel cobalt and copper electrolytes.[8,24,31–35] Hence, this popular dye class became the foundation of the study.

It was also essential that the large CDCA substituent did not induce any ring twisting of the conjugated system, which could negatively affect the optical properties of the sensitizers. To minimize any potential ring twisting, the CDCA substituent was attached in the bay region between two five-membered heterocycles.

2.1. Dye Synthesis

2.1.1. Donor Moiety

The complexity of the target sensitizers meant the preparation resembled more of a total synthesis than the synthesis of a simple dye. The preparation of the donor fragments however was relatively uncomplicated, as shown in **Scheme 1**. Synthesis routes based on those reported by Gabrielsson et al. and Zhang et al. were used to prepare the triarylamine donor fragments.[10,36] While (2,4-dipropoxyphenyl)boronic acid was commercially available, 2-(2,4-bis(hexyloxy)phenyl)-pinacol boronic ester had to be prepared in-house, using the convenient palladium-catalyzed borylation reaction developed by Billingsley and Buchwald.[37] The crude pinacol boronic ester was used without further purification to yield triarylamine **3**. The last bromination step by N-bromosuccinimide (NBS) proved regiospecific with high yields of the advanced intermediates **4** and **5**.

Figure 1. Dye and additive distribution concepts.
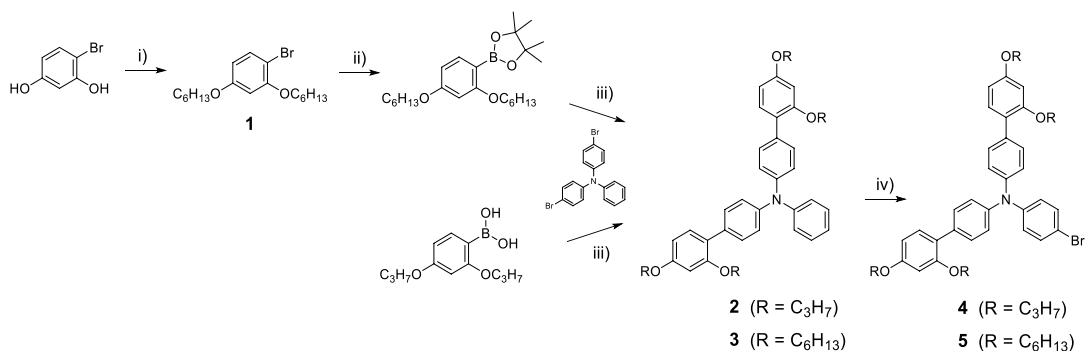
Scheme 1. Synthesis route of triphenylamine donor fragments. i) KOH, DMSO, 1-bromohexane, r.t., ii) HBpin, PdCl$_2$(CH$_3$CN)$_2$, SPhos, Et$_3$N/1,4-dioxane, 110 °C, iii) Pd(OAc)$_2$, SPhos, K$_2$CO$_3$, H$_2$O/1,4-dioxane, iv) NBS, CH$_2$Cl$_2$, r.t.

2.1.2. π-Spacer Moiety

Our strategy to arrive at the CDCA-functionalized π-spacer involved several different reactions, from old textbook chemistry to more modern coupling reactions (see **Scheme 2**). First, CDCA was converted to its methyl ester **6**, in a Fischer esterification. Second, the hydroxyl groups of **6** were protected as *tert*-butyldimethylsilane ethers (TBDMS), and compound **7** was further reduced by LiAlH$_4$ in tetrahydrofuran (THF) to yield the primary alcohol **8**. To install the CDCA moiety onto the π-spacer, a Williamson ether synthesis between compound **8** and 2-bromo-3-(bromomethyl)thiophene based on the procedure reported by Bjørnholm et al. was performed.[38] Subsequently, the removal of the TBDMS protected groups by HCl gave compound **9**. The first four steps were all quantitative in terms of yields (97–99%). The introduction of the furan moiety proved to be a challenging step, but a Suzuki coupling catalyzed by [1,1′-bis(diphenylphosphino)ferrocene]dichloropalladium(II) (PdCl2(dppf)) using three equivalents of (5-formylfuran-2-yl)boronic acid was eventually

developed, giving compound **10** in a satisfactory yield of 68%. The final step in the synthesis of the CDCA π-spacer building block **11** was bromination by NBS. Despite the low yield of 25% due to a challenging purification, enough material was prepared for the target sensitizers to be synthesized in sufficient amounts.

Preparation of the π-spacer without the CDCA substituent required two steps. First, a Suzuki coupling between 2-bromothiophene and 5-formylfuran-2-yl boronic acid gave compound **12** in 48% yield, confirming it was not the steric bulk of the CDCA substituent that caused the low yield in the same reaction to compound **10**. Finally, a bromination by NBS in 59% yield completed the reference π-spacer building block **13**.

2.1.3. Dye Assembly

The triarylamine donor fragments **4** and **5** were converted to boronic esters again by the procedure of Billingsley and Buchwald.[37] They were then coupled to the π-spacer building
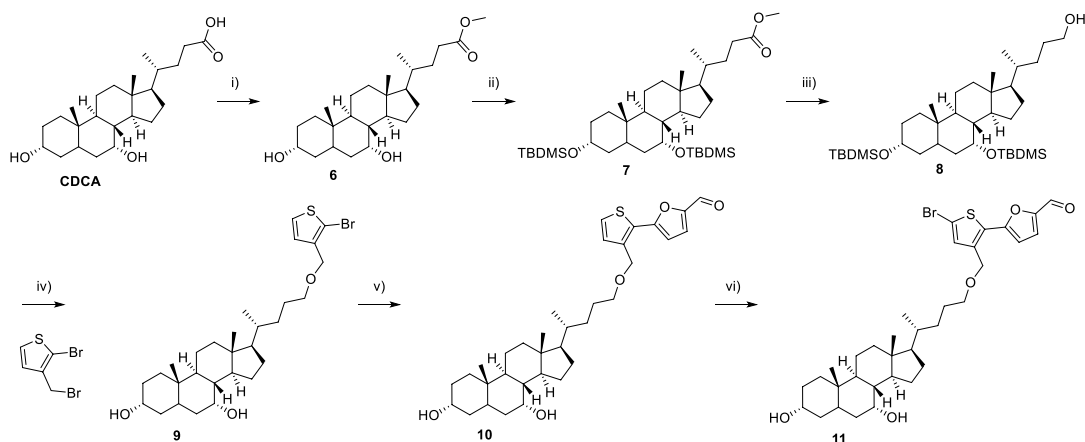
Scheme 2. Synthesis route for CDCA-functionalized π-spacer **11**. i) MeOH, H$_2$SO$_4$, r.t., ii) TBDMS triflate, 2,6-lutidine, DCM, r.t., iii) LiAlH$_4$, THF, r.t., iv) NaH, THF, 60 °C followed by deprotection by HCl, v) (5-formylfuran−2-yl)boronic acid, PdCl$_2$(dppf), K$_2$CO$_3$, H$_2$O/1,4-dioxane, 80 °C, vi) NBS, CHCl$_3$/AcOH, 0 °C.
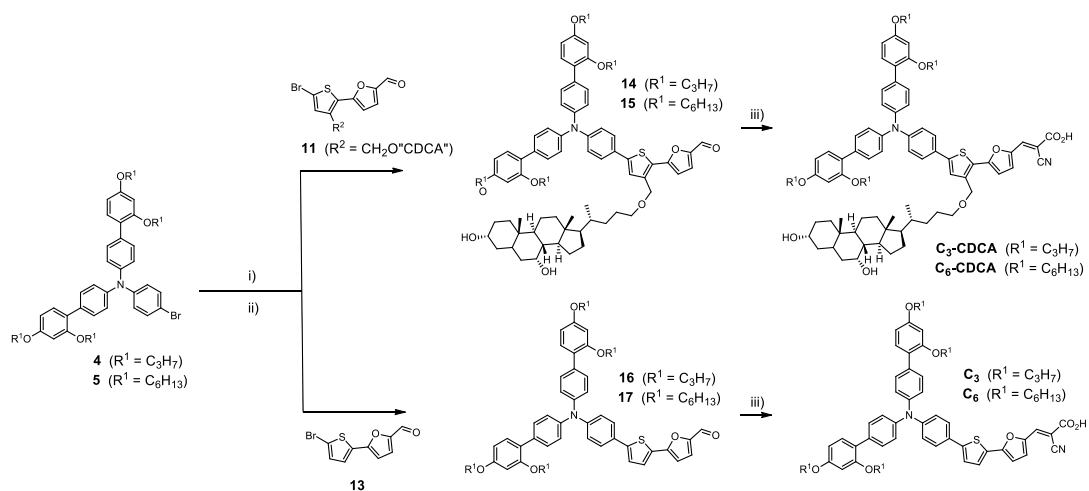
Scheme 3. Fusion of triphenylamine donors **4** and **5** with the CDCA-functionalized π-spacer **11** and reference π-spacer **13**. i) HBpin, PdCl$_2$(CH$_3$CN)$_2$, SPhos, Et$_3$N/1,4-dioxane, 110 °C, ii) Pd(OAc)$_2$, SPhos, 1,4-dioxane/H$_2$O, 80 °C, iii) cyanoacetic acid, piperidine, ACN/THF, 65 °C.

blocks **11** and **13**, giving the carboxaldehydes **14–17**, as shown in **Scheme 3**. The Knoevenagel condensation installed the cyanoacrylic acid anchoring group in yields from 54% to 95%, successfully concluding the synthesis of the first two sensitizers bearing CDCA substituents and their two corresponding reference dyes.

2.2. Photophysical Properties

One aim with the design of the sensitizers is that the CDCA substituent does not negatively affect their photophysical and electrochemical properties. The CDCA moiety should simply be an inert substituent, affecting only the aggregation properties of the dyes. The UV–vis spectra shown in **Figure 2** show only minor differences in absorption between the four sensitizers. The reference dyes C$_3$ and C$_6$ have slightly higher molar extinction coefficients, and the internal charge transfer (ICT) transition
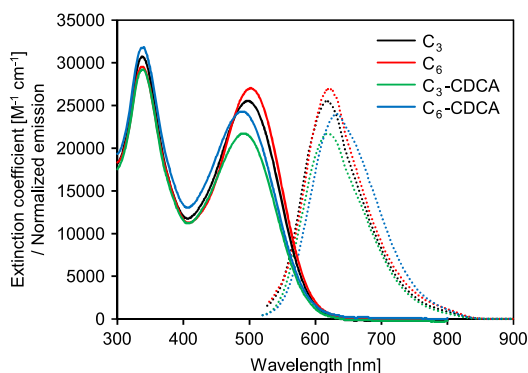
Figure 2. UV–vis measurements and normalized emission spectra of all dyes in dichloromethane solution.

peaks are redshifted by about 10 nm. These changes can simply be explained by the large CDCA substituent introducing a slight ring twist between the thiophene and furan rings. Of the four dyes, the two with C$_6$ chains have 6–12% higher molar extinction coefficients compared with the C$_3$ analogs. Although the reason for this is unknown, the phenomenon of higher molar extinction coefficients for longer alkyl chains has been previously observed for triarylamine,[39] phenothiazine,[40] and ruthenium complex dyes.[41]

When anchored on TiO$_2$ without additional coadsorbents (Figure S1, Supporting Information), the ICT transition peaks of the reference sensitizers are blueshifted by 53–59 nm, indicating they could be prone to H aggregation.[9] Sensitizers C$_3$–CDCA and C$_6$–CDCA are also affected but by a reduced margin of 35–44 nm. This suggests that the CDCA substituents prevent aggregation to a certain extent and that additional CDCA added to the staining solution may be required when fabricating devices. The free OH groups of the tethered CDCA substituent may well interact with the semiconductor surface, due to the flexibility of the linker, but the extent and effect of this has not been investigated.

Optical bandgaps extracted from the intersections of the absorption and emission curves in Figure 2 are in the range of 2.18–2.20 eV for all four sensitizers, further indicating that CDCA substituents do not significantly affect the photophysical properties. Integration of the 1 sun AM1.5 G solar spectrum gives the maximum short-circuit current obtainable from a sensitizer with a specific absorption onset or bandgap. For the sensitizers in this work, with a bandgap around 2.20 eV, a maximum J_{SC} value of 10.4 mA cm^{-2} is expected. All the measured photophysical and electrochemical properties are shown in **Table 1**.

2.3. Electrochemical Properties

The four dyes adsorbed onto TiO$_2$ films were investigated by cyclic voltammetry (CV) to determine the oxidation potentials.

Table 1. Photophysical properties of the triarylamine dyes C_3, C_6, C_3–CDCA, and C_6–CDCA.

Dye	λ_{abs}[a] [nm]	ε [M^{-1} cm^{-1}]	Em.[b] [nm]	λ_c[c] on TiO$_2$ [nm]	Rel. ε on TiO$_2$	E_{0-0}[d] [eV]	E_{ox}[e] [V vs SHE]	E_{LUMO}[f] [V]
C_3	498	25 500	617	442	1.43	2.20	1.09	−1.11
C_6	502	27 000	621	445	1.29	2.19	1.12	−1.07
C_3–CDCA	492	21 700	619	448	1.00	2.20	1.11	−1.09
C_6–CDCA	489	24 300	632	451	1.01	2.18	1.11	−1.07

[a]Maximum of most redshifted peak; [b]Emission when ICT band is excited, in DCM solution; [c]Maximum of most redshifted peak on TiO$_2$ (2.5 μm, GreatcellSolar 18NR-T); [d]Calculated from the intersection of the absorption and normalized emission spectra; [e]Measured versus Fc$^+$/Fc on stained TiO$_2$ electrodes in acetonitrile with 0.1 M LiTFSI, converted to V versus SHE by 0.624. Scan rate 20 mV s^{-1}; [f]Calculated from $E_{ox}-E_{0-0}$.

The 2.5 μm thick films were prepared by 30NR-D TiO$_2$ screen printed on FTO glass. The stained photoanodes were attached to the working electrode of the potentiostat, with a carbon graphite rod used as a counter electrode. The reference electrode was Ag/AgCl and the supporting electrolyte was 0.1 M lithium bis(trifluoromethanesulfonyl)imide (LiTFSI) in dry acetonitrile. Cyclic voltammograms are shown in **Figure 3**, and the extracted electrochemical information is found in Table 1. All the dyes display a single reversible oxidation and very similar electrochemical behavior. This indicates that neither the presence of the CDCA substituent nor the length of the alkoxy chains greatly

Figure 3. CVs of the four sensitizers and ferrocene. Sensitizers measured on TiO$_2$ films (2.5 μm on FTO glass), carbon counter electrode, Ag/AgCl reference, 0.1 M LiTFSI supporting electrolyte. Ferrocene (Fc) was measured with a glassy carbon working electrode and used for calibration with a value of 0.624 V versus SHE.[42]

affects the electrochemical properties of the sensitizers. When the ferrocene standard was measured, the working electrode was replaced by a glassy carbon electrode, and the $E_{1/2}$ of ferrocene was found at 0.36 V versus Ag/AgCl. The calculated values for the oxidation potentials of the four sensitizers were all in the range of 1.09–1.12 V versus standard hydrogen electrode (SHE), suggesting that they should be compatible with the redox potential of the $[Cu^{+/2+}(tmby)_2](TFSI)_{1/2}$ electrolyte (tmby = 4,4′,6,6′-tetramethyl-2,2′-bipyridine), reported at 0.87 V versus SHE.[24] Excited state energies calculated from the E_{0-0} values and E_{ox} were found between −1.07 and −1.11 V versus SHE, suggesting that all sensitizers provide a sufficient driving force for efficient electron injection into the conduction band of TiO$_2$, commonly reported around −0.5 V versus SHE. The energy levels would also be compatible with the I$^-$/I$_3^-$ electrolyte, but this would lower the V_{OC} significantly, and we are of the opinion that the same relative effects on performance would be observed.

2.4. Photovoltaic Properties

The four sensitizers were evaluated in DSSCs alongside the structurally related reference dye D35 reported by Hagberg et al.[43] The fabrication procedure for the DSSCs is described in the Experimental Section. The complete set of photovoltaic data is reported in **Table 2**, while a selection of J–V curves is shown in **Figure 4**a,b.

First, the effect of CDCA as a coadsorbent for the reference sensitizers C_3 and C_6 was determined by testing a range of CDCA concentrations (0, 1, 5, 10, and 50 equivalents relative to the sensitizers). The results of this study are shown in **Figure 5** and in the top part of Table 2. The full set of J–V curves and the incident photon-to-current conversion efficiency (IPCE) spectra of all CDCA concentrations are included in the Supporting Information (Figure S2, Supporting Information).

Generally, C_6 outperforms C_3 in all performance characteristics in the CDCA concentration study, despite having a 19% reduction in dye loading compared with C_3 (Table S1, Supporting Information). Further, the performance of C_3 is also affected to a greater extent by the CDCA concentration than that of C_6. The most noticeable difference between the two dyes, differing only by the alkoxy chain length, is the open-circuit voltage. Without the CDCA additive, the difference in V_{OC} is 99 mV in favor of dye C_6. When including the D35 reference dye, which has butoxy
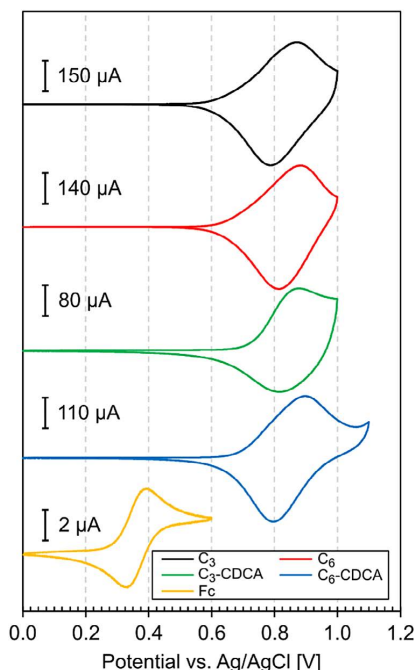
Table 2. Photovoltaic performance of all dyes in 1 sun AM 1.5 G illumination and from IPCE measurements. Electrolyte composition 0.09 M [Cu(tmby)$_2$] TFSI$_2$, 0.20 M [Cu(tmby)$_2$]TFSI, 0.1 M LiTFSI, and 0.6 M 1-methylbenzimidazole in dry acetonitrile.

Dye	CDCA [eq.]	TiO$_2$ [μm]	IPCE J_{SC} [mA cm^{-2}][a]	J_{SC} [mA cm^{-2}]	V_{OC} [mV]	Fill factor [%]	PCE [%]
C$_3$	0	4 + 2	6.31	6.53 ± 0.13	965 ± 3	0.72 ± 0.01	4.55 ± 0.12
	1	4 + 2	6.91	6.88 ± 0.43	965 ± 10	0.73 ± 0.01	4.91 ± 0.42
	5	4 + 2	7.04	7.29 ± 0.27	955 ± 14	0.72 ± 0.01	5.05 ± 0.28
	10	4 + 2	6.88	7.60 ± 0.14	962 ± 20	0.73 ± 0.02	5.37 ± 0.23
	50	4 + 2	6.32	6.88 ± 0.40	937 ± 8	0.72 ± 0.04	4.69 ± 0.50
C$_6$	0	4 + 2	7.68	7.09 ± 0.14	1064 ± 5	0.72 ± 0.01	5.48 ± 0.14
	1	4 + 2	7.96	7.27 ± 0.32	1038 ± 28	0.74 ± 0.02	5.64 ± 0.26
	5	4 + 2	6.96	7.56 ± 0.08	970 ± 21	0.73 ± 0.02	5.39 ± 0.20
	10	4 + 2	7.26	7.56 ± 0.18	1000 ± 22	0.74 ± 0.01	5.65 ± 0.14
	50	4 + 2	6.18	7.19 ± 0.09	959 ± 13	0.76 ± 0.01	5.29 ± 0.15
C$_3$–CDCA	0	4 + 2	6.49	5.55 ± 0.09	1025 ± 5	0.70 ± 0.01	4.03 ± 0.04
	0	8 + 4	6.98	6.21 ± 0.43	961 ± 11	0.74 ± 0.02	4.49 ± 0.46
	10	4 + 2	7.27	7.12 ± 0.17	1013 ± 15	0.73 ± 0.01	5.34 ± 0.24
	10	8 + 4	8.05	7.50 ± 0.39	1000 ± 2	0.76 ± 0.01	5.81 ± 0.32
C$_6$–CDCA	0	4 + 2	6.77	7.07 ± 0.08	1044 ± 3	0.72 ± 0.02	5.39 ± 0.07
	0	8 + 4	8.54	7.84 ± 0.47	1008 ± 25	0.76 ± 0.01	6.11 ± 0.44
	10	4 + 2	7.81	8.00 ± 0.09	1035 ± 15	0.74 ± 0.00	6.20 ± 0.02
	10	8 + 4	8.54	8.30 ± 0.30	992 ± 14	0.77 ± 0.02	6.44 ± 0.35
D35	0	4 + 2	7.40	7.51 ± 0.22	1016 ± 23	0.73 ± 0.00	5.60 ± 0.31

[a]Obtained by integration of the IPCE spectrum over the 1 sun AM 1.5 G spectrum.
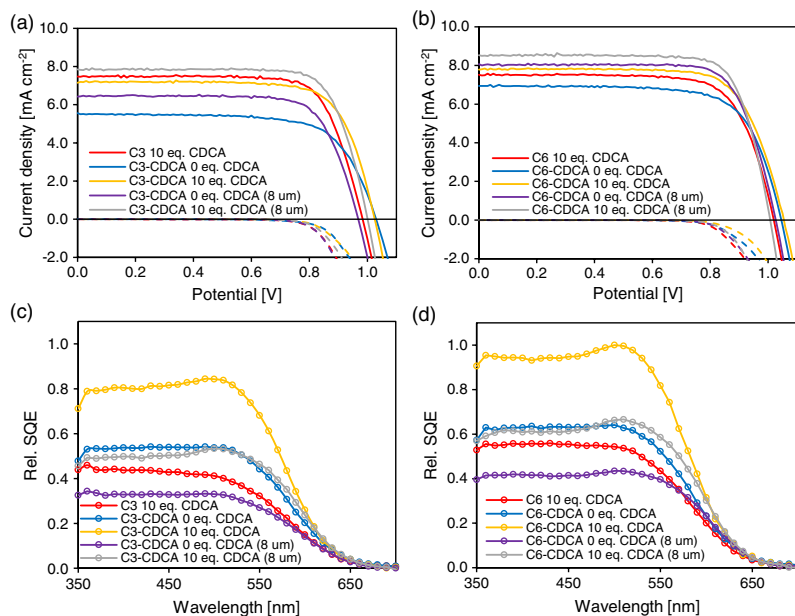
Figure 4. a,b) Current density versus applied potential plots under 1 sun AM1.5 G illumination (lines) and in the dark (dashed lines). c,d) SQE spectra, essentially dye-loading-adjusted incident photon-to-current conversion efficiency curves. Curves are scaled relative to the highest-performing device. Comment of 8 μm means 8 + 4 μm TiO$_2$ was used, whereas no specification implies 4 + 2 μm TiO$_2$ electrodes. Original IPCE measurements available in the Supporting Information.
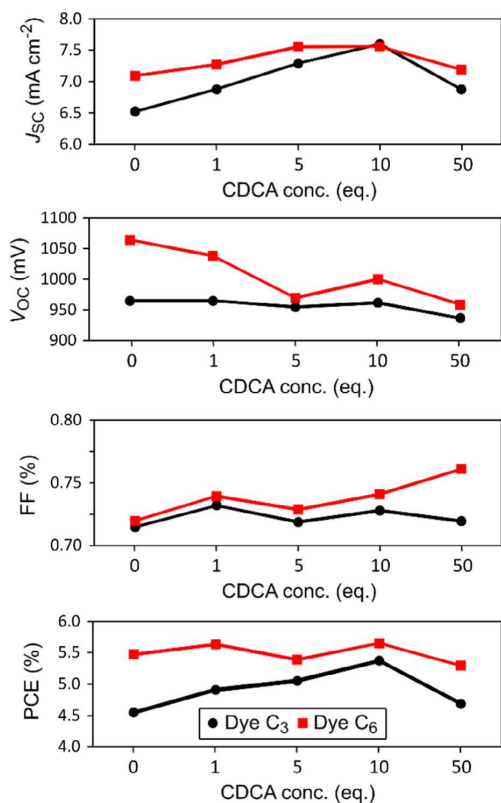
Figure 5. Screening of CDCA concentration for dyes C_3 and C_6. Each data point is the average of three devices.

chains, the following trend of V_{OC} is found: C_3 (965 mV) < C_4 (1016 mV) < C_6 (1064 mV). As the CDCA concentration is increased, the V_{OC} of both dyes decreases. This is explained by a lowered conduction band edge due to protonation of TiO_2 by the carboxylic acid of CDCA. The maximum short-circuit current density is found for 5–10 equivalents of CDCA, leading to the highest PCEs being obtained for 10 equivalents of CDCA for both chain lengths.

With the coadsorbent dependence of the reference sensitizers determined, the dyes with CDCA substituents were tested with no additional CDCA additive. Compared with the optimized C_3 and C_6 devices, the relative efficiencies were 75% and 95% for C_3–CDCA and C_6–CDCA. This is particularly notable when considering that the CDCA substituent reduces the dye loading by 39–45%. Perhaps most strikingly, the increase in V_{OC} from C_3 to C_3–CDCA was measured at 60 mV. In other studies, the use of longer alkoxy chains has produced the same V_{OC}-enhancing behavior,[44] and thus we conclude that the CDCA substituent blocks electron recombination from TiO_2 to the electrolyte and thereby improves the photovoltage. This is supported by a slight improvement in electron lifetimes (see Figure 6c). A similar behavior has previously been reported for the introduction of

an alkyl chain in the same position of a dye with a comparable structure. The LEG3 dye, with the hexyl entity attached to the π-spacer, displayed increased J_{SC}, V_{OC}, and fill factor, attributed to the reduced recombination when compared with the reference dye LEG1.[36] Following the same arguments, for the C_6 dyes, no change in V_{OC} was observed, or expected, as the longer alkoxy chains already sufficiently block the recombination.

We then tested the optimized CDCA coadsorbent concentrations (10 equivalents) with the dyes C_3–CDCA and C_6–CDCA. To our surprise, this further improved the efficiencies significantly. In the case of C_3–CDCA with 10 equivalent CDCA, a near-identical PCE as for the optimized C_3 was achieved, an improvement of 33%. For C_6–CDCA, the additional coadsorbent gave an improvement in PCE of 10%. Obviously, more than one unit of CDCA per dye molecule is required for the sensitizer to operate efficiently. Furthermore, because C_6–CDCA is more efficient than C_6 with the same amount of CDCA in the staining solution, it could indicate an improved distribution of CDCA, so a higher short-circuit current can be obtained despite lowered dye-loading values (see Table S1, Supporting Information).

Finally, for dyes C_3–CDCA and C_6–CDCA, we attempted to double the thickness of the TiO_2 layers, from $4 + 2$ to $8 + 4\,\mu m$ (see Table 2). This resulted in an increased average PCE of 9%, suggesting that the optimal thickness of active TiO_2 in this study is between 4 and 8 μm. The observed reduction in the open-circuit voltage can be explained by a more restricted diffusion for the redox shuttle in the TiO_2 network, increasing recombination and thus lowering the electron lifetime and V_{OC}. Surprisingly, the fill factors of the devices increased with thicker TiO_2 films, which is not expected under full illumination if there are diffusion issues in the devices.

The IPCE spectra in Figure S3, Supporting Information, show that light harvest is less than optimal for all devices fabricated with these sensitizers, as the maximum IPCE value is only 70%. This is a consequence of modest molar extinction coefficients, paired with thin TiO_2 layers required for the slow diffusing copper complex redox couple in the electrolyte. However, for the purpose of testing the CDCA substituents, this is of little importance. The IPCE spectra resemble the UV–vis absorption spectra, but the onset is redshifted by up to 50 nm, compared with the absorption spectra, likely an effect of different solvents in device operation and the photophysical measurements. From Table 2, the values for the integrated short-circuit current from the IPCE spectra are in good agreement with the values obtained from the J–V sweeps.

It was desirable to develop a technique capable of distinguishing between devices fabricated with varying quality SAMs but with similar performance characteristics. This should also be of wider interest to the DSSC community, as there are currently few techniques for assessing the SAM quality. Our solution to this issue was to adjust the IPCE spectra for the respective dye-loading values, the results of which are shown in Figure 4c,d. This way, the photovoltaic contribution per sensitizer molecule can be displayed and compared, with the plot resembling an absorbed photon-to-current conversion efficiency (APCE) spectrum, as $IPCE = APCE \cdot LHE$, where LHE is the light-harvesting efficiency defined by International Union of Pure and Applied Chemistry (IUPAC) as $1 - 10^{-A}$, (where A is absorptance), which again is a product of the extinction

coefficient and dye loading of the sensitizer on the TiO_2 surface. However, for most thicker films, the LHE is close to 1 regardless of the sensitizer, making dye-loading values the more sensible choice for scaling the IPCE spectra. In addition, when comparing dyes of similar extinction coefficients, any differences in absorptance occur from the respective dye-loading values. To the best of our knowledge, this approach has not been used to investigate the individual efficiency contributions of sensitizers, and thus we suggest the term "sensitizer quantum efficiency" (SQE) for the technique. Although the use of absolute units like milliampere per centimeter square per mol dye is possible for SQE, we here chose relative SQE to compare the different sensitizers.

High SQE values in these plots indicate high efficiencies of the individual sensitizer molecules, and low values can be an indication of recombination, diffusion issues, or poor absorption properties. Here, the performance advantage of the CDCA-substituted dyes is very clear for both the C_3 and C_6 dyes. First, with the same concentration of CDCA in the staining solutions, the C_3/C_6–CDCA dyes are remarkably more efficient than their unsubstituted analogs. This suggests a more optimized molecular environment for the CDCA dyes in the SAM. Second, by increasing the thickness of TiO_2, the individual sensitizer performance is lowered. The mechanism behind this behavior must be related to either the increased redox shuttle diffusion resistance, electron transport resistance, or complete light attenuation, leaving a portion of the active layer without any illumination.

Charge extraction and electron lifetime measurements were used to further investigate the properties of the dye monolayers in the devices. In the charge extraction measurements of the C_3 dyes, the same V_{OC} trend observed from the J–V sweeps can be

seen. The CDCA substituent shifts the curves toward higher V_{OC} values, as well as toward higher Q_{OC} values. For the C_6 dyes (**Figure 6**b), the trend is not as clear; this would be expected from the very similar photovoltaic performance. However, the devices with an 8 μm thick active TiO_2 layer deliver slightly higher Q_{OC} values compared to the 4 μm devices.

The effect of different CDCA concentrations (0, 10, and 50 equivalents) has the same effect on the electron lifetime behavior for both C_3 and C_6. An increased amount of CDCA causes a drop in electron lifetime, even though the relative conduction band shift associated with the protonation from the carboxylic acid of CDCA is accounted for. The same separated grouping of C_3 and C_3–CDCA dyes is observed, suggesting the CDCA substituent is contributing to an overall denser dye/CDCA monolayer, restricting the access to TiO_2 for the Cu^{2+} species. However, C_6 and C_6–CDCA do not display the same trend. The reason for this could be superior antiaggregation properties of the hexyl chains over the propyl chains or a more efficient blocking effect of TiO_2. Somewhat surprisingly, the thicker TiO_2 electrodes display the highest electron lifetimes in both C_3 and C_6 dye series. We expected the hindered diffusion of the copper redox species in and out of the TiO_2 layer to facilitate recombination of injected electrons to the electrolyte, but it appears that the quality of the monolayer is sufficiently high to block this recombination pathway.

To investigate the linearity of the devices, the photovoltaic performance of the highest-performing solar cells was measured under a range of light intensities (see **Figure 7**). A nonlinear short-circuit current density (as a function of light intensity) would indicate diffusion limitations. We suspected that the
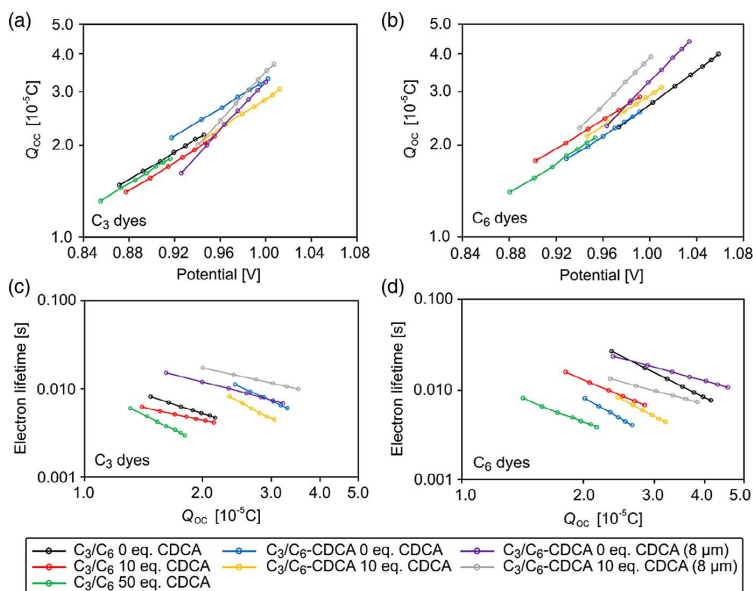
Figure 6. a,b) Charge extraction measurements at different light intensities. C_3 dyes in (a) and C_6 dyes in (b). c,d) Lifetime measurements at different light intensities, plotted against collected charge for the same devices at the same potentials. C_3 dyes in (c) and C_6 dyes in (d). Measured with the Dyenamo Toolbox instrument.
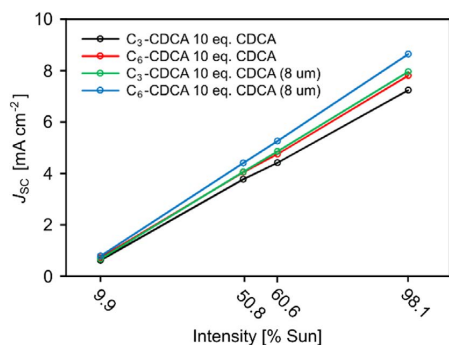
Figure 7. Short-circuit current measurements for four devices at light intensities from 0.1 to 1 sun. Comment of 8 μm means $8 + 4$ μm TiO_2 was used, whereas no specification implies $4 + 2$ μm TiO_2 electrodes.

thicker devices with an 8 μm active TiO_2 layer would be limited by diffusion issues, but all the devices behaved linearly from 0.1 to 1 sun AM1.5 G illumination. This indicates that diffusion does not limit the performance of the $8 + 4$ μm devices. It should be noted that the thicker scattering layer of the 8 μm devices can play a role in enhancing the short-circuit current density and fully or partially mask any diffusion issues.

It is also possible that complete light attenuation in the thicker devices could be a limiting factor. This can explain the marginal performance enhancement, but not the lack of diffusion issues. To circumvent this, a sensitizer with a wider absorption spectrum or several dyes with complementary spectra will have to be used to increase the overall efficiency.

3. Conclusions

To solve the challenges often faced when using CDCA as an anti-aggregation additive in DSSCs, we reported a novel sensitizer design concept. By covalently attaching the CDCA moiety to the sensitizer, improved control of the dye monolayer composition was achieved. Two triarylamine dyes, carrying CDCA substituents, were prepared through a convergent 10–12-step synthesis. A thiophene–furan-linked π-spacer was found to be a convenient point of attachment of the CDCA moiety. Fortunately, the large bulk of the CDCA substituent did not affect the optical and electrochemical properties of the sensitizers, compared with the non-CDCA reference dyes.

First, it was established that the length of the alkoxy chains was of extreme importance in the devices fabricated with $[Cu^{+/2+}(tmby)_2](TFSI)_{1/2}$ electrolyte. The V_{OC} of the C_3 dye was significantly lower than that of the C_6 dye. Although the V_{OC} of both dyes decreased upon addition of CDCA, 10 equivalents was found to yield the highest PCE values for the reference dyes. The covalent CDCA substituent of C_6–CDCA was found to increase the V_{OC} compared with the optimized reference dye, and despite significantly lowering the dye loading, the PCE increased by 10%. This result is attributed to a higher-quality dye monolayer, as can be rationalized by SQE plots, a dye-loading-corrected IPCE measurement.

The dye molecules reported here are predominantly considered model compounds solely for testing the concept; however, larger effects are to be expected if this approach is implemented for severely aggregating dyes. Furthermore, the authors are of the opinion that the structure of CDCA should also be subject to optimization. Through synthetic efforts, the excellent antiaggregation properties of CDCA may well be retained in a more compact unit.

4. Experimental Section

Dye Synthesis: The synthetic details for compounds **9**, **10**, **11**, **14**, and **15** and sensitizers C_3–CDCA and C_6–CDCA are included below. The synthetic procedures and spectroscopic data for the remaining compounds can be found in the Supporting Information. The reference list includes citations to works referenced in the Supporting Information.[45–50]

Materials: All chemicals and reagents used for the synthesis and device fabrication of the sensitizers were sourced from Sigma Aldrich. TiO_2 pastes were bought from GreatCell Solar and the D35 reference dye, $[Cu(tmby)_2]TFSI$, and $[Cu(tmby)_2]TFSI_2$ were bought from Dyenamo.

Solar Cell Assembly: The working electrodes of the devices were fabricated from FTO glass (NSG10, Nippon Sheet Glass), cut to size, and washed with Deconex 21 ($2 g L^{-1}$) in an ultrasonic bath for 45 min. Following UV/O_3 cleaning for 15 min (Novascan PSD-UV), a dense blocking layer of TiO_2 was deposited by immersion in aqueous $TiCl_4$ solution (40 mM) for 30 min at 70 °C. The glass slides were rinsed with deionized water and ethanol before the procedure was repeated and before heating the glass slides on a hotplate at 250 °C for 1 h. The titania pastes were screen printed onto the FTO glass with a 120 T mesh (Seritec Services S.A.), giving each electrode an active area of 0.283 cm². For the $4 + 2$ μm electrodes, two layers of 30NR-D and one layer of scattering paste were printed, and for the electrodes with $8 + 4$ μm, four layers of 30NR-D and two layers of scattering paste were printed. Between each layer, the FTO glass slides were heated at 125 °C for 5 min and then cooled back to room temperature before printing the next layer. The working electrodes were finished by sintering on a programmable hotplate at 125, 250, 375, 450, and 500 °C for 5, 5, 5, 15, and 30 min with 5 min ramping between each step.

Counter electrodes were made from TEC15 FTO glass. Holes were drilled with a diamond drill bit, and the glass slides were washed in an ultrasonic bath for 15 min in each of the following solutions: Hellmanex 2% detergent solution, deionized water, ethanol, and acetone. A layer of poly(3,4-ethylenedioxythiophene) (PEDOT) was electrochemically deposited on the FTO glass from an aqueous solution of 3,4-ethylenedioxythiophene (EDOT), as described by Ellis et al.[51]

The solvent mixture used for the dye-staining solutions was acetonitrile/*tert*-butanol/tetrahydrofuran (1:1:1, v/v), with a dye concentration of 0.1 mM and various amounts of the coadsorbent CDCA, as specified in the Results and Discussion section. The staining time for all experiments was 20 h, and the electrodes were rinsed in acetonitrile and air dried in a dry box before assembly. Surlyn gaskets (35 μm) were melted between the working and counter electrodes (50 W heating element, 2×9 s for sufficient sealing).

The electrolyte contained 0.09 M $[Cu(tmby)_2]TFSI_2$, 0.20 M $[Cu(tmby)_2]$ TFSI, 0.1 M LiTFSI, and 0.6 M 1-methylbenzimidazole in dry acetonitrile, and the DSSCs were filled with electrolyte by vacuum backfilling. The filling hole was sealed by Surlyn and a glass cover slip, before the protruding edges of the electrodes were covered with soldering tin for increased conductivity.

Component and Device Characterization: The UV–vis absorption measurements were recorded on a Hitachi U−1900 spectrophotometer, emission spectra were recorded with a FS5 Spectrofluorometer from Edinburgh Instruments, and electrochemical experiments were recorded with a Versastat 3 potentiostat from Princeton Applied Research. Dye-loading experiments were conducted in duplicates by desorption of stained photoanodes in a solution of 40 mM tetrabutylammonium

hydroxide in stabilized THF. Separate molar extinction coefficients of the dyes in the basic media were measured for increased accuracy. The J–V characteristics of the devices under 1 sun AM1.5 G illumination were recorded with an Oriel xenon lamp solar simulator (300 W), connected to a Keithley 2400, scanned from open circuit to short circuit with a settling time of 100 ms at each voltage step of 10 mV. IPCE measurements were recorded on a commercial Arkeo-Ariadne setup (Cicci Research s.r.l., 300 W xenon light source) with 50% sun bias light. For the J–V sweeps and IPCE measurements, the devices were masked with a 0.158 cm^2 aperture black metal mask. Charge extraction and electron lifetime measurements were conducted using the Dyenamo Toolbox (Dyenamo, Sweden).

Synthesis of (3S,7S,8S,9R,10R,13S,14R,17S)-17-((S)-5-((2-bromothiophen-3-yl)methoxy)pentan-2-yl)-10,13-dimethylhexadecahydro-1H-cyclopenta[a]phenanthrene-3,7-diol (9): Compound **8** (3.01 g, 4.96 mmol), NaH (357 mg, 14.9 mmol), and THF (14 mL) were placed in a flask under nitrogen atmosphere and stirred for 1 h at 0 °C. 2-Bromo-3-bromomethylthiophene (1.90 g, 7.44 mmol) was added dropwise for 5 min before the reaction was heated to 60 °C and stirred for 19 h. The reaction mixture was cooled to room temperature and was quenched by addition of aqueous NH$_4$Cl (5 wt%, 15 mL). The aqueous phase was extracted by ethyl acetate (3 × 50 mL), washed with brine (50 mL), and dried over anhydrous Na$_2$SO$_4$ before the solvents were removed in vacuo. The crude product (light yellow oil) was then suspended in methanol (200 mL) and heated to 60 °C. HCl (37%, 10 mL) was added and the reaction stirred overnight. All solids dissolved during the reaction and TLC confirmed full conversion after 17 h. Aqueous NaHCO$_3$ solution (10 wt%, 150 mL) was added, and the aqueous phase was extracted by ethyl acetate (3 × 100 mL). The combined organic phases were washed with brine and dried over anhydrous Na$_2$SO$_4$ before being concentrated in vacuo. The crude product was purified by silica gel column chromatography (ethyl acetate, R_f = 0.38) to yield compound **9** as a white solid (2.73 g, 4.93 mmol, 99%), mp 80–82 °C. ^{1}H NMR (600 MHz, acetone-d$_6$) δ: 7.50 (d, J = 5.6 Hz, 1 H), 7.04 (d, J = 5.6 Hz, 1H), 4.42 (s, 2H), 3.82–3.79 (m, 1H), 3.44 (t, J = 6.2 Hz, 2H), 3.36–3.30 (m, 1.4H*), 3.16 (d, J = 3.2 Hz, 0.3H*), 2.38–2.31 (m, 1H), 2.02–1.05 (m, 25H), 0.95 (d, J = 6.3 Hz, 3H), 0.92 (s, 3H), 0.69 (s, 3 H); ^{13}C NMR (150 MHz, acetone-d$_6$) δ: 140.3, 129.5, 127.4, 110.8, 72.1, 71.6, 68.1, 67.3, 57.2, 51.4, 43.3, 43.0, 40.86, 40.85, 40.6, 36.5, 36.02, 36.01, 33.8, 33.2, 31.7, 30.6, 29.2, 27.1, 24.4, 23.5, 21.6, 19.2, 12.3; IR (neat, cm^{-1}) ν: 3394 (br), 2929 (m), 2863 (m), 1449 (w), 1374 (w), 1221 (w), 1108 (w), 1079 (w), 998 (w), 689 (w); HRMS (ESI+, m/z): found 575.2177 (calcd. C$_{29}$H$_{45}$^{79}BrO$_3$S 575.2170, [M + Na]$^+$). The asterisk in (H*) indicates exchange observed for the OH protons.

Synthesis of 5-(3-((((4S)-4-((3S,7S,8S,9R,10R,13S,14R,17S)-3,7-dihydroxy-10,13-dimethylhexadecahydro-1H-cyclopenta[a]phenanthren-17-yl)pentyl)oxy)methyl)thiophen-2-yl)furan-2-carbaldehyde (10): Compound **9** (500 mg, 0.903 mmol), (5-formylfuran-2-yl)boronic acid (379 mg, 2.71 mmol), PdCl$_2$(dppf) (33 mg, 0.045 mmol), and K$_2$CO$_3$ (499 mg, 3.61 mmol) were mixed. 1,4-Dioxane (6 mL) and water (6 mL) were degassed and added in a nitrogen atmosphere. The reaction mixture was heated to 80 °C and stirred for 25 min before being cooled to room temperature. Water (10 mL) was added and the aqueous phase extracted by ethyl acetate (3 × 50 mL). The combined organic phases were washed with brine (30 mL) and dried over anhydrous Na$_2$SO$_4$, filtered, and the solvents were removed in vacuo. The crude product was purified by silica gel column chromatography (ethyl acetate, R_f = 0.32) to obtain compound **10** as a light brown solid (350 mg, 0.615 mmol, 68%), mp 70–72 °C. ^{1}H NMR (600 MHz, acetone-d$_6$) δ: 9.65 (s, 1H), 7.61 (d, J = 5.0 Hz, 1H), 7.54 (d, J = 3.7 Hz, 1H), 7.24 (d, J = 5.0 Hz, 1H), 6.92 (d, J = 3.7 Hz, 1H), 4.69 (s, 2H), 3.82–3.77 (m, 1H), 3.52 (t, J = 6.3 Hz, 2H), 3.37–3.30 (m, 1H), 3.38–3.31 (m, 1.5H*), 3.16 (d, J = 3.2 Hz, 0.4H*), 2.40–2.29 (m, 1H), 2.00–0.95 (m, 25H), 0.94 (d, J = 6.6 Hz, 3H), 0.91 (s, 3H), 0.67 (s, 3H); ^{13}C NMR (150 MHz, acetone-d$_6$) δ: 177.6, 154.4, 152.8, 140.3, 131.4, 128.6, 127.6, 124.8, 110.7, 72.1, 71.6, 68.1, 67.2, 57.1, 51.2, 43.2, 42.9, 40.8, 40.7, 40.5, 36.4, 35.92, 35.90, 33.7, 33.2, 31.7, 30.3, 29.0, 27.1, 24.3, 23.4, 21.4, 19.1, 12.2; IR (neat, cm^{-1}) ν: 3410 (br), 2930 (m), 2864 (m), 1673 (m), 1499 (w), 1377 (w), 1109 (w), 1079 (w), 1028 (w), 997 (w), 766 (w), 736 (w); HRMS (ESI+, m/z): found

591.3120 (calcd. C$_{34}$H$_{48}$O$_5$S 591.3120, [M + Na]$^+$). The asterisk in (H*) indicates exchange observed for the OH protons.

Synthesis of 5-(5-bromo-3-((((4S)-4-((3S,7S,8S,9 R,10 R,13S,14 R,17S)-3,7-dihydroxy-10,13-dimethylhexadecahydro-1H-cyclopenta[a]phenanthren-17-yl)pentyl)oxy)methyl)thiophen-2-yl)furan-2-carbaldehyde (11): Compound **10** (230 mg, 0.404 mmol) was dissolved in a mixture of chloroform (3 mL) and glacial acetic acid (3 mL) in a nitrogen atmosphere at 0 °C. NBS (120 mg, 0.667 mmol) was added and the reaction was stirred in the dark, at 0 °C for 17 h, slowly reaching room temperature, before water (20 mL) was added and the aqueous phase was extracted by chloroform (3 × 30 mL). The combined organic phases were washed with brine (30 mL), dried over anhydrous Na$_2$SO$_4$, filtered, and concentrated in vacuo. Purification by silica gel column chromatography (ethyl acetate, R_f = 0.33) gave compound **11** as a brown solid (76 mg, 0.117 mmol, 29%), mp 83–85 °C. ^{1}H NMR (600 MHz, acetone-d$_6$) δ: 9.66 (s, 1H), 7.54 (d, J = 3.8 Hz, 1H), 7.29 (s, 1H), 6.93 (d, J = 3.8 Hz, 1H), 4.66 (s, 2H), 3.82–3.77 (s, 1H), 3.52 (t, J = 6.3 Hz, 2H), 3.36–3.30 (m, 1H), 2.39–2.31 (m, 1H), 2.02–1.05 (m, 27H), 0.94 (d, J = 6.5 Hz, 3H), 0.92 (s, 3H), 0.68 (s, 3H); ^{13}C NMR (150 MHz, acetone-d$_6$) δ: 177.8, 153.0, 152.7, 140.9, 134.2, 130.1, 124.6, 113.9, 111.3, 72.1, 71.7, 68.1, 66.9, 57.0, 51.3, 43.2, 42.9, 40.9, 40.8, 40.5, 36.44, 36.42, 35.95, 35.90, 33.7, 33.1, 31.7, 29.0, 27.0, 24.3, 23.4, 21.4, 19.1, 12.2; IR (neat, cm^{-1}) ν: 3456 (br), 2932 (m), 2865 (m), 1710 (m), 1674 (m), 1497 (w), 1375 (w), 1243 (w), 1179 (w), 1021 (w), 978 (w), 766 (w), 735 (w); HRMS (ASAP+, m/z): found 611.2189 (calcd. C$_{34}$H$_{44}$O$_3$S^{79}Br 611.2195, [M − 2H$_2$O + H]$^+$).

Synthesis of 5-(5-(4-(bis(2′,4′-dipropoxy-[1,1′-biphenyl]-4-yl)amino)phenyl)-3-((((4S)-4-((3S,7S,8S,9R,10R,13S,14R,17S)-3,7-dihydroxy-10,13-dimethylhexadecahydro-1H-cyclopenta[a]phenanthren-17-yl)pentyl)oxy)methyl)thiophen-2-yl)furan-2-carbaldehyde (14): Compound **4** (72 mg, 0.10 mmol), PdCl$_2$(CH$_3$CN)$_2$ (0.53 mg, 2.04 μmol), and SPhos (3.4 mg, 8.2 μmol) were added to a Schlenk tube before it was evacuated, and a N$_2$ atmosphere established. Dry 1,4-dioxane (0.2 mL) was used to dissolve the compounds and the reaction mixture was stirred at room temperature before 4,4,5,5-tetramethyl-1,3,2-dioxaborolane (20 μL, 0.165 mmol) and dry triethylamine (130 μL) were added. The reaction mixture was heated to 80 °C and stirred for 1 h before cooling to room temperature. The reaction mixture was filtered through Celite using ethyl acetate as the eluent; the solvents were removed in vacuo. The crude mixture obtained was a yellow oil and was used without further purification.

The crude product from borylation, compound **11** (55 mg, 0.085 mmol), Pd(OAc)$_2$ (0.38 mg, 1.70 μmol), SPhos (1.4 mg, 3.4 μmol), and K$_2$CO$_3$ (47 mg, 0.34 mmol) were mixed. 1,4-Dioxane (1 mL) and water (1 mL) were degassed and added in a nitrogen atmosphere. The reaction mixture was heated to 80 °C and stirred for 2 h before cooling to room temperature. Water (20 mL) was added and the aqueous phase extracted by ethyl acetate (3 × 25 mL). The combined organic phases were dried with brine (25 mL) and over anhydrous Na$_2$SO$_4$, filtered, and the solvents were removed in vacuo. The crude product was purified by silica gel column chromatography (n-pentane/ethyl acetate, 1:1, R_f = 0.16) to obtain compound **14** as a yellow solid (33 mg, 0.028 mmol, 33%), mp 108–110 °C. ^{1}H NMR (600 MHz, acetone-d$_6$) δ: 9.65 (s, 1H), 7.65 (d, J = 8.8 Hz, 2H), 7.55–7.53 (m, 5H), 7.49 (s, 1H), 7.28 (d, J = 8.4 Hz, 2H), 7.18–7.15 (m, 4H), 7.13 (d, J = 8.7 Hz, 2H), 6.92 (d, J = 3.8 Hz, 1H), 6.64 (d, J = 2.3 Hz, 2H), 6.60 (dd, J = 8.5, 2.3 Hz, 2H), 4.69 (s, 2H), 3.99 (t, J = 6.5, Hz, 4H), 3.98 (t, J = 6.5, Hz, 4H), 3–80–3.75 (m, 1H), 3.56 (t, J = 6.1 Hz, 2H), 3.36–3.30 (m, 1.8H)*, 3.09 (s. br., 0.7H)*, 2.37–2.30 (m, 1H), 2.00–1.06 (m, 33H), 1.04 (t, J = 7.4 Hz, 6H), 1.00 (t, J = 7.4 Hz, 6H), 0.94 (d, J = 6.6 Hz, 3H), 0.90 (s, 3H), 0.66 (s, 3H); ^{13}C NMR (150 MHz, acetone-d$_6$) δ: 177.4, 160.8 (2C), 158.0 (2C), 154.4, 152.6, 149.1, 146.2 (2C), 145.5, 141.5, 135.1 (2C), 131.6 (2C), 131.3 (4C), 127.6, 127.4 (2C), 126.4, 126.3, 125.1 (5C), 123.6 (2C), 123.4 (2C), 110.7, 106.8 (2C), 101.1 (2C), 72.1, 71.6, 70.6 (2C), 70.2 (2C), 68.1, 67.4, 57.1, 51.2, 43.2, 42.9, 40.8, 40.7, 40.5, 36.4, 35.91, 35.89, 33.6, 33.2, 31.7, 30.3, 29.0, 27.1, 24.3, 23.4, 23.33 (2C), 23.32 (2C), 21.4, 19.1, 12.2, 11.1 (2C), 10.8 (2C); IR (neat, cm^{-1}) ν: 3413 (br), 2960 (m), 2928 (m), 2868 (m), 1672 (m), 1601 (m), 1490 (s), 1387 (s), 1271 (m), 1182 (s), 1133 (w), 1001 (w), 978 (m), 830 (m); HRMS (ESI+, m/z): found 1196.6631 (calcd. C$_{76}$H$_{94}$NO$_9$S 1196.6649, [M + H]$^+$).

Synthesis of 5-(5-(4-(bis(2',4'-bis(hexyloxy)-[1,1'-biphenyl]-4-yl)amino) phenyl)-3-((((4S)-4-((3S,7S,8S,9R,10R,13S,14R,17S)-3,7-dihydroxy-10,13-dimethylhexadecahydro-1H-cyclopenta[a]phenanthren-17-yl)pentyl)oxy)methyl)thiophen-2-yl)furan-2-carbaldehyde (15): Compound **5** (133 mg, 0.151 mmol), PdCl₂(CH₃CN)₂ (0.8 mg, 3.0 μmol), and SPhos (5 mg, 12.0 μmol) were added to a Schlenk tube before it was evacuated, and an N₂ atmosphere was established. Dry 1,4-dioxane (0.3 mL) was used to dissolve the compounds and the reaction mixture was stirred at room temperature before 4,4,5,5-tetramethyl-1,3,2-dioxaborolane (33 μL, 0.227 mmol) and dry triethylamine (0.2 mL) were added. The reaction mixture was heated to 80 °C and stirred for 2.5 h before cooling to room temperature. The reaction mixture was filtered through Celite using ethyl acetate as the eluent. The solvents were removed in vacuo, giving the crude material as a yellow oil.

The crude product from borylation, compound **11** (70 mg, 0.108 mmol), Pd(OAc)₂ (0.5 mg, 2.161 μmol), SPhos (1.8 mg, 4.3 μmol), and K₂CO₃ (60 mg, 0.43 mmol) were mixed. 1,4-Dioxane (1 mL) and water (1 mL) were degassed and added in a nitrogen atmosphere. The reaction mixture was heated to 80 °C and stirred for 35 min before cooling to room temperature. Water (20 mL) was added and the aqueous phase extracted by ethyl acetate (4 × 25 mL). The combined organic phases were dried with brine (30 mL) and over anhydrous Na₂SO₄, filtered, and the solvents were removed in vacuo. The crude product was purified by silica gel column chromatography (ethyl acetate, $R_f = 0.48$) to obtain compound **15** as a yellow solid (46 mg, 0.034 mmol, 31%), mp 78–79 °C. ¹H NMR (600 MHz, acetone-d₆) δ: 9.65 (s, 1H), 7.65 (d, *J* = 8.7 Hz, 2H), 7.56–7.52 (m, 5H), 7.49 (s, 1H), 7.28 (d, *J* = 8.5 Hz, 2H), 7.19–7.15 (m, 4H), 7.14 (d, *J* = 8.7 Hz, 2H), 6.92 (d, *J* = 4.0 Hz, 1H), 6.65 (d, *J* = 2.4 Hz, 2H), 6.60 (dd, *J* = 8.5, 2.4 Hz, 2H), 4.70 (s, 2H), 4.05–4.02 (m, 8H), 3.79–3.75 (m, 1H), 3.56 (t, *J* = 6.1 Hz, 2H), 3.35–3.30 (m, 1H), 2.33 (q, *J* = 12.2 Hz, 1H), 2.00–1.01 (m, 60H), 0.94 (d, *J* = 6.6 Hz, 3H), 0.92 (t, *J* = 7.0 Hz, 6H), 0.90 (s, 3H), 0.87 (t, *J* = 7.0 Hz, 6H), 0.66 (s, 3H); ¹³C NMR (150 MHz, acetone-d₆) δ:177.4, 160.8 (2C), 158.0 (2C), 154.3, 152.7, 149.2, 146.2 (2C), 145.5, 141.5, 135.1 (2C), 131.6 (2C), 131.3 (4C), 127.6, 127.4 (2C), 126.34, 126.29, 125.0 (2C), 123.6 (2C), 123.4 (2C), 110.7, 106.8 (2C), 101.1 (2C), 72.0, 71.6, 69.0 (2C), 68.6 (2C), 68.0, 67.5, 57.1, 51.2, 43.2, 42.9, 40.8, 40.7, 40.5, 36.43, 36.36, 35.9, 33.7, 33.2, 32.4 (2C), 32.3 (2C), 31.7, 30.3, 30.0 (2C), 29.9 (2C), 29.0, 27.1, 26.6 (2C), 26.5 (2C), 24.3, 23.4, 23.3 (4C), 21.4, 19.1, 14.4 (2C), 14.3 (2C), 12.2; IR (neat, cm⁻¹) ν: 3458 (br), 2931 (m), 2862 (m), 1675 (m), 1603 (m), 1492 (m), 1288 (m), 1182 (m), 830 (m); HRMS (ESI+, *m/z*): found 1364.8512 (calcd. C₈₈H₁₁₈NO₉S 1364.8527, [M + H]⁺).

Synthesis of (E)-3-(5-(5-(4-(bis(2',4'-dipropoxy-[1,1'-biphenyl]-4-yl)amino) phenyl)-3-((((4S)-4-((3S,7S,8S,9R,10R,13S,14R,17S)-3,7-dihydroxy-10,13-dimethylhexadecahydro-1H-cyclopenta[a]phenanthren-17-yl)pentyl)oxy)methyl)thiophen-2-yl)furan-2-yl)-2-cyanoacrylic acid (Dye C₃–CDCA): Compound **14** (32 mg, 0.027 mmol) and cyanoacetic acid (46 mg, 0.54 mmol) were dissolved in degassed acetonitrile (12 mL) and THF (2 mL) in a nitrogen atmosphere. Piperidine (32 μL, 27 mg, 0.321 mmol) was added and the reaction was heated to 80 °C for 2 h before cooling to room temperature and quenched in HCl (1 M, 50 mL). Ethyl acetate (30 mL) was added and the organic phase was washed with water (3 × 200 mL), then dried with brine (30 mL) and over anhydrous Na₂SO₄, filtered, and the solvents were removed in vacuo. The crude product was purified by silica gel column chromatography (gradient: 0–20% MeOH in ethyl acetate). The solvents were removed, the product redissolved in ethyl acetate, and then filtered before complete removal of the solvents yielded sensitizer C₃–CDCA as a dark solid (18 mg, 0.014 mmol, 54%), mp 153–154 °C (dec. 173 °C). ¹H NMR (600 MHz, THF-d₈) δ: 7.86 (s, 1H), 7.46 (d, *J* = 8.3 Hz, 2H), 7.38–7.35 (m, 5H), 7.32 (s, 1H), 7.13 (d, *J* = 8.4 Hz, 2H), 7.04–7.01 (m, 6H), 6.80 (br. s, 1H), 6.48 (d, *J* = 2.3 Hz, 2H), 6.43 (dd, *J* = 8.4, 2.2 Hz, 2H), 4.65 (s, 2H), 3.85–3.80 (m, 8H), 3.59 (s, 1H), 3.50–3.40 (m, 3H), 3.35 (s, br, 0.4H*), 3.14–3.08 (m, 1H), 2.23–2.15 (m, 1H), 1.89–0.97 (m, 33H), 0.94 (t, *J* = 7.4 Hz, 6H), 0.89 (t, *J* = 7.5 Hz, 6H), 0.84 (d, *J* = 6.6 Hz, 3H), 0.78 (s, 3H), 0.56 (s, 3H) (CO₂H proton missing); ¹³C NMR (150 MHz, acetone-d₆) δ: 163.0, 159.5 (2C), 156.6 (2C), 154.0, 147.9, 147.7, 145.0 (2C), 144.8, 140.7, 136.4, 133.7 (2C), 130.1 (2C), 129.8, 129.7 (4C), 126.6, 125.9 (2C), 124.6, 123.6, 123.5 (5C), 122.5 (2C), 122.3

(2C), 115.0, 110.3, 105.0 (2C), 99.8 (2C), 70.7, 70.4, 69.3 (2C), 68.7 (2C), 66.8, 66.7, 55.9, 50.0, 41.9, 41.8, 39.6, 39.5, 39.4, 35.35, 35.32, 34.9, 34.7, 32.3, 32.0, 30.6, 27.9, 26.0, 23.1, 22.2 (2C), 22.13 (2C), 22.05, 20.2, 17.8, 10.9, 9.8 (2C), 9.5 (2C); IR (neat, cm⁻¹) ν: 3400 (br), 2961 (m), 2931 (m), 2870 (m), 2217 (w), 1704 (w), 1601 (m), 1488 (s), 1387 (m), 1264 (m), 1181 (s), 1030 (m), 829 (m), 734 (s); HRMS (APPI-, *m/z*): found 1261.6573 (calcd. C₇₉H₉₃N₂O₁₀S 1261.6551, [M - H]⁻). The asterisk in (H*) indicates exchange observed for the OH protons.

Synthesis of (E)-3-(5-(5-(4-(bis(2',4'-bis(hexyloxy)-[1,1'-biphenyl]-4-yl) amino)phenyl)-3-((((4S)-4-((3S,7S,8S,9R,10R,13S,14R,17S)-3,7-dihydroxy-10,13-dimethylhexadecahydro-1H-cyclopenta[a]phenanthren−17-yl)pentyl)oxy) methyl)thiophen-2-yl)furan-2-yl)-2-cyanoacrylic acid (Dye C₆–CDCA): Compound **15** (45 mg, 0.033 mmol) and cyanoacetic acid (56 mg, 0.66 mmol) were dissolved in degassed acetonitrile (35 mL) and THF (5 mL) in a nitrogen atmosphere. Piperidine (39 μL, 34 mg, 0.396 mmol) was added and the reaction was heated to 80 °C for 1 h before cooling to room temperature and quenched in HCl (1 M, 100 mL). Ethyl acetate (30 mL) was added and the organic phase was washed with water (3 × 200 mL), then dried with brine (30 mL) and over anhydrous Na₂SO₄, filtered, and the solvents were removed in vacuo. The crude product was purified by silica gel column chromatography (gradient: 0–30% MeOH in ethyl acetate). The solvents were removed, the product redissolved in ethyl acetate, and then filtered before complete removal of the solvents yielded the sensitizer C₆–CDCA as a dark solid (45 mg, 0.031 mmol, 95%), mp 132–134 °C (dec. 163 °C). ¹H NMR (600 MHz, THF-d₈) δ: 7.85 (s, 1H), 7.45 (d, *J* = 8.50 Hz, 2H), 7.39–7.33 (m, 5H), 7.31 (s, 1H), 7.12 (d, *J* = 8.4 Hz, 2H), 7.05–7.00 (m, 6H), 6.78 (br. s, 1H), 6.47 (d, *J* = 2.1 Hz, 2H), 6.43 (dd, *J* = 8.5, 2.1, 2H), 4.64 (s, 2H), 3.89–3.84 (m, 8H), 3.61–3.58 (m, 1H), 3.44–3.40 (m, 2H), 3.15–3.09 (m, 2H), 2.23–2.15 (m, 1H), 1.90–0.84 (m, 58H), 0.84–0.71 (m, 18H), 0.56 (s, 3H) (CO₂H proton missing); ¹³C NMR (150 MHz, THF-d₈) δ: 163.2, 159.5 (2C), 156.6 (2C), 153.6, 147.8 (2C), 144.9 (2C), 144.7, 140.5, 136.1, 133.7 (2C), 130.0 (2C), 129.8, 129.7 (4C), 126.6, 125.9 (2C), 124.6, 123.8, 123.5 (5C), 122.5 (2C), 122.3 (2C), 115.2, 110.2, 104.9 (2C), 99.8 (2C), 70.7, 70.4, 67.7 (2C), 67.2 (2C), 66.8, 66.7, 55.9, 50.0, 41.9, 41.8, 39.6, 39.5, 39.4, 35.33, 35.31, 34.9, 34.6, 32.3, 32.0, 31.2 (2C), 31.1 (2C), 30.6, 28.9 (2C), 28.7 (2C), 27.8, 26.0, 25.4 (4C), 23.1, 22.2 (2C), 22.14 (2C), 22.05, 20.2, 17.8, 13.1 (2C), 13.0 (2C), 10.9; IR (neat, cm⁻¹) ν: 3387 (br), 2927 (m), 2858 (m), 2217 (w), 1700 (w), 1601 (m), 1489 (s), 1380 (m), 1263 (s), 1180 (s), 1030 (m), 794 (m), 735 (m); HRMS (ESI, *m/z*): found 1429.8400 (calcd. C₉₁H₁₁₇N₂O₁₀S 11429.8429, [M–H]⁻).

Supporting Information

Supporting Information is available from the Wiley Online Library or from the author.

Conflict of Interest

The authors declare no conflict of interest.

Keywords

antiaggregation, chenodeoxycholic acid, dye design, dye distributions, sensitizer quantum efficiencies

[1] B. O'Regan, M. Grätzel, *Nature* **1991**, *353*, 737.

[2] A. Hagfeldt, G. Boschloo, L. Sun, L. Kloo, H. Pettersson, *Chem. Rev.* **2010**, *110*, 6595.

[3] M. Freitag, J. Teuscher, Y. Saygili, X. Zhang, F. Giordano, P. Liska, J. Hua, S. M. Zakeeruddin, J.-E. Moser, M. Grätzel, A. Hagfeldt, *Nat. Photonics* **2017**, *11*, 372.

[4] D. Joly, L. Pelleja, S. Narbey, F. Oswald, T. Meyer, Y. Kervella, P. Maldivi, J. N. Clifford, E. Palomares, R. Demadrille, *Energy Environ. Sci.* **2015**, *8*, 2010.

[5] N. Robertson, *Angew. Chem. Int. Ed.* **2006**, *45*, 2338.

[6] Y. S. Tingare, N. S. Vinh, H.-H. Chou, Y.-C. Liu, Y.-S. Long, T.-C. Wu, T.-C. Wei, C.-Y. Yeh, *Adv. Energy Mater.* **2017**, *7*, 1700032.

[7] E. Mosconi, J.-H. Yum, F. Kessler, C. J. Gómez García, C. Zuccaccia, A. Cinti, M. K. Nazeeruddin, M. Grätzel, F. De Angelis, *J. Am. Chem. Soc.* **2012**, *134*, 19438.

[8] S. M. Feldt, E. A. Gibson, E. Gabrielsson, L. Sun, G. Boschloo, A. Hagfeldt, *J. Am. Chem. Soc.* **2010**, *132*, 16714.

[9] L. Zhang, J. M. Cole, *J. Mater. Chem. A* **2017**, *5*, 19541.

[10] X. Zhang, Y. Xu, F. Giordano, M. Schreier, N. Pellet, Y. Hu, C. Yi, N. Robertson, J. Hua, S. M. Zakeeruddin, H. Tian, M. Grätzel, *J. Am. Chem. Soc.* **2016**, *138*, 10742.

[11] K. Kakiage, Y. Aoyama, T. Yano, K. Oya, J.-i. Fujisawa, M. Hanaya, *Chem. Commun.* **2015**, *51*, 15894.

[12] A. Yella, R. Humphry-Baker, B. F. E. Curchod, N. Ashari-Astani, J. Teuscher, L. E. Polander, S. Mathew, J.-E. Moser, I. Tavernelli, U. Rothlisberger, M. Grätzel, M. K. Nazeeruddin, J. Frey, *Chem. Mater.* **2013**, *25*, 2733.

[13] M. Xu, R. Li, N. Pootrakulchote, D. Shi, J. Guo, Z. Yi, S. M. Zakeeruddin, M. Grätzel, P. Wang, *J. Phys. Chem. C* **2008**, *112*, 19770.

[14] J.-H. Yum, D. P. Hagberg, S.-J. Moon, K. M. Karlsson, T. Marinado, L. Sun, A. Hagfeldt, M. K. Nazeeruddin, M. Grätzel, *Angew. Chem. Int. Ed.* **2009**, *48*, 1576.

[15] S. Mathew, A. Yella, P. Gao, R. Humphry-Baker, B. F. E. Curchod, N. Ashari-Astani, I. Tavernelli, U. Rothlisberger, K. Nazeeruddin, M. Grätzel, *Nat. Chem.* **2014**, *6*, 242.

[16] N. Manfredi, M. Monai, T. Montini, F. Peri, F. De Angelis, P. Fornasiero, A. Abbotto, *ACS Energy Lett.* **2018**, *3*, 85.

[17] A. Kay, M. Grätzel, *J. Phys. Chem.* **1993**, *97*, 6272.

[18] J. M. Donkers, R. L. P. Roscam Abbing, S. F. J. van de Graaf, *Biochem. Pharmacol.* **2019**, *161*, 1.

[19] N. A. Malik, *Appl. Biochem. Biotechnol.* **2016**, *179*, 179.

[20] R. Cisneros, M. Beley, F. Lapicque, *Phys. Chem. Chem. Phys.* **2016**, *18*, 9645.

[21] A. F. Buene, E. E. Ose, A. G. Zakariassen, A. Hagfeldt, B. H. Hoff, *J. Mater. Chem. A* **2019**, *7*, 7581.

[22] Y. Hong, Z. Iqbal, X. Yin, D. Cao, *Tetrahedron* **2014**, *70*, 6296.

[23] H. Cheema, A. Baumann, E. K. Loya, P. Brogdon, L. E. McNamara, C. A. Carpenter, N. I. Hammer, S. Mathew, C. Risko, J. H. Delcamp, *ACS Appl. Mater. Interfaces* **2019**, *11*, 16474.

[24] Y. Saygili, M. Söderberg, N. Pellet, F. Giordano, Y. Cao, A. B. Muñoz-García, S. M. Zakeeruddin, N. Vlachopoulos, M. Pavone, G. Boschloo, L. Kavan, J.-E. Moser, M. Grätzel, A. Hagfeldt, M. Freitag, *J. Am. Chem. Soc.* **2016**, *138*, 15087.

[25] Y. Saygili, M. Stojanovic, N. Flores-Díaz, S. M. Zakeeruddin, N. Vlachopoulos, M. Grätzel, A. Hagfeldt, *Inorganics* **2019**, *7*, 30.

[26] J. T. Lin, P.-C. Chen, Y.-S. Yen, Y.-C. Hsu, H.-H. Chou, M.-C. P. Yeh, *Org. Lett.* **2009**, *11*, 97.

[27] J. Zhao, T. Jin, A. Islam, E. Kwon, M. Akhtaruzzaman, N. Asao, L. Han, K. A. Alamry, S. A. Kosa, A. M. Asiri, Y. Yamamoto, *Tetrahedron* **2014**, *70*, 6211.

[28] H. Zhu, Y. Wu, J. Liu, W. Zhang, W. Wu, W.-H. Zhu, *J. Mater. Chem. A* **2015**, *3*, 10603.

[29] K.-M. Lu, W.-M. Li, P.-Y. Lin, K.-T. Liu, C.-Y. Liu, *Adv. Synth. Catal.* **2017**, *359*, 3805.

[30] A. Baumann, H. Cheema, M. A. Sabuj, L. E. McNamara, Y. Zhang, A. Peddapuram, S. T. Nguyen, D. L. Watkins, N. I. Hammer, N. Rai, J. H. Delcamp, *Phys. Chem. Chem. Phys.* **2018**, *20*, 17859.

[31] Y. Cao, Y. Liu, S. M. Zakeeruddin, A. Hagfeldt, M. Grätzel, *Joule* **2018**, *2*, 1108.

[32] Y. Hao, J. Saygili, J. Cong, A. Eriksson, W. Yang, J. Zhang, E. Polanski, K. Nonomura, S. M. Zakeeruddin, M. Grätzel, A. Hagfeldt, G. Boschloo, *ACS Appl. Mater. Interfaces* **2016**, *8*, 32797.

[33] M. Freitag, F. Giordano, W. Yang, M. Pazoki, Y. Hao, B. Zietz, M. Grätzel, A. Hagfeldt, G. Boschloo, *J. Phys. Chem. C* **2016**, *120*, 9595.

[34] J.-H. Yum, E. Baranoff, F. Kessler, T. Moehl, S. Ahmad, T. Bessho, A. Marchioro, E. Ghadiri, J.-E. Moser, C. Yi, M. K. Nazeeruddin, M. Grätzel, *Nat. Commun.* **2012**, *3*, 631.

[35] M. Freitag, Q. Daniel, M. Pazoki, K. Sveinbjörnsson, J. Zhang, L. Sun, A. Hagfeldt, G. Boschloo, *Energy Environ. Sci.* **2015**, *8*, 2634.

[36] E. Gabrielsson, H. Ellis, S. Feldt, H. Tian, G. Boschloo, A. Hagfeldt, L. Sun, *Adv. Energy Mater.* **2013**, *3*, 1647.

[37] K. L. Billingsley, S. L. Buchwald, *J. Org. Chem.* **2008**, *73*, 5589.

[38] T. Bjørnholm, D. R. Greve, N. Reitzel, T. Hassenkam, K. Kjaer, P. B. Howes, N. B. Larsen, J. Bøgelund, M. Jayaraman, P. C. Ewbank, R. D. McCullough, *J. Am. Chem. Soc.* **1998**, *120*, 7643.

[39] Q.-Y. Yu, J.-Y. Liao, S.-M. Zhou, Y. Shen, J.-M. Liu, D.-B. Kuang, C.-Y. Su, *J. Phys. Chem. C* **2011**, *115*, 22002.

[40] Y. Hua, S. Chang, D. D. Huang, X. Zhou, X. J. Zhu, J. Z. Zhao, T. Chen, W. Y. Wong, W. K. Wong, *Chem. Mater.* **2013**, *25*, 2146.

[41] L. Schmidt-Mende, J. E. Kroeze, J. R. Durrant, M. K. Nazeeruddin, M. Grätzel, *Nano Lett.* **2005**, *5*, 1315.

[42] V. V. Pavlishchuk, A. W. Addison, *Inorganica Chim. Acta* **2000**, *298*, 97.

[43] D. P. Hagberg, X. Jiang, E. Gabrielsson, M. Linder, T. Marinado, T. Brinck, A. Hagfeldt, L. Sun, *J. Mater. Chem.* **2009**, *19*, 7232.

[44] Y. Saygili, M. Stojanovic, H. Michaels, J. Tiepelt, J. Teuscher, A. Massaro, M. Pavone, F. Giordano, S. M. Zakeeruddin, G. Boschloo, J.-E. Moser, M. Grätzel, A. B. Muñoz-García, A. Hagfeldt, M. Freitag, *ACS Appl. Energy Mater.* **2018**, *1*, 4950.

[45] J.-H. Yum, T. W. Holcombe, Y. Kim, J. Yoon, K. Rakstys, M. K. Nazeeruddin, M. Grätzel, *Chem. Commun.* **2012**, *48*, 10727.

[46] Md. K. Nazeeruddin, M. Grätzel, E. Baranoff, F. Kessler, J.-H. Yum, EP2492277A1, École Polytechnique Fédérale de Lausanne **2011**.

[47] L. Huang, Y. Sun, Y. Zhu, Y. Zhang, J. Xu, Y.-M. Shen, *Steroids* **2009**, *74*, 701.

[48] C. D'Amore, F. S. Di Leva, V. Sepe, B. Renga, C. Del Gaudio, M. V. D'Auria, A. Zampella, S. Fiorucci, V. Limongelli, *J. Med. Chem.* **2014**, *57*, 937.

[49] P. R. Parry, M. R. Bryce, B. Tarbit, *Org. Biomol. Chem.* **2003**, *1*, 1447.

[50] S.-H. Kim, R. D. Rieke, *J. Org. Chem.* **2013**, *78*, 1984.

[51] H. Ellis, R. Jiang, S. Ye, A. Hagfeldt, G. Boschloo, *Phys. Chem. Chem. Phys.* **2016**, *18*, 8419.

1900569 (12 of 12)

Supporting Information

First Report of CDCA-Substituted Dyes Improving the Dye Monolayer Quality in Dye-Sensitized Solar Cells

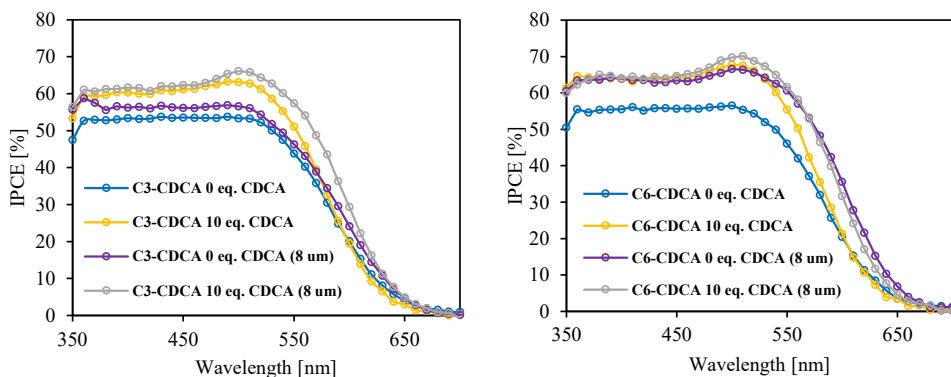*Audun F. Buene, David M. Almenningen, Anders Hagfeldt, Odd R. Gautun, Bård H. Hoff**
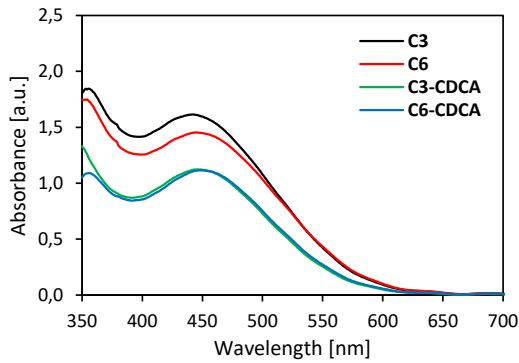
Figure S1. Absorption spectra of the four dyes on TiO$_2$ films (2.5 µm thickness).
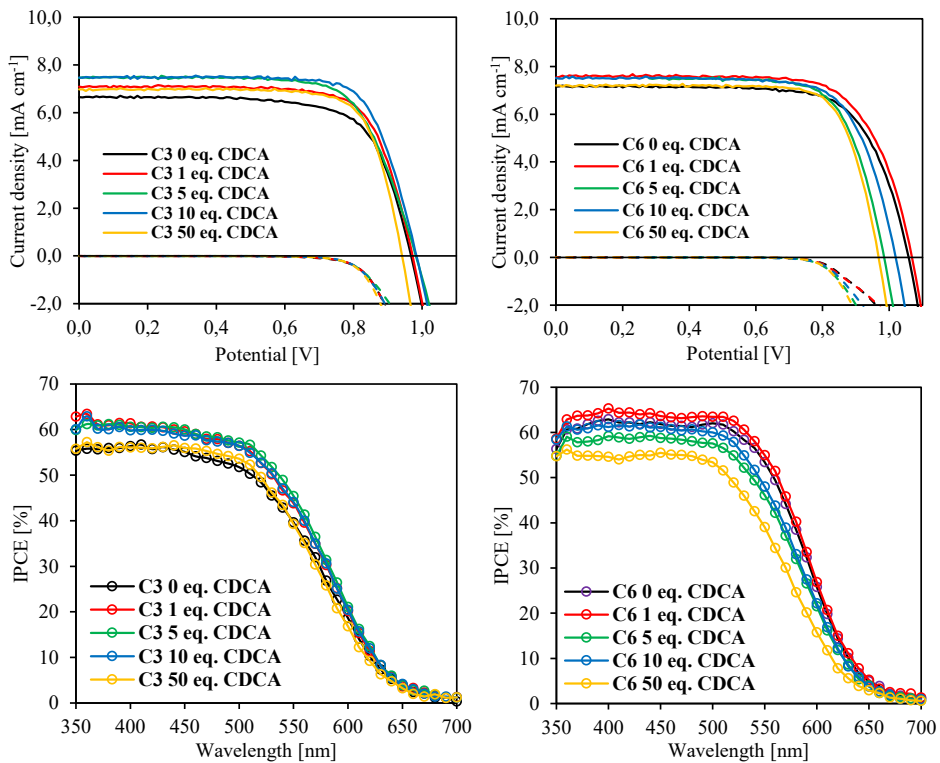
Figure S2. Photovoltaic performance of optimization process of dyes **C3** and **C6** with different amounts of chenodeoxycholic acid (0, 1, 5, 10 and 50 eq. of CDCA).

Figure S3. Photocurrent action spectra of the dyes with CDCA substituents, with different additional CDCA concentrations and thickness of TiO_2.

Table S1. Dye loading experiments for a selection of staining solutions and film TiO_2 film thicknesses.

Dye	ε [M^{-1} cm^{-1}] [a]	CDCA [eq.]	TiO_2 [μm]	Dye loading[b] [10^{-8} mol cm^{-2}]
C_3	34700	10	4 + 2	8.52 ± 0.33
C_6	36300	10	4 + 2	6.86 ± 0.03
C_3-CDCA	31200	0	4 + 2	6.17 ± 0.07
		0	8 + 4	10.65 ± 0.12
		10	4 + 2	4.66 ± 0.19
		10	8 + 4	7.70 ± 0.49
C_6-CDCA	33500	0	4 + 2	5.48 ± 0.11
		0	8 + 4	9.51 ± 0.20
		10	4 + 2	4.21 ± 0.21
		10	8 + 4	6.54 ± 0.19

[a] Average extinction coefficient from two solutions of dye in 40 mM TBAOH in stabilized THF.

[b] Average of two stained electrodes separately desorbed.

Synthesis details

Materials and reagents: All reactions were carried out under nitrogen atmosphere, and all synthesis reagents were acquired from Sigma Aldrich.

Analytical instruments: NMR spectroscopy (^{1}H and ^{13}C) was recorded on 400 and 600 MHz Bruker instruments, and all chemical shifts are reported relative to the respective solvent signals. Mass determination was performed on a Waters "Synapt G2-S" QTOF instrument in positive and negative modes. UV-vis spectra were recorded on a Hitachi U-1900 instrument using quarts cuvettes for the solution samples, while fluorescence spectroscopy was recorded on an Edinburgh instruments FS5 Spectrofluorometer. Infrared spectra were recorded on a Bruker Alpha FT-IR spectrometer with an ATR module.

Synthesis of 1-bromo-2,4-bis(hexyloxy)benzene (1)[46]
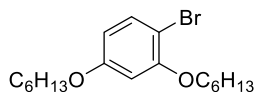
4-Bromoresorcinol (3.00 g, 15.9 mmol) and KOH (2.42 g, 43.1 mmol) were dissolved in DMSO (20 mL), before 1-bromohexane (6.7 mL, 47.7 mmol) was added. The resulting mixture was stirred at room temperature overnight. The product was extracted from DMSO using pentane (4 × 40 mL), the combined pentane phases were washed with water (4 × 40 mL), before drying with brine solution (40 mL) and ultimately dried over anhydrous Na_2SO_4. The pentane phase was then filtered, and the solvents were removed *in vacuo*. The crude product was purified by silica gel column chromatography (dichloromethane/*n*-pentane, 1:4, R_f = 0.27). Compound **1** was isolated as a clear oil (5.29 g, 14.8 mmol, 93%). ^{1}H NMR (400 MHz, DMSO-d_6) δ: 7.39 (d, J = 8.7 Hz, 1H), 6.62 (d, J = 2.6 Hz, 1H), 6.46 (dd, J = 8.7, 2.7 Hz, 1H), 4.01 (t, J = 6.4 Hz, 2H), 3.94 (t, J = 6.5 Hz, 2H), 1.74-1.64 (m, 4H), 1.47-1.35 (m, 4H), 1.34-1.26 (m, 8H), 0.89-0.85 (m, 6H).

Synthesis of *N*-(2',4'-dipropoxy-[1,1'-biphenyl]-4-yl)-*N*-phenyl-2',4'-dipropoxy-[1,1'-biphenyl]-4-amine (2)
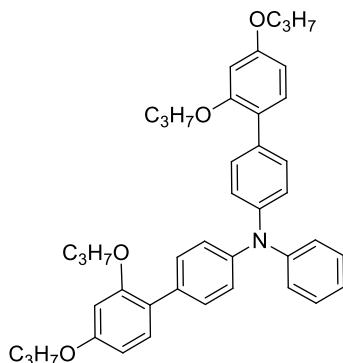
4-Bromo-*N*-(4-bromophenyl)-*N*-phenylaniline (1.00 g, 0.992 mmol), (2,4-dipropoxyphenyl)boronic acid (1.48 g, 5.55 mmol), Pd(OAc)$_2$ (22 mg, 0.098 mmol), SPhos (81 mg, 0.197 mmol) and K$_2$CO$_3$ (1.37 g, 9.9 mmol) were mixed. 1,4-Dioxane (8 mL) and water (8 mL) were degassed and added under nitrogen. The reaction mixture was heated to 80 °C and left stirring for 20 hours before cooling to room temperature. Water (40 mL) was added and the aqueous phase extracted by ethyl acetate (3 × 40 mL). The combined organic phases were dried with brine (40 mL) and over anhydrous Na$_2$SO$_4$, filtered and the solvents were removed *in vacuo*. The crude product was purified by silica gel column chromatography (CH$_2$Cl$_2$, R_f = 0.67) to obtain compound **2** as a clear oil (1.45 g, 2.12 mmol, 85%). ^{1}H NMR (400 MHz, CDCl$_3$) δ: 7.46-7.40 (m, 4H), 7.30-7.22 (m, 4H), 7.20-7.16 (m, 2H), 7.15-7.10 (m, 4H), 7.00 (t, *J* = 6.6 Hz, 1H), 6.57-6.51 (m, 4H), 3.98-3.87 (m, 8H), 1.88-1.72 (m, 8H), 1.05 (t, *J* = 7.3 Hz, 6H), 0.98 (t, *J* = 7.3 Hz, 6H); ^{13}C NMR (100 MHz, CDCl$_3$) δ: 159.5 (2C), 157.0 (2C), 148.0, 146.0 (2C), 132.7 (2C), 130.8 (2C), 130.1 (4C), 129.1 (2C), 124.2 (2C), 123.5 (4C), 123.1 (2C), 122.4, 105.4 (2C), 100.5 (2C), 70.0 (2C), 69.6 (2C), 22.7 (2C), 22.6 (2C), 10.8 (2C), 10.6 (2C); IR (neat, cm^{-1}) ν: 2963 (w), 2935 (w), 2875 (w), 1602 (m), 1491 (s), 1468 (m), 1243 (s), 1180 (s), 1132 (m), 908 (w), 731 (w); HRMS (ASAP+, *m/z*): HRMS (ASAP+, *m/z*): found 630.3574 (calcd. C$_{42}$H$_{48}$NO$_4$ 630.3583, [M+H]$^+$).

Synthesis of *N*-(2',4'-bis(hexyloxy)-[1,1'-biphenyl]-4-yl)-2',4'-bis(hexyloxy)-*N*-phenyl-[1,1'-biphenyl]-4-amine (3)
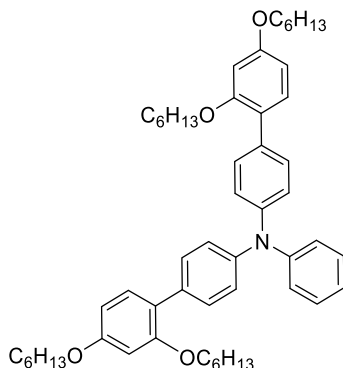
Compound **1** (1.98 g, 5.54 mmol), PdCl$_2$(CH$_3$CN)$_2$ (43 mg, 0.17 mmol) and SPhos (136 mg, 0.33 mmol) were added to a two-neck round-bottom flask before it was evacuated, and a N$_2$-atmosphere established. Dry 1,4-dioxane (15 mL) was used to dissolve the compounds and the reaction mixture was stirred at rt. before 4,4,5,5-tetramethyl-1,3,2-dioxaborolane (1.7 mL, 11.7 mmol) and dry triethyl amine (2.4 mL, 17.2 mmol) were added. The reaction mixture was heated to 110 °C and left stirring for 90 minutes before cooling to room temperature. The reaction mixture was filtered through Celite using ethyl acetate as eluent, the solvents were removed *in vacuo*. The crude mixture obtained was a yellow oil and was used without further purification.

The aforementioned crude product was added to a single neck round-bottom flask along with 4-bromo-*N*-(4-bromophenyl)-*N*-phenylaniline (0.90 g, 2.23 mmol), Pd(OAc)$_2$ (24 mg, 0.11 mmol), SPhos (81 mg, 0.20 mmol) and K$_2$CO$_3$ (1.23 g, 8.90 mmol). 1,4-Dioxane (8 mL) and

water (8 mL) were degassed and added under nitrogen. The reaction mixture was heated to 80 °C and stirred for 24 hours before cooling to room temperature. Water (50 mL) was added and the aqueous phase extracted by dichloromethane (3 × 50 mL). The combined organic phases were dried over anhydrous Na_2SO_4, filtered and the solvents were removed *in vacuo*. The crude product was purified by silica gel column chromatography (dichloromethane/*n*-pentane, 1:4, R_f = 0.19) and recrystallized from acetonitrile to yield compound **3** as a white solid (1.11 g, 1.38 mmol, 62%). ^{1}H NMR (400 MHz, CDCl3) δ: 7.45-7.40 (m, 4H), 7.28-7.22 (m, 4H), 7.20-7.16 (m, 2H), 7.15-7.10 (m, 4H), 7.00 (t, *J* = 6.8 Hz, 1H), 6.56-6.51 (m, 4H), 4.00-3.92 (m, 8H), 1.84-1.69 (m, 8H), 1.52-1.44 (m, 4H), 1.44-1.23 (m, 20H), 0.91 (t, *J* = 7.1 Hz, 6H), 0.86 (t, *J* = 6.9 Hz, 6H); ^{13}C NMR (100 MHz, CDCl3) δ: 159.5 (2C), 157.0 (2C), 148.0, 146.0 (2C), 132.7 (2C), 130.8 (2C), 130.1 (4C), 129.1 (2C), 124.2 (2C), 123.5 (4C), 123.1 (2C), 122.4, 105.3 (2C), 100.4 (2C), 68.4 (2C), 68.1 (2C), 31.6 (2C), 31.5 (2C), 29.3 (2C), 29.1 (2C), 25.78 (2C), 25.76 (2C), 22.63 (2C), 22.57 (2C), 14.1 (2C), 14.0 (2C). IR (neat, cm[-1]) ν: 2927 (m), 2857 (m), 1603 (m), 1491 (s), 1467 (m), 1271 (s), 1178 (s), 1134 (m), 1045 (m), 835 (m). HRMS (ASAP+, *m/z*): HRMS (ASAP+, *m/z*): found 798.5456 (calcd. $C_{54}H_{72}NO_4$ 798.5461, [M+H]$^+$).

Synthesis of *N*-(4-bromophenyl)-*N*-(2',4'-dipropoxy-[1,1'-biphenyl]-4-yl)-2',4'-dipropoxy-[1,1'-biphenyl]-4-amine (4)
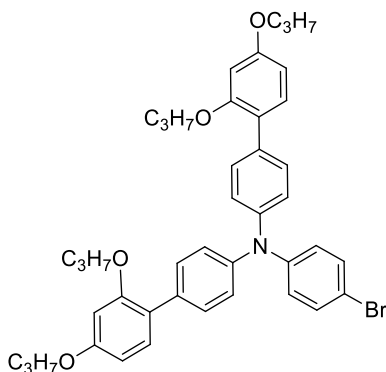
Compound **2** (0.65 g, 1.03 mmol) and NBS (0.19 g, 1.08 mmol) were added to a round-bottom flask under dark conditions. Dichloromethane (20 mL) was degassed and added under nitrogen at 0 °C. The reaction mixture was then allowed to warm to rt. while stirring for 5 hours. Water (40 mL) was added and the aqueous phase was extracted using dichloromethane (3 × 20 mL). The combined organic phases were dried over anhydrous Na_2SO_4, filtered and the solvents were removed *in vacuo*. The crude product was purified by silica gel column chromatography (dichloromethane, R_f = 0.74). Compound **4** was isolated as a clear oil (0.60 g, 0.85 mmol, 82%). ^{1}H NMR (400 MHz, CDCl3) δ: 7.45-7.41 (m, 4H), 7.36-7.31 (m, 2H), 7.27-7.23 (m, 2H), 7.14-7.09 (m, 4H), 7.07-7.02 (m, 2H), 6.56-6.51 (m, 4H), 3.97-3.89 (m, 8H), 1.88-1.73 (m, 8H), 1.05 (t, *J* = 7.0 Hz, 6H), 0.99 (t, *J* = 7.0 Hz, 6H); ^{13}C NMR (100 MHz, CDCl3) δ: 159.6 (2C), 157.0 (2C), 147.2, 145.5 (2C), 133.3 (2C), 132.0 (2C), 130.9 (2C), 130.3 (4C), 125.2 (2C), 123.7 (4C), 122.9 (2C), 114.4, 105.4 (2C), 100.4 (2C), 70.0 (2C), 69.6 (2C), 22.7 (2C), 22.6 (2C), 10.7 (2C), 10.6 (2C); IR (neat, cm[-1]) ν: 2962 (w), 2934 (w),

2874 (w), 1605 (m), 1580 (m), 1485 (s), 1269 (s), 1180 (s), 1133 (m), 1002 (m), 795 (m), 731 (m); HRMS (ASAP+, *m/z*): HRMS (ASAP+, *m/z*): found 708.2681 (calcd. $C_{42}H_{47}NO_4Br$ 708.2688, $[M+H]^+$).

Synthesis of *N*-(2',4'-bis(hexyloxy)-[1,1'-biphenyl]-4-yl)-N-(4-bromophenyl)-2',4'-bis(hexyloxy)-[1,1'-biphenyl]-4-amine (5)[47]
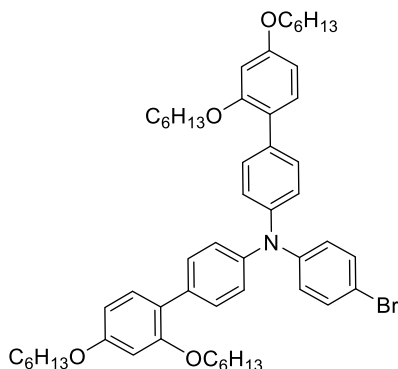
Compound **3** (1.00 g, 1.25 mmol) and NBS (0.22 g, 1.25 mmol) were added to a round-bottom flask under dark conditions. Dichloromethane (25 mL) was degassed and added under nitrogen at 0 °C. The reaction mixture was then allowed to warm to room temperature while stirring for 15 hours. Water (40 mL) was added and the aqueous phase was extracted using dichloromethane (3 × 30 mL). The combined organic phases were dried over anhydrous Na_2SO_4, filtered and the solvents were removed *in vacuo*. The crude product was purified by silica gel column chromatography (dichloromethane, R_f = 0.8). Compound **5** was isolated as a clear oil (0.99 g, 1.12 mmol, 90%). ^{1}H NMR (400 MHz, CDCl$_3$) δ: 7.46-7.41 (m, 4H), 7.35-7.30 (m, 2H), 7.27-7.23 (m, 2H), 7.14-7.08 (m, 4H), 7.06-7.02 (m, 2H), 6.56-6.51 (m, 4H), 4.00-3.92 (m, 8H), 1.84-1.70 (m, 8H), 1.52-1.44 (m, 4H), 1.44-1.25 (m, 20H), 0.91 (t, *J* = 6.5 Hz, 6H), 0.87 (t, *J* = 6.5 Hz, 6H); ^{13}C NMR (100 MHz, CDCl$_3$) δ: 159.6 (2C), 157.0 (2C), 147.2, 145.5 (2C), 133.3 (2C), 132.0 (2C), 130.8 (2C), 130.3 (4C), 125.1 (2C), 123.7 (4C), 122.9 (2C), 114.4, 105.3 (2C), 100.3 (2C), 68.4 (2C), 68.1 (2C), 31.6 (2C), 31.5 (2C), 29.3 (2C), 29.1 (2C), 25.78 (2C), 25.76 (2C), 22.64 (2C), 22.58 (2C), 14.1 (2C), 14.0 (2C); IR (neat, cm^{-1}) ν: 2928 (m), 2858 (m), 1606 (m), 1581 (m), 1487 (s), 1468 (m), 1281 (m), 1180 (m), 1135 (w); HRMS (ASAP+, *m/z*): HRMS (ASAP+, *m/z*): found 876.4559 (calcd. $C_{54}H_{71}NO_4Br$ 876.4566, $[M+H]^+$).

Synthesis of methyl (4*S*)-4-((3*S*,7*S*,8*S*,9*R*,10*R*,13*S*,14*R*,17*S*)-3,7-dihydroxy-10,13-dimethylhexadecahydro-1*H*-cyclopenta[*a*]phenanthren-17-yl)pentanoate (6)[48]
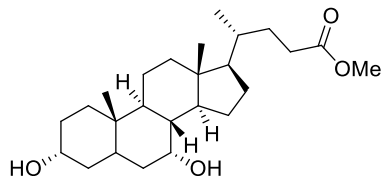
Chenodeoxycholic acid (10.0 g, 25.5 mmol) was dissolved in methanol (300 mL), and while stirring, conc. H_2SO_4 (1.5 mL) was added slowly. Then, the reaction mixture was stirred at room temperature for 1 hour. The reaction mixture was poured into aqueous $NaHCO_3$ solution (0.5 M, 150 mL) and extracted with ethyl acetate (3 × 150 mL). Upon removal of the solvents *in vacuo*, compound **6** was obtained as white solid (10.1 g, 24.7 mmol, 97%), mp 69-73 °C (lit.[48] 85.2-86.0 °C). ^{1}H NMR (400 MHz, DMSO-d_6) δ: 4.31 (d, *J* = 4.7 Hz, 1H), 4.11 (d, *J* = 3.7 Hz, 1H), 3.64-3.60 (m, 1H), 3.57 (s, 3H), 3.23-3.13 (m, 1H), 2.37-2.27 (m, 1H), 2.25-2.13 (m, 2H), 1.93-1.61 (m, 7H), 1.50-0.95 (m, 16H), 0.88 (d, *J* = 6.5 Hz, 3H), 0.83 (s, 3H), 0.60 (s, 3H); HRMS (ESI+, *m/z*): found 371.2946 (calcd. $C_{25}H_{42}O_4Na$ 429.2981, [M+Na]+).

Synthesis of methyl (4*S*)-4-((3*S*,7*S*,8*S*,9*R*,10*R*,13*S*,14*R*,17*S*)-3,7-bis((tert-butyldimethylsilyl)oxy)-10,13-dimethylhexadecahydro-1*H*-cyclopenta[*a*]phenanthren-17-yl)pentanoate (7)
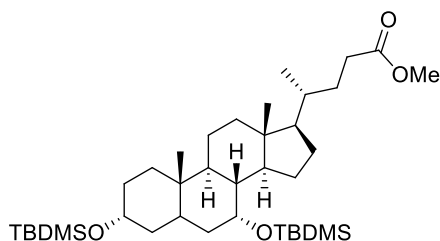
Compound **6** (6.00 g, 14.8 mmol), 2,6-lutidine (17.2 mL, 148 mmol) and dichloromethane (216 mL) were added to a flask at 0 °C under nitrogen atmosphere. *tert*-Butyl dimethylsilyltrifluoromethanesulphonate (10.2 mL, 44.3 mmol) was added and the reaction was stirred for 22 hours. The reaction mixture was quenched in aqueous $NaHSO_4$ solution (1 M, 150 mL) and the water phase was extracted with CH_2Cl_2 (3 × 150 mL). The combined organic phases were washed with aqueous $NaHSO_4$ solution (1 M, 3 × 100 mL) and brine (100 mL), then dried over anhydrous Na_2SO_4. Compound **7** was obtained as a clear oil (9.30 g, 14.6 mmol, 99%) upon the removal of the solvents *in vacuo*. The material contained a *tert*-butyl trimethylsilyl containing impurity of unknown structure. ^{1}H NMR (400 MHz, acetone-d_6) δ: 3.89-3.89 (m, 1H), 3.60 (s, 3H), 3.53-3.45 (m, 1H), 2.39-2.29 (m, 2H), 2.26-2.18 (m, 1H), 2.03-1.01 (m, 20H), 0.97-0.92 (m, 15H), 0.90-0.87 (m, 12H), 0.69 (s, 3H), 0.15 (s, 3H), 0.10 (s, 3H), 0.053 (s, 3H), 0.046 (s, 3H); ^{13}C NMR (100 MHz, acetone-d_6) δ: 174.5, 73.3, 70.6, 56.9, 51.5, 51.0, 43.2, 42.7, 41.6, 41.4, 40.6, 36.3, 36.2, 35.8, 35.3, 33.3, 31.89, 31.86,

31.5, 28.7, 26.6 (3C), 26.2 (3C), 24.6, 23.3, 21.3, 19.0, 18.7, 18.6, 12.3, -1.9, -4.37, -4.40, -5.4; IR (neat, cm^{-1}) ν: 2952 (m), 2929 (m), 2855 (m), 1739 (m), 1462 (m), 1436 (m), 1373 (m), 1263 (s), 1252 (s), 1088 (s), 1026 (s), 834 (s), 770 (s), 736 (s), 701 (s); HRMS (ASAP+, *m/z*): found 657.4713 (calcd. $C_{37}H_{70}O_4NaSi_2$ 657.4710, [M+Na]$^+$).

Synthesis of (4*S*)-4-((3*S*,7*S*,8*S*,9*R*,10*R*,13*S*,14*R*,17*S*)-3,7-bis((tert-butyldimethylsilyl)oxy)-10,13-dimethylhexadecahydro-1*H*-cyclopenta[*a*]phenanthren-17-yl)pentan-1-ol (8)[49]
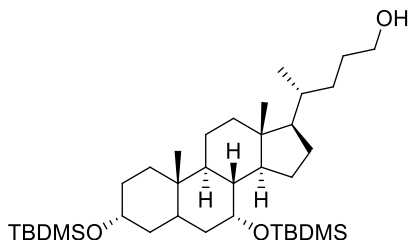
Compound **7** (9.00 g, 14.2 mmol) was dissolved in THF (210 mL) under nitrogen atmosphere at 0 °C. Lithium aluminium hydride in THF solution (2 M, 21.2 mL, 42.5 mmol) was added, and the reaction was stirred for 19 hours while reaching room temperature, before work-up by a modified Fieser work-up procedure. Addition of water (1.6 mL) causing vigorous bubbling, then aqueous NaOH (4 M, 1.6 mL) was added which formed a white granulate. Water (5 mL) was added and the reaction mixture was stirred for 10 minutes, before addition of anhydrous Na$_2$SO$_4$ and 10 minutes stirring before removal of solids by filtration. The solvents were removed *in vacuo* to yield compound **8** as a white solid (8.43 g, 13.9 mmol, 98%), mp 116-117 °C (lit. not reported). ^{1}H NMR (400 MHz, acetone-d_6) δ: 3.89-3.88 (m, 1H), 3.52-3.46 (m, 3H), 3.36 (t, *J* = 5.4 Hz, 0.5H*), 2.39-2.29 (m, 1H), 2.01-1.01 (m, 24H), 0.96-0.93 (m, 15H), 0.88 (s, 10H), 0.69 (s, 3H), 0.15 (s, 3H), 0.10 (s, 3H), 0.052 (s, 3H), 0.045 (s, 3H); ^{13}C NMR (100 MHz, acetone-d_6) δ: 72.3, 69.6, 62.0, 61.9, 56.3, 50.0, 42.1, 41.7, 40.6, 40.4, 39.7, 35.7, 35.2, 34.8, 34.3, 32.4, 32.0, 30.9, 27.8, 25.6 (3C), 25.2 (3C), 23.6, 22.3, 20.3, 18.2, 18.0, 17.6, 11.3, -2.9, -5.38, -5.42, -6.4; IR (neat, cm^{-1}) ν: 3324 (w (br), OH), 2928 (s), 2855 (s), 1462 (m), 1373 (m), 1251 (s), 1091 (s), 1026 (s), 930 (s), 834 (s), 770 (s); HRMS (ESI+, *m/z*): found 629.4751 (calcd. $C_{36}H_{70}O_3NaSi_2$ 629.4761, [M+Na]$^+$). * Exchange of protons observed for OH.

Synthesis of 5-(thiophen-2-yl)furan-2-carbaldehyde (12)[50]
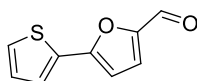
2-Bromothiophene (842 mg, 5.16 mmol), (5-formylfuran-2-yl)boronic acid (1.08 g, 7.75 mmol), PdCl$_2$(dppf) (113 mg, 0.155 mmol) and K$_2$CO$_3$ (2.86 g, 20.7 mmol) were mixed, and degassed water (18 mL) and degassed 1,4-dioxane (18 mL) were added under nitrogen

atmosphere. The reaction was heated to 80 ºC and stirred for 24 hours. Upon cooling to room temperature, the solvents were removed from the reaction mixture *in vacuo*, then deionized water (30 mL) and ethyl acetate (30 mL) were added and the phases separated. The aqueous phase was extracted with ethyl acetate (3 × 50 mL) before the combined organic phases were washed with brine (50 mL), dried over anhydrous Na_2SO_4, filtered and the solvents were removed *in vacuo*. The crude product was purified by silica gel column chromatography (*n*-pentane/ethyl acetate 1:1, R_f = 0.60) to yield compound **12** as a yellow oil (445 mg, 2.502 mmol, 48%). ^{1}H NMR (400 MHz, acetone-d_6) δ: 9.63 (s, 1H), 7.67 (dd, *J* = 5.0, 1.1 Hz, 1H), 7.64 (dd, *J* = 3.7, 1.0 Hz, 1H), 7.52 (d, *J* = 3.7 Hz, 1H), 7.20 (dd, *J* = 5.0, 3.7 Hz, 1H), 6.98 (d, *J* = 3.7 Hz, 1H); HRMS (ASAP+, *m/z*): found 179.0164 (calcd. $C_9H_7O_2S$ 179.0167, [M+H]$^+$).

Synthesis of 5-(5-bromothiophen-2-yl)furan-2-carbaldehyde (13)[51]
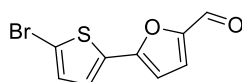
Compound **12** (203 mg, 1.139 mmol) was dissolved in a mixture of chloroform (6 mL) and glacial acetic acid (6 mL) under nitrogen atmosphere at 0 °C. *N*-Bromosuccinimide (NBS) (250 mg, 1.405 mmol) was added and the reaction was stirred under darkness, at 0 °C for 17 hours. Due to incomplete conversion, another portion of NBS (71 mg, 0.399 mmol) was added and the reaction stirred for another 2 hours before water (10 mL) was added and the aqueous phase was extracted by chloroform (3 × 30 mL). The combined organic phases were washed with brine (30 mL), dried over anhydrous Na_2SO_4, filtered and concentrated *in vacuo*. Purification by silica gel column chromatography (*n*-pentane/ethyl acetate 1:1, R_f = 0.57) gave compound **13** as a light brown solid (173 mg, 0.673 mmol, 59%), mp 90-91 °C (lit.[51] 91-92 °C). ^{1}H NMR (400 MHz, acetone-d_6) δ: 9.64 (s, 1H), 7.52 (d, *J* = 3.8 Hz, 1H), 7.46 (d, *J* = 4.0 Hz, 1H), 7.27 (d, *J* = 4.0 Hz, 1H), 7.01 (d, *J* = 3.8 Hz, 1H); HRMS (ASAP+, *m/z*): found 256.9269 (calcd. $C_9H_6O_2S^{79}Br$ 256.9272, [M+H]$^+$).

Synthesis of 5-(5-(4-(bis(2',4'-dipropoxy-[1,1'-biphenyl]-4-yl)amino)phenyl)thiophen-2-yl)furan-2-carbaldehyde (16)
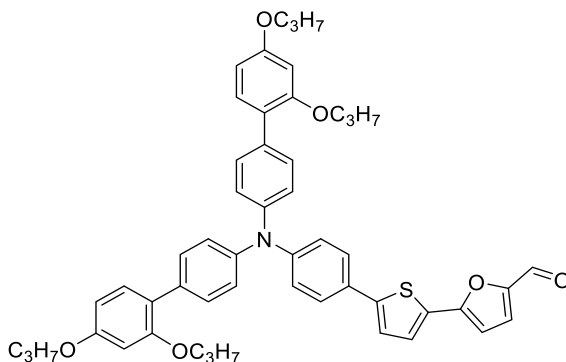
Compound **4** (373 mg, 0.53 mmol), PdCl$_2$(CH$_3$CN)$_2$ (4 mg, 16 µmol) and SPhos (13 mg, 32 µmol) were added to a Schlenk-tube before it was evacuated, and N$_2$-atmosphere established. Dry 1,4-dioxane (1.5 mL) was used to dissolve the compounds and the reaction mixture was stirred at rt. before 4,4,5,5-tetramethyl-1,3,2-dioxaborolane (160 µL, 1.11 mmol) and dry triethyl amine (230 µL, 1.65 mmol) were added. The reaction mixture was heated to 110 °C and left stirring for 60 minutes before cooling to room temperature. The reaction mixture was filtered through Celite using ethyl acetate as eluent, the solvents were removed *in vacuo*. The crude mixture obtained was a yellow oil and was reacted without further purification.

The crude product from the borylation, compound **13** (57 mg, 0.22 mmol), Pd(OAc)$_2$ (2.4 mg, 11 µmol), SPhos (9 mg, 22 µmol) and K$_2$CO$_3$ (122 mg, 0.88 mmol) were mixed. 1,4-Dioxane (4 mL) and water (4 mL) were degassed and added under nitrogen atmosphere. The reaction mixture was heated to 80 °C and left stirring for 16 hours before cooling to room temperature. Water (40 mL) was added and the aqueous phase extracted by dichloromethane (3 × 40 mL). The combined organic phases were dried over anhydrous Na$_2$SO$_4$, filtered and the solvents were removed *in vacuo*. The crude product was purified by silica gel column chromatography (*n*-pentane/dichloromethane, 1:4, R_f = 0.13) to obtain compound **16** as a red solid (72 mg, 89 µmol, 41%), mp 82-84 °C. ^{1}H NMR (400 MHz, CDCl$_3$) δ: 9.60 (s, 1H), 7.52-7.45 (m, 7H), 7.29 (d, J = 3.7 Hz, 1H), 7.28-7.26 (m, 2H), 7.22 (d, J = 4.2 Hz, 1H), 7.20-7.15 (m, 6H), 6.66 (d, J = 4.2 Hz, 1H), 6.57-6.53 (m, 4H), 3.99-3.91 (m, 8H), 1.88-1.74 (m, 8H), 1.06 (t, J = 7.0 Hz, 6H), 1.00 (t, J = 7.0 Hz, 6H); ^{13}C NMR (100 MHz, CDCl$_3$) δ: 176.7, 159.6 (2C), 157.0 (2C), 155.0, 151.4, 148.2 (2C), 147.0, 145.4 (2C), 133.3 (2C), 130.9 (2C), 130.3 (4C), 129.3, 127.4, 126.8, 126.6 (2C), 124.2 (5C), 123.1 (2C), 123.0, 122.9, 107.2, 105.4 (2C), 100.5 (2C), 70.0 (2C), 69.6 (2C), 22.7 (2C), 22.6 (2C), 10.7 (2C), 10.6 (2C); IR (neat, cm^{-1}) ν: 2964 (m), 2876 (m), 1672 (m), 1600 (m), 1517 (s), 1273 (s), 1135 (s), 833 (m); HRMS (ASAP+, *m/z*): found 806.3521 (calcd. C$_{51}$H$_{52}$NO$_6$S 806.3515, [M+H]$^+$).

Synthesis of 5-(5-(4-(bis(2',4'-bis(hexyloxy)-[1,1'-biphenyl]-4-yl)amino)phenyl)thiophen-2-yl)furan-2-carbaldehyde (17)
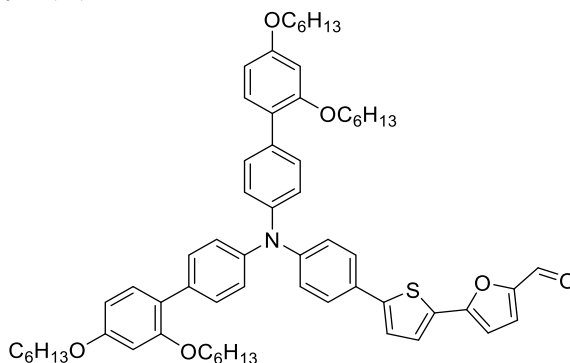
Compound **5** (312 mg, 0.36 mmol), PdCl$_2$(CH$_3$CN)$_2$ (3 mg, 12 µmol) and SPhos (9 mg, 22 µmol) were added to a Schlenk-tube before it was evacuated, and N$_2$-atmosphere established. Dry 1,4-dioxane (1 mL) was used to dissolve the compounds and the reaction mixture was

stirred at rt. before 4,4,5,5-tetramethyl-1,3,2-dioxaborolane (110 µL, 0.75 mmol) and dry triethyl amine (150 µL, 1.10 mmol) were added. The reaction mixture was heated to 110 °C and left stirring for 60 minutes before cooling to room temperature. The reaction mixture was filtered through Celite using ethyl acetate as eluent, the solvents were removed *in vacuo*. The crude mixture obtained was a yellow oil and was reacted without further purification.

The crude product from the borylation, compound **13** (57 mg, 0.222 mmol), Pd(OAc)$_2$ (2.5 mg, 0.011 mmol), SPhos (9.1 mg, 0.022 mmol) and K$_2$CO$_3$ (188 mg, 1.36 mmol) were mixed. 1,4-Dioxane (4 mL) and water (4 mL) were degassed and added under nitrogen atmosphere. The reaction mixture was heated to 80 °C and left stirring for 17 hours before cooling to room temperature. Water (40 mL) was added and the aqueous phase extracted by ethyl acetate (3 × 40 mL). The combined organic phases were dried with brine (40 mL) and over anhydrous Na$_2$SO$_4$, filtered and the solvents were removed *in vacuo*. The crude product was purified by silica gel column chromatography (CH$_2$Cl$_2$, R_f = 0.39) to obtain compound **17** as a red resin (135 mg, 0.138 mmol, 62%). ^{1}H NMR (600 MHz, CDCl$_3$) δ: 9.60 (s, 1H), 7.50-7.44 (m, 7H), 7.29 (d, J = 3.8 Hz, 1H), 7.27-7.25 (m, 2H), 7.22 (d, J = 3.9 Hz, 1H), 7.18-7.15 (m, 6H), 6.66 (d, J = 3.8 Hz, 1H), 6.56-6.53 (m, 4H), 4.00-3.95 (m, 8H), 1.83-1.72 (m, 8H), 1.51-1.45 (m, 4H), 1.44-1.39 (m, 4H), 1.38-1.34 (m, 8H), 1.32-1.28 (m, 8H), 0.92 (t, J = 7.8 Hz, 6H), 0.87 (t, J = 7.3 Hz, 6H); ^{13}C NMR (150 MHz, CDCl$_3$) δ: 176.7, 159.6 (2C), 157.0 (2C), 155.0, 151.4, 148.3 (2C), 147.0, 145.3 (2C), 133.6 (2C), 130.9 (2C), 130.3 (4C), 129.3, 127.4, 126.7, 126.6 (2C), 124.2 (5C), 123.1 (2C), 122.92, 122.88, 107.2, 105.3 (2C), 100.4 (2C), 68.4 (2C), 68.1 (2C), 31.6 (2C), 31.5 (2C), 29,3 (2C), 29.1 (2C), 25.78 (2C), 22.76 (2C), 22.63 (2C), 22.58 (2C), 14.0 (4C); IR (neat, cm^{-1}) ν: 2952 (m), 2858 (m), 1674 (m), 1601 (m), 1491 (s), 1287 (s), 1182 (s), 833 (m); HRMS (ASAP+, *m/z*): found 974.5391 (calcd. C$_{63}$H$_{76}$NO$_6$S 974.5393, [M+H]$^+$).

Synthesis of (*E*)-3-(5-(5-(4-(bis(2',4'-dipropoxy-[1,1'-biphenyl]-4-yl)amino)phenyl)thiophen-2-yl)furan-2-yl)-2-cyanoacrylic acid (Dye C$_3$)
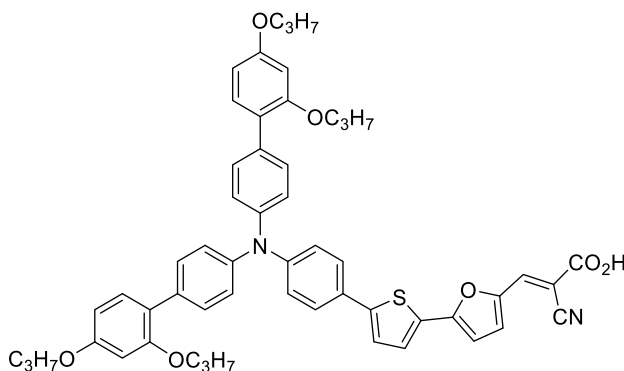
Compound **16** (59 mg, 73 µmol) and cyanoacetic acid (125 mg, 1.46 mmol) were dissolved in degassed acetonitrile (17 mL) under nitrogen atmosphere. Piperidine (87 µL, 75 mg, 0.88

mmol) was added and the reaction was heated to 80 °C for 1 hour before cooling to room temperature and quenched in HCl (4 M, 30 mL). Dichloromethane (50 mL) was added and the organic phase was washed with water (4 × 100 mL), then dried over anhydrous Na_2SO_4, filtered and the solvents were removed *in vacuo*. The crude product was purified by silica gel column chromatography (gradient: 0-15% MeOH in CH_2Cl_2), the dye-containing fractions were washed with HCl (1 M, 2 × 30 mL) to obtain sensitizer **C₃** as a dark solid (58 mg, 66 μmol, 91%), mp 125-127 °C (dec. 178 °C). ^{1}H NMR (600 MHz, CD_2Cl_2) δ: 8.00-7.96 (m, 1H), 7.58-7.51 (m, 3H), 7.50-7.46 (m, 4H), 7.42-7.36 (m, 1H), 7.30-7.22 (m, 3H), 7.19-7.11 (m, 6H), 6.81-6.75 (m, 1H), 6.58-6.52 (m, 4H), 3.97-3.91 (m, 8H), 1.84-1.75 (m, 8H), 1.05 (t, J = 7.5 Hz, 6H), 1.00 (t, J = 7.4 Hz, 6H) (CO₂$\underline{H}$ proton missing); ^{13}C NMR (150 MHz, CD_2Cl_2) δ: 168.1, 160.3 (2C), 157.6 (2C), 156.6, 148.9, 148.4, 147.9, 145.9 (2C), 138.9, 134.4 (2C), 131.4 (4C), 130.9 (4C), 129.6, 129.1, 127.2 (2C), 124.8 (4C), 124.0, 123.4 (2C), 123.2 (2C), 116.3, 109.8, 106.1 (2C), 100.8 (2C), 95.1, 70.6 (2C), 70.2 (2C), 23.2 (2C), 23.1 (2C), 11.1 (2C), 10.9 (2C); IR (neat, cm^{-1}) ν: 3030 (m), 2963 (m), 2932 (m), 2874 (m), 2218 (w), 1687 (w), 1601 (m), 1555 (m), 1474 (s), 1267 (m), 1181 (s), 1025 (m), 793 (m); HRMS (TOF MS ES+, *m/z*): found 873.3561 (calcd. $C_{54}H_{53}N_2O_7S$ 873.3573, [M+H]$^+$).

Synthesis of (*E*)-3-(5-(5-(4-(bis(2',4'-bis(hexyloxy)-[1,1'-biphenyl]-4-yl)amino)phenyl)thiophen-2-yl)furan-2-yl)-2-cyanoacrylic acid (Dye C$_6$)
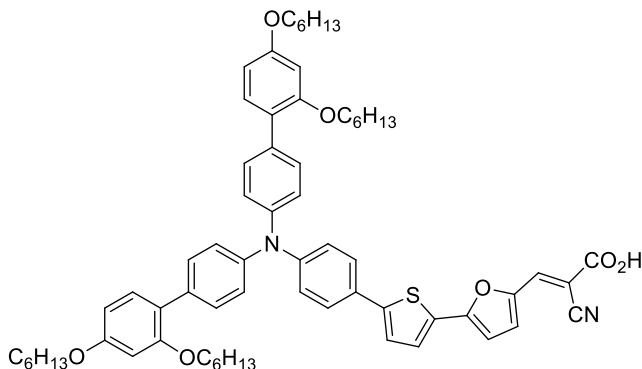
Compound **17** (110 mg, 0.11 mmol) and cyanoacetic acid (192 mg, 2.26 mmol) were dissolved in degassed acetonitrile (26 mL) under nitrogen atmosphere. Piperidine (134 µL, 115 mg, 1.35 mmol) was added and the reaction was heated to 80 °C for 1 hour before cooling to room temperature and quenched in HCl (4 M, 50 mL). Dichloromethane (100 mL) was added and the organic phase was washed with water (4 × 100 mL), then dried over anhydrous Na$_2$SO$_4$, filtered and the solvents were removed *in vacuo*. The crude product was purified by silica gel column chromatography (gradient: 0-20% MeOH in CH$_2$Cl$_2$), the dye-containing fractions were washed with HCl (1 M, 2 × 20 mL) to obtain sensitizer **C$_6$** as a dark solid (96 mg, 92 µmol, 82%), mp 97-99 °C (dec. 142 °C). ^{1}H NMR (600 MHz, CD$_2$Cl$_2$) δ: 8.00-7.97 (m, 1H), 7.60-7.58 (m, 1H), 7.57-7.52 (m, 2H), 7.50-7.46 (m, 4H), 7.44-7.37 (m, 1H), 7.33-7.22 (m, 4H), 7.21-7.10 (m, 5H), 6.82-6.79 (m, 1H), 6.57-6.53 (m, 4H), 4.00-3.96 (m, 8H), 1.82-1.73 (m, 8H), 1.51-1.46 (m, 4H), 1.45-1.41 (m, 4H), 1.38-1.34 (m, 8H), 1.33-1.29 (m, 8H), 0.92 (t, J = 7.1 Hz, 6H), 0.88 (t, J = 7.0 Hz, 6H) (CO$_2$<u>H</u> proton missing); ^{13}C NMR (150 MHz, CD$_2$Cl$_2$) δ: 168.0, 160.4 (2C), 157.6 (2C), 156.7, 149.1, 148.6, 147.9, 145.8 (2C), 139.0, 134.5 (2C), 131.3 (4C), 130.9 (4C), 129.6, 129.2, 127.2 (2C), 124.9 (4C), 124.0, 123.3 (2C), 123.1 (2C), 116.2, 109.8, 106.0 (2C), 100.8 (2C), 95.0, 69.0 (2C), 68.7 (2C), 32.2 (2C), 32.1 (2C), 29.9 (2C), 29.7 (2C), 26.4 (2C), 26.3 (2C), 23.21 (2C), 23.17 (2C), 14.40 (2C), 10.38 (2C); IR (neat, cm^{-1}) ν: 3400 (br), 3031 (w), 2926 (m), 2856 (m), 222 (w), 1685 (m), 1599 (s), 1492 (s), 1418 (s), 1286 (s), 1025 (s), 792 (m), 705 (m); HRMS (ASAP+, *m/z*): found 997.5543 (calcd. C$_{65}$H$_{77}$N$_2$O$_5$S 997.5553, [M-CO$_2$+H]$^+$).

NMR
Compound 1
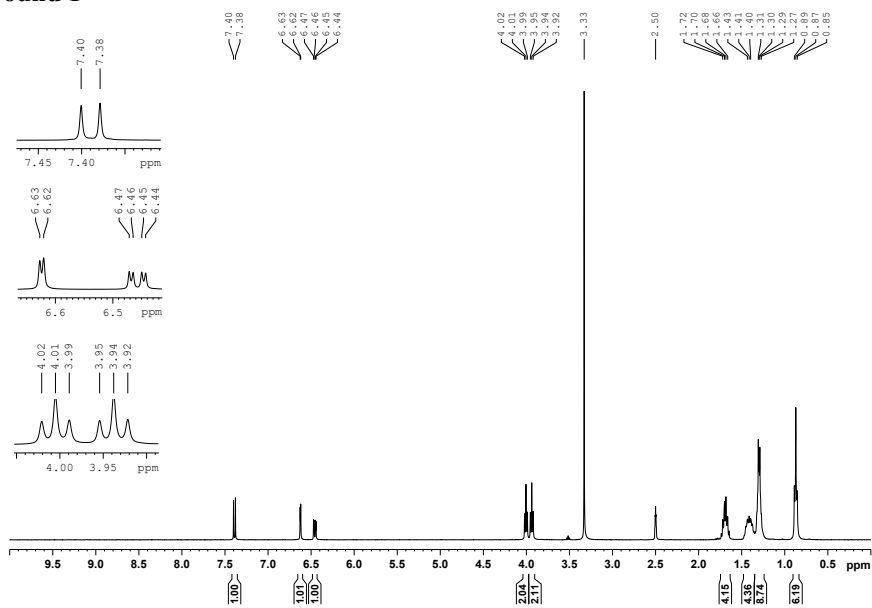
Figure S4. ^{1}H NMR (400 MHz, DMSO-d_6) spectrum for compound **1**.

Compound 2

Figure S5. ^{1}H NMR (400 MHz, CDCl$_3$) spectrum for compound **2**.

Figure S6. ^{1}H NMR (100 MHz, CDCl$_3$) spectrum for compound **2**.

Compound 3

Figure S7. ^{1}H NMR (400 MHz, CDCl$_3$) spectrum for compound **3**.

Figure S8. ^{13}C NMR (100 MHz, CDCl$_3$) spectrum for compound **3**.
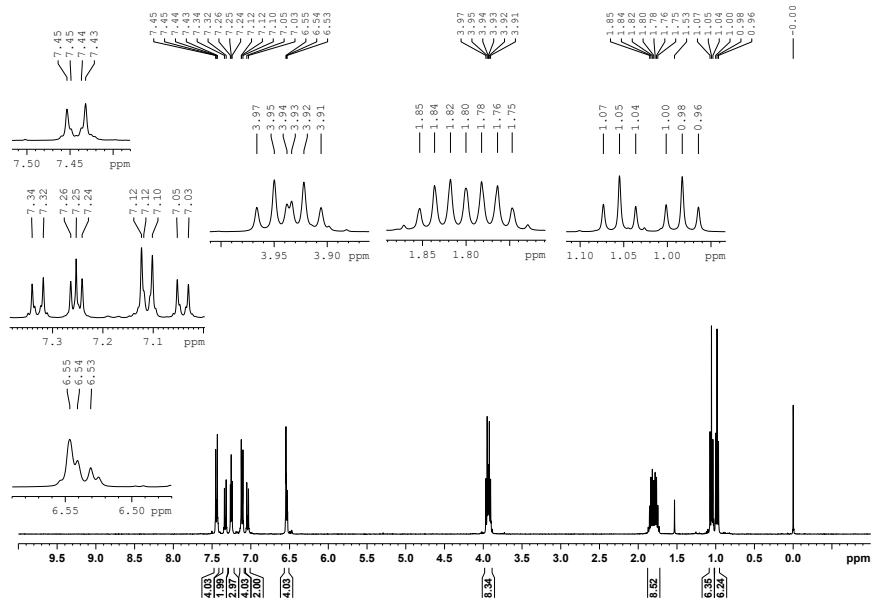
Compound 4

Figure S9. ^{1}H NMR (400 MHz, CDCl$_3$) spectrum for compound **4**.
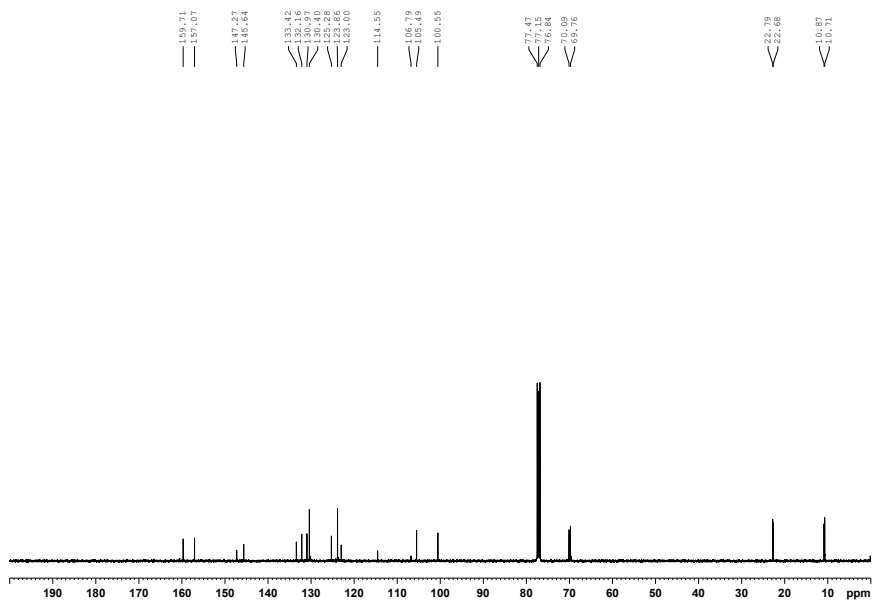
Figure S10. ^{13}C NMR (100 MHz, CDCl$_3$) spectrum for compound **4**.

Compound 5
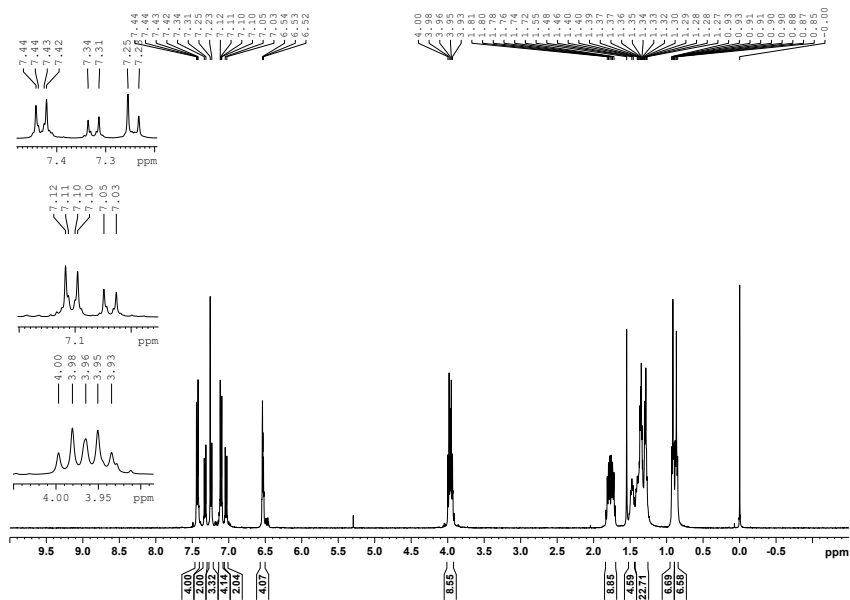
Figure S11. ^{1}H NMR (400 MHz, CDCl$_3$) spectrum for compound **5**.
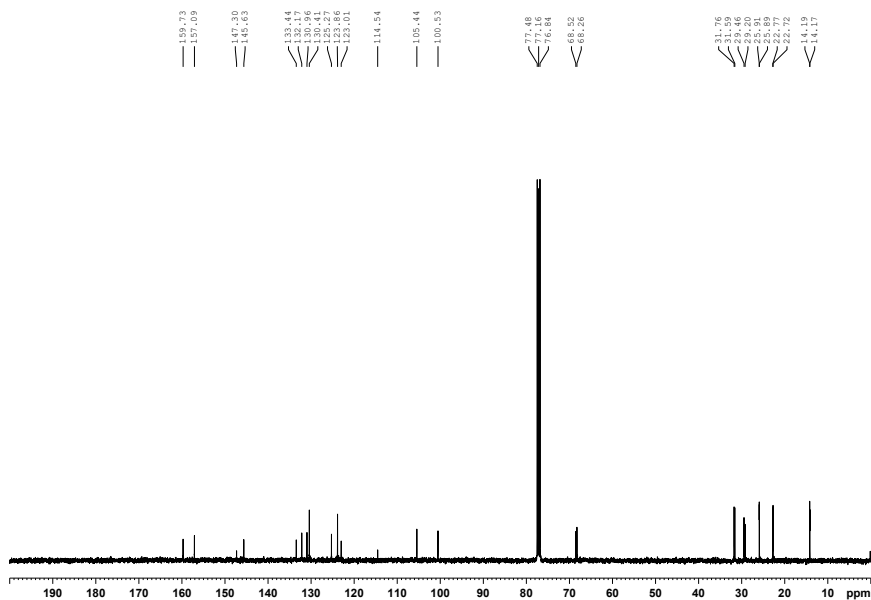
Figure S12. ^{13}C NMR (100 MHz, CDCl$_3$) spectrum for compound **5**.

Compound 6
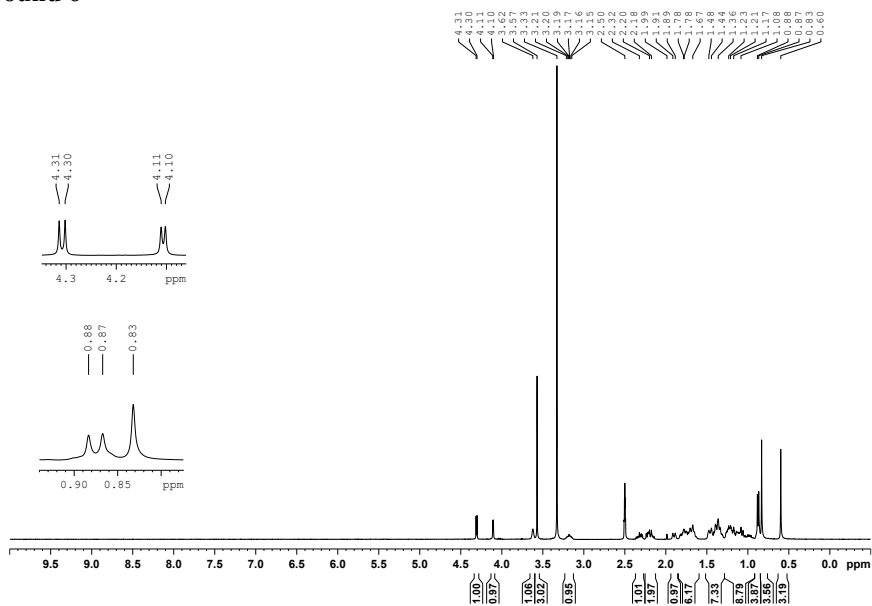
Figure S13. ^{1}H NMR (400 MHz, DMSO-d_6) spectrum for compound **6**.

Compound 7
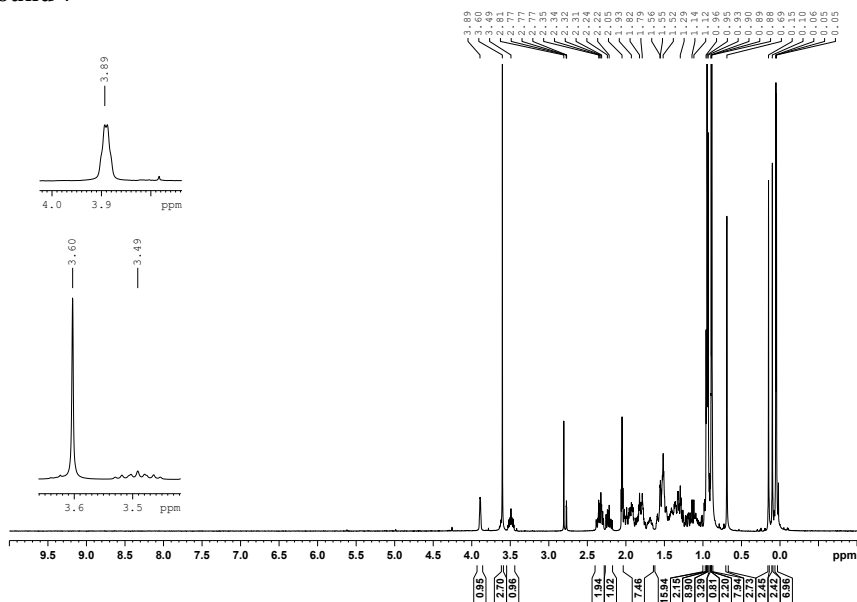
Figure S14. ^{1}H NMR (400 MHz, acetone-d_6) spectrum for compound **7**. The material contained a *tert*-butyl trimethylsilyl containing impurity of unknown structure.
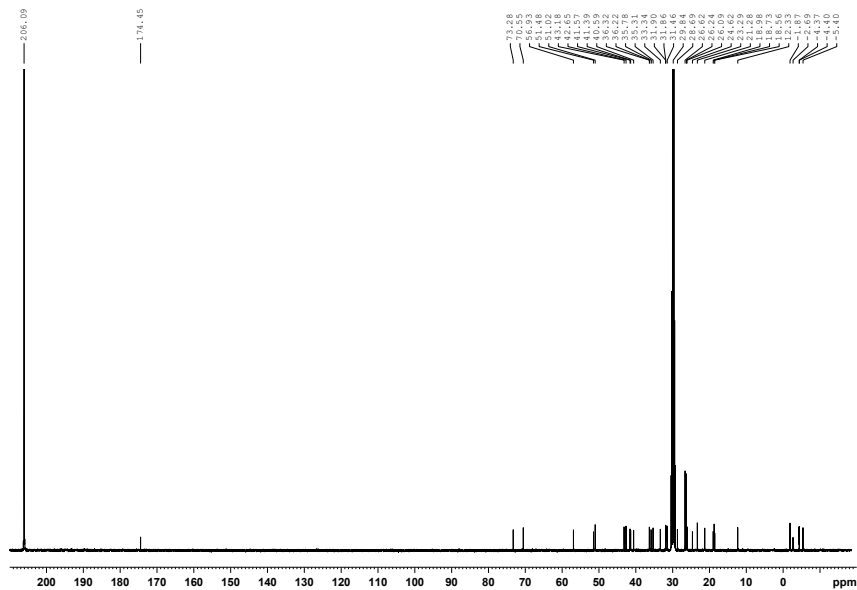
Figure S15. ^{13}C NMR (100 MHz, acetone-d_6) spectrum for compound **7**. (Impurity visible at 26.1 and -2.7 ppm)

Compound 8
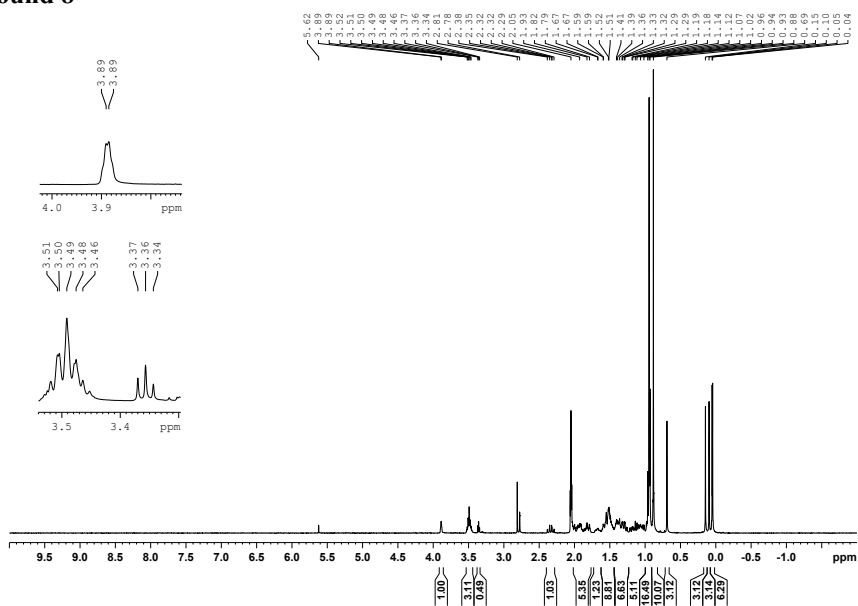
Figure S16. ^{1}H NMR (400 MHz, acetone-d_6) spectrum for compound **8**.

Figure S17. ^{13}C NMR (100 MHz, acetone-d_6) spectrum for compound **8**.
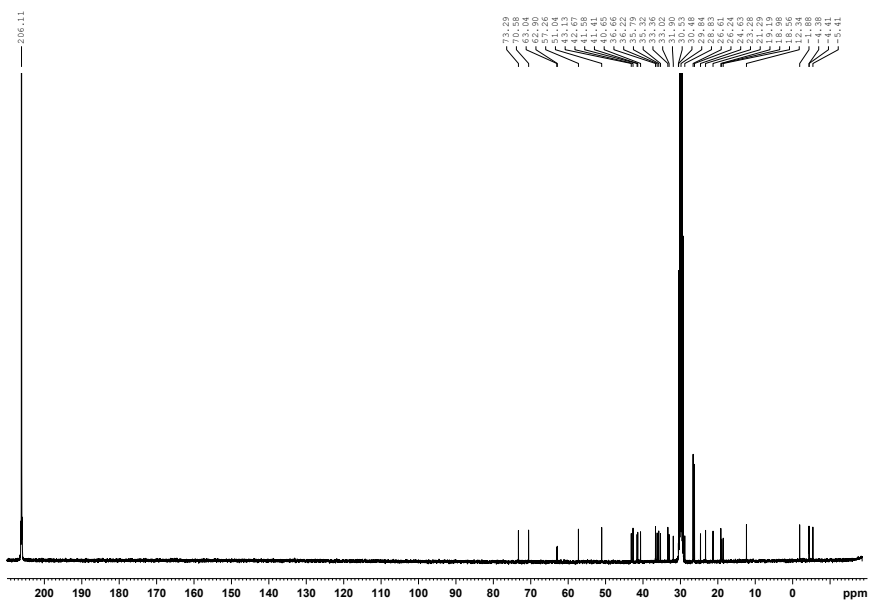
Compound 9
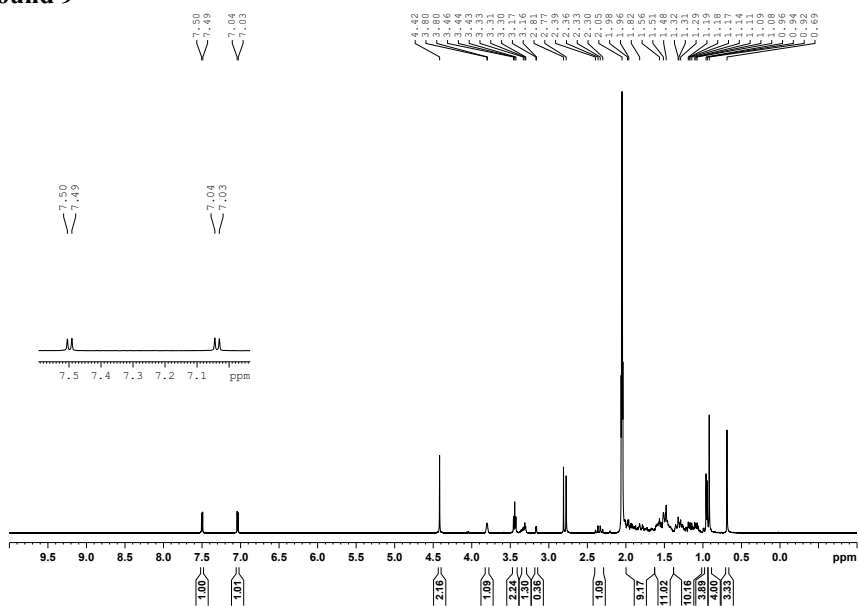
Figure S18. ^{1}H NMR (600 MHz, acetone-d_6) spectrum for compound **9**.
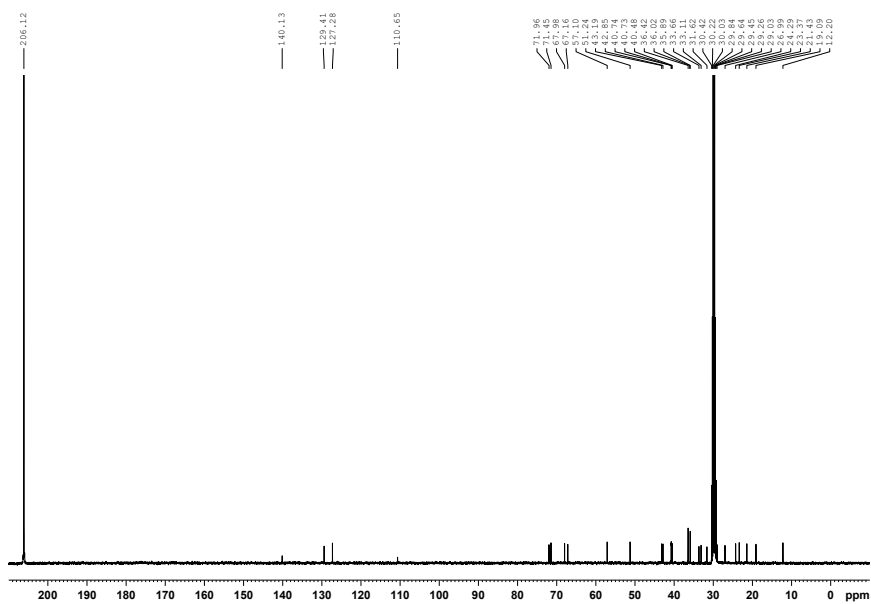
Figure S19. ^{13}C NMR (150 MHz, acetone-d_6) spectrum for compound **9**.

Compound 10
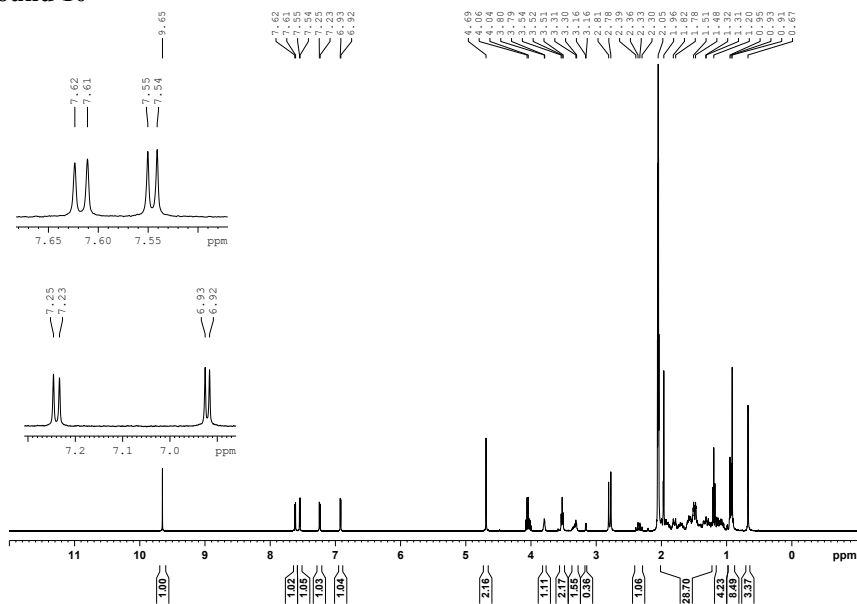
Figure S20. ^{1}H NMR (600 MHz, acetone-d_6) spectrum for compound **10**. The analyzed material contained EtOAc.
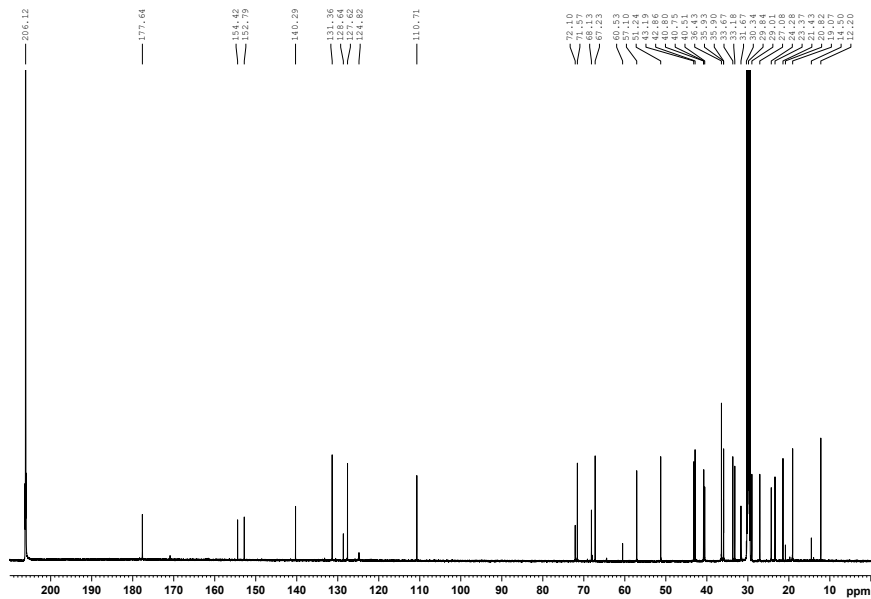
Figure S21. ^{13}C NMR (150 MHz, acetone-d_6) spectrum for compound **10**. The analyzed material contained EtOAc.

Compound 11
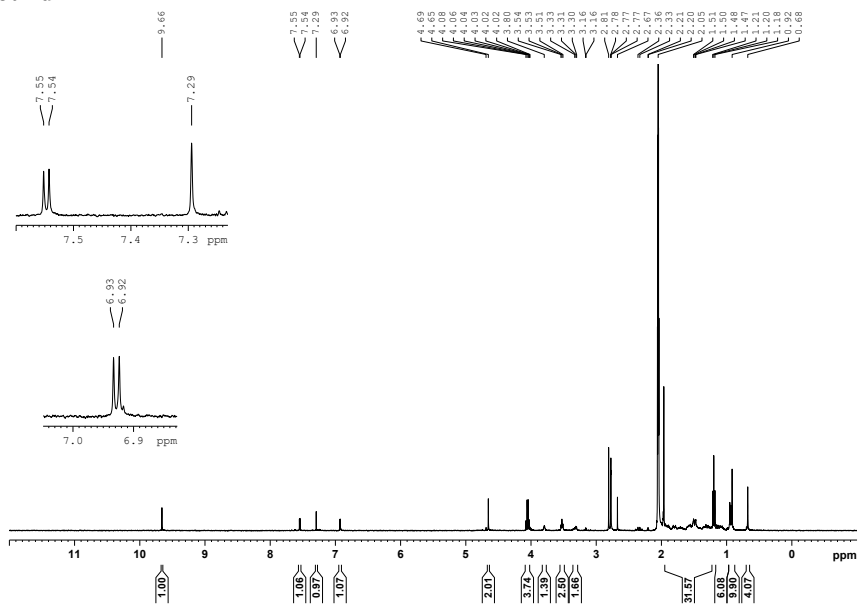
Figure S22. ^{1}H NMR (600 MHz, acetone-d_6) spectrum for compound **11**. The analyzed material contained EtOAc.
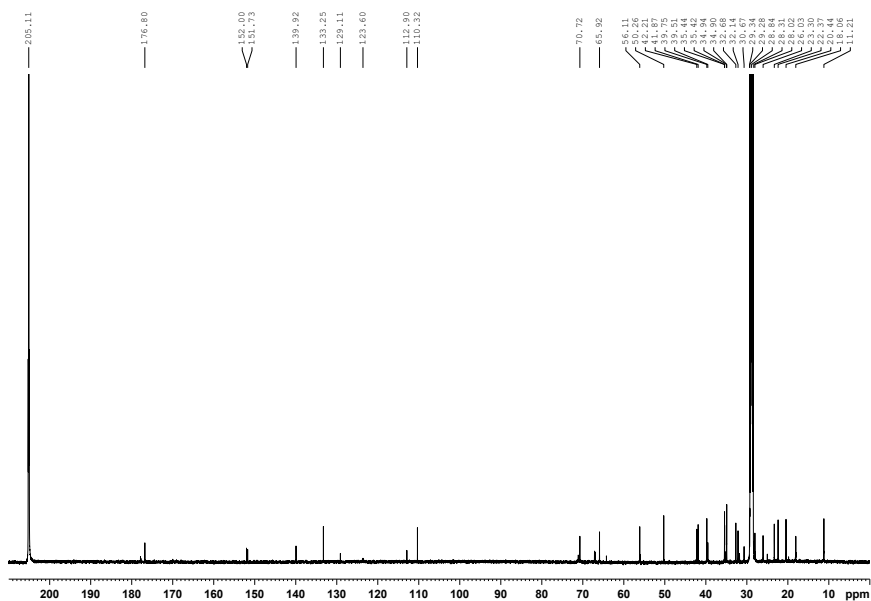
Figure S23. ^{13}C NMR (150 MHz, acetone-d_6) spectrum for compound **11**. The analyzed material contained EtOAc.

Compound 12
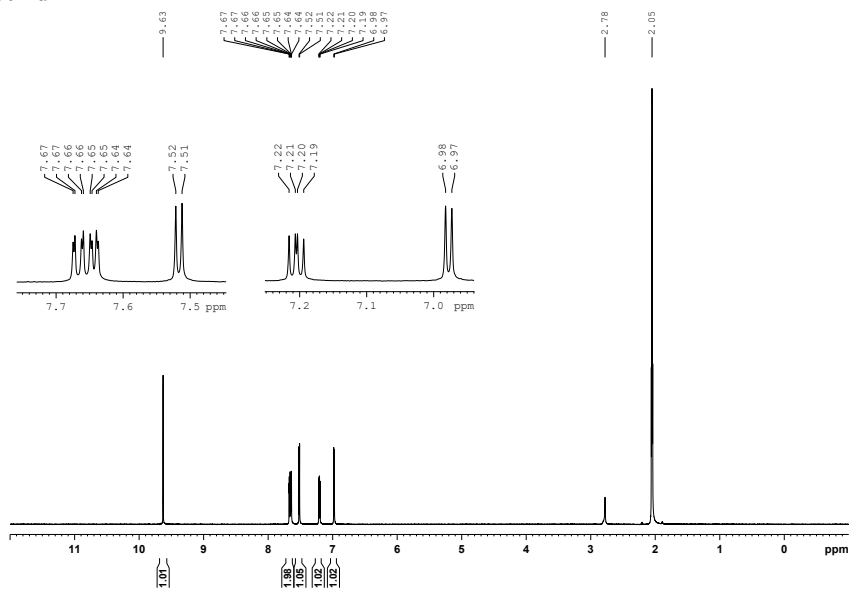
Figure S24. ^{1}H NMR (400 MHz, acetone-d_6) spectrum for compound **12**.

Compound 13
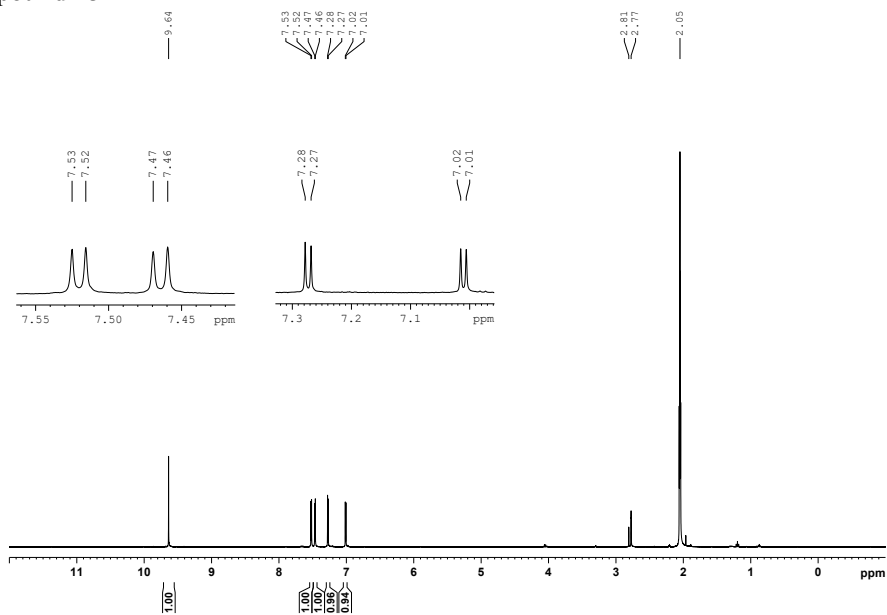
Figure S25. ^{1}H NMR (400 MHz, acetone-d_6) spectrum for compound **13**.

Compound 14
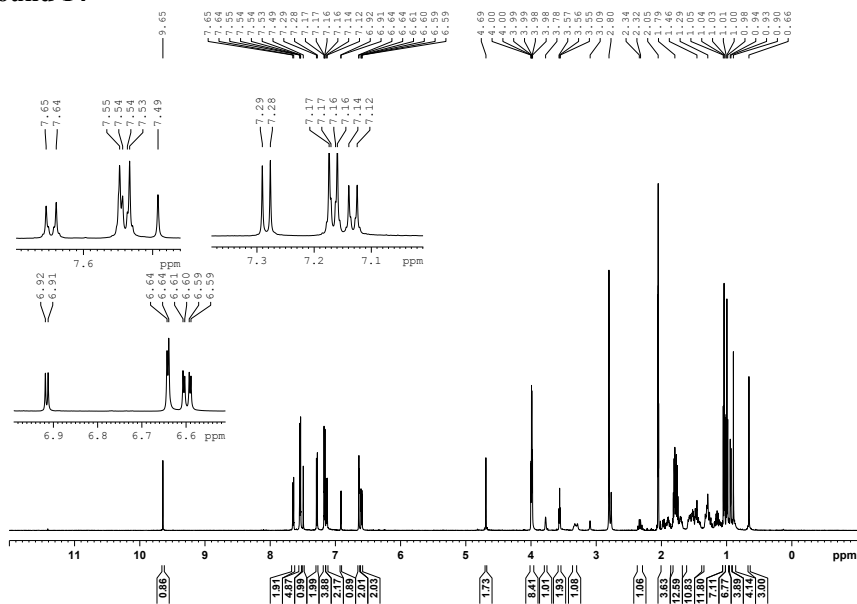
Figure S26. ^{1}H NMR (600 MHz, acetone-d_6) spectrum for compound **14**.
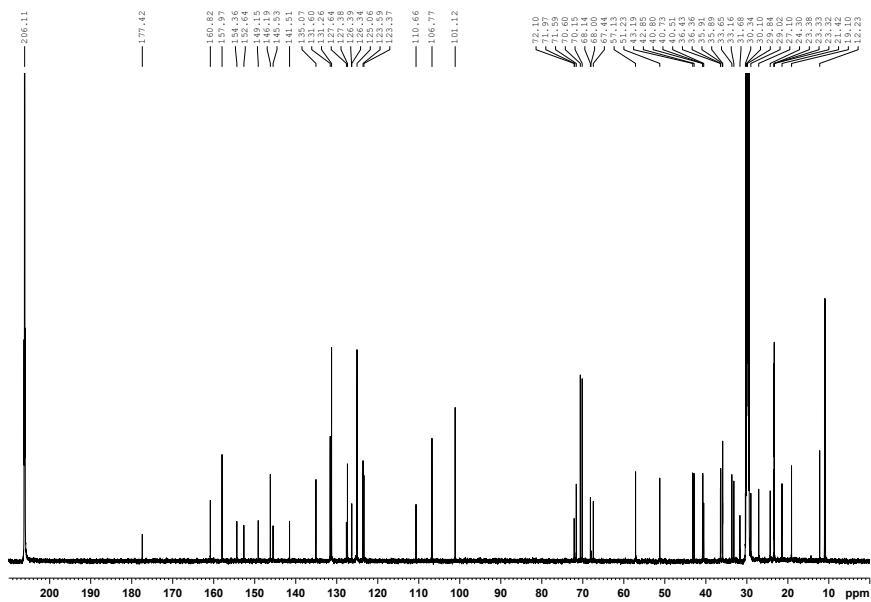
Figure S27. ^{13}C NMR (150 MHz, acetone-d_6) spectrum for compound **14**.

Compound 15

Figure S28. ^{1}H NMR (600 MHz, acetone-d_6) spectrum for compound **15**.

Figure S29. ^{13}C NMR (150 MHz, acetone-d_6) spectrum for compound **15**.
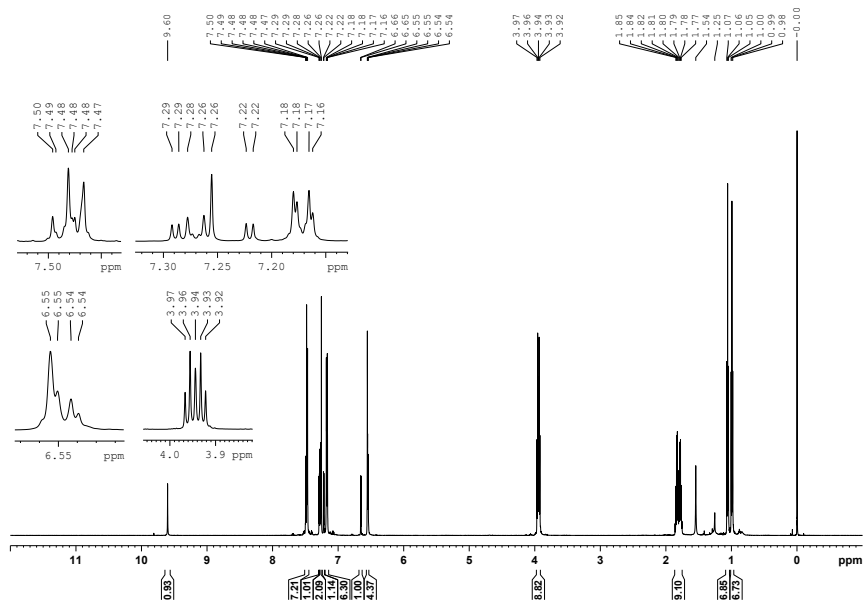
Compound 16

Figure S30. ^{1}H NMR (600 MHz, CDCl$_3$) spectrum for compound **16**.
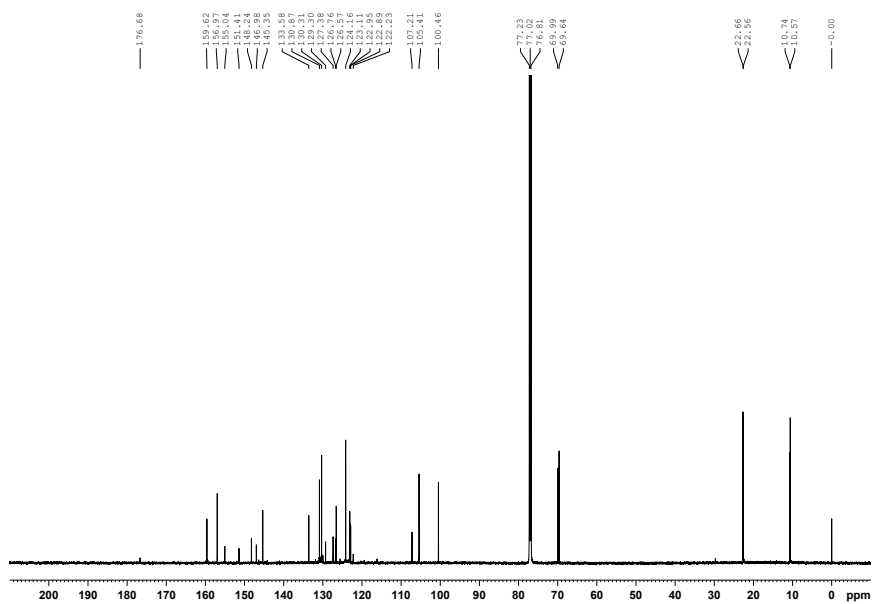
Figure S31. ^{13}C NMR (150 MHz, CDCl$_3$) spectrum for compound **16**.

Compound 17

Figure S32. ^{1}H NMR (600 MHz, CDCl$_3$) spectrum for compound **17**.

Figure S33. ^{13}C NMR (150 MHz, CDCl$_3$) spectrum for compound **17**.
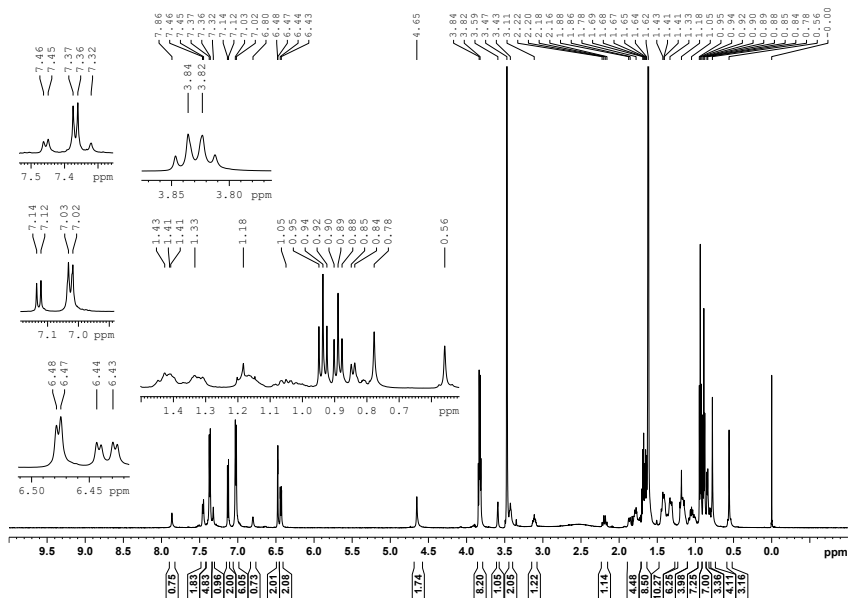
Sensitizer C₃-CDCA

Figure S34. ^{1}H NMR (600 MHz, THF-d_8) spectrum for compound **C₃-CDCA**.

Figure S35. ^{13}C NMR (150 MHz, THF-d_8) spectrum for sensitizer **C₃-CDCA**.
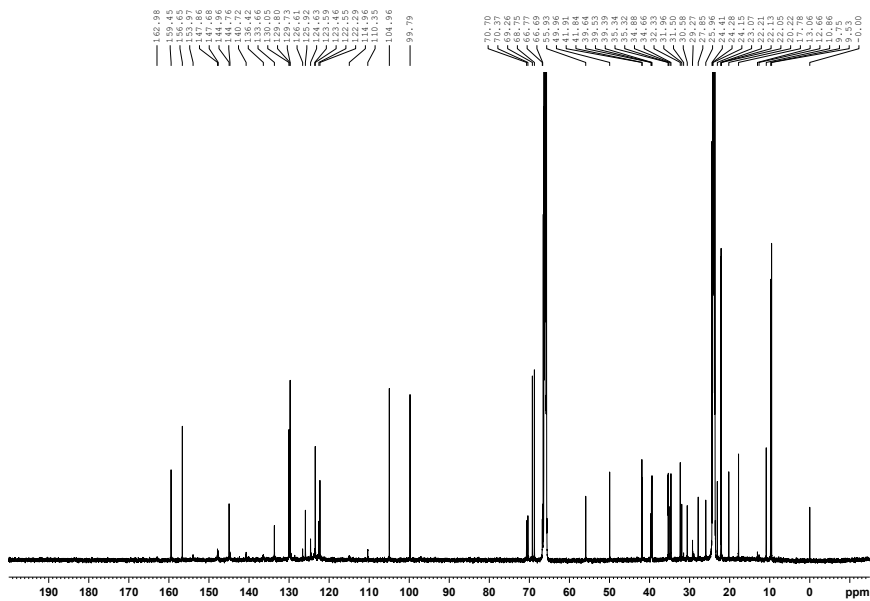
Sensitizer C₆-CDCA
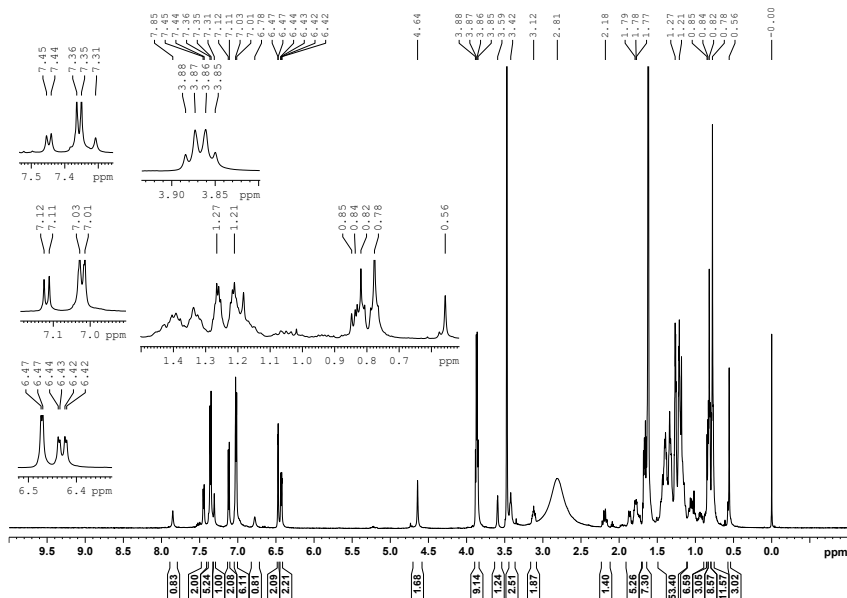
Figure S36. ¹H NMR (600 MHz, THF-d_8) spectrum for sensitizer **C₆-CDCA**.
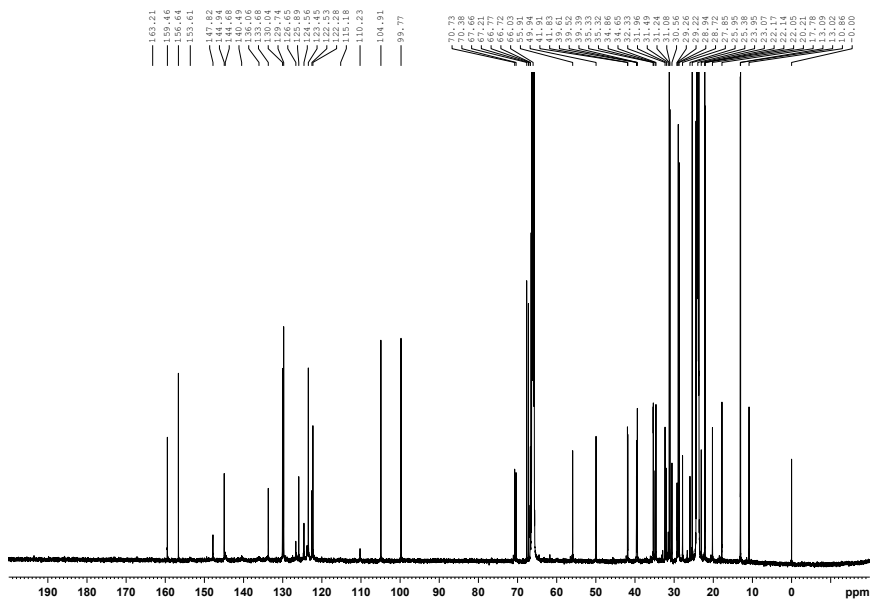
Figure S37. ¹³C NMR (150 MHz, THF-d_8) spectrum for sensitizer **C₆-CDCA**.

Sensitizer C₃
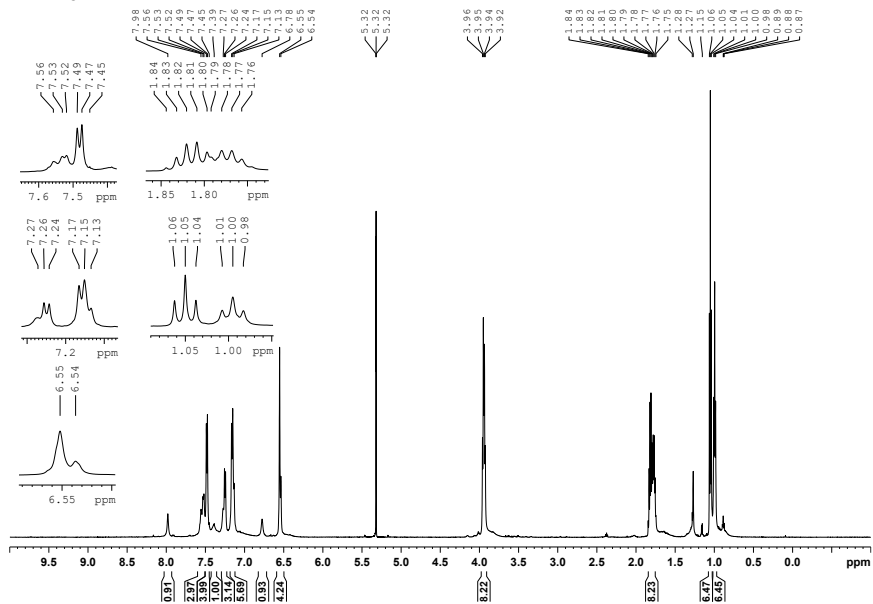
Figure S38. ^{1}H NMR (600 MHz, CD$_2$Cl$_2$) spectrum for sensitizer **C₃**.
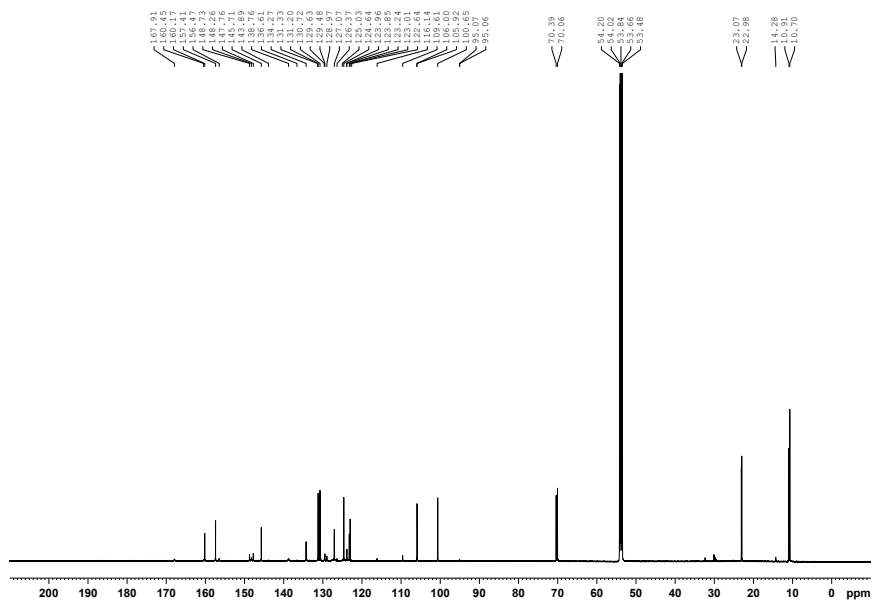
Figure S39. ^{13}C NMR (600 MHz, CD$_2$Cl$_2$) spectrum for sensitizer **C₃.**

Sensitizer C₆
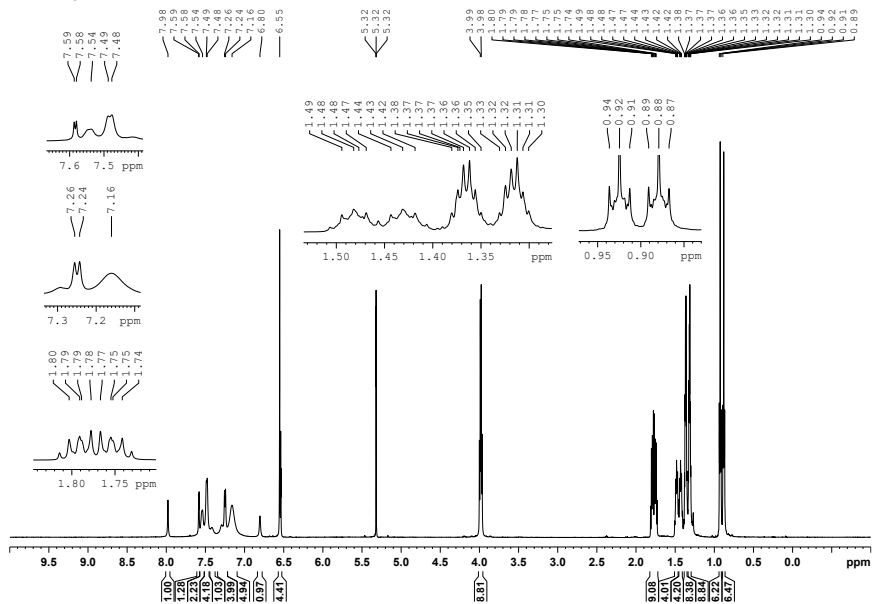
Figure S40. ¹H NMR (600 MHz, CD₂Cl₂) spectrum for sensitizer **C₆**.
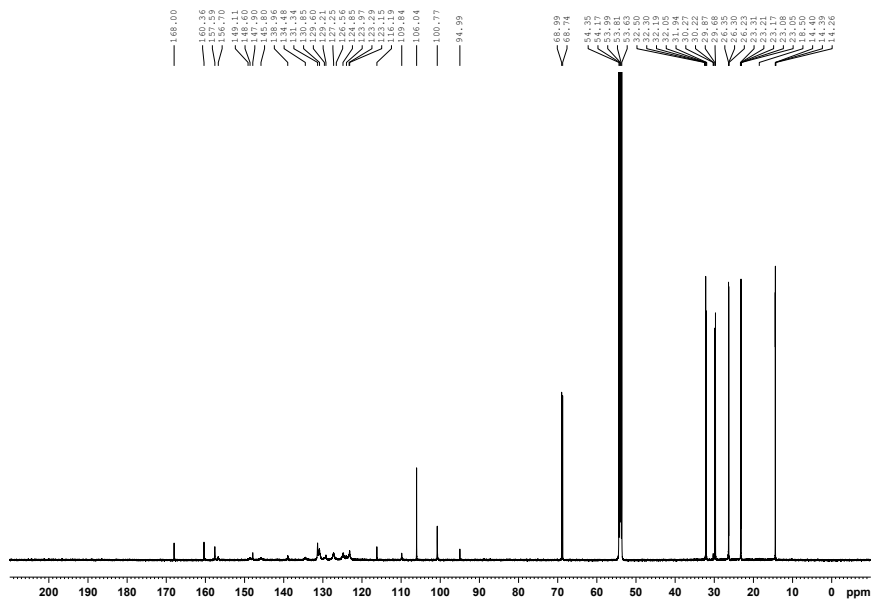
Figure S41. ¹³C NMR (150 MHz, CD₂Cl₂) spectrum for sensitizer **C₆**.

34

Paper V

D. M. Almenningen, B. S. Haga, H. E. Hansen, A. F. Buene, B. H. Hoff and O. R. Gautun

Adamantyl Side-Chains as Anti-aggregating Moieties in Dyes for Dye-Sensitized Solar Cells,

Paper V

Chemistry A European Journal

Accepted Article

Title: Adamantyl Side-Chains as Anti-aggregating Moieties in Dyes for Dye-Sensitized Solar Cells

Authors: David Moe Almenningen, Brita Susanne Haga, Henrik Erring Hansen, Audun Formo Buene, Bård Helge Hoff, and Odd Reidar Gautun

This manuscript has been accepted after peer review and appears as an Accepted Article online prior to editing, proofing, and formal publication of the final Version of Record (VoR). The VoR will be published online in Early View as soon as possible and may be different to this Accepted Article as a result of editing. Readers should obtain the VoR from the journal website shown below when it is published to ensure accuracy of information. The authors are responsible for the content of this Accepted Article.

WILEY-VCH

WILEY-VCH

Adamantyl Side-Chains as Anti-aggregating Moieties in Dyes for Dye-Sensitized Solar Cells

David Moe Almenningen[a], Brita Susanne Haga[a], Henrik Erring Hansen[b], Audun Formo Buene[c], Bård Helge Hoff[a], Odd Reidar Gautun[a]*

D. M. A. Author 1, B. S. H. Author 2, Prof. Dr. B. H. H. Author 5, Prof. Dr. O. R. G. Corresponding author

Department of Chemistry, Norwegian University of Science and Technology, Høgskoleringen 5, 7491 Trondheim, Norway
E-mail: odd.r.gautun@ntnu.no

H. E. H. Author 3

Department of Materials Science and Engineering, Norwegian University of Science and Technology, Sem Sælands vei 12, 7491 Trondheim, Norway

Dr. A. F. B Author 4

Department of Civil and Environmental Engineering, Norwegian University of Science and Technology, Høgskoleringen 7a, 7034 Trondheim, Norway.

Designing and evaluating novel dye concepts is crucial for the development of the field of dye-sensitized solar cells (DSSCs). In our recent report, the novel concept of tethering the anti-aggregation additive chenodeoxycholic acid (CDCA) to dyes for DSSC was introduced. Based on the performance improvements seen for this modification, the aim of this study is to see if a simplified anti-aggregation unit could achieve similar results. The following study reports the synthesis and photovoltaic characterization of two novel dyes decorated with the steric ethyladamantyl moiety on the π-spacer, and on the triarylamine donor. This modification is demonstrated to be successful in increasing the photovoltages in devices employing copper-based electrolytes compared to the non-modified reference dye. The best photovoltaic performance is achieved by a device prepared with the adamantyl decorated donor dye and CDCA, this device achieves a power conversion efficiency of 6.1% (*Short-circuit current* = 8.3 mA cm^{-2}, *Open-circuit voltage* = 1054 mV, *Fill factor* = 0.69). The improved photovoltaic performance seen for the adamantyl decorated donor demonstrate the potential of ethyladamantyl side chains as a tool to ensure surface protection of TiO$_2$.

1

Introduction

The dye-sensitized solar cell (DSSC), a technology that recently turned 30 years since its original report in 1991, has shown remarkable promise in recent years for ambient light photovoltaics.[1, 2] The typical device consists of three key components: a layer of mesoporous semiconducting metal-oxide (most commonly TiO_2), a light-absorbing dye which is attached on the metal-oxide, and a redox mediator responsible for regenerating the oxidized sensitizers.[3] Owing to this multifaceted nature, where optimization of the devices can be achieved through tuning of the separate parts, the technology still remains relevant and under constant development today. The introduction of novel copper-based redox mediators where the energy levels of the electrolyte (0.87-0.97 V vs. the standard hydrogen electrode (SHE)) are more closely matched to the energy levels of the dyes, has led to a drastic reduction in overpotential losses of the devices compared to the traditional I^-/I_3^--electrolyte (0.5 V vs. SHE).[4] These new mediators have enabled devices with power conversion efficiencies (PCE) of more than 13% under standard AM1.5G sunlight, and efficiencies surpassing 30% under lowlight conditions.[5, 6] The development of novel dyes displaying photochromic behavior,[7] and dyes displaying near-infrared (NIR) absorption facilitate devices with tunable transparency.[8] This property lends itself nicely for the use of DSSC in building integrated photovoltaics (BIPV), where transparency of the devices is important to make them visually non-intrusive.[9, 10]

Fully organic dyes offer a unique opportunity to tailor optical and or electronical properties on a molecular level. The absorption properties of dyes that adopt a donor - π-spacer - acceptor (D-π-A) motif is easily modified by varying the acceptor or donor strength of the building blocks, or through modification of the π-conjugated linker.[11] Expanding the π-conjugated system broadens the spectral response of dyes, and increases the attainable short-circuit current of the solar cells.[12-14] However, such an expansion of the aromatic system leaves the dyes susceptible to aggregate on the surface of TiO_2. This blue-shifts the absorption of the dyes and facilitates quenching of the excited states of the dyes.[15] Implementing measures to combat the undesirable aggregation effects has been a topic for many studies over the years and a wide variety of approaches has been designed and evaluated. Linking multiple dyes together has proven valuable in reducing aggregation,[16-18] optimizing the bulkiness of the sidechains on the aromatic system is another proven method.[19-21] It is also quite common to add anti-aggregation additives to the staining solution, the most common additive for DSSC is chenodeoxycholic acid (CDCA).[22] In our previous study on anti-aggregation measures for DSSC, see Figure 1, we prepared two dyes with CDCA tethered to their π-spacer (**C₃-CDCA** and **C₆-CDCA**), and found this to be beneficial for photovoltaic performance compared to the reference dyes (**C₃** and **C₆**).[23] Our previous study also highlighted the anti-aggregational effect of the alkoxy chains on the donor side of the molecules, where superior performance was seen for the dyes with longer side chains (**C₆** and **C₆-**

2

CDCA vs. **C₃** and **C₃-CDCA**). Some of the improvements seen for this structural modification is likely due to another closely related aspect of solar cell performance, namely the recombination of electrons in TiO_2 with the oxidized species of the electrolyte. This loss process is known to lower the Fermi level of TiO_2, effectively reducing the attainable open-circuit voltage (V_{oc}) of the dye-sensitized solar cell.[24] Ever since moving to one-electron redox mediators, such as Co^{2+}/Co^{3+} and Cu^{+}/Cu^{2+} complexes, the retardation of recombination has been a key goal for molecular engineering of novel dyes, as Co^{3+} and Cu^{2+} species of the novel electrolytes undergo a more rapid recombination with electrons in TiO_2 compared to the conventional I_3^--complex.[25-27] The dye **MS5**, a striking example of successful molecular engineering to circumvent the effect of recombination, was presented in a recent paper by Zhang et al.[6] This dye employs dodecyloxy side chains that suppresses recombination expertly to allow for copper-based devices with a record photovoltage of 1.24 V.

With the promising results from our initial study of tethering the highly steric CDCA on the π-spacer, we set out to investigate if a simplified blocking group could achieve similar performance improvements. It has been shown that introducing too large side chains is bad for overall photovoltaic performance.[20] We therefore prepared a dye (**BSH-2**), shown in Figure 1, which had 1-ethyladamantyl tethered to the π-spacer in an analogous manner to the previously reported CDCA-dyes. Adamantane is a rather unique hydrocarbon consisting of three fused cyclohexane rings in a rigid but strain-free ring system.[28] Adamantyl substitutions are common structural motifs in the field of antiviral pharmaceuticals.[29-32] Besides this, adamantyl's unique properties have also been utilized in organic optoelectronic materials such as organic hole-transporting materials (HTM),[33, 34] or as a side chain on diketopyrrolopyrrole (DPP) pigments.[35, 36] In the field of DSSC we have also seen some use of adamantane derivatives, where 1-admantane acetic acid (ADAA) has been evaluated as an anti-aggregation additive,[22] the nitroxide radical 2-azaadamantan-*N*-oxyl (AZA) has been employed as a redox mediator,[37] and most notably AZA has found use in a tandem redox system with a $Co^{2+/3+}$ complex to achieve V_{oc} values above 1 V.[38] With the illustrious properties of the dodecyloxy substituted donor of **MS5** in mind, we also set out to prepare a dye (**BSH-3**), shown in Figure 1, which is fitted with adamantylethyloxy (another 12-carbon moiety) substituents on the triarylamine donor. The effects of the ethyladamantyl substituents on **BSH-2** and **BSH-3** will be compared with the performance of the reference dye **JK-305**, a standard triarylamine dye bearing hexyloxy side chains and a 2',2-bithiophene π-spacer. The dye **JK-305**, displayed a PCE of 7.3% (J_{sc} = 13.1 mA cm⁻², V_{oc} = 760 mV, FF = 0.73) in an iodine-based electrolyte.[39] The results presented will serve as a model study to illustrate the potential merits, and eventual pitfalls of the steric ethyladamantyl substitutions on the π-spacer and on the donor of dyes for DSSC.

3

Our previous work: *Sol. RRL* 2020, **4**, 1900569
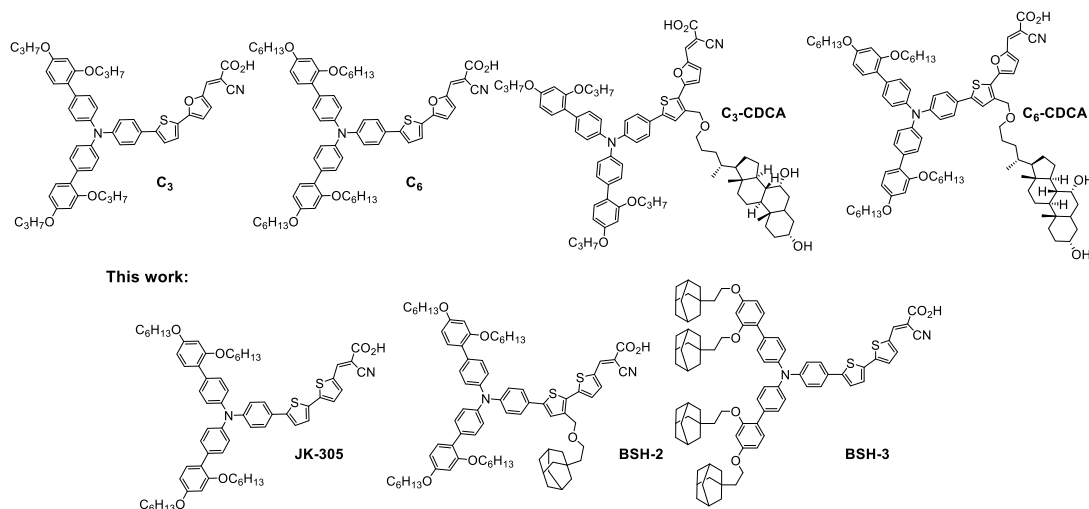
Figure 1. The sensitizers prepared in our previous work represented the first report of the common anti-aggregation additive CDCA tethered to a dye covalently. The dyes prepared in study is the first report of ethyladamantyl as side chains in dyes for DSSC.

Results and Discussion

Dye Synthesis

The synthesis of the dyes is based on the route used for the CDCA-dyes previously reported by our group.[23] However, in contrast to CDCA, the adamantyl-moiety bears no additional heteroatoms and this simplified the synthesis somewhat as it made protection chemistry redundant. The preparation of the adamantyl-functionalized π-spacer is shown in Scheme 1, starting from the commercially available adamantyl acetic acid (ADAA). The acid was subjected to a Fischer esterification, yielding the methyl ester **1** and a reduction giving the adamantyl ethanol **2**. Compound **2** was used to prepare the bromide **3** needed for the synthesis of the adamantyl decorated donor, which will be discussed later. Further, the alcohol **2** was fused with bromo-3-(bromomethyl)thiophene using a Williamson ether synthesis under Finkelstein conditions, to produce **4**. A Suzuki-Miyaura cross-coupling catalyzed by XPhos Pd G3 reported by Bruno et al. [40] was used to produce bithiophene **5**. A final bromination using NBS yielded the finished π-spacer building block **6**.

4
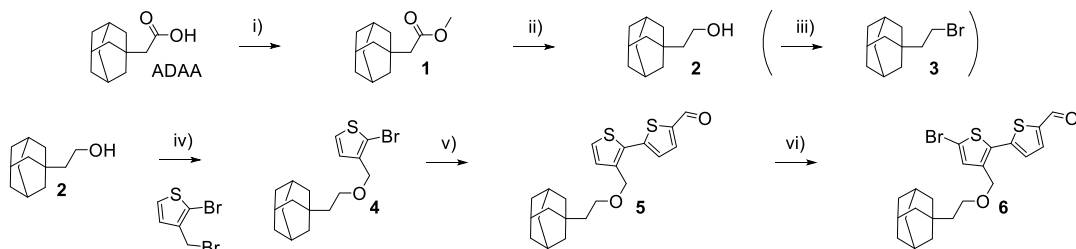
Scheme 1. Synthesis of π-spacer building block **6**, and key intermediate **3** used in the synthesis of the adamantyl-donor. *i) MeOH, H₂SO₄, r.t., 79%, ii) LiAlH₄, THF, r.t., 79%, iii) HBr, 100 °C, 94%, iv) NaH, NaI THF, 50 °C, 75% v) (5-formylthiophene-2-yl)boronic acid, XPhos Pd G3, K₃PO₄, H₂O/1,4-dioxane, 80 °C, 54%, vi) NBS, CH₂Cl₂, 0 °C, 66%.*

The synthesis of the adamantyl donor followed our previously reported synthesis of triarylamine donors, shown in Scheme 2. Interestingly, the Williamson ether synthesis involving the adamantyl bromide **3** suffered from a competing elimination reaction. As a result of this, the yield of **9** was 49% which is considerably lower than the yield of **7** at 82%. The subsequent Pd-catalyzed borylation reaction reported by Billingsley and Buchwald, [41] showed full conversion to the corresponding boronates **8** and **10**. A Suzuki-Miyaura reaction of 4,4'-dibromotriphenylamine yielded the functionalized triarylamines **11** and **12**, in yields of 87% and 56%, respectively. The ultimate step in the donor synthesis was a regiospecific bromination using NBS, where **13** and **14** were prepared in yields of 99% and 95%, respectively.
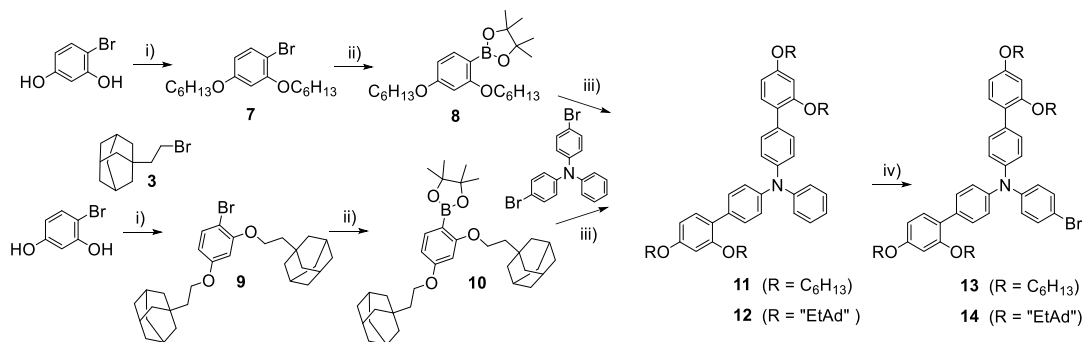
Scheme 2. Synthesis of key donor intermediates **13** and **14**. *i) KOH, DMSO, 1-bromohexane/intermediate 3, r.t., 82%/49%, ii) HBpin, PdCl₂(CH₃CN)₂, SPhos, Et₃N/1,4-dioxane, 110 °C, iii) Pd(OAc)₂, SPhos, K₂CO₃, H₂O/1,4-dioxane, 80 °C, 87%/56%, iv) NBS, CH₂Cl₂, r.t., 99%/95%.*

The π-spacer and the donor moieties were merged, and the dyes completed as shown in Scheme 3. Firstly, the brominated triarylamines were converted to the corresponding boronic esters using the Pd-catalyzed borylation reaction. The crude boronate products were then used in a Susuki-Miyaura cross coupling, yielding the dye precursors **15-17** in yields of 29-48% over two steps from the brominated triarylamine. The final step was a Knoevenagel condensation, introducing the cyano acetic acid anchoring group giving the sensitizers **JK-305**, **BSH-2**, and **BSH-3** in yields of 57-79%.

5
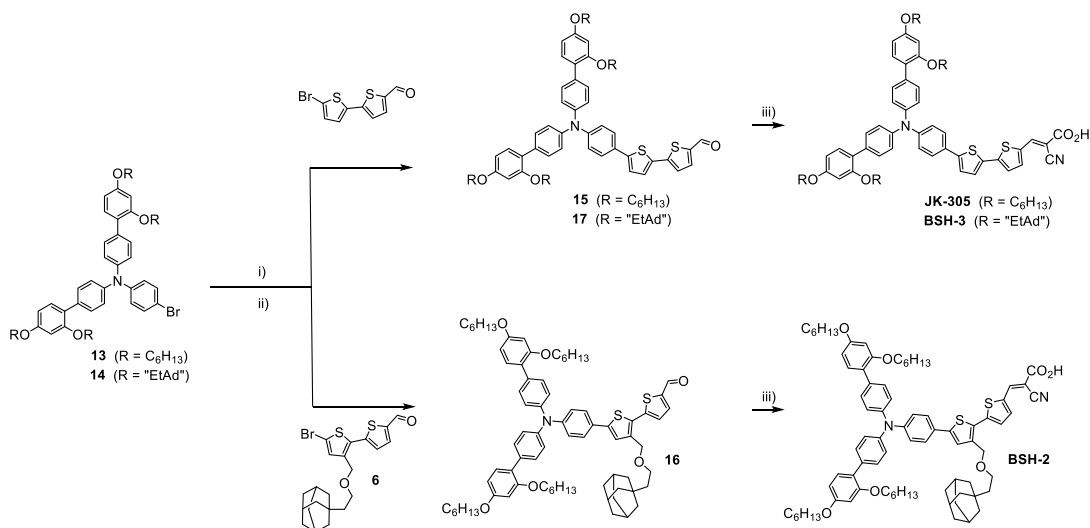
Scheme 3. *Synthesis route for the merging of donor and π-spacer moieties and preparation of dyes **JK-305**, **BSH-2**, and **BSH-3**. i) HBpin, PdCl$_2$(CH$_3$CN)$_2$, SPhos, Et$_3$N/1,4-dioxane, 110 °C, ii) Pd(OAc)$_2$, SPhos, 1,4-dioxane/H$_2$O, 80 °C, 43%(**15**)/48%(**16**)/29%(**17**), iii) cyanoacetic acid, piperidine, CH$_3$CN, 80 °C, 79%(**JK-305**)/67%(**BSH-2**)/57%(**BSH-3**).*

Photophysical properties

The photophysical properties of dyes are essential for their performance as sensitizers in dye-sensitized solar cells. It is crucial that modifications done on the dye molecules does not adversely affect their absorption properties in solution or when attached on TiO$_2$. UV/Vis measurements of the dyes were performed on the dyes in dichloromethane solution ($2 \cdot 10^{-5}$ M), and adsorbed on a TiO$_2$ film (2.5 μm, 18NR-T, Greatcell Solar). The results from these measurements are shown in Figure 2, and Figure 3 and are summarized in Table 1.
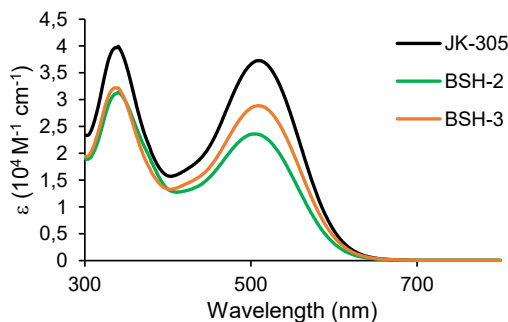
Figure 2. *Absorption spectra of all dyes in dichloromethane solution.*
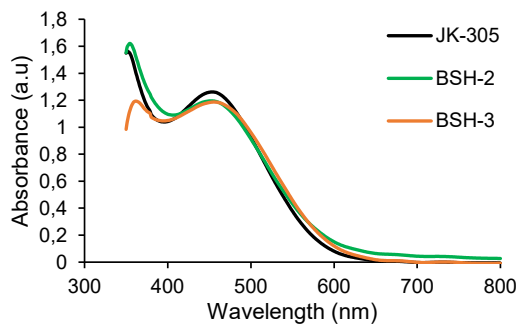
Figure 3. UV/vis measurements of all dyes on TiO$_2$ films (2.5 μm, 18NR-T, Greatcell Solar).

Comparing the data obtained from our measurements with the previously reported data of the dye **JK-305**, a solvatochromic effect on the absorption properties is seen.[39] The absorption maximum is found at 510 nm in dichloromethane, a redshift of 59 nm compared to the previously reported data in ethanol. The optical band gap is also found to be smaller from the measurements done in dichloromethane (2.12 eV) compared to the measurements in ethanol (2.30 eV). The optical properties of the adamantyl-functionalized dyes in solution are similar to the reference dye **JK-305**, where the absorption maxima are found within 5 nm of each other. However, the molar extinction coefficient of **JK-305** is approximately 9000-13000 M^{-1}cm^{-1} higher than that of **BSH-2** and **BSH-3**. The slightly bigger optical band gap of **BSH-2** could suggest that the adamantyl-moiety forces a slight out-of-plane ring twist between the two thiophenes, as previous quantum calculations has demonstrated that side chain modified thiophenes display larger dihedral angles than non-modified ones.[42] The absorption properties of the dyes on TiO$_2$ films are also remarkably similar, where a 52-56 nm blueshift of absorption maxima is seen for the dyes in this series when adsorbed on TiO$_2$. This blueshift is frequently attributed to a combination of deprotonation of the carboxylic acid, and formation of H-aggregated dye clusters on the TiO$_2$ surface.[43, 44]

When comparing **JK-305** to our previously reported dye **C$_6$**, which is entirely similar except for a thiophene-furan π-spacer instead, we see that absorption maximum is redshifted by 8 nm and the intensity of absorption is increased by 10000 M^{-1}cm^{-1}. When we introduced the CDCA-moiety on the π-spacer of **C$_6$-CDCA** we saw a blueshift of 13 nm compared to the reference dye, while the introduction of adamantyl on the π-spacer of **BSH-2** blue-shifted absorption by 5 nm. Introduction of adamantyl on the donor of **BSH-3**, had negligible effect on the absorption maximum compared to the reference dye. This shows that the adamantyl-functionalization is even more useful in terms of absorption properties than the CDCA-functionalization in our previous study.

7

***Table 1.** Photophysical and electrochemical properties of dyes in the series.*

Dye	$\lambda_{abs}{}^a$ (nm)	ε ($_M{}^{-1}cm^{-1}$)	Em.[b] (nm)	$\lambda_{abs}{}^c$ on TiO$_2$ (nm)	$E_{0-0}{}^d$ (eV)	$E_{ox}{}^e$ (V vs. SHE)	$E_{LUMO}{}^f$ (V vs. SHE)
JK-305	510	37300	632	454	2.12	1.10	-1.02
BSH-2	505	23600	629	453	2.19	1.11	-1.08
BSH-3	509	28900	634	456	2.13	1.14	-0.99

[a] Maximum of most red-shifted peak measured in dichloromethane solution (2 · 10^{-5} M). [b] Emission when ICT band is excited, in dichloromethane solution. [c] Maximum of most red-shifted peak on TiO$_2$ (2.5 μm, GreatcellSolar 18NR-T). [d] Calculated from the intersection of the absorption and normalized emission spectra. [e] Measured vs. F$_c{}^+$/F$_c$ on stained TiO$_2$ electrodes in acetonitrile with 0.1 M LiTFSI, converted to V vs. SHE by 0.624 V. Scan rate 10 mV s^{-1}. [f] Calculated from E$_{ox}$-E$_{0-0}$.

Electrochemical properties

Another crucial performance parameter for the sensitizers in dye-sensitized solar cells is their electronic properties. The HOMO energy level of the dye should leave sufficient driving force for the oxidized dye to be regenerated by the redox shuttle. Additionally, the excited state energy level should have a sufficient driving force for electron injection into the metal oxide. The oxidation potentials of the dyes were found through cyclic voltammetry (CV) experiments of the dyes sensitized on TiO$_2$ films. The LUMO level was calculated by subtracting the optical band gap from the measured oxidation potential. The energy levels of the frontier orbitals of the dyes in relation to the electrolyte and the conduction band of TiO$_2$ is shown in Figure 4.

All the dyes displayed reversible oxidation peaks around 1.10-1.14 V vs. SHE, suggesting that the modifications done on the dyes had minor effect on their frontier orbitals. This is also seen in our previous publication, where the CDCA-moiety had little or no effect on the oxidation potential of the dye. The CV measurements revealed that all the dyes would be compatible for use in a device with a Cu$^+$/Cu^{2+} redox shuttle, as the HOMO energy levels are sufficiently deep. The dye which displayed the highest oxidation potential of 1.10 V vs. SHE (**JK-305),** still had a driving force of 0.23 V which is more than the 0.1 V previously established to be sufficient.[4]

8
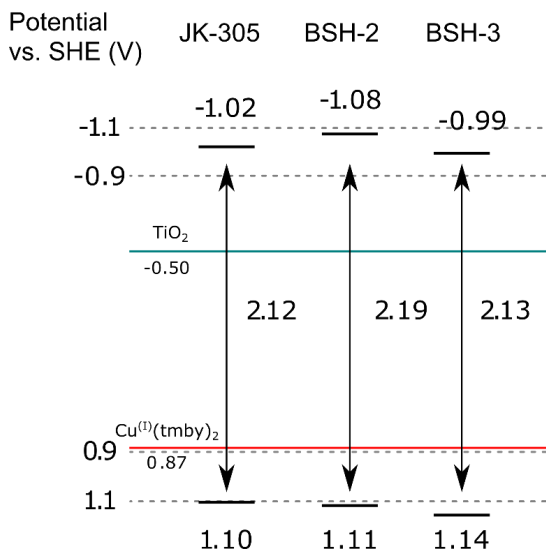
Figure 4. Energy levels of the frontier orbitals for the sensitizers in this study.

Photovoltaic properties

The fabrication and characterization of DSSC-devices sensitized with the dyes, revealed that insertion of adamantyl-groups was beneficial for increasing the V_{oc} of the devices. The data from the photovoltaic characterization is summarized in Table 2, the data presented is the average values obtained from three separate devices. The *J-V* curves of the best performing devices from each parallel are shown in Figure 5 and Figure 6. In our recent review on the class of phenothiazine dyes, we saw that one dye (**H-PTZ**) had been investigated in 13 separate papers with PCE values ranging from 3.1% to 6.6%.[45] This showed us the value of using known reference sensitizers to provide a benchmark for the findings presented in a study. In this study we prepared devices sensitized with the known dye **Y123** to serve as a reference, the efficiency of the **Y123** solar cell was 6.5% (J_{sc} = 10.0 mA cm^{-2}, V_{oc} = 992 mV, FF = 0.65).

When comparing the performance of the devices without any additives in the staining solution the best performing dye was the reference dye **JK-305** (5.7%), narrowly outperforming the dye with a modified π-spacer, **BSH-2** (5.5%). The dye with a modified donor, **BSH-3**, displayed a worse performance under these conditions owing to a remarkably low fill factor of 45%. It should be noted, however, that the open-circuit voltages of all three dyes under these conditions exceeded 1.0 V which was fairly promising with regards to the dyes' ability to insulate the surface of TiO$_2$ and prevent recombination. In our previous work we saw that all the dyes, even the CDCA-substituted dyes, benefitted from 10 equivalents of additional CDCA added in the staining solution. With this in mind we set out to prepare a set of new devices with 10 equivalents of CDCA added in the staining solution. For the reference dye **JK-305**, a slight improvement in PCE was seen, mainly due to an improved fill factor of the devices.

9

The devices prepared with **BSH-2** and CDCA revealed a surprising outcome, where the additive reduced the overall performance of the device significantly. It is the only dye in this and the previous study which has not benefitted from the addition of CDCA. This could suggest that there are some undesirable interactions between the adamantyl-substituents and CDCA occurring on the surface of TiO$_2$. Furthermore, the adamantyl-donor dye, **BSH-3**, benefitted immensely from addition of CDCA, and improvement of all performance parameters was seen. The most pronounced effect was seen for the fill factor which increased from 45% to 69%. As a consequence of this drastic improvement, the **BSH-3**/CDCA combination was the most efficient device in the series (J_{sc} = 8.3 mA cm^{-2}, V_{oc} = 1054 mV, FF = 0.69, PCE = 6.1%). This shows that the adamantyl groups could offer an improvement over the conventional hexyl chains, due to the higher photovoltages that this modification allows.

The excellent photovoltage of **BSH-2** (1.07 V) led us to wonder whether adamantyl acetic acid (ADAA) introduced in the staining solution could work as an anti-aggregation additive. Therefore, we prepared a set of devices where we added the same amount of ADAA (10 equiv.) to the staining solution of **JK-305**. The devices prepared with ADAA saw a reduction in all performance parameters. Excluding **BSH-3**, the devices fabricated with additives produce lower photovoltages in all cases. This can be explained by increased protonation that lowers the Fermi level of TiO$_2$.[46] The deleterious interactions between dye and additive seen for the **BSH-2**/CDCA and **JK-305**/ADAA might also facilitate recombination which would also explain the lower photovoltage observed. When considering the dye loading experiments, the addition of CDCA reduced dye loading by ≈ 20% in all three cases. The addition of ADAA reduced dye loading by only 4%. In addition, the reduced fill factor and J_{sc} seen for the devices prepared with **JK-305** and ADAA suggest that this additive has no anti-aggregation effect. When combining this with the adverse effect that increased protonation has on the photovoltage, we do not recommend adding ADAA to future staining solutions. In a previous study on the anti-aggregation effect of ADAA, a similar reduction of photovoltage was seen.[22]

The IPCE-spectra of the devices fabricated in this study are shown in Figure 7 and Figure 8. The maxima for all the dyes are found at 60-70% which shows that the devices suffer from suboptimal light harvesting. It seems that the molar extinction coefficient is not the only cause for the limited light harvesting ability, as **Y123** (ε = 48000 M^{-1} cm^{-1}) and **BSH-3** (ε = 28900 M^{-1} cm^{-1}) both display similar maxima of around 70%.

The effect of the adamantyl modifications was also apparent when considering the results of the dye loading experiments. We see that the ethyladamantyl substitutions lower the dye loading by ≈ 25% compared to the reference dye, independently of added anti-aggregation additives. It also shows that one substituent on the π-spacer lowers the dye loading by the same amount as four substituents on the donor. The dye **BSH-2** display a considerably higher dye loading (6.8 · 10^{-8} mol cm^{-2}), than its CDCA-

10

WILEY-VCH

substituted analogue **C$_6$-CDCA** (4.2 · 10^{-8} mol cm^{-2}) under similar conditions. This suggest that the more compact adamantyl substituent has a smaller steric impact than the CDCA-substituent.

Table 2. *Photovoltaic performance of all dyes under 1 sun AM 1.5G illumination, and from IPCE measurements. Results from dye loading experiments are also included.*

Dye	Additive (10 equiv.)	IPCE J_{SC} (mA cm^{-2})[a]	J_{SC} (mA cm^{-2})	V_{OC} (mV)	FF	PCE (%)	Dye Loading (10^{-8} mol cm^{-2})[b]
JK-305	-	8.94	8.6 ± 0.1	1035 ± 4	0.64 ± 0.02	5.7 ± 0.2	11.2 ± 0.1
	CDCA	8.32	8.4 ± 0.3[c]	972 ± 19[c]	0.70 ± 0.01[c]	5.8 ± 0.2[c]	9.0 ± 0.5
	ADAA	7.83	7.5 ± 0.2	955 ± 4	0.55 ± 0.03	3.9 ± 0.2	10.8 ± 0.03
BSH-2	-	8.24	8.2 ± 0.2	1067 ± 5	0.63 ± 0.01	5.5 ± 0.1	8.6 ± 0.02
	CDCA	6.11	7.4 ± 0.2	975 ± 8	0.49 ± 0.03	3.5 ± 0.2	6.8 ± 0.3
BSH-3	-	8.84	7.9 ± 0.2	1045 ± 3	0.45 ± 0.04	3.7 ± 0.3	8.4 ± 0.03
	CDCA	8.38	8.3 ± 0.4	1054 ± 14	0.69 ± 0.01	6.1 ± 0.2	6.8 ± 0.2
Y123[d]	CDCA (4 eq.)	9.92	10.0	992	0.65	6.5	8.2 ± 0.2

[a] *Obtained by integration of the IPCE spectrum over the 1 sun AM 1.5 G spectrum.* [b] *Values averaged of two desorbed TiO$_2$-electrodes.* [c] *Average values of two cells.* [d] *Values from best-performing device.*
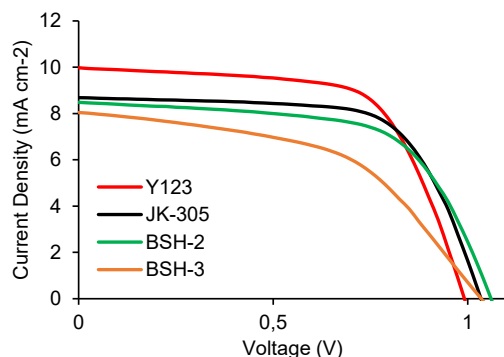
Figure 5. *J-V curves for the best parallel of each dye in devices without anti-aggregation additives, obtained under 1 sun AM 1.5G illumination. Also included is the benchmark dye **Y123** with 4 eq. CDCA.*
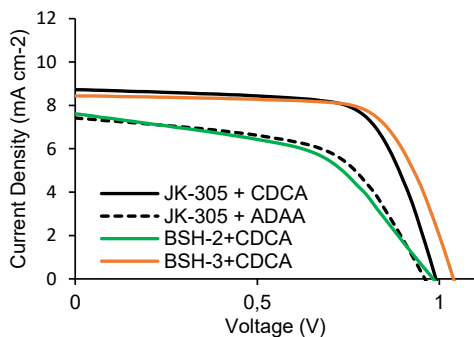
Figure 6. *J-V curves for the best parallel of each dye in devices with anti-aggregation additives, obtained under 1 sun AM 1.5G illumination.*

11
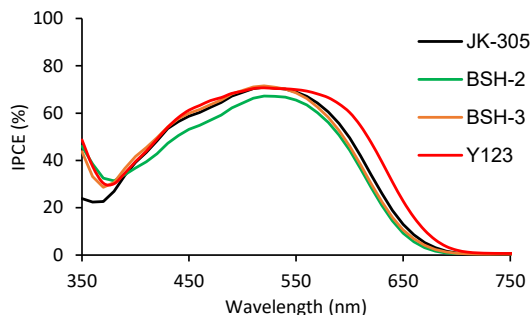
Figure 7. IPCE spectra of the best performing parallel for each dye.
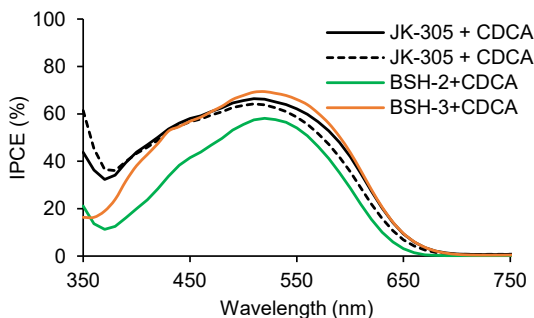
Figure 8. IPCE spectra of the best performing parallel for each dye.

Electrochemical impedance spectroscopy

To further evaluate the anti-recombination properties of the adamantyl moieties we performed impedance spectroscopy experiments on the different devices. The complex plane plots of the devices are shown in Figure S3 in the ESI, and the recombination resistance as a function of applied voltage is shown in Figure 9. In the devices prepared without any additives, **JK-305** and **BSH-2** display higher recombination resistances than the adamantyl donor dye **BSH-3**. This is in stark contrast to the devices prepared with additives, where **BSH-3** display marginally the highest recombination resistance in the series. This further highlights the benefit of added CDCA in staining solution to improve device performance through surface passivation in addition to its anti-aggregational effect.[47] Meanwhile, the addition of CDCA to **BSH-2** resulted in a facilitation of recombination which could stem from undesired interactions between the adamantyl on the π-spacer and CDCA. This is in contrast to the results from our previous study, where the CDCA-substituted π-spacer dyes showed improved electron lifetimes from addition of CDCA to the staining solution. The use of ADAA as an additive in the staining solution of **JK-305** also proved to be detrimental, as it lowered the recombination resistance compared to the additive-free **JK-305** device, and the **JK-305**/CDCA device. The results from EIS support the hypothesis that the lower photovoltage measured for devices prepared with anti-aggregation additives is due to a facilitation of recombination.

12
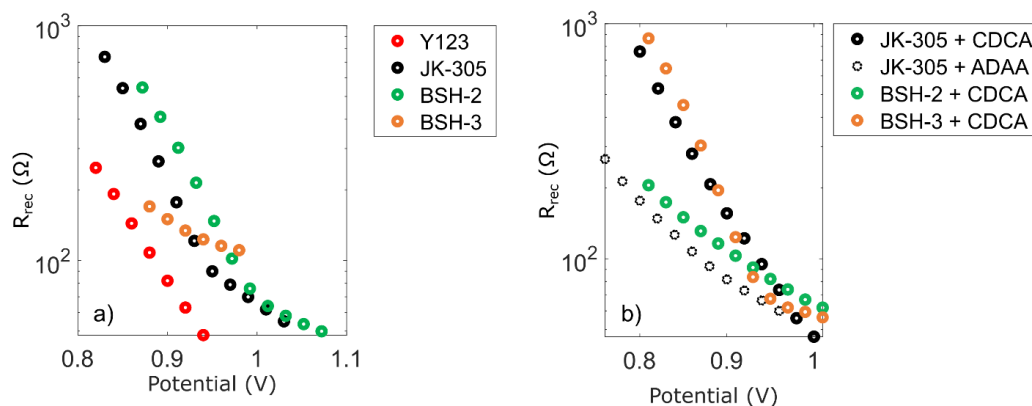
Figure 9. The recombination resistances of the dyes, obtained from EIS under monochromatic light, plotted against applied voltage for a) the devices without anti-aggregation additives and the benchmark dye *Y123*, b) the devices with anti-aggregation additives.

Conclusion

By introducing ethyladamantyl substitutions on two different locations of the triarylamine dye scaffold, namely the π-spacer and the donor, we designed and synthesized two novel dyes **BSH-2** and **BSH-3**. The effects of these substitutions were evaluated by comparing them to the performance of a reference dye without any modifications, the previously reported **JK-305** dye. Overall, we saw that the ethyladamantyl substituted dyes produced higher photovoltages than the reference dye in all cases. The photovoltaic performance of the dye with an adamantyl-substituted π-spacer, **BSH-2**, showed sign of deleterious interactions between the substituent and CDCA. The EIS measurements revealed that the **BSH-2**/CDCA device suffered from a lower recombination resistance compared to the additive-free **BSH-2** device. Conversely, the adamantyl donor dye, **BSH-3**, got a significant boost in photovoltaic performance from added CDCA, EIS measurements showed that CDCA had increased the recombination resistance considerably. The best photovoltaic performance, and the highest recombination resistance was seen from the **BSH-3**/CDCA device, which suggest that this donor could be of use for future dye designs.

Experimental Section

Materials and reagents

All reactions were performed under inert N_2-atmosphere. The chemicals used were all purchased from Merck. A full account of the synthetic procedures is given in the ESI.

Analytical instruments

13

^{1}H and ^{13}C NMR was performed using either a BRUKER 400 MHz or 600 MHz magnet, the spectra obtained are calibrated against residual solvent peak of CDCl$_3$ (7.26/77.16 ppm), CD$_2$Cl$_2$ (5.32/53.84 ppm), DMSO-d_6 (2.50/39.52 ppm), Acetone-d_6 (2.05/29.84 ppm) or THF-d_8 (1.72/25.31 ppm). The IR-spectra are obtained using a BRUKER Alpha Eco-ATR FTIR spectrometer, the data is reported with wavenumber and intensity of the signal. Mass determination was performed by MS-analysis in positive ionization mode on a Synapt G2-S Q-TOF-instrument for Waters, the samples were ionized by an ASAP-probe (APCI) without prior chromatographic separation. UV-Vis spectroscopy was performed using a Hitachi U-1900 spectrometer, and photoluminescence characterization was carried out on an Edinburgh Instruments FS5-spectrofluorometer. CV experiments were carried out using a Versastat 3 Potentiostat, the data was acquired using the Versastudio software. The three-electrode system consisted of a stained TiO$_2$ photoanode as the working electrode, a graphite carbon counter electrode, and a Ag/AgCl reference. The supporting electrolyte was 0.1 M LiTFSI in dry acetonitrile.

Fabrication of dye-sensitized solar cells

The anodes were prepared from FTO glass (NSG10, Nippon Sheet Glass), which was first cleaned in a Deconex 21-solution (2 g/L) under sonication for 45 minutes. Next the FTO was treated with UV/O$_3$ (Novascan PSD-UV) for 15 minutes. Immersion of the glass in aqueous TiCl$_4$-solution (40 mM) at 70 °C for 2 × 30 minutes followed by rinsing with deionized water and ethanol was carried out before sintering the TiO$_2$ for 1 hour at 250 °C on hotplate to deposit a blocking layer on the FTO-sample. Pastes of TiO$_2$ were screen printed onto the FTO (120 T mesh, area 0.2826 cm^2, Seritec Services S.A.), first two active layers (30NR-D, Dyesol) were printed with 5 minutes heating on a hotplate at 125 °C after each layer. A scattering layer (WER2-O, Dyesol) was ultimately printed, and the TiO$_2$ was sintered on a programmable hotplate at set temperatures of 125, 250, 375, 450, and 500 °C for 5, 5, 5, 15, and 30 minutes with a ramping time of 5 minutes. This yielded electrodes consisting of a 4 μm thick active layer and 2 μm thick scattering layer measured by a Bruker DekTak XT profilometer. Before staining the electrodes were annealed at 500 °C for 30 minutes, using a hotplate.

The counter electrodes were prepared from TEC10 FTO glass supplied by Sigma Aldrich. Holes were drilled into the electrodes from the FTO-side using a diamond drill bit, this procedure was carried out under water. The glass plates were then cleaned using Deconex 21 (aq., 2 g/L), deionized water, ethanol, and acetone, in an ultrasonic bath for 15 minutes for each. An electrocatalytic layer of poly(3,4-ethylenedioxythiophene) was deposited on the FTO following the previously reported procedure by Ellis et al.[48]

The photoanodes were placed in the dye bath while still holding ~ 80 °C from the annealing-procedure and stored in a chamber at 30 °C overnight. The dye baths were prepared using a mixture of acetonitrile,

14

WILEY-VCH

t-butanol, and THF (1:1:1, v/v) to make a solution of dye (0.1 mM) and any eventual co-adsorbent CDCA or ADAA (1 mM). The staining of the reference **Y123** was done similarly, but the solvent mixture used was in this case *t*-butanol and acetonitrile (1:1, v/v) and the concentration was CDCA was reduced (0.4 mM). Following 15 hours of staining the electrodes were rinsed in acetonitrile for 2 minutes, then sealed to the counter electrode using Surlyn (25 μm, Solaronix) in a drybox. A 4 × 20 second treatment of the cell using a 50 W PTC heat element was sufficient to seal the cells. The electrolyte was vacuum backfilled into the device, the filling-hole was sealed with Surlyn and a glass cover disk. To complete the devices, the electrodes were painted with silver conducting paint (Electrolube, SCP). The electrolyte employed was a previously reported electrolyte, consisting of $[Cu^{(I)}(tmby)_2]TFSI$ (0.20 M), $[Cu^{(II)}(tmby)_2](TFSI)_2$ (0.10 M), LiTFSI (0.10 M), and , *N*-methylbenzimidazole (0.60 M) dissolved in dry acetonitrile.[6]

Device characterization

J-V curves were obtained under 1 sun illumination AM 1.5G illumination provided by a Sciencetech SP300B solar simulator, calibrated with a Newport Reference Cell (91150V), connected to a Keithley 2450 SourceMeter. A mask with an active area of 0.238 cm^2 was used on all the J-V measurements. IPCE measurements were carried out using a halogen lamp (Ocean Optics HL-2000) and a monochromator (Spectral Products CM110) connected to the Keithley 2450. The devices and the reference photodiode (Thorlabs, FDS100-CAL) were covered with a mask with a size of 0.049 cm^2. The electrochemical impedance properties were measured in a light-exclusion box containing a Zahner CIMPS QE/IPCE TLS03 tunable light source. The light source was connected to a Zahner XPOT potentiostat, the devices were connected to a Zahner IM6ex potentiostat, both potentiostats were controlled by the Thales software. EIS was performed under constant illumination at wavelength 479 nm with an intensity of 12.6 mW/cm^2. The voltage across the cells was oscillating with an amplitude of 10 mV over a 100mHz – 100 kHz frequency range. The measurements were distributed logarithmically over this range with 8 measurements per decade for frequencies higher than 66 Hz and 3 measurements per decade for frequencies lower than 66 Hz. The results above 66 Hz were also averaged over 20 measurements for every frequency while the results below 66 Hz were averaged over 2 measurements per frequency. The oscillating voltage across the DSSCs had an applied DC-bias during the measurements which was decreased by 20 mV between measurements starting at the open circuit voltage of the cells. All DSSCs were measured 10 times each, with the DC-bias voltage as the variable.

15

WILEY-VCH

The resulting Nyquist plots were fitted to a transmission line model as shown by Fabregat et.al[49] using the nonlinear Levenberg-Marquardt least square fitting method. From the fitted curves, the recombination resistance was extracted and plotted as a function of applied potential.

Supporting Information

Supporting Information is available from the Wiley Online Library or from the author.

Acknowledgements

Received: ((will be filled in by the editorial staff))

Revised: ((will be filled in by the editorial staff))

Published online: ((will be filled in by the editorial staff))

References

[1] O'Regan B, Grätzel M, *Nature*, **1991**, *353*, 737.

[2] Freitag M, Teuscher J, Saygili Y, Zhang X, Giordano F, Liska P, Hua J, Zakeeruddin SM, Moser J-E, Grätzel M, Hagfeldt A, *Nat Photonics*, **2017**, *11*, 372.

[3] Hagfeldt A, Boschloo G, Sun L, Kloo L, Pettersson H, *Chem Rev*, **2010**, *110*, 6595.

[4] Saygili Y, Söderberg M, Pellet N, Giordano F, Cao Y, Muñoz-García AB, Zakeeruddin SM, Vlachopoulos N, Pavone M, Boschloo G, Kavan L, Moser J-E, Grätzel M, Hagfeldt A, Freitag M, *J Am Chem Soc*, **2016**, *138*, 15087.

[5] Cao Y, Liu Y, Zakeeruddin SM, Hagfeldt A, Grätzel M, *Joule*, **2018**, *2*, 1108.

[6] Zhang D, Stojanovic M, Ren Y, Cao Y, Eickemeyer FT, Socie E, Vlachopoulos N, Moser J-E, Zakeeruddin SM, Hagfeldt A, Grätzel M, *Nat Commun*, **2021**, *12*, 1777.

[7] Huaulmé Q, Mwalukuku VM, Joly D, Liotier J, Kervella Y, Maldivi P, Narbey S, Oswald F, Riquelme AJ, Anta JA, Demadrille R, *Nat Energy*, **2020**, *5*, 468.

[8] Naim W, Novelli V, Nikolinakos I, Barbero N, Dzeba I, Grifoni F, Ren Y, Alnasser T, Velardo A, Borrelli R, Haacke S, Zakeeruddin SM, Graetzel M, Barolo C, Sauvage F, *JACS Au*, **2021**, *1*, 409.

16

[9] Yoon S, Tak S, Kim J, Jun Y, Kang K, Park J, *Build Environ*, **2011**, *46*, 1899.

[10] Grifoni F, Bonomo M, Naim W, Barbero N, Alnasser T, Dzeba I, Giordano M, Tsaturyan A, Urbani M, Torres T, Barolo C, Sauvage F, *Adv Energy Mater*, **2021**, *11*, 2101598.

[11] Bureš F, *RSC Adv*, **2014**, *4*, 58826.

[12] Li R, Lv X, Shi D, Zhou D, Cheng Y, Zhang G, Wang P, *J Phys Chem C*, **2009**, *113*, 7469.

[13] Liu J, Li R, Si X, Zhou D, Shi Y, Wang Y, Jing X, Wang P, *Energy Environ Sci*, **2010**, *3*, 1924.

[14] Almenningen DM, Hansen HE, Vold MF, Buene AF, Venkatraman V, Sunde S, Hoff BH, Gautun OR, *Dyes Pigm*, **2021**, *185*, 108951.

[15] Zhang L, Cole JM, *J Mater Chem A*, **2017**, *5*, 19541.

[16] Sirohi R, Kim DH, Yu S-C, Lee SH, *Dyes Pigm*, **2012**, *92*, 1132.

[17] Akula SB, Tingare YS, Su C, Chen H-S, Li W-Q, Lekphet W, Li W-R, *Dyes Pigm*, **2021**, *186*, 108985.

[18] Colom E, Andrés-Castán JM, Franco S, Garín J, Montoya JF, Orduna J, Villacampa B, Blesa MJ, *Dyes Pigm*, **2017**, *136*, 505.

[19] Joly D, Godfroy M, Pellejà L, Kervella Y, Maldivi P, Narbey S, Oswald F, Palomares E, Demadrille R, *J Mater Chem A*, **2017**, *5*, 6122.

[20] Wang J, Liu S, Chai Z, Chang K, Fang M, Han M, Wang Y, Li S, Han H, Li Q, Li Z, *J Mater Chem A*, **2018**, *6*, 22256.

[21] Sivasankaran L, Pradhan SC, Mishra RK, Soman S, Ajayaghosh A, *Sol Energy*, **2022**, *236*, 182.

[22] Kay A, Graetzel M, *J Phys Chem*, **1993**, *97*, 6272.

[23] Buene AF, Almenningen DM, Hagfeldt A, Gautun OR, Hoff BH, *Sol RRL*, **2020**, *4*, 1900569.

[24] Pazoki M, Cappel UB, Johansson EMJ, Hagfeldt A, Boschloo G, *Energy Environ Sci*, **2017**, *10*, 672.

[25] Feldt SM, Gibson EA, Gabrielsson E, Sun L, Boschloo G, Hagfeldt A, *J Am Chem Soc*, **2010**, *132*, 16714.

[26] Gabrielsson E, Ellis H, Feldt S, Tian H, Boschloo G, Hagfeldt A, Sun L, *Adv Energy Mater*, **2013**, *3*, 1647.

[27] Baumann A, Curiac C, Delcamp JH, *ChemSusChem*, **2020**, *13*, 2503.

[28] Fort RC, Schleyer PvR, *Chem Rev*, **1964**, *64*, 277.

[29] Wanka L, Iqbal K, Schreiner PR, *Chem Rev*, **2013**, *113*, 3516.

[30] Davies WL, Grunert RR, Haff RF, McGahen JW, Neumayer EM, Paulshock M, Watts JC, Wood TR, Hermann EC, Hoffmann CE, *Science*, **1964**, *144*, 862.

[31] Maassab HF, Cochran KW, *Science*, **1964**, *145*, 1443.

[32] Butterworth RF, *Drugs in R&D*, **2021**, *21*, 267.

[33] Watson Brian L, Rolston N, Bush KA, Taleghani L, Dauskardt RH, *J Mater Chem A*, **2017**, *5*, 19267.

[34] Zhang K, Wang L, Liang Y, Yang S, Liang J, Cheng F, Chen J, *Synth Met*, **2012**, *162*, 490.

[35] Cigánek M, Heinrichová P, Kovalenko A, Kučerík J, Vala M, Weiter M, Krajčovič J, *Dyes Pigm*, **2020**, *175*, 108141.

[36] Kovalenko A, Yumusak C, Heinrichova P, Stritesky S, Fekete L, Vala M, Weiter M, Sariciftci NS, Krajcovic J, *J Mater Chem C*, **2017**, *5*, 4716.

[37] Kato F, Kikuchi A, Okuyama T, Oyaizu K, Nishide H, *Angew Chem Int Ed*, **2012**, *51*, 10177.

[38] Flores-Díaz N, Bahng H-w, Vlachopoulos N, Moser J-E, Zakeeruddin SM, Grätzel M, Hagfeldt A, *J Mater Chem A*, **2019**, *7*, 10998.

17

WILEY-VCH

[39] Lim K, Ju MJ, Song J, Choi IT, Do K, Choi H, Song K, Kim HK, Ko J, *ChemSusChem*, **2013**, *6*, 1425.

[40] Bruno NC, Tudge MT, Buchwald SL, *Chem Sci*, **2013**, *4*, 916.

[41] Billingsley KL, Buchwald SL, *J Org Chem*, **2008**, *73*, 5589.

[42] Feng Q, Zhou G, Wang Z-S, *J Power Sources*, **2013**, *239*, 16.

[43] Tian H, Yang X, Chen R, Zhang R, Hagfeldt A, Sun L, *J Phys Chem C*, **2008**, *112*, 11023.

[44] Dentani T, Kubota Y, Funabiki K, Jin J, Yoshida T, Minoura H, Miura H, Matsui M, *New J Chem*, **2009**, *33*, 93.

[45] Buene AF, Almenningen DM, *J Mater Chem C*, **2021**, *9*, 11974.

[46] Wu K-j, Shen K, Yu Y, Wang D-l, *Chin J Chem Phys*, **2012**, *25*, 733.

[47] Salvatori P, Marotta G, Cinti A, Anselmi C, Mosconi E, De Angelis F, *J Phys Chem C*, **2013**, *117*, 3874.

[48] Ellis H, Vlachopoulos N, Häggman L, Perruchot C, Jouini M, Boschloo G, Hagfeldt A, *Electrochim Acta*, **2013**, *107*, 45.

[49] Fabregat-Santiago F, Bisquert J, Palomares E, Otero L, Kuang D, Zakeeruddin SM, Grätzel M, *J Phys Chem C*, **2007**, *111*, 6550.

Accepted Manuscript

18

WILEY-VCH

We report two novel triarylamine dyes that are decorated with ethyladamantyl side chains on the π-spacer (**BSH-2**), and on the donor (**BSH-3**).

The ethyladamantyl modified dyes display higher photovoltages than the non-modified reference dye (**JK-305**).

DSSC devices prepared with the adamantyl decorated donor dye (**BSH-3**) and the anti-aggregation additive CDCA display the best PCE of the series, at 6.1%.

D. M. A. Author 1, B. S. H. Author 2, H. E. H. Author 3, A. F. B. Author 4, B. H. H. Author 5, O. R. G. Corresponding Author*

Adamantyl Side-Chains as Anti-aggregating Moieties in Dyes for Dye-Sensitized Solar Cells
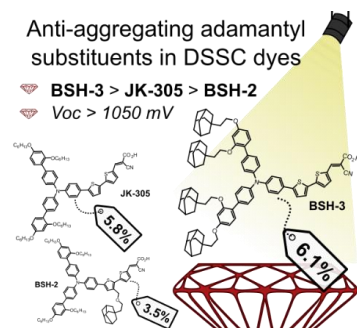
Supporting Information

Adamantyl Side-Chains as Anti-aggregating Moieties in Dyes for Dye-Sensitized Solar Cells

David Moe Almenningen[a], Brita Susanne Haga[a], Henrik Erring Hansen[b], Audun Formo Buene[c], Bård Helge Hoff[a], Odd Reidar Gautun[a]*

List of contents

Absorption and emission
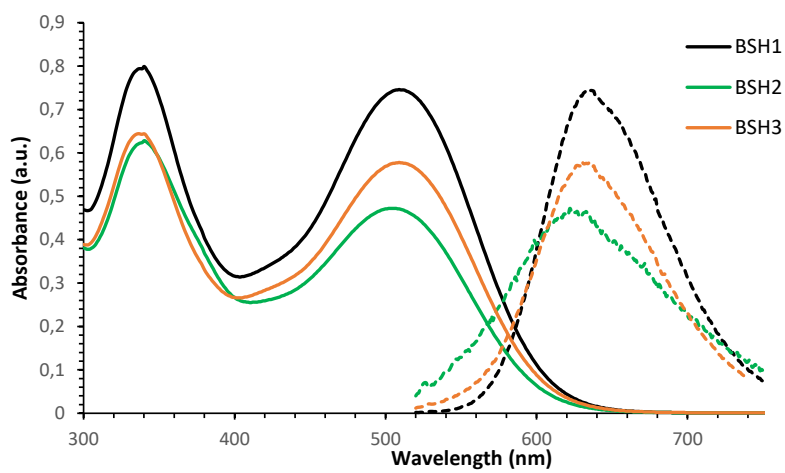
Figure S1. Normalized absorption (-) and emission (--) spectra of the dyes in DCM solution.

Cyclic voltammetry
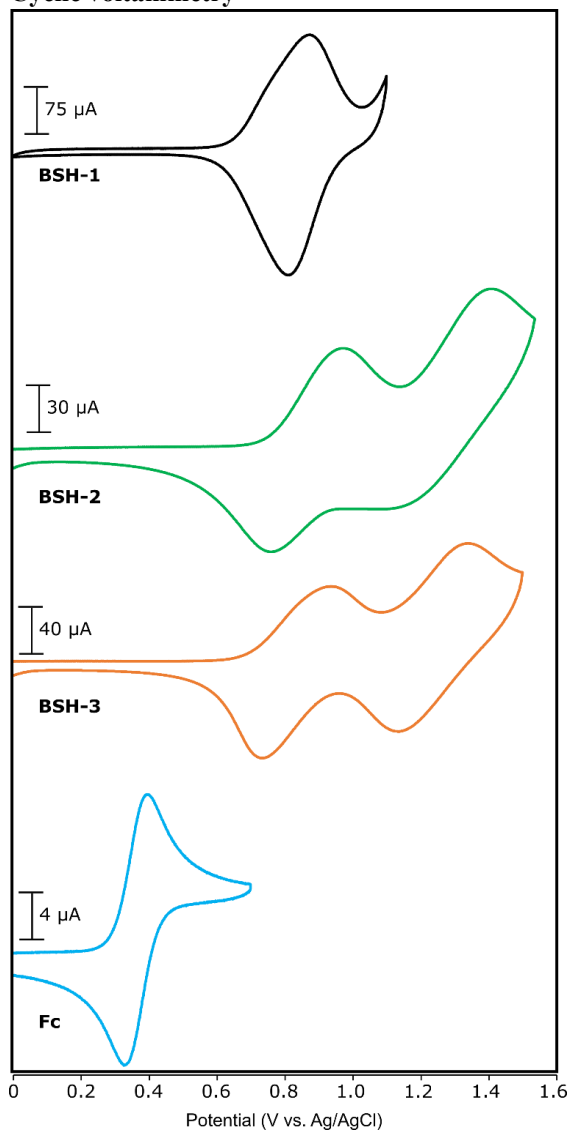
Figure S2. CVs of the dyes and ferrocene. Sensitizers measured on TiO_2 films (2.5 μm on FTO glass), carbon counter electrode, Ag/AgCl reference, 0.1 M LiTFSI supporting electrolyte. Ferrocene (Fc) was measured with a glassy carbon working electrode and used for calibration with a value of 0.624 V versus SHE.[1]

Electrochemical impedance spectroscopy
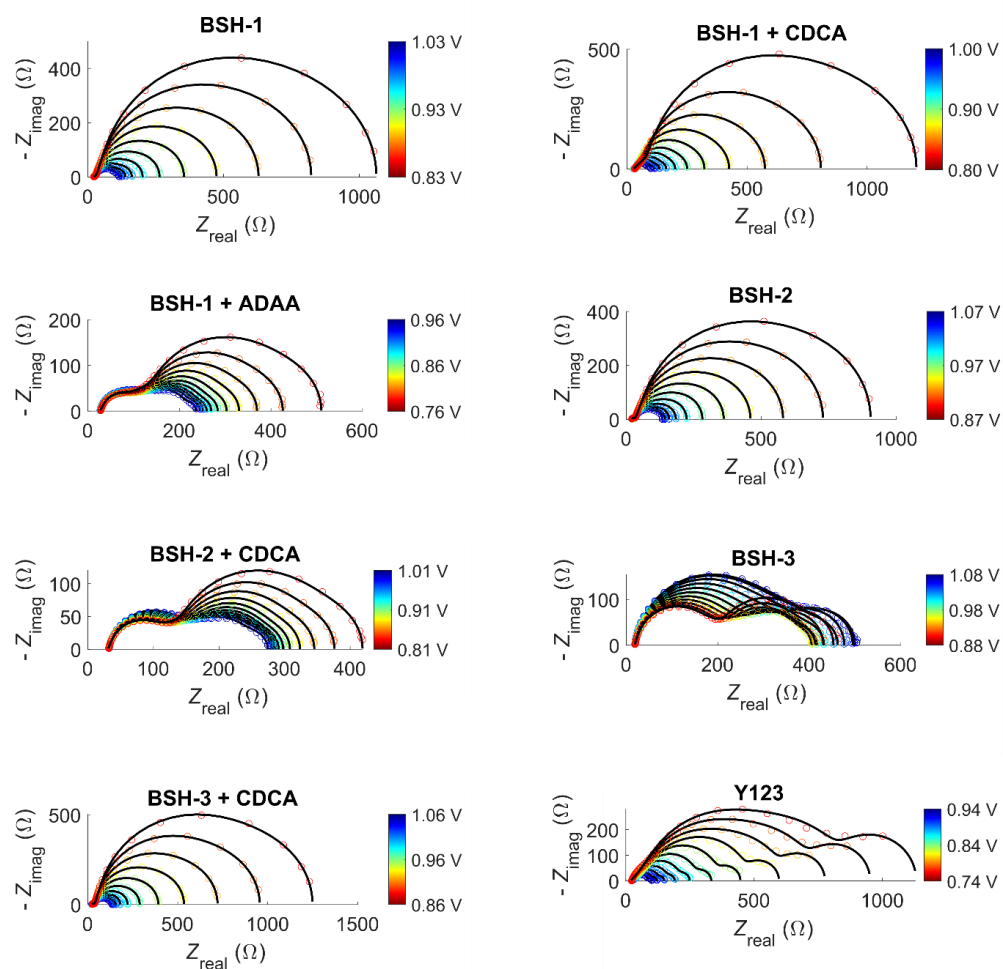
Figure S3. Complex plane diagrams obtained from electrochemical impedance spectroscopy under monochromatic light of 479 nm.

Experimental

Materials and reagents

All reactions were carried out under nitrogen atmosphere, and all synthesis reagents were acquired from Merck.
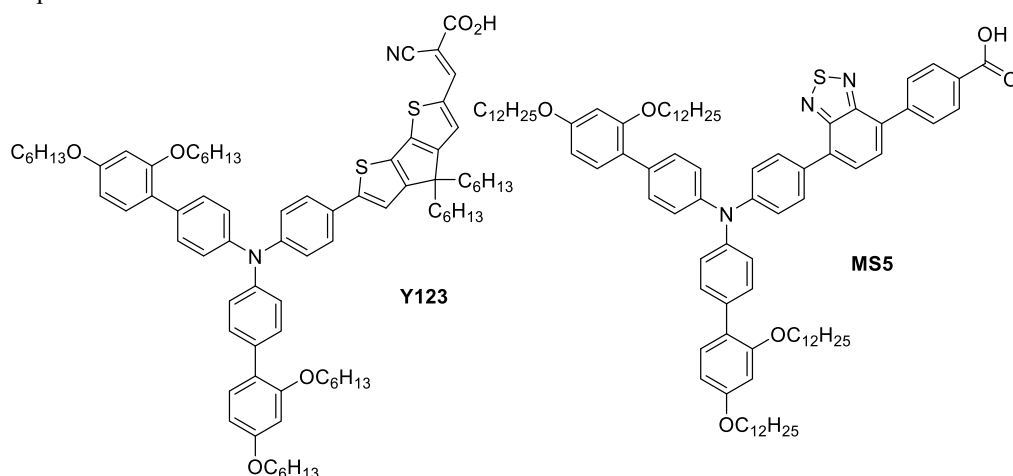
Figure S4. Structure of the benchmark dye **Y123**[2] and the dye **MS5**[3] which was a source of inspiration for the **BSH-3** dye.

Analytical instruments

NMR spectroscopy (^{1}H and ^{13}C) was recorded on 400 and 600 MHz Bruker instruments, and all chemical shifts are reported relative to the respective solvent signals. Mass determination was performed on a Waters "Synapt G2-S" QTOF instrument in positive and negative modes. UV/Vis spectra were recorded on a Hitachi U-1900 instrument using quarts cuvettes for the solution samples, while fluorescence spectroscopy was recorded on a Cary Eclipse Fluorescence Spectrophotometer. Infrared spectroscopy was recorded on an FTIR Thermo Nicolet Nexus FT-IR spectrophotometer.

Synthesis of methyl 2-(adamantan-1-yl)acetate (1)
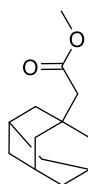
1-Adamantaneacetic acid (6.00 g, 30.9 mmol) was dissolved in methanol (110 mL), before dropwise addition of H_2SO_4 (95%, 1.6 mL). The resulting mixture was stirred at r.t. overnight. Following this, the solvent was removed under reduce pressure. The residue was dissolved in ethyl acetate (120 mL) before being washed with an aqueous solution of $NaHCO_3$ (0.5 M, 120 mL) The aqueous phase was extracted using ethyl acetate (3 × 100 mL), and the combined organic phases dried over Na_2SO_4. The organic phase was then filtered, and the solvents were removed *in vacuo*. The crude product was purified by silica gel column chromatography (dichloromethane, R_f = 0.8). The product **1** was isolated as a clear oil (5.10 g, 24.5 mmol, 79%). ^{1}H NMR (400 MHz, CDCl$_3$) δ: 3.63 (s, 3H), 2.06 (s, 2H), 1.98-1.90 (m, 3H), 1.72-1.54 (m, 12H); ^{13}C NMR (150 MHz, CDCl$_3$) δ: 172.4, 51.1, 48.9, 42.5 (3C), 36.8 (3C), 32.8, 28.7 (3C);

IR (neat, cm^{-1}) ν: 2899 (s), 2847 (m), 1734 (s), 1448 (m), 1325 (m), 1137 (s), 1018 (s); HRMS (ASAP+, *m/z*): found 209.1544 (calcd. $C_{13}H_{21}O_2$ 209.1542, [M+H]$^+$).

Synthesis of 1-adamantaneethanol (2)
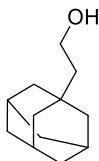
A suspension was of LiAlH$_4$ (1.34 g, 35.3 mmol) in anhydrous THF (50 mL) was kept at 0 °C, to which a solution of **1** (5.10 g, 24.5 mmol) in anhydrous THF (15 mL) was added slowly. The resulting mixture was stirred overnight while being warmed to room temperature. The reaction was stopped following a modified Fieser work-up procedure where water (3.2 mL), then aqueous NaOH (4 M, 3.2 mL) was added to form a white granulate. Water (8 mL) was then added and the reaction mixture was stirred for 10 minutes, before addition of anhydrous Na2SO4 and 10 minutes stirring before removal of solids by filtration. The solvents were removed *in vacuo,* yielding the product **2** as a white solid (3.48 g, 19.3 mmol, 79%). ^{1}H NMR (400 MHz, CDCl$_3$) δ: 3.69 (t, *J* = 7.5 Hz, 2H), 1.96-1.89 (m, 3H), 1.73-1.58 (m, 6H) 1.54-1.49 (m, 6H), 1.37 (t, *J* = 7.5 Hz, 2H) (-O<u>H</u> proton missing). The NMR spectrum is in accordance with previously reported data.[4]

Synthesis of 1-(2-bromoethyl)adamantane (3)
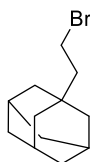
Compound **2** (2.00 g, 11.1 mmol) was added aqueous HBr (47%, 30 mL) and refluxed at 100 °C overnight. After being cooled to room temperature the reaction mixture was diluted with water (50 mL). The aqueous phase was extracted using dichloromethane (3 × 80 mL), and the combined organic phases were dried over Na$_2$SO$_4$. The organic phase was then filtered, and the solvents were removed *in vacuo*, yielding **3** as a white solid (2.54 g, 10.5 mmol, 94%). ^{1}H NMR (400 MHz, CDCl$_3$) δ: 3.44-3.36 (m, 2H), 1.99-1.91 (m, 3H), 1.75-1.57 (m, 8H), 1.53-1.47 (m, 6H). The NMR spectrum is in accordance with previously reported data.[5]

Synthesis of 3-((2-(adamantan-1-yl)ethoxy)methyl)-2-bromothiophene (4)
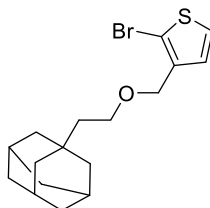
Compound **3** (3.48 g, 19.3 mmol), NaH (460 mg, 19.3 mmol), NaI (580 mg, 3.9 mmol) and anhydrous THF (28 mL) were placed in a flask under nitrogen atmosphere and stirred at 0 °C. A solution of 2-bromo-3-bromomethylthiophene (4.9 mL, 19.3 mmol) in anhydrous THF (30 mL) was added dropwise before the reaction was heated to 50 °C and stirred overnight. The reaction mixture was cooled to room temperature and was quenched by addition of water (60 mL). The aqueous phase was extracted with ethyl acetate (3 × 60 mL) and dried over

6

anhydrous Na$_2$SO$_4$ before the solvents were removed in vacuo. The crude product was purified by silica gel column chromatography (*n*-pentane, R_f = 0.58) to obtain **4** as a yellow oil (5.16 g, 14.6 mmol, 75%). ^{1}H NMR (400 MHz, CDCl$_3$) δ: 7.23 (d, *J* = 5.8 Hz, 1H), 6.98 (d, *J* = 5.8 Hz, 1H), 4.42 (s, 2H), 3.52 (t, *J* = 8.3 Hz, 2H), 1.97-1.90 (m, 3H), 1.73-1.59 (m, 6H), 1.53-1.48 (m, 6H), 1.41 (t, *J* = 8.3 Hz, 2H); ^{13}C NMR (100 MHz, CDCl$_3$) δ: 138.8, 128.4, 126.0, 110.9, 67.0, 66.6, 43.7, 42.9 (3C), 37.3 (3C), 31.9, 28.8 (3C); IR (neat, cm^{-1}) ν: 2896 (s), 2844 (s), 1449 (m), 1103 (s), 686 (m).

Synthesis of 3'-((2-(adamantan-1-yl)ethoxy)methyl)-[2,2'-bithiophene]-5-carbaldehyde (5)
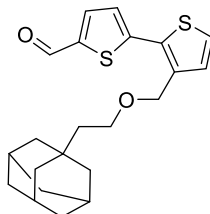
Compound **4** (300 mg, 0.84 mmol) and 5-formyl-2-thiopheneboronic acid (190 mg, 1.27 mmol), K$_3$PO$_4$ (1.54 g, 11.1 mmol), and the precatalyst XPhos Pd G3 (22 mg, 26 µmol) were added to a Schlenk tube and N$_2$-atmosphere established. 1,4-Dioxane (3 mL) and water (3 mL) were degassed and added under nitrogen, the reaction mixture was stirred at 80 °C for 2 hours. After cooling to room temperature, water (10 mL) was added and the aqueous phase was extracted with ethyl acetate (3 x 10 mL). The combined organic phases were dried with brine (10 mL) and over anhydrous Na$_2$SO$_4$, filtered and the solvents were removed *in vacuo*. The residue was purified by silica gel column chromatography (ethyl acetate/*n*-pentane, 1:10, R_f = 0.31). The product **5** was isolated as an orange oil (170 mg, 0.45 mmol, 54%). ^{1}H NMR (400 MHz, CDCl$_3$) δ: 9.84 (s, 1H), 7.67 (d, *J* = 3.4 Hz, 1H), 7.27 (d , *J* = 5.4 Hz, 1H), 7.25 (d, *J* = 3.4 Hz, 1H), 7.11 (d, *J* = 5.4 Hz, 1H), 4.52 (s, 2H), 3.54 (t, *J* = 7.6 Hz, 2H) 1.93-1.84 (m, 3H), 1.69-1.53 (m, 6H), 1.49-1.44 (m, 6H), 1.40 (t, *J* = 7.6 Hz, 2H); ^{13}C NMR (100 MHz, CDCl$_3$) δ: 182.8, 145.7, 143.2, 138.1, 137.0, 132.6, 130.8, 127.0, 126.1, 66.82, 66.75, 43.7, 42.8 (3C), 37.2 (3C), 31.9, 28.8 (3C); IR (neat, cm^{-1}) ν: 2899 (s), 2845 (s), 1666 (s), 1449 (s), 1226 (w); HRMS (ASAP+, *m/z*): found 387.1452 (calcd. C$_{22}$H$_{27}$O$_2$S$_2$ 387.1452, [M+H]$^+$).

Synthesis of 3'-((2-(adamantan-1-yl)ethoxy)methyl)-5'-bromo-[2,2'-bithiophene]-5-carbaldehyde (6)
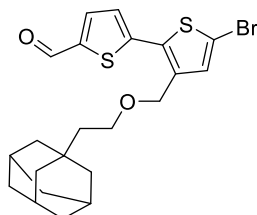
Compound **5** (170 mg, 0.48 mmol) and NBS (110 mg, 0.58 mmol) were added to a round-bottom flask under dark conditions. Degassed dichloromethane (8 mL) was degassed and added under nitrogen at 0 °C. The reaction mixture was then allowed to warm to room temperature while stirring for 15 hours. Water (20 mL) was added and the aqueous phase was extracted
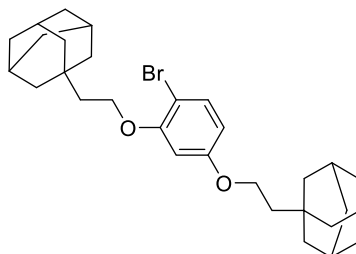
using dichloromethane (3 × 15 mL). The combined organic phases were dried over anhydrous Na$_2$SO$_4$, filtered and the solvents were removed *in vacuo*. The crude product was purified by silica gel column chromatography (ethyl acetate/*n*-pentane 1:10, R_f = 0.34). Compound **6** was isolated as a red oil (140 mg, 0.31 mmol, 66%). ^{1}H NMR (400 MHz, CDCl$_3$) δ: 9.89 (s, 1H), 7.70 (d, *J* = 4.0 Hz, 1H), 7.21 (d , *J* = 4.0 Hz, 1H), 7.13 (s, 1H), 4.49 (s, 2H), 3.56 (t, *J* = 7.4 Hz, 2H) 1.96-1.91 (m, 3H), 1.73-1.59 (m, 6H), 1.52-1.51 (m, 6H), 1.43 (t, *J* = 7.4 Hz, 2H); ^{13}C NMR (100 MHz, CDCl$_3$) δ: 182.7, 144.0, 143.5, 138.7, 136.8, 133.6, 133.3, 127.1, 113.4, 67.0, 66.5, 43.7, 42.8 (3C), 37.2 (3C), 31.9, 28.8 (3C); IR (neat, cm^{-1}) ν: 2899 (s), 2845 (s), 1668 (s), 1450 (s), 1220 (w); HRMS (ASAP+, *m/z*): found 465.0558 (calcd. C$_{22}$H$_{26}$BrO$_2$S$_2$ 465.0557, [M+H]$^+$).

Synthesis of 1-bromo-2,4-bis(hexyloxy)benzene (7)
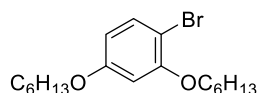
4-Bromoresorcinol (2.99 g, 15.8 mmol) and KOH (7.84 g, 47.5 mmol) were dissolved in DMSO (30 mL), before 1-bromohexane (6.7 mL, 47.5 mmol) was added. The resulting mixture was stirred at r.t. overnight. Following this, the mixture was quenched in water (20 mL). The aqueous phase was extracted using *n*-pentane (4 × 30 mL), the combined organic phases were washed with water (3 x 40 mL) before being dried with brine (50 mL) and over Na$_2$SO$_4$. The organic phase was then filtered, and the solvents were removed *in vacuo*. The crude product was purified by silica gel column chromatography (dichloromethane/*n*-pentane, 1:5, R_f = 0.27). The product **7** was isolated as a clear oil (4.65 g, 13.0 mmol, 82%). ^{1}H NMR (400 MHz, DMSO-*d*$_6$) δ: 7.39 (d, *J* = 8.7 Hz, 1H), 6.62 (d, *J* = 2.6 Hz, 1H), 6.46 (dd, *J* = 8.7, 2.7 Hz, 1H), 4.01 (t, *J* = 6.4 Hz, 2H), 3.94 (t, *J* = 6.5 Hz, 2H), 1.74-1.64 (m, 4H), 1.47-1.35 (m, 4H), 1.34-1.26 (m, 8H), 0.89-0.85 (m, 6H). The NMR spectrum is in accordance with previously reported data.[6]

Synthesis of 1,1'-(((4-bromo-1,3-phenylene)bis(oxy))bis(ethane-2,1-diyl))bis(adamantane) (9)

4-Bromoresorcinol (0.52 g, 2.7 mmol), compound **3** (2.00 g, 8.2 mmol) and KOH (0.46 g, 8.2 mmol) were dissolved in DMSO (50 mL). The resulting mixture was stirred at r.t. overnight. Following this, the mixture was quenched in water (100 mL). The aqueous phase was extracted using *n*-pentane (4 × 50 mL), the combined organic phases were washed with water (3 x 40 mL) before being dried with brine (40 mL) and over Na$_2$SO$_4$. The organic phase was then filtered, and the solvents were removed *in vacuo*. The crude product was purified by silica gel column chromatography (dichloromethane/*n*-pentane, 1:5, R_f = 0.24). The product **9** was isolated as a white solid (0.69 g, 1.3 mmol, 49%) mp 85-88 °C. ^{1}H NMR (600 MHz, CDCl$_3$) δ: 7.37 (d, *J* = 8.7 Hz, 1H), 6.45 (d, *J* = 2.7 Hz, 1H), 6.36 (dd, *J* = 8.7, 2.7 Hz, 1H), 4.05 (t, *J* = 7.2

Hz, 2H), 3.99 (t, J = 7.2 Hz, 2H), 1.98-1.95 (m, 6H), 1.74-1.69 (m, 6H), 1.68-1.63 (m, 8H), 1.62-1.55 (m, 14H); ^{13}C NMR (150 MHz, CDCl$_3$) δ: 159.7, 156.3, 133.2, 106.4, 102.8, 101.4, 65.2, 64.5, 43.1, 42.84 (3C), 42.83 (3C), 37.21 (3C), 37.19 (3C), 32.0, 28.81 (3C), 28.78 (3C); IR (neat, cm^{-1}) ν: 2945 (s), 2845 (m), 1597 (w), 1305 (w), 1019 (w); HRMS (ASAP+, m/z): found 513.2361 (calcd. C$_{30}$H$_{42}$BrO$_2$ 513.2368, [M+H]$^+$).

Synthesis of N-(2',4'-bis(hexyloxy)-[1,1'-biphenyl]-4-yl)-2',4'-bis(hexyloxy)-N-phenyl-[1,1'-biphenyl]-4-amine (11)
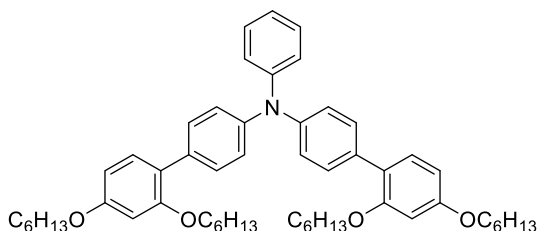
Compound **7** (1.99 g, 12.9 mmol) was added along with PdCl$_2$(CH$_3$CN)$_2$ (44 mg, 170 µmol), SPhos (138 mg, 336 µmol). The compounds were dissolved in 1,4-dioxane (17 mL), then 4,4,5,5-tetramethyl-1,3,2-dioxaborolane (1.6 mL, 11.8 mmol) and NEt$_3$ (2.3 mL, 17.6 mmol) were added. The reaction mixture was heated to 80 °C and left stirring for two hours before the reaction mixture was cooled to room temperature. The contents of the reaction were filtered through a Celite plug using EtOAc as eluent, the solvents were then removed in vacuo. The crude boronate ester **8** was a brown viscous oil that was used without further purification.

4,4′-Dibromotriphenylamine (471 mg, 1.2 mmol), K$_2$CO$_3$ (1.54 g, 11.1 mmol), Pd(OAc)$_2$ (19 mg, 84 µmol), SPhos (69 mg, 168 µmol) along with 1.51 g of the crude boronate **8** were added. 1,4-Dioxane (5 mL) and water (5 mL) were degassed and added under nitrogen, the reaction mixture was stirred at 80 °C for 24 hours. After cooling to room temperature, water (50 mL) was added and the aqueous phase was extracted with ethyl acetate (3 x 50 mL). The combined organic phases were dried with brine (50 mL) and over anhydrous Na$_2$SO$_4$, filtered and the solvents were removed *in vacuo*. The residue was purified by silica gel column chromatography (dichloromethane/n-pentane, 1:1, R_f = 0.40). The product **11** was isolated as a yellow oil (810 mg, 1.00 mmol, 87%). ^{1}H NMR (400 MHz, CDCl$_3$) δ: 7.45-7.40 (m, 4H), 7.28-7.22 (m, 4H), 7.20-7.16 (m, 2H), 7.15-7.10 (m, 4H), 7.00 (t, J = 6.8 Hz, 1H), 6.56-6.51 (m, 4H), 4.00-3.92 (m, 8H), 1.84-1.69 (m, 8H), 1.52-1.44 (m, 4H), 1.44-1.23 (m, 20H), 0.91 (t, J = 7.1 Hz, 6H), 0.86 (t, J = 6.9 Hz, 6H). The NMR spectrum is in accordance with previously reported data.[6]

Synthesis of 2',4'-bis(2-(adamantan-1-yl)ethoxy)-*N*-(2',4'-bis(2-(adamantan-1-yl)ethoxy)-[1,1'-biphenyl]-4-yl)-*N*-phenyl-[1,1'-biphenyl]-4-amine (12)
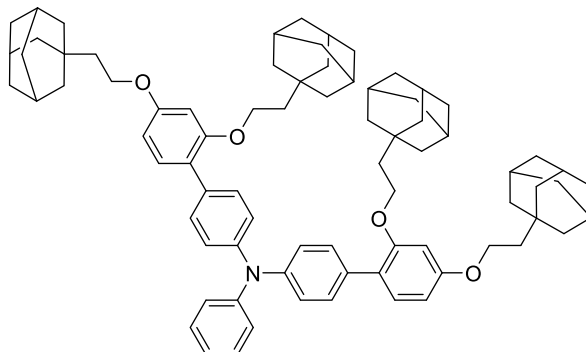
Compound **9** (686 mg, 1.3 mmol) was added along with PdCl$_2$(CH$_3$CN)$_2$ (19 mg, 72 µmol), SPhos (59 mg, 144 µmol). The compounds were dissolved in 1,4-dioxane (6 mL), then 4,4,5,5-tetramethyl-1,3,2-dioxaborolane (0.42 mL, 2.9 mmol) and NEt$_3$ (0.6 mL, 4.3 mmol) were added. The reaction mixture was heated to 80 °C and left stirring for two hours before the reaction mixture was cooled to room temperature. The contents of the reaction were filtered through a Celite plug using EtOAc as eluent, the solvents were then removed in vacuo. The crude boronate **10** was a brown viscous oil and was used without further purification.

4,4′-Dibromotriphenylamine (250 mg, 0.62 mmol), K$_2$CO$_3$ (750 mg, 5.4 mmol), Pd(OAc)$_2$ (9 mg, 40 µmol), SPhos (69 mg, 80 µmol) along with 0.74 g of the crude boronate **10** were added. 1,4-Dioxane (3 mL) and water (2 mL) were degassed and added under nitrogen, the reaction mixture was stirred at 80 °C for 24 hours. After cooling to room temperature, water (50 mL) was added and the aqueous phase was extracted with dichloromethane (3 x 30 mL). The combined organic phases were dried over anhydrous Na$_2$SO$_4$, filtered and the solvents were removed *in vacuo*. The residue was purified by silica gel column chromatography (dichloromethane/*n*-pentane, 1:4, R_f = 0.14). The product **12** was isolated as a white solid (390 mg, 0.35 mmol, 56%) mp 120-124 °C. ^{1}H NMR (600 MHz, CDCl$_3$) δ: 7.41 (app. d, J = 8.6 Hz, 4H), 7.27-7.24 (m, 4H), 7.17 (d, J = 8.3 Hz, 2H), 7.12 (app. d, J = 8.6 Hz, 4H), 7.00 (t, J = 8.3 Hz, 1H), 6.55-6.52 (m, 4H), 4.06 (t, J = 7.0 Hz, 4H), 4.01 (t, J = 7.0 Hz, 4H), 2.00-1.97 (m, 6H), 1.94-1.92 (m, 6H), 1.75-1.64 (m, 24H), 1.62-1.59 (m, 16H), 1.58-1.54 (m, 4H), 1.53-1.50 (m, 12H); ^{13}C NMR (150 MHz, CDCl$_3$) δ: 159.6 (2C), 157.2 (2C), 148.2, 146.2 (2C), 133.0 (2C), 131.0 (2C), 130.4 (4C), 129.3 (2C), 124.3 (2C), 123.7 (4C), 123.4 (2C), 122.5, 105.3 (2C), 100.5 (2C), 64.7 (2C), 64.2 (2C), 43.2 (2C), 43.0 (2C), 42.9 (6C), 42.8 (6C), 37.2 (12C), 32.0 (2C), 31.9 (2C), 28.81 (6C), 28.80 (6C); IR (neat, cm^{-1}) ν: 2897 (s), 1845 (m), 1606 (m), 1492 (m), 1175 (m); HRMS (ASAP+, *m/z*): found 1109.7261 (calcd. C$_{78}$H$_{95}$NO$_4$ 1109.7240, [M]$^+$).
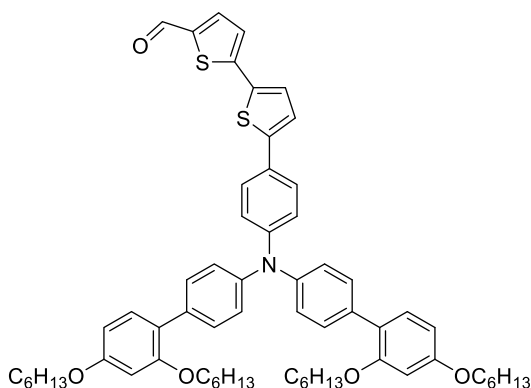
Synthesis of *N*-(2',4'-bis(hexyloxy)-[1,1'-biphenyl]-4-yl)-*N*-(4-bromophenyl)-2',4'-bis(hexyloxy)-[1,1'-biphenyl]-4-amine (13)
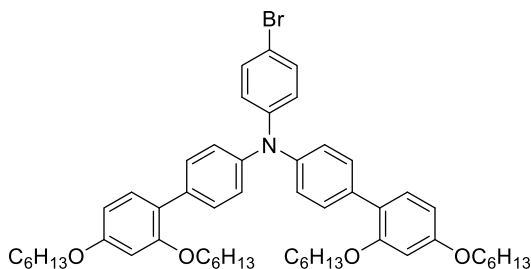
Compound **11** (0.81 g, 1.01 mmol) and NBS (0.18 g, 1.01 mmol) were added to a round-bottom flask under dark conditions. Dichloromethane (20 mL) was degassed and added under nitrogen at 0 °C. The reaction mixture was then allowed to warm to room temperature while stirring for 15 hours. Water (40 mL) was added and the aqueous phase was extracted using dichloromethane (3 × 30 mL). The combined organic phases were dried over anhydrous Na$_2$SO$_4$, filtered and the solvents were removed *in vacuo*. The crude product was purified by silica gel column chromatography (dichloromethane, R_f = 0.8). Compound **13** was isolated as a clear oil (0.87 g, 0.99 mmol, 99%). ^{1}H NMR (400 MHz, CDCl$_3$) δ: 7.46-7.41 (m, 4H), 7.35-7.30 (m, 2H), 7.27-7.23 (m, 2H), 7.14-7.08 (m, 4H), 7.06-7.02 (m, 2H), 6.56-6.51 (m, 4H), 4.00-3.92 (m, 8H), 1.84-1.70 (m, 8H), 1.52-1.44 (m, 4H), 1.44-1.25 (m, 20H), 0.91 (t, *J* = 6.5 Hz, 6H), 0.87 (t, *J* = 6.5 Hz, 6H). The NMR spectrum is in accordance with previously reported data.[6]

Synthesis of *N*-(2',4'-bis(hexyloxy)-[1,1'-biphenyl]-4-yl)-*N*-(4-bromophenyl)-2',4'-bis(hexyloxy)-[1,1'-biphenyl]-4-amine (14)
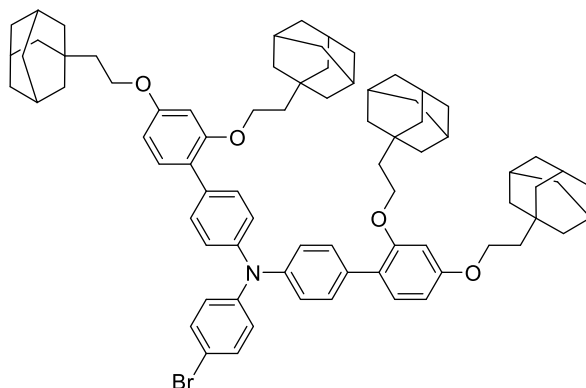
Compound **12** (370 mg, 0.34 mmol) and NBS (64 mg, 0.36 mmol) were added to a round-bottom flask under dark conditions. Dichloromethane (8 mL) was degassed and added under nitrogen at 0 °C. The reaction mixture was then allowed to warm to room temperature while stirring for 15 hours. Water (20 mL) was added and the aqueous phase was extracted using dichloromethane (3 × 15 mL). The combined organic phases were dried over anhydrous Na$_2$SO$_4$, filtered and the solvents were removed *in vacuo*. The crude product was purified by silica gel column chromatography (dichloromethane, R_f = 0.84). Compound **14** was isolated as

a white solid (0.38 g, 0.32 mmol, 95%) mp 139-141 °C. ^{1}H NMR (600 MHz, CDCl$_3$) δ: 7.42 (d, J = 9.5 Hz, 4H), 7.32 (d, J = 9.1 Hz, 2H), 7.24 (d, J = 8.1 Hz, 2H), 7.10 (d, J = 9.5 Hz, 4H), 7.03 (d, J = 9.1 Hz, 2H), 6.55-6.52 (m, 4H), 4.06 (t, J = 7.4 Hz, 4H), 4.02 (t, J = 7.2 Hz, 4H), 2.00-1.96 (m, 6H), 1.95-1.90 (m, 6H), 1.76-1.64 (m, 20H), 1.64-1.58 (m, 20H), 1.56 (t, J = 7.3 Hz, 4H), 1.52-1.49 (m, 12H); ^{13}C NMR (150 MHz, CDCl$_3$) δ: 159.6 (2C), 157.2 (2C), 147.4, 145.6 (2C), 133.6 (2C), 132.2 (2C), 131.0 (2C), 130.5 (4C), 125.2 (2C), 123.9 (4C), 123.1 (2C), 114.5, 105.3 (2C), 100.5 (2C), 64.7 (2C), 64.2 (2C), 43.2 (2C), 43.0 (2C), 42.9 (6C), 42.8 (6C), 37.22 (6C), 37.21 (6C), 32.0 (2C), 31.9 (2C), 28.81 (6C), 28.80 (6C); IR (neat, cm^{-1}) ν: 2896 (s), 2844 (m), 1604 (m), 1580 (m), 1468 (m), 1264 (s), 1174 (m), 1019 (m), 835 (m), 737 (s); HRMS (ASAP+, m/z): found 1187.6365 (calcd. C$_{78}$H$_{94}$NO$_4$Br 1187.6366, [M]$^+$).

Synthesis of 5'-(4-(bis(2',4'-bis(hexyloxy)-[1,1'-biphenyl]-4-yl)amino)phenyl)-[2,2'-bithiophene]-5-carbaldehyde (15)

Compound 1**3** (270 mg, 0.31 mmol) was added along with PdCl$_2$(CH$_3$CN)$_2$ (2.4 mg, 9 µmol), SPhos (7.5 mg, 18 µmol). The compounds were dissolved in 1,4-dioxane (1 mL), then 4,4,5,5-tetramethyl-1,3,2-dioxaborolane (0.1 mL, 0.69 mmol) and NEt$_3$ (0.15 mL, 1.08 mmol) were added. The reaction mixture was heated to 110 °C and left stirring for one hour before the reaction mixture was cooled to room temperature. The contents of the reaction were filtered through a Celite plug using EtOAc as eluent, the solvents were then removed in vacuo. The crude boronic ester was a brown viscous oil that was used without further purification.

5'-Bromo-2,2'-bithiophene-5-carboxaldehyde (76 mg, 0.3 mmol), K$_2$CO$_3$ (254 mg, 1.8 mmol), Pd(OAc)$_2$ (3.5 mg, 15 µmol), SPhos (12.6 mg, 30 µmol) along with 0.28 g of the crude boronate product were added. 1,4-Dioxane (5 mL) and water (5 mL) were degassed and added under nitrogen, the reaction mixture was stirred at 80 °C for 18 hours. After cooling to room temperature, water (50 mL) was added, and the aqueous phase was extracted with dichloromethane (3 x 40 mL). The combined organic phases were dried over anhydrous Na$_2$SO$_4$, filtered and the solvents were removed *in vacuo.* The residue was purified by silica gel column chromatography (dichloromethane/*n*-pentane, 1:4, R_f = 0.48). The product **15** was isolated as an orange wax (130 mg, 0.13 mmol, 43%). ^{1}H NMR (600 MHz, CDCl$_3$) δ: 9.86 (s, 1H), 7.67 (d, J = 4.0 Hz, 1H), 7.50-7.45 (m, 6H), 7.33 (d, J = 4.0 Hz, 1H), 7.27 (app. d, J = 8.9 Hz, 2H), 7.24 (d, J = 3.7 Hz, 1H) 7.20-7.15 (m, 7H), 6.57-6.53 (m, 4H), 4.02-3.95 (m, 8H), 1.81 (q, J = 8.2 Hz, 4H), 1.76 (q, J = 8.2 Hz, 4H), 1.52-1.45 (m, 4H), 1.44-1.39 (m, 4H), 1.39-

1.34 (m, 8H), 1.34-1.28 (m, 8H), 0.93 (t, J = 7.0 Hz, 6H), 0.88 (t, J = 7.0 Hz, 6H); ^{13}C NMR (150 MHz, CDCl$_3$) δ: 182.5, 159.8 (2C), 157.1 (2C), 148.4, 147.7, 146.7, 145.5 (2C), 141.4, 137.6, 134.0, 133.8 (2C), 131.0 (2C), 130.5 (4C), 127.4, 126.9, 126.7 (2C), 124.3 (4C), 123.8, 123.20, 123.17 (2C), 123.0 (2C), 105.5 (2C), 100.6 (2C), 68.6 (2C), 68.3 (2C), 31.8 (2C), 31.6 (2C), 29.5 (2C), 29.2 (2C), 25.9 (2C), 22.8 (2C), 22.7 (2C), 14.2 (4C); IR (neat, cm^{-1}) ν: 2928 (m), 2857 (m), 1665 (m), 1453 (s), 1288 (m), 1181 (m), 1048 (m), 832 (m), 795 (m); HRMS (ASAP+, m/z): found 989.5075 (calcd. C$_{63}$H$_{75}$NO$_5$S$_2$ 989.5087, [M]$^+$). The NMR spectra are in accordance with previously reported data.[7]

Synthesis of 3'-((2-(adamantan-1-yl)ethoxy)methyl)-5'-(4-(bis(2',4'-bis(hexyloxy)-[1,1'-biphenyl]-4-yl)amino)phenyl)-[2,2'-bithiophene]-5-carbaldehyde (16)
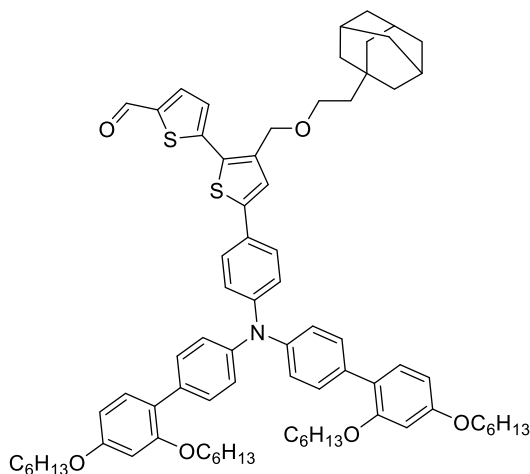
Compound 1**3** (270 mg, 0.31 mmol) was added along with PdCl$_2$(CH$_3$CN)$_2$ (2.4 mg, 9 µmol), SPhos (7.5 mg, 18 µmol). The compounds were dissolved in 1,4-dioxane (1 mL), then 4,4,5,5-tetramethyl-1,3,2-dioxaborolane (0.1 mL, 0.69 mmol) and NEt$_3$ (0.15 mL, 1.08 mmol) was added. The reaction mixture was heated to 110 °C and left stirring for one hour before the reaction mixture was cooled to room temperature. The contents of the reaction were filtered through a Celite plug using EtOAc as eluent, the solvents were then removed in vacuo. The crude boronic ester was a brown viscous oil that was used without further purification.

Compound **6** (129 mg, 0.28 mmol), K$_2$CO$_3$ (254 mg, 1.8 mmol), Pd(OAc)$_2$ (3.5 mg, 15 µmol), SPhos (12.6 mg, 30 µmol) along with 0.28 g of the crude boronate product were added. 1,4-Dioxane (5 mL) and water (5 mL) were degassed and added under nitrogen, the reaction mixture was stirred at 80 °C for 18 hours. After cooling to room temperature, water (50 mL) was added, and the aqueous phase was extracted with dichloromethane (3 x 40 mL). The combined organic phases were dried over anhydrous Na$_2$SO$_4$, filtered and the solvents were removed *in vacuo*. The residue was purified by silica gel column chromatography (dichloromethane, R_f = 0.48). The product **16** was isolated as a yellow-orange wax (170 mg, 0.15 mmol, 48%). ^{1}H NMR (600 MHz, CD$_2$Cl$_2$) δ: 9.87 (s, 1H), 7.73 (d, J = 3.8 Hz, 1H), 7.52 (d, J = 8.9 Hz, 2H), 7.48 (app. d, J = 8.3 Hz, 4H) 7.33 (d, J = 3.8 Hz, 1H), 7.32 (s, 1H), 7.25 (d, J = 8.1 Hz, 2H), 7.19-7.14 (m, 6H), 6.57-6.53 (m, 4H), 4.57 (s, 2H), 4.02-3.95 (m, 8H), 3.62 (t, J = 7.4 Hz, 2H), 1.96-1.91 (m, 3H), 1.83-1.74 (m, 8H), 1.73-1.62 (m, 6H), 1.55 (d, J = 2.5 Hz, 6H) 1.52-1.40 (m, 10H), 1.39-

1.35 (m, 8H), 1.34-1.29 (m, 8H), 0.93 (t, J = 7.0 Hz, 6H), 0.8 (t, J = 7.0 Hz, 6H); ^{13}C NMR (150 MHz, CD$_2$Cl$_2$) δ: 182.9, 160.2 (2C), 157.4 (2C), 148.6, 145.81 (2C), 145.78, 144.8, 143.1, 139.8, 137.4, 134.2 (2C), 131.2 (2C), 130.8 (4C), 130.73, 127.1, 126.9 (2C), 126.8, 125.9, 124.6 (4C), 123.4 (2C), 123.0 (2C), 105.9 (2C), 100.6 (2C), 68.8 (2C), 68.6 (2C), 67.3, 67.1, 44.1, 43.1 (3C), 37.5 (3C), 32.2, 32.1 (2C), 31.9 (2C), 29.7 (2C), 29.5 (2C), 29.3 (3C), 26.21 (2C), 26.16 (2C), 23.1 (2C), 23.0 (2C), 14.3 (2C), 14.2 (2C); IR (neat, cm^{-1}) ν: 2906 (m), 2848 (w), 1665 (m), 1602 (s), 1493 (s), 1291 (m), 1182 (m), 1055 (m); HRMS (ASAP+, m/z): found 1181.6589 (calcd. C$_{76}$H$_{95}$NO$_6$S$_2$ 1181.6601, [M]$^+$).

Synthesis of 5'-(4-(bis(2',4'-bis(2-(adamantan-1-yl)ethoxy)-[1,1'-biphenyl]-4-yl)amino)phenyl)-[2,2'-bithiophene]-5-carbaldehyde (17)
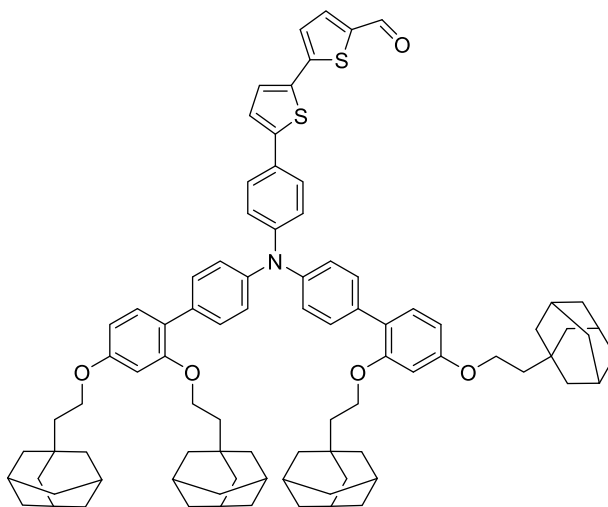
Compound 1**4** (290 mg, 0.24 mmol) was added along with PdCl$_2$(CH$_3$CN)$_2$ (2.4 mg, 9 µmol), SPhos (7.5 mg, 18 µmol). The compounds were dissolved in 1,4-dioxane (1 mL), then 4,4,5,5-tetramethyl-1,3,2-dioxaborolane (0.1 mL, 0.69 mmol) and NEt$_3$ (0.15 mL, 1.08 mmol) were added. The reaction mixture was heated to 110 °C and left stirring for one hour before the reaction mixture was cooled to room temperature. The contents of the reaction were filtered through a Celite plug using EtOAc as eluent, the solvents were then removed in vacuo. The crude boronic ester was a brown viscous oil that was used without further purification.

5′-Bromo-2,2′-bithiophene-5-carboxaldehyde (60 mg, 0.24 mmol), K$_2$CO$_3$ (200 mg, 1.5 mmol), Pd(OAc)$_2$ (3.5 mg, 15 µmol), SPhos (12.6 mg, 30 µmol) along with 0.30 g of the crude boronate product were added. 1,4-Dioxane (5 mL) and water (5 mL) were degassed and added under nitrogen, the reaction mixture was stirred at 80 °C for 18 hours. After cooling to room temperature, water (50 mL) was added, and the aqueous phase was extracted with dichloromethane (3 x 40 mL). The combined organic phases were dried over anhydrous Na$_2$SO$_4$, filtered and the solvents were removed *in vacuo.* The residue was purified by silica gel column chromatography (dichloromethane/n-pentane, 1:8, R_f = 0.67). The product **17** was isolated as a red-orange solid (93 mg, 0.07 mmol, 29%) mp 159-161 °C. ^{1}H NMR (600 MHz, CD$_2$Cl$_2$) δ: 9.84 (s, 1H), 7.69 (d, 1H, J = 4.0 Hz), 7.51 (app. d, J = 8.7 Hz, 2H), 7.46 (app. d, J = 8.6 Hz, 4H), 7.36 (d, 1H, J = 3.9 Hz), 7.28 (d, 1H, J = 3.9 Hz), 7.25-7.22 (m, 3H), 7.16-7.12

(m, 6H), 6.55-6.52 (m, 4H), 4.07 (t, 4H, J = 7.2 Hz), 4.04 (t, 4H, J = 7.2 Hz), 1.99-1.97 (m, 6H), 1.95-1.91 (m, 6H), 1.76-1.64 (m, 24H), 1.64-1.61 (m, 12H), 1.61-1.56 (m, 8H), 1.56-1.54 (m, 12H); ^{13}C NMR (150 MHz, CD$_2$Cl$_2$) δ: 182.9, 160.3 (2C), 157.6 (2C), 148.8, 147.6, 146.9, 145.9 (2C), 142.0, 138.1, 134.52, 134.50 (2C), 131.3 (2C), 131.0 (4C), 127.9, 127.3 (2C), 127.1 (2C), 124.8 (4C), 124.4, 123.7(2C), 123.5 (2C), 123.2 (2C), 106.0 (2C), 100.7 (2C), 65.1 (2C), 64.7 (2C), 43.7 (2C), 43.5 (2C), 43.24 (6C), 43.21 (6C), 37.6 (12C), 32.4 (2C), 32.3 (2C), 29.44 (6C), 29.42 (6C); IR (neat, cm^{-1}) ν: 2900 (s), 2846 (m), 1668 (m), 1601, 1493, 1453 (s), 1177, 1048; HRMS (ASAP+, m/z): found 1301.6940 (calcd. C$_{87}$H$_{99}$NO$_5$S$_2$ 1301.6965, [M]$^+$).

Synthesis of (*E*)-3-(5'-(4-(bis(2',4'-bis(hexyloxy)-[1,1'-biphenyl]-4-yl)amino)phenyl)-[2,2'-bithiophen]-5-yl)-2-cyanoacrylic acid (JK-305)
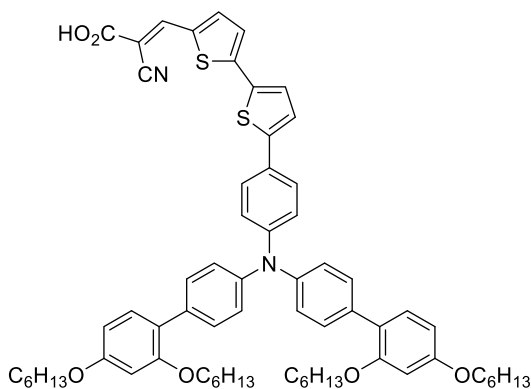
Compound **15** (75 mg, 0.08 mmol) and cyanoacetic acid (130 mg, 1.51 mmol) were dissolved in degassed acetonitrile (22 mL) under nitrogen atmosphere. Piperidine (0.09 mL, 0.9 mmol) was added, and the reaction was heated to 80 °C for 60 minutes before cooling to room temperature and quenched in aqueous HCl (4 M, 50 mL). Dichloromethane (3 × 70 mL) was used to extract the aqueous phase, and the combined organic phases were washed with water (4 × 100 mL), then dried over anhydrous Na$_2$SO$_4$, filtered and the solvents were removed *in vacuo*. The crude product was purified by silica gel column chromatography (gradient: 0-15% MeOH in CH$_2$Cl$_2$), to obtain sensitizer **BSH-1** as a dark solid (63 mg, 0.06 mmol, 79%), 153-155 °C. ^{1}H NMR (600 MHz, DMSO-d_6, 80 °C) δ: 8.40 (s, 1H), 7.93 (d, J = 4.1 Hz, 1H), 7.61 (d, J = 9.2 Hz, 2H), 7.56 (d, J = 4.9 Hz, 1H), 7.52 (d, J = 4.9 Hz, 1H), 7.48-7.42 (m, 5H), 7.23 (d, J = 8.4 Hz, 2H), 7.10 (d, J = 8.5 Hz, 4H), 7.06 (d, J = 9.2 Hz, 2H), 6.62 (d, J = 2.8 Hz, 2H), 6.58 (dd, J = 2.8, 8.4 Hz, 2H), 4.01 (t, J = 6.7 Hz, 4H), 3.98 (t, J = 6.4 Hz, 4H), 1.74 (q, J = 6.7 Hz, 4H), 1.66 (q, J = 6.4 Hz, 4H), 1.48-1.42 (m, 4H), 1.39-1.32 (m, 12H), 1.29-1.23 (m, 8H), 0.90 (t, J = 6.7 Hz, 6H), 0.83 (t, J = 6.4 Hz, 6H) (CO$_2$<u>H</u> proton missing); ^{13}C NMR (150 MHz, DMSO-d_6, 80 °C) δ: 163.0, 159.0 (2C), 156.4 (2C), 147.3, 145.4, 145.3, 145.2, 144.4 (2C), 140.1, 133.5, 133.3 (2C), 132.9, 130.1 (2C), 129.7 (4C), 127.7, 126.23 (2C), 126.16, 124.3, 123.8, 123.4 (4C), 122.2 (2C), 122.0 (2C), 116.0, 106.2 (2C), 100.6 (2C), 98.2, 67.9 (2C), 67.5 (2C), 30.5 (2C), 30.4 (2C), 28.3 (2C), 28.2 (2C), 24.74 (2C), 24.72 (2C), 21.50 (2C), 21.47 (2C), 13.3 (2C), 13.2 (2C); IR (neat, cm^{-1}) ν: 3411 (br w), 2927 (m), 2856 (m), 1658 (m), 1606 (m), 1492 (m), 1446 (s), 1272 (m), 1023 (m), 1002 (s), 823 (w), 761 (w); HRMS (ASAP+, m/z): found 1057.5205 (calcd. C$_{66}$H$_{77}$N$_2$O$_6$S$_2$ 1057.5223, [M+H]$^+$).

Synthesis of (*E*)-3-(3'-((2-(adamantan-1-yl)ethoxy)methyl)-5'-(4-(bis(2',4'-bis(hexyloxy)-[1,1'-biphenyl]-4-yl)amino)phenyl)-[2,2'-bithiophen]-5-yl)-2-cyanoacrylic acid (BSH-2)
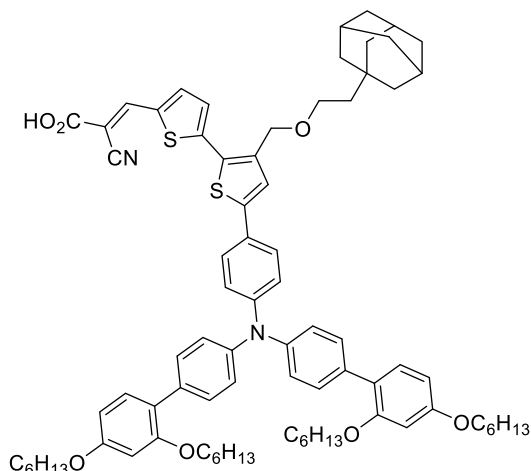
Compound **16** (120 mg, 0.10 mmol) and cyanoacetic acid (170 mg, 2.1 mmol) were dissolved in degassed acetonitrile (45 mL) under nitrogen atmosphere. Piperidine (0.20 mL, 1.2 mmol) was added and the reaction was heated to 80 °C for 1 hour before cooling to room temperature and quenched in aqueous HCl (4 M, 50 mL). Dichloromethane (3 × 70 mL) was used to extract the aqueous phase, and the combined organic phases were washed with water (4 × 100 mL), then dried over anhydrous Na_2SO_4, filtered and the solvents were removed *in vacuo*. The crude product was purified by silica gel column chromatography (gradient: 0-15% MeOH in CH_2Cl_2), to obtain sensitizer **BSH-2** as a dark solid (87 mg, 0.07 mmol, 67%), mp 75-77 °C (dec.).^{1}H NMR (600 MHz, Acetone-d_6) δ: 8.44 (s, 1H), 7.97 (d, *J* = 4.3 Hz, 1H), 7.60 (d, *J* = 8.7 Hz, 2H), 7.51 (d, *J* = 9.0 Hz, 4H), 7.49-7.47 (m, 2H), 7.25 (d, *J* = 8.8 Hz, 2H), 7.14 (d, *J* = 9.0 Hz, 4H), 7.11 (d, *J* = 8.7 Hz, 2H), 6.63 (d, *J* = 2.3 Hz, 2H), 6.57 (dd, *J* = 2.3, 8.8 Hz, 2H), 4.61 (s, 2H), 4.03-3.99 (m, 8H), 3.66 (t, *J* = 7.1 Hz, 2H), 1.92-1.88 (m, 3H), 1.78 (app. q, *J* = 8.1 Hz, 4H), 1.73 (app. q, *J* = 7.7 Hz, 4H), 1.71-1.61 (m, 6H), 1.56 (d, *J* = 2.4 Hz, 6H), 1.52-1.40 (m, 12H), 1.40-1.25 (m, 20H), 0.91 (t, *J* = 8.1 Hz, 6H), 0.86 (t, *J* = 7.7 Hz, 6H) (CO$_2$<u>H</u> proton missing); ^{13}C NMR (150 MHz, Acetone-d_6) δ: 163.9, 160.8 (2C), 158.0 (2C), 149.2, 147.2, 146.3, 146.1 (2C), 145.3, 140.89, 140.87, 136.2, 135.1 (2C), 131.6 (2C), 131.3 (4C), 131.2, 127.51, 127.45, 127.4 (2C), 127.2, 125.0 (4C), 123.6 (2C), 123.4 (2C), 116.9, 106.7 (2C), 101.1 (2C), 98.9, 69.0 (2C), 68.6 (2C), 67.4, 67.2, 44.5, 43.4 (3C), 37.8 (3C), 32.5, 32.4 (2C), 32.3 (2C), 29.8 (4C)*, 29.5 (3C)*, 26.6 (2C), 26.5 (2C), 23.3 (4C), 14.4 (2C), 14.3 (2C); IR (neat, cm^{-1}) ν: 3500 (br w), 2902 (m), 2849 (m), 2218 (w), 1686 (m), 1599 (m), 1490 (m), 1408 (s), 1262 (m), 1178 (s), 825 (m), 734 (s); HRMS (ASAP+, *m/z*): found 1248.6650 (calcd. $C_{79}H_{96}N_2O_7S_2$ 1248.6659, [M]$^+$). *The ^{13}C signals were found using ^{1}H-^{13}C HSQC spectroscopy due to their overlap with the residual solvent signal.
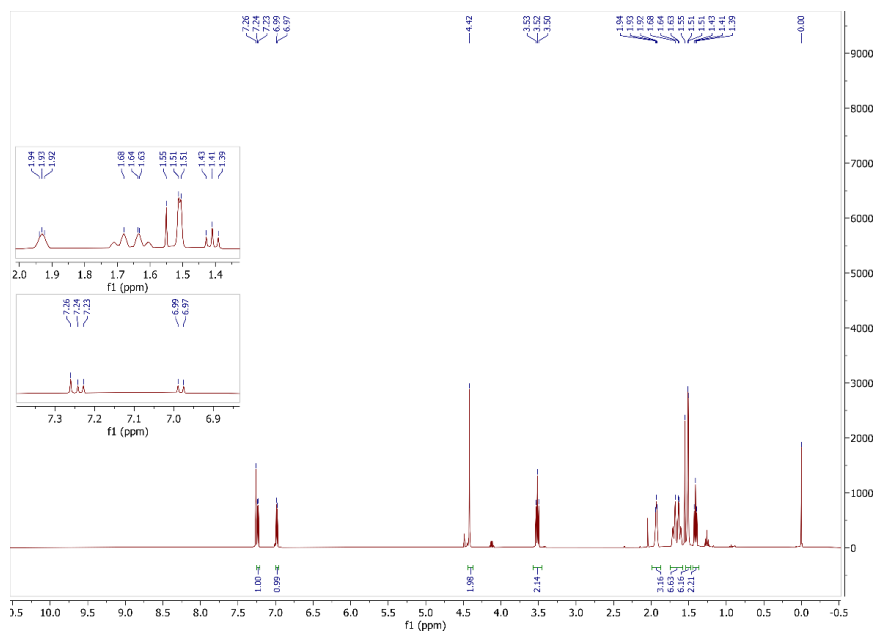
Synthesis of (*E*)-3-(5'-(4-(bis(2',4'-bis(2-(adamantan-1-yl)ethoxy)-[1,1'-biphenyl]-4-yl)amino)phenyl)-[2,2'-bithiophen]-5-yl)-2-cyanoacrylic acid (BSH-3)
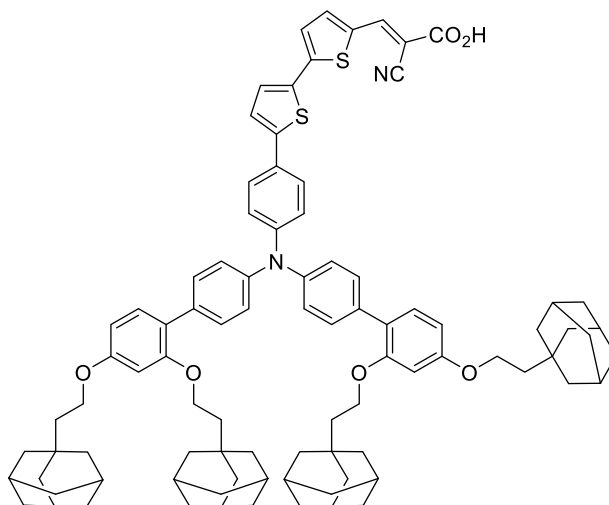

Compound **17** (66 mg, 0.05 mmol) and cyanoacetic acid (90 mg, 1.1 mmol) were dissolved in degassed acetonitrile (40 mL) under nitrogen atmosphere additionally chloroform (5 ml) was added to dissolve **17**. Piperidine (0.10 mL, 0.64 mmol) was added, and the reaction was heated to 80 °C for 3 hours before cooling to room temperature and quenched in aqueous HCl (4 M, 50 mL). Dichloromethane (3 × 70 mL) was used to extract the aqueous phase, and the combined organic phases were washed with water (4 × 100 mL), then dried over anhydrous Na_2SO_4, filtered and the solvents were removed *in vacuo*. The crude product was purified by silica gel column chromatography (gradient: 0-15% MeOH in CH_2Cl_2), to obtain sensitizer **BSH-3** as a dark purple solid (39 mg, 0.03 mmol, 57%), 206-207 °C (dec.). ^{1}H NMR (600 MHz, THF-d_8) δ: 8.32 (s, 1H), 7.79 (d, J = 4.1 Hz, 1H), 7.56 (app. d, J = 8.7 Hz, 2H), 7.48 (d, J = 3,9 Hz, 1H), 7.44 (app. d, J = 8.6 Hz, 4H), 7.38 (d, J = 4,0 Hz, 1H), 7.34 (d, J = 3,9 Hz, 1H), 7.20 (d, J = 8.4 Hz, 2H), 7.14-7.11 (m, 6H), 6.56 (d, J = 2.3 Hz, 2H), 6.53 (dd, J = 2.3, 8.4 Hz, 2H), 4.08-4.02 (m, 8H), 1.99-1.95 (m, 6H), 1.94-1.90 (m, 6H), 1.78-1.67 (m, 24H), 1.66-1.64 (m, 12H), 1.61-1.58 (m, 4H), 1.56-1.54 (m, 16H) (CO$_2$H proton missing); ^{13}C NMR (150 MHz, THF-d_8) δ: 164.0, 160.7 (2C), 158.0 (2C), 149.3, 147.6, 147.3, 146.4, 146.3 (2C), 140.3, 135.3, 135.2 (2C), 134.7, 131.4 (2C), 131.2 (4C), 128.5, 127.9 (2C), 127.3, 124.9, 124.8 (4C), 124.4, 123.8 (2C), 123.8 (2C), 116.6, 106.1 (2C), 101.1 (2C), 99.4, 65.1 (2C), 64.2 (2C), 44.2 (2C), 43.9 (2C), 43.6 (6C), 43.5 (6C), 38.0 (12C), 32.7 (2C), 32.6 (2C), 29.88 (6C), 29.87 (6C); IR (neat, cm^{-1}) ν: 2896 (s), 2844 (m), 2217 (w), 1681 (m), 1578 (m), 1491 (m), 1436 (s), 1264 (s), 1181 (m), 1052 (m), 795 (m), 735 (s); HRMS (ASAP+, *m/z*): found 1324.7125 (calcd. $C_{89}H_{100}N_2O_4S_2$ 1324.7125, [M-CO$_2$]$^+$).
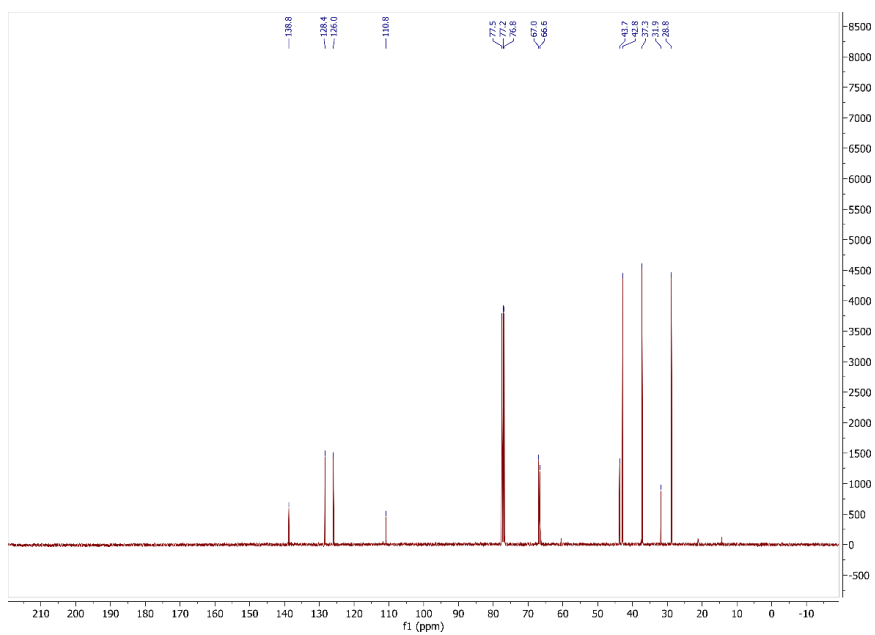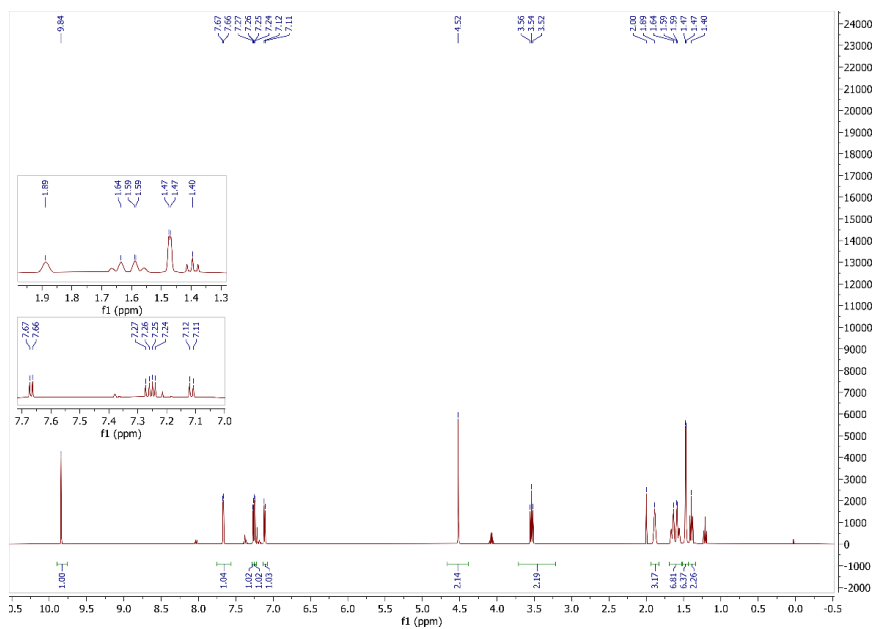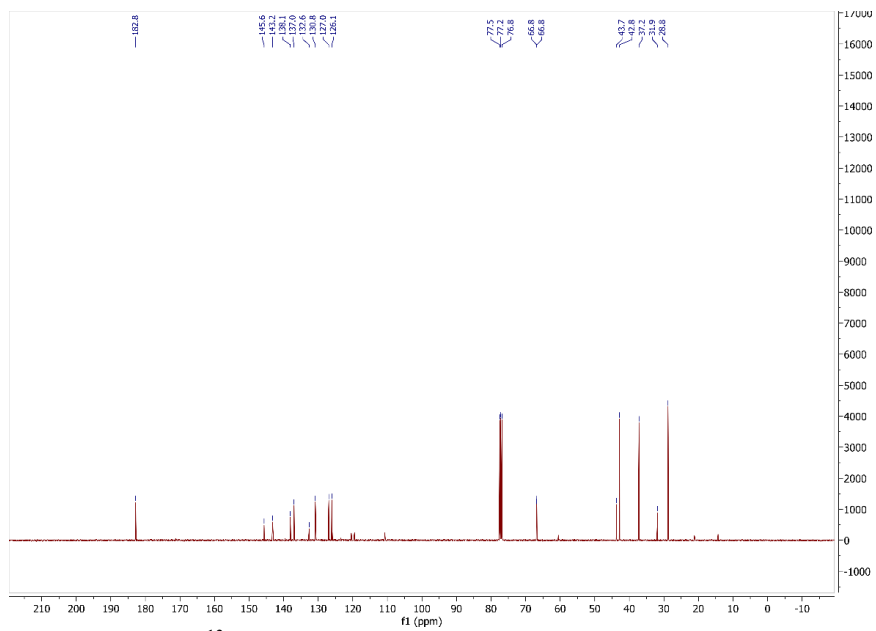
NMR

Figure S5. ^{1}H NMR (400 MHz, CDCl$_3$) spectrum for compound **1**.

Figure S6. ^{13}C NMR (100 MHz, CDCl$_3$) spectrum for compound **1**.

Figure S7. ^{1}H NMR (400 MHz, CDCl$_3$) spectrum for compound **4**.

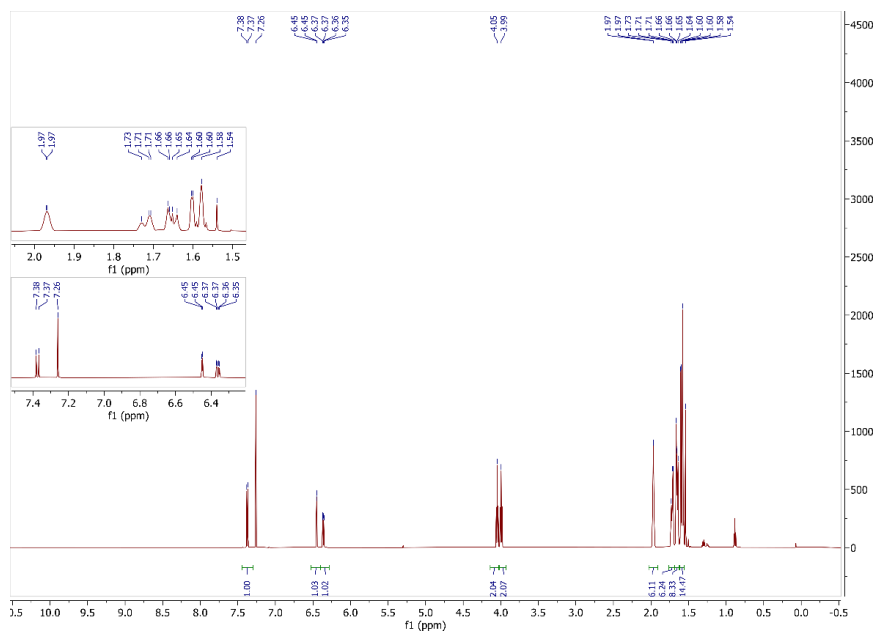**Figure S8.** ^{13}C NMR (100 MHz, CDCl$_3$) spectrum for compound **4**.

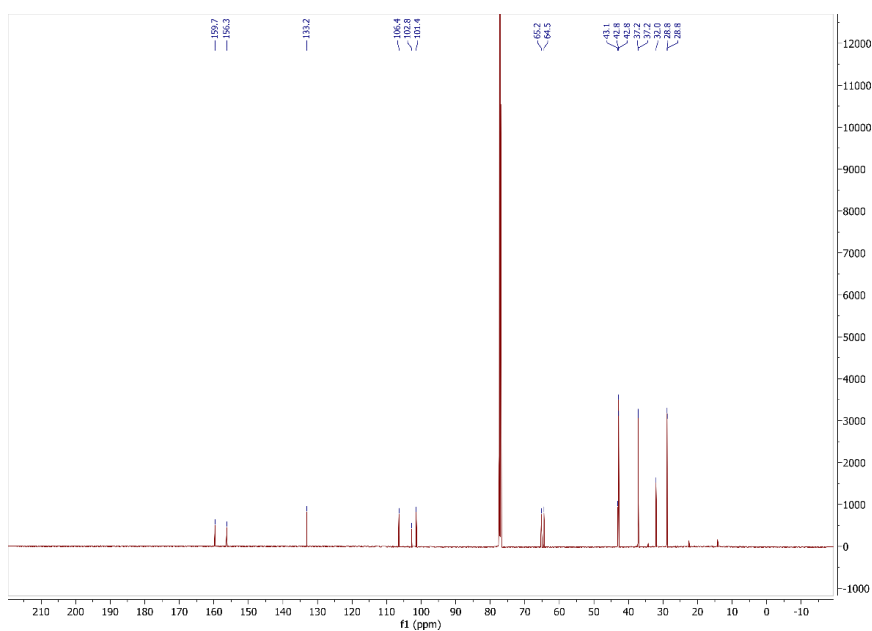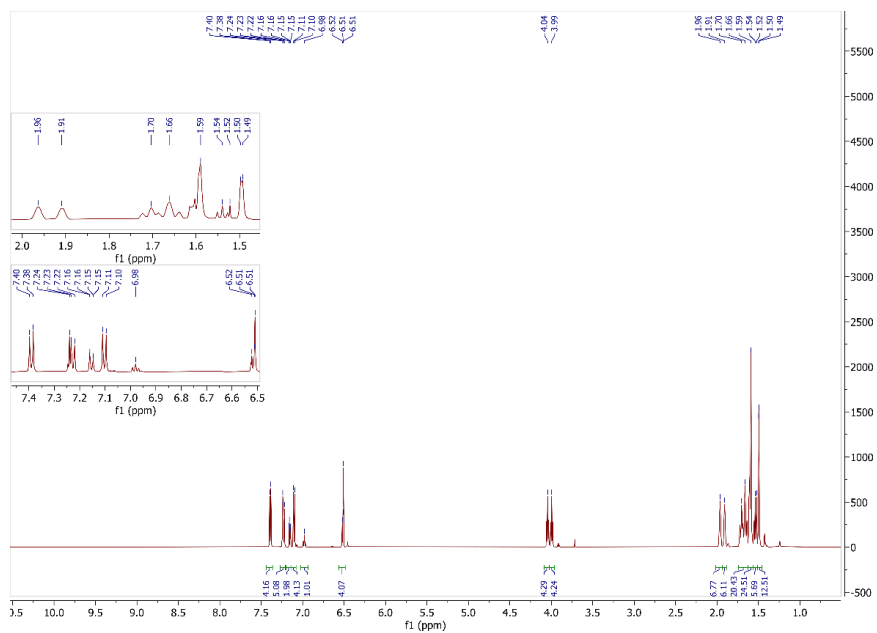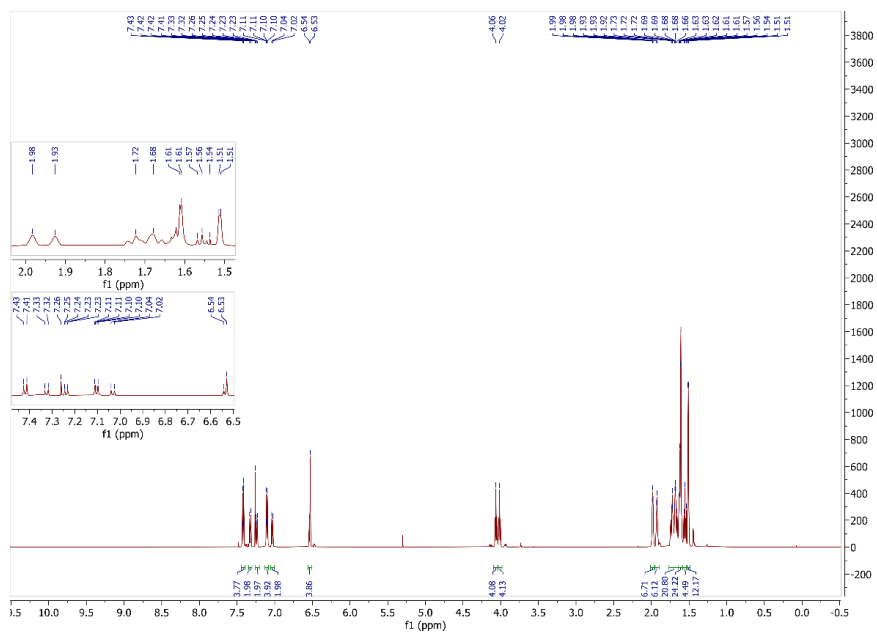**Figure S9.** ^{1}H NMR (400 MHz, CDCl$_3$) spectrum for compound **5**.

Figure S10. ^{13}C NMR (100 MHz, CDCl$_3$) spectrum for compound **5**.

Figure S11. ^{1}H NMR (400 MHz, CDCl$_3$) spectrum for compound **6**.

Figure S12. ^{13}C NMR (100 MHz, CDCl$_3$) spectrum for compound **6**.
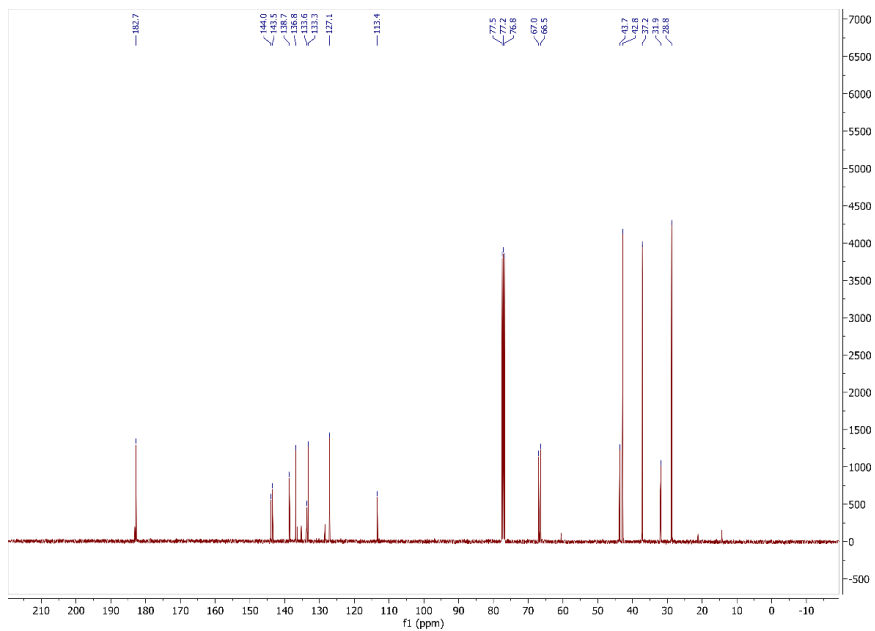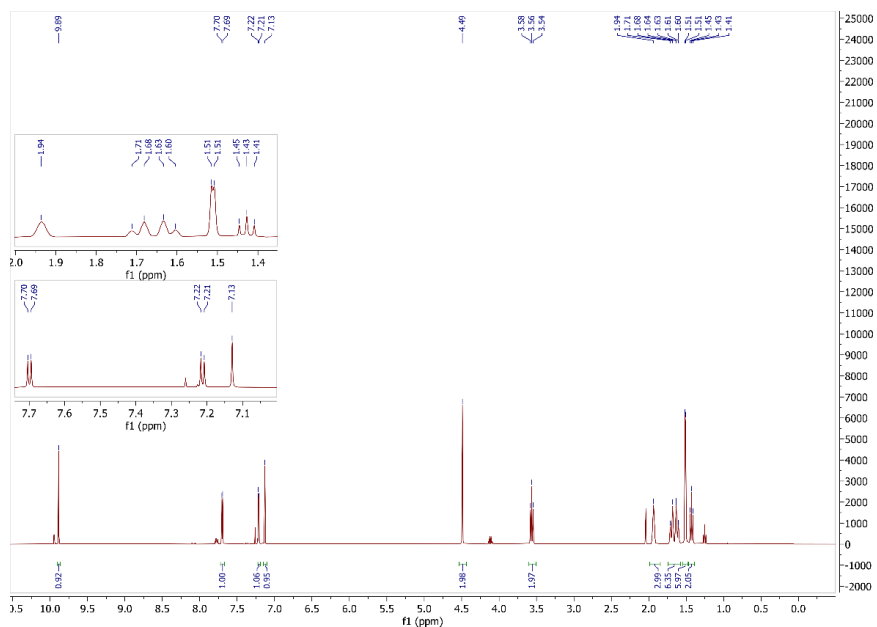
Figure S13. ^{1}H NMR (600 MHz, CDCl$_3$) spectrum for compound **9**.

Figure S14. ^{13}C NMR (150 MHz, CDCl$_3$) spectrum for compound **9**.

Figure S15. ^{1}H NMR (600 MHz, CDCl$_3$) spectrum for compound **12**.
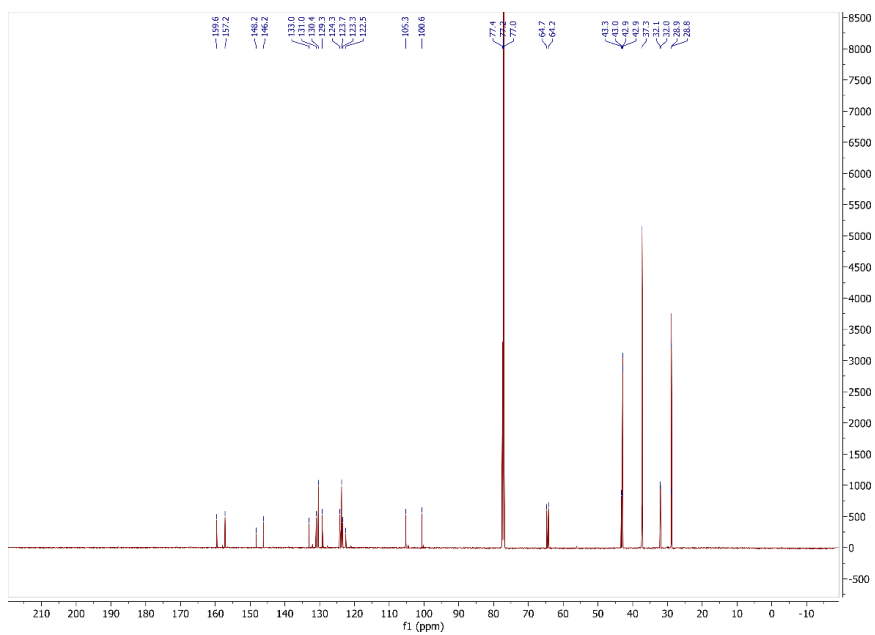
Figure S16. ^{13}C NMR (150 MHz, CDCl$_3$) spectrum for compound **12**.

Figure S17. ^{1}H NMR (600 MHz, CDCl$_3$) spectrum for compound **14**.
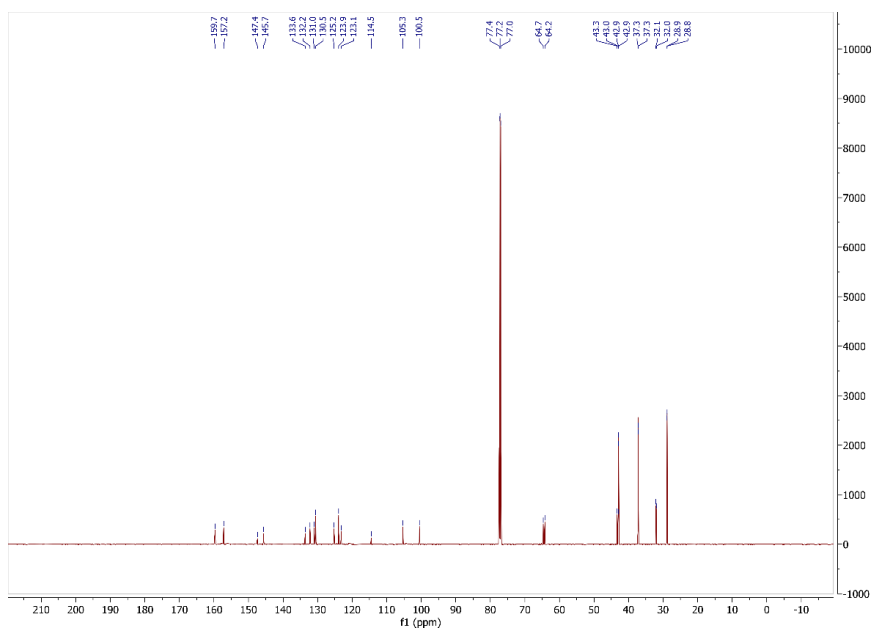
Figure S18. ^{13}C NMR (150 MHz, CDCl$_3$) spectrum for compound **14**.
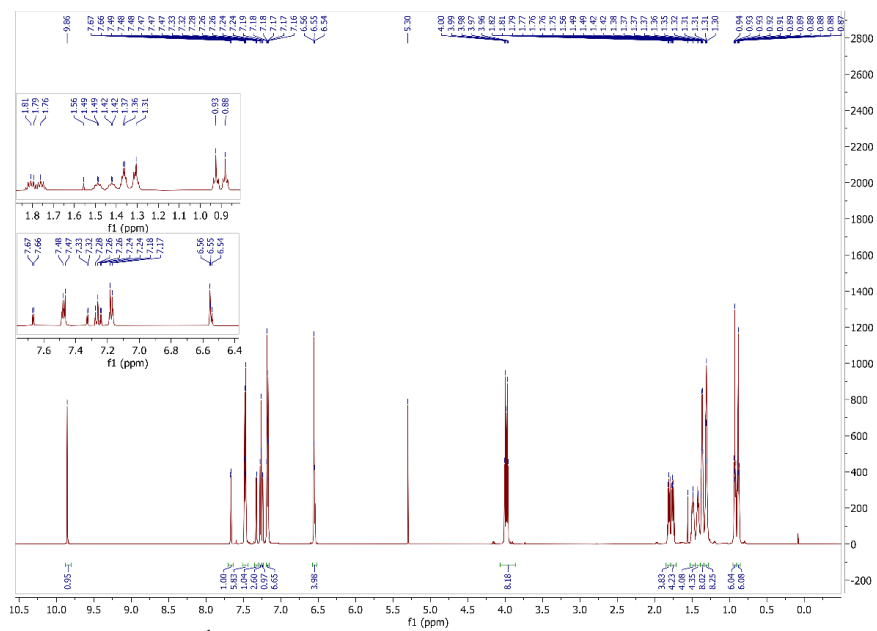
Figure S19. ^{1}H NMR (600 MHz, CDCl$_3$) spectrum for compound **15**.
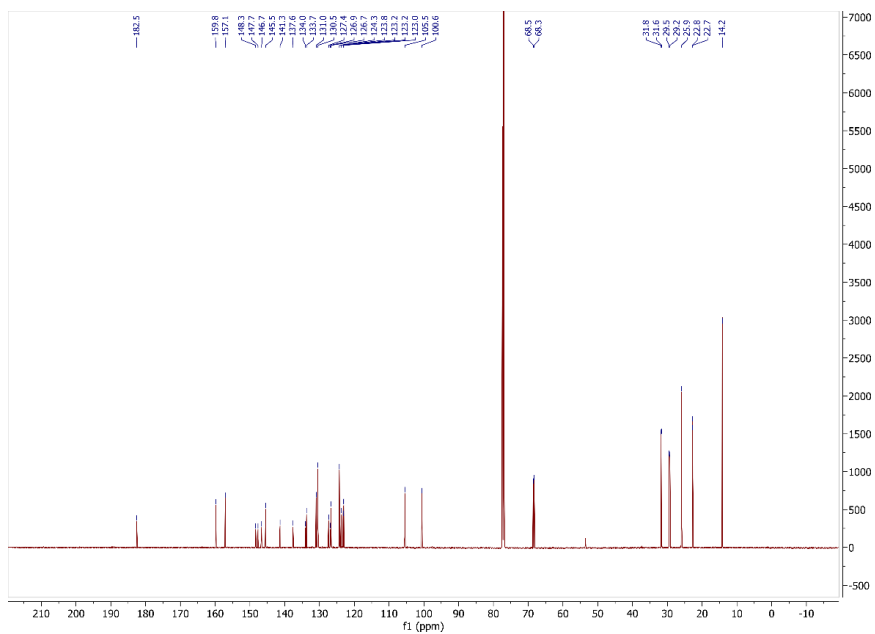
Figure S20. ^{13}C NMR (150 MHz, CDCl$_3$) spectrum for compound **15**.
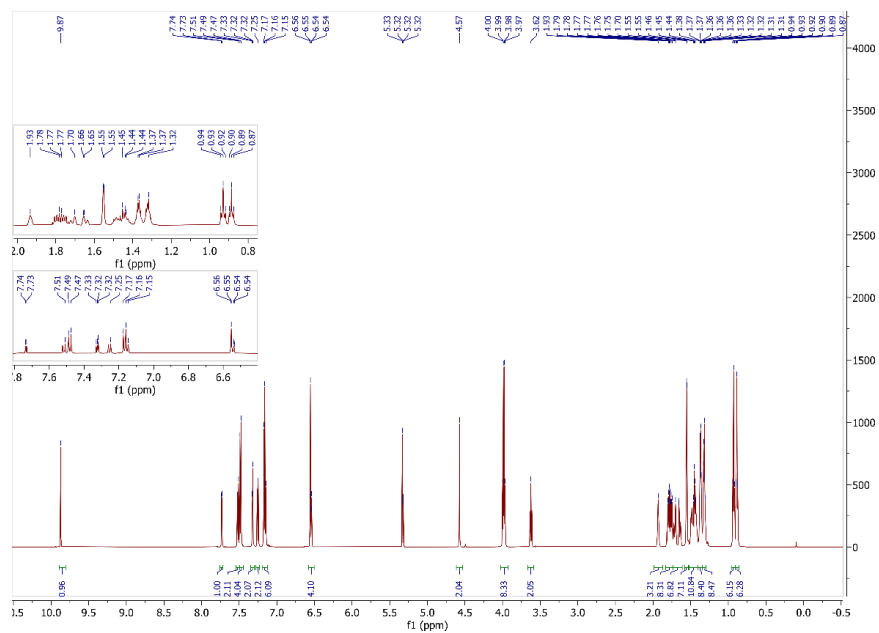
Figure S21. ^{1}H NMR (600 MHz, CD$_2$Cl$_2$) spectrum for compound **16**.

Figure S22. ^{13}C NMR (150 MHz, CD$_2$Cl$_2$) spectrum for compound **16**.

Figure S23. ^{1}H NMR (600 MHz, CD$_2$Cl$_2$) spectrum for compound **17**.

Figure S24. ^{13}C NMR (150 MHz, CD$_2$Cl$_2$) spectrum for compound **17**.

Figure S25. ^{1}H NMR (600 MHz, DMSO-d_6, 80 °C) spectrum for dye **JK-305**.

Figure S26. ^{13}C NMR (150 MHz, DMSO-d_6, 80 °C) spectrum for dye **JK-305**.

Figure S27. ^{1}H NMR (600 MHz, Acetone-d_6) spectrum for dye **BSH-2**.

Figure S28. ^{13}C NMR (150 MHz, Acetone-d_6) spectrum for dye **BSH-2**.
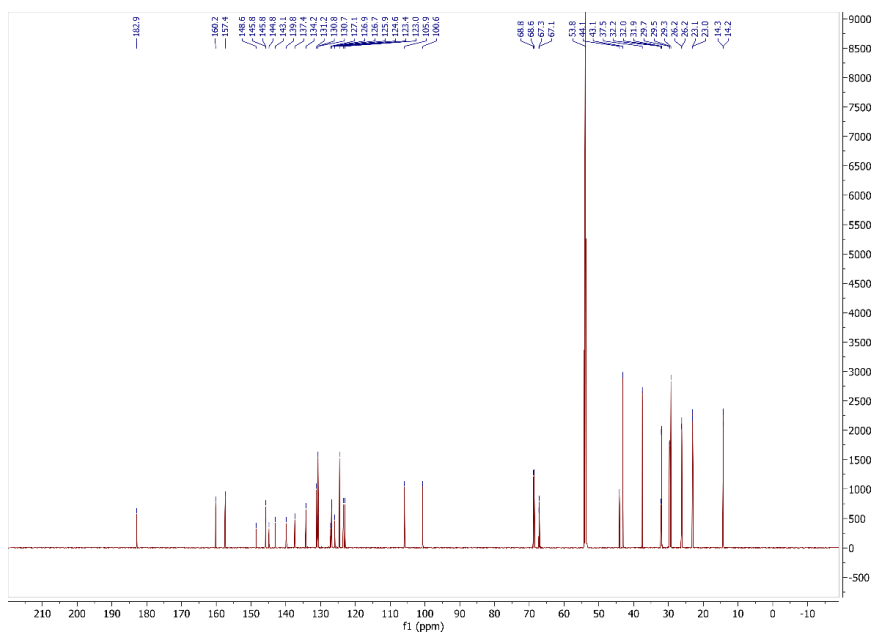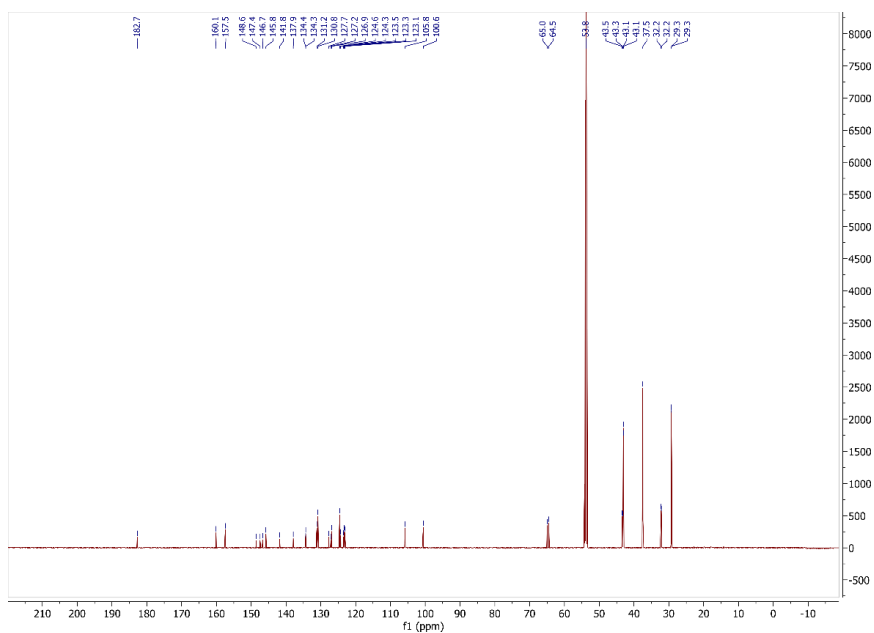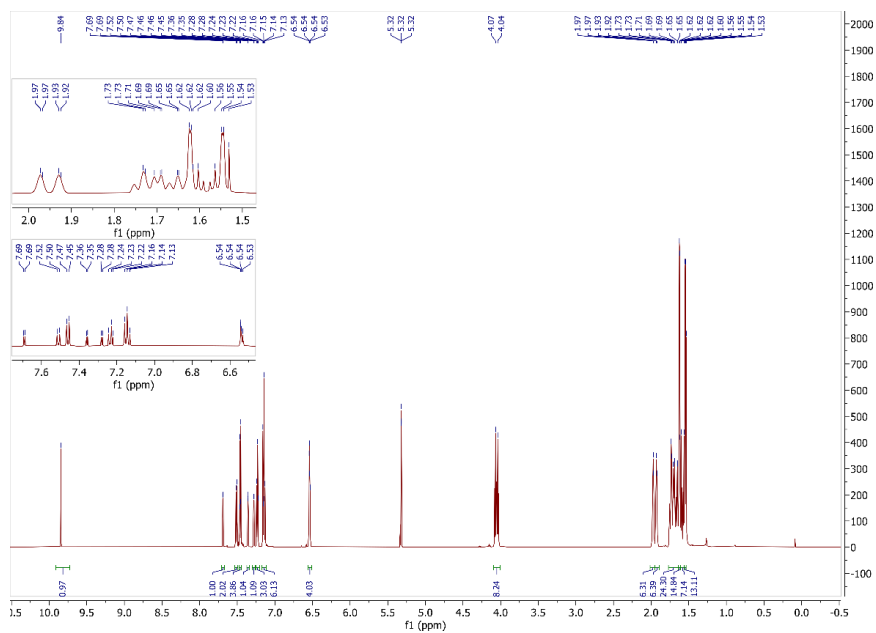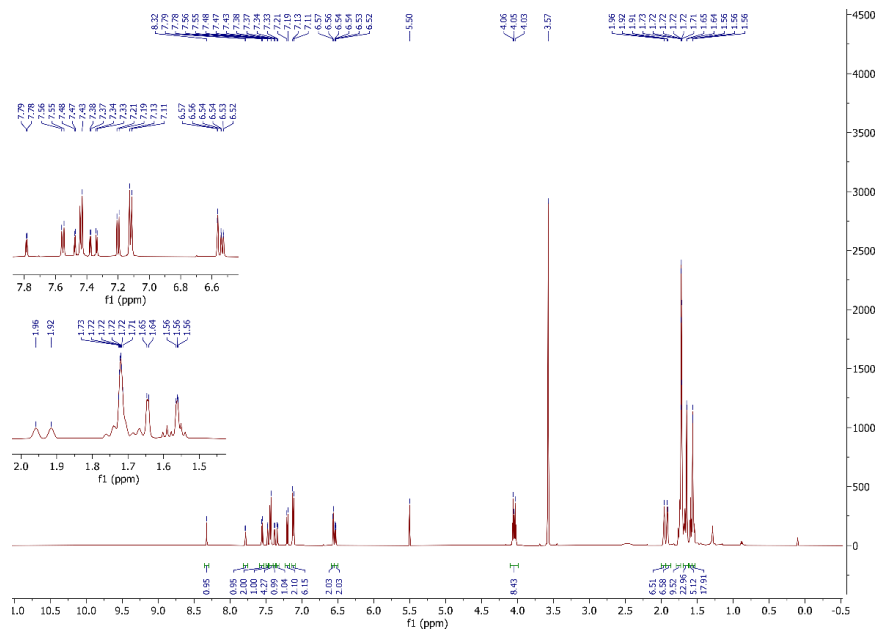
Figure S29. ^{1}H NMR (600 MHz, THF-d_8) spectrum for dye **BSH-3**.

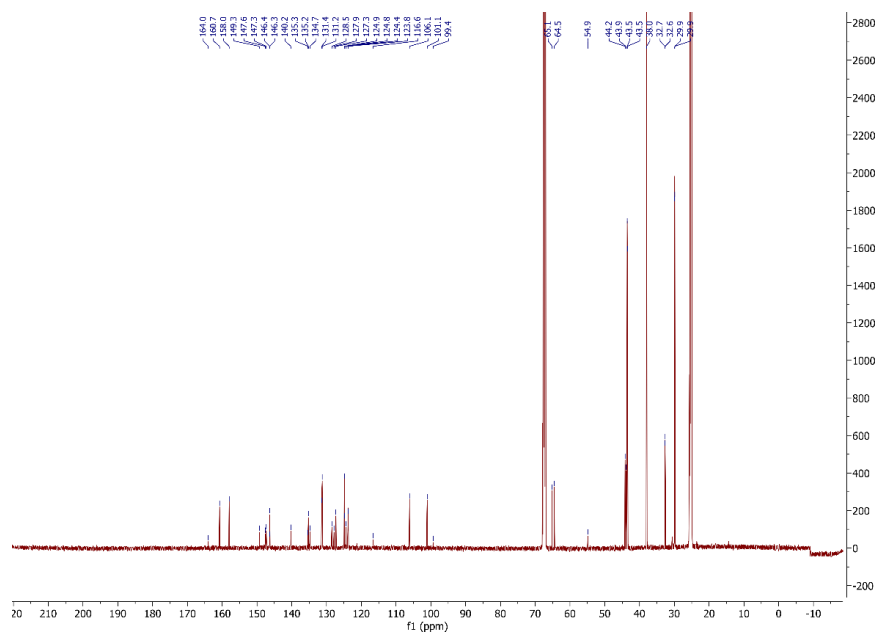**Figure S30.** ^{13}C NMR (150 MHz, THF-d_8) spectrum for dye **BSH-3**.

References

[1] Pavlishchuk VV, Addison AW, *Inorg Chim Acta*, **2000**, *298*, 97.

[2] Tsao HN, Yi C, Moehl T, Yum J-H, Zakeeruddin SM, Nazeeruddin MK, Grätzel M, *ChemSusChem*, **2011**, *4*, 591.

[3] Zhang D, Stojanovic M, Ren Y, Cao Y, Eickemeyer FT, Socie E, Vlachopoulos N, Moser J-E, Zakeeruddin SM, Hagfeldt A, Grätzel M, *Nature Communications*, **2021**, *12*, 1777.

[4] Cloutier M, Mamone M, Paquin J-F, *Chem Commun*, **2020**, *56*, 5969.

[5] Belser T, Stöhr M, Pfaltz A, *J. Am. Chem. Soc.*, **2005**, *127*, 8720.

[6] Buene AF, Almenningen DM, Hagfeldt A, Gautun OR, Hoff BH, *Sol. RRL*, **2020**, *4*, 1900569.

[7] Lim, K, Ju, MJ, Song, J, Choi, IT, Do, K, Choi, H, Song, K, Kim, HK, Ko, J, *ChemSusChem*, **2013**, *6*, 1425.